DOE/MC/23075 -- 5031
(DE96003016)
Vol. II

Measurement and Modeling of Advanced Coal Conversion Processes Volume II

User's Manual 93-PCGC-2: Pulverized Coal Gasification and Combustion Model (2-Dimensional) with a Generalized Coal Reactions Submodel (FG-DVC)

Peter R. Solomon
Michael A. Serio
David G. Hamblen
Ziaul Huque
Andrew M. Eaton
Sylvie Charpenay
Zhen Zhong Yu

L. Douglas Smoot
B. Scott Brewster
Richard D. Boardman
Susana K. Berrondo
Yuxin Zhao
Philip E. Best

June 1993

Work Performed Under Contract No.: DE-AC21-86MC23075

For
U.S. Department of Energy
Office of Fossil Energy
Morgantown Energy Technology Center
Morgantown, West Virginia

By
Advanced Fuel Research, Inc.
East Hartford, Connecticut
and
Brigham Young University
Provo, Utah

DISCLAIMER

DOE/MC/23075 -- 5031

MEASUREMENT AND MODELING OF ADVANCED COAL CONVERSION PROCESSES
Volume II -- 93-PCGC-2 User's Manual

DOE

DOE/MC/23075 -- 5031
(DE96002316)
Vol. II
Distribution Category UC-109

Measurement and Modeling of Advanced Coal Conversion Processes Volume II

User's Manual 93-PCGC-2: Pulverized Coal Gasification and Combustion Model (2-Dimensional) with a Generalized Coal Reactions Submodel (FG-DVC)

Peter R. Solomon
Michael A. Serio
David G. Hamblen
Ziaul Huque
Andrew M. Eaton
Sylvie Charpenay
Zhen Zhong Yu
L. Douglas Smoot
B. Scott Brewster
Richard D. Boardman
Susana K. Berrondo
Yuxin Zhao
Philip E. Best

Work Performed Under Contract No.: DE-AC21-86MC23075

For
U.S. Department of Energy
Office of Fossil Energy
Morgantown Energy Technology Center
P.O. Box 880
Morgantown, West Virginia 26507-0880

By
Advanced Fuel Research, Inc.
87 Church Street
East Hartford, Connecticut 06108
and
Brigham Young University
Provo, Utah 84602

June 1993

Abstract

A two-dimensional, steady-state model for describing a variety of reactive and non-reactive flows, including pulverized coal combustion and gasification, is presented. Recent code revisions and additions are described. The model, referred to as 93-PCGC-2, is applicable to cylindrical, axi-symmetric systems. Turbulence is accounted for in both the fluid mechanics equations and the combustion scheme. Radiation from gases, walls, and particles is taken into account using a discrete ordinates method. The particle phase is modeled in a Lagrangian framework, such that mean paths of particle groups are followed. A new coal-general devolatilization submodel (FG-DVC) with coal swelling and char reactivity submodels has been added. The heterogeneous reaction scheme allows for both diffusion and chemical reaction. Major gas-phase reactions are modeled assuming local instantaneous equilibrium, and thus the reaction rates are limited by the turbulent rate of mixing. A thermal and fuel NO_x finite rate chemistry submodel is included which integrates chemical kinetics and the statistics of the turbulence. A sorbent injection submodel with sulfur capture is included. The gas phase is described by elliptic partial differential equations that are solved by an iterative line-by-line technique. Under-relaxation is used to achieve numerical stability. Both combustion and gasification environments are permissible. User information and theory are presented, along with sample problems.

Preface

Considerable effort has been made to produce a computer code which will converge to a solution under as wide a variety of input conditions as possible. First elements of this code have been operating at Brigham Young University since 1977, with improvements having been made continuously since that time. Hundreds of predictions have been made with the code; however, the complex nature of the physical processes being modeled results in a numerical computer program that is sensitive to input conditions. Users are cautioned that arbitrary sets of input parameters will not necessarily produce converged solutions. A thorough understanding of the model equations and the numerical solution technique will give the user a better understanding of how to adjust appropriate numerical parameters to obtain a converged solution. 93-PCGC-2 is still considered to be a "specialist usable" code.

This code has been developed to apply to a variety of reacting and non-reacting flows, including pulverized coal combustion and coal gasification. Gasification can be interpreted as fuel-rich combustion, with little or no differences in the basic governing processes. Recent extensions have included the ability to predict laminar and near-laminar systems.

Key improvements and changes in the code include the following: 1) coal-general devolatilization submodel (FG-DVC) with coal swelling and char reactivity submodels; 2) robust, user-friendly energy equation option; 3) laminar-flow option and laminarization with turbulence; 4) generalized solids feeding in inlets other than the primary; 5) condensed-phase equilibrium algorithm; 6) thermal NO submodel; 7) sorbent particle injection with sulfur capture; and 8) graphical pre-processor. In order to differentiate among various versions of the code, the version associated with this user's manual is referred to as 93-PCGC-2, the "93" indicating the year of release. The code is referred to herein as simply "PCGC-2."

Acknowledgments

This document is the user's manual for the improved computer model for Pulverized Coal Gasification and Combustion in Two Dimensions (93-PCGC-2). The code is so named in order to differentiate it from the earlier version, 87-PCGC-2, and because it was completed in 1993. Work on this code was initiated originally under contracts from the U.S. Department of Energy and the Electric Power Research Institute in December of 1974. Research and development on this technology has continued since that time.

Work during 1982 through 1984 was supported by the U.S. Department of Energy, Morgantown Energy Technology Center (METC), Morgantown, West Virginia, under Contract No. DE-AC21-81MC-16518 with Mr. Gary R. Friggens and subsequently Dr. Holmes A. Webb, Jr., and then Dr. Lily Herskovits as Technical Project Officers; Grant No. DE-FG22-80PC-30306 with Mr. James Hickerson as Technical Project Officer; and Contract No. DE-AC21-80MC-14368 with Mr. Kenneth Markel as Technical Project Officer; The Electric Power Research Institute, Palo Alto, California, under Contract No. RP-364-3 with Mr. John Dimmer as Contract Officer. Work during the period from 1985 to April 30, 1987 was sponsored in part by METC under Contract No. DE-AC21-85MC-22059. Mr. Gary Friggens was the DOE technical project officer until the summer of 1986 when Mr. Leland E. Paulson became the technical project officer for DOE.

Work from 1985 to 1987 was also sponsored by Technical Associates and Affiliates of the University's Advanced Combustion Engineering Research Center who were in alphabetical order: Advanced Fuel Research, Babcock and Wilcox, Chevron Research Co., Combustion Engineering Co., Consolidation Coal Co., Convex Computer Corp., Corning Glass Works, Dow Chemical U.S.A., Electric Power Research Institute, Empire State Electric Energy Research Corp., Foster Wheeler Development Co., Gas Research Institute, General Electric Corp., General Motors Corp., Idaho National Engineering Laboratory, International Fuel Cells, Morgantown Energy Technology Center (METC), Pittsburgh Energy Technology Center, Pyropower Corp., Questar Development Corp., Shell Development Co.,

Southern California Edison Co., Tennessee Valley Authority, The National Science Foundation, The State of Utah, TRW, Inc. and Utah Power and Light Co.

During the last six years, work continued jointly by BYU and Advanced Fuel Research, Inc. (AFR) under sponsorship of METC. Mr. Justin Beeson, Dr. Richard Johnson, and Dr. Norman Holcomb were Contracting Office Technical Representatives (COTRs). Financial cost sharing from the Research Division of Brigham Young University for development of this code during the entire period of development is gratefully acknowledged.

Table of Contents

APPENDICES

List of Figures

List of Tables

Chapter One

Introduction

This manual presents the details of the improved and revised two-dimensional computer code referred to as 93-PCGC-2 (Pulverized Coal Gasification and Combustion: 2-Dimensional), which can be used to describe a variety of reacting and non-reacting flows, including pulverized coal combustion and gasification. This version of PCGC-2 has also been used to describe the combustion of gaseous diffusion flames and isothermal, two-phase fluid mechanics. Previous versions of the code have also been applied to liquid sprays, coal slurries, and other oxidation/reduction reaction chambers.

The modeling scheme is based on an Eulerian framework for the gas phase and a mixed Eulerian/Lagrangian framework for the particle phase. The approach emphasizes the turbulent fluid mechanics and the turbulent combustion processes in a turbulent flame. Most gas-phase reactions are assumed to be mixing-limited, so that gaseous combustion is modeled with a statistical probability density function based on mixture fractions. A two-equation (k-ε) turbulence model is used for closure. The particle phase includes the effects of aerodynamic particle drag and turbulent particle dispersion. Particle reactions are considered to be slow with respect to the gas-phase turbulence time scale. Rate processes for slurry liquid vaporization, coal devolatilization, and char reaction are included, based on time-

mean gaseous properties. Particle and gas radiation, with anisotropic and multiple scattering, are included.

The description that follows applies to entrained-flow, pulverized-coal reaction processes, where particles are small (<150 μm) and heating rates are high (10^3-10^6 K s^{-1}). This treatment would not necessarily apply to fixed- or fluidized-bed processes without modification.

Code Development

Formulation, numerical solution and evaluation of 93-PCGC-2, or just PCGC-2 as it is commonly called herein, has been completed over the past 12-13 years. Development has reached a point where the code is being applied to systems of practical interest. However, appropriate use of this comprehensive code requires a thorough understanding of the basic code foundations and operation. Our experience suggests that a person with an advanced (i.e. graduate) engineering degree and a strong background in fluid mechanics, heat and mass transfer, thermodynamics, and numerical analysis requires at least six months to a year (full time) to effectively understand and use the code. Results can be obtained faster with the guidance of experienced users.

Code Improvements and Revisions

The 1993 release of PCGC-2 contains several improvements over the previous (1987) release, including a generalized coal reactions submodel with a database of coal reaction parameters for the eight coals in the Argonne Premium Coal Sample Program, improved applicability to fuel-rich systems (e.g. gasification) due to a new condensed-phase chemical equilibrium submodel, an extended pollutant submodel, generalized solids feeding with capability for sorbent injection and sulfur capture, a laminar-flow option and laminarization with turbulence, effects of gas buoyancy, improved robustness and user-friendliness, and improved code graphics. Each of these improvements is briefly described below.

The generalized coal reactions submodel was developed by Solomon and coworkers (Solomon et al., 1988) at Advanced Fuel Research, Inc., and is referred to herein and in the literature as the FG-DVC model. It is basically a combination of two submodels, a function group (FG) submodel for predicting evolution of light gases and tar, and a char formation submodel based on the processes of char depolymerization, tar vaporization, and char cross-linking (DVC). Information from FG-DVC is also used in the particle submodel to predict swelling and char reactivity. A database of submodel parameters for the eight standard Argonne coals is provided with the code, so that the user need only specify the type of coal he or she wishes to use. Coals other than the Argonne coals are accommodated through an interpolation scheme.

The new condensed-phase equilibrium submodel was based on the METCEC code. It was developed by METC based on the NASA-Lewis equilibrium code CEC. It's incorporation into 93-PCGC-2 has improved code predictions for fuel-rich cases where solid carbon is a significant species for very fuel-rich stoichiometric mixtures. The new submodel was incorporated as an option, preserving the older CREE chemical equilibrium option which is faster and which is still applicable to gaseous combustion and fuel-lean coal systems.

The full energy equation option is considerably more robust, user-friendly, and accurate, than in the previous version of PCGC-2. Full energy equation solutions can now be accomplished fairly routinely. The basic theory regarding the treatment of enthalpy in turbulent flows has remained unchanged, but the particle-gas interaction term is calculated more accurately, and the table look-up scheme for gas properties is more accurate, robust, efficient, and user-friendly.

The pollutant submodel was extended to calculate fuel NO_x with additional mechanisms that are applicable to fuel-rich (gasification) conditions. In addition, capability was added for calculating thermal NO_x. A sorbent reactions submodel was added to calculate the capture of SO_2 or H_2S by injected sorbent particles.

The solids feed submodel was generalized to allow solids feeding in the secondary and additional (e.g. sidewall) inlets. In addition, capability was added

for injecting and tracking sorbent particles and their reactions after the main combusting coal particle/gas flowfield has been computed.

An option was added to PCGC-2 for modeling laminar flow. This option still assumes gas mixing to be rate limiting (i.e. infinite-rate gas kinetics). A laminarization extension was also added to the k-ε turbulence submodel to calculate transitional flow. A gas buoyancy term was added to the axial gas momentum equation to allow free convection effects to be included in these types of flows.

Significant improvements were also been made in the area of code graphics. An X-windows-based pre-processor, which uses software available for license under an independent arrangement, was developed for quickly generating code input files for "standard" cases. A standard case is defined as one which has no additional inlets (i.e. only a primary and a secondary), no intrusions (reactor diameter is constant except for the quarl region), and coal properties can be modeled by one of the Argonne coals. The pre-processor provides default values for most of the code options and input parameters, and is a considerable step forward in making the code usable by a person who has a technical background, but no experience with PCGC-2. In addition to the pre-processor, an improved post-processor, which also uses software available for license under an independent arrangement, provides plotting capability for gas and particle properties, as well as results of pollutant calculations. There is also an option for converting output data into a format compatible with spreadsheet plotting programs.

Limitations

The following limitations apply to PCGC-2.

- The flowfield, geometry (e.g. inlets and intrusions), and body forces (gravity) are axisymmetric.
- The flow is subsonic (dilatation is ignored). The maximum Mach number should be less than about 0.3.

- Chemical reaction rates are limited by turbulent mixing and not by kinetics (with the exception of nitrogen oxides).
- Particles are dispersed in the gas phase, and particle-particle interactions are ignored.

These assumptions are discussed in the next chapter.

The submodels dealing with turbulence issues are at best tenuous. Specifically, the turbulence (k-ε), turbulent particle dispersion, and turbulence-chemistry interactions, are not yet capable of producing accurate results in all cases.

Document Format

This users manual is organized into two parts. Part One documents the theory (Chapter 2), the solution of the model equations (Chapter 3), and the generalized particle reactions submodel (Chapter 4). An understanding of the theoretical foundations of the code is prerequisite to its correct application, and potential users are encouraged to study this material carefully. Part Two describes the use of the code (Chapters 5 and 6), it's implementation on computer hardware (Chapter 7), and sample problems illustrating code application (Chapter 8). While significant effort has been expended to make the code user-friendly and robust, it must be recognized that PCGC-2 is still very much a "user-specialist" code requiring a significant amount of experience beyond simple theoretical understanding for efficient management and use. Laboratories interested in extensive use of PCGC-2 should plan on committing a technical person full-time for approximately six months to a year to learn to use this code. Training is available as described below.

Code Availability and Training

The 1993 version of PCGC-2 with FG-DVC submodel was developed jointly by Brigham Young University and Advanced Fuel Research, Inc. under contract to the

Department of Energy (Contract No. DE-AC21-86MC23075). It is a shared product of the Advanced Combustion Engineering Research Center and is subject to Center distribution policy for shared products. The code will be available starting approximately May 1, 1993.

Organizations wishing to obtain the code should contact

Dr. Andrew M. Eaton
ACERC Software Specialist
75 CTB
Brigham Young University
Provo, Utah 84602
(801) 378-5008
Fax: (801) 378-3831

The source code and sample problems are available on magnetic tape. The code has been developed on Convex and Sun Microsystems computers with the UNIX operating system. The code is not guaranteed to run on any particular computer system, however, and users should plan on making modifications, particularly if their system is not one of the above. The extent of the required modifications varies with each installation.

Training in the use of the code is also available through the Advanced Combustion Engineering Research Center (ACERC). This training is best accomplished on an individual basis. Interested scientists and engineers are encouraged to visit the laboratory for a short period (4-6 weeks) during which time they will receive assistance in learning to use the code and apply it to a problem of interest. All travel and living expenses during this period will be the responsibility of the visiting scientist/engineer[1]. On-campus housing may be available, especially during the non-academic (summer) months. BYU will provide office space and computer resources and assist in making suitable housing arrangements.

[1]Industrial Associate trainees can request partial financial support from ACERC for their visit to the Center.

Chapter Two

Theoretical Development

The mathematical modeling of turbulent combustion and gasification has been recognized as a difficult problem not only due to the numerical challenges associated with solving the differential equation set but also the challenges of physically describing the important chemical and physical processes, such as chemistry-turbulence interactions, turbulent particle dispersion, particle reactions, etc. PCGC-2 uses currently available mathematical technology to combine knowledge of fluid mechanics with a reasonable approach to the reaction processes. Care has been taken to maintain the scope of the simplifying approximations on a consistent level.

Model Basis

PCGC-2 has been applied to non-reacting flow systems, gaseous diffusion flames, pulverized coal-fired combustion, entrained-flow gasification, droplet combustion, and slurry combustion or gasification (including coal-water mixtures) in axisymmetric coordinates. Variations in the properties are considered only in the axial and radial directions. Symmetry is assumed in the angular direction. A

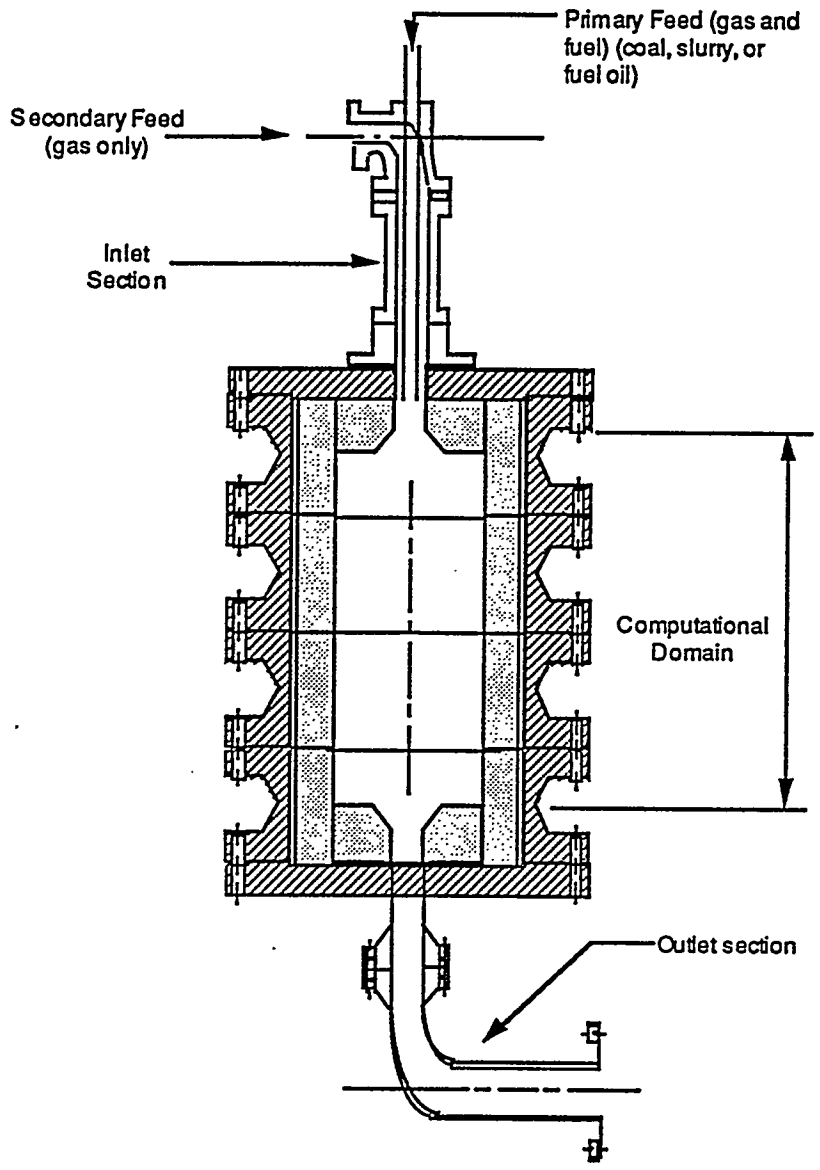

Figure 2-1. Two-dimensional reactor schematic.

schematic of a typical reactor modeled by PCGC-2 is shown in Figure 2-1 (Smith, 1979; Thurgood, 1979). This particular cylindrical reactor is coaxial, with coal entering the reactor in the central (primary) stream and the majority of the oxidizer entering in the outer (secondary) stream or annulus. The code has been generalized to include multiple inlets that can be located along any of the walls and to include arbitrary shapes within the axisymmetric assumption. Typical pulverized coal particles range in size from two micrometers (microns) to one hundred fifty micrometers. Slurry droplets can reach several hundred micrometers. The model predicts the mean gas field properties for axisymmetric, steady-state, turbulent flames (i.e., local velocity, temperature, density, and species composition). Particle properties are also computed, such as coal burnout, particle or droplet velocity and temperature, and coal/droplet component composition. Figure 2-2 illustrates the various submodels incorporated into PCGC-2.

The gas phase is assumed to be a turbulent, reacting continuum field that can be described locally by general conservation equations. The flow is assumed to be time-steady. Gas properties (i.e., density, temperature, species composition) are assumed to fluctuate randomly according to a probability density function (PDF) characteristic of the turbulence. Gas-phase body forces are neglected. The gas is assumed to be Newtonian and dilatation is neglected.

The gas field is treated in an Eulerian framework. Turbulence is modeled by breaking the variables into fluctuating and time-mean components in the conventional manner (Hinze, 1967; Tennekes and Lumley, 1972). The two-equation k-ε model is used for closure (Launder and Spalding, 1972). PCGC-2 is coded to handle either Reynolds- or Favre-averaging. The effect of particles on the gas-phase turbulence is modeled with an empirical correlation. Gas-phase reactions are assumed to be limited by mixing rates for major species and not by kinetics; gaseous properties are calculated assuming local instantaneous equilibrium. For non-equilibrium reactions, such as occur in methane flames or in coal gasifiers, partial (frozen) equilibrium can be used to describe mixing-limited reactions.

The pulverized coal flame radiation field is a multicomponent, non-uniform, emitting, absorbing, scattering gas-particle system (Smith et al., 1981). The coal particles cause anisotropic and multiple scattering. The flame may be surrounded

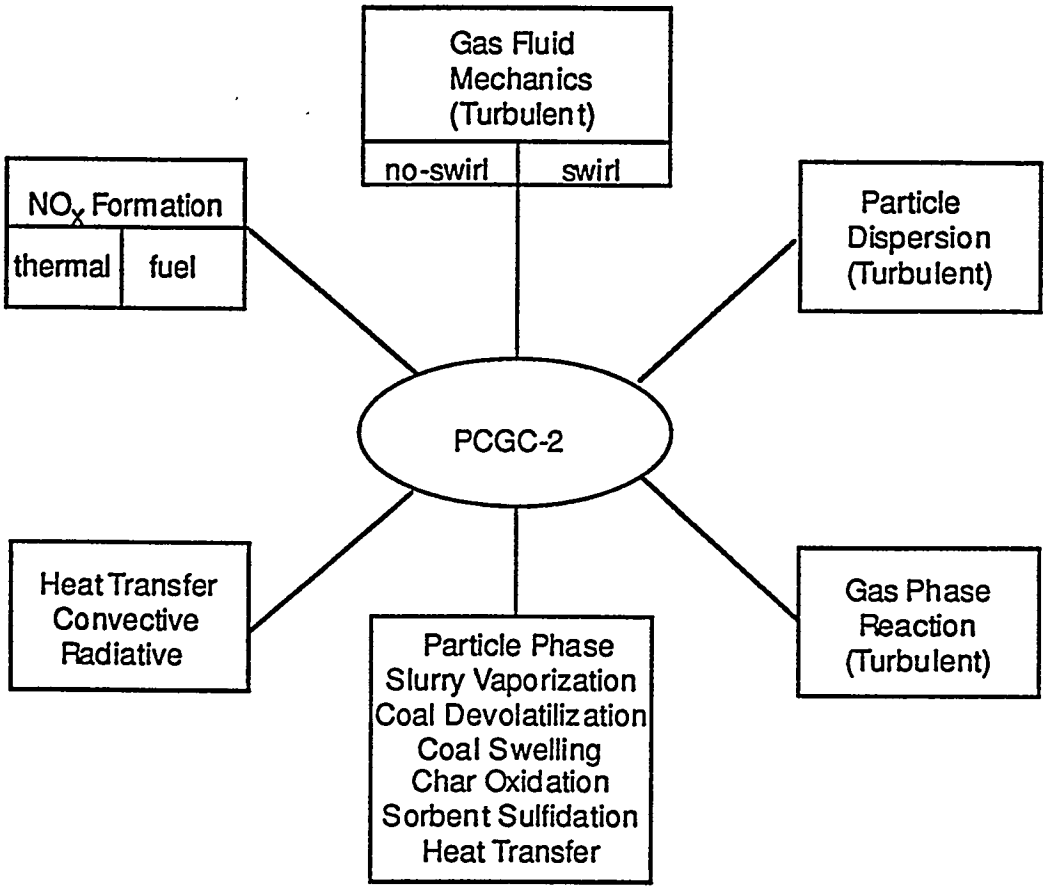

Figure 2-2. Submodels in PCGC-2.

by non-uniform, emitting, reflecting, absorbing surfaces. Optical coefficients for the gas, walls, and particles are difficult to obtain in flames (Sarofim and Hottel, 1978) and PCGC-2 uses the recommendations of Varma and Pratt (1978) to calculate the optical coefficients necessary for a pulverized coal flame. An Eulerian framework is used to model the radiation, which facilitates incorporation of radiation properties into gas-phase equations. The Lagrangian particle field does

not mesh completely with the Eulerian radiation equations, since a bulk particle density is difficult to obtain from Lagrangian systems.

The particle phase is not considered a continuum as is the gas phase (Smith et al., 1981; Fletcher, 1980). Different particles at the same location may exhibit different properties due to their different histories. In PCGC-2, Lagrangian treatment of the particles is performed, representing the particle field as a series of mean trajectories. Particle properties can be obtained along the mean trajectories by integration of the governing particle equations. The effect of turbulent fluctuations on the trajectories of the particles is treated in a mixed Eulerian-Lagrangian framework. The effect of turbulent fluctuations in the gas phase on particle reaction rates is ignored.

PCGC-2 assumes that the off-gas from the coal is of constant elemental composition. The particle reaction submodel is discussed by Smith (Smith, 1979) (see also Smoot and Pratt, 1979; Fletcher, 1983). Particles are defined to consist of slurry liquid, raw coal, char, and ash. Ash is inert by definition; volatile mineral matter is considered as part of the volatile matter of the coal. Coal reaction rates can be characterized by multiple parallel reaction rates with fixed activation energies, or by a general coal reactions submodel (FG-DVC) based on a functional group description of the coal for gas evolution, and a network description for depolymerization, tar vaporization, and cross-linking. In the former case, coal particle swelling is predicted empirically. In the latter case, it can be predicted from gas evolution rate and viscosity of the melt (see Chapter 4). The particles are assumed to be isothermal. The parameters which describe the coal reaction rates are part of the input to the code. Default values can also be supplied by the code for some of the parameters, based on coal type.

Gas Differential Equations

All of the gas-phase equations are Eulerian, steady-state, second-order, non-linear, elliptical partial differential equations. Each of these may be conveniently cast into one finite difference form, so that only one solution technique is required. Table 2-1 contains a summary of this form for all of the gas phase equations. Note that the particles are accounted for only by appropriate particle source terms for mass (S_p^m) ,

momentum (S_p^u and S_p^v), and enthalpy (S_p^h). These terms represent the addition of mass, momentum, and energy to the gas phase from the particles. The source terms are found along a particle trajectory by taking the difference in the particle properties on each side of a computational cell and dividing by the cell volume (see Chapter III).

The following sections describe each of the equations in Table 2-1 in more detail. The equations for the radiation field and the particle number-density field do not fit the form of the gas-phase equations and are discussed separately. The method used to solve these equations is discussed in Chapter 3.

TABLE 2-1

GAS PHASE DIFFERENTIAL EQUATIONS

$$\frac{\partial}{\partial x}(\bar{\rho}\tilde{u}\phi)+\frac{1}{r}\frac{\partial}{\partial r}(r\bar{\rho}\tilde{v}\phi)-\frac{\partial}{\partial x}\left(\Gamma_\phi\frac{\partial\phi}{\partial r}\right)-\frac{1}{r}\frac{\partial}{\partial r}\left(r\Gamma_\phi\frac{\partial\phi}{\partial r}\right)=S_\phi$$

ϕ	Γ_ϕ	S_ϕ
1	0	S_p^m
$\tilde{u}$	μ_e	$-\frac{\partial\bar{p}}{\partial x}+\frac{\partial}{\partial x}\left(\mu_e\frac{\partial\tilde{u}}{\partial x}\right)$ $+\frac{1}{r}\frac{\partial}{\partial r}\left(r\mu_e\frac{\partial\tilde{v}}{\partial x}\right)\begin{cases}+\bar{\rho}g\ \text{(down - fired)}\\ -\bar{\rho}g\ \text{(up - fired)}\\ +0\ \text{(horizontally fired)}\end{cases}+S_p^u+\tilde{u}S_p^m$
$\tilde{v}$	μ_e	$-\frac{\partial\bar{p}}{\partial r}+\frac{\partial}{\partial x}\left(\mu_e\frac{\partial\tilde{u}}{\partial r}\right)+\frac{1}{r}\frac{\partial}{\partial r}\left(r\mu_e\frac{\partial\tilde{v}}{\partial r}\right)-2\mu_e\frac{\tilde{v}}{r^2}+\frac{\bar{\rho}}{r}\tilde{w}\tilde{w}+S_p^v+\tilde{v}S_p^m$
$\tilde{w}$	μ_e	$-\frac{\rho\tilde{v}\tilde{w}}{r}-\frac{\tilde{w}}{r^2}\frac{\partial}{\partial r}(r\mu_e)$

TABLE 2-1 (continued)

$$\frac{\partial}{\partial x}(\bar{\rho}\tilde{u}\phi)+\frac{1}{r}\frac{\partial}{\partial r}(r\bar{\rho}\tilde{v}\phi)-\frac{\partial}{\partial x}\left(\Gamma_\phi\frac{\partial\phi}{\partial r}\right)-\frac{1}{r}\frac{\partial}{\partial r}\left(r\Gamma_\phi\frac{\partial\phi}{\partial r}\right)=S_\phi$$

ϕ	Γ_ϕ	S_ϕ
k	μ_e/σ_k	$\Phi-\bar{\rho}\varepsilon$
ε	μ_e/σ_ε	$\frac{\varepsilon}{k}[C_1\Phi-C_2\bar{\rho}\varepsilon]$
$\tilde{f}_p$	μ_e/σ_f	S_p^f
g_f	μ_e/σ_g	$\frac{C_{g1}\mu_e}{\sigma_g}\left[\left(\frac{\partial\tilde{f}}{\partial x}\right)^2+\left(\frac{\partial\tilde{f}}{\partial r}\right)^2\right]-\frac{C_{g2}\bar{\rho}\varepsilon g_f}{k}$
$\tilde{\eta}$	μ_e/σ_η	S_p^η
g_η	μ_e/σ_g	$\frac{C_{g1}\mu_e}{\sigma_g}\left[\left(\frac{\partial\tilde{\eta}}{\partial x}\right)^2+\left(\frac{\partial\tilde{\eta}}{\partial r}\right)^2\right]-\frac{C_{g2}\bar{\rho}\varepsilon g_\eta}{k}$
$\tilde{h}$	μ_e/σ_h	$q'_{rg}+\tilde{u}\frac{\partial\bar{p}}{\partial x}+\tilde{v}\frac{\bar{p}}{\partial r}+S_p^h$

where $\Phi=\mu_e\left\{2\left[\left(\frac{\partial\tilde{u}}{\partial x}\right)^2+\left(\frac{\partial\tilde{v}}{\partial r}\right)^2+\left(\frac{\tilde{v}}{r}\right)^2\right]+\left[\frac{\partial\tilde{u}}{\partial r}+\frac{\partial\tilde{v}}{\partial x}\right]^2+\left[r\frac{\partial}{\partial r}\left(\frac{\tilde{w}}{r}\right)\right]^2+\left(\frac{\partial\tilde{w}}{\partial x}\right)^2\right\}$

$$\mu_e=\mu^t+\mu^\ell$$

$$\mu^t = C_\mu \bar{\rho} k^2/\varepsilon \qquad\qquad S_p^m = S_p^f + S_p^n$$

Gas-Phase Fluid Mechanics

The instantaneous gas-phase equations of continuity and momentum (Bird et al., 1960) are presented here with the particle reaction source terms (Smoot and Pratt, 1979). Equations for turbulence properties, mixture fractions, and energy can be similarly derived. The equations of continuity and motion are:

$$\frac{D\rho}{Dt} = -\rho\left(\vec{\nabla}\cdot\vec{v}\right) + S_p^m \tag{2-1}$$

$$\rho\frac{D\vec{v}}{Dt} = -\vec{\nabla}p - \vec{\nabla}\cdot\bar{\bar{\tau}} + \rho\vec{g} + \vec{S}_p^v \tag{2-2}$$

where D/Dt is the substantial derivative. The S_p terms represent the coupling between the gas phase and the particle phase, i.e. the particle source/sink terms. All variables are defined in the Nomenclature.

The equations are reduced with following simplifications: 1) cylindrical coordinates, 2) 2-dimensional axisymmetric geometry, 3) body forces only in the axial direction, 4) steady-state, and 5) Newtonian fluid. Equations 2-1 and 2-2 become:

$$\frac{\partial}{\partial x}(\rho u) + \frac{1}{r}\frac{\partial}{\partial r}(r\rho v) = S_p^m \tag{2-3}$$

$$\begin{aligned}&\frac{\partial}{\partial x}(\rho uu) + \frac{1}{r}\frac{\partial}{\partial r}(r\rho vu) - \frac{\partial}{\partial x}\left(\mu\frac{\partial u}{\partial x}\right) - \frac{1}{r}\frac{\partial}{\partial r}\left(\mu r\frac{\partial u}{\partial r}\right)\\ &= -\frac{\partial p}{\partial x} + \frac{\partial}{\partial x}\left(\mu\frac{\partial u}{\partial x}\right) + \frac{1}{r}\frac{\partial}{\partial r}\left(\mu r\frac{\partial v}{\partial x}\right) - \frac{\partial}{\partial x}\left(\frac{2}{3}\mu\, div\,\vec{v}\right) + \psi\rho g + S_p^u + u_{pg}S_p^m\end{aligned} \tag{2-4}$$

$$\frac{\partial}{\partial x}(\rho uv)+\frac{1}{r}\frac{\partial}{\partial r}(r\rho vv)-\frac{\partial}{\partial x}\left(\mu\frac{\partial v}{\partial x}\right)-\frac{1}{r}\frac{\partial}{\partial r}\left(\mu r\frac{\partial v}{\partial r}\right)$$
$$=-\frac{\partial p}{\partial r}+\frac{\partial}{\partial x}\left(\mu\frac{\partial u}{\partial r}\right)+\frac{1}{r}\frac{\partial}{\partial r}\left(\mu r\frac{\partial v}{\partial r}\right)-2\frac{\mu v}{r^2} \qquad (2\text{-}5)$$
$$-\frac{1}{r}\frac{\partial}{\partial r}\left(\frac{2}{3}\mu r\, div\,\vec{v}\right)+\frac{2}{3}\frac{\mu}{r}\, div\,\vec{v}+S_p^v+v_{pg}S_p^m$$

$$\frac{\partial}{\partial x}(\rho uw)+\frac{1}{r}\frac{\partial}{\partial r}(r\rho vw)-\frac{\partial}{\partial x}\left(\mu\frac{\partial w}{\partial x}\right)-\frac{1}{r}\frac{\partial}{\partial r}\left(\mu r\frac{\partial w}{\partial r}\right)$$
$$=-\frac{\rho vw}{r}-\left(\frac{w}{r^2}\right)\frac{\partial}{\partial r}(r\mu) \qquad (2\text{-}6)$$

where ψ is equal to 1 for downfired, -1 for upfired, and 0 for horizontally fired.

One more approximation is made before arriving at the equations used in PCGC-2. The *div* $\vec{v}$ term in Eqns. 2-4 and 2-5 are associated with the dilatation of the fluid. These terms describe the volume change of a fluid element due to expansion or compression. For perfectly incompressible fluids, the equation of continuity can be used to prove that those terms are identically zero. For a compressible fluid, the effect is minimal at low velocities (less than 0.25 Mach No.) and is often neglected (Bird et al., 1960; Smoot and Pratt, 1979). This convention is also followed in PCGC-2.

It is useful to understand the significance of each term in the equation set. The first two terms in the equation of continuity (Eqn. 2-3) represent the net rate of mass addition to the volume element by convection from the axial and radial components respectively. The S_p^m term represents the net rate of mass addition per unit volume due to particle reaction. The first two terms in the momentum equations (Eqns. 2-4, 5 and 6) are the convection terms. They represent the net rate of convected momentum to the volume element attributed to the axial and radial components. Equation 2-4 describes the momentum contributed by the axial component of the velocity, Eqn. 2-5 describes that contributed by the radial component, and Eqn. 2-6 describes that contributed by the tangential component. The third and fourth terms in each of these equations may conveniently be thought

of as the corresponding diffusion terms. When turbulence is modeled using Reynolds stresses, they are not strictly molecular diffusion terms because of the contribution to the momentum due to turbulent transfer. The diffusion appearance of second-order derivatives makes it natural to refer to them in this way. The first term on the right-hand side of the axial and radial momentum equations represents the pressure force on the volume element. All other terms on the right-hand side of these equations are considered source or sink terms, representing other sources or sinks of momentum. The S_p^u and S_p^v terms represent the aerodynamic drag effects of the particles on the axial and radial components of momentum. The $u_{pg}S_p^m$ and $v_{pg}S_p^m$ terms represent the momentum exchange due to particle mass efflux. In this version of the code, u_{pg} and v_{pg} are assumed to be equal to the gas velocity and S_p^w and $w_{pg}S_p^m$ are neglected. These assumptions will be relaxed in future versions of the code. The reasons for these physical meanings for each term are more apparent because each differential equation is cast into the standard form of Table 2-1. The numerical method for solving these equations is discussed Chapter 3.

Equations 2-3 through 2-6 must be solved for u, v, w, and p. Historically, the pressure term caused numerical solution difficulties, and thus a transformation was used to change the four variables and four partial differential equations into two partial differential equations and two variables, namely, the stream function and vorticity. The pressure term was then eliminated. This approach had difficulties with defining the physical boundary conditions. The numerical approach discussed in Chapter 3 obviates the difficulties with the pressure term, and thus the primitive variable formulation (u, v, w, p) is solved in PCGC-2.

The Eulerian equation set, along with the appropriate boundary conditions (see Chapter 3), is sufficient to permit solution for the flow field, provided that the density and viscosity are known everywhere in the field. In an isothermal, constant-density fluid, these variables are known a priori. However, in the combustion system of interest, these variables are position dependent. It is through these terms alone that coupling of the combustion model to the fluid mechanics model occurs. This subject is discussed later in this chapter. Also, the problem of time-averaging changes the equation set somewhat. This is the topic of the next section.

Turbulence Model

The Closure Problem

In laminar flows, velocity gradients are sufficiently mild that the fluid can dynamically adjust to imposed shear stresses through molecular (viscous) forces. When imposed shear forces are too great for the fluid to adjust through molecular processes, the fluid is "torn" into largely coherent regions (turbulent eddies), which can rotate and thus relieve the shear forces caused by the imposed velocity differences. A review of turbulence and its associated closure problem can be found in Tennekes and Lumley (1972), and for applications to coal combustion modeling, in Smoot and Smith (1985). A particularly pertinent review of turbulence models and their applications to swirling flow is given by Sloan et al. (1986).

k-ε Turbulence Model Used in PCGC-2

PCGC-2 uses the approach to this closure problem credited to Boussinesq (1877) which is derived by analogy to the laminar Newtonian viscosity. It is assumed that

$$\overline{u'v'} = -\nu_g^t\left(\frac{\partial \bar{u}}{\partial r} + \frac{\partial \bar{v}}{\partial x}\right) \qquad (2\text{-}7)$$

where ν_g^t is the turbulent kinematic eddy viscosity. The correlation of fluctuating variables is thus expressed in terms of the mean field variables. Although Eqn. 2-7 is convenient, it does not have a sound theoretical basis. However, this approach has been widely used in turbulent gaseous systems, and is therefore applied in PCGC-2 for lack of a better model (Smith, 1979; Tennekes and Lumley, 1972; Pratt, 1976). A review of the accuracy of the approach in these applications with comparisons to more sophisticated approaches is given by Sloan, et al. (1986). The turbulence closure model used in PCGC-2 (Launder and Spalding, 1972) relates the turbulent kinetic energy (k) and its rate of dissipation (ε) by:

$$\nu_g^t = \frac{C_\mu k^2}{\varepsilon} \tag{2-8}$$

where:

$$k = \frac{\left(\overline{u''^2} + \overline{v''^2} + \overline{w''^2}\right)}{2} \tag{2-9}$$

Transport equations for k and ε can be derived from basic principles (Launder and Spalding, 1972), although some terms must be modeled empirically. The k and ε equations used in PCGC-2 are:

$$\frac{\partial}{\partial x}\left(\bar{\rho}\tilde{\mu}k\right) + \frac{1}{r}\frac{\partial}{\partial r}\left(r\bar{\rho}\tilde{v}k\right) - \frac{\partial}{\partial x}\left(\frac{\mu_e}{\sigma_k}\frac{\partial k}{\partial x}\right) - \frac{1}{r}\frac{\partial}{\partial r}\left(r\frac{\mu_e}{\sigma_k}\frac{\partial k}{\partial r}\right)$$
$$= \mu_e\left\{2\left[\left(\frac{\partial\tilde{\mu}}{\partial x}\right)^2 + \left(\frac{\partial\tilde{v}}{\partial r}\right)^2 + \left(\frac{\tilde{v}}{r}\right)^2\right] + \left(\frac{\partial\tilde{\mu}}{\partial r} + \frac{\partial\tilde{v}}{\partial x}\right)^2 + \left(r\frac{\partial}{\partial r}\frac{\tilde{w}}{r}\right)^2 + \left(\frac{\partial\tilde{w}}{\partial x}\right)^2\right\} - \bar{\rho}\varepsilon \tag{2-10}$$

$$\frac{\partial}{\partial x}\left(\bar{\rho}\tilde{\mu}\varepsilon\right) + \frac{1}{r}\frac{\partial}{\partial r}\left(r\bar{\rho}\tilde{v}\varepsilon\right) - \frac{\partial}{\partial x}\left(\frac{\mu_e}{\sigma_e}\frac{\partial\varepsilon}{\partial x}\right) - \frac{1}{r}\frac{\partial}{\partial r}\left(\frac{\mu_e}{\sigma_e}\frac{\partial\varepsilon}{\partial r}\right)$$
$$= \left(\frac{\varepsilon C_1}{k}\right)\mu_e\left\{2\left[\left(\frac{\partial\tilde{\mu}}{\partial x}\right)^2 + \left(\frac{\partial\tilde{v}}{\partial r}\right)^2 + \left(\frac{\tilde{v}}{r}\right)^2\right] + \left(\frac{\partial\tilde{\mu}}{\partial r} + \frac{\partial\tilde{v}}{\partial x}\right)^2\right. \tag{2-11}$$
$$\left. + \left(r\frac{\partial}{\partial r}\frac{\tilde{w}}{r}\right)^2 + \left(\frac{\partial\tilde{w}}{\partial x}\right)^2\right\} - \frac{\varepsilon^2 C_2\bar{\rho}}{k}$$

where:

$$\mu_e = \mu^\ell + \mu^t \tag{2-12}$$

and:

$$\mu^t = \overline{\rho}\mu_g^t \tag{2-13}$$

The constants C_μ, C_1, C_2, σ_k and σ_ε are "universal" constants and have been optimized by comparison with experimental observations of both isothermal and reacting flows (Kahlil et al., 1975). The recommended values of these constants are found in Table 2-2. The k-ε model is the most popular method for turbulence closure for both gaseous and particle-laden systems (Bilger, 1974; Spalding, 1975; Smoot and Smith, 1987). Models which account for combustion-generated turbulence, coherent structures, and gas-particle interaction (Bilger, 1976; Spalding, 1975) are needed.

TABLE 2-2

TURBULENCE MODEL CONSTANTS

Constant	Value
C_μ	0.09
C_1	1.44
C_2	1.92
σ_k	0.9
σ_ε	1.22

Melville and Bray (1979) note that the presence of particles has only a slight effect on the gas-phase turbulence. They suggest a correlation using the ratio of the mean particle bulk density to the mean gas density, as follows:

$$v_{g\ particles}^t = v_{g\ no\ part.}^t \left(1 + \frac{\overline{\rho}_b}{\overline{\rho}_g}\right)^{-0.5} \tag{2-14}$$

According to this equation, the amount of turbulence decreases as the bulk particle density increases. PCGC-2 is coded to allow for this empirical correction of gas-

phase turbulence due to particles. The correction is limited to a minimum value of 0.95.

Laminarization and laminar flow

Some 2-D reactors have zones where the local Reynolds number is low and laminar effects are significant. An option is therefore provided in PCGC-2 for including laminarization effects in the k-ε model according to the extension of Jones and Launder (1972, 1973). This extension includes the following modifications:

(i) Viscous diffusion of k and ε are included.
(ii) The terms containing the *C*'s in eqns. 2-8 and 2-11 become dependent upon the Reynolds number of turbulence.
(iii) Terms are added to account for the fact that the dissipation processes are not isotropic.

The complete form of the turbulence model with the laminarization extension is given below.

Turbulence energy

$$\frac{\partial}{\partial x}(\bar{\rho}\tilde{\mu}k)+\frac{1}{r}\frac{\partial}{\partial r}(r\bar{\rho}\tilde{v}k)-\frac{\partial}{\partial x}\left(\frac{\mu_e}{\sigma_k}\frac{\partial k}{\partial x}\right)-\frac{1}{r}\frac{\partial}{\partial r}\left(r\frac{\mu_e}{\sigma_k}\frac{\partial k}{\partial r}\right)$$

$$=\mu_e\left\{2\left[\left(\frac{\partial\tilde{\mu}}{\partial x}\right)^2+\left(\frac{\partial\tilde{v}}{\partial r}\right)^2+\left(\frac{\tilde{v}}{r}\right)^2\right]+\left(\frac{\partial\tilde{\mu}}{\partial r}+\frac{\partial\tilde{v}}{\partial x}\right)^2+\left(r\frac{\partial}{\partial r}\frac{\tilde{w}}{r}\right)^2+\left(\frac{\partial\tilde{w}}{\partial x}\right)^2\right\}$$

$$-\bar{\rho}\varepsilon-2\mu^{\ell}\left(\frac{\partial k^{\frac{1}{2}}}{\partial x}+\frac{\partial k^{\frac{1}{2}}}{\partial r}\right)^2 \qquad (2\text{-}15)$$

Energy dissipation

$$\frac{\partial}{\partial x}(\bar{\rho}\bar{\mu}\bar{\varepsilon})+\frac{1}{r}\frac{\partial}{\partial r}(r\bar{\rho}\bar{v}\bar{\varepsilon})-\frac{\partial}{\partial x}\left(\frac{\mu_e}{\sigma_e}\frac{\partial\varepsilon}{\partial x}\right)-\frac{1}{r}\frac{\partial}{\partial r}\left(\frac{\mu_e}{\sigma_e}\frac{\partial\varepsilon}{\partial r}\right)$$

$$=\left(\frac{\varepsilon C_1 f_1}{k}\right)\mu_e\left\{2\left[\left(\frac{\partial\bar{\mu}}{\partial x}\right)^2+\left(\frac{\partial\bar{v}}{\partial r}\right)^2+\left(\frac{\bar{v}}{r}\right)^2\right]+\left(\frac{\partial\bar{\mu}}{\partial r}+\frac{\partial\bar{v}}{\partial x}\right)^2+\left(r\frac{\partial}{\partial r}\frac{\bar{w}}{r}\right)^2+\left(\frac{\partial\bar{w}}{\partial x}\right)^2\right\}$$

$$-\frac{\varepsilon^2 C_2 f_2\bar{\rho}}{k}+\underline{\underline{2.0\mu^t\mu^t\left(\frac{\partial^2 u}{\partial x^2}+\frac{\partial^2 u}{\partial r^2}+\frac{\partial^2 v}{\partial x^2}+\frac{\partial^2 v}{\partial r^2}+\frac{\partial^2 w}{\partial x^2}+\frac{\partial^2 w}{\partial r^2}\right)^2}} \qquad (2\text{-}16)$$

Turbulent viscosity formula

$$\nu_g^t=\frac{C_\mu f_\mu k^2}{\varepsilon} \qquad (2\text{-}17)$$

In the above equation set, the C's and σ's retain the values assigned to them in Table 2-2; the influence of Reynolds number mentioned under (ii) above is introduced by way of the f's, which are assigned the following forms:

$$f_1=1.0$$

$$f_2=1.0-0.3\exp\left[\left(-Re^t\right)^2\right]$$

$$f_\mu=\exp\left(-\frac{2.5}{1+\frac{Re}{50}}\right) \qquad (2\text{-}18)$$

where $Re\equiv\rho k^2/\mu\varepsilon$ is interpreted as the Reynolds number of turbulence.

For purely laminar reactors, the k-ε calculations may be turned completely off in the model, thus allowing diffusion to be calculated according to purely molecular forces.

Particle Phase Mechanics

Background

A distinguishing feature among pulverized coal models is the treatment of the dispersed particle phase. In large-scale furnaces there are large recirculation zones. Swirling inlet flows can also have a major influence on the particle motion. Gas molecules tend to equilibrate locally. However, particles exist locally with different properties due to the varying history of each particle.

The approach used in PCGC-2 is based on the PSI-CELL technique of Crowe, et al. (1977). Care is taken to account for all modes of gas-particle coupling. The method does not account for particle-particle interactions and thus would not be applicable to highly loaded, dense-phase flow. It is intended to be applied to dispersed-flow systems. The model is based on calculating the trajectories or paths of representative particles through the gas phase (continuum) field in a Lagrangian fashion. These particles are used to calculate sources of mass, momentum, and energy to the gas phase. These source terms were introduced in the previous section. Crowe, et al. (1977) discuss the basic concept, the derivation of the gas and particle equations, and calculation of the source terms. Briefly, mean particle velocities, trajectories, temperatures, and compositions are obtained by integrating representative equations for the mean motion, energy, and component continuity for an ensemble of particles in the gas flow field. Total momentum, energy, and mass of the particle cloud are recorded on crossing cell boundaries. The net difference in the particle properties between leaving and entering any given cell then provides the particle source terms for the gas flow equations. While the mean location of the particle ensemble is being tracked, the statistical spatial distribution about this mean is currently modeled only by a delta function at the mean. Work is currently underway to include the variance (Baxter, 1987).

Particle Momentum Equation

The particle momentum equation for a single particle in the Lagrangian framework is given by:

$$\alpha_j \; d\left(\vec{v}_j\right)/dt = \vec{f}_j + \alpha_j \, \vec{g} \tag{2-19}$$

The reaction rate term is accounted for by assuming the particle mass leaves the particle with equal mass and velocity in all directions. The drag term $\left(\vec{f}_p\right)$ is related to the difference in gas and particle velocities by:

$$\vec{f}_j = \Gamma_d\left(\vec{v}_g - \vec{v}_j\right) \tag{2-20}$$

where Γ_d is some time constant based on the drag coefficient (C_d), as shown below:

$$\Gamma_d = \frac{\left(\frac{\pi D_j^2}{4}\right)\rho_g C_d \left\|\vec{v}_j - \vec{v}_g\right\|}{2} \tag{2-21}$$

For spherical particles, the following correlation is suggested for the drag coefficient (Wallis, 1969):

$$C_{do} = \left(\frac{24}{Re}\right)\left(1 + 0.15\,Re^{0.687}\right) \tag{2-22}$$

It has been shown that high particle reaction rates can alter the drag coefficient (Bird et al., 1960). The relationship used in PCGC-2 is that suggested by Bailey et al. (1970):

$$C_d = \frac{C_{do}}{1 + B_m} \tag{2-23}$$

$$B_m = \sum \frac{r_i}{k_i} \tag{2-24}$$

where B_m is the particle blowing parameter for mass transfer, which will be discussed later in this chapter.

In a turbulent system, the equation of motion for an individual particle becomes more complicated. The approach taken to account for turbulence in Eqn. 2-19 is to decompose the particle velocity into convective and diffusive components:

$$\vec{v}_j = \vec{v}_{jc} + \vec{v}_{jd} \tag{2-25}$$

The convective component of velocity ($\vec{v}_{jc}$)is defined as the velocity that would arise in the absence of turbulence, or the ballistic velocity based on the mean gas velocity. Therefore, Eqn. 2-19 is used to find $\vec{v}_{jc}$ along a trajectory by numerical integration. The diffusive component of velocity ($\vec{v}_{jd}$) is added to account for the turbulence effects on particle motion.

In the Lagrangian framework, the diffusive velocity $\vec{v}_{jd}$ is modeled using the mean particle bulk density gradient:

$$\vec{v}_{jd}\overline{\rho}_{jb} = -\Gamma_j \vec{\nabla}\overline{\rho}_{jb} \tag{2-26}$$

Equation 2-26 can be viewed as a particle diffusivity equation, since the left-hand side can be thought of as a turbulent mass flux (relative to the convective velocity):

$$\vec{j}_j = \left(\vec{v}_j - \vec{v}_{jc}\right)\overline{\rho}_{jb} = \vec{v}_{jd}\overline{\rho}_{jb} \tag{2-27}$$

Equation 2-26 now defines the transport coefficient Γ_j as a turbulent particle diffusivity, which can also be expressed as:

$$\Gamma_j = D_j^t = \frac{\nu_j^t}{\sigma_j^t} \tag{2-28}$$

where D_j^t is the turbulent particle diffusivity, ν_j^t is the turbulent particle kinematic viscosity, and σ_j^t is the turbulent particle Schmidt number. Much research is currently being conducted by the scientific community on how to obtain the turbulent particle kinematic viscosity (ν_j^t).

An expression for ν_j^t should account for particle size, so that larger particles are not affected by the turbulence as much as are smaller particles. The ν_j^t expression should also include some term to account for the level of turbulence intensity. The model selected for use in PCGC-2 is that of Melville and Bray (1979), which relates ν_j^t to ν_g^t as follows:

$$\nu_j^t = \frac{\nu_g^t}{\left[1+\left(t_j / t^t\right)\right]} \tag{2-29}$$

The particle relaxation time (t_j) is related to the Stokesian particle drag (Melville and Bray, 1979; Longwell and Weiss, 1980; Lockwood et al., 1980; Lilly, 1973) by:

$$t_j = \frac{\alpha_j}{3\pi\mu_g d_j} \tag{2-30}$$

The turbulence time scale (t^t) is related to the local turbulence by:

$$t^t = \frac{\nu_g^t}{\overline{u_g'^2}} \tag{2-31}$$

Assuming isotropic turbulence ($\overline{u_g'^2} = 2/3\ k$) and substituting Eq. 2-17 for ν_g^t, Eqn. 2-31 becomes

$$t^t = \frac{3C_\mu k}{2\varepsilon} \tag{2-32}$$

The value of the turbulent particle Schmidt number σ_j^t is not well characterized. Comparisons of predictions to data can be used to empirically determine this parameter. Best results were obtained by Fletcher (1983) using $\sigma_j^t = 0.35$. This value compares well with the results of Lilly (1973), where $\sigma_j^t = 0.34$,

but not as well with the results of Melville and Bray (1979), who recommended a value of *0.7*.

Several other particle dispersion models are also found in the current literature. Lockwood, et al. (1980) used an empirical approach to get v_{jd} from u'^2 and v'^2. Longwell and Weiss (1980) considered that the ratio of particle eddy diffusivity to gas eddy diffusivity followed a sinusoidal pattern involving t_j and t^t. Lilly (1973) gives evidence that $\upsilon_j^t/\upsilon_g^t$ decreases as t_j/t^t increases, especially for small particles (6 to 16 μm). Lilly's results are surprising, since the large particles were more dispersed than the smaller particles. The model of Melville and Bray (1979) was selected here because it seemed to be more complete than the other models and is applicable to the size range of interest (10 to 100 μm).

Bulk Particle Density

The bulk particle density is needed to calculate the radiation field (discussed later) and to calculate particle velocities (Eqn. 2-26). However, the Eulerian bulk particle density field cannot be calculated directly from the Lagrangian particle trajectory information. Methods used for obtaining this gradient by counting particles and smoothing Lagrangian density information have not been completely acceptable. The bulk particle mass, and number densities are related as follows:

$$\overline{\rho}_b = \alpha_j \overline{n}_j \tag{2-33}$$

The number density $(\overline{n}_j)$ is easier to calculate than the mass density $(\overline{\rho}_b)$ because the number of particles represented by each trajectory is constant throughout the computational domain. The mass density changes due to particle reaction. Equation 2-26 then becomes:

$$\vec{v}_{jd}\,\overline{n}_j = \Gamma_j\,\vec{\nabla}\overline{n}_j \tag{2-34}$$

Equation 2-34 is thought to approximate $\vec{v}_{jd}$ just as well as Eqn. 2-26. However, $\overline{n}_j$ cannot be calculated from the Lagrangian particle-phase information, and can only be approximated using the Eulerian gas-phase information. The Eulerian equation of continuity for the particle number density in turbulent flow (steady-state) is:

$$\frac{\partial}{\partial x}\left(\bar{u}_j\bar{n}_j\right)+\frac{1}{r}\frac{\partial}{\partial r}\left(r\bar{v}_j\bar{n}_j\right)-\frac{\partial}{\partial x}\left(\Gamma_j\frac{\partial\bar{n}_j}{\partial x}\right)-\frac{1}{r}\frac{\partial}{\partial r}\left(r\Gamma_j\frac{\partial\bar{n}_j}{\partial r}\right)=0 \qquad (2\text{-}35)$$

The diffusion coefficient $\left(\Gamma_j\right)$ in Eqn. 2-35 is the same as in Eqn. 2-28, and can be approximated on an Eulerian basis assuming an average size for the particle as it reacts. The equation, however, requires the Eulerian particle velocity field for its solution. For the purposes of Eqn. 2-35 the gas-phase velocity components are used to approximate u_j and v_j. With the small particles of interest to pulverized coal conversion processes, the particle and gas velocities are similar. Reynolds numbers for the particles relative to the gas are often less than 0.01. This approximation is only used for the purposes of Eq. 2-35, since the Lagrangian solution yields the particle velocity including the effects of particle drag.

Gas Phase Reactions

The Turbulent Reaction Rate

The importance of properly accounting for the turbulent interactions with the combustion chemistry in diffusion flames cannot be overemphasized (Bilger, 1974). In writing conservation equations for individual species in turbulent reacting systems, time-averaging is required as has been shown earlier. The instantaneous form of these equations can be found in several sources (Bird et al., 1960; Smoot and Pratt, 1979; Williams, 1965). All of these species conservation equations contain reaction rate terms of the form.

$$r_i = m_i m_j \rho^2 A \; exp\left(-\frac{E}{RT}\right) \qquad (2\text{-}36)$$

Proper time-averaging of such terms is accomplished by decomposing the instantaneous variables into their main and fluctuating components, giving rise to terms of the form:

$$\overline{r_i} = \overline{m_i m_j \rho^2 A \; exp\left(-\frac{E}{RT}\right)} = \rho^{-2}\overline{m_i}\,\overline{m_j} A \; exp\left(-\frac{E}{RT}\right)\left\{1 + \frac{\overline{\rho'^2}}{\rho'^2} + \frac{\overline{m_i' m_j'}}{\overline{m_i}\,\overline{m_j}}\right.$$

$$\left. + \frac{\overline{2\rho' m_i'}}{\overline{\rho}\,\overline{m_i}} + 2\frac{\overline{\rho' m_j'}}{\overline{\rho}\,\overline{m_j}} + \frac{E}{R\overline{T}}\left[\frac{\overline{m_i' T'}}{\overline{m_i}\,\overline{T}} + \frac{\overline{m_j' T'}}{\overline{m_j}\,\overline{T}} + \left(\frac{E}{2R\overline{T}} - 1\right)\frac{\overline{T'^2}}{\overline{T}^2}\right] + \ldots\right\} \qquad (2\text{-}37)$$

The other terms which appear involve triple correlations of the fluctuating variables. It is to be remembered that for any realistic reaction scheme, scores of these equations must necessarily appear.

Historically, two approaches have been used to solve this problem. At one extreme, complex finite-rate chemistry is considered but turbulent mixing is disregarded. Bowman (1975) and Caretto (1976) reviewed this literature. At the other extreme, turbulent mixing is treated in detail as described earlier, but local instantaneous (infinite rate) chemistry is assumed. Bilger (1974) reviewed this literature. Very few attempts have been made to combine finite-rate chemistry and detailed turbulent mixing. Borghi (1974) applied turbulent chemical reaction rate calculations to a CO-containing plume. He introduced the concept of the contact index. Spalding (1978) proposed a combined Eulerian/Lagrangian formulation. Even with these difficulties, in many situations simplified combustion models can predict gaseous turbulent combustion processes with acceptable engineering accuracy (Spalding, 1978; Gosman et al., 1978; Libby, 1976; Spalding, 1971). Each of these references suggests different forms of a combustion model. Simplifications are usually made by assigning properties to the bulk fuel and oxidizer streams.

The Mixture Fraction

In gaseous diffusion flames, the fuel and oxidizer are fed in separate streams. They enter the reactor in separate eddies which must be intimately contacted on a molecular level before reaction can occur. The assumption is then made that this micro-mixing process is rate-limiting, not the kinetic process. This allows the chemistry to be computed from equilibrium. Only one differential equation is required to describe the degree of "mixedness" or "unmixedness" at a point, a great

simplification as compared to the immense system of equations described above for the kinetic scheme.

For cases where there are two identifiable streams or states that have uniform properties, it is convenient to describe a conservative scalar f, the mixture fraction:

$$f = \frac{M_p}{M_p + M_s} = \textit{mass fraction of fluid atoms originating in primary stream} \quad (2\text{-}38)$$

The advantage of the mixture fraction approach lies in its ability to calculate any conserved scalar (s) from the local value of f:

$$s = fs_p + (1-f)s_s \quad (2\text{-}39)$$

An example of a conserved scalar is the mass fraction of a given element.

The following sections develop an approach to comprehensive calculations which use the concept of mixture fractions. The application of this concept requires that the turbulent diffusivities of all gas phase species be equal and that their boundary conditions be the same. These properties taken together constitute what is sometimes called Crocco similarity (Smith, 1979). The mixture fraction approach greatly reduces the number of conserved scalars required to describe a combustion system.

Scalar Transport

The differential equation for the transport of a scalar variable is shown here in its Favre-averaged form:

$$\frac{\partial}{\partial x}\left(\bar{\rho}\tilde{u}\tilde{f}\right) + \frac{1}{r}\frac{\partial}{\partial r}\left(r\bar{\rho}\tilde{v}\tilde{f}\right) - \frac{\partial}{\partial x}\left(\frac{\mu_e}{\sigma_f}\frac{\partial \tilde{f}}{\partial x}\right) - \frac{1}{r}\frac{\partial}{\partial r}\left(\frac{r\mu_e}{\sigma_f}\frac{\partial \tilde{f}}{\partial r}\right) = 0 \quad (2\text{-}40)$$

The solution of this equation, together with the fluid mechanics model, will prescribe the mean fluid values for the flow and the mixing, provided the appropriate mean density is available. The advantage of knowing $\tilde{f}$ is that with the

aid of a probability density function (pdf) for f, the time-mean values may be found for any arbitrary value β which is only a function of f.

$$\bar{\beta} = \alpha_p \beta_p + \alpha_s \beta_s + \int_0^T \beta(f) P(f) df \tag{2-41}$$

The mean of the distribution of the mixture fraction (first moment about the origin) is given by Eqn. 2-40. The variance (second moment about the mean, or the mean square fluctuation) of the mixture fraction is defined as:

$$g_f = \overline{\left(f - \bar{f}\right)^2} = \frac{1}{T}\int_0^T \left[f(t) - \bar{f}\right]^2 dt \tag{2-42}$$

where T is large compared with the time scale of the local turbulence. Launder and Spalding (1972) show how a transport equation for g_f can be derived and appropriate terms modeled in a manner analogous to, and consistent with the other two equations in the k-ε turbulence model. The resulting equation is:

$$\frac{\partial}{\partial x}\left(\bar{\rho}\tilde{u}g_f\right) + \frac{1}{r}\frac{\partial}{\partial r}\left(r\bar{\rho}\tilde{v}g_f\right) - \frac{\partial}{\partial x}\left(\frac{\mu_e}{\sigma_g}\frac{\partial g}{\partial x}f\right) - \frac{1}{r}\frac{\partial}{\partial r}\left(\frac{r\mu_e}{\sigma_g}\frac{\partial g}{\partial r}r\right)$$
$$= \frac{C_{g1}\mu_e}{\sigma_g}\left[\left(\frac{\partial \tilde{f}}{\partial x}\right)^2 + \left(\frac{\partial \tilde{f}}{\partial r}\right)^2\right] - C_{g2}\frac{\bar{\rho}\varepsilon g}{k} \tag{2-43}$$

Appropriate constants for the combustion submodel, introduced by Eqns. 2-40 and 2-42, are given in Table 2-3.

TABLE 2-3

TURBULENT COMBUSTION MODEL CONSTANTS

Constant	Value
C_{g1}	2.8
C_{g2}	1.92
σ_f	0.9
σ_g	0.9
σ_{h_t}	0.9
σ_{h_t}	0.8
E^*	9.793

*These constants arise from boundary conditions

Besides $\tilde{f}$ and g_f, the pdf shape is needed. In regions of small g_f the shape of the pdf makes little difference. The pdf shape is determined from experimentally observed fluctuations in coal flames. Smith (1979), for example, used a top-hat (uniform) distribution, while forms of the Gaussian distribution and the Beta distribution have also been used. Kent and Bilger (1977) used a "clipped" Gaussian distribution which accounts for intermittency, and noted significant sensitivity of the predictions to the form of the pdf, particularly for nitric oxide predictions. Other references pertaining to pdf shape are found in Smith (1979), Fletcher (1980), Kuo (1986), Lockwood and Naguib (1975), and Kent and Bilger (1976).

PCGC-2 is presently coded to use the clipped Gaussian distribution, (i.e. adjusted for intermittency) similar to that used in the last two references. The parameters needed to calculate this Gaussian pdf are as follows: The continuous portion of the probability curve is given by

$$P(f) = (2\pi G_f)^{-1/2} \exp(-Z_f^2 / 2) \qquad (2\text{-}43)$$

where

$$Z_f = \frac{(f - F)}{\sqrt{G_f}} \qquad (2\text{-}44)$$

and F and Gf come from:

$$\tilde{f} = \alpha_p + \frac{1}{\sqrt{2\pi G_f}} \int_{0+}^{1-} f \exp\left[-\frac{(f-F)^2}{2G_f}\right] df \qquad (2\text{-}45)$$

and

$$g_f = \alpha_p - (\tilde{f})^2 + \frac{1}{\sqrt{2\pi G_f}} \int_{0+}^{1-} f^2 \exp\left[-\frac{(f-F)^2}{2G_f}\right] df \qquad (2\text{-}46)$$

The area under the clipped portions are given by

$$\alpha_p = \frac{1}{\sqrt{2\pi}} \int_{\frac{1-F}{\sqrt{G_f}}}^{\infty} \exp\left(-\frac{Z_f^2}{2}\right) dZ_f \qquad (2\text{-}47)$$

and

$$\alpha_s = \frac{1}{\sqrt{2\pi}} \int_{-\infty}^{-\frac{F}{\sqrt{G_f}}} \exp\left(-\frac{Z_f^2}{2}\right) dZ_f \qquad (2\text{-}48)$$

where α_p and α_s are the intermittency of the primary and secondary streams, respectively.

Chemical Equilibrium

In a combustor which is assumed locally adiabatic (no gas radiation, external heat loss, or compressible heating/cooling), the standard enthalpy is a conserved scalar, and thus with the assumption of equal diffusivities, the instantaneous local enthalpy h may be calculated directly from f:

$$h = fh_p + (1-f)h_s \qquad (2\text{-}49)$$

If the local turbulent diffusivities are equal, the elemental mass fractions (b_k) are also conserved scalars and are given by:

$$b_k = f b_{kp} + (1-f) b_{ks} \tag{2-50}$$

Equations 2-49 and 2-50 are not dependent on the assumption of chemical equilibrium but only on the equality of diffusivities, and in the case of Eqn. 2-49, on the assumption of locally adiabatic operation. These assumptions comprise what is called Crocco similarity (Smith, 1979). For non-adiabatic operation, the energy equation (Eqn. 2-89) must be solved.

If local, instantaneous, equilibrium is assumed (micro-mixing is limiting rather than chemical kinetics), all thermodynamic properties can be obtained. For a Gibbs free energy reduction scheme, the required parameters are the energy level, pressure, and elemental composition. The equilibrium properties are then functions of f alone:

$$T = T(b_k, h) = T[b_k(f), h(f)] = T(f) \tag{2-51}$$

$$\rho = \rho(b_k, h) = \rho[b_k(f), h(f)] = \rho(f) \tag{2-52}$$

$$y_i = y_i(b_k, h) = y_i[b_k(f), h(f)] = y_i(f) \tag{2-53}$$

The turbulent flow mean compositions and other properties are obtained by weighting with the pdf of f, as in Eqn. 2-41:

Thus
$$\tilde{y}_i = \alpha_p y_{ip} + \alpha_s y_{is} + \int_{0+}^{1-} y_i(f) P(f) df \tag{2-54}$$

$$\tilde{\rho} = \alpha_p \rho_p + \alpha_s \rho_s + \int_{0+}^{1-} \rho(f) P(f) df \tag{2-55}$$

$$\tilde{T} = \alpha_p T_p + \alpha_s T_s + \int_{0+}^{1-} T(f)P(f)df \qquad (2\text{-}56)$$

This approach to find the mean properties is dependent on the enthalpy (h) and the element mass fractions (b_k) being functions only of the mixture fraction (f). When heat losses (due to radiation, external heat loss, or compression/expansion) are significant, then Crocco similarity must be abandoned for the conservation equation in h (Eqn. 2-89). In this situation, Eqns. 2-51 through 2-53 are no longer valid, and in general, the properties become functions of both f and h:

$$\beta = \beta(b_k, h) = \beta[b_k(f), h] = \beta(f, h) \qquad (2\text{-}57)$$

Favre-averaged properties are obtained by convolution with a joint pdf:

$$\tilde{\beta} = \int_h \int_f (f,h)P(f,h)dfdh \qquad (2\text{-}58)$$

This equation is valid for locally adiabatic operation as well, in which case the enthalpy is a function of f alone, and Eqn. 2-58 reduces to Eqn. 2-41.

The problem of obtaining $P(f,h)$ is greatly simplified by partitioning the enthalpy into: 1) the energy which would be convected if there were no local heat losses or gains (h_f), and 2) the residual energy due to the local heat losses/gains (h_r).

$$h = h_f + h_r \qquad (2\text{-}59)$$

$$h = \left[fh_p + (1-f)h_s\right] + h_r \qquad (2\text{-}60)$$

In practice, the residual enthalpy can be calculated directly from the known field values of h and f from the inlet conditions:

$$\tilde{h}_r = \tilde{h} - \tilde{f}h_p - (1-\tilde{f})h_s \qquad (2\text{-}61)$$

Finally, it is assumed that the effects of the fluctuations of h_r are small compared with the effects of the fluctuations of hf as implied by Eqn. 2-61.

$$\dot{h_r} = 0 \tag{2-62}$$

Thus

$$\tilde{h_r} = h_r \tag{2-63}$$

This means that the fluctuations are correlated by the single variable f as before

$$\tilde{\beta} = \alpha_p\beta_p + \alpha_s\beta_s + \int_{0+}^{1-} \beta(f,h_r)P(f)df \tag{2-64}$$

where h_r is constant with respect to the fluctuations in f. Since h_r will often be small relative to hf, this approximation is thought to be reasonable in many cases. Without the above assumption, it would be necessary to include transport equations for both h and the mean square fluctuation of h_r. In addition, Eqn. (2-64) would need to be convoluted over the joint probability density function $P(f,h_r)$.

A special case arises if it is assumed that the heat loss from the reactor is uniform throughout the reactor. The total amount of sensible heat potentially in the reactor is

$$Q_s = \int_{T_{ref}}^{T_a} C_p dT \tag{2-65}$$

where T_a is the adiabatic gas temperature and T_{ref} is the inlet gas temperature (ambient). The heat loss factor (γ) is defined to be the fraction of the total sensible heat lost from the reactor:

$$\gamma = \frac{h_a - h}{Q_s} \tag{2-66}$$

where h_a is the adiabatic enthalpy calculated from Eqn. 2-49. The enthalpy can now be calculated as a function of the heat loss:

$$h = h_a - \gamma Q_s \tag{2-67}$$

For a constant value of γ, Eqn. 2-67 maintains Crocco similarity while allowing for an approximation to non-adiabatic operation.

Reacting Particles

The gas model development to this point has assumed that no particles are present. When reacting particles are accounted for, it is convenient to define a new progress variable "η" (similar to f) which describes the mass fraction of gas originating from the burning coal. This progress variable is called the coal-gas mixture fraction, and is defined as shown below:

$$\eta = \frac{M_c}{M_p + M_s + M_c} = \text{mass fraction of fluid atoms originating from the coal} \tag{2-68}$$

If the only source of fuel for the combustion or gasification system of interest is from the coal particles or slurry droplets, and if all of the remaining transporting fluid is composed of the same fluid with the same energy level, then η is the only required progress variable. Such is the case for practical combustors where the coal particles are transported with air in the primary stream, and the secondary stream is composed of air at the same temperature as the primary stream. In such systems the primary and secondary streams have exactly the same composition and energy level. In this limiting case, the coal gas mixture fraction (η) is adequate to describe the progress of mixing in the chemical field since the components of the gas can be broken into only two parts, namely the coal offgas and the inlet gas.

A more general approach is adopted in PCGC-2. A mixture fraction is included to allow primary carrier gas fluid different than the secondary gas in either composition and/or enthalpy level. Alternatively, the mixture fraction may be used to track a vaporizing liquid (e.g. coal-oil, coal-water mixtures), which evolves at a different rate and has a different composition and heating value than the coal offgas. In either case, the gas phase must be broken into three components: 1) mass of gas

originating from the primary gas or a slurry liquid, 2) gas originating from the secondary gas, and 3) the coal offgas. A minimum of two progress variables are required to describe the gas field at any one point in this approach. The variable η is used to describe the mass fraction of coal offgas. In addition, the mixture fraction f provides the information regarding the amount of primary carrier gas fluid or slurry liquid. Whether the variable f is used to track the mixing of the primary and secondary streams or the mixing of vaporizing liquid in the combustion gases, there is a significant advantage in defining it as a mass ratio rather than a mass fraction. That is

$$f = \frac{\dot{m}_p}{\dot{m}_p + \dot{m}_s} \tag{2-69}$$

or, in the case of slurry combustion,

$$f = \frac{\dot{m}_\ell}{\dot{m}_\ell + \dot{m}_{p+s}} \tag{2-70}$$

In this case, f is not the local mass fraction of gas originating from the primary stream or slurry liquid, but instead is the *mass fraction of this quantity in the local mixture of primary plus secondary or vaporized slurry liquid plus inlet gas.* Since the mixture fraction f contains only information of the intermixing of the primary and secondary gas streams, or inlet gas with vaporized liquid, it is somewhat insensitive to local fluctuations of η, and thus is much more independent of η than is the local mass fraction of primary fluid or slurry liquid. This statistical independence is useful in calculating the local chemical composition. Thus, f and η can be considered statistically independent to a first-order approximation.

Although f, as defined in Eqns. 2-69 or 2-70, is a useful quantity for the calculational procedure, the local mass fraction of primary fluid or vaporizing liquid is also an important parameter. This quantity is defined as f_p:

$$f_p = \frac{\dot{m}_p}{\dot{m}_p + \dot{m}_s + \dot{m}_c} \tag{2-71}$$

or
$$f_p = \frac{\dot{m}_\ell}{\dot{m}_\ell + \dot{m}_{p+s} + \dot{m}_c} \tag{2-72}$$

where f_p is the conserved scalar for the reacting particle or droplet-laden system. The variable f as defined in Eqns. 2-69 or 2-70 is not a conserved scalar in reacting, particle-laden systems. The importance of f_p is obvious from this conservative principle. Its mean value can be calculated from a Favre-averaged ($\tilde{f}_p$) conservation equation which includes convection and turbulent diffusion terms. There is no source term for the $\tilde{f}_p$ equation when fp is defined as in Eqn. 2-71. When f_p is defined by Eqn. 2-72, the source term is given by the mass of vaporizing liquid. From these definitions, the relationship between f and f_p is:

$$f = \frac{f_p}{1-\eta} \tag{2-73}$$

The progress variables f and η are useful quantities for partitioning the characteristics of the gas field. In order to obtain the mean temperature, density, composition, etc. of the gas field, we must understand the statistical distribution of these variables due to the turbulent fluctuations (i.e. the probability density function). In addition, each of the three components (coal offgas, primary carrier gas and secondary gas or slurry vapor) can react chemically to form new products.

In coal combustion/gasification systems, $\tilde{f}$ can be obtained from a non-conservative (i.e., with a source term) transport equation. Alternatively, f_p can be calculated from a conservative transport equation and f obtained through the relationship shown in Eqn. 2-73. Of course, Eqn. 2-73 relates the instantaneous values of f and f_p. But if f_p can be considered statistically independent of η, then the relationship also holds true in the mean:

$$\tilde{f} = \frac{\tilde{f}_p}{1-\tilde{\eta}} \tag{2-74}$$

The assumption of Crocco similarity applies here as well as in the case of gaseous diffusion flames. With the above assumptions, any local property that is a function of f and η, can be calculated directly.

$$\beta = \beta_c \eta + (1-\eta)\left[f\beta_p + (1-f)\beta_s\right] \tag{2-75}$$

The subscript c stands for pure coal off-gas. Time-mean gas properties (i.e. species composition, density, and temperature) can be obtained for any values of η and f by convolution over a joint probability density function:

$$\tilde{\beta} = \int_{-\infty}^{\infty}\int_{-\infty}^{\infty} \beta(\eta, f) P(\eta, f) d\eta df \tag{2-76}$$

Note that Eqn. 2-76 is analogous to Eqn. 2-41. Assuming η and f are independent, the joint probability density function, $P(\eta,f)$, can be separated:

$$P(\eta, f) = P(\eta) P(f) \tag{2-77}$$

Intermittency can occur for both η and f, and must be handled carefully (Fletcher, 1980). Intermediate steps to the final formulation are shown for completeness. By substituting Eqn. 2-77 into 2-76 and expanding:

$$\tilde{\beta} = \int_{-\infty}^{\infty}\int_{-\infty}^{\infty} P(f)\beta(\eta, f) df]P(\eta) d\eta \tag{2-78}$$

$$\tilde{\beta} = \int_{-\infty}^{\infty}\left[\alpha_p \beta(\eta,1) + \alpha_s \beta(\eta,0) + \int_{0+}^{1-} P(f)\beta(\eta, f) df\right] P(\eta) d\eta \tag{2-79}$$

Finally:

$$\begin{aligned}\tilde{\beta}(\eta, f) &= \alpha_c \beta_c + \alpha_I\left[\alpha_p \beta_p + \alpha_s \beta_s + \int_{0+}^{1+} P(f)\beta(0, f) df\right] \\ &+ \alpha_p \int_{0+}^{1-} P(\eta)\beta(\eta,1) d\eta + \alpha_s \int_{0+}^{1-} P(\eta)\beta(\eta,0) d\eta + \int_{0+}^{1-}\int_{0+}^{1-} P(\eta)P(f)\beta(\eta, f) d\eta df\end{aligned} \tag{2-80}$$

where it has been recognized that

$$\alpha_p + \alpha_s + \int_{0+}^{1-} P(f)df = 1 \tag{2-81}$$

Intermittency of the coal off-gas stream, α_c and α_I, are given by

$$\alpha_c = \frac{1}{\sqrt{2\pi}} \int_{\frac{1-H}{\sqrt{G_\eta}}}^{\infty} \exp\left(-\frac{Z_\phi^2}{2}\right) dZ_\phi \tag{2-82}$$

and

$$\alpha_I = \frac{1}{\sqrt{2\pi}} \int_{-\infty}^{\frac{H}{\sqrt{G_\eta}}} \exp\left(-\frac{Z_\phi^2}{2}\right) dZ_\phi \tag{2-83}$$

where Z_ϕ is given by

$$Z_\phi = \frac{\eta - H}{\sqrt{G_\eta}} \tag{2-84}$$

The subscript I represents pure inlet gas from both the primary and secondary streams. H and G_η are determined from:

$$\tilde{\eta} = \alpha_c + \frac{1}{\sqrt{2\pi G_f}} \int_{0+}^{1-} \eta \exp\left[-\frac{(\eta - H)^2}{2G_\eta}\right] d\eta \tag{2-85}$$

$$g_\eta = \alpha_c - (\tilde{\eta})^2 + \frac{1}{\sqrt{2\pi G_\eta}} \int_{0+}^{1-} \eta^2 \exp\left[-\frac{(\eta - H)^2}{2G_\eta}\right] d\eta \tag{2-86}$$

Equations for $\tilde{\eta}$ and g_η are necessary to obtain the pdf, and are derived in a manner which is analogous to the equations for $\tilde{f}$ and g_f.

$$\frac{\partial(\bar{\rho}\tilde{u}\tilde{\eta})}{\partial x}+\frac{1}{r}\frac{\partial(r\bar{\rho}\tilde{v}\tilde{\eta})}{\partial r}-\frac{\partial}{\partial x}\left(\frac{\mu_e\partial\tilde{\eta}}{\sigma_\eta\partial x}\right)-\frac{1}{r}\frac{\partial}{\partial r}\left(r\frac{\mu_e\partial\tilde{\eta}}{\sigma_\eta\partial r}\right)=S_p^\eta \qquad (2\text{-}87)$$

$$\frac{\partial(\bar{\rho}\tilde{u}g_\eta)}{\partial x}+\frac{1}{r}\frac{\partial(r\bar{\rho}\tilde{v}g_\eta)}{\partial r}-\frac{\partial}{\partial x}\left(\frac{\mu_e}{\sigma_g}\frac{\partial g_\eta}{\partial x}\right)-\frac{1}{r}\frac{\partial}{\partial r}\left(r\frac{\mu_e}{\sigma_g}\frac{\partial g_\eta}{\partial r}\right)$$
$$=\frac{C_{g1}\mu_e}{\sigma_g}\left[\left(\frac{\partial\tilde{\eta}}{\partial x}\right)^2+\left(\frac{\partial\tilde{\eta}}{\partial r}\right)^2\right]-\frac{C_{g2}\bar{\rho}\varepsilon g_\eta}{k} \qquad (2\text{-}88)$$

For lack of better constants, the "universal" constants from Table 2-3 (e.g. C_{g1}, C_{g2}) are used in Eqns. 2-87 and 2-88. These constants are semi-empirical, and need to be investigated further. The S_p^η term in Eqn. 2-87 represents the local mass addition to the gas phase from coal reactions (one component of the total particle mass source term).

When the adiabatic assumption is relaxed, the enthalpy must be calculated from a transport equation. Gas properties will then be functions of η, f, and h, so that (η,f) in Eqn. 2-77 must be replaced by (η,f,h). Equation 2-77 must also be convoluted with $P(h)$ if fluctuations in h are important (Smith, 1979). The gas-phase energy conservation equation is listed here for completeness:

$$\frac{\partial(\bar{\rho}\tilde{u}\tilde{h})}{\partial x}+\frac{1}{r}\frac{\partial(r\bar{\rho}\tilde{v}\tilde{h})}{\partial r}-\frac{\partial}{\partial x}\left(\frac{\mu_e}{\sigma_h}\frac{\partial\tilde{h}}{\partial x}\right)-\frac{1}{r}\frac{\partial}{\partial r}\left(r\frac{\mu_e}{\sigma_h}\frac{\partial\tilde{h}}{\partial r}\right)=q'_{rg}+\tilde{u}\frac{\partial\bar{p}}{\partial x}+\tilde{v}\frac{\partial\bar{p}}{\partial r}+S_p^h \qquad (2\text{-}89)$$

The q'_{rg} term represents the net volumetric heat addition due to radiation. The S_p^h term represents the heat given to the gas by the particles due to particle reaction and convection. The other two terms on the right-hand side represent the net heat addition due to expansion/contraction.

Formally, the gas phase properties are a function of the elemental composition, the total enthalpy and the local pressure. The enthalpy fluctuations due to the presence of the particles can be accounted for by partitioning the total gas enthalpy into the contributions by η, by f, and by the residual enthalpy contributions.

To this point, the elemental composition of the coal offgas has been assumed constant. This assumption could be relaxed, and each reaction involved (i.e., high activation energy pyrolysis, heterogeneous oxidation, etc.) could produce different gaseous elemental compositions by defining a new η_m for each reaction. In this case, η_m would be a local mass ratio of gas originating from the m^{th} reaction, defined in such a way as to preserve (if possible) their statistical independence. The instantaneous local gaseous properties would then be obtained from $f, \eta_1, \eta_2, ..., \eta_m$. Intermittency of each mixture fraction would need to be properly included as before. Brewster et al. (1988) have formalized a general approach for an arbitrary number of mixture fractions, including intermittency and accounting for fluctuations, assuming mutual independence among the mixture fractions. The added complexity in solving transport equations for each new η_m and for each new g_η, and then convolving the instantaneous properties over the probability density functions of all mixture fractions would significantly increase computational time and storage. The approximations involved in the statistical model might then nullify any advantage achieved by way of increased flexibility in specification of the coal offgas composition unless η fluctuations were ignored.

Particle Phase Reactions

This section describes the modeling of single, reacting coal particles in pulverized coal combustion and gasification processes. The description includes vaporization, devolatilization, char oxidation, and gas-particle interchange of momentum, heat, and mass. The resulting model describes the response of a coal particle to its thermal, chemical, and physical environment.

Development of an analytical treatment of pulverized coal-char behavior in reacting systems is based largely on independent experimental observations and kinetic parameters deduced from these observations. The description that follows applies to pulverized coal reaction processes, where particles are small (<150 μm), and heating rates are high (10^3-10^6 K s^{-1}). The treatment is intended for application to pulverized-coal furnaces and entrained-coal gasifiers and would not necessarily apply to fixed or fluidized-bed processes without modification.

Particle reactions can be described by one of two approaches: 1) simple kinetics models for weight loss or 2) a comprehensive chemical model for devolatilization, particle swelling, and char reactivity (FG-DVC). The latter approach is described in Section ?.

Particle Continuity Equations

In the case of simple weight-loss kinetics, the coal particle (droplet) is considered to consist of four components: Slurry liquid, coal, char, and ash. Ash is defined as that part of the particle (droplet) that is inert. Char is the residue left in the coal particle when the volatile products are released plus that portion of the particle which cannot undergo devolatilization.

The process by which each particle reacts is schematically presented in Fig. 2-3. The continuity equations for the components are listed below for the j^{th} particle size:

$$\frac{d\alpha_{wj}}{dt} = -r_{wj} \tag{2-90}$$

$$\frac{d\alpha_{cj}}{dt} = r_{cj} \tag{2-91}$$

$$\frac{d\alpha_{hj}}{dt} = r_{hj} \tag{2-92}$$

$$\frac{d\alpha_{aj}}{dt} = 0 \tag{2-93}$$

The slurry liquid vaporizes in accordance with classical expressions.

$$liquid \rightarrow vapor \tag{2-94}$$

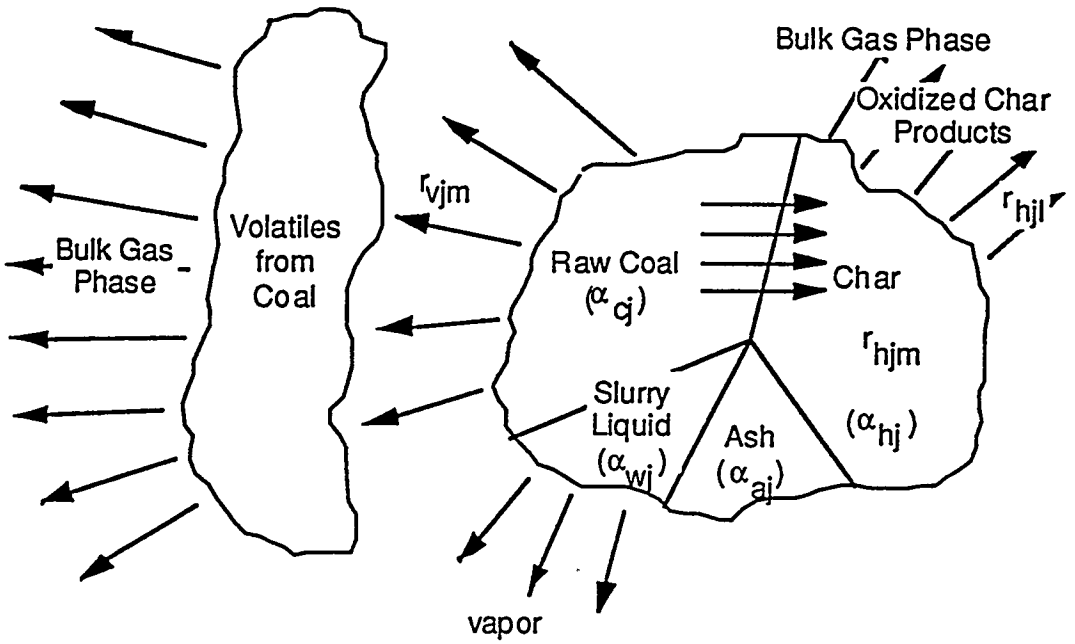

Fig. 2-3. Schematic of coal particle/droplet illustrating components and reaction processes.

The vaporization rate is modeled such that it can be controlled by either heat or mass transfer. In practice, the vaporization rate is nearly always controlled by the heat transfer rate. The mass transfer driving force, i.e. the difference between the vapor concentration at the droplet surface and that in the bulk gas, has a larger impact on the droplet temperature than on the vaporization rate. The fraction of the droplet surface covered with liquid is specified.

The raw coal, or the dry, ash-free portion of the coal, undergoes devolatilization to volatiles and char by one or more reactions (M in total number) of the form:

$$(raw\ coal)_j \xrightarrow{k_{jm}} Y_{jm}(volatiles) + (1 - Y_{jm})(char) \qquad (2\text{-}95)$$

The volatiles react further in the gas phase. The char reacts heterogeneously, after diffusion of the reactant (i.e. O_2, CO_2, H_2O, H_2) to the particle surface, by one or more reactions (L in total number) of the form:

$$\phi_\ell(\text{char}) + (\text{oxidizer})_\ell \xrightarrow{k_\ell} (\text{gaseous products})_\ell \qquad (2\text{-}96)$$

ϕ_ℓ is the stoichiometric coefficient (moles carbon required per mole of oxidizer). Values of ϕ_ℓ usually assumed for O_2, CO_2, H_2O, and H_2, are 1.74, 1.0, 1.0, and 0.5, respectively. Hence, 15 percent CO_2 is assumed to form heterogeneously for O_2 oxidation, following the recommendations of Mitchell (1988). The oxidation reactions are assumed to be first-order with respect to the oxidizer concentration.

An overview of this coal submodel is presented in the following sections, and further detail is given elsewhere (Smoot and Pratt, 1979; Smith, 1979; Fletcher, 1980, Smoot and Smith, 1985).

Particle Energy Equation

The Lagrangian equation for particle energy is:

$$\frac{d(\alpha_j h_j)}{dt} = Q_{rj} - Q_j - (1-\chi) r_j h_{jg} \qquad (2\text{-}97)$$

where Q_{rj} represents the net radiation to the particle, Q_j represents convection and conduction from the particle to the gas phase, h_{jg} is the enthalpy of the coal offgas and accounts for heats of reaction, and χ is the fraction of the volatile enthalpy that gets directly fed back to the particle from the volatiles combustion. At the present time, χ is an empirical parameter of the model. The third term on the right represents the net enthalpy lost to the gas by transfer of mass due to particle reaction. The heats of reaction for the heterogeneous reactions are given to the particle. Note that the radiative and convective heat transfer terms have opposite signs. That is, if both are heating the particle, radiation is positive and convection is negative. This is a consequence of sign conventions used in the code.

Physical Properties. This section discusses the equations proposed to obtain the particle and gas phase properties needed for the particle reactions submodel. The gas phase properties discussed are necessary in order to incorporate

diffusion limitations on particle reaction rates. These properties are not determined from the statistical PDF approach since incorporation of turbulent fluctuating effects on such physical properties is not justifiable. Table 2-4 shows the calculation procedures used for the gas phase properties. These procedures are discussed elsewhere (Smith, 1979; Baxter, 1987) and may be found in standard text books on transport properties (e.g. Bird et al., 1960).

The physical characteristics of the j^{th} particle type are calculated as follows: During vaporization, slurry droplets maintain diameters which are essentially equal to their original diameter (Baxter, 1987). Fuel oil droplets decrease in diameter with constant density. The particle is allowed to swell linearly with the extent of devolatilization:

$$\frac{d_j}{d_{jo}} = 1 + \gamma \frac{\alpha_{cjo} - \alpha_{cj}}{\alpha_{cjo}} \qquad (2\text{-}105)$$

The swelling coefficient γ must be specified. This swelling during devolatilization is an experimentally observed phenomenon (Anson et al., 1971). The average particle diameter increase is often on the order of 10 percent for highly volatile bituminous coals (Smoot and Horton, 1978).

Char particles are assumed to burn out according to (Mitchell, 1989)

$$\frac{d_j}{d_{jo}} = \left(\frac{\alpha_j}{\alpha_{jo}}\right)^b \quad ; \quad \frac{\rho_j}{\rho_{jo}} = \left(\frac{\alpha_j}{\alpha_{jo}}\right)^a \qquad (2\text{-}106)$$

where ρ_{jo}, d_{jo}, and α_{jo} are the density, diameter, and mass, respectively, of the j^{th} particle size after complete devolatilization (i.e., when $\alpha_{cj} = 0$). For spherical particles, $a+3b=1.0$. For constant density burning, $a=0$, and for constant diameter burning, $a=1.0$. For values between 0 and 1, both the size and diameter of the particle decrease with burnout. Following Mitchell's recommendation, a is normally taken as 0.25. Constant density burning is recommended for fuel oil combustion.

TABLE 2-4

PHYSICAL PROPERTIES FOR PARTICLE MODEL

Description	Equation	No.
Gas species conductivity	$k_i = \left(C_{pi} + \frac{5R}{4M_i} \right) \mu_i$	(2-98)
Gas mixture conductivity	$k_g = \sum_i \frac{X_i k_i}{\sum_k X_k \phi_{ik}}$	(2-99)
Gas species viscosity	$\mu_i = \frac{2.67 \times 10^{-6} \left(M_i T_g \right)^{1/2}}{\sigma_i^2 \Omega_\mu}$	(2-100)
Interaction parameter	$\phi_{ik} = \frac{1}{2\sqrt{2}} \left[1 + \frac{M_i}{M_k} \right]^{1/2} \left[1 + \left(\frac{\mu_i}{\mu_k} \right)^{1/2} \left(M_k M_i \right)^{1/4} \right]^2$	(2-101)
Gas mixture viscosity	$\mu_g = \sum_i \frac{X_i \mu_i}{\sum_k X_k \phi_{ik}}$	(2-102)
Species diffusivity	$D_{ik} = \frac{1.83 \times 10^{-12} T_g^{3/2} \left[\frac{1}{M_k} + \frac{1}{M_i} \right]^{1/2}}{p \sigma_{ik}^2 \Omega_d}$	(2-103)
Mixture diffusivity	$D_{im} = \frac{1 - X_i}{\sum_{i \neq k} \frac{X_k}{D_{ik}}}$	(2-104)

The predicted particle temperature and reaction rates change with changing heat capacity. Particle heat capacity is calculated according to:

$$C_{pj} = \frac{\alpha_{wj} C_{pwj} + \alpha_{hj} C_{phj} + \alpha_{cj} C_{pcj} + \alpha_{aj} C_{paj}}{\alpha_j} \qquad (2\text{-}107)$$

Coal and char heat capacity are calculated according to (Merrick, 1983):

$$c_v = \left(\frac{R}{a}\right)\left[g_1\left(\frac{380}{T}\right) - 2g_1\left(\frac{1800}{T}\right)\right] \qquad (2\text{-}108)$$

where R is the universal gas constant (8314.4 J/kg-mol/K), a is the average atomic weight of the coal or char (kg/kg-mol), T is the temperature (K), and g_1 is the following function:

$$g_1(z) = \frac{e^z}{\left(\frac{e^z - 1}{z}\right)^2} \qquad (2\text{-}109)$$

The average atomic weight of the coal is given by

$$a = \frac{1}{\sum_i^n \frac{y_i}{\mu_i}} \qquad (2\text{-}110)$$

where y_i is the mass fraction of element i, μ is the atomic weight of element i, and n is the number of elements in the organic portion of the coal. Merrick compared his heat capacity model with experimental data and found agreement within about 10% in the temperature range of 273–573 K. The heat capacity of ash is taken as

$$C_v = 593.3 + 0.586\,T \qquad (2\text{-}111)$$

where T is in K. Predicted particle temperatures can differ by as much at 500 K depending on the choice of heat capacity models used (Baxter, 1988).

The equilibrium mole fraction of liquid at the temperature, T, of the droplet is calculated from the Clapeyron equation and Raoult's law:

$$x_1 = \frac{P(T_1)}{P_{tot}} exp\left[\int_{T_1}^{T} \frac{\int_{T^o}^{T} \Delta C_p dT'' + \Delta h(T^o)}{RT'^2} dT' \right] \qquad (2\text{-}112)$$

ΔC_p is the difference in the vapor and liquid heat capacities, and $\Delta h(T^o)$ is the difference in specific enthalpies at the specified temperature T^o. All quantities needed for this equation are input variables. An option for an Antoine equation is also included.

The actual mole fraction of the vaporizing liquid at the surface of the droplet is not equal to the equilibrium value but is a function of it. If the droplet temperature is greater than or equal to its boiling temperature, the vaporization rate is given by an equation which does not depend on the surface concentration. The heat of vaporization as a function of temperature is calculated according to

$$\Delta H_v^T = \int_{T^o}^{T} \Delta C_p dT'' + \Delta h(T^o) \qquad (2\text{-}113)$$

Convective and Conductive Heat Transfer. The particle energy is computed from Eqn. 2-97. Auxiliary relationships needed to describe the heat transfer processes are shown in Table 2-5. The temperature of the particle is obtained by integrating Eqn. 2-97 formally with the definition of C_{pg} given in Eqn. 2-107 and h_{fj}^o in Eqn. 2-126. The resulting nonlinear equation is solved with a combined bisection-regula falsi technique.

Equation 2-115 of Table 2-5 represents the heat transfer rate for a single particle between the j^{th} particle and the gas phase. Nu_{jg} represents the mean conductive Nusselt number for heat transfer from spheres without the effects of mass transfer. The term enclosed between brackets is the mass transfer correction. The derivation of this term based on classical film theory is discussed elsewhere (Smith, 1979). A reasonable expression for Nu_{jg} is given in Eqn. 2-116 (Kreith, 1973). The blowing transpiration parameter for heat transfer (B_j) is given in Eqn. 2-117. The relationship of this parameter to that for mass transfer is also discussed by Smith (1979). The definitions of Re_{jg} and Pr_g are given in Eqns. 2-118 and 2-

119. The resulting Q_j is required for the particle differential energy equation (Eqn. 2-97).

Equations 2-120 through 2-123 show how the enthalpy of each of the particle constituents is calculated for use in the particle enthalpy calculation (Eqn. 2-114). The functional form of the heat capacity correlation depends on input parameters, as discussed earlier. The enthalpy of the volatile matter from each of the M devolatilization reactions is calculated from an energy balance as shown in Eqn. 2-124. The enthalpy of the particle products for use in Eqn. 2-97 is shown in Eqn. 2-125. The first three terms in Eqn. 2-125 represent the enthalpy of coal volatiles, oxidized char, and slurry liquid, respectively, assuming negligible heat of reaction for the devolatilization and char oxidation reactions and negligible heat of vaporization for the slurry liquid. The last three terms (multiplied by ζ) represent the heats of reaction for devolatilization and char oxidation and the heat of vaporization of the slurry liquid, respectively, a fraction (ζ) of which is added to the product gas enthalpy. Since heats of reaction and vaporization are negative when heat is given off (exothermic) ζ represents the fraction of these heats which is given to the particle phase. When ζ equals one, the heats of reaction and vaporization are given entirely to the particle phase. When ζ equals zero, they are given entirely to the gas phase. The proper value of ζ is thought to be 1.0.

Particle Reactions

This section discusses each of the reactions involved in the reaction model of the j^{th} particle classification. The rate expression for each is presented and the effects of oxidizer diffusion and high rates of mass transfer or particle blowing are incorporated. As presented schematically in Fig. 2-3, the three overall mass loss processes for each particle are vaporization, devolatilization, and heterogeneous reaction. The corresponding equations are shown in Table 2-6. The model allows one vaporization reaction, M devolatilization reactions, and L char oxidation reactions of the form shown in Eqn. 2-96 per particle type. Each of these reaction sets will be discussed in turn. The total reaction rate of the j^{th} particle classification per unit reactor volume is then the sum of each of these reactions, $(1 + L + M)$ in total number, as shown in Eqn. 2-129.

TABLE 2-5

CONVECTIVE AND CONDUCTIVE HEAT TRANSFER FOR PARTICLE MODEL

Type	Equation	
Particle enthalpy	$h_j = \frac{\alpha_{wj}h_{wj} + \alpha_{cj}h_{cj}\alpha_{hj}h_{hj} + \alpha_{aj}h_{aj}}{\alpha_j}$	(2-114)
Particle-gas heat transfer	$Q_j = Nu_{jg}\pi\left(\frac{B_j}{exp\ B_j - 1}\right)K_g\left(T_j - T_g\right)d_j$	(2-115)
Nusselt No.	$Nu_{jg} = 2.0 + 0.65\ Re_{jg}^{0.5}\ Pr_g^{0.333}$	(2-116)
Transpiration parameter	$B_j = \frac{r_j C_{pg}}{2\pi d_j k_g}$	(2-117)
Reynolds No.	$Re_{jg} = \frac{d_j\left\|\vec{v}_g - \vec{v}_j\right\|\rho_g}{\mu_g}$	(2-118)
Prandtl No.	$Pr_g = \frac{C_{pg}\mu_g}{k_g}$	(2-119)
Liquid enthalpy	$h_{wj} = h_{fwj}^0 + \int_{298}^{T_j} C_{pwj}dT_j$	(2-120)
Raw coal enthalpy	$h_{cj} = h_{fcj}^o + \int_{298}^{T_j} C_{pcj}dT_j$	(2-121)
Char enthalpy	$h_{hj} = h_{fhj}^o + \int_{298}^{T_j} C_{phj}dT_j$	(2-122)

TABLE 2-5 (continued)

Type	Equation	
Ash enthalpy	$h_{aj} = h^o_{faj} + \int_{298}^{T_j} C_{paj} dT_j$	(2-123)
Volatiles enthalpy	$h_{vjm} = \frac{h_{cj} - h_{hj}\left(1 - Y_{jm}\right)}{Y_{jm}}$	(2-124)
Total particle product gas enthalpy	$h_{jg} = \frac{1}{r}\left[\sum_m r_{vjm} h_{vjm} + h_{hj} \sum_l r_{hjl} + r_{wj} h_{wj} + \zeta\left(\sum_m r_{vjm} \Delta h^r_{jm} + \sum_l r_{hjl} \Delta h^r_{jl} + r_{wj} \Delta h^v_w\right)\right]$	(2-125)
Particle heat of formation	$h^o_{fj} = \frac{\alpha_{wj} h^o_{fwj} + \alpha_{hj} h^o_{fhj} + \alpha_{cj} h^o_{fcj} + \alpha_{aj} h^o_{faj}}{\alpha_j}$	(2-126)

The equations for the vaporization reactions are shown in Table 2-6. Vaporization is controlled by either heat transfer or mass transfer. The vaporization rate for non-boiling liquid (Eqn. 2-128) is the sum of diffusive and convective components. K_w in the diffusion term is the mass transfer coefficient uncorrected for mass transfer. w is the mass transfer correction factor. S_f is the fraction of the particle surface area over which evaporation is taking place. The contribution of oxidizer-char reactions to the total mass flux from the particle has been neglected in the correction term because char oxidation is not usually important during slurry liquid vaporization. Slurry droplets often are not predicted to boil unless the local gas phase mass fraction of slurry liquid (e.g. water) reaches a high value (Baxter, 1987). However, the vaporization rate is normally heat-transfer-limited.

TABLE 2-6

PARTICLE REACTIONS FOR PARTICLE MODEL

Type	Equation	
Liquid vaporization rate (non-boiling)	$r_{wj} = \dfrac{S_f A_j k_{jw} \rho_g \left(X_{wjs} - X_{wb}\right) + X_{wjs} \sum_m S_f r_{vjm}}{1 - X_{wjs}}$	(2-127)
Liquid vaporization rate (boiling)	$r_{wj} = \dfrac{-Q_j + Q_{rj} + r_{cj}\left(h_{jg} - h_{cj}\right)\zeta + r_{hj}\zeta\left(h_{jg} - h_{hj}\right)}{\zeta\left(h_{jg} - h_{wj}\right)}$	(2-128)
Particle reaction rate to gas phase	$r_j = \sum_l r_{hjl} + \sum_m r_{vjm} + r_{wj}$	(2-129)
Net char reaction rate	$r_{hj} = \sum_m r_{hjm} - \sum_l r_{hjl}$	(2-130)
Oxidizer-char reaction rate	$r_{hjl} = \dfrac{A_j^2 M_{hj} M_g \phi_l k_{cji} k_{jl} \zeta_j C_{olg} C_g}{M_g A_j C_g \left(\zeta_j k_{jl} + k_{cjl}\right) + r_j}$	(2-131)
Kinetic char reaction rate coefficient	$k_{jl} = A_{jl} T_j^n \, exp\left(\dfrac{-E_{jl}}{RT_j}\right)$	(2-132)
Transpiration parameters for mass transfer	$B_{ji} = \dfrac{r_j}{2\pi D_{im} \rho_g d_j}$	(2-133)
Mass transfer coefficient	$k_{cji} = \dfrac{Sh_{jg} D_{im} B_{ji}}{d_j\left(exp\, B_{ji} - 1\right)}$	(2-134)
Total coal reaction rate	$r_{cj} = \sum_m -r_{cjm} = -\sum_m \left(r_{hjm} + r_{vjm}\right)$	(2-135)

TABLE 2-6 (continued)

Type	Equation	
Volatile production rate	$r_{vjm} = k_{mj} Y_{mj} \alpha_{cj}$	(2-136)
Char production rate	$r_{hjm} = \frac{r_{vjm}\left(1 - Y_{mj}\right)}{Y_{mj}}$	(2-137)
Coal kinetic rate coefficient	$k_{mj} = A_{mj}\, exp\left(\frac{-E_{mj}}{RT_j}\right)$	(2-138)

The kinetic rate of production of volatiles from the m^{th} reaction is given in Eqn. 2-137, where the reaction rate constant is given in Eqn. 2-138. Diffusional effects only become important when the volatiles repolymerize or condense prior to diffusion into the gas phase. Equation 2-137 is used because of uncertainties in the repolymerization rate coefficients, the nature of the volatiles diffusion process, and because techniques and models used to correlate existing pyrolysis data most often have taken forms like Eqn. 2-137.

The recommended rate constants for devolatilization are shown in Table 2-7. The two-step model (Ubhayakar et al., 1976) is a reasonable compromise between a simple one-step model (e.g. Godridge and Read, 1976), which would not account for the effects of particle size and pressure, and a more complex, multistep mechanism. The rates of Ubhayakar have been most often used in the past.

In accordance with Eqn. 2-95, the devolatilization of the raw coal can produce char. A simple mass balance results in the rate of formation of char from the j^{th} particle type from the m^{th} reaction as shown in Eqn. 2-138. Finally, the net rate of disappearance of the raw coal in the j^{th} particle class may be obtained by summing over all M devolatilization reactions. The rate of raw coal disappearance is the rate of char plus volatiles formation according to Eqn. 2-95 and as shown in Eqn. 2-136.

Char is assumed to react heterogeneously with gaseous oxidizers that diffuse to the particle surface from the bulk gas phase. Two rate-limiting steps are considered for this process: 1) gas phase diffusion and 2) heterogeneous reaction. The combined reaction rate is given in Eqn. 2-132. In this form of the equation, the surface reaction has been assumed to be first-order in the surface concentration of the oxidizer The Arrhenius expression for the rate constant is given in Eqn. 2-133.

TABLE 2-7

DEVOLATILIZATION RATE EXPRESSIONS AND PARAMETERS

Single-Step Model:

$$raw\ coal \xrightarrow{k} Y\ (volatiles) + (1-Y)\ (char)$$

Rank	Reference	Y	A (s^{-1})	E (J/kmol)
Lignite	Solomon et al., 1986	0.4	4.3×10^{14}	2.29×10^{8}
	Kobayashi et al., 1977	0.7	6.6×10^{4}	1.05×10^{8}
	Anthony et al., 1976	0.4	2.83×10^{2}	4.64×10^{7}
	Truelove & Jamaluddin, 1986	0.4	6.2×10^{3}	4.64×10^{7}
Bituminous	Solomon et al., 1986	0.4	4.3×10^{14}	2.29×10^{8}
	Kobayashi et al., 1977	0.7	6.6×10^{4}	1.05×10^{8}
	Anthony et al., 1976	0.4	7.1×10^{2}	4.94×10^{7}
	Truelove & Jamaluddin, 1986	0.4	2.0×10^{4}	4.94×10^{7}
	Wiser et al., 1967	0.5	4.8×10^{1}	6.27×10^{7}
	Badzioch & Hawksley, 1970	0.4	1.14×10^{5}	7.45×10^{7}
	Badzioch & Hawksley, 1970	0.4	3.12×10^{5}	7.45×10^{7}

TABLE 2-7 (continued)

Two-Step Model:

$$raw\ coal \begin{cases} \xrightarrow{k_1} Y_1(volatiles) + (1 - Y_1)(char) \\ \xrightarrow{k_2} Y_2(volatiles) + (1 - Y_2)(char) \end{cases}$$

Rank	Reference	i	Y_i	A (s^{-1})	E (J/kmol)
Lignite	Kobayashi et al., 1977	1	0.3	2.0×10^5	1.05×10^8
		2	1.0	1.3×10^7	1.67×10^8
Bituminous	Kobayashi et al., 1977	1	0.3	2.0×10^5	1.05×10^8
		2	1.0	1.3×10^7	1.67×10^8
	Ubhayakar et al., 1977[1]	1	0.4	3.7×10^5	7.36×10^7
		2	0.8	1.5×10^{13}	2.51×10^8

Values of the rate parameters to use for char reaction with oxygen and carbon dioxide in PCGC-2 are shown in Table 2-8 A sample calculation for A_{jl} is given in Appendix K. Given the lack of reliable data for char reaction with steam and hydrogen, the assumptions of Hobbs et al. (1992) are recommended. They assumed that the steam-char reaction rate is the same as the carbon dioxide reaction rate and that the char gasification rate by hydrogen is three orders of magnitude smaller than the gasification rate by carbon dioxide. Their assumptions were based on the data of Walker et al. (1959), Yoon (1978), Wen et al. (1982), Wen and Chaung (1979), and Blackwood (1959). The mass transfer coefficient, which is also required, must be corrected for particle blowing or high rates of mass transfer. The mass transfer coefficient without blowing may be calculated from an empirical correlation for the Sherwood Number (Sh) (Bird et al., 1960):

$$Sh_{jg} = \frac{k_{ji} d_j}{D_{im}} = 2.0 + 0.6\left(Re_{jg}\right)^{1/2} (Sc)^{1/3} \qquad (2\text{-}139)$$

TABLE 2-8

COEFFICIENTS FOR CHAR REACTION WITH O_2 AND CO_2

$$k_{jl} A_{jl} T_j^n \exp\left(\frac{-E_{jl}}{RT_j}\right)$$

Oxidizer	Rank	Reference	n	A_{jl} (m/K^{n}s)	E_{jl} (J/kmol)
O_2	all ranks[1]	Goetz et al. (1982) data recorrelated by Baxter et al. (1986)	1.0	2.30	9.29×10^7
	all ranks	Field, et. al., 1967	1.0	298	1.49×10^8
	hv Bituminous A	Goetz et al. (1982) data recorrelated by Baxter et al. (1986)	1.0	1.03	7.49×10^7
	hv Bituminous C	"	1.0	0.479	5.25×10^7
	Subbituminous C	"	1.0	10.4	9.31×10^7
	hv Bituminous A	Goetz, et. al., 1982	1.0	2.25	8.52×10^7
	hv Bituminous C	"	1.0	2.02	7.18×10^7
	Subbituminous C	"	1.0	4.96	8.36×10^7
CO_2	Lignite	Goetz et al. (1982) data recorrelated by Baxter et al. (1986)	1.0	3.419	1.30×10^8
	hv Bituminous A	"	1.0	1160.0	2.59×10^8
	hv Bituminous C	"	1.0	4890.0	2.60×10^8
	Subbituminous C	"	1.0	6188.0	2.40×10^8
	Lignite	Goetz, et al., 1982	1.0	45.0	1.65×10^8
	hv Bituminous A	"	1.0	95.14	2.25×10^8
	hv Bituminous C	"	1.0	88.5	2.36×10^8
	Subbituminous C	"	1.0	70.95	1.78×10^8

where the Schmidt Number (Sc) is $\frac{\mu_g}{\rho_g D_{im}}$, and the Reynolds Number (Re) is based on the difference in velocity between the particle and gas phases. If the Reynolds

number is zero, this expression reduces to the theoretical value of 2.0 for molecular diffusion. The resulting expression for k_{co}, corrected for particle blowing, is given in Eqn. 2-135. In this case, the blowing parameter is that for mass transfer (Eqn. 2-123).

Since char is being formed by each of the M devolatilization reactions and depleted by each of the L oxidation reactions, the net rate of char reaction is given in Eqn. 2-92. Further, since the heterogeneous reaction is zero order with respect to the char concentration, heterogeneous ignition is permitted. The ignition phenomenon of the coal is not limited to devolatilization. Heterogeneous surface ignition is possible even if devolatilization has not been initiated.

Radiation

Background

Radiative transfer becomes increasingly important as the furnace dimensions are increased, and in a typical coal-fired furnace environment, radiation includes contributions from both particulates (coal/char, ash and soot) and the gas phase (mainly CO_2 and H_2O). The accuracy of the radiation calculation depends on a combination of the accuracy of the calculation method, and the degree of certainty with which the radiative properties of the medium and surrounding walls are known. The radiative properties of the particulates depend on their concentration, size distribution, and complex refractive indices; those of the gases depend on their temperature, partial pressures and the optical thickness of the enclosure. Considerable uncertainties exist, in particular, regarding the size and concentration of soot, and the refractive index of ash. A recent study (Jamaluddin and Smith, 1987) of the sensitivity of predicted radiation fluxes to variations in the inputs indicated that these predictions are most sensitive to the particle concentration and size distribution, while the effect of the absorption and scattering efficiencies of the particles are rather insignificant. As for the gas phase radiation, emissivity data (Sarofim and Hottel, 1978) are known with more certainty than the local variations in gas temperature and species concentrations.

Radiative heat transfer models of gas- or oil-fired (Field et al., 1967; Bueters et al., 1974), and pulverized coal-fired furnaces (Lowe et al., 1974) have been reported using zone and flux methods with simple empirical assumptions for flow characteristics, temperatures, heat release rates, and gas composition. Recent radiation modeling has focused on the more efficient but less fundamental flux methods.

The flux methods commonly used are the four-flux type (Gosman and Lockwood, 1973; Lowes et al., 1973; DeMarco and Lockwood, 1975; Varma, 1979). Most of these models suffer from a lack of coupling between the directional fluxes. The discrete ordinates method (an extension of the flux method) corrects this defect, and still offers an equation form which is amenable to numerical methods consistent with the fluid mechanics. The consequences of the lack of effective coupling between the directional fluxes on the predictions of the radiation models has been demonstrated earlier (Jamaluddin and Smith, 1986). PCGC-2 uses either the Varma axisymmetric six-flux method (VFM), or the discrete ordinates method (DOM).

Formulation

Radiation calculations are based on an energy balance for a beam of radiation passing through a volume element (see Fig. 2-4) containing an absorbing-emitting-scattering medium:

$$(\mu_m/r)\left[\partial(rI_m)/\partial r\right]-(1/r)\left[\partial(n_m I_m)/\partial\psi\right]+\xi_m(\partial I_m/\partial z)$$
$$=-(k_a+k_s)I_m+k_a I_b+\frac{k_s}{4\pi}\int_{4\pi}p\left(\underline{\Omega},\underline{\Omega}^l\right)I_m d\Omega' \qquad (2\text{-}140)$$

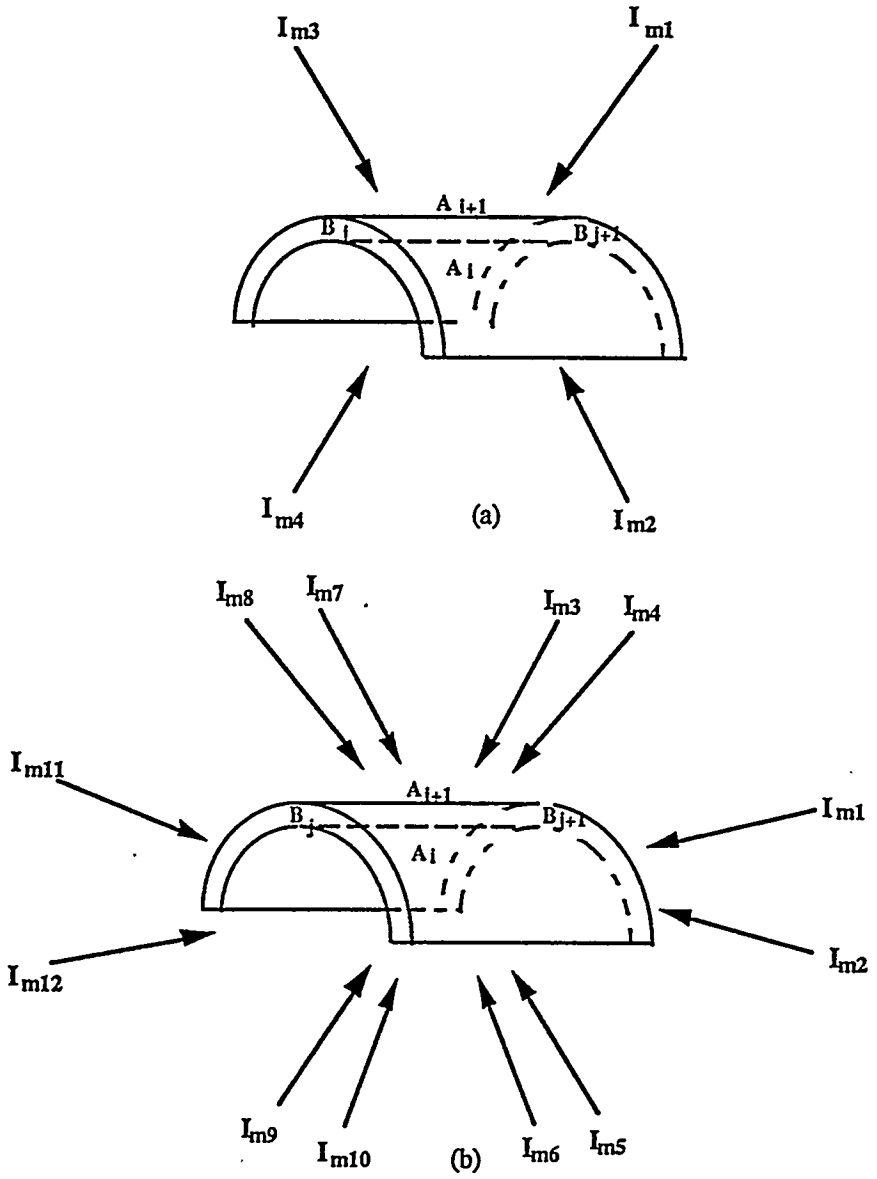

Figure 2-4. Directional intensities reaching a volume\element. (a) S_2 (b) S_4.

The left side of Eqn. 2-140 represents the gradients of intensity in the direction of propagation, and the right side represents, respectively, the attenuation of intensity due to absorption and out-scattering, and the contribution to the direction intensity due to emission by the medium, and in-scattering. $P(\Omega,\Omega')$ is a probability density function, formally known as the phase function, which determines the distribution of the scattered intensity. Eqn. 2-140 is better known as the radiation transport equation. The quantities μ_m, η_m, and ξ_m represent the direction cosines for the direction $\underset{\sim}{\Omega}$, and are expressed as (see Fig. 2-5)

$$\mu_m = \sin\theta\cos\psi, \quad \eta_m = \sin\theta\sin\psi, \quad \xi_m = \cos\theta \tag{2-141}$$

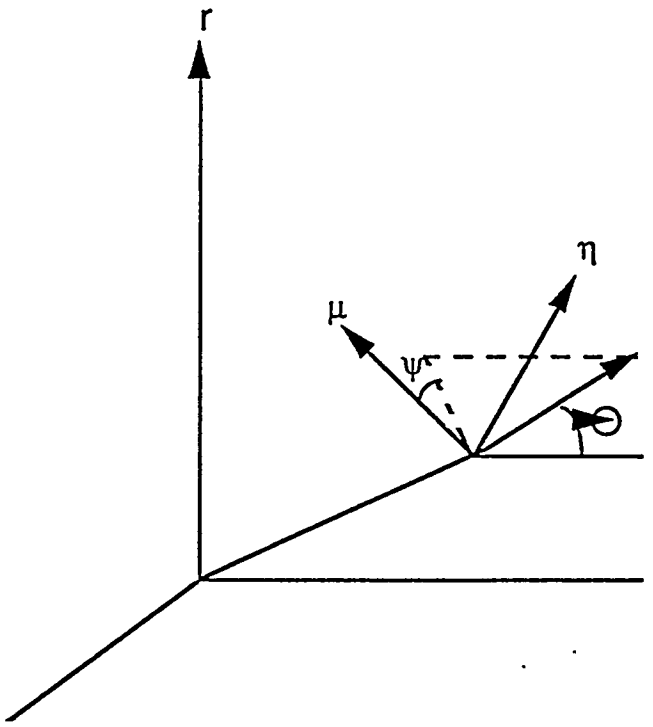

Figure 2-5. The direction cosines.

The flux methods (including the discrete ordinates method) solve Eqn. 2-140 in a number of pre-determined directions. The number of directions, N_m, depends on the order of the approximation. In discrete ordinates method, this is given by $N_m=n(n+2)$ (Carlson and Lathrop, 1968), where n represents the order of the discrete ordinates approximation (the number of values for the direction cosines considered within the range ± 1.0). The angular integral is evaluated using numerical quadrature. Each direction Ω_m is pictured as a point on the surface of a unit sphere with which a surface area w_m is associated. w_m can be viewed as the angular quadrature weight, with the requirement that

$$\sum_m w_m = 4\pi \tag{2-142}$$

In the conventional flux methods (e.g., VFM), the quadrature weight is assumed to be uniform for all directions. In the VFM this is assigned a value of $4\pi/6$. In the discrete ordinates method, the entire quadrature scheme (i.e., the direction cosines and the weights) is obtained using the "moment matching" technique of Carlson and Lathrop (1968). The quadrature schemes for the S_2 and S_4 discrete ordinates, where radiation transport equation is solved in 4 and 12 directions, respectively, ($N_m/2$ directions required due to axial symmetry), are reported in Tables 2-9 and 2-10 (Truelove, 1976, 1978). These direction cosines establish a coupling between the directional intensities. In the orthogonal flux methods (like the VFM), the directions chosen to solve the radiative transport equation coincide with the coordinate directions, and therefore the coupling between the directional intensities is lost (for every direction, one of the direction cosines has a value of unity, while the other two are zeroes).

Considering the surrounding surfaces to be diffusely emitting-reflecting, the boundary conditions for the above equation are

$$
\begin{aligned}
&at\ r = R: \quad I_m = \varepsilon_w I_{bw} + (1-\varepsilon_w)\frac{q_r^+}{\pi} \ ; \ \mu_m < 0 \\
&at\ r = 0: \quad I_m = I_{m'} \ ; \ \mu_{m'} = \mu_m \\
&at\ z = 0: \quad I_m = \varepsilon_w I_{bw} + (1-\varepsilon_w)\frac{q_z^-}{\pi} \ ; \ \xi_m > 0 \\
&at\ z = L: \quad I_m = \varepsilon_w I_{bw} + (1-\varepsilon_w)\frac{q_z^+}{\pi} \ ; \ \xi_m < 0
\end{aligned}
\qquad (2\text{-}143)
$$

TABLE 2-9

THE S_2 QUADRATURE FOR AXISYMMETRIC CYLINDRICAL ENCLOSURES

m	μ	η	ξ	w_m
1	-0.5	0.7071	-0.5	π
2	0.5	0.7071	-0.5	π
3	-0.5	0.7071	0.5	π
4	0.5	0.7071	0.5	π

TABLE 2-10

THE S_4 QUADRATURE FOR AXISYMMETRIC CYLINDRICAL ENCLOSURES

m	μ	η	ξ	w_m
1	-0.2959	0.2959	-0.9082	$\pi/3$
2	0.2959	0.2959	-0.9082	$\pi/3$
3	-0.9082	0.2959	-0.2959	$\pi/3$
4	-0.2959	0.9082	-0.2959	$\pi/3$
5	0.2959	0.9082	-0.2959	$\pi/3$
6	0.9082	0.2959	-0.2959	$\pi/3$

TABLE 2-10 (continued)

m	μ	η	ξ	w_m
7	-0.9082	0.2959	0.2959	$\pi/3$
8	0.2959	0.9082	0.2959	$\pi/3$
9	0.2959	0.9082	0.2959	$\pi/3$
10	0.9082	0.2959	0.2959	$\pi/3$
11	-0.2959	0.2959	0.9820	$\pi/3$
12	0.2959	0.2959	0.9820	$\pi/3$

with the hemispherical fluxes given by

$$q_r^+ = \sum_m W_m \mu_m I_m \quad ; \quad \mu_m > 0$$
$$q_r^- = \sum_m W_m |\mu_m| I_m \quad ; \quad \mu_m < 0$$
$$q_z^+ = \sum_m W_m \xi_m I_m \quad ; \quad \xi_m > 0$$
$$q_z^- = \sum_m W_m |\xi_m| I_m \quad ; \quad \xi_m < 0 \qquad (2\text{-}144)$$

In the VFM, these fluxes are obtained as

$$q^+ = \frac{F+q}{2}$$
$$q^- = \frac{F-q}{2} \qquad (2\text{-}145)$$

the flux-sums and the net fluxes being those from the previous iteration.

Assuming scatter to be linearly anisotropic, the phase function may be represented by

$$P\left(\underline{\Omega},\underline{\Omega}'\right)=1+a_0\cos\phi \tag{2-146}$$

where ϕ is the angle between the incident and the scattered intensities, and a_0 is an asymmetry factor with a value between +1.0 and -1.0. In terms of the direction cosines, $P\left(\underline{\Omega},\underline{\Omega}'\right)$ can be written as

$$P\left(\underline{\Omega},\underline{\Omega}'\right)=1+a_0\left(\mu_m\mu_{m'}+\xi_m\xi_{m'}\right) \tag{2-147}$$

In the VFM, the directional contributions due to scatter are evaluated as

$$\begin{aligned}\bar{f}&=2\pi\int_o^{\pi/2}P\left(\underline{\Omega},\underline{\Omega}'\right)\sin\phi\cos^2\phi d\phi\\ \bar{b}&=2\pi\int_{\pi/2}^{\pi}P\left(\underline{\Omega},\underline{\Omega}'\right)\cos^2\phi\sin\phi d\phi\\ \bar{s}&=\left(1-\bar{f}-\bar{b}\right)/4\end{aligned} \tag{2-148}$$

where $\bar{f}$, $\bar{b}$, *and* $\bar{s}$ are the forward-, backward-, and side-scattered components.

The angular derivative term in Eqn. 2-140 is evaluated using a direct-differencing technique (Carlson and Lathrop (1968)). Using this technique, the second term on the left hand side of Eqn. 2-140 can be re-written as

$$(1/r)\left[\partial\left(\eta_m I_m\right)/\partial\psi\right]=(1/r)\left[\left(\alpha_{m+1/2}I_m+1/2-\alpha_{m-1/2}I_m-1/2\right)\right]/w_m \tag{2-150}$$

The direction $m\pm1/2$ define the edges of the angular range of w_m, the two terms representing, respectively, the flow out of and into the angular range. A direct relationship between α_m and w_m can be drawn on the basis of isotropic radiation

$$\alpha_{m+1/2}-\alpha_{m-1/2}=w_m\mu_m \tag{2-151}$$

The α's are chosen so that the radiation intensity is only redistributive in the azimuthal direction (i.e., no net transfer). In the Varma method this is achieved by

letting $dI_{\psi}^{+}/d\psi = dI_{\psi}^{-}/d\psi = 0.0$, which eliminates two of the six first-order equations of intensity distribution and reduces them to algebraic form.

Working Equations

The working equations for DOM and VFM are quite different, and deserve separate discussion.

Discrete Ordinates Method (DOM). Multiplying both sides of Eqn. 2-140 by 2π rdrdz, and integrating over the volume element (Fig. 2-4), we obtain

$$\mu_m\left(A_{i+1}I_{i+1} - A_iI_i\right) - \left(A_{i+1} - A_i\right)\left[\left(\alpha_{m+1/2}I_{m+1/2} - \alpha_{m-1/2}I_{m-1/2}\right)/w_m\right]$$
$$+\xi_m\left(B_{j+1}I_{j-1} - B_jI_j\right) = -\left(k_a + k_s\right)V_pI_m + k_aV_pI_b$$
$$+\frac{k_sV_p}{r\pi}\sum_m\left[1 + a_o\left(\mu_m\mu_{m'} + \xi\xi_{m'}\right)\right]w_m \qquad (2\text{-}152)$$

The intensities I_{i+1}, I_{j+1} and $I_{m+1/2}$ can be expressed in terms of the discrete intensities I_i, I_j and $I_{m-1/2}$ using central differencing:

$$I_i + I_{i+1} = I_j + I_{j+1} = I_{m-1/2} + I_{m+1/2} = 2I_m \qquad (2\text{-}153)$$

I_m intensity at the center of the volume element can therefore be evaluated as

$$I_m = \frac{\mu_mAI_i + \beta_mI_{m-1/2} + \xi_mBI_j + V_p\left(k_aI_b + k_sI_s\right)}{\mu_mA - \beta_m + \xi_mB + V_p\left(k_a + k_s\right)} \qquad (2\text{-}154)$$

where

$$
\begin{aligned}
A &= A_i + A_{i+1} \\
B &= B_j + B_{j+1} \\
B_m &= -\left(\alpha_{m+1/2} + \alpha_{m-1/2}\right)\left(A_{i+1} - A_i\right)/w_m \\
I_s &= \sum_m w_m I_m \left[\frac{1 + a_o\left(\mu_m \mu_{m'} + \xi_m \xi_{m'}\right)}{4\pi}\right]
\end{aligned}
$$

Eqn. 2-151 is strictly applicable to the case where both μ_m and ξ_m are positive. For other combinations of μ_m and ξ_m, the equation changes.

Varma Six-Flux Method. The four first-order equations for the r- and x-directed intensities are combined into two second-order equations following the approach of Gosman and Lockwood (1973). The radiation flux sum and the net radiation are defined as

$$F = q^+ + q^- \tag{2-154}$$

$$q = q^+ - q^- \tag{2-155}$$

Combining each pair of radiation flux equations results in an expression of the following form (for the x-component):

$$q_x = -\Gamma_x \left(dF_x/dx\right) \tag{2-156}$$

where

$$\Gamma_x = \left[k_a + k_s\left(1 - \bar{b} - \bar{f}\right)\right]^{-1}$$

Adding each pair, and combining with Eqn. 2-156, the following equation for the x-component results

$$-\frac{d}{dx}\left(\Gamma_x \frac{dF_x}{dx}\right) = \left(c_1 + c_2\right)F_x + 2c_3 F_r + 2c_4 E_b \tag{2-157}$$

The corresponding equations for the r and ψ components are

$$\frac{1}{r}\frac{d}{dx}(rF_r) = (c_1 + c_2)F_r + 2c_3F_x + 2c_4E_b \tag{2-158}$$

$$F_\theta = 2c_5(F_x + F_r) + 2c_6E_b \tag{2-159}$$

The necessary coefficients are defined in Table 2-11. The extinction coefficient and the albedo of scatter are given by

$$k_t = k_a + k_s \tag{2-160}$$

$$\omega_o = \frac{k_s}{k_t} \tag{2-161}$$

TABLE 2-11

COEFFICIENTS FOR FLUX SUMS

$$c_1 = -k_t(1 - \omega_o f) + k_t\left(\frac{2\omega_o^2 s^2}{1 - \omega_o f - \omega_o b}\right)$$

$$c_2 = k_t\omega_o b + k_t\left(\frac{2\omega_o^2 s^2}{1 - \omega_o f - \omega_o b}\right)$$

$$c_3 = k_t\omega_o s + k_t\left(\frac{2\omega_o^2 s^2}{1 - \omega_o f - \omega_o b}\right)$$

TABLE 2-11 (continued)

$$c_4 = k_t\left(\frac{1-\omega_o}{6}\right)\left(1+\frac{2\omega_o s}{1-\omega_o f-\omega_o b}\right)$$

$$c_5 = \frac{\omega_o s}{1-\omega_o f-\omega_o b}$$

$$c_6 = \frac{1-\omega_o}{6(1-\omega_o f-\omega_o b)}$$

Radiative Properties

To carry out the above calculations, information is needed on the absorption and scattering cross-sections for the particulates, as well as the scattering phase functions. These can be calculated using Mie theory (Mie, 1908) if the particle size, the wavelength of the radiation, and the complex refractive index of the particle are known. Sample results from such calculations, using a published program (Dave, 1968), are presented in Fig. 2-6 for size parameters $(\pi dj/\lambda)$ in the range of 0-100. In this figure, the refractive index of char is taken as 1.93 (1.0-0.53i) at a wavelength of 2 μm.

Optical properties of coal are not well characterized (Solomon et al., 1986; Brewster and Kunitomo, 1984; Baxter et al., 1988). The absorption and scattering efficiencies depend strongly on these properties. Once the absorption and scattering efficiencies are known from Mie theory, the absorption and scattering coefficients of the particulates for a cell can be evaluated as

$$k_{ap,cell} = \sum_i \sum_j k_{aij,cell} = (\pi/4)\sum_i \sum_j \dot{n}_{ij} \int_{cell} Q_{aj} d_j^2 dt \qquad (2\text{-}162)$$

$$k_{sp,cell} = \sum_i \sum_j k_{sij,cell} = (\pi/4) \sum_i \sum_j \dot{n}_{ij} \int_{cell} Q_{sj} d_j^2 dt \qquad (2\text{-}163)$$

where t is the time along a Lagrangian trajectory, and $\dot{n}_{ij}$ is the particle number flowrate for the i^{th} starting location and j^{th} particle size. The scattering efficiency plotted in Fig. 2-6 includes a contribution of 1.0 due to diffraction which must be discounted in heat transfer calculations (Varma, 1979). This makes the value of Q_s used in Eqn. 2-163 equal to 1.0 less than that plotted in Fig. 2-6. Soot particles absorb, but do not scatter radiation significantly due to their microscopic size. Soot radiation is considered below.

The absorption coefficients for the gases are evaluated from gas emissivity data:

$$k_{ag} = (1/L_e)\left[ln\left(1-\varepsilon_g\right)\right] \qquad (2\text{-}164)$$

where

$$\varepsilon_g = C_{co_2}\varepsilon_{co_2} + C_{H_2O}\varepsilon_{H_2O} - \Delta\varepsilon \qquad (2\text{-}165)$$

and the mean (effective) beam length (a single overall value is used in PCGC-2) is given by

$$L_e = 3.5(V_F/A_F) \qquad (2\text{-}166)$$

C_{CO_2} and C_{H_2O} represent the pressure corrections to the gas emissivities, and $\Delta\varepsilon$ represents the spectral overlap correction. The gas emissivity data are taken from Hottel and Sarofim (1967) and Siegel and Howell (1981). The overall absorption coefficient for a cell can therefore be obtained as

$$k_{a,cell} = k_{ap,cell} + k_{ag,cell} \qquad (2\text{-}167)$$

and the total heat absorption by the cell as

$$q_{r,cell} = k_{a,cell}\left(F_x + F_r + F\psi - E_b\right)_{cell} \qquad (2\text{-}168)$$

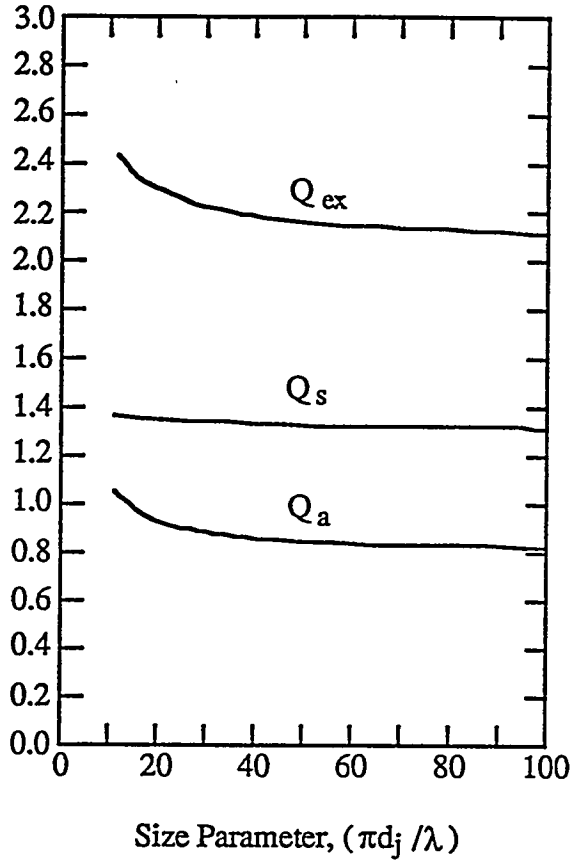

Fig. 2-6. The absorption, scattering, and extinction efficiencies of char particles at wavelength of 2μm and refractive index of 1.93 [1-i(0.53)].

out of which a fraction $q_{rg} = (k_{ag}/k_a)q_r$ is absorbed by the gas phase, and the remainder $q_{rp} = (k_{ap}/k_a)q_r$ is absorbed by the particle phase within the cell. The radiation transfer rate to the Lagrangian particles is given by

$$Q_{rj} = \frac{\pi d_j^2}{4} Q_{aj}\left(F_x + F_r + F_\psi - E_b\right) \qquad (2\text{-}169)$$

The blackbody emissive power, E_b, is given by (Siegel and Howell, 1981, p. 36)

$$E_b = 4\sigma T_g^4 \qquad (2\text{-}170)$$

where T_g is the local gas temperature (Siegel and Howell, 1981, p.36).

Soot Radiation

When soot radiation is included, Eqn. 2-153 becomes

$$I_m = \frac{\mu_m A I_i + \beta_m I_{m-1/2} + \xi_m B I_j + V_p\left(k_a I_b + k_s I_s + k_{soot\,em} I_b\right)}{\mu_m A - \beta_m + \xi_m B + V_p\left(k_a + k_s + k_{soot\,abs}\right)} \qquad (2\text{-}171)$$

The values of $k_{soot\,em}$ and $k_{soot\,abs}$ are given by (Kent and Honnery, 1990)

$$k_{soot\,em} = 1.9 \times 10^3 f_v T_e \ (m^{-1}) \qquad (2\text{-}172)$$

and

$$k_{soot\,abs} = 1.9 \times 10^3 f_v T_b \ (m^{-1}) \qquad (2\text{-}173)$$

where f_v is the volume fraction of soot, and the volume of soot (which does not include entrained gas) = (moles of soot) x 12 grams per mole/soot density. The Favre-averaged mole fraction of solid, condensed carbon is taken as the mean soot concentration since there is currently no kinetics-based soot formation and decay model in PCGC-2. With this assumption, the model will probably underpredict the contribution due to soot radiation, since soot formation kinetics are fairly rapid, but decay is fairly slow. These values are for small soot particles and are averaged over wavelength and temperature. T_e is the local gas temperature in Kelvins, and T_b is the effective blackbody temperature of the radiation incident on the local volume.

The correction due to spectral overlap of soot and gas radiation is given by (Hottel and Sarofim, 1967)

$$\Delta\varepsilon = \sum_i \varepsilon_i - \left[1 - \prod_i (1 - \varepsilon_i)\right] \quad (2\text{-}174)$$

With a three-component model for continuum radiation (soot, H_2O, and CO_2), the correction becomes

$$\Delta\varepsilon = \varepsilon_{H_2O} c_{H_2O} + \varepsilon_{CO_2} c_{CO_2} + \varepsilon_{soot} - \left[1 - \left(1 - \varepsilon_{H_2O} c_{H_2O}\right)\left(1 - \varepsilon_{CO_2} c_{CO_2}\right)\left(1 - \varepsilon_{soot}\right)\right] \quad (2\text{-}175)$$

With the correction due to the overlap of CO_2 and H_2O lines already included, the additional correction simplifies to two pairwise corrections, for soot-CO_2 and soot-H_2O:

$$\Delta\varepsilon_{soot,CO_2} = \varepsilon_{soot} \times \varepsilon_{CO_2} \quad (2\text{-}176)$$

and

$$\Delta\varepsilon_{soot,H_2O} = \varepsilon_{soot} \times \varepsilon_{H_2O} \quad (2\text{-}177)$$

However, Eqn. 2-174 only applies if all but one of the species is a grey-body radiator; not the case for soot. The correct calculation for the correction term is shown below. Equations 2-176 and 2-177 calculate the correction to within 4 percent for all temperatures and concentrations of interest.

Nitrogen Pollutants

Background

The development of an effective model to predict nitrogen pollutant formation during pulverized coal combustion requires an adequate description of nitrogen conversion from coal, char, and soot to volatile gaseous nitrogen species and subsequent homogeneous and heterogeneous reactions among the nitrogen, fuel, and oxidizer species. The kinetic mechanism must be limited to sufficiently few homogeneous reactions to allow for coupling with the turbulent mixing process. The approach used for calculating each reaction rate is dependent on the relative time scales of reaction and turbulent fluctuation.

Reaction Mechanisms

Two simplified fuel-NO mechanisms are available for predicting the conversion of coal-bound nitrogen to HCN, NH_3, NO and N_2 as illustrated by the schematics in Figure 2-7. Either mechanism can be coupled with the Zel'dovich mechanism. One mechanism is an extension of the NO_x model in previous versions of PCGC-2. It allows volatile coal and char nitrogen to be partitioned between HCN and NH_3 (see Figure 2-7a). The second mechanism (see Figure 2-7b) is based on the general concept that HCN decays to NH_3 which is subsequently oxidized to NO or competitively reduced to N_2. The Zel'dovich mechanism is used to predict thermal NO formation. Thermal NO formation can also be predicted for gaseous fuel cases. Joint or separate prediction of fuel NO and thermal NO can be made for coal-containing cases.

a) Expanded mechanism

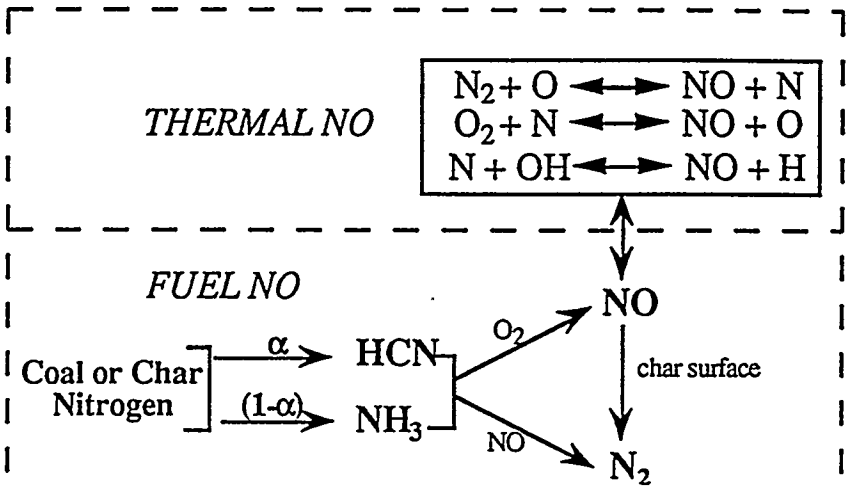

b) Alternative mechanism

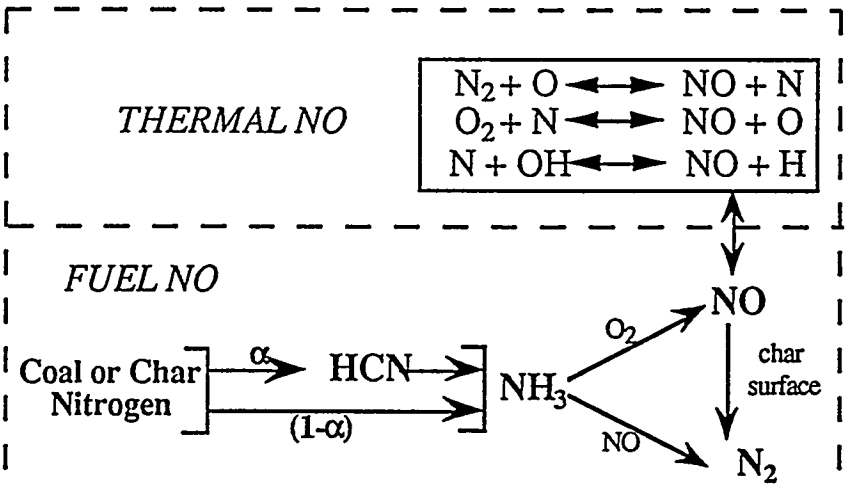

Figure 2-7. Kinetic mechanisms for prediction of fuel and thermal NO.

Prompt NO formation occurs in coal flames, but since coal generally contains 1-2% nitrogen, prompt NO is likely to be overshadowed by fuel NO. It is estimated that prompt NO typically accounts for less than 5% of the total NO formed. However, prompt NO formation may be significant during gaseous combustion. Reactions describing the interaction of nitrogen species with fuel fragments, called "reburning" reactions, may be important in fuel-rich flame conditions. Neither prompt NO nor reburning reactions are currently modeled in this version of the NO_x submodel.

The global rate expressions reported by de Soëte (1975) and Bose et al., (1988) and the empirical rate correlations by Mitchell and Tarbell (1982) appear to be the best available rates for predicting the homogeneous fuel NO mechanism steps. The user has the flexibility of selecting the rate expressions to fit the alternative fuel NO mechanisms. The rate parameters for the thermal NO reactions were taken from Bowman (1975) and Miller and Bowman (1989). An empirical rate expression is used to predict char/NO reaction. Table 2-11 documents the rate parameters for the individual reaction steps.

It is generally agreed that the reaction network for thermal NO is correctly described by the modified Zel'dovich mechanism based on research originally carried out by Zel'dovich (1947).

$$N_2 + O \leftrightarrow NO + N \qquad (2\text{-}178)$$

$$N + O_2 \leftrightarrow NO + O \qquad (2\text{-}179)$$

In fuel-rich environments (stoichiometric ratios of air to fuel < 1.0), at least one additional step should be included in this mechanism (Lavoie et al., 1970).

$$N + OH \leftrightarrow NO + H \qquad (2\text{-}180)$$

The following thermal NO rate expression is derived by Westenberg, (1971)

$$\frac{d[NO]}{dt} = 2[O]\left\{\frac{k_{A6}[N_2] - \frac{k_{-A6}k_{-A7}[NO]^2}{k_{A7}[O_2]}}{1 + \frac{k_{-A6}[NO]}{k_{A7}[O_2]+k_{A8}[OH]}}\right\} \quad \text{gmole cm}^{-3}\,\text{s}^{-1} \qquad (2\text{-}181)$$

For most lean flames, the reaction in Eqn. 2-180 may be neglected. In early stages of the flame, NO concentrations are very low; thus, the reverse reactions for Reactions in eqns. 2-178 and 2-179 are negligible. This yields a simpler thermal NO rate expression when the "steady state assumption" for atomic nitrogen is also invoked.

$$\frac{d[NO]}{dt} = 2k_{A6}[O][N_2] \quad \text{gmole cm}^{-3}\,\text{s}^{-1} \qquad (2\text{-}182)$$

Both eqns. 2-181 and 2-182 have been made available in the NO_X submodel. Both expressions are coupled to the combustion kinetics through competition for the oxygen atom. In fuel lean, secondary combustion zones, where CO is oxidized to CO_2, O is often assumed to be only in equilibrium with O_2.

$$O_2 + M \leftrightarrow 2O + M \qquad (2\text{-}183)$$

$$[O] = \left\{K'_{eq}[O_2]\right\}^{1/2} \qquad (2\text{-}184)$$

Another approach, which accounts for [O] and [OH] in excess of their equilibrium values, is assumed to be valid in regions where hydrocarbons are consumed (Iverach et al., 1973; Sarofim and Pohl, 1973; and Thompson et al., 1981).

$$[O] = K_{eq}^{\cdot} \frac{[O_2][CO]}{[CO_2]} \qquad (2\text{-}185)$$

Both options for calculating O concentrations have been included in the NO_x submodel.

When the global rate expressions of Wendt and coworkers are selected to predict fuel NO formation, OH concentrations must be estimated for the HCN oxidation reaction (see Table 2-12). Two options are available in the NO_x submodel. The default option is to use the gaseous equilibrium OH concentrations calculated by PCGC-2. The second option is to predict the deviation from equilibrium using a empirical expression. Wendt et al. (1989) presented an equation for estimating the "overshoot" in radical OH concentration as a function of temperature for their reactor system and conditions.

$$OH = OH_{eq}\left[1.1x10^{-4} exp\left(\frac{15469}{T}\right)\right] \qquad (2\text{-}186)$$

This expression is included in the revised NO_x submodel and can be used to adjust OH concentrations. When experimental OH data are available for a particular flame condition, the temperature-dependent constants can be changed.

TABLE 2-12

REACTION EXPRESSION ALTERNATIVES FOR THE GENERALIZED NITRIC OXIDE MODEL

Thermal NO Mechanism Reactions[£]

$k = A\,T^{\beta}\,exp(-E/RT)$ $(cm^3\ gmole^{-1}\ s^{-1})$

Reaction Expression	Concentration	A	β	E (J/gmole)
$O + N_2 \rightarrow NO + N$	$X_{N_2} X_O$	$1.36x10^{14}$	0	315,900
$N + NO \rightarrow N_2 + O$	$X_{NO} X_N$	$3.27x10^{12}$	0.300	-
$N + O_2 \rightarrow NO + O$	$X_{O_2} X_N$	$6.40x10^{9}$	1.000	26,300
$O + NO \rightarrow O_2 + N$	$X_{NO} X_O$	$1.50x10^{9}$	1.000	162,100
$N + OH \rightarrow NO + H$	$X_{OH} X_N$	$3.80x10^{13}$	0	-
$H + NO \rightarrow OH + N$	$X_{NO} X_H$	$2.00x10^{14}$	0	196,600

TABLE 2-12 (continued)

Fuel NO Mechanism Reactions

$k = Aexp(-E/RT)$ $(cm^3\ gmole^{-1}\ s^{-1})$

Reaction Expression	Reference	Concentration	*A*	*E* (J/gmole)
$HCN \rightarrow NO$	DeSoëte (1975)§	$X_{HCN} X^b_{O_2}$	3.50×10^{10}	280,300
$HCN \rightarrow N_2$	DeSoëte (1975)	$X_{HCN} X_{NO}$	3.00×10^{12}	251,000
$HCN \rightarrow NH_3$	Bose *et al.*, (1988)	$X_{HCN} X_{OH}$	parameters are coal dependent	
	Mitchell and Tarbell (1982)	$X_{HCN} X_{O_2}$	(see Mitchell and Tarbell, 1982)	
$NH_3 \rightarrow NO$	DeSoëte (1975)§	$X_{NH_3} X^b_{O_2}$	4.00×10^6	133,900
	Mitchell and Tarbell (1982)	$X_{NH_3} X_{O_2}$	(see Mitchell and Tarbell, 1982)	
$NH_3 + NO \rightarrow N_2$	DeSoëte (1975)	$X_{NH_3} X_{NO}$	1.80×10^8	113,000
	Bose *et al.* (1988)	$X_{NH_3} X_{NO}$	1.92×10^4	94,100
	Mitchell and Tarbell (1982)	$X_{NH_3} X_{NO}$	6.22×10^{14}	230,100

Char/NO Reaction¶

$$d[NO]/dt = 4.18 \times 10^4 exp(-17{,}500/T) A_E P_{NO}\ gmol \cdot s^{-1}$$

£ Rate parameters are from Miller and Bowman (1989) and Bowman (1975).

§ The power for oxygen concentrations is determined from an auto correlation, $b = f(O_2)$, given by

DeSoëte (1975).

¶ Levy et al., (1981)

Working Equations

The Favre-averaged species continuity equation is used to calculate the Favre-mean mass fractions of the nitrogen pollutants (NO, HCN, and NH_3) throughout the turbulent reactor.

$$\overline{W}_i = \overline{\rho}\tilde{u}\left(\frac{\partial \tilde{Y}_i}{\partial x}\right) + \overline{\rho}\tilde{v}\left(\frac{\partial \tilde{Y}_i}{\partial r}\right) - \left(\frac{\partial}{\partial x}\right)\left(\tilde{D}_Y \frac{\partial \tilde{Y}_i}{\partial x}\right) - \frac{1}{r}\left(\frac{\partial}{\partial r}\right)\left(r\tilde{D}_Y \frac{\partial \tilde{Y}_i}{\partial r}\right) \quad (2\text{-}187)$$

Here, $\overline{W}_i$ is the overall mean chemical reaction source or sink term calculated by summing all individual (global and elementary-step) mean reaction rates, $\overline{\omega}_j$, involving formation or destruction of species i by the jth reaction.

$$\overline{W}_i = \sum_j \overline{\omega}(X_i, X_k, T)_j \quad (2\text{-}188)$$

Smith et al. (1982) assumed that ω_j for turbulent reacting gases could be approximated by convolving the instantaneous rates over the random fluctuations of the two mixture fraction progress variables f and η.

$$\overline{\omega}_i = \overline{\rho}\int_f \int_\eta (\omega_i(f,\eta,h)/\rho(f,\eta,h))\tilde{P}(f)\tilde{P}(\eta)d\eta df \quad (2\text{-}189)$$

In order to jointly integrate the chemical kinetics and turbulent fluctuations, local instantaneous species concentrations must be known for every probable state of "mixedness". The overall fractional conversion of each species is tracked in the revised NO_X submodel. Individual species are bounded between their maximum and minimum values, depending on their initial concentrations and the limiting reactants. The fractional conversion of individual species reactions between these bounds is used to calculate the desired instantaneous concentrations.

The maximum amount of HCN or NH_3 available for reaction at a location in the reactor is determined by the local instantaneous extent of coal mass loss, tracked by the coal off-gas mixture fraction. The maximum HCN and NH_3 concentrations are determined from the ultimate yield of fuel nitrogen at each location in the reactor. The local minimum HCN and NH_3 concentrations are determined by the local availability of oxidizer. Thus, the local fractional conversion, ζ_i, is bounded between 0.0 and 1.0 and is expressed as:

$$\zeta_i = \left(\frac{X_i^f - X_i}{X_i^f - X_i^{min}}\right) \qquad i = HCN, NH_3 \quad (2\text{-}190)$$

Here X_i^f represents the local maximum concentration for HCN or NH_3 and X_i^{min} represents the local minimum. When HCN or NH_3 is the limiting reactant, X_i^{min} is 0.0. Except in fuel-rich regions, X_i^{min} is typically 0.0 for coal combustion. During coal gasification, X_i^{min} is frequently not zero.

The maximum amount of fuel NO that can be formed locally is determined from the maximum concentrations of HCN and NH_3 combined, since in the limit, where enough oxygen is available, all of the HCN and NH_3 can be converted to NO. When NO does not enter the reactor with any inlet stream, the minimum amount of NO is zero and the fractional conversion of NO reduces to the following equation:

$$\zeta_{NO}^{fuel} = \left(\frac{X_{NO}}{X_{NO}^f} \right) \tag{2-191}$$

The formation of thermal NO is bounded by the local equilibrium concentrations since the extended Zel'dovich mechanism contains reversible elementary-step reactions. The reaction progress for thermal NO reactions is determined by scaling the local instantaneous NO concentration by the local equilibrium quantity. Local NO equilibrium concentrations is calculated by an equilibrium subroutine in PCGC-2. The fractional conversion for thermal NO may be viewed as an equilibrium deviation factor and is not bounded by unity.

$$\zeta_{NO}^{thermal} = \left(\frac{X_{NO}}{X_{NO}^{eq}} \right) \tag{2-192}$$

When $\zeta_{NO}^{thermal}$ is less than 1.0, the thermal NO mechanism favors NO formation; conversely, when the value of $\zeta_{NO}^{thermal}$ is greater than unity, thermal NO shifts back to atomic and molecular oxygen and nitrogen according to the extended Zel'dovich mechanism.

When joint thermal and fuel NO predictions are made, the maximum NO concentration possible is calculated as the sum of the maximum amount of fuel NO and maximum thermal NO possible. The maximum concentration of thermal NO possible can be calculated by the sum of the forward reaction steps of the Zel'dovich mechanism, neglecting reverse mechanism reactions. The fuel NO and

thermal NO mechanisms couple in such a manner that final NO concentrations rarely equal the sum of thermal NO and fuel NO concentrations when predicted separately. Both mechanisms compete for oxygen concentrations and NO is destroyed simultaneously by both mechanisms, regardless of the origin of NO.

It is assumed that the local instantaneous reaction progress variables are approximately equal to their time-mean values; in other words, turbulent fluctuations do not affect the local extent-of-reaction. Thus, the local extent-of-reaction is calculated using time-mean values. For example;

$$\zeta_i = \tilde{\zeta}_i = \left(\frac{\tilde{X}_i^f - \tilde{X}_i}{\tilde{X}_i^f - \tilde{X}_i^{min}} \right) \qquad i = HCN, NH_3 \qquad (2\text{-}193)$$

Once the local fractional conversion of a species is known, the local instantaneous concentrations are calculated by scaling the local instantaneous maximum or equilibrium concentrations with the appropriate fractional conversion variable. For example;

$$X_i = X_i^f - \left(X_i^f - X_i^{min} \right) \tilde{\zeta}_i \qquad i = HCN, NH_3 \qquad (2\text{-}194)$$

The amount of nitrogen released from the coal is calculated directly from the source of particle mass added to the gas phase $\left(S_p^{\eta} \right)$. Experimental evidence shows that HCN and NH_3 are rapidly produced and exist as relatively long lived species under all coal flame conditions. Several investigators have reported that HCN precedes the appearance of NH_3 for both high and low rank coals over a broad range of stoichiometries (Ghani and Wendt, 1990, Haussmann and Kruger, 1989, Freihaut and Proscia, 1991). However, other investigations (Peck et al., 1991 and Chen et al., 1982) observed that NH_3 may be a direct pyrolysis product in subbituminous flames and that light-gas NH_3 may also be produced by heterogeneous processes. Until a comprehensive nitrogen pyrolysis model is incorporated into the NO_x submodel, the fraction of coal and char nitrogen released as HCN or NH_3 is specified by adjustable parameters. The FG/DVC model has not been adapted into the submodel in this version of the code.

Two adjustable parameters are available in the model to control nitrogen release to the gas phase. The parameter ζ_n specifies the fractional conversion of

coal and/or char nitrogen to gaseous nitrogen while the adjustable parameter α_n is used to partition the initial volatile nitrogen between HCN and NH_3. In the model, the coal off-gas mixture fraction tracks the extent of coal and char conversion to the gas phase. Hence, the yield of coal-nitrogen released to the gas phase is expressed by the equations:

$$\left(Y_{HCN}\right)_{max} = \eta \cdot \zeta_n \cdot \alpha_n \cdot bcn \cdot MW_{HCN} \qquad (2\text{-}195)$$

$$\left(Y_{NH_3}\right)_{max} = \eta \cdot \zeta_n \cdot (1-\alpha_n) \cdot bcn \cdot MW_{NH_3} \qquad (2\text{-}196)$$

Here, *bcn*, is the percentage of nitrogen in the coal and is determined by ultimate analysis of the coal. η is the fraction of coal off-gas at a position in the reactor. The fractional nitrogen release parameters are bounded to $(0.0 \leq \zeta_n \leq 1.0)$ and $(0.0 \leq \alpha_n \leq 1.0)$.

Submodel Summary

All of the equations that are solved by the NO_x submodel are listed in Table 2-12. The following is a summary of the key model assumptions.

i. The formation of nitrogen pollutant species does not impact the governing flame structure.
ii. NO formation/destruction mechanisms other than thermal NO and fuel NO are neglected.
iii. Fuel NO formation is adequately described by global mechanisms explicit only in HCN, NH_3, NO, and N_2.
iv. Thermal NO is adequately predicted by the extended Zel'dovich mechanism. Two rate expressions are available.
v. Atomic oxygen can be predicted using quasi-equilibrium expressions dependent on major species concentrations (O_2, CO_2, and CO). Two expressions are available.
vi. Nitrogen is devolatilized or released from char at a rate proportional to the rate of total coal weight loss. The proportionality constant is an adjustable parameter.

vii. Volatile nitrogen is instantaneously converted to HCN and/or NH_3 once it is released to the gas. The partition between HCN and NH_3 is specified by an adjustable parameter.
viii. Instantaneous species concentrations can be tracked using fractional conversion expressions.
ix. Instantaneous and Favre-average fractional conversions are approximately equal.
x. Mean homogeneous reaction rates are obtained by convolving over the probability of mixture fraction progress variables.
xi. Heterogeneous char/NO reactions are not affected by turbulence.
xii. Soot/NO interaction are neglected.

TABLE 2-13

EQUATION SET FOR A GENERALIZED NO MODEL

Equation	Definition
$\overline{W}_i = \overline{\rho}\tilde{u}\left(\frac{\partial \tilde{Y}_i}{\partial x}\right) + \overline{\rho}\tilde{v}\left(\frac{\partial \tilde{Y}_i}{\partial r}\right) - \left(\frac{\partial}{\partial x}\right)\left(\tilde{D}_Y \frac{\partial \tilde{Y}_i}{\partial x}\right) - \frac{1}{r}\left(\frac{\partial}{\partial r}\right)\left(r\tilde{D}_Y \frac{\partial \tilde{Y}_i}{\partial r}\right)$	Species Continuity for i = HCN, NH_3, and NO
$\overline{W}_i = \sum_j \overline{\omega}(X_i, X_k, T)_j$	Overall mean reaction rate for i = HCN, NH_3, and NO; j = 1-6
$\overline{\omega}_i = \overline{\rho}\int_f \int_\eta (\omega_i(f,\eta,h)/\rho(f,\eta,h))\tilde{P}(f)\tilde{P}(\eta)d\eta df$	Joint convolution of chemical kinetics and turbulence fluctuations
$\omega_i = k_{ij} X_j X_k^b (\rho/M_{mix})$	Instantaneous reaction rate for fuel NO mechanism reactions i = 1-4, j and k = HCN, NH_3, NO, O_2, or OH

TABLE 2-13 (continued)

$\omega_5 = 2X_O\left[\dfrac{k_{1r}X_{N_2} - \left(\dfrac{k_{-1r}k_{-2r}X_{NO}^2}{k_{2r}X_{O_2}}\right)}{1+\left(\dfrac{k_{-1r}X_{NO}}{k_{2r}X_{O_2}+k_{3r}X_{OH}}\right)}\right]\left(\dfrac{P}{RT}\right)$	Instantaneous reaction options for thermal NO formation
or $\omega_5 = 2k_{A6}X_O X_{N_2}\left(\dfrac{P}{RT}\right)$	
$\omega_6 = \alpha_p n_p k_{1k} A_E \tilde{\rho}_{NO}$	Mean and instantaneous reaction of NO decay by char surface
$\tilde{\zeta}_{O_2} = \left(\dfrac{\tilde{X}_{O_2}^{eq} - \tilde{X}_{O_2}}{\tilde{X}_{O_2}^{eq} - \tilde{X}_{O_2}^{\min}}\right)$ $\tilde{\zeta}_{OH} = \left(\dfrac{\tilde{X}_{OH}^{eq} - \tilde{X}_{OH}}{\tilde{X}_{OH}^{eq} - \tilde{X}_{OH}^{\min}}\right)$	Mean fractional conversion progress variables
$\tilde{\zeta}_{N_2} = \left(\dfrac{\tilde{X}_{N_2}}{\tilde{X}_{N_2}^{eq}}\right)$ $\tilde{\zeta}_{NO}^{thermal} = \left(\dfrac{\tilde{X}_{NO}}{\tilde{X}_{NO}^{eq}}\right)$ $\tilde{\zeta}_{NO}^{fuel} = \left(\dfrac{\tilde{X}_{NO}}{\tilde{X}_{NO}^{f}}\right)$	
$\tilde{\zeta}_{HCN} = \left(\dfrac{\tilde{X}_{HCN}^{f} - \tilde{X}_{HCN}}{\tilde{X}_{HCN}^{f} - \tilde{X}_{HCN}^{\min}}\right)$ $\tilde{\zeta}_{NH_3} = \left(\dfrac{\tilde{X}_{NH_3}^{f} - \tilde{X}_{NH_3}}{\tilde{X}_{NH_3}^{f} - \tilde{X}_{NH_3}^{\min}}\right)$	
$\tilde{Y}_i = \tilde{Y}_i^{eq} - \tilde{Y}_{NO}\dfrac{M_i}{M_{NO}}$ $i = N_2, O_2$	Species mole fractions from atom balance
$\tilde{Y}_{OH} = \tilde{Y}_{OH}^{eq} - \left(\tilde{Y}_{HCN}^{f} - \tilde{Y}_{HCN}\right)\dfrac{M_{OH}}{M_{HCN}}$ *(when HCN is oxidized by OH)*	
$\tilde{X}_i = \tilde{Y}_i\dfrac{M_{wtx}}{M_i}$. i = *all mechanistic species*	Mean species mass fractions
$X_i = \tilde{X}_i^{eq}$ $i = CO_2, CO, H_2O,$ *and* H_2	Instantaneous species mass fractions

TABLE 2-13 (continued)

$X_{O_2} = X_{O_2}^{eq} - \left(X_{O_2}^{eq} - X_{O_2}^{\min}\right)\tilde{\zeta}_{O_2}$ $\qquad$ $X_{OH} = X_{OH}^{eq} - \left(X_{OH}^{eq} - X_{OH}^{\min}\right)\tilde{\zeta}_{OH}$ $X_{N_2} = \left(X_{N_2}^{eq}\right)\tilde{\zeta}_{N_2}$ $X_i = X_i^f - \left(X_i^f - X_i^{\min}\right)\tilde{\zeta}_i \qquad i = HCN, NH_3$ $X_{NO} = \left(X_{NO}^{eq}\right)\tilde{\zeta}_{NO}^{thermal}$ or $X_{NO} = \left(X_{NO}^f\right)\tilde{\zeta}_{NO}^{fuel}$ $X_i^{\min} = \max\left(0.0, X_i^{eq} - \left(\frac{X_{HCN}^f}{M_{HCN}} + \frac{X_{NH_3}^f}{M_{NH_3}} + \frac{X_{NO}^{eq}}{M_{NO}}\right)\frac{M_i}{2}\right) \qquad i = O_2, N_2$ $X_i^{\min} = \max\left(0.0, X_i^f - \left(X_{O_2}^{eq} 4 M_i / M_{O_2}\right)\right) \qquad i = HCN, NH_3$ [3] $X_{OH}^{\min} = \max\left(0.0, X_{OH}^{eq} - X_{HCN}^f \frac{M_{OH}}{M_{HCN}}\right)$ $X_{HCN}^f = \alpha_N (bcn)\eta \qquad X_{NH_3}^f = (1-\alpha_N)(bcn)\eta$ $X_{NO}^f = X_{HCN}^f + X_{NH_3}^f + \left(X_{NO}^{thermal}\right)$ [§] $X_O = \left[K_{eq} X_{O_2}\right]^{1/2}$ or $X_O = K_{eq}\frac{X_{O_2} X_{CO}}{X_{CO_2}}$	Quasi-equilibrium expressions for estimating radical oxygen concentrations

[3] A factor of 4 is used since every molecule of NO formed by oxidation of HCN or NH_3 can reduce another NH_3 or HCN molecule to N_2.

§ Term added to the maximum concentration of NO possible when joint fuel and thermal NO calculations are made.

Sulfur Pollutants and Sorbent Reactions Submodel

Background

Sulfur-containing pollutants formed by burning fossil fuels include SO_2, SO_3, H_2S, COS, and CS_2. Under normal boiler operating conditions, with excess

oxygen, virtually all of the sulfur is oxidized to SO_2 with small quantities of SO_3. Fuel-rich species (primarily H_2S) exist only in regions of the reactor where the coal particles are rapidly devolatilizing and oxygen is depleted. When coal is gasified under oxygen-deficient conditions, the principal sulfur-containing species is H_2S, with SO_2 also occurring locally in various regions of the gasifier.

Sulfur pollutants can be captured during the combustion process or in the flue gas ducts by injecting sorbents. Calcium-based sorbents are particularly attractive due to their low cost and the inertness of the calcium sulfate (in the case of SO_2 capture) or calcium sulfide (in the case of H_2S capture) by-product. The calcium sorbents first undergo calcination followed by particle sulfation. The reacted sorbents are typically collected with the fly ash by the bag house or electrostatic precipitator.

SO_x Pollutant Species

Local instantaneous equilibrium is assumed for the homogeneous chemistry; thus, the volatile sulfur is assumed to be locally equilibrated with the gas prior to capture by the sorbents. This information is provided by the chemical equilibrium subroutines of PCGC-2. The model does not currently allow for the conversion of SO_2 to H_2S or visa versa once it is formed or after one species is preferentially captured by the sorbents.

Sorbent Reactions Model

When hydrated lime [$Ca(OH)_2$] and limestone [calcium carbonate ($CaCO_3$)] sorbent particles are injected into the combustor and thermally heated, calcination occurs:

$$CaCO_3(s) \rightarrow CaO(s) + CO_2(g) \qquad (2\text{-}197)$$

$$Ca(OH)_2(s) \rightarrow CaO(s) + H_2O(g) \qquad (2\text{-}198)$$

Complete calcination of a $CaCO_3$ particle yields a particle of CaO with about 50 percent free pore volume. Once calcined material is produced, sulfur capture can

occur, provided the temperature is conducive for sulfation reactions. The following simplified reactions are generally accepted to occur:

$$CaO(s) + \frac{1}{2}O_2(g) + SO_2(g) \rightarrow CaSO_4(s) \qquad (2\text{-}199)$$

$$CaO(s) + H_2S(g) \rightarrow CaS(s) + H_2O(g) \qquad (2\text{-}200)$$

$$CaO(s) + SO_3(g) \rightarrow CaSO_4(s) \qquad (2\text{-}201)$$

Some simplifying assumptions which have made in the current sorbent reactions submodel include: 1) The sorbent particles are assumed to be instantaneously calcined to CaO; 2) The sorbent particles are isothermal and in thermal equilibrium with the local gas; and 3) Sulfation is considered irreversible.

A shrinking-core grain model developed and evaluated by Silcox et al. (1985, 1989) is used to predict the capture of SO_2 and H_2S. This model assumes that calcined sorbent particles consist of an agglomeration of small spherical grains of CaO. Sulfation occurs by the following sequence of physical and chemical events:

(1) diffusion of reactants from the bulk gas to the particle surface.
(2) pore diffusion of reactants to the particle internal (i.e., grain) surface.
(3) solid-state diffusion through the product layer (except at the onset of reaction).
(4) reaction of with CaO

Figure 2-8 gives a conceptual view of the shrinking-core grain model for a sorbent particle with a radius of R_p. The enlargement of an area of grains at an internal radius of R (or a subshell) illustrates the band of reaction product (e.g $CaSO_4$) with product radius of r_g', extended beyond the original grain radius, r_g, and the core radius, r, of the unreacted calcined material.

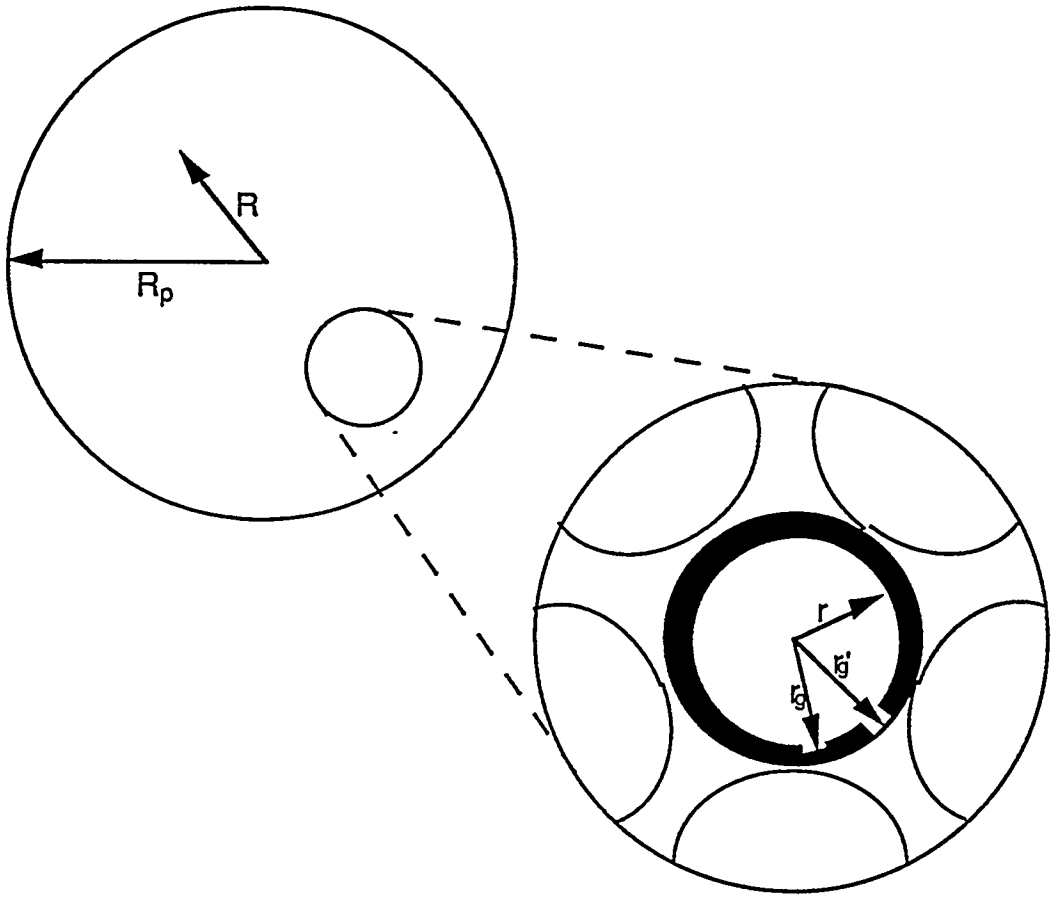

Figure 2-8. Conceptual view of the shrinking-core grain model. (Figure adapted with permission from Silcox (1985)

For sorbent particles which are spherical in shape, a material balance for the reacting gas in a concentric shell of the particle yields,

$$\frac{d^2C}{dR^2}+\left(\frac{2}{R}+\frac{1}{D_{eff}}\frac{dD_{eff}}{dR}\right)\frac{dC}{dR}-\frac{N}{D_{eff}}=0 \qquad (2\text{-}202)$$

where C is the SO_2 concentration, R is the radial coordinate of the sorbent, $\bar{D}_{eff}$ is the effective pore diffusivity, and N is the rate of reaction of SO_2 per unit volume of porous solid. The boundary conditions which satisfy this equation are,

$$R=R_p \qquad D_{eff}\frac{dC}{dR}=k_m(C_b-C) \qquad (2\text{-}203)$$

$$R=0 \qquad \frac{\partial C}{\partial R}=0 \qquad (2\text{-}204)$$

Here C_b is the bulk gas SO_2 concentration and k_m is a mass transfer coefficient which can be obtained from a suitable Sherwood number.

The reaction term, N, is given for reaction of order n, with respect to the sulfur-containing reactant, by,

$$N=\frac{C^n}{\dfrac{1}{k_f}+\dfrac{r^2}{D_{sp}}\left(\dfrac{1}{r}-\dfrac{1}{r_g}\right)}(A), \qquad mol\ cm^{-3}\ s^{-1} \qquad (2\text{-}205)$$

where k_f is the forward heterogeneous reaction expression, D_{sp} is the diffusion coefficient of SO_2 in the solid product layer, and A is the interfacial area available for reaction per unit volume. The reaction order, n, has been not been generalized in the current version. First and half-order reactions can be selected for SO_2 capture and only a first order reaction is allowable for H_2S capture. The first order reaction expressions have been tested and found to converge without difficulty.

The sulfation grain model is solved at discrete time steps as the particles progress through the combustor. Thus, the instantaneous sorbent particle conversion (sulfation) is dependent on the local gaseous properties (composition, temperature, etc.).

Working Equation

The Favre-averaged species continuity equation is used to calculate the Favre-mean mass fraction of the sulfur pollutants (SO_2 and H_2S) throughout the turbulent reactor.

$$\overline{W}_i = \bar{\rho}\tilde{u}\left(\frac{\partial \tilde{Y}_i}{\partial x}\right) + \bar{\rho}\tilde{v}\left(\frac{\partial \tilde{Y}_i}{\partial r}\right) - \left(\frac{\partial}{\partial x}\right)\left(\tilde{D}_Y \frac{\partial \tilde{Y}_i}{\partial x}\right) - \frac{1}{r}\left(\frac{\partial}{\partial r}\right)\left(r\tilde{D}_Y \frac{\partial \tilde{Y}_i}{\partial r}\right) \qquad (10)$$

$\overline{W}_i$ is the mean chemical reaction source or sink term for the species mass fraction, either SO_2 or H_2S, depending on the dominant species formed in the gas phase. The source term for each finite-difference cell is comprised of two contributions; 1) the sink due to sorbent capture by particles passing through the cell, and 2) the contribution of sulfur released to the cell by reacting coal particles within the cell.

Lagrangian trajectories for the reacting sorbent particles, analogous to the method of tracking coal particles, are calculated simultaneously with solution of the sorbent reaction grain model. The effects of the sorbent particles on the gas velocity and radiation fluxes are neglected. The particles are also assumed to follow the motion of the gas.

Chapter Three

Solution Technique

Approach

An information flow diagram for PCGC-2 is shown in Figure 3-1. The basic approach is to decouple the gas and particle equations using the particle source terms as "tear" variables. After initializing the flow field and geometric quantities, the gas variables are first solved for an assumed set of source terms. After converging the gas phase, the gas properties are updated, the Eulerian particle number density fields are calculated, and the radiation field is solved. The Lagrangian particle trajectories are then solved one at a time. New values of the source terms are calculated from particle mass, enthalpy, and velocity, when trajectories cross cell boundaries. Based on the previously guessed values of the source terms and the newly calculated values, an improved guess of the source terms is made, the gas phase reconverged, the particle trajectories recalculated, and so forth, until overall convergence of both phases is achieved. An option is also provided (INEACH = T) for solving the gas and particle phases simultaneously, in semi-coupled form, rather than in nested form as described above. The approaches for solving the gas and particle phases are discussed in more detail below.

Gas Phase

All of the gas phase equations are Eulerian, steady-state, second order, non-linear, elliptical partial differential equations. All of the gas phase equations are conveniently cast into one finite difference form, so that only one solution technique

is required. Table 2-1 contains a summary of this form for all of the gas phase equations.

The gas field is solved using a line-by-line technique; a tri-diagonal algorithm is used to solve the finite difference equations along a line using appropriate boundary conditions. PCGC-2 is coded to calculate the gas field line-by-line in either direction, or else in alternate directions. The tri-diagonal algorithm is solved iteratively for a specific variable until convergence is achieved. These iterations on a specific variable are termed "micro-iterations"; generally only three micro-iterations are necessary to obtain convergence for each variable. Each variable in Table 2-1 is solved in succession, starting with u and ending with h. A "macro-iteration" is completed after the complete set of variables has been calculated once (Steps 2 and 3 in Fig. 3-1) . Between 200 and 1000 macro-iterations are required to completely converge the gas phase (Steps 2-4 in Fig 3-1; this comprises one "gas-phase iteration").

The particles are accounted for only by appropriate particle source terms of mass $\left(S_p^m\right)$, momentum $\left(S_p^u \text{ and } S_p^v\right)$, and enthalpy $\left(S_p^h\right)$. These terms represent the addition of mass, momentum, and energy to the gas phase by the particles. The source terms are found along a particle trajectory by taking the difference in the particle properties on each side of a computational cell and dividing by the cell volume.

Roache (1976) presents a good review of techniques for solving fluid dynamics problems. The particular fluid flow problem solved by PCGC-2 consists of a recirculating fluid, and this type of problem has been heavily investigated by researchers at Imperial College. A method similar to the TEACH technique (Gosman and Pun, 1973) developed at Imperial College is used in PCGC-2 to solve the gas equations in the primitive variables. This technique is an iterative, steady-state, finite difference approach, and is widely used (Lockwood et al., 1980; Smith, 1979; Smoot and Pratt, 1979). Recently, finite element methods have been applied successfully to fluid flow problems (Gallagher et al., 1975). These methods have some strong advantages, particularly pertaining to arbitrary boundary shapes, but they are still in a developing stage and have not been applied extensively to compressible recirculating flows.

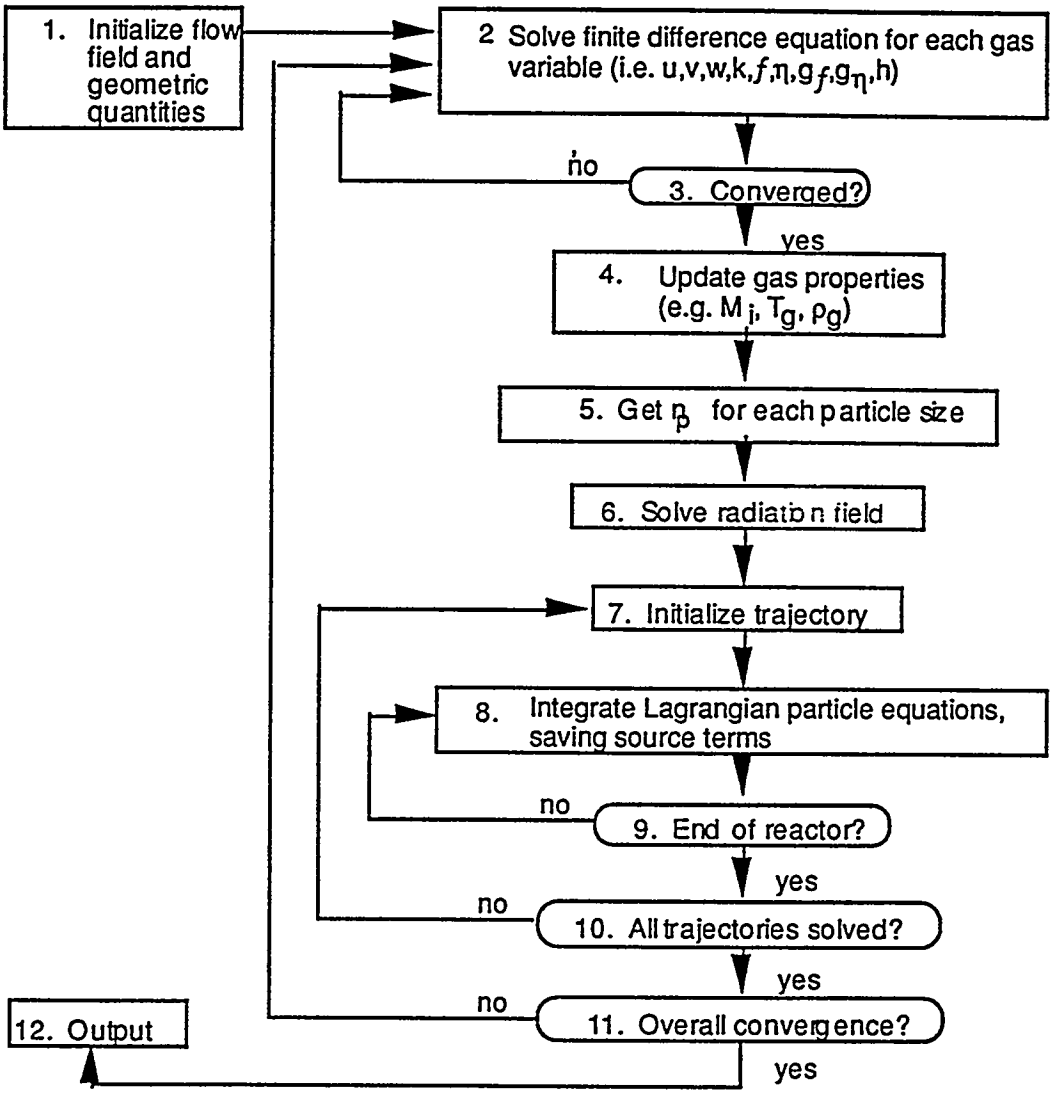

Fig. 3-1. Information flow diagram.

Each of the differential equations must be cast in finite difference form and solved over some appropriate grid spacing. A series of grid lines running orthogonally to the coordinate directions define at their intersection, node points, where the values of the dependent variables are usually identified. Roach (1976) has reviewed application of the flow equations to various possible mesh systems and show that in the (u, v, p) formulation, the variables u and v are most conveniently and accurately evaluated with node points lying on the boundary and with p and ρ being placed at one-half grid spacing off the boundary. This staggered-mesh system is shown in Fig. 3-2 as it is applied in PCGC-2. The grid spacing may be non-uniform, with grid points concentrated in areas of steep gradients. This spacing increases the convergence rate and accuracy of the computations. PCGC-2 locates all faces midway between node points. Arithmetic averaging is used to obtain property values at mesh boundaries between node points. Throughout PCGC-2, the distance between nodes is stored and used in the differencing scheme. Completely arbitrary grid spacing is thus permitted.

It is has already been mentioned that special difficulties arise in the primitive variable approach in that the momentum equations contain the pressure gradient terms, yet pressure does not explicitly appear in the continuity equation. Roach (1976) used the Los Alamos Marker and Cell (MAC) method for solving this problem. Patankar (1975, 1980) developed a semi-implicit method for pressure-linked equations (SIMPLE). PCGC-2 has been coded to include the SIMPLE algorithm and two of its variants (SIMPLER and SIMPLEC). A brief outline of the basic technique is presented here. More complete derivations may be found in the next section.

Figure 3-2 shows a typical computational cell. Attention is focused on the node point P and its nearest neighbors (N, S, E, W). The pressure, along with other variables, is calculated for these nodes. The velocity components associated with this node point are calculated at cell faces as shown. This staggered grid helps in writing the mass conservation equation for a cell since the velocities at the cell faces are needed in the convection terms. In addition, the difference of pressure between two adjacent nodes is used to derive the velocity component for the point midway between them.

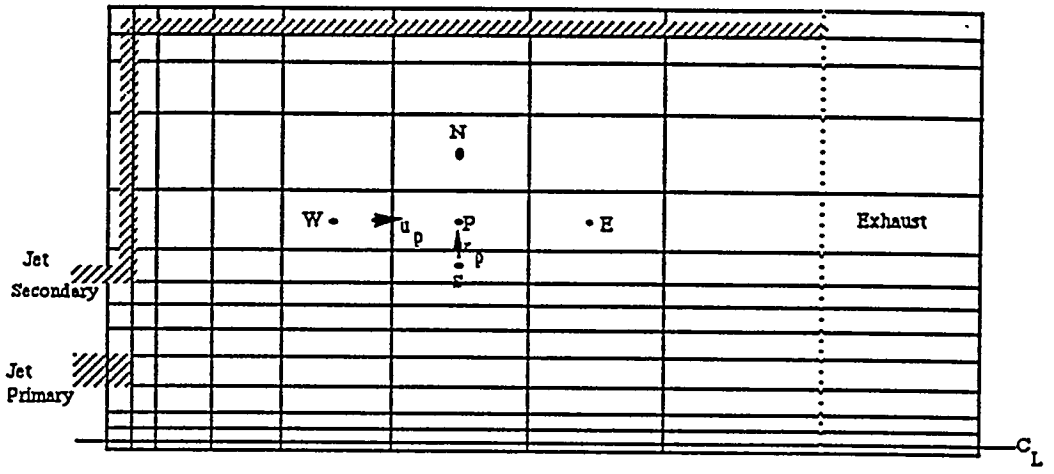

Figure 3-2. Sample grid pattern for PCGC-2.

When the momentum equations are cast in finite difference form (discussed in the next section) the unknown pressure terms will appear. At this point, the true pressure $\overline{p}$ is decomposed into a best estimate p^* and a pressure correction term $\overline{p}^c$.

$$\overline{p} = \overline{p}^* + \overline{p}^c \tag{3-1}$$

With the help of this decomposition of the true pressure and the two momentum difference equations, expressions may be found for two velocity components in terms of starred velocity components and pressure-correction variables $\left(\overline{p}^c\right)$. The continuity equation permits closure of the problem. By writing it in infinite difference form and substituting the velocity equation in terms of $\overline{p}^c$, a finite difference equation for the pressure correction is formed. In other words, the continuity equation is written in terms of the unknown pressure corrections in Eqn. 3-1.

The overall iterative solution procedure for the SIMPLE algorithm is:

1. Begin with the best available initial guess for all variables including pressure $(\bar{p}^*)$.
2. Calculate auxiliary variables such as density, temperature, etc., from the associated combustion mode.
3. Solve the momentum difference equations for the starred velocity field.
4. Solve the pressure correction form of the continuity equation for $\bar{p}^c$.
5. Calculate the pressure (from Eqn. 3-1) and corrected velocities.
6. Solve the difference equations for all other associated variables (i.e., k, ε, g_f, η, g_η, $\tilde{h}$).
7. With the new updated variables, return to Step 2 and continue iteration until convergence is achieved.

The overall iterative solution procedure for the SIMPLER algorithm is similar to the procedure for the SIMPLE algorithm (as shown above). The continuity equation is used in connection with the momentum equations to formulate an equation for pressure $(\bar{p})$ instead of the pressure correction $(\bar{p}^c)$. The iterative scheme is discussed later in the text. The SIMPLEC method (Van Doormaal and Raithby, 1984) corrects an inconsistency in the derivation of the pressure correction equation and results in faster convergence.

Particle Phase

The particle source-in-cell (PSI-CELL) technique of Crowe and coworkers (1977) has been followed directly to account for the Lagrangian particle field in the Eulerian gas field. The procedure is outlined below:

1. The Eulerian gas field is solved without particles using the above algorithm.
2. The radiation field is solved using the flux method.
3. The Lagrangian particle field is solved with a representative number of trajectories and the particle source term field is calculated.
4. The gas is solved with the updated particle source term field.
5. Step 2 is repeated and iteration continued until overall convergence is achieved.

The PSI-CELL technique is very efficient with respect to storage and computational time required. The only significant storage requirement is for the particle source term field. Steps 2 through 4 represent one "particle iteration" (Steps 7 through 11

in Fig. 3-1). Convergence is achieved when the gas phase does not change significantly between particle iterations.

Finite Difference Scheme

The majority of this section was taken originally from another source with the author's permission (Wormeck, 1976). Modifications to the original material were made as appropriate.

Introduction

This section presents the basic fluid flow solution procedure. This derivation brings to light various questions and possible alternative routes to take. The pressure is usually the variable giving the most trouble and can be eliminated by cross-differentiation of the momentum equations and introducing vorticity ξ as a dependent variable. The two velocity components are then removed by defining the stream function ψ. The resultant (ψ, ξ) system requires two equations to be solved for the unknown vorticity and stream function. If the flow is compressible, then the pressure must be recovered by the usual technique of integrating one of the momentum equations, after which the density can be updated by an equation of state.

The (ψ, ξ) system has been developed and published elsewhere (Gosman et al., 1969), but because of difficulties with boundary conditions, failure for many compressible flows, and not being readily extendible to three-dimensional flows, the method was abandoned in favor of a new algorithm (Gosman and Pun, 1973) which solves the flow equations in the primitive variables. The latter method is discussed in this section.

Differential Equations

The gas-phase equation set was presented in Chapter 2, illustrating that the equations can be cast into one standard form. The presentation in this section will focus on this general form and on deviations from this form for the momentum equations due to the staggered grid. The continuity and momentum equations are presented here in their customary form (Bird et al., 1960) with particle source terms:

$$MASS\ (continuity):\ \frac{\partial \rho}{\partial t} + \vec{\nabla} \bullet (\rho \vec{v}) = S_p^m \tag{3-2}$$

$$MOMENTUM:\ \rho \frac{D\vec{v}}{Dt} = -\vec{\nabla} p - \vec{\nabla} \bullet \vec{\vec{\tau}} + \rho \vec{g} + \vec{v}_{pg} S_p^m + S_p^{\vec{v}} \tag{3-3}$$

where D/Dt is the substantive derivative, and $\vec{\vec{\tau}}$ is the stress tensor. The S_p terms are the source terms due to the particle phase. After the complete derivation, an analysis will be performed to modify the finite-difference equations such that total mass is conserved.

Neglecting body forces, this system of equations can be expanded in terms of cylindrical coordinates for steady, axi-symmetric flows (Gosman et al., 1969):

$$CONTINUITY:\ \frac{\partial}{\partial x}(\rho u) + \frac{1}{r}\frac{\partial}{\partial r}(r \rho v) = S_p^m \tag{3-4}$$

U-MOMENTUM (direction x):

$$\begin{aligned} &\frac{\partial}{\partial x}(\rho u u) + \frac{1}{r}\frac{\partial}{\partial r}(r \rho u v) - \frac{\partial}{\partial x}\left(\mu \frac{\partial u}{\partial x}\right) - \frac{1}{r}\frac{\partial}{\partial r}\left(\mu r \frac{\partial u}{\partial r}\right) \\ &= -\frac{\partial p}{\partial x} + \frac{\partial}{\partial x}\left(\mu \frac{\partial u}{\partial x}\right) + \frac{1}{r}\frac{\partial}{\partial r}\left(\mu r \frac{\partial v}{\partial x}\right) - \frac{\partial}{\partial x}\left(\frac{2}{3}\mu\, div\, \vec{v}\right) + u_{pg} S_p^m + S_p^u \end{aligned} \tag{3-5}$$

V-MOMENTUM (direction r):

$$\begin{aligned} &\frac{\partial}{\partial x}(\rho u v) + \frac{1}{r}\frac{\partial}{\partial r}(r \rho v v) - \frac{\partial}{\partial x}\left(\mu \frac{\partial v}{\partial x}\right) - \frac{1}{r}\frac{\partial}{\partial r}\left(\mu r \frac{\partial v}{\partial r}\right) = \\ &-\frac{\partial p}{\partial r} + \frac{\partial}{\partial x}\left(\mu \frac{\partial u}{\partial r}\right) + \frac{1}{r}\frac{\partial}{\partial r}\left(\mu r \frac{\partial v}{\partial r}\right) - \frac{2\mu v}{r^2} - \frac{1}{r}\frac{\partial}{\partial r}\left(\frac{2}{3}\mu r\, div\, \vec{v}\right) \\ &+ \frac{2}{3}\frac{\mu\, div\, \vec{v}}{r} + \frac{\rho w w}{r} + v_{pg} S_p^m + r S_p^v \end{aligned} \tag{3-6}$$

W-MOMENTUM (tangential direction):

$$\frac{\partial}{\partial x}(\rho uw)+\frac{1}{r}\frac{\partial}{\partial r}(r\rho vw)-\frac{\partial}{\partial x}\mu\frac{\partial w}{\partial x}-\frac{1}{r}\frac{\partial}{\partial r}\left(r\mu\frac{\partial w}{\partial r}\right)=-\frac{\rho vw}{r}$$
$$-\frac{1}{r^2}\frac{\partial}{\partial r}r^3\mu\frac{\partial w}{\partial r}+W_{pg}S_p^m+S_p^w \qquad (3\text{-}7)$$

All of the above equations can be cast into a standard form:

$$div\,(\rho\vec{v}\phi)-div\,(\Gamma\,grad\,\phi)=S \qquad (3\text{-}8)$$

where ϕ is taken as the dependent variable, Γ as the exchange coefficient relating the force with the flux in the transport law for ϕ, and S as the source term that includes all terms not contained in the first two terms. The first term is generally referred to as the convection term while the second term is the diffusion term. Writing Eqn. 3-8 in cylindrical two-dimensional coordinates,

$$\frac{1}{r}\left[\frac{\partial}{\partial x}(r\rho u\phi)+\frac{\partial}{\partial r}(r\rho v\phi)\right]-\frac{1}{r}\left[\frac{\partial}{\partial x}\left(r\Gamma\frac{\partial\phi}{\partial x}\right)+\frac{\partial}{\partial r}\left(r\Gamma\frac{\partial\phi}{\partial r}\right)\right]=S \qquad (3\text{-}9)$$

The corresponding terms in Eqns. 3-4 to 3-7 are easily identified.

Note that the diffusion terms are simply the divergence of a gradient and that any other form of a transport law must be contained in the source term. In particular, the $(\partial/\partial r)[2\mu r(\partial v/\partial r)]$ term in the second momentum equation has been split, with half of it becoming the second diffusion term in Eqn. 3-6 while the remainder becomes the third source term on the right. This is required for success of the method; the reasoning will follow once the two modifications for correcting mass conservation are developed below.

Therefore our equation system becomes

CONTINUITY *($\phi = 1$)*:

$$\frac{\partial}{\partial x}(\rho u)+\frac{1}{r}\frac{\partial}{\partial r}(r\rho v)=S_p^m \qquad (3\text{-}10)$$

U-MOMENTUM ($\phi = u$):

$$\frac{\partial}{\partial x}(\rho uu)+\frac{1}{r}\frac{\partial}{\partial r}(r\rho uv)-\frac{\partial}{\partial x}\left(\mu\frac{\partial u}{\partial x}\right)-\frac{1}{r}\frac{\partial}{\partial r}\left(r\mu\frac{\partial u}{\partial r}\right)=-\frac{\partial p}{\partial x}+S^u \tag{3-11}$$

V-MOMENTUM ($\phi = v$):

$$\frac{\partial}{\partial x}(\rho uv)+\frac{1}{r}\frac{\partial}{\partial r}(r\rho vv)-\frac{\partial}{\partial x}\left(\mu\frac{\partial v}{\partial x}\right)-\frac{1}{r}\frac{\partial}{\partial r}\left(r\mu\frac{\partial v}{\partial r}\right)=-\frac{\partial p}{\partial r}+S^v \tag{3-12}$$

W-MOMENTUM ($\phi = w$):

$$\frac{\partial}{\partial x}(\rho uw)+\frac{1}{r}\frac{\partial}{\partial r}(r\rho vw)-\frac{\partial}{\partial x}\left(\mu\frac{\partial w}{\partial x}\right)-\frac{1}{r}\frac{\partial}{\partial r}\left(r\mu\frac{\partial w}{\partial r}\right)=S^w \tag{3-13}$$

where the three source terms are given by:

$$S^u=\frac{\partial}{\partial x}\left(\mu\frac{\partial u}{\partial x}\right)+\frac{1}{r}\frac{\partial}{\partial r}\left(r\mu\frac{\partial v}{\partial x}\right)-\frac{\partial}{\partial x}\left(\frac{2}{3}\mu\, div\,\vec{v}\right)+u_{pg}S_p^m+rS_p^u \tag{3-14}$$

$$S^v=\frac{\partial}{\partial x}\left(\mu\frac{\partial u}{\partial r}\right)+\frac{1}{r}\frac{\partial}{\partial r}\left(r\mu\frac{\partial v}{\partial r}\right)-\frac{2\mu v}{r^2}-\frac{1}{r}\frac{\partial}{\partial r}\left(\frac{2}{3}r\mu\, div\,\vec{v}\right)+\frac{2}{3}\frac{\mu\, div\,\vec{v}}{r}+\frac{\rho ww}{r}+v_{pg}S_p^m+S_p^v \tag{3-15}$$

$$S^w=-\frac{\rho vw}{r}-\frac{1}{r^2}\frac{\partial}{\partial r}r^3\mu\frac{\partial w}{\partial r}+w_{pg}S_p^m+S_p^w \tag{3-16}$$

The $div\ \vec{v}$ term is always dropped in the TEACH program. The effect of particle mass source terms on tangential momentum is ignored in this version of the code.

Finite-Difference Equations

There are at least four methods of deriving finite-difference equations from the differential equations. These include Taylor series expansions, polynomial fitting, integral methods, and the control volume approach. The approach taken here is to use the integral technique (Gosman et al., 1969).

Grid. Before integrating the standard equations over the flow domain, a satisfactory grid is required. The boundaries of the flow domain are made to coincide with one of the constant coordinate directions, with only the Cartesian and cylindrical geometries considered.

A series of grid lines orthogonal to the coordinate directions define (at their intersections) node points where the values of the dependent variables will usually be identified. TEACH incorporates non-uniform spacing between these grid points to obtain higher resolution (and therefore accuracy) in regions where the flow gradients are expected to be severe, but does not utilize the more numerically accurate coordinate-stretching transformations, e.g. exponential stretch.

The choice of mesh system depends on whether the node points are to lie on the flow boundary or one-half grid spacing away from it. Roache (1976) derives and compares all of the flow equations in these various mesh systems and shows that in the (u, v, p) formulation, the variable u and v are most conveniently and accurately evaluated in the mesh system with node points laying on the boundary, while p and ρ are most conveniently and accurately evaluated when node values are one-half grid spacing off the walls. The use of a hybrid- or staggered-mesh system thus suggests itself.

A staggered grid is used as shown in Fig. 3-3, where a boomerang-shaped structure has been drawn to emphasize the field positions of the dependent variables u, v, p, and ϕ (a general variable) that correspond to FORTRAN indices I and J.

It should be noted that the flow domain is a continuous field which has been discretized by a mesh to perform a numerical analysis. All dependent variables and fluid properties are stored in two-dimensional FORTRAN arrays and all grid coordinates and distances are stored in one-dimensional arrays. Referencing a variable requires consideration of the field location specified by subscripts and its representation in the computer code.

The various computational cells are centered at the point of definition of the variable of interest and extend halfway to the four adjacent (in two-dimensional) neighboring node points. Thus we speak of the p-cell (main cell), u-cell and v-cell. The practice in TEACH is to name the node point of interest as P and the neighboring nodes as the four points of a compass.

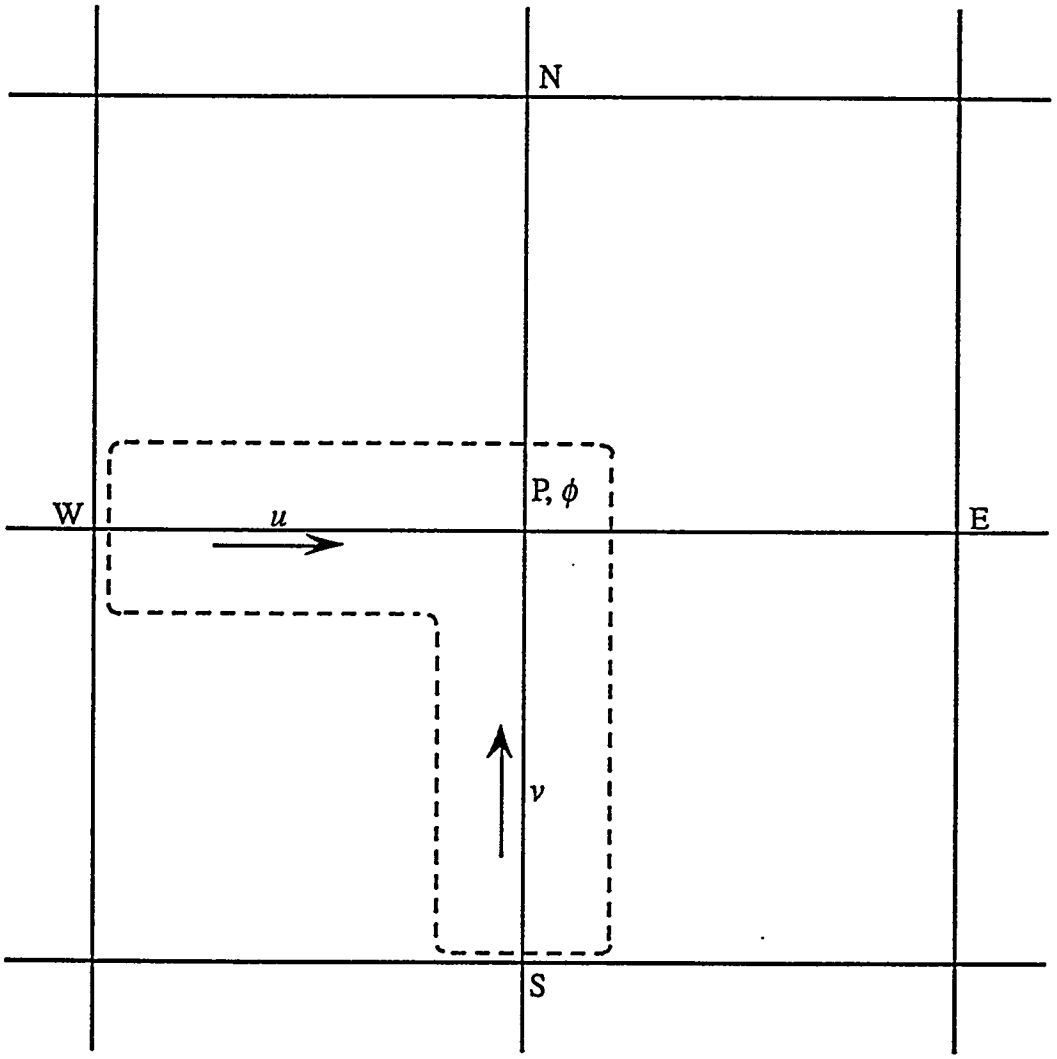

Fig. 3-3. The boomerang-shaped structure enclosing the points of definition of u, v, p, and ϕ corresponding to FORTRAN index I, J.

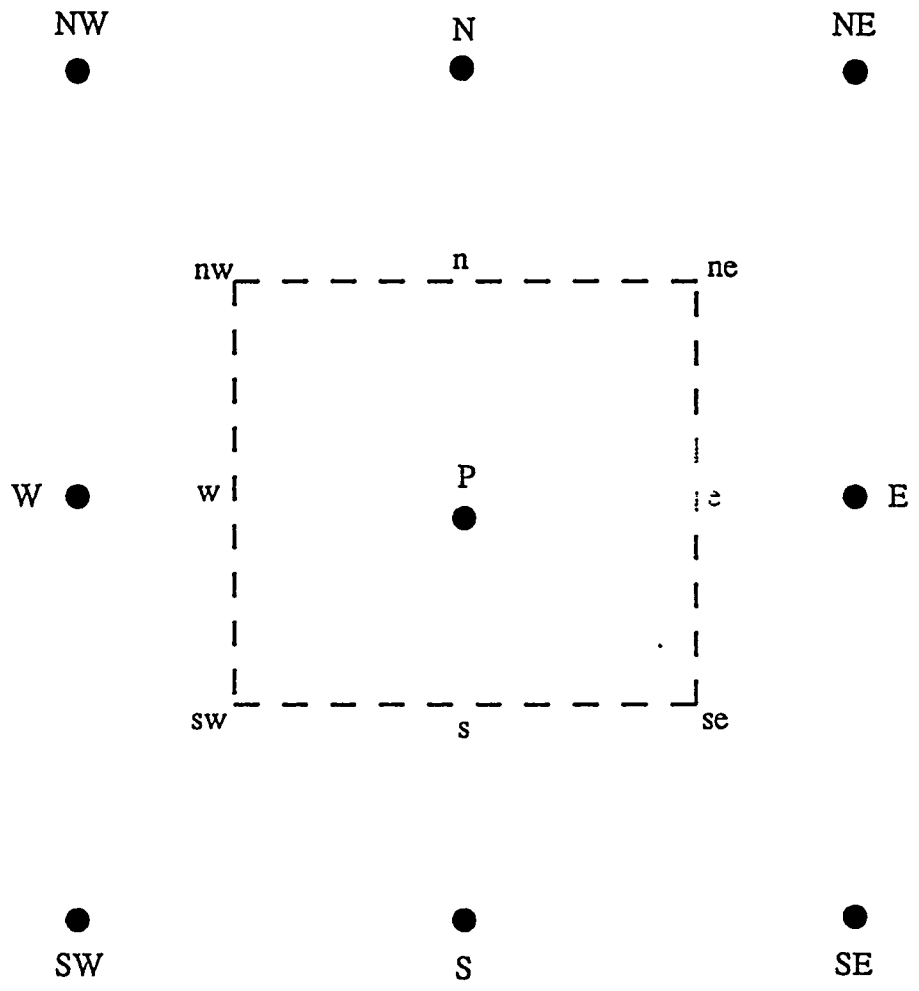

Fig. 3-4. Illustration of the grid symbols for a computational cell.

The mathematical description is illustrated in Fig. 3-4, where the absence of a subscript on these compass points signifies the main cell and addition of u or v superscripts implies the u- or v-cell respectively. Figs. 3-5, 3-6, and 3-7 illustrate

the FORTRAN description of these three computational cells. Note how the velocity cells "overlap" the grid lines when the grid spacing is non-uniform.

Three computational cells are associated with each node point. The node points are specified by the FORTRAN indices I and J. The main cell center is denoted by subscript p and is located at (x_p, r_p) [FORTRAN symbols X(I) and R(J)]. The u-cell center has the same radial location as the p-cell and is referenced automatically by subscript p and superscript u. It is located at x_p^u, r_p in the mathematical developments and in FORTRAN by coordinates [XU(I), R(J)]. With the v-cell, the center has the same x location as the main cell, but the radial coordinate is r_p^v [RV(J)]. Thus Fig. 3-5 is a template which, when centered on grid location X(I), R(J), references the main cell (no superscripts). Adding a superscript u to the symbols will describe the field if node P is moved to the center of the u-cell at coordinates XU(I), R(J). Similarly, the v-cell notation is shown by moving Fig. 3-5 to the center of the v-cell [X(I), RV(J)] and addition of the v superscript to all variables.

A location can be referenced in several ways; for example, consider the center of the west face of the main cell. A variable ϕ is referenced there mathematically by either ϕ_w or ϕ_p and approximately (exactly in a uniform grid) by ϕ_{nw}^v. In the derivation of the finite-difference equations which will follow, these different notations will be utilized to reference the same position. When writing the computer code, the best available FORTRAN variables are employed.

Use of the staggered grid also has the convenient feature that velocity is defined at the locations where it is needed in the convective terms. Pressure is defined so as to make it easy to compute the pressure gradients in the two momentum equations.

Integration of the Standard Equation

The standard equation (Eqn. 3-9) will be developed first, followed by the momentum equations and the equation for pressure.

General Finite-Difference Equation (ϕ-Equation). Fig. 3-8 displays a typical internal main cell where the ϕ-equation (Eqn. 3-9) can be integrated over the volume obtained by rotating the area, represented by the dotted lines, about the symmetry axis to give:

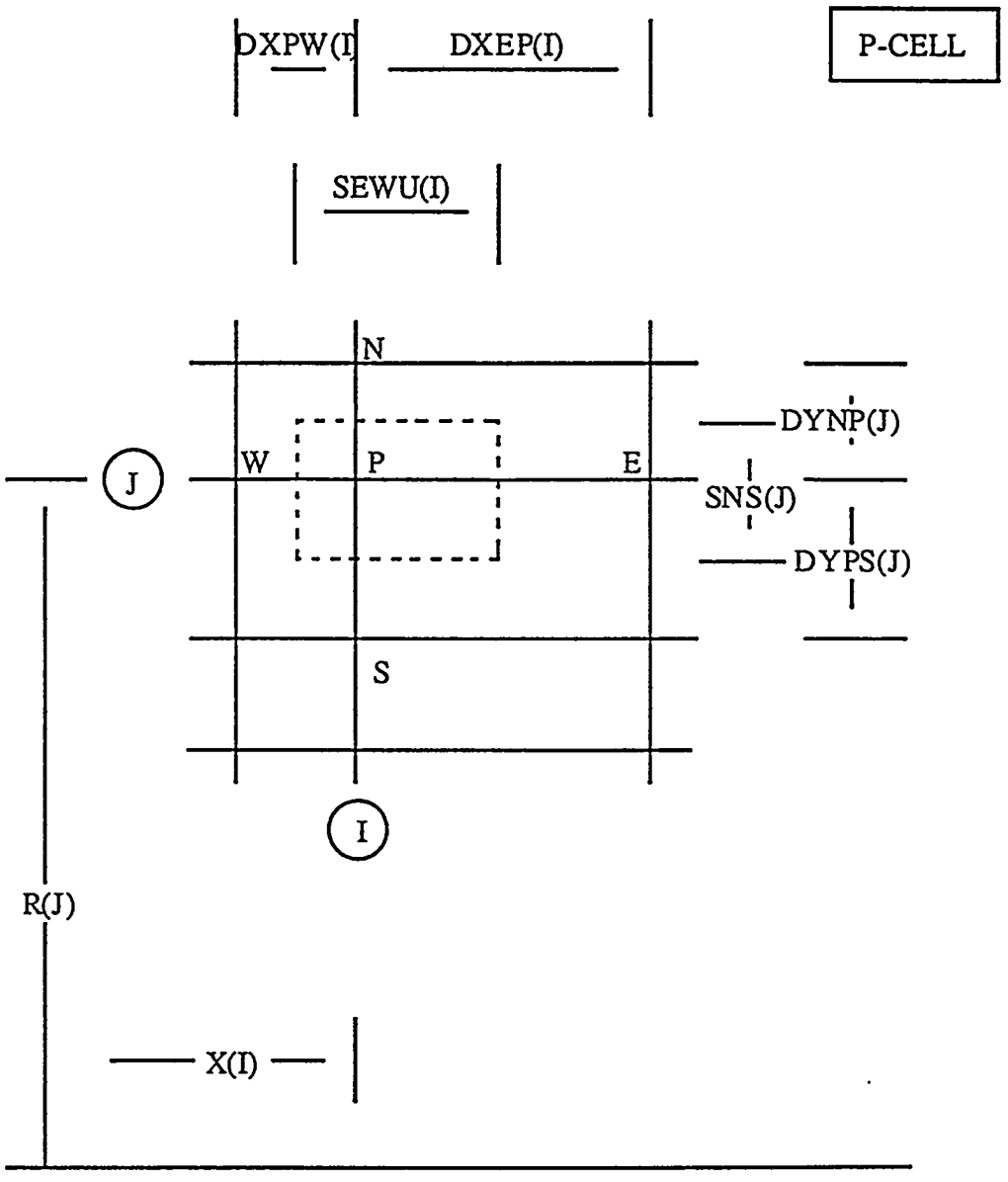

Fig. 3-5. FORTRAN symbols for p-cell.

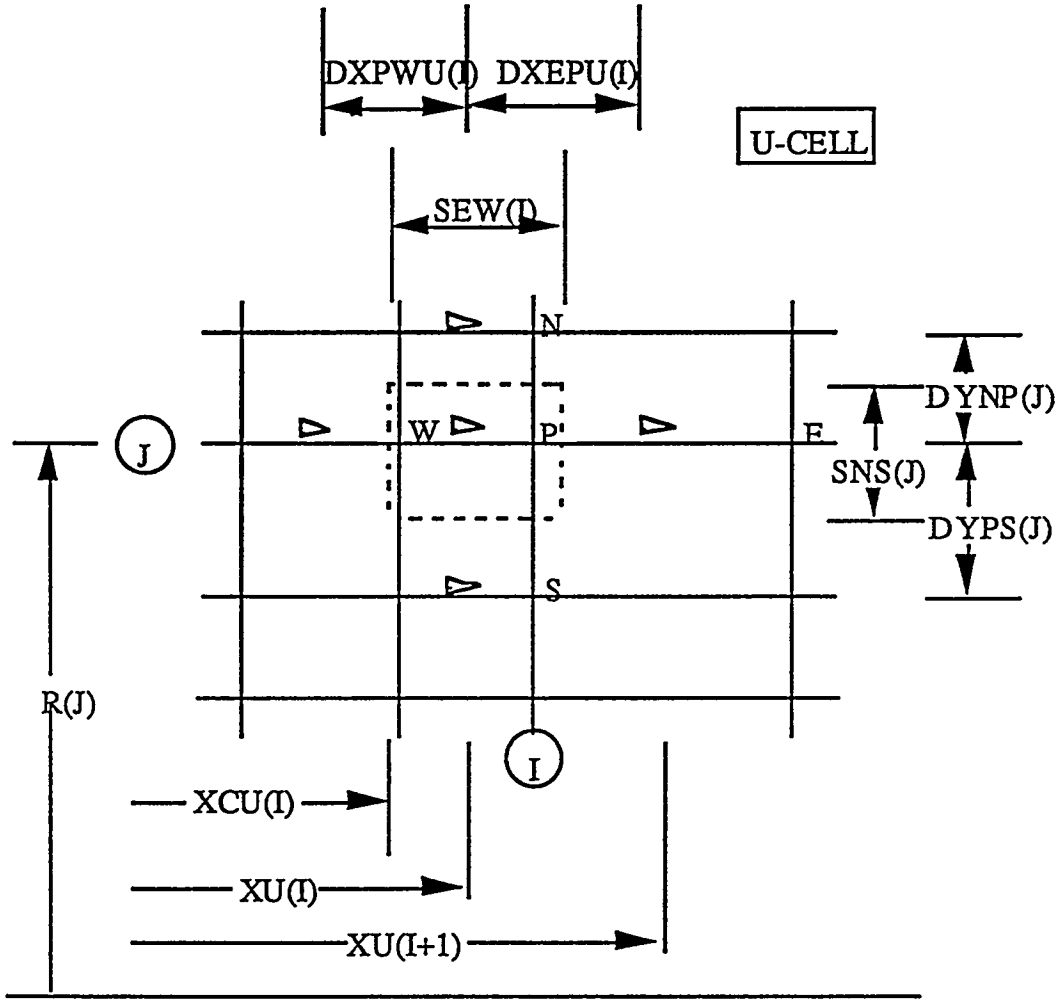

Fig. 3-6. FORTRAN symbols for *u*-cell.

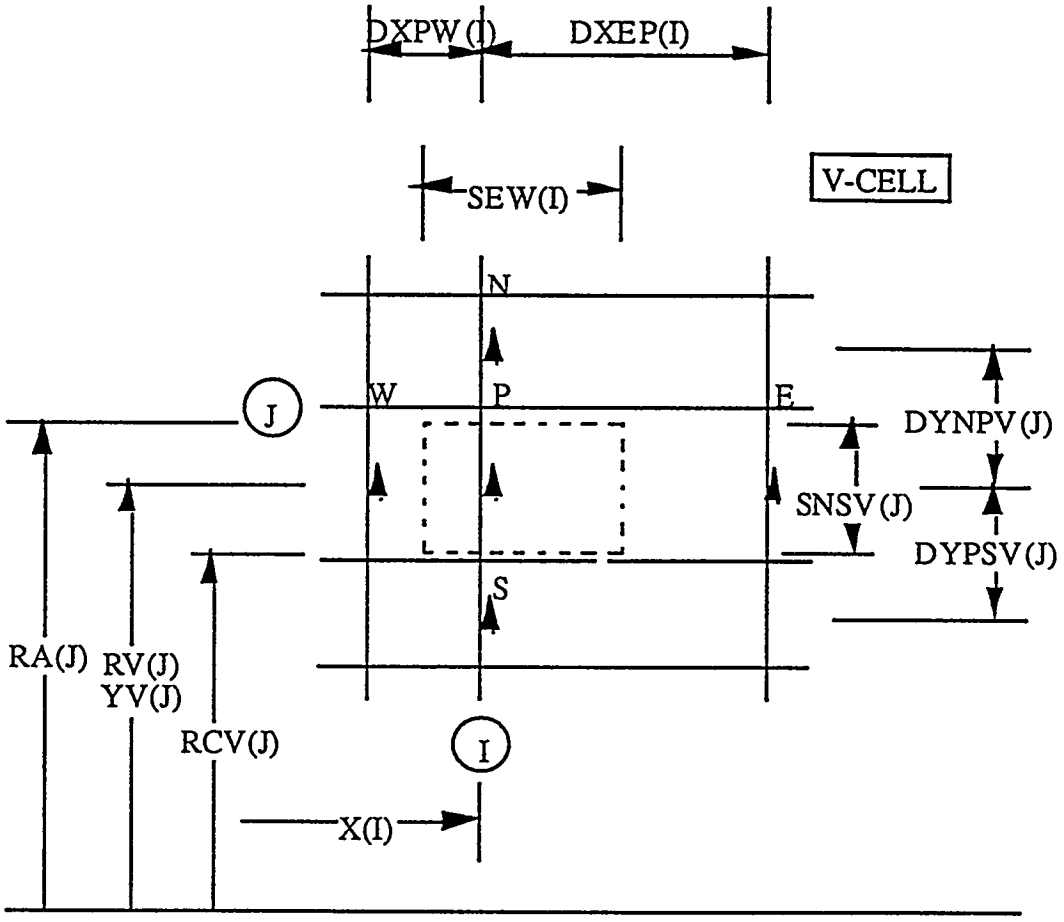

Fig. 3-7. FORTRAN symbols for *v*-cell.

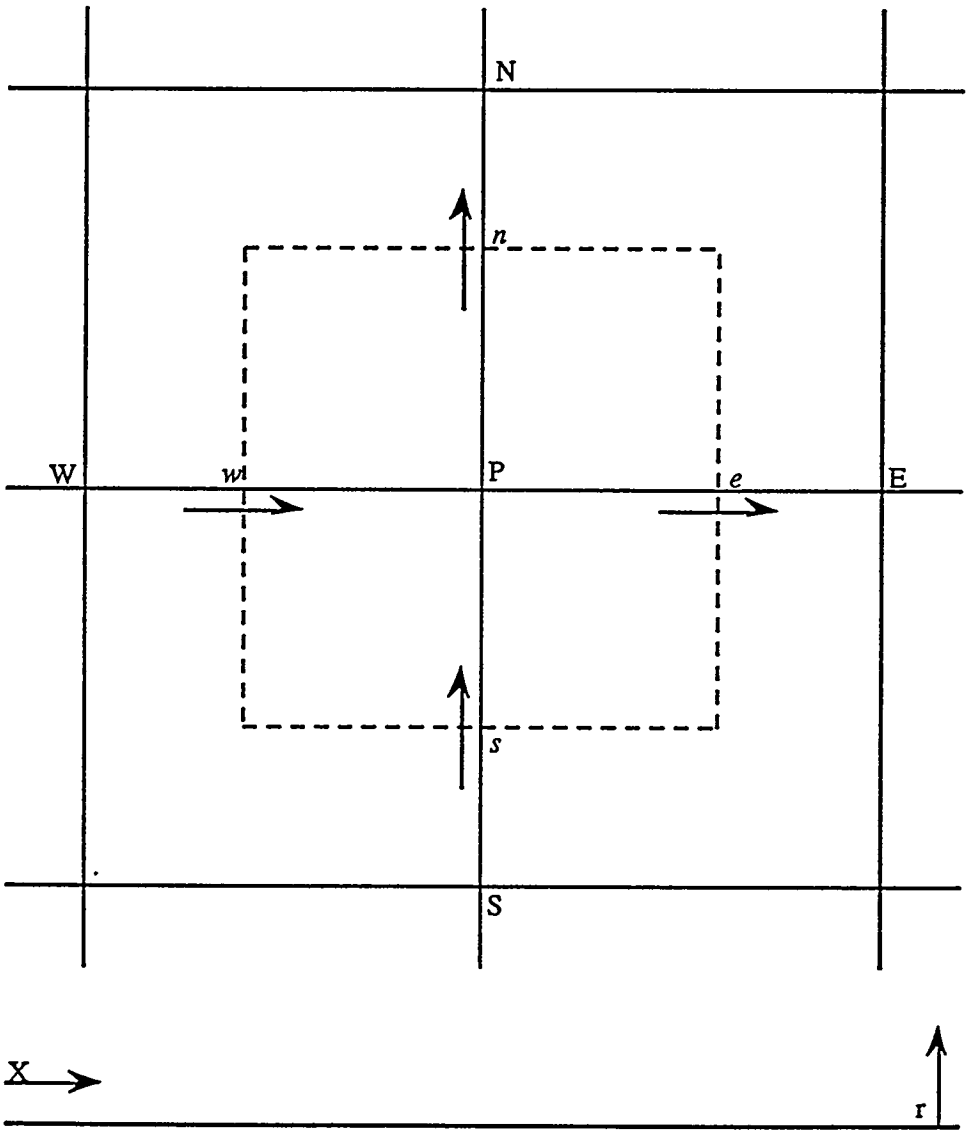

Fig. 3-8. Illustration of the main cell finite-difference grid showing the node point labeling.

$$\int_{x_w}^{x_e}\int_{r_s}^{r_n}\int_{0}^{1}\left[\frac{\partial}{\partial x}(\rho ur\phi)+\frac{\partial}{\partial r}(\rho vr\phi)-\frac{\partial}{\partial x}\left(r\Gamma\frac{\partial\phi}{\partial x}\right)-\frac{\partial}{\partial r}\left(r\Gamma\frac{\partial\phi}{\partial r}\right)-rS^{\phi}\right]dxdrd\xi_3=0$$

(3-17)

where the third coordinate, ξ_3, has the integration limits of 0 and 1 radians for convenience instead of 0 to 2π radians, because of assumed axial symmetry (i.e. the final overall equation is divided by 2π).

Considering the first convection term in Eqn. 3-17

$$\int_{x_w}^{x_e}\int_{r_s}^{r_n}\int_{0}^{1}\frac{\partial}{\partial x}(\rho ur\phi)dxdrd\xi_3 \tag{3-18}$$

and noting that all properties are uniform in the third direction, we can perform two exact integrations, giving

$$\int_{r_s}^{r_n}[\rho ur\phi]_w^e dr \tag{3-19}$$

where *e* and *w* indicate that the expression is to be evaluated at the east and west faces, respectively. The derivation to this point is exact. Factoring *r* from the integrand and applying the mean-value theorem

$$\int_{r_s}^{r_n}[\rho ur\phi]_w^e dr=\int_{r_s}^{r_n}[\rho u\phi]_w^e rdr=\int_{r_s}^{r_n}\{[\rho u\phi]_e-[\rho u\phi]_w\}rdr \tag{3-20}$$

$$\equiv\{[\overline{\rho u\phi}]_e-[\overline{\rho u\phi}]_w\}\frac{r_n^2-r_s^2}{2} \tag{3-21}$$

where the subscript stands for evaluation at that particular face. The right-hand side of Eqn. 3-21 may be rewritten as

$$\left\{\left[\overline{\rho u \phi}\right]_e - \left[\overline{\rho u \phi}\right]_w\right\} A_{ew} \tag{3-22}$$

where A_{ew}, the area of the east or west face of the cell, is given by

$$A_{ew} = \int_{r_s}^{r_n}\int_{0}^{1} r\, dr\, d\xi_3 = \frac{1}{2}\left(r_n^2 - r_s^2\right) \tag{3-23}$$

or

$$A_{ew} = \frac{1}{2}(r_n - r_s)(r_n + r_s) = r_{ap}(r_n - r_s) \tag{3-24}$$

where

$$r_{ap} = \frac{r_n + r_s}{2} \tag{3-25}$$

For arbitrary grid spacing, r_{ap} is not the same as r_p. Thus r_{ap} is stored throughout the entire calculational domain.

In the staggered grid system, the u velocities are defined at the cell boundaries where they are required ($u_e = u_E$, $u_w = u_p$) and the first convection term now becomes

$$\rho_e \phi_e u_E A_{ew} - \rho_w \phi_w u_p A_{ew} \tag{3-26}$$

We can define convection coefficients as

$$C_E = \rho_e u_E A_{ew} \tag{3-27}$$

$$C_W = \rho_w u_p A_{ew} \tag{3-28}$$

which gives the mass flowrate through the face corresponding to the subscript.

Both ρ and ϕ are defined at the main grid nodes and some sort of interpolation is needed to determine their values at the faces midway between node

points. The practice typically employed is to linearly interpolate dependent variables and use simple averaging for fluid properties. Thus,

$$\rho_e = \frac{1}{2}(\rho_p + \rho_E),\ \rho_w = \frac{1}{2}(\rho_w + \rho_p) \tag{3-29}$$

and

$$x_P < x_\phi < x_E \quad \phi_e = (1 - f_E)\phi_P + f_E\phi_E,\ \ f_E = \frac{x - x_P}{x_E - x_P} \tag{3-30}$$

$$x_W < x_\phi < x_P \quad \phi_w = (1 - f_W)\phi_W + f_W\phi_P,\ \ f_W = \frac{x - x_W}{x_P - x_W} \tag{3-31}$$

$$r_P < r_\phi < r_N \quad \phi_n = (1 - f_N)\phi_P + f_N\phi_N,\ \ f_N = \frac{r - r_P}{r_N - r_P} \tag{3-32}$$

$$r_S < r_\phi < r_P \quad \phi_s = (1 - f_S)\phi_S + f_S\phi_P,\ \ f_S = \frac{r - r_S}{r_P - r_S} \tag{3-33}$$

Since PCGC-2 always employs cell faces halfway between node points, this interpolation is identical to simple averaging, even for non-uniform grid spacing, since the *f*'s are always equal to 0.5. Using these relationships, with all *f*'s set equal to 0.5, the convection coefficients become

$$C_E = \frac{1}{2}(\rho_P + \rho_E)u_E A_{ew} \tag{3-34}$$

$$C_W = \frac{1}{2}(\rho_P + \rho_w)u_P A_{ew} \tag{3-35}$$

The first convection term in the *f*-equation (Eqn. 3-17) then becomes (upon substitution)

$$C_E f_E \phi_E - C_W (1 - f_W)\phi_W + \left[C_E (1 - f_E) - C_W f_W\right]\phi_P \tag{3-36}$$

Similarly, the second convection term in Eqn. 3-17 is

$$\int_{x_w}^{x_e}\int_{r_s}^{r_n}\int_0^1 \frac{\partial}{\partial r}(\rho v r \phi)\, dx\, dr\, d\xi_3 \tag{3-37}$$

Again, two exact integrations can be performed to give

$$\int_{x_w}^{x_e} [\rho v r \phi]_s^n\, dx \tag{3-38}$$

From the mean-value theorem this term becomes

$$\left\{[\rho v \phi]_n r_n - [\rho v \phi]_s r_s\right\}(x_e - x_w) \tag{3-39}$$

In terms of the geometric quantities

$$A_n = r_n (x_e - x_w) \tag{3-40}$$

$$A_s = r_s (x_e - x_w) \tag{3-41}$$

the convection coefficients are defined as:

$$C_N = \rho_n v_n A_n = \frac{1}{2}(\rho_N + \rho_P) v_N A_n \tag{3-42}$$

$$C_S = \rho_s v_s A_s = \frac{1}{2}(\rho_S + \rho_P) v_P A_s \tag{3-43}$$

The final form of the second convection term of the ϕ-equation becomes:

$$C_N f_N \phi_N - C_S(1-f_S)\phi_S + \left[C_N(1-f_N) - C_S f_S\right]\phi_P \tag{3-44}$$

Considering the diffusion terms in Eqn. 3-17 separately, we have:

$$\int_{x_w}^{x_e}\int_{r_s}^{r_n}\int_{0}^{1}\left[-\frac{\partial}{\partial x}\left(r\Gamma\frac{\partial\phi}{\partial x}\right)-\frac{\partial}{\partial r}\left(r\Gamma\frac{\partial\phi}{\partial r}\right)\right]dx\,dr\,d\xi_3 \tag{3-45}$$

and integrating twice gives:

$$-\int_{r_s}^{r_n}\left[r\Gamma\frac{\partial\phi}{\partial x}\right]_w^e dr - \int_{x_w}^{x_e}\left[r\Gamma\frac{\partial\phi}{\partial r}\right]_s^n dx \tag{3-46}$$

Using the same technique as presented for convection terms, these last integrals can be evaluated as:

$$-\Gamma_e\left(\frac{\partial\phi}{\partial x}\right)_e r_{ap}(r_n - r_s) + \Gamma_w\left(\frac{\partial\phi}{\partial x}\right)_w r_{ap}(r_n - r_s) \tag{3-47}$$

$$-\Gamma_n\left(\frac{\partial\phi}{\partial r}\right)_n r_n(x_e - x_w) + \Gamma_s\left(\frac{\partial\phi}{\partial r}\right)_s r_s(x_e - x_w) \tag{3-48}$$

As expected, the same geometric quantities appear as in the convection terms; substituting Eqns. 3-26, 3-40, and 3-41 yields:

$$-\Gamma_e\left(\frac{\partial\phi}{\partial x}\right)_e A_{ew} + \Gamma_w\left(\frac{\partial\phi}{\partial x}\right)_w A_{ew} - \Gamma_n\left(\frac{\partial\phi}{\partial r}\right)_n A_n + \Gamma_s\left(\frac{\partial\phi}{\partial r}\right)_s A_s \tag{3-49}$$

The derivatives at the four faces must be expressed in terms of variables at the main node points. Employing central differences (which are second-order accurate) (Dave, 1968) gives:

$$-\Gamma_e\left(\frac{\phi_E-\phi_P}{\delta x_{PE}}\right)A_{ew}+\Gamma_w\left(\frac{\phi_P-\phi_W}{\delta x_{PW}}\right)A_{ew}$$
$$-\Gamma_n\left(\frac{\phi_N-\phi_P}{\delta y_{NP}}\right)A_n+\Gamma_s\left(\frac{\phi_P-\phi_S}{\delta y_{PS}}\right)A_s \qquad (3\text{-}50)$$

Where the δx and δy stand for coordinate distance between the node points indicated by their corresponding subscripts.

Diffusion coefficients can be defined and calculated as:

$$D_E=\Gamma_e\frac{A_{ew}}{\delta x_{PE}}=\left(\frac{\Gamma_P+\Gamma_E}{2}\right)\left(\frac{A_{ew}}{\delta x_{PW}}\right) \qquad (3\text{-}51)$$

$$D_W=\Gamma_w\frac{A_{ew}}{\delta x_{PW}}=\left(\frac{\Gamma_P+\Gamma_W}{2}\right)\left(\frac{A_{ew}}{\delta x_{PW}}\right) \qquad (3\text{-}52)$$

$$D_N=\Gamma_n\frac{A_n}{\delta y_{NP}}=\left(\frac{\Gamma_P+\Gamma_N}{2}\right)\left(\frac{A_n}{\delta y_{NP}}\right) \qquad (3\text{-}53)$$

$$D_S=\Gamma_s\frac{A_s}{\delta y_{PS}}=\left(\frac{\Gamma_P+\Gamma_S}{2}\right)\left(\frac{A_s}{\delta y_{PS}}\right) \qquad (3\text{-}54)$$

Thus the diffusion terms can be expressed as

$$-D_E(\phi_E-\phi_P)+D_W(\phi_P-\phi_W)-D_N(\phi_N-\phi_P)+D_S(\phi_P-\phi_S) \qquad (3\text{-}55)$$

Note the similarity with a control-volume formulation: the exchange coefficients and geometric quantities are contained in the diffusion coefficients D, while the

difference in ϕ, which drives the diffusion, is explicitly shown with the correct sign (ϕ enters the cell when the ϕ-difference is negative).

Finally, we are left with the source terms in Eqn. 3-17,

$$\int_{x_w}^{x_e}\int_{r_s}^{r_n}\int_{0}^{1} r\, S^{\phi}\, dx\, dr\, d\xi_3 \tag{3-56}$$

One of the major reasons for the success of the TEACH formulation is the linearization of this source term. Thus

$$\int_{x_w}^{x_e}\int_{r_s}^{r_n}\int_{0}^{1} r\, S^{\phi}\, dx\, dr\, d\xi_3 = S_U^{\phi} + S_P^{\phi}\, \phi_P \tag{3-57}$$

which defines two source term coefficients, S_U^{ϕ} and S_P^{ϕ}. If the source term happens to be nonlinear in terms of the dependent variable, ϕ_P, the technique calls for ϕ_P to be factored from the expression (if possible) and to appear with the S_P^{ϕ} coefficient in Eqn. 3-57. Thus, ϕ_P appears implicitly while the remaining factored expression involving ϕ_P will be considered as known (explicit, based on previous values) and lumped together in the S_U^{ϕ} coefficient of Eqn. 3-57. Furthermore, as shown later in this chapter, S_P^{ϕ} must be negative to guarantee stable convergence.

In general, S^{ϕ} will be a function of all the dependent variables and other fluid properties as well as various types of derivatives involving these quantities. When integrating this source term, the value prevailing at the cell center will be used for all quantities. Any derivatives will be evaluated by central differencing. Therefore, the source term is considered constant, and:

$$\int_{x_w}^{x_e}\int_{r_s}^{r_n}\int_{0}^{1} r\, S^{\phi}\, dx\, dr\, d\xi_3 = S^{\phi}(\Delta V) = S_U^{\phi} + S_P^{\phi}\, \phi P \tag{3-58}$$

where ΔV is the volume of the cell.

Upon substitution of these newly defined coefficients, the general ϕ-equation becomes

$$[C_E f_E - D_E]\phi_E - [C_W(1-f_W) + D_W]\phi_W + [C_N f_N - D_N]\phi_N - [C_S(1-f_S) + D_S]\phi_S$$
$$+[C_E(1-f_E) + D_E - C_W f_W + D_W + C_N(1-f_N) + D_N - C_S f_S + D_S]\phi_P = S_U + S_P\phi_P$$

(3-59)

Adding and subtracting C_E - C_W + C_N - C_S from the bracket preceding ϕ_P and rearranging to obtain common expressions yields:

$$[(C_E - C_W + C_N - C_S) + D_W + (1-f_W)C_W$$
$$+D_E - f_E C_E + D_S + (1-f_S)C_S + D_N - f_N C_N]\phi_P$$
$$= [D_W + (1-f_W)C_W]\phi_W + [D_E - f_E C_E]\phi_E + [D_S + (1-f_S)C_S]\phi_S$$
$$+[D_N - f_N C_N]\phi_N + S_U + S_P\phi_P \qquad (3\text{-}60)$$

It is convenient to define new total coefficients to replace these common expressions:

$$A_E = D_E - f_E C_E \qquad (3\text{-}61)$$

$$A_W = D_W + (1-f_W)C_W \qquad (3\text{-}62)$$

$$A_N = D_N - f_N C_N \qquad (3\text{-}63)$$

$$A_S = D_S + (1-f_S)C_S \qquad (3\text{-}64)$$

The A's with the single subscript are not area coefficients, but convection/diffusion coefficients. In terms of these total coefficients, the finite-difference form of the ϕ-equation becomes

$$[C_E - C_W + C_N - C_S + A_E + A_W + A_N + A_S]\phi_P$$
$$= A_E\phi_E + A_W\phi_W + A_N\phi_N + A_S\phi_S + S_U + S_P\phi_P \qquad (3\text{-}65)$$

5. First Modification (Stability)

Checking to see if mass is conserved, we can express the continuity equation in finite-difference form as follows. From Eqn. 3-10

$$\int_{x_w}^{x_e}\int_{r_s}^{r_n}\int_0^1 \left[\frac{\partial}{\partial x}(r\rho u) + \frac{\partial}{\partial r}(r\rho v) - rS_p^m\right] dx\, dr\, d\xi_3 = 0 \qquad (3\text{-}66)$$

or

$$\int_{r_s}^{r_n} [r\rho u]_w^e dr + \int_{x_w}^{x_e} [r\rho v]_s^n dx = S_p^m(\Delta V) \qquad (3\text{-}67)$$

and in terms of convection coefficients,

$$C_E - C_W + C_N - C_S - S_p^m(\Delta V) = \dot{M}_{net} \qquad (3\text{-}68)$$

At steady-state, $\dot{M}_{net}$ should equal zero in a converged solution. During the course of iterating to obtain a converged solution, the quantity $\left(C_E - C_W + C_N - C_S - S_p^m(\Delta V)\right)$ will not in general vanish. In addition, a situation may arise where all of the total coefficients (A's) are zero, thus causing the finite-difference ϕ-equation (Eqn. 3-65) to become singular. Therefore, we cannot allow this grouping of convection coefficients on the LHS of Eqn. 3-65 to become equal to zero. From the definitions of these coefficients (Eqns. 3-61 to 3-64), if $\dot{M}_{net}$ is positive, then mass is being lost in the cell and a mass flow rate of $C_E - C_W + C_N - C_S - S_p^m(\Delta V)$ is carrying the property of ϕ out of the cell. Under such conditions, it is reasonable to set $\dot{M}_{net}$ to zero and to include an additional term corresponding to the mass flow rate $C_E - C_W + C_N - C_S - S_p^m(\Delta V)$ carrying the (old) property ϕ_p^{old} with it. The other possibility (of $\dot{M}_{net}$ being negative)

implies accumulation of mass in the cell, with ϕ being transported from the neighboring cells. Since Eqn 3-65 predicts this, no modification is necessary. Combining this modification into the source coefficients, Eqn. 3-65 becomes

$$[A_E + A_W + A_N + A_S]\phi_P = A_E\phi_E + A_W\phi_W + A_N\phi_N + A_S\phi_S + S_U + S_P\phi_P \tag{3-69}$$

with

$$S_U = max\left\{C_E - C_W + C_N - C_S - S_P^m(\Delta V),\ 0\right\}\phi_P^{old} + S_U^{rest} \tag{3-70}$$

$$S_P = -max\left\{C_E - C_W + C_N - C_S - S_P^m(\Delta V),\ 0\right\} + S_P^{rest} - S_P^m(\Delta V) \tag{3-71}$$

where

$$\phi_P^{old} = \text{old or known value of } \phi \text{ at node } P \tag{3-72}$$

$$S_U^{rest},\ S_P^{rest} = \text{source coefficients of the original equation given by Eqn. III.B-57 times the volume of the cell} \tag{3-73}$$

This modification will ensure that the finite-difference equation will behave reasonably when the mass flow rates for the control volume do not satisfy continuity.

Equation 3-69 can be written more compactly by introducing a subscript d for the four directions (E, W, N, S), and combining the coefficients of the ϕ_P term:

$$\left[\left(\sum_d A_d\right) - S_P\right]\phi_P = \sum_d A_d\phi_d + S_U \tag{3-74}$$

where S_U and S_P are given by Eqns. 3-70 and 3-71. Another coefficient can be defined as

$$A_P = \sum_d A_d - S_P \tag{3-75}$$

and the standard equation form which TEACH solves is expressed as

$$A_P\phi_P = \sum_d A_d\phi_d + S_U \tag{3-76}$$

6. Second Modification (Improved Differencing Scheme)

Thus far the derivation resulting in Eqn. 3-76 has used central differencing for all terms. Because of non-linearities in the transport equations, central differencing is not exact. For problems in computational fluid mechanics with large convection terms (i.e. cell Reynolds numbers greater than 2), central differencing causes problems in some locations (Roache, 1976; Patankar, 1980).

A simple, one-dimensional analysis, for which a known exact solution exists, can be performed (Wormeck, 1976; Patankar, 1980). It can be concluded from such an analysis that central differencing is preferable for small cell Reynolds numbers, and upwind differencing is performed for large values, but neither is satisfactory for all Reynolds numbers. Equation 3-76 is therefore modified to conform to these non-linearities while at the same time conserving mass. This approach is discussed in more detail by Patankar (1980). Questions and modifications concerning stability and convergence rates will be discussed in the next section.

The technique employed by PCGC-2 alters the differencing scheme according to the local value of the cell Reynolds Number (*Re*). For example, for a west face we note that:

$$G_w A_w = (\rho u A)_w = C_W \tag{3-77}$$

$$Re_w = \left(\frac{\rho u \delta}{\mu}\right)_w = \left(\frac{\rho u A}{\frac{\mu}{\delta}A}\right)_w = \frac{C_W}{D_W} \tag{3-78}$$

Therefore, the local cell Reynolds number is a measure of the relative magnitude of convection and diffusion. When convection terms are very small relative to diffusion terms (small *Re*), then central differencing is preferred. However, when convection terms are large relative to diffusion terms (large *Re*) then upwind differencing is preferred. In middle regions of *Re*, some combination is preferred. PCGC-2 uses either 1) hybrid differencing or 2) power-law differencing.

The mathematical representation of the alternate schemes is as follows. The total coefficients for each direction are rewritten as:

$$A_N = \Omega_N + max\ (0,\ -C_N) \tag{3-79}$$

$$A_S = \Omega_S + max\ (0,\ C_S) \tag{3-80}$$

$$A_E = \Omega_E + max\ (0,\ -C_E) \tag{3-81}$$

$$A_W = \Omega_E + max\ (0,\ C_W) \tag{3-82}$$

where Ω depends on the differencing scheme used. For upwind differencing:

$$\Omega_d = D_d \tag{3-83}$$

For central differencing:

$$\Omega_d = D_d - 0.5|C_d| \tag{3-84}$$

For hybrid differencing:

$$\Omega_d = max\left[0,\ \left(D_d - 0.5|C_d|\right)\right] \tag{3-85}$$

For power-law differencing:

$$\Omega_d = max\left\{0,\ D_d\left[\frac{D_d - 0.1|C_d|}{D_d}\right]^5\right\} \tag{3-86}$$

The difference between the various differencing schemes can be summarized as follows: in upwind differencing, the finite difference is taken in the direction from which the velocity vector is arriving. Central differencing has already been

discussed. Hybrid differencing uses upwind differencing when cell Reynolds Numbers are larger than 2 or less than -2 and central differencing when -2<Re<2. Power-law differencing uses the fifth-order-power-law expression for -10<Re<10 and upwind differencing outside this range. For both power-law and hybrid differencing, the appropriate differencing is applied to convection terms. Diffusion terms are ignored for high Reynolds numbers (pure upwind differencing). These advanced differencing options allow for greater accuracy with less grid resolution than is permissible with central differencing. The power-law scheme is recommended in all cases.

Convergence Test

The finite-difference equations will now be analyzed for convergence criteria. Writing Eqn. 3-76 as

$$\phi_p = \sum_d A_d^{'} \phi_d + S_U^{'} \tag{3-87}$$

where $A_d^{'} = A_d / A_p$ and $S_U^{'} = S_U / A_p$, we have a system of linear algebraic equations of the form

$$x_i = \sum_{j, j \neq i} \left(a_{ij} x_j \right) + b_i \tag{3-88}$$

From the theory of linear equations (Gosman et al., 1969; Patankar and Spalding, 1970) if the a_{ij} and b_i are constants, the sufficient conditions for convergence are:

$$\sum_{j, j \neq i} |a_{ij}| \begin{cases} < 1 \text{ for all } i \\ < 1 \text{ for at least one } i \end{cases} \tag{3-89}$$

Since $A_d^{'}$ and $S_U^{'}$ in Eqn. 3-87 are not constant, the criteria in Eqn. 3-89 do not apply exactly. However, as an approximation, we may expect convergence if

$$\sum_d \frac{A_d}{A_d - S_p} \begin{cases} < 1 \text{ for all } i \\ < 1 \text{ for at least one } i \end{cases} \tag{3-90}$$

which implies that S_p must be less than zero. The S_p term is the source term involving the dependent variable implicitly (based on new value). Therefore, to insure a negative value for S_p, if any source term containing the dependent variable is positive, the old value of ϕ must be used and the term combined this term with the S_U quantity (i.e., appearing explicitly).

Since the coefficients are not constant, convergence is not guaranteed by Eqn. 3-88 but is reasonably assured if $S_p < 0$. If divergence is encountered, under-relaxation may be used as discussed later. PCGC-2 generally converges if the source terms are linear or mildly nonlinear. Highly nonlinear source terms may not converge or require very small (0.1-0.3) under-relaxation factors.

Solution of the Finite-Difference Equations (TDMA)

PCGC-2 has a large system of linear algebraic finite-difference equations to solve, and vast numbers of techniques are available (Carnahan et al., 1969) to solve this system of equations. Some of the more popular methods to solve the fluid flow type of equation systems are presented elsewhere (Roache, 1976).

Matrix inversion and other direct techniques are out of the question because of the large number of equations involved, and therefore iterative methods must be employed. The formulation in terms of vorticity and stream function (Gosman, et al., 1969) utilized a Gauss-Seidel algorithm, which is a point-by-point method. The equations are solved one at a time, passing from node point to node point throughout the flow field. New values of the variables are used as soon as they become available, and the complete flow field is solved for each dependent variable before going to the next dependent variable.

The technique used in PCGC-2 is to solve simultaneously a line of node points in a so-called line-by-line method. This line-by-line technique is implemented in a very efficiently numbered scheme, the Tri-Diagonal Matrix Algorithm (TDMA). The equations are of the form:

$$D_i\phi_i = A_i\phi_{i+1} + B_i\phi_{i-1} + C_i \qquad (3\text{-}91)$$

where i=2,N-1 and the values of the constant coefficients A_i, B_i, C_i, and D_i are given for i=2,N-1 together with the boundary values ϕ_1 and ϕ_N. The procedure calls for rewriting Eqn. 3-91 as:

$$\phi_i = A_i' \phi_{i+1} + C_i' \qquad (3\text{-}92)$$

and obtaining a solution by successive substitution, starting with $i=N-1$ and working backwards to $i=2$. The transformed coefficients $A_i^{'}$ and $C_i^{'}$ are given by the recurrence relations:

$$A_i^{'} = \frac{A_i}{D_i - B_i A_{i-1}^{'}} \tag{3-93}$$

$$C_i^{'} = \frac{C_i + C_{i-1}^{'} B_i}{D_i - B_i A_{i-1}^{'}} \tag{3-94}$$

with the starting values of $A_1^{'} = 0$ and $C_1^{i} = \phi_1$.

The TDMA can be implemented to solve Eqn. 3-76 by considering the equations for all the control volumes along a grid line with the last or best estimates for the values of ϕ along the two neighboring grid lines, and hence constructing an equation set which can be solved by the TDMA. In this manner, we can first traverse along all the grid lines in, say, the x direction; then, using this solution as the best estimate, go over lines in the r direction.

For the r-direction sweep, Eqn. 3-76 is written as:

$$A_P \phi'_P = A_N \phi'_N + A_S \phi'_S + \left(A_E \phi_E + A_W \phi_W + S_U\right) \tag{3-95}$$

where the term in the parentheses is considered known and TDMA can be applied. The superscript $'$ denotes the values obtained from this first phase of solution, while the second phase, the x-direction sweep, is the solution of:

$$A_P \phi''_P = A_E \phi''_E + A_W \phi''_W + \left(A_N \phi'_N + A_S \phi'_S + S_U\right) \tag{3-96}$$

in a similar manner.

It must be remembered that the TDMA is an iterative solution technique to solve the finite-difference equations, the coefficients of which are only tentative and require updating to account for the changes in the values of the variables. The number of sweeps needed for an accurate solution of the finite-difference equations before the coefficients are recalculated is arbitrary and problem-dependent. Convergence criteria are used to converge the equations uniformly (van Doormaal and Raithby, 1984).

Final Form

The final form of the *f*-finite-difference equation in PCGC-2 is:

$$A_P\phi_P = A_E\phi_E + A_W\phi_W + A_N\phi_N + A_S\phi_S + S_U \tag{3-97}$$

where

$$A_P = A_E + A_W + A_N + A_S - S_P \tag{3-98}$$

$$A_E = \Omega_E + max(0,\ -C_E) \tag{3-99}$$

$$A_W = \Omega_W + max(0,\ C_W) \tag{3-100}$$

$$A_N = \Omega_N + max(0,\ -C_N) \tag{3-101}$$

$$A_S = \Omega_S + max(0,\ C_S) \tag{3-102}$$

$$\Omega_d = \begin{cases} max\left[0,\ D_d\left(\dfrac{D_d - 0.1|C_d|}{D_d}\right)^5\right] & \text{for power - law differencing} \\ max\left[0,\ D_d - 0.5|C_d|\right] & \text{for hybrid differencing} \end{cases} \tag{3-103}$$

where $d = E, W, N,$ or S

$$D_E = \frac{\frac{1}{2}(\Gamma_P + \Gamma_E)(A_{ew})}{\delta x_{PE}} \tag{3-104}$$

$$D_W = \frac{\frac{1}{2}(\Gamma_P + \Gamma_W)(A_{ew})}{\delta x_{PW}} \tag{3-105}$$

$$D_N = \frac{\frac{1}{2}(\Gamma_P + \Gamma_N)(A_n)}{\delta x_{NP}} \tag{3-106}$$

$$D_S = \frac{\frac{1}{2}(\Gamma_P + \Gamma_S)(A_S)}{\delta x_{PS}} \tag{3-107}$$

$$C_E = \frac{\frac{1}{2}(\rho_P + \rho_E)(A_{ew})}{u_E} \tag{3-108}$$

$$C_W = \frac{\frac{1}{2}(\rho_P + \rho_W)(A_{ew})}{u_P} \tag{3-109}$$

$$C_N = \frac{\frac{1}{2}(\rho_P + \rho_N)(A_N)}{v_N} \tag{3-110}$$

$$C_S = \frac{\frac{1}{2}(\rho_P + \rho_S)(A_S)}{v_P} \tag{3-111}$$

$$S_U = max\left[C_E - C_W + C_N - C_S - S_P^m(\Delta V),\ 0\right]\phi_P^{old} + S_U^{rest}(vol) \tag{3-112}$$

$$S_P = -max\left[C_E - C_W + C_N - C_S - S_P^m(\Delta V),\ 0\right] + S_P^{rest}(vol) - S_P^m(\Delta V) \tag{3-113}$$

$$S_U^{rest} + S_P^{rest}\phi_P = S^{\phi} \qquad (3\text{-}114)$$

and the grid definition implies that all the fs are equal to 0.5.

Finite-Difference Form of the Momentum Equation

The finite-difference form of the momentum equation closely resembles Eqn. 3-97 for the general ϕ-equation, with two exceptions. First, as mentioned previously, a staggered-velocity grid is employed for the definition of the velocity components (see Figs. 3-9 and 3-10), and therefore control volumes centered at these velocity locations are defined which are different from those for the other dependent variables. Secondly, the pressure gradient term, which may be regarded as a source of momentum, is treated in a special manner, and the geometric coefficient which relates a velocity component to the pressure difference between the adjacent nodes is stored for use in the pressure equation.

If the pressure distribution were known, the momentum equations (Eqns. 3-11 to 3-13) would be uncoupled from the continuity equation (Eqn. 3-10) and could be solved in a straightforward manner. Unfortunately , the pressures are not known in advance.

PCGC-2 employs the SIMPLE (Semi-Implicit Method for Pressure-Linked Equations) algorithm and two of its variants: SIMPLER (SIMPLE-Revised) and SIMPLEC (Patankar and Spalding, 1970, 1972; Patankar, 1980; van Doormaal and Raithby, 1984). In these techniques, the pressure distribution is guessed (i.e. assumed known) and denoted by p^*. The solution of the momentum equations for the two velocity components that correspond with this guessed (or "starred") pressure field becomes the "starred" velocity field. Corrections are then made to the "starred" pressure field so as to bring the velocity field into conformity with the continuity equation.

u-Equation. From Eqn. 3-11, the u-equation is:

$$\frac{\partial}{\partial x}(r\rho uu)+\frac{\partial}{\partial r}(r\rho uv)-\frac{\partial}{\partial x}\left(r\mu\frac{\partial u}{\partial x}\right)-\frac{\partial}{\partial r}\left(r\mu\frac{\partial u}{\partial r}\right)=-r\frac{\partial p}{\partial x}+rS^{u} \qquad (3\text{-}115)$$

where the source term is given by Eqn. 3-14. The convection and diffusion terms are identical to the ϕ-equation with $\phi = u$ and $\Gamma = \mu$, and hence the derivation of the finite-difference equations is similar to the f-equation, but the integration is performed over the u-control volume, which is staggered from the main ϕ-cell. The pressure term is handled explicitly. Figure 3-9 shows a typical u-cell, and the

superscript u means that reference to this u-cell is being made instead of to the main control volume.

Integrating Eqn. 3-115 over the u-cell in the same manner as the ϕ-equation was integrated over the main or p-cell, the first convection term becomes:

$$\int_{x_w^u}^{x_e^u}\int_{r_s^u}^{r_n^u}\int_0^1 \frac{\partial}{\partial x}(r\rho uu)d\xi_3 dr dx \tag{3-116}$$

or

$$(\rho uu)_e^u A_{ew}^u - (\rho uu)_w^u A_{ew}^u \tag{3-117}$$

A problem arises here as to which way to expand the density and velocity. For example, one method would be to linearly interpolate the velocities and simply average the density. Another method would be to linearly interpolate the product $\rho u = G$ as well as the remaining u. The former method results in:

$$\rho_e^u \left(u_e^u\right)^2 = \rho_e^u \left[\left(1 - f_E^u\right)u_p + f_E^u u_E\right]^2 \tag{3-118}$$

and, for $f_e^u = \frac{1}{2}$, the east face convection term is:

$$\tfrac{1}{4} A_{ew}^u \rho_P \left(u_P + u_E\right)^2 \tag{3-119}$$

The latter method yields

$$(\rho u)_e^u u_e^u = \left[\left(1 - f_E^u\right)(\rho u)_P + f_E^u (\rho u)_E\right]\left[\left(1 - f_E^u\right)u_P + f_E^u u_E\right] \tag{3-120}$$

requiring the densities midway between their points of definition. By averaging them and taking $f_e^u = \frac{1}{2}$, the convection coefficient through the east face is given by:

$$\tfrac{1}{2} A_{ew}^u \left[\left(\frac{\rho_E + \rho_P}{2}\right)u_E + \left(\frac{\rho_P + \rho_W}{2}\right)u_P\right] \tag{3-121}$$

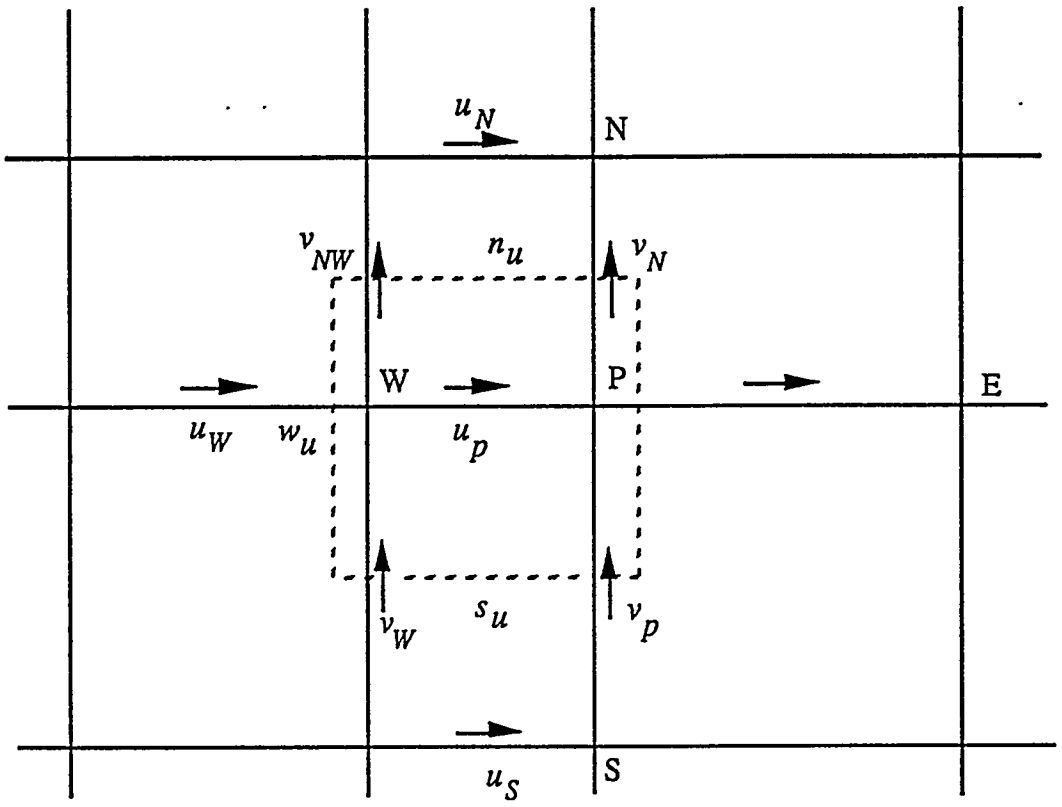

Fig. 3-9. A typical *u*-cell showing adjacent velocities. Other symbols define the location of the control volume over which the first momentum equation is integrated.

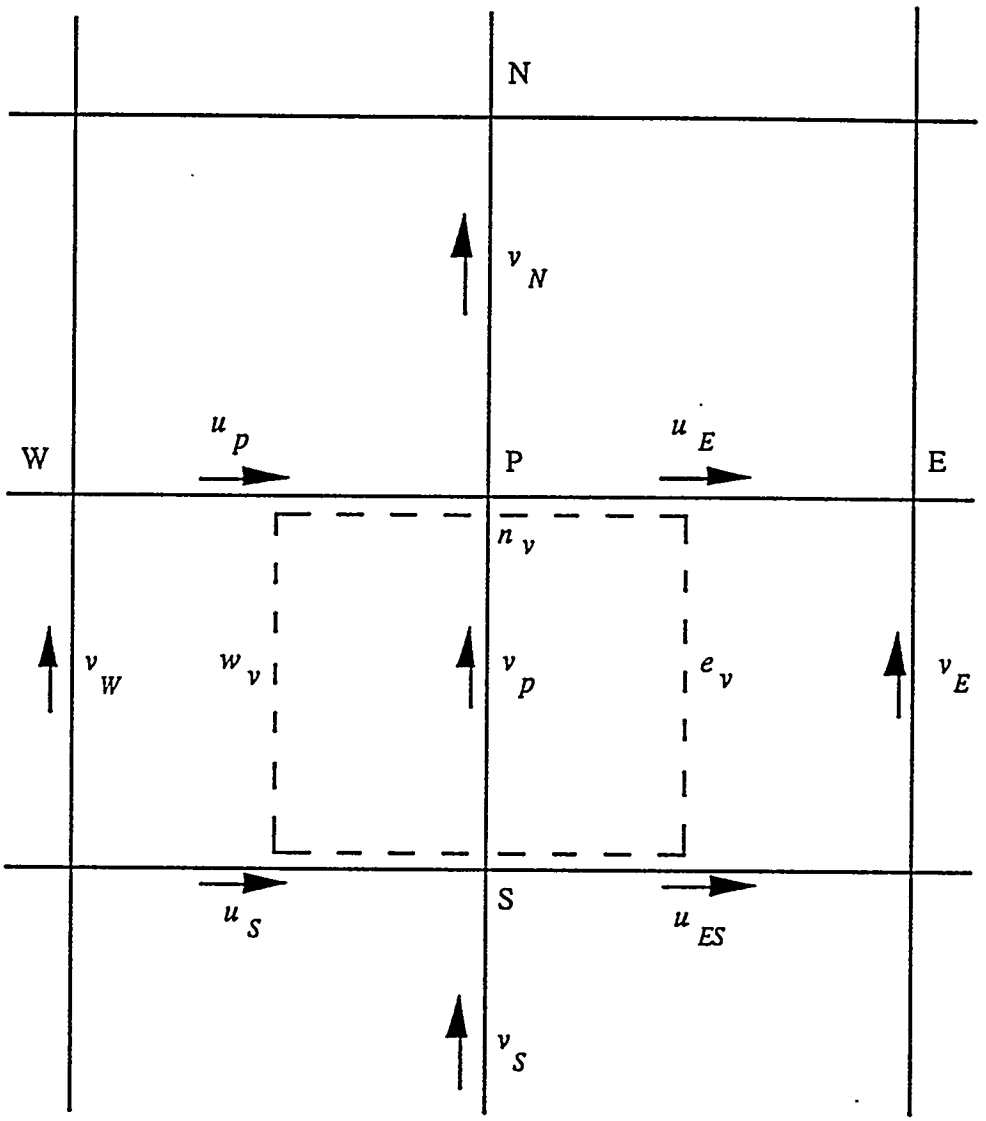

Fig. 3-10. A typical v-cell showing adjacent velocities. Other symbols define the location of the control volume over which the second momentum equation is integrated.

The second convection term integrates to

$$(\rho vu)_n^u A_n^u - (\rho vu)_s^u A_s^u \tag{3-122}$$

where the ρv products are linearly interpolated between the points of definition of the v velocities as:

$$(\rho v)_n^u = \left(1 - f_W^u\right)\left(\frac{\rho_W + \rho_{NW}}{2}\right)v_{NW} + f_W^u\left(\frac{\rho_N + \rho_P}{2}\right)v_N \tag{3-123}$$

$$(\rho v)_s^u = \left(1 - f_W^u\right)\left(\frac{\rho_W + \rho_{SW}}{2}\right)v_W + f_W^u\left(\frac{\rho_S + \rho_P}{2}\right)v_P \tag{3-124}$$

where

$$f_W^u = \frac{x_P^u - x_W}{x_P - x_W} \tag{3-125}$$

PCGC-2 defines the velocities midway between the main node points at cell faces $\left(f_w^u = \frac{1}{2}\right)$, and the four u-equation convection coefficients are:

$$C_E^u = \tfrac{1}{4}\left[(\rho_P + \rho_E)u_E + (\rho_P + \rho_W)u_P\right]A_{ew}^u \tag{3-126}$$

$$C_W^u = \tfrac{1}{4}\left[(\rho_P + \rho_W)u_P(\rho_W + \rho_{WW})u_W\right]A_{ew}^u \tag{3-127}$$

$$C_N^u = \tfrac{1}{4}\left[(\rho_P + \rho_N)v_N + (\rho_W + \rho_{NW})v_{NW}\right]A_n^u \tag{3-128}$$

$$C_S^u = \tfrac{1}{4}\left[(\rho_P + \rho_S)v_P + (\rho_W + \rho_{SW})v_W\right]A_s^u \tag{3-129}$$

where

$$\rho_{WW} = \rho_{i-2,j} \tag{3-130}$$

The diffusion terms for the u-equation are defined as:

$$D_E^u = \frac{\mu_e^u A_{ew}^u}{\delta x_{EP}^u} \tag{3-131}$$

$$D_W^u = \frac{\mu_w^u A_{ew}^u}{\delta x_{PW}^u} \tag{3-132}$$

$$D_N^u = \frac{\mu_n^u A_n^u}{\delta y_{NP}} \tag{3-133}$$

$$D_S^u = \frac{\mu_s^u A_s^u}{\delta y_{PS}} \tag{3-134}$$

where the viscosities are interpolated as:

$$\mu_e^u \approx \mu_P \tag{3-135}$$

$$\mu_w^u \approx \mu_W \tag{3-136}$$

$$\mu_n^u = \tfrac{1}{4}\left(\mu_{NW} + \mu_N + \mu_W + \mu_P\right) \tag{3-137}$$

$$\mu_s^u = \tfrac{1}{4}\left(\mu_W + \mu_P + \mu_{SW} + \mu_S\right) \tag{3-138}$$

Considering the pressure term in Eqn. 3-115

$$\int_{x_w^u}^{x_e^u}\int_{r_s^u}^{r_n^u}\int_0^1\left(-r\frac{\partial p}{\partial x}\right)d\xi_3\,dr\,dx \tag{3-139}$$

and integrating twice yields:

$$-\int_{x_w^u}^{x_e^u}\left[\tfrac{1}{2}\left(r_n^u\right)^2-\left(r_s^u\right)^2\left(\frac{\partial p}{\partial x}\right)\right]dx \tag{3-140}$$

$$=-\tfrac{1}{2}\left(r_n^u-r_s^u\right)\left(r_n^u+r_s^u\right)\left[p\right]_{x_w^u}^{x_e^u} \tag{3-141}$$

and since

$$r_P=\tfrac{1}{2}\left(r_n^u+r_s^u\right) \tag{3-142}$$

$$A_{ew}^u\left(-p_e^u+p_w^u\right) \tag{3-143}$$

where these pressures are already defined at their required locations to give:

$$A_{ew}\left(p_W-p_P\right) \tag{3-144}$$

Since the leading coefficient will be needed in the pressure equation, it is stored as a new area coefficient, $D^u=A_e^u$. The expression

$$D^u\left(p_W-p_P\right) \tag{3-145}$$

will be incorporated into the S_U term. Also note that for turbulent flow, the normal stress (pressure) is augmented by $\frac{2}{3}\rho k$.

Evaluating the source terms the same way, the final u-equation is

$$A_P u_P = \sum_d A_d u_d + D^u(p_W - p_P) + S_U \tag{3-146}$$

where[1]

$$A_P = \sum_d A_d - S_p \tag{3-147}$$

$$A_d = \Omega_d + max(0, -C_d) \; for \; d = E \; or \; N \tag{3-148}$$

$$A_d = \Omega_d + max(0, C_d) \; for \; d = W \; or \; S \tag{3-149}$$

$$\Omega_d = max\left[0,\; D_d\left(\frac{D_d - 0.1|C_d|}{D_d}\right)^5\right] \tag{3-150}$$

$$S_U = max\left\{C_E - C_W + C_N - C_S - S_p^m(\Delta V),\; 0\right\} u_P + S_U^{rest}(vol) \tag{3-151}$$

$$S_P = -max\left\{C_E - C_W + C_N - C_S - S_p^m(\Delta V),\; 0\right\} + \left(S_P^{rest}\right)(vol) - S_p^m(\Delta V) \tag{3-152}$$

and C_d and D_d are given by Eqns. 3-126 to 3-134.

<u>v and w Equations</u>. Following a similar procedure, the second momentum equation, Eqn. 3-12 can be expressed as:

$$A_p v_p = \sum_d A_d v_d + S_U \tag{3-153}$$

---

[1]This Ω_d is for power-law differencing. If hybrid differencing is used, $\Omega_d = max\left[0,\; D_d - 0.5|C_d|\right]$.

where the total coefficients are defined in the usual manner, but S_U is given as:

$$S_U = max\left\{C_E - C_W + C_N - C_S - S_p^m(\Delta V),\ 0\right\}v_p + D_v\left(p_s - p_p\right) + \left(S_U^{rest}\right)(vol) \tag{3-154}$$

The v-equation coefficients are:

$$C_E = \tfrac{1}{4}\left[\left(\rho_P + \rho_E\right) u_E + \left(\rho_S + \rho_{SE}\right) u_{SE}\right] \tag{3-155}$$

$$C_W = \tfrac{1}{4}\left[\left(\rho_P + \rho_W\right) u_P + \left(\rho_S + \rho_{SW}\right) u_S\right] \tag{3-156}$$

$$C_N = \tfrac{1}{4}\left[\left(\rho_P + \rho_N\right) v_N + \left(\rho_P + \rho_S\right) v_P\right] \tag{3-157}$$

$$C_S = \tfrac{1}{4}\left[\left(\rho_P + \rho_S\right) v_P \left(\rho_S + \rho_{SS}\right) \mathrm{v_S}\right] \tag{3-158}$$

The diffusion coefficients are given by:

$$D_E = \frac{\mu_e^v A_{ew}^v}{\delta x_{EP}} \tag{3-159}$$

$$D_W = \frac{\mu_w^v A_{ew}^v}{\delta x_{PW}} \tag{3-160}$$

$$D_N = \frac{\mu_p A_n^v}{\delta y_{NP}^v} \tag{3-161}$$

$$D_S = \frac{\mu_S A_s^v}{\delta y_{PS}^v} \tag{3-162}$$

Figure 3-10 shows a typical v control volume and notation. Similar results can be obtained for the tangential momentum equation.

Pressure Correction Equation (Continuity)

The next task in the SIMPLE/R/C algorithms is to correct the starred pressure and velocity fields such that the continuity equation is satisfied. The two finite-difference momentum equations are from Eqns 3-146 and 3-153:

$$A_p^u u_p = \sum_d A_d^u u_d + D^u\left(p_W + p_p\right) + S_U^u \tag{3-163}$$

$$A_p^v v_p = \sum_d A_d^v v_d + D^v\left(p_S - p_p\right) + S_U^v \tag{3-164}$$

Lacking knowledge of the pressure distribution, the pressures in the above momentum equations are guessed (denoted by a star superscript) to allow the computation of the two velocity components u^* and v^* corresponding to the p^* distribution. This true pressure is

$$p = p^* + p' \tag{3-165}$$

where p' is the pressure correction which, when summed with the guessed pressure, will give the correct pressure.

The SIMPLE algorithm utilizes the continuity equation to determine the pressure corrections. The equations expressing the true velocities in terms of the guessed velocities and pressure corrections are developed below. Substituting the guessed pressures in Eqns. 3-163 and 3-164 yields:

$$A_p^u u_p^* = \sum_d A_d^u u_d^* + D^u\left(p_W^* - p_P^*\right) + S_U^u \tag{3-166}$$

$$A_p^v v_p^* = \sum_d A_d^v v_d^* + D^v\left(p_S^* - p_p^*\right) + S_U^v \tag{3-167}$$

These equations are solved for the "starred" velocity fields. Subtracting the corresponding Eqns. 3-166 and 3-167 from Eqns. 3-163 and 3-164 and substituting the pressure corrections, we have:

$$A_p^u\left(u_p - u_p^*\right) = \sum_d A_d^u\left(u_d - u_d^*\right) + D^u\left(p_W' - p_P'\right) \tag{3-168}$$

$$A_p^v\left(v_p - v_p^*\right) = \sum_d A_d^v\left(v_d - v_d^*\right) + D^v\left(p_S' - p_P'\right) \tag{3-169}$$

which gives the true velocities as:

$$u_p = u_p^* + \frac{D^u}{A_p^u}\left(p_W' - p_P'\right) + \sum_d \frac{A_d^u}{A_p^u}\left(u_d - u_d^*\right) \tag{3-170}$$

$$v_p = v_p^* + \frac{D^v}{A_p^v}\left(p_S' - p_P'\right) + \sum_d \frac{A_d^v}{A_p^v}\left(v_d - v_c^*\right) \tag{3-171}$$

A similar derivation applied to the neighboring nodes leads to

$$u_E = u_E^* + \left(\frac{D^u}{A_p^u}\right)_E \left(p_P' - p_E'\right) + \sum_{d_E}\left(\frac{A_d^u}{A_p^u}\right)_E \left(u_d - u_d^*\right) \tag{3-172}$$

$$v_N = v_N^* + \left(\frac{D^v}{A_p^v}\right)_N \left(p_P' - p_N'\right) + \sum_{d_N}\left(\frac{A_d^v}{A_p^v}\right)_N \left(v_d - v_d^*\right) \tag{3-173}$$

where the new subscript refers to total coefficients at the node point.

From Eqn. 3-68, the finite-difference form of the continuity equation is

$$\rho_e u_E A_e - \rho_w u_p A_w + \rho_n v_N A_n - \rho_s v_P A_s - S_p^m(\Delta V) = 0 \tag{3-174}$$

In the so-called incompressible pressure-correction equation, the density does not depend on pressure; this derivation follows.

Equation 3-174 calls for substitution of Eqns. 3-170 to 3-173 for the velocities, but the last term in each of these equations is lengthy and complicated, so that it will be dropped to give the true velocities as:

$$u_P = u_P^* + D_P^u(p'_W - p'_P) \tag{3-175}$$

$$v_P = v_P^* + D_P^v(p'_S - p'_P) \tag{3-176}$$

$$u_E = u_E^* + D_E^u(p'_P - p'_E) \tag{3-177}$$

$$v_N = v_N^* + D_N^v(p'_P - p'_N) \tag{3-178}$$

where the new pressure coefficients include the corresponding A_P terms. Now substituting these velocities, the continuity equation becomes:

$$\left(\rho_e A_e D_E^u + \rho_w A_w D_P^u + \rho_n A_n D_N^v + \rho_s A_s D_P^v\right)p'_P = \left(\rho_e A_e D_E^u\right)p'_E + \left(\rho_w A_w D_P^u\right)p'_W + \left(\rho_n A_n D_N^v\right)p'_N + \left(\rho_s A_s D_S^v\right)p'_S - \rho_e A_e u_E^* + \rho_w A_w u_P^* - \rho_n A_n v_N^* + \rho_s A_s v_P^* + S_p^m(\Delta V) \tag{3-179}$$

This equation allows the pressure corrections to be determined from known quantities, and furthermore has a similar form to the standard finite-difference equation. Defining the following pressure-correction coefficients:

$$A_E = \rho_e A_e D_E^u \tag{3-180}$$

$$A_W = \rho_w A_w D_P^u \tag{3-181}$$

$$A_N = \rho_n A_n D_N^v \tag{3-182}$$

$$A_S = \rho_s A_s D_P^v \tag{3-183}$$

$$S_U = -\rho_e A_e u_E^* + \rho_w A_w u_P^* - \rho_n A_n v_N^* + \rho_s A_s v_P^* + S_p^m(\Delta V) \tag{3-184}$$

the pressure-correction equation becomes simply:

$$\left(\sum_d A_d\right) p_p' = \sum_d A_d p_d' + S_U \tag{3-185}$$

which can be solved by the TDMA. Note that no hybrid differencing is required.

The quantity S_U defined above is the net mass source resulting from the starred velocity field which, in general, does not satisfy continuity. The aim of the pressure correction equation is to reduce this mass source to zero; indeed, by monitoring this quantity, the extent of convergence is known, with complete convergence occurring when the sum of these pressure source terms throughout the flow domain is less than some input tolerance (typically 0.001-0.0001).

After resolving the pressure correction equation by the TDMA, the correct pressure and velocities are given by

$$p = p^* + p' \tag{3-186}$$

$$u_p = u_p^* + D_u(p_W' - p_P') \tag{3-187}$$

$$v_p = v_p^* + D_v(p_S' - p_P') \tag{3-188}$$

It should be pointed out that the pressure correction equation calculates just the corrections to the pressure field; and in a converged solution these corrections vanish, and therefore, the dropping of the last terms in the momentum equations, to arrive at Eqns. 3-175 to 3-179, has no effect on the accuracy of the solution. Also, it must be noted that under-relaxation is required (~0.5) so that only a portion of these corrections is added at a time.

The SIMPLER (SIMPLE-Revised) algorithm was developed by Patankar (1980) to allow faster convergence than the SIMPLE algorithm. Solving Equations 3-163 and 3-164 for u_p and v_p yields:

$$u_p = \frac{\sum_d A_d^u u_d + D_P^u (p_W - p_P) - S_U^u}{A_P^u} \tag{3-189}$$

$$v_p = \frac{\sum_d A_d^v v_d + D_P^v (p_S - p_P) - S_U^v}{A_P^v} \tag{3-190}$$

Pseudo-velocities $(\hat{u}_p,\ \hat{v}_p)$ are defined to simplify Eqns. 3-188 and 3-189:

$$\hat{u}_P = \frac{\sum_d A_d^u u_d + S_U^u}{A_P^u} \tag{3-191}$$

$$\hat{v}_P = \frac{\sum_d A_d^v v_d + S_U^v}{A_P^v} \tag{3-192}$$

Similar equations are easily derived for $\hat{u}_E$ and $\hat{v}_N$. Using Eqns. 3-191 and 3-192, Eqns. 3-188 and 3-189 are reduced to:

$$u_P = \hat{u}_P + D_P^u (p_W - p_P) \tag{3-193}$$

$$v_P = \hat{v}_P + D_P^v(p_S - p_P) \tag{3-194}$$

Equations 3-193 and 3-194 are very similar to Eqns. 3-175 and 3-176. Substituting the velocities from Eqns. 3-193 and 3-194 into the continuity equation yields an equation similar to Eqn. 3-185, except that the pseudo velocities are used instead of the starred velocities:

$$\left(\sum_d A_d\right) p_P = \sum_d A_d p_d + S_u^P \tag{3-195}$$

where the A's are given by Eqns. 3-180 through 3-183, and S_u^P is defined by:

$$S_u^P = -\rho_e A_e \hat{u}_E + \rho_w A_w \hat{u}_P - \rho_n A_n \hat{v}_N + \rho_s A_s \hat{v}_P + S_p^m(\Delta V) \tag{3-196}$$

The SIMPLER algorithm is summarized below (Patankar, 1980):

1. Start with a guessed velocity field.
2. Calculate the coefficients for the axial and radial momentum equations and then calculate the pseudo-velocities from Eqns. 3-191 and 3-192 using the guessed velocity field.
3. Calculate the pressure coefficients and solve for the pressure field using Eqn. 3-195.
4. Treating this pressure field as p^*, solve for the starred velocity field using Eqns. 3-166 and 3-167.
5. Solve the pressure correction equation (Eqn. 3-185) to get p'.
6. Correct the starred velocity field using Eqns. 3-175 and 3-176, but do not correct the pressure field.
7. Solve the other conservation equations, as necessary (w, k, ε, f, μ, etc.).
8. Return to step 2 and repeat as necessary.

The SIMPLER algorithm has been shown to reduce the convergence time in PCGC-2 by nearly one-half of that required by the SIMPLE algorithm (Fletcher, 1983). It should be pointed out that in Eqn. 3-194, S_U^P should not necessarily vanish when convergence is achieved like S_U in Eqn. 3-185. Also, it must be noted that best results are achieved when under-relaxation is not used for either the pressure (Eqn. 3-195) or the pressure correction (Eqn. 3-185) when the SIMPLER

algorithm is used. The SIMPLER algorithm makes it possible to use much larger values for all other under-relaxation factors in the model (i.e. less under-relaxation). A typical value is 0.7 instead of 0.5.

Dropping the last term in Eqns. 3-170 through 3-173 is equivalent to dropping the first term on the right-hand side of Eqns. 3-168 and 3-169, which has been pointed out to be inconsistent since this term is equivalent in magnitude to a term on the left-hand side that results when Eqn. 3-147 is substituted for A_p^u (van Doormaal and Raithby, 1984). A "consistent" approximation which still leads to a suitable expression for p' can be obtained by subtracting the term $\sum_d A_d^u\left(u_p - u_p^*\right)$ from both sides of Eqn. 3-168:

$$\left(A_p^u - \sum_d A_d^u\right)u_p' = \underline{\sum_d A_d^u\left(u_d' - u_p'\right)} + D^u\left(p_W' - p_P'\right) \qquad (3\text{-}197)$$

A similar equation can be obtained for Eqn. (3-169). In the SIMPLEC approximation, the underlined term $\sum_d A_d^u\left(u_d' - u_p'\right)$ is neglected. A "C" is appended to the name SIMPLE as a reminder that this is a "consistent" approximation. Equation 3-197 then becomes equivalent to Eqn. 3-174, where

$$D_p^u = \frac{A_e^u}{A_p^u - \sum_d A_d^u} \qquad (3\text{-}198)$$

p' should not be under-relaxed in SIMPLEC.

Under-Relaxation

The solution of the finite-difference equations in the form of Eqn. 3-195 generally diverges unless the iterative corrections are under-relaxed. The conventional practice in computational fluid dynamics is to under-relax the dependent variables to avoid numerical instabilities. However, based on considerable experience, under-relaxation in this code is accomplished by under-relaxing the source terms.

If f_{UR} is the under-relaxation factor, then under-relaxation is accomplished as follows:

$$A_P^{new} = \frac{A_P^{old}}{f_{UR}} \tag{3-199}$$

$$S_U^{new} = S_U^{old} + \frac{(1-f_{UR})\phi_P^{old} A_P^{new}}{f_{UR}} \tag{3-200}$$

where ϕ_{old}^P is the known value of ϕ computed during the previous iteration.

These modifications are performed before solution of the finite-difference equations by TDMA. All dependent variables are relaxed by this method, where the under-relaxation factor can be different for each variable. In the pressure-correction equation (Eqn. 3-185), the pressure coefficients can also be under-relaxed:

$$D^u = \left(D^u\right) f_{UR}^u / A_P^u \tag{3-201}$$

$$D^v = \left(D^v\right) f_{UR}^v / A_P^v \tag{3-202}$$

It may also be required to under-relax the fluid properties if they change rapidly as is the case with viscosity in turbulent flow and the density in compressible flow. If $\phi^{(n)}$ is the value of the property used in iteration $n+1$, and $\phi^{(n+1)}$ is the value computed in the $n+1^{st}$ iteration, the value used in the $n+1^{st}$ iteration is computed from

$$\phi = f_{UR}\, \phi^{(n+1)} + \left(1-f_{UR}\right) \phi^{(n)} \tag{3-203}$$

The values of the under-relaxation factors must be between zero and one, and for computational efficiency, should be the largest value allowing a stable solution. The optimum values of the under-relaxation factors are problem-dependent. Should divergence occur, smaller values may be required.

Boundary Conditions

There exist an infinite number of solutions to the governing equations, and only the boundary conditions distinguish one solution from another. Thus, the boundary conditions play an important role. An excellent presentation of many types of boundary conditions occurring in fluid dynamic calculations and a discussion of their effects on numerical stability and accuracy have been given elsewhere (Roache, 1976).

In PCGC-2, all boundaries coincide with the control volume sides as illustrated in Fig. 3-11. The implementation of the boundary conditions in the numerical procedure is accomplished by modifying the finite-difference equations for the boundary cells:

$$\left(\sum_d A_d - S_p\right)\phi_p = A_E\phi_E + A_W\phi_W + A_N\phi_N + A_S\phi_S + S_U \qquad (3\text{-}204)$$

The four total coefficients (A's) and the two source term coefficients S_U and S_p in the above equation are altered in such a way that the boundary conditions are satisfied. This technique, generally referred to as "breaking the link," is illustrated by rewriting the equation as

$$A_E(\phi_P - \phi_E) + A_W(\phi_P - \phi_W) + A_N(\phi_P - \phi_N) + A_S(\phi_P - \phi_S) = S_U + S_P\,\phi_P \qquad (3\text{-}205)$$

It may be seen that ϕ_p may be considered as being "linked" to its four neighbors. The above equation is correct for interior cells; for boundary cells, the appropriate total coefficients (A's) must be set to zero, and the correct conditions of convection and diffusion at the boundary included by modifying the two source terms. Thus the procedure calls for specifying the boundary conditions as linear functions of the dependent variable. All three types of boundary conditions for elliptic equations are permissible, and will be discussed in turn.

Dirichlet conditions, or prescribed values of the function, are inserted by calculating the correct convection and diffusion coefficients based on the prescribed values of the dependent variable on the boundary, and using the hybrid differencing scheme to obtain a new total coefficient $A^{(new)}$.

Hence:

$$A_d^{(old)} = 0 \tag{3-206}$$

$$D_d = \frac{\Gamma_B A_B}{\delta_{BP}} \tag{3-207}$$

$$C_d = \rho_B vel_B A_B \tag{3-208}$$

$$A_d^{(new)} = HYBRID[C_d, D_d] \tag{3-209}$$

$$S_U^{(new)} = S_U^{(old)} + A_d^{(new)} \phi_B \tag{3-210}$$

$$S_P^{(new)} = S_P^{(old)} - A_d^{(new)} \tag{3-211}$$

where the subscript B refers to the conditions at the boundary located at a distance of δ_{BP} from the cell center in the d direction, ϕ_B is the prescribed boundary value, A_B is the area of the control volume on the boundary, and C_d and D_d are the convection and diffusion coefficients at the control volume face on the boundary. If the velocity at the boundary, vel_B, is zero (as in the case of a solid wall), then Eqns. 3-206 to 3-211 reduce to:

$$A_d^{(new)} = 0 \tag{3-212}$$

$$S_U^{(new)} = S_U^{(old)} + \left(\frac{\Gamma_B A_B}{\delta_{BP}} \right) \phi_B \tag{3-213}$$

$$S_P^{(new)} = S_P^{(old)} - \left(\frac{\Gamma_B A_B}{\delta_{BP}} \right) \tag{3-214}$$

where A_B is the area of the bounding face.

For Neumann conditions, for which the normal derivative of the function is specified, the usual "links" to all the adjacent exterior cells are broken by setting to zero the appropriate A's and inserting the prescribed boundary fluxes, as follows:

$$S_U^{(new)} = S_U^{(old)} + \left(c \frac{\partial \phi}{\partial n} \right)_B (area)_B \tag{3-215}$$

$$S_P^{(new)} = S_P^{(old)} \tag{3-216}$$

where $\left(c \frac{\partial \phi}{\partial n} \right)_B$ is the specified flux at the boundary.

The third type of boundary condition is the mixed or Robbin's type with the linear combination of the function value and normal gradient specified (for example, in a convective heat transfer calculation). Consider heat conduction occurring from node W in Fig. 3-11 to the boundary, where convection takes place with a heat transfer coefficient α. Then the required boundary condition (for steady state) is:

$$q = \alpha A_W (T_B - T_P) = k_B A_W \frac{T_W - T_B}{\delta_{WB}} \tag{3-217}$$

where k_B is the conductivity of the conducting media, T_B is the boundary temperature, and δ_{WB} is the distance between node W and the boundary. The boundary temperature can be eliminated in the above equation to give:

$$q = \frac{T_W - T_P}{\frac{1}{\alpha A_W} + \frac{k_B A_W}{\delta_{WB}}} \tag{3-218}$$

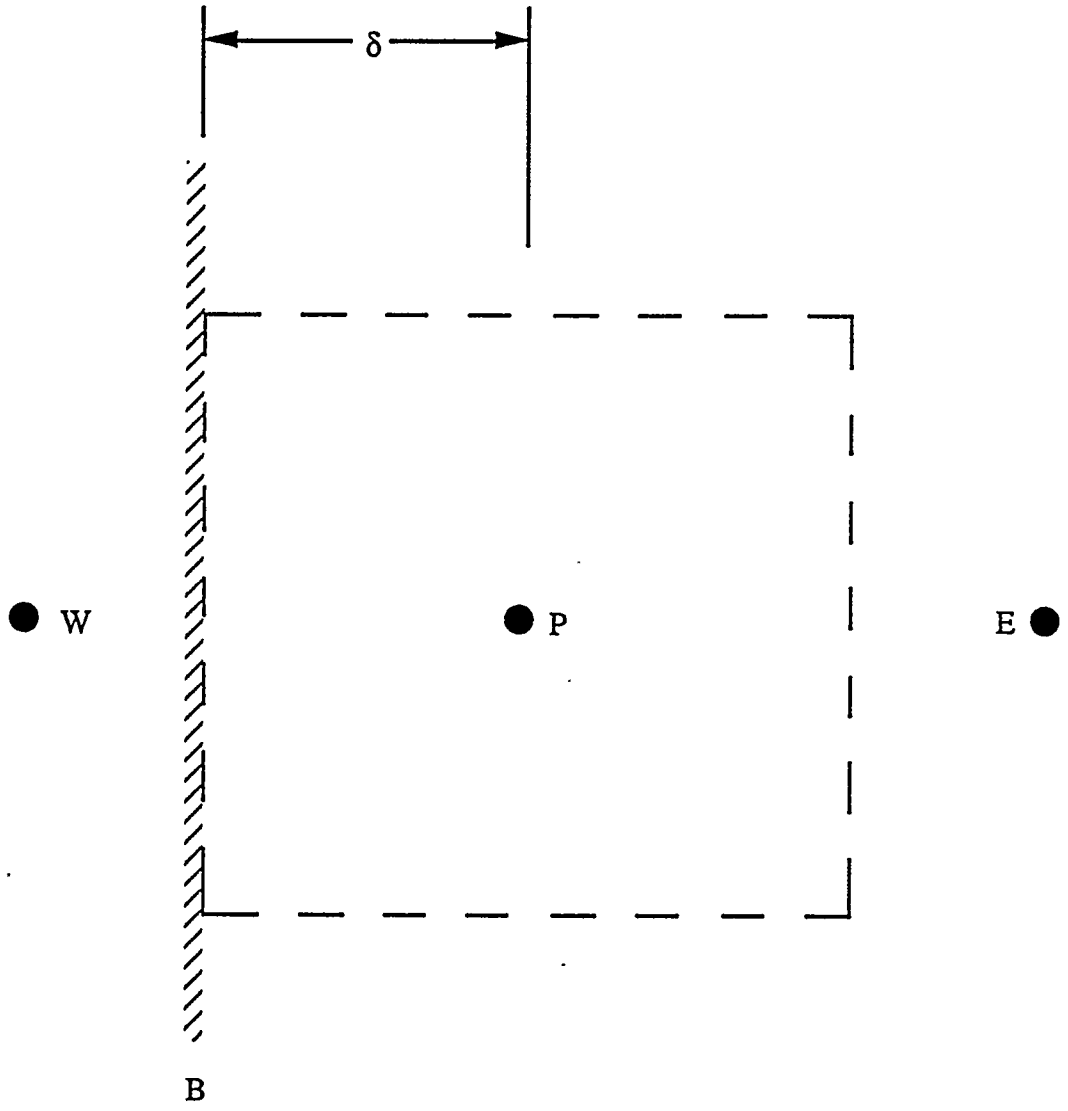

Fig. 3-11. A typical main boundary cell.

and the two source terms become:

$$S_U^{T(new)} = S_U^{T(old)} + \frac{T_W}{R_T} \tag{3-219}$$

$$S_P^{T(new)} = S_P^{T(old)} - \frac{1}{R_T} \tag{3-220}$$

where

$$R_T = \frac{1}{\alpha A_w} + \frac{k_B A_w}{\delta_{WB}} \tag{3-221}$$

Normally, PCGC-2 iterates on a rectangular domain (being controlled by FORTRAN do-loops) and if this domain contains node points which are outside the flow field domain, either the computer code can be altered to skip these nodes or the following technique can be employed to fix the value of ϕ at the node:

$$S_U = (\gamma \phi_p) \tag{3-222}$$

$$S_P = (-\gamma) \tag{3-223}$$

where γ is a large number (10^{30}) and ϕ_p is the value desired at the node point. Boundary conditions must be inserted for each boundary cell.

Numerical Diffusion

The hybrid differencing scheme introduces numerical errors in the convection terms of order OΔx) when upwind differencing is used and O(Δx^2) when central differencing is used. When upwind differencing is used, the error introduced from the finite-difference approximation can be viewed as an artificial numerical diffusion (Roache, 1976). This numerical diffusion is a function of the Courant number:

$$C_x = \frac{u\Delta t}{\Delta x} \tag{3-224}$$

If $C_x = 1$, the numerical diffusion terms will be identically zero (Roache, 1976), meaning that the finite-difference approximation is exact. The errors introduced by upwind differencing should be investigated by using a different finite-differencing scheme. Central-differencing, however, is thought to be unstable for elliptical partial differential equations (Roache, 1976).

Several authors (Leonard, 1979; Castro, 1978; Raithby, 1976; Argarwal, 1981; Leschiziner, 1980; Lillington, 1978) have developed methods to eliminate numerical diffusion in simple flow systems. Significant numerical diffusion has been shown to arise in predictions where convection dominates physical diffusion and where there is a streamline-to-grid skewness (Leschiziner, 1980). The above-referenced predictions were made when the streamlines were at a 45-degree angle to the grid. Significant numerical diffusion has also been reported when gradients exist normal to the streamlines in the dependent variable and source terms (Lillington, 1978). It was also noted that higher-order differencing schemes could have poor convergence in some elliptical flow regimes. Raithby (1976) found that numerical diffusion was significant only when the source terms take a certain form and if the streamlines were skew to the grid. Leonard (1979) showed predictions where significant numerical diffusion occurred when streamlines were at an 18-degree angle to the grid. Leonard and co-workers also argued that their scheme allows larger grid spacing since it was more accurate.

Fletcher (1983) incorporated the method of Leonard (1979) into PCGC-2 to determine the effect of numerical diffusion in typical PCGC-2 predictions. The basis for the differencing scheme of Leonard (1979) is a second-order interpolation scheme for the values for the variable of interest (ϕ) at the cell wall. The predictions made using Leonard's higher-order differencing scheme required 10 to 15 times the computational time required for the prediction made using upwind differencing. The results for the non-reacting flow system indicated that numerical diffusion does not seriously affect PCGC-2 predictions, and that the hybrid differencing prediction is sufficiently accurate for this particular flow system. However, it is important to note that this observation was made for only a single computation, and was not achieved in a reacting or particle-laden system.

The negligible effect of numerical diffusion is somewhat surprising, since the streamlines in the recirculation zone of the reactor were definitely skew to the grid. Roache (1976) states that if the grid size is small enough, the effects of numerical diffusion will not be significant. He also says that a free outflow boundary condition (such as that used in PCGC-2) tends to reduce upstream error in elliptical systems.

In light of these results, the effects of numerical diffusion in PCGC-2 predictions for this particular geometry (namely the BYU Combustor) are thought to be of secondary importance. The higher-order differencing algorithm of Leonard (1979) was not used in PCGC-2 for any other predictions. Other higher-order differencing methods should not be used unless they are first demonstrated for reacting flows.

Boundary Conditions

A discussion of the numerical approach used in PCGC-2 is not complete without a discussion of the boundary conditions for all of the equations used. Each variable must have a boundary condition specified at each of the boundaries for elliptic equations. Symmetry conditions are imposed along the centerline, while other types of boundary conditions must be specified at the reactor walls, inlets, and exits.

Inlet Streams

The inlet mass flow rate is used to set the inlet velocities, with assumed parallel injection ($v_{pri}=v_{sec}=0$). This gives a Dirichlet condition for u and v. Turbulence intensities must be specified for the inlet streams in order to get Dirichlet boundary conditions for k. Turbulence intensities are defined as follows:

$$I=\frac{\left[\overline{(u')}^2+\overline{(v')}^2\right]^{\frac{1}{2}}}{\left[\bar{u}^2+\bar{v}^2\right]^{\frac{1}{2}}}=\frac{[2k]^{1/2}}{\|\vec{v}\|} \tag{3-225}$$

where $\|\vec{v}\|$ is the magnitude of vector $\vec{v}$. Since $\bar{u}$ and $\bar{v}$ are known in the inlet streams, k is specified when I is set. The dissipation level (ε) must be estimated at the inlet from empirical correlations (Syed and Sturgess, 1980):

$$\varepsilon=\frac{C_\mu k^{1.5}}{0.03D_e} \tag{3-226}$$

where D_e is the effective inlet diameter. The mixture fraction is known by definition in each of the inlet streams, and the mixture fraction fluctuations (g_f) are assumed zero in the inlet streams. The coal is not allowed to react in the inlet streams, so that η and g_η are both zero at the inlet boundary.

PCGC-2 is coded to allow user-specified inlet profiles of u, v, w, r, k, and ε in both the primary and/or secondary streams. Theoretical or experimental velocity profiles can be used. Theoretical inlet velocity profiles are calculated according to Bird, et al. (1960). The inlet velocity profile is normalized to match continuity with the specified inlet mass flowrate.

Centerline

Symmetry conditions are imposed at the centerline on all variables, meaning that the radial component of the gradient of any variable is zero $\left(\frac{\partial \beta}{\partial r} = 0\right)$ at the centerline. This specifies a Neumann condition at the axis or symmetry for all variables. The only exception to this rule is the radial radiation flux (F_r). The quantity (rF_r) is assumed zero along the centerline.

Outlet Stream

The radial component of the velocity $(\vec{v})$ is set to zero at the reactor exit, while the axial component $(\vec{u})$ is adjusted to satisfy over-all continuity with the inlet gas mass flow rates. The outlet values of f and η are set to force continuity with the inlet particle mass droplet flow rate. It is assumed that all of the other variables have smooth axial profiles at each radial location near the reactor exit. The outlet condition for these variables is determined by setting the axial gradient equal to zero.

Walls

The wall boundary conditions are of special interest. Of course, it would be possible to use parabolic boundary layer equations and solve them all the way to the wall; however, to reduce computer storage and run times, it is convenient to bridge over the wall region. The Van Driest hypothesis on turbulent flow near a wall is used to derive wall functions which are consistent with the logarithmic law of the

wall. Launder and Spalding (1972) outline the derivation and Patankar and Spalding (1970) give more details. In this way the dependent variables at the wall are linked to those in the logarithmic region (also see Khalil et al., 1975). For the velocity component normal to the wall in question, a Neumann condition is used and the gradient is set equal to zero (i.e., $\partial v/\partial r = 0$ for the north wall). For the component of velocity parallel to the wall in question, a no-slip boundary condition is assumed. A Dirichlet condition is imposed and the velocity component is set equal to zero (i.e., $\bar{u} = 0$ for the north wall; however, in this near-wall region, the fully developed turbulent exchange coefficient is not valid, and an exchange coefficient (effective turbulent viscosity) is calculated from the logarithmic law of the wall as given below and derived by Launder and Spalding (1972) (for a north wall, u velocity):

$$\Gamma_u = \mu_e = \frac{\tau_w \Delta r}{\Delta u} = \frac{\tau_w \Delta r}{u_p} = \frac{\rho C_\mu^{1/4} k^{1/2} \kappa \Delta r}{ln\left[\frac{E C_\mu^{1/4} k^{1/2} \Delta r \rho}{\mu}\right]} \tag{3-227}$$

When the reactor is non-adiabatic and convective/conductive heat losses must be considered, a Neumann condition is specified for the enthalpy *(h)*. The normal derivative is calculated from a universal temperature profile in the logarithmic region for the near-wall turbulence (for the north wall)

$$\Gamma \frac{\partial h}{\partial r} = -\left(\Gamma \frac{\partial h}{\partial r}\right)_w = -\left(\frac{C_p \Gamma \partial T}{\partial r}\right)_w = q_w \tag{3-228}$$

$$q_w = \left(T_p - T_w\right) \rho C_\mu^{1/4} k^{1/2} \sigma_{h,t} C_{pmix} \left[P + \frac{1}{\kappa} ln\left(\frac{E \Delta r\, C_\mu^{1/4} k^{1/2} \rho}{\mu}\right)\right] \tag{3-229}$$

where P is the extra resistance to heat transfer that arises due to the difference in σ_h and $\sigma_{h,t}$. Jayatilleke (1969) gives the following correlation for P:

$$P = 9.24\left[\left(\frac{\sigma_h}{\sigma_{h,t}}\right)^{3/4} - 1\right] \tag{3-230}$$

where $\sigma_{h,t} = 0.9$. Equation 3-230 was found to cause numerical instability in PCGC-2, apparently due to some nodes being too close to the wall. Rather than sacrifice the accuracy of the bulk flow solution by moving all nodes farther away from the wall, a constant value of unity is used for P. No instability is caused when P is non-negative. For $\sigma_h = 0.8$, the available data (Jayatilleke, 1969) are extremely scattered, and P ranges from -8 to +23. The value predicted by Eqn. 3-230 is -0.78, however the correlation is thought to be inaccurate at the low value of σ_h due to the scatter in the data. Therefore, a constant value of unity is reasonable. The quantity $\left[\Gamma(\partial h/\partial r)\right]_w$ is the total turbulent flux of enthalpy to or from the wall and is the quantity needed by the numerical scheme for the Neumann condition.

At the walls, the normal derivative of the turbulent energy is zero:

$$\frac{\partial k}{\partial x_i} = 0 \tag{3-231}$$

However, the production of turbulent kinetic energy *(P)* and the dissipation *(ε)* near the walls require modification. Near a wall in axi-symmetric, polar-cylindrical coordinates,

$$P_W = -\overline{u_x' u_x'}\frac{\partial \bar{u}_x}{\partial x} - \overline{u_r' u_r'}\frac{\partial (r\bar{u}_r)}{\partial r} + \frac{\tau_w}{\rho}\left(\frac{\partial \bar{u}_x}{\partial r} + \frac{\partial \bar{u}_r}{\partial x}\right) \tag{3-232}$$

When the wall is parallel to the u_x direction, $\partial \bar{u}_r/\partial x = 0$. For a wall perpendicular to u_x, $\partial u_x/\partial x = 0$. An extension of Eqn. 3-332 to include axi-symmetric, swirling flows is discussed by Lilly and Rhode (1982).

The wall shear stress (τ_w) can be estimated from turbulent Couette flow near a wall. The modified log-law is used:

$$u^+ = \frac{1}{\kappa} ln\left(Ey^+\right) \tag{3-233}$$

where

$$y^+ = \frac{y\rho\left(C_\mu^{\frac{1}{4}}k\right)^{\frac{1}{2}}}{\mu} \tag{3-234}$$

and

$$u^+ = \frac{\overline{u}}{\sqrt{\frac{\tau_w}{\rho}}} \tag{3-235}$$

Thus, the wall shear stress can be calculated directly:

$$\tau_w = \frac{\overline{u}\kappa\left(C_\mu^{\frac{1}{4}}k\right)^{\frac{1}{2}}\rho}{\ell n\left[\frac{E\Delta r\left(C_\mu^{\frac{1}{4}}k\right)^{\frac{1}{2}}\rho}{\mu}\right]} \tag{3-236}$$

Equation 3-336 is substituted for Eqn. 3-332 for the production of turbulent energy near a wall (P_w).

The dissipation rate at solid boundaries is harder to evaluate. In this case, it is suggested that the last node point in the flow field near a wall be set according to the following mixing length approximation.

$$\ell_m = \kappa\Delta y_i \tag{3-237}$$

where κ is a mixing length constant (= 0.42) and Δy_i is the distance from the wall:

$$\varepsilon = \frac{C_\mu^{\frac{3}{4}}k^{\frac{3}{2}}}{\kappa\Delta y_i} \tag{3-238}$$

The dissipation in the k-equation can also be altered accordingly. The wall boundary conditions on $\tilde{f}$, $\tilde{g}_f$, $\tilde{\eta}$, and $\tilde{g}_\eta$ are simply Neumann conditions of zero normal derivative ($\partial\phi/\partial r = 0$, or $\partial\phi/\partial x = 0$).

Summary

A summary of the boundary conditions for each variable is found in Table 3-1.

TABLE 3-1

PCGC-2 BOUNDARY CONDITIONS

	Primary jet	Secondary jet	Symmetry axis	North wall	South wall	West wall	East wall	Outlet
$\tilde{u}$	uniform at u_p, or profile	uniform at u_s, or profile	$\tilde{u}_{i,1}=\tilde{u}_{i,2}$	τ_w from wall function	τ_w from wall function	0	0	$\tilde{u}_{i,j}=\tilde{u}_{i-1,j}$
$\tilde{v}$	0, or profile	uniform at v_s, or profile	0	0	0	τ_w from wall function	τ_w from wall function	0
$\tilde{w}$	0, or profile	0, or profile	0, or $\tilde{w}_{i,1}=\tilde{w}_{i,2}$	τ_w from wall function	τ_w from wall function	τ_w from wall function	τ_w from wall function	$\tilde{w}_{i,j}=\tilde{w}_{i-1,j}$
$\tilde{k}$	from primary turbulence intensity	from secondary turbulence intensity	$\tilde{k}_{i,1}=\tilde{k}_{i,2}$	Near-wall values from wall function	Near-wall values from wall function	Near-wall values from wall function	Near-wall values from wall function	$\tilde{k}_{i,j}=\tilde{k}_{i-1,j}$
$\tilde{\varepsilon}$	from empirical correla-tions	from empirical correla-tions	$\tilde{\varepsilon}_{i,1}=\tilde{\varepsilon}_{i,2}$	Near-wall values from length scale	Near-wall values from length scale	Near-wall values from length scale	Near-wall values from length scale	$\tilde{\varepsilon}_{i,j}=\tilde{\varepsilon}_{i-1,j}$
g_f, g_η	0	0	$g_{i,1}=g_{i,2}$	$\tilde{g}_{i,1}=\tilde{g}_{i,j-1}$	$\tilde{g}_{i,j}=\tilde{g}_{i,j+1}$	$\tilde{g}_{i,j}=\tilde{g}_{i+1,j}$	$\tilde{g}_{i,j}=\tilde{g}_{i-1,j}$	$\tilde{g}_{i,j}=\tilde{g}_{i-1,j}$
$\tilde{h}$	uniform at h_p	uniform at h_s	$\tilde{h}_{i,1}=\tilde{h}_{i,2}$	q_w from wall function	q_w from wall function	q_w from wall function	q_w from wall function	$\tilde{h}_{i,j}=\tilde{h}_{i-1,j}$

TABLE 3-1 (continued)

	Primary jet	Secondary jet	Symmetry axis	North wall	South wall	West wall	East wall	Outlet
$\tilde{f}$	specified in input data	specified in input data	$\tilde{f}_{i,1} = \tilde{f}_{i,2}$	$\tilde{f}_{i,j} = \tilde{f}_{i,j-1}$	$\tilde{f}_{i,j} = \tilde{f}_{i,j+1}$	$\tilde{f}_{i,j} = \tilde{f}_{i+1,j}$	$\tilde{f}_{i,j} = \tilde{f}_{i-1,j}$	$\tilde{f}_{i,j} = \tilde{f}_{i-1,j}$
$\tilde{\eta}$	0	0	$\tilde{\eta}_{i,1} = \tilde{\eta}_{i,2}$	$\tilde{\eta}_{i,j} = \tilde{\eta}_{i,j-1}$	$\tilde{\eta}_{i,j} = \tilde{\eta}_{i,j+1}$	$\tilde{\eta}_{i,j} = \tilde{\eta}_{i+1,j}$	$\tilde{\eta}_{i,j} = \tilde{\eta}_{i-1,j}$	$\tilde{\eta}_{i,j} = \tilde{\eta}_{i-1,j}$

NOTE: Saying $\phi_{i,1} = \phi_{i,2}$, etc., is the differencing scheme for $(\partial\tilde{\phi}/\partial n) = 0$.

Generalized Geometry

The principal purpose of this section is to describe the treatment of axi-symmetric combustors with non-uniform cross-sections. Modern pulverized combustors and gasifiers and CWM combustors cannot always be represented in two dimensions using a cylindrical reactor vessel. Some reactors incorporate radiation baffles, "wasp waists," exit constrictions, and other extensions of the wall into the flow field. When modeling such reactors, the boundary conditions must be modified to account for these flow field "intrusions." PCGC-2 allows for generalized wall boundary conditions. Figure 3-12 shows sample reactor configurations that are possible with the code.

Approach

Eulerian gas phase equations are steady-state, yielding an elliptic system of partial differential equations. Such systems require boundary conditions at every boundary surrounding the flow domain. In a two-dimensional, axi-symmetric framework, boundary conditions are set at the inlets, along the centerline, along the exit, and along the walls. Cell faces are labeled like the directions of a compass (north, south, east, west) for ease of description. The flow chambers are generally modeled with inlets in the west wall, the centerline along the south boundary, and the exit along the east boundary, as if the reactor were horizontal.

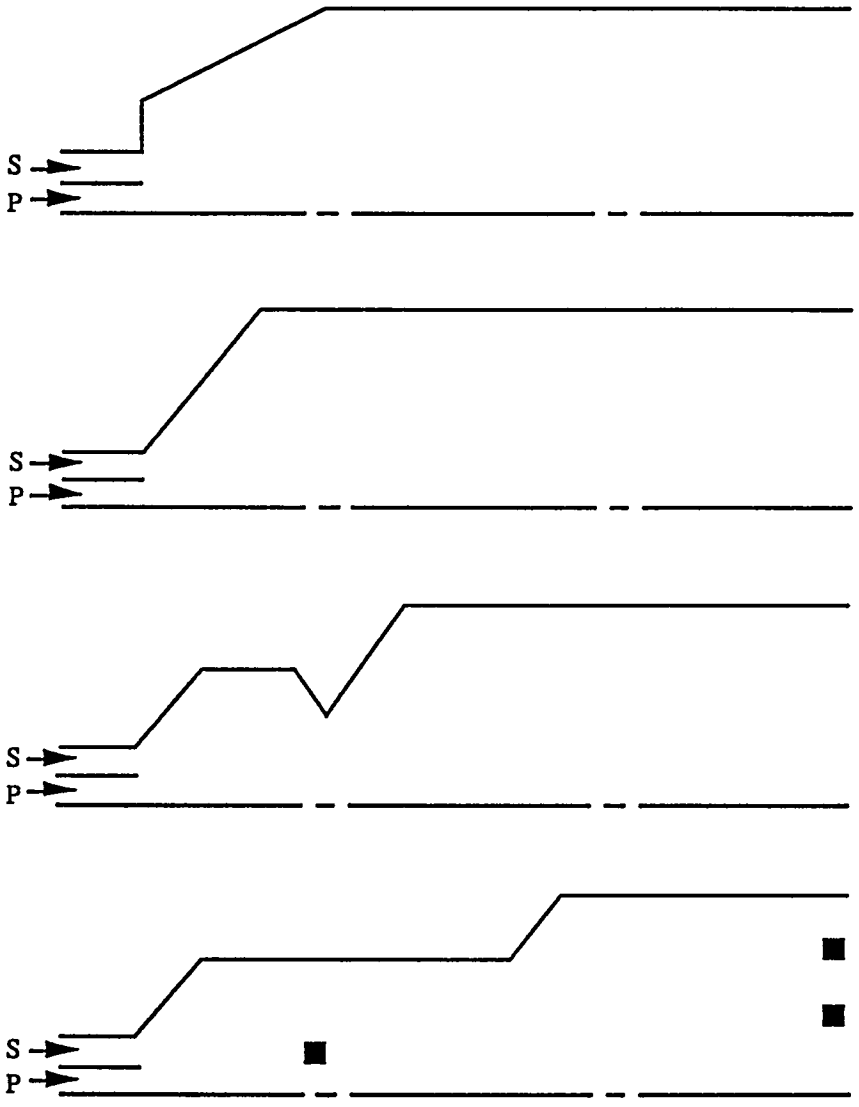

Figure. 3-12. Sample reactor configurations possible with modified PCGC-2. (■ are intrusions)

Gas phase equations are transformed into algebraic form using power-law finite differencing (Patankar, 1980). A staggered grid is used in the finite difference approach, with velocities stored at cell faces and other variables (e.g. density, mixture fraction) stored at cell centers. Figure 3-2 showed a sample grid used for PCGC-2 calculations.

Table 3-1 shows typical boundary conditions used in PCGC-2 for the main gas field variables. In this formulation, any deviation from the cylinder wall is termed an "intrusion" into the flow field. All intrusions must be symmetrical and around the centerline of the reactor. For example, a triangular exit constriction is modeled as a cone when rotated around the centerline.

Intrusions are allowed in any part of the computational domain, and need not be connected to the outer wall in this formulation. The only restriction to this geometric formulation is that each grid cell is rectangular (in two dimensions), and not triangular. This means that any smooth intrusions must be modeled in a saw-tooth manner, as shown in Fig. 3-13. In the limit, if grid spacing is small, smooth intrusions can be accurately modeled. However, computational time and memory requirements generally limit the fineness of the grid.

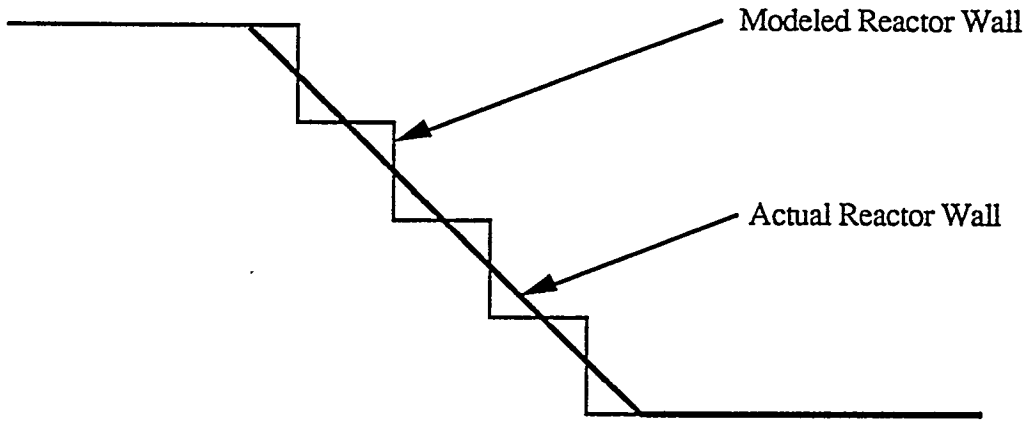

Figure 3-13. Example of saw-tooth representation of reactor wall.

Numerical Method

An arbitrary grid cell is pictured in Fig. 3-14 along with the eight adjacent cells. The center cell has location *X(I)* and *R(J)*, and the surrounding cells are therefore described in terms of *I+1*, *I-1*, *J+1*, and *J-1*. The array INTR(*I,J*) is defined to be 1 if the cell is an intrusion (wall) and 0 if the cell is part of the flow field. The value of INTR(*I,J*) is checked at each cell in the computational domain to see where the intrusions are located. When an intrusion is located, the boundary conditions of the surrounding cells are adjusted accordingly.

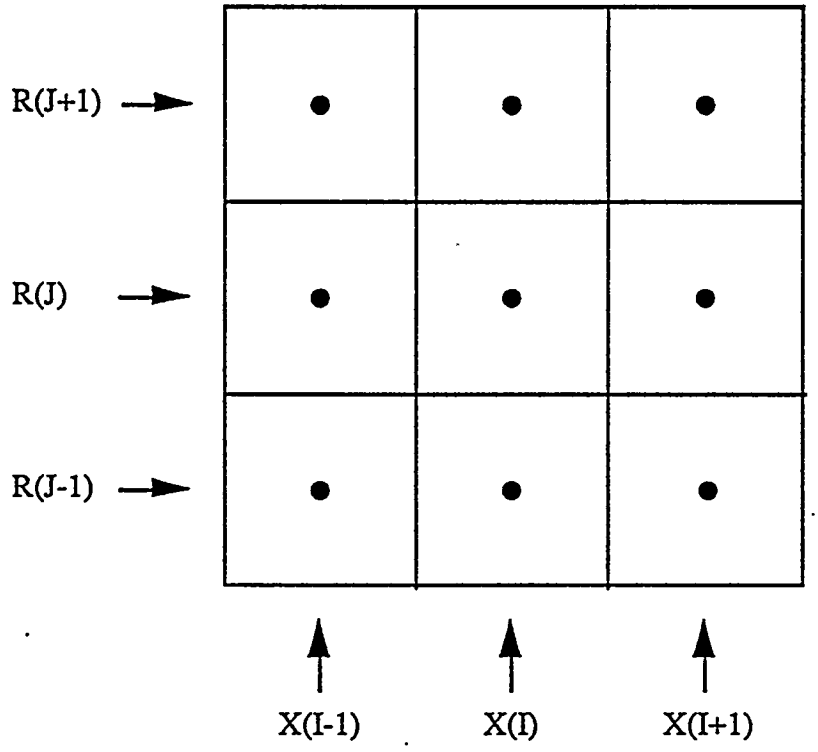

Figure 3-14. Arbitrary grid cell showing location of X, R, I and J.

Suppose that cell (I,J) is an intrusion and that we are solving the mixture fraction (F) equation. The value of $F(I,J)$ is set to zero as follows:

$$SU(I,J)=0 \tag{3-239}$$

$$SP(I,J)=-1.0\times 10^{30} \tag{3-240}$$

Table 3-1 indicates that boundary conditions are satisfied for the f equation by setting the gradient at the wall to zero. For the f equation, this done by setting the appropriate "A" coefficient (i.e. AE, AW, AN, or AS) to zero in the neighboring cell. For example, the north neighbor cell $(I,J+1)$ to an intrusion at (I,J) must have the south boundary modified so that

$$AS(I,J+1)=0 \tag{3-241}$$

Similarly, the other neighbor cells to an intrusion are modified as follows:

$$AN(I,J-1)=0 \tag{3-242}$$

$$AW(I+1,J)=0 \tag{3-243}$$

$$AE(I-1,J)=0 \tag{3-244}$$

If a neighboring cell is also an intrusion, the boundary between the cells is not modified at all, since Eqns. 3-239 and 3-240 negate the effect of the A coefficients.

Intrusions are used to describe the reactor walls as well as intrusions into the main flow field. When modifying the boundary conditions around the cells at the outer wall, care is taken not to exceed the dimensions of the arrays. For example at the north wall (I,NJ), the north neighbor cell is not used and hence is not modified.

All P-cell variables (w, k, ε, g_f, g_η, h, f, η, p, p') are adjusted for intrusions as described above using the boundary conditions from Table 3-1 and the north, south, east and west neighboring cells. However, since a staggered grid is used, u and v are defined on the faces of the P-cells. Intrusions are also defined on

the P-cells, which complicates the boundary conditions for u and v (U-cells and V-cells).

Figure 3-15 shows an intrusion with the u velocity locations at the neighboring cells. Both *U(I,J)* and *U(I+1,J)* are zero because they are located on the edge of the intrusion. The S_u and S_p terms are modified as shown in Eqns. 3-239 and 3-240 for these two cells. The east and west neighbor cell boundary conditions for the u velocity are set as follows:

$$AE(I-1,J)=0 \tag{3-245}$$

$$AW(I+2,J)=0 \tag{3-246}$$

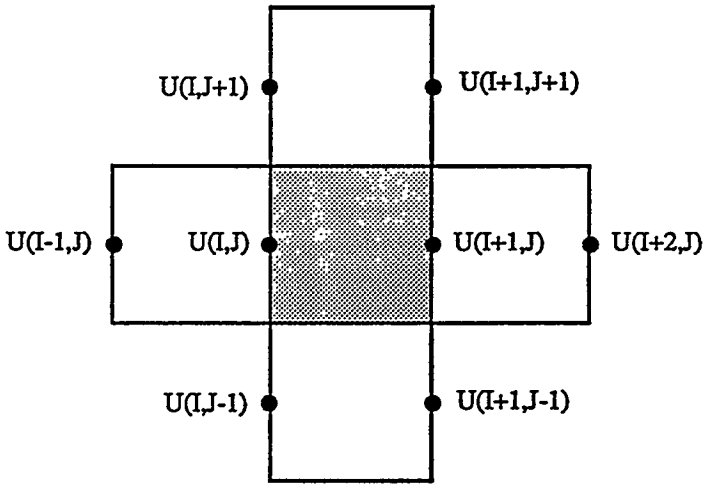

Figure 3-15. Arbitrary U-cell showing locations of cells affected by intrusion at (I,J).

For a single cell intrusion, u velocity boundary conditions must also be applied to the northeast, northwest, southeast, and southwest neighboring u cells. These boundaries are located at the corners of the intrusion, and hence have characteristics of both boundary cells and free flow field cells. Khalil et al. (1975)

suggest some type of averaging for the corner cells so that "inclined" walls can be modeled. The approach here is to treat the corner cells as if they were bounded by the wall along the entire cell boundary. The northeast (*I+1,J+1*) and northwest (*I,J+1*) U-cells therefore have south wall boundary conditions (see Table 3-1), and the southeast (*I+1,J-1*) and southwest (*I,J-1*) U-cells have north wall boundary conditions. In the course of development, these corner cells were also treated as free-flow field cells, but results did not merit the use of this approach.

Figure 3-16 shows an arbitrary V-cell with the location of the six neighboring V-cells. The ν at the north and south edges of the intrusions are set to zero for (*I,J*) and (*I,J+1*). The north and south neighbor cell boundary conditions simply become:

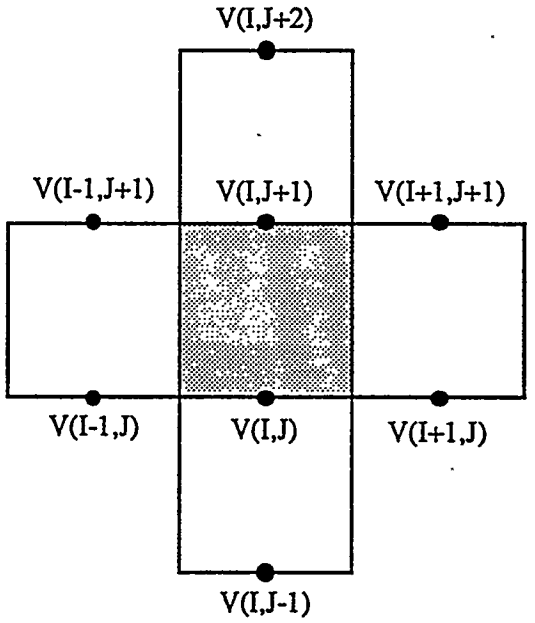

Figure 3-16. Arbitrary V-cell showing locations of cells affected by intrusion at (I,J).

$$AN(I,J-1)=0 \tag{3-247}$$

$$AS(I,J+2)=0 \tag{3-248}$$

The northeast ($I+1,J+1$) and southeast ($I+1,J$) V-cells have west wall boundary conditions based on the logarithmic wall function (see Table 3-1) and the northwest ($I-1,J+1$) and southwest ($I-1,J$) V-cells have east wall boundary conditions.

Input and Output for Intrusions

The locations of the intrusions in the flow field are read from the grid data file (also used to read in the locations of grid points). A sample grid data file is shown in Appendix G. A two-dimensional array of *X*'s and *O*'s is found at the bottom of the grid data file; the *X*'s represent intrusions and walls and the *O*'s represent the free flow field. This two-dimensional array is also used to govern the location of the additional inlets, as described in the next section. Each location in this two-dimensional array represents a single computational cell, and the *x-y* coordinates of the cells are given at the top of the grid file.

There are two logical parameters that govern the use of the intrusions in the flow field: INRDGD and INTRUS. Table 3-2 shows how these two variables affect the code operation. When starting from scratch (without a restart), setting both variables to .FALSE. will allow the code to generate a new grid data file which can then be modified to allow for intrusions. The modified grid data file will then be used with both variables .TRUE. in order to read the data file and look for intrusions.

TABLE 3-2

USE OF FORTRAN INPUT VARIABLES INRDGD AND INTRUS

INRDGD	INTRUS	Reads New X's & Y's	Reads New Intrusions	Allows (INQRL=T)	Writes Out New Grid File (GRDOUT=T)
T	T	yes	yes	yes	yes
T	F	yes	no	yes	yes
*F	*T	no	no	yes	yes
F	F	no	no	\ yes	yes

*Use of these variables not recommended with these values.

Additional Inlets

The principal purpose of this section is to describe the formulation which permits multiple feed streams at arbitrary locations along the combustor boundaries. A primary stream located symmetrically about the centerline, one secondary stream, and up to three additional streams in either the north or west walls of the reactor vessel are allowed. Any stream can contain particles or droplets. Figure 3-17 shows sample feed stream configurations possible with the code. Since this is a 2-D, axi-symmetric formulation, all geometries must be rotated around the centerline. A north wall inlet, therefore, is really modeled as a slit all the way around the outer reactor wall.

Approach

Table 3-1 showed boundary conditions used for the primary and secondary streams. Additional inlets along the west wall have similar boundary conditions, except for the inlet gas mixture fraction *f*. As discussed previously in the approach to gas phase chemistry, only two mixing variables are solved. This allows definition of three independent sources of mass to the gas phase. Inlet compositions and temperatures for all inlet streams must be a function of the two mixing variables. Since one mixing variable η is generally used to account for coal off-gas, the inlets are usually specified with the remaining mixing variable *f*. For example, some inlets may contain high temperature air while others contain low-temperature air. The three sources of mass would then be 1) coal off-gas, 2) high-temperature air, and 3) low-temperature air. The mixture fraction would be the flow ratio of high-temperature air to total inlet air, and the *f* value for each inlet stream would determine the mixture of air entering the reactor from that stream. For CWM computations, all inlets are regarded as having the same composition and energy level, and *f* is the mass addition of water into the gas phase from the droplets.

The staggered grid used in PCGC-2 makes the determination of inlet velocities different from P-cell variables. For west wall inlets, grid node I=1 is a false boundary used to establish velocities. Figure 3-18 shows a west wall inlet with 3 different grid nodes in the axial direction. The velocity *U(1,J)* is specified by knowing the inlet mass flow rate, density, and cross-sectional area (in FORTRAN variables):

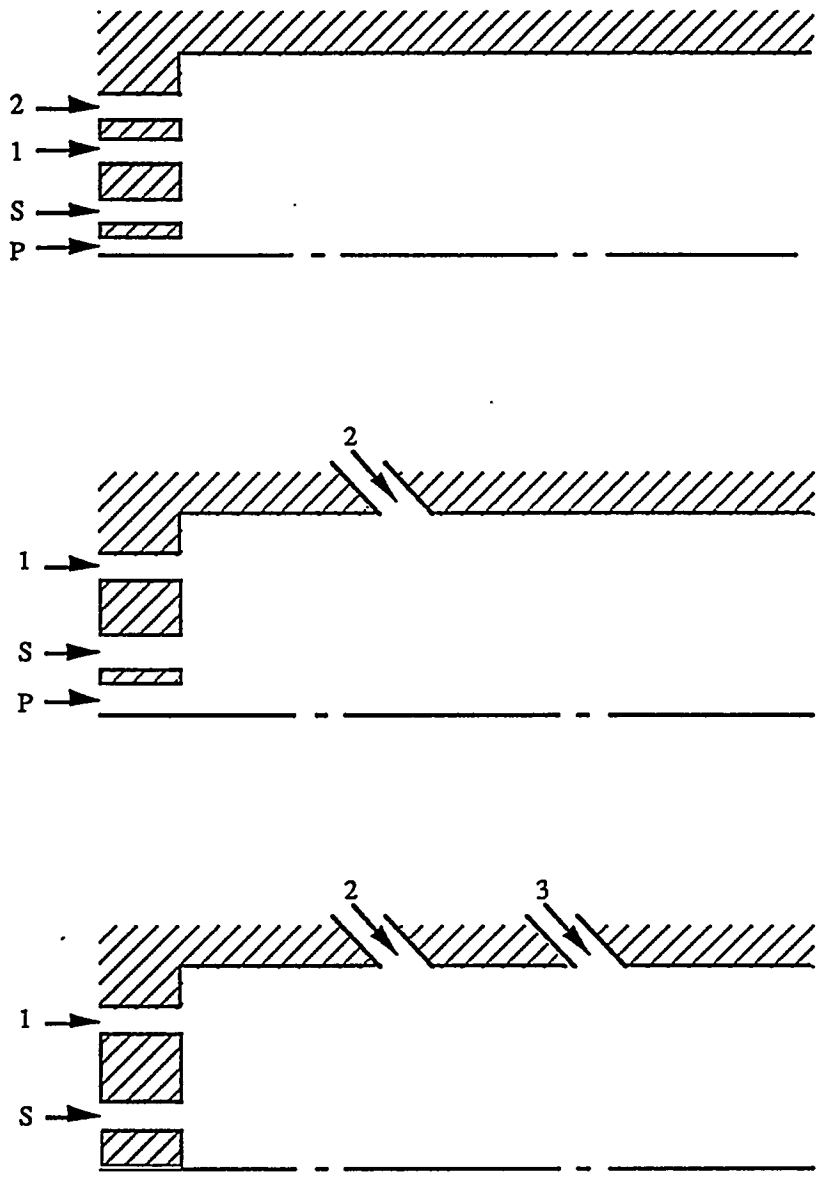

Figure 3-17. Example feed stream configurations.

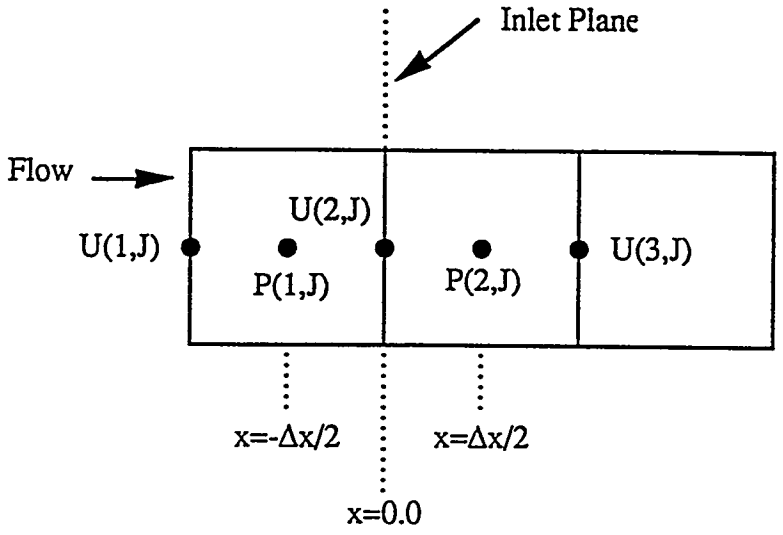

Figure 3-18. Axial grid locations for west wall inlets.

$$U(1,J) = \dot{m}_{cell} / RHO(1,J) / A_{cell} \tag{3-249}$$

The velocity at *U(2,J)* is different than *U(1,J)* due to a change in density, but continuity yields the following equation:

$$U(1,J) * RHO(1,J) = U(2,J) * [RHO(1,J) + RHO(2,J)]/2.0 \tag{3-250}$$

or

$$U(2,J) = U(1,J) * \frac{RHO(I,J) * 2.0}{RHO(1,J) + RHO(2,J)} \tag{3-251}$$

The value of *U(2,J)* changes at every gas phase iteration because *RHO(2,J)* changes.

Figure 3-19 shows a north wall inlet with 3 different grids in the radial direction. However, the maximum dimension on the *V* array is *NJ*, so the location of the *V(I,NJ+1)* is undefined. The array, *VINLT(I)*, stores the velocities in the false boundary above the north wall. The inlet velocity at the inlet plane is then:

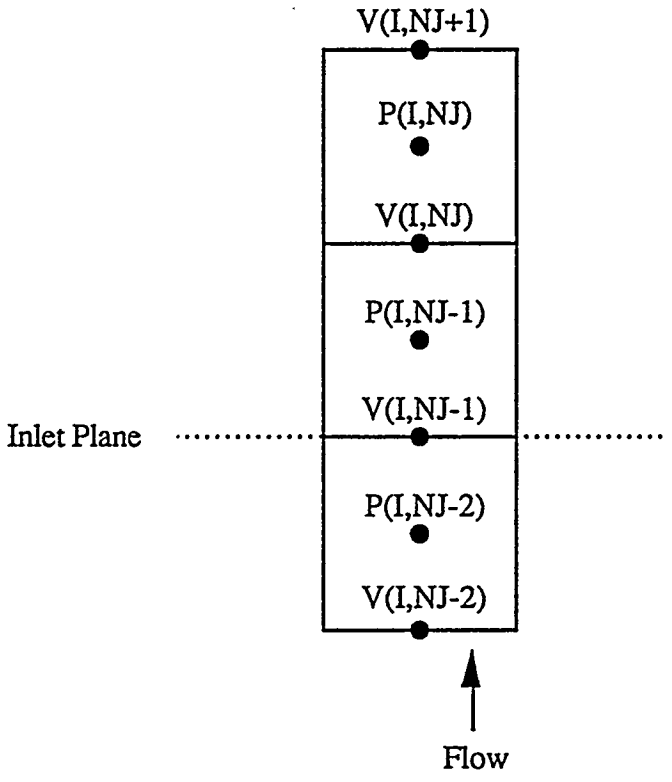

Figure 3-19. Radial grid locations for north wall inlets.

$$V(I,NJ) = VINLT(I) * \frac{RHO(I,NJ) * 2.0}{RHO(I,NJ) + RHO(I,NJ-1)} \qquad (3\text{-}252)$$

Provisions are made to allow for non-parallel injection in the additional inlets, but detailed velocity profiles in each additional inlet were not incorporated. The only detailed velocity profiles allowed are in the primary and secondary streams.

All inlets must be in the outer reactor shell with paths to the main flow field. Inlets are calculated only in the false boundary along the west and north walls. No inlets are permitted in the east wall (the east reactor wall is considered an exit).

Input and Output for Additional Inlets

A mixture fraction for each inlet stream, including primary and secondary streams is read from the main input data file. The f value in the primary and secondary streams need not be 1.0 and 0.0. Flow rates and turbulence intensities for each inlet stream are also read from the main data file.

The locations of the primary and secondary streams are read from the main data file, but the additional inlet stream locations are specified by the grid data file. P represents a cell in the primary stream, the S represents a cell in the secondary stream, and the numbers 1, 2, or 3 represent the first, second, or third additional inlets. Primary and secondary stream locations can be changed using either the main data file or the grid data file.

Gas Phase Properties

In Chapter 2, the theory was introduced for finding the mean turbulent properties such as species mole fraction, density, etc. The approach requires instantaneous values of the energy level (h) and the weight fraction of the elements (b_k) to be calculated from the instantaneous values of the mixture fraction and (in the case of non-adiabatic reactors) residual enthalpy. From this input, the Gibb's free energy is minimized to give the instantaneous local equilibrium properties. These properties are then convoluted over the complete probability density function with proper account for intermittency to produce the mean properties. This can be done for either Reynolds-averaging or Favre-averaging.

The largest computational portion of this algorithm is the equilibrium computations. Pratt and Wormeck (1976) have developed a code (CREK, Combustion Reaction Equilibrium and Kinetics) for either complex kinetic or equilibrium computations. This code was developed as a module for incorporation into larger fluid mechanics schemes. The approach for equilibrium computations is the same as was described in Chapter 2 of Pratt and Wormeck (1976). CREK was

used as a base but was stripped of all statements pertaining to the kinetic computations. The input was also restructured to receive local element mass fractions (b_k) as required by the above approach. The resulting submodel was named CREE (Chemical Reaction Equilibrium for Elements). The FORTRAN comment statements are profuse and with reference to Pratt and Wormeck (1976), the user explanation should be more than sufficient.

CREE is applicable to gaseous combustion or fuel-lean coal combustion. Because it does not treat condensed-phases, it does not give good predictions for fuel-rich coal systems (e.g. gasification) where solid carbon is a significant species at equilibrium. Therefore, another chemical equilibrium option has been provided based on the METCEC code developed by Nicoletti (1986). METCEC was based on the NASA-Lewis CEC code and properly accounts for condensed phases. It requires more time to converge than does CREE, and therefore both algorithms are provided as options in PCGC-2.

Computational efficiency is enhanced significantly by constructing table search procedures for the equilibrium properties. When the equilibrium properties are functions of only two independent variables (f and η), a table is constructed listing each property as a function of f and η. The inlet and coal gas mixture fractions are physically restricted to lie between the values of 0 and 1. A table is constructed once at the beginning of the code calculations using CREE. All subsequent calls for equilibrium properties are performed by interpolation within the table. The subroutine TABLE in PCGC-2 does all the table construction and retrieval. This subroutine uses knowledge of the stoichiometric mixture fraction for each η even though intervals of f may be different.

Chapter 2 showed how the PDF approach is altered when the system is non-adiabatic. In this case, the equilibrium properties are a function of three variables: the mixture fraction (f), the coal gas mixture fraction (η), and the residual enthalpy (h_r). The table look-up approach is still used; however, the table is three- rather than two-dimensional. Since the three-dimensional table is quite large, it is saved from one calculation to the next.

Two types of PDF's have been used in PCGC-2; a Gaussian distribution and a top-hat or uniform distribution. The Gaussian distribution produces slightly smoother gas property profiles, but the uniform distribution requires slightly less time to obtain a converged gas-phase solution. The present version of PCGC-2 uses only the Gaussian distribution.

The convolution of gas properties with a PDF requires numerical integration (see Eqn. 2-80). This integration is time-consuming because the particle properties have to be either repeatedly calculated or interpolated from a table of values (Smith, 1979). The integration must be performed with a minimum of function evaluations.

The method used to perform these integrations is five-point Gaussian quadrature (Abramowitz and Stegun, 1972). This method combines reasonable accuracy with a minimum number of function evaluations.

Intermittency for the Gaussian PDF is calculated as shown in Eqns. 2-47, 2-48, 2-82, and 2-83. It is easily seen that the equations for α give the area under the normal curve, which is tabulated in standard math handbooks. Tabulated values of the area under the normal curve were fitted using a cubic spline routine.

Radiation

Equation 2-141 is solved in each direction, forming a set of N differential equations (coupled pde's in DOM, uncoupled ode's in VFM). Due to the different forms of the working equations, the solution techniques used in the DOM and VFM are also quite different.

Discrete Ordinates Method (DOM)

The calculation is started at the top right-hand corner of the computational domain using the boundary conditions (Eqn. 2-143). The boundary condition on the axis is based on the conservation of flux (i.e., a reflective boundary). An initial estimate of the azimuthal component of intensity, before starting with the recursive solution scheme, is obtained by solving Eqn. 2-140 in the special direction where η_m=0.0. The solution thus obtained is assigned a zero weight. The directions of traverse are chosen so that the values of the direction cosines gradually increase, a change in the sign of the direction cosine signifying a reversal in the corresponding direction of integration.

The solution to the discrete ordinates equations must be obtained iteratively, as the calculated intensities enter the boundary conditions and the in-scattering term (Eqn. 2-140). Once the intensity at a cell-center is known (from Eqn. 2-154), the intensity at the downstream surface of the volume element can be obtained by extrapolation using Eqn. 2-153. However, the central differencing scheme used in Eqn. 2-153 often results in negative intensities (particularly in the presence of steep gradients, or where spatial resolution is not high enough). Such negative intensities are impossible on physical grounds, and my be avoided using a combination of central and upwind differencing (Truelove, 1978):

$$I_{i+1} = (1+f)\, I_m - f I_i, \; etc., \; {}^{0 \le f \le 1.0}_{\mu_m,\, \varepsilon_m > 0} \tag{3-253}$$

where f = 1.0 yields central differencing, and f = 0.0 yields pure upwind differencing. If negative intensities are encountered during calculations, f is gradually decreased from its initial value of 1.0 till the negativity is removed. For f = 0.0, the intensity is always non-negative, and special directions are not required to initiate the recursive solution.

In the case of a scattering medium, an approximate solution is first obtained without the in- and out-scattering terms. The scattering terms are then included as a perturbation to the approximate solution to obtain the final, converged solution for the absorbing-emitting-scattering case.

Varma Flux Method

The two ordinary differential equations (Eqns. 2-157 and 2-158) are cast into finite difference form as shown in Table 3-3. The 'C' coefficients are defined in Table 2-11. These equations are solved using a line-by-line technique as in the gas phase. The tridiagonal matrix algorithm (TDMA) gives an exact solution on each line. The radiation calculations generally converge quickly, and do not take much computational time relative to the gas-phase calculations. Axial symmetry is used for the centerline boundary condition, and the wall boundary conditions (see Eqn. 2-143) are treated in the same way as those for the gas-phase calculations.

TABLE 3-3

FINITE DIFFERENCE FOR THE RADIATION FLUX SUMS

ϕ	Equation
F_x	$A_p^x \phi_p = A_E \phi_E + A_W \phi_W + S_U^x$
F_r	$A_p^r \phi_p = A_N \phi_N + A_S \phi_S + S_U^r$

$$A_p^x = A_E + A_W - S_p^x$$

$$A_p^r = A_N + A_S - S_p^n$$

TABLE 3-3 (continued)

$$A_E = \frac{\Gamma_P + \Gamma_E}{2\delta x_{PE}}$$

$$A_W = \frac{\Gamma_W + \Gamma_P}{2\delta x_{PW}}$$

$$A_N = \frac{\Gamma_P + \Gamma_N}{2\delta r_{NP}}$$

$$A_S = \frac{\Gamma_S + \Gamma_P}{2\delta r_{PS}}$$

$$S_u^x = 2(C_3 F_r + C_4 I_b)(SEW)$$

$$S_u^r = 2r(C_3 F_x + C_4 I_b)(SNS)$$

$$S_p^x = (C_2 + C_1)(SEW)$$

$$S_p^r = (C_2 + C_1)(SNS)$$

Integration of Particle Equations

Approach

The particle source-in-cell (PSI-CELL) technique of Crowe and coworkers (Crowe et al., 1977) has been followed directly to account for the Lagrangian particle field in the Eulerian gas field. The procedure is outlined below:

1. The Eulerian gas field is solved without particles as described earlier.
2. The radiation field is solved using the flux method, as described earlier.
3. The Lagrangian particle field is solved with a representative number of trajectories and the particle source term field is calculated.
4. The gas field is solved with the updated particle source term field.
5. Step 2 is repeated and iteration continued until overall convergence is achieved.

The PSI-CELL technique is very efficient with respect to storage and computational time required. The only significant storage requirement is for the particle source term field. Steps 2 through 4 represent one "particle iteration" (steps 7 through 11 in Fig. 3-1). Convergence is achieved when the gas field does not change between particle iterations.

The Lagrangian particle equation of motion (Eqn. 2-19) is integrated once analytically to save computational time. The x-component of the equation can be written as

$$\frac{du_j}{dt} = \frac{\Gamma_d\left(u_g - u_j\right)}{\alpha_j} \pm g \qquad (3\text{-}254)$$

where the gravitational force term assumes the reactor is vertical (+ for down-fired, - for up-fired). Substituting Eqn. 2-21 for Γ_d and rearranging, Eqn. 3-353 becomes

$$\frac{du_j}{dt} = \frac{C_d Re}{24 t_j}\left(u_g - u_j\right) \pm g \qquad (3\text{-}255)$$

where C_d is given by Eqns. 2-22 through 2-24, Re is given by

$$Re = \frac{\rho_g \left\| \vec{v}_j - \vec{v}_g \right\| d_j}{\mu_g} \tag{3-256}$$

and t_j is given by Eqn. 2-30. Taking u_g and $\frac{C_d Re}{t_j}$ constant, Eqn. 3-255 may be integrated to obtain

$$ln\left[\frac{A\left(u_g - u_j^{new}\right) \pm g}{A\left(u_g - u_j^{old}\right) \pm g}\right] = -A(\Delta t) \tag{3-257}$$

where $A = \frac{C_d Re}{24 t_j}$. Equation 3-257 may be solved for u_j^{new} to obtain

$$u_j^{new} = u_g - \left(u_g - u_j^{old}\right) e^{-A(\Delta t)} \pm \frac{g}{A}\left(1 - e^{-A(\Delta t)}\right) \tag{3-258}$$

A similar treatment of the r-component of Eqn. 2-19 leads to

$$v_j^{new} = v_g - \left(v_g - v_j^{old}\right) e^{-A(\Delta t)} \tag{3-259}$$

where the gravitational force term is missing because of the assumed vertical orientation of the reactor. Equations 3-357 and 3-358 are integrated by the simple Euler method to obtain particle position as a function of time.

The simple Euler's method was found satisfactory for calculating the particle trajectory, but unsatisfactory for integrating the particle continuity (Eqns. 2-90 through 2-94) and energy (Eqn. 2-97) equations; hence, the modified Euler's method is used to integrate the latter. The step-size for the integration scheme must be small enough so that the particle does not cross more than one cell boundary between function evaluations. Step sizes must be small in regions of rapid coal reaction in order to achieve numerical accuracy, but large enough in all regions to be numerically efficient. PCGC-2 uses a self-adjusting step-size control based on the difference between the predictor and corrector of the modified Euler's method.

The diffusive component of particle velocity is determined from Eqn. 2-34:

$$\vec{v}_{jd} = -\Gamma_j \frac{\vec{\nabla}\,\overline{n}_j}{\overline{n}_j} \tag{3-260}$$

In practice, $\vec{\nabla}\,\overline{n}_j$ is difficult to calculate on the computer, because $\overline{n}_j$ is a large number. The calculation becomes inaccurate because of computer roundoff and taking the difference of two large numbers. To overcome this computer limitation, $\vec{\nabla}\,\overline{n}_j$ is calculated as follows:

$$\vec{v}\,\overline{n}_j = \overline{n}_j\,\vec{\nabla}\left(ln\,\overline{n}_j\right) \tag{3-261}$$

Equation 3-359 becomes

$$\vec{v}_{jd} = -\Gamma_j\,\vec{\nabla}\left(ln\,\overline{n}_j\right) \tag{3-262}$$

When a particle collides with the wall, the particle is allowed to 1) stick to the wall (in which case the particle trajectory calculation stops), or 2) bounce off the wall. The particles are arbitrarily allowed to exit from recirculation zones by setting the diffusion velocity to zero after three loops, if such a situation occurs.

Stiffness

Problems with stability occur in the integration of the energy equation when the integrand changes slowly. In such areas, oscillations in the energy level occur that generally increase in amplitude until solution is no loner feasible (these are called numerically "stiff" equations). When the integrand begins to change slowly, a numerical approximation is made in which the left-hand side and 3rd term on the right-hand side of Eqn. 2-97 are set to zero and the particle properties are solved with an algebraic equation for the temperature:

$$T_{pj} = T_g + \frac{Q_{rp}}{Nu_j\,\pi\,k_g\,d_j} \tag{3-263}$$

This equation can also be viewed from a physical standpoint. In downstream regions of the reactor, temperature gradients are small and radiation is the main cause of differences between gas and particle temperatures.

The particle energy stiffness assumption was validated by comparison with a prediction using very small step sizes. This stiffness assumption greatly decreases computational time for each trajectory without significant loss of accuracy. Care is taken to de-dimensionalize the criteria for employing the stiffness assumption in PCGC-2, in order to simplify manipulation by the user. Smith (1979) found that the errors introduced in 1-DICOG from the stiffness assumption are negligible, and that significant computational time is saved because larger integration steps can then be taken. The same conclusions are found true of the particle energy equation in PCGC-2 (Fletcher, 1980).

Particle Temperature

The particle temperature depends on its composition and enthalpy. All of the components of the particle, i.e. composition and enthalpy, are predicted as independent quantities. At each time step, these properties are used to solve for particle temperature. Because there are several options in the code for expressing the particle heat capacity and its dependence on temperature, an efficient and robust algorithm is used which is based on a combination of bisection and regula-falsi techniques.

Particle Reactions

Calculation of the particle reaction rates and heat fluxes is iterative. Oxidizer-char reaction rates (Eqn. 2-131) depend on the char mass transfer coefficient (Eqn. 2-134) which, in turn, depends on the transpiration parameter for mass transfer (Eqn. 2-133) and the reaction rate. The transpiration parameter and mass transfer coefficient are calculated using assumed reaction rates, and the reactions are then iterated on until converged. Under-relaxation is used to make the calculation more stable.

Particle-Gas Coupling

Mixed Eulerian-Lagrangian Particle Model

An information flow diagram for the mixed Eulerian-Lagrangian particle model is shown in Fig. 3-20. Eulerian particle number density is needed by the radiation

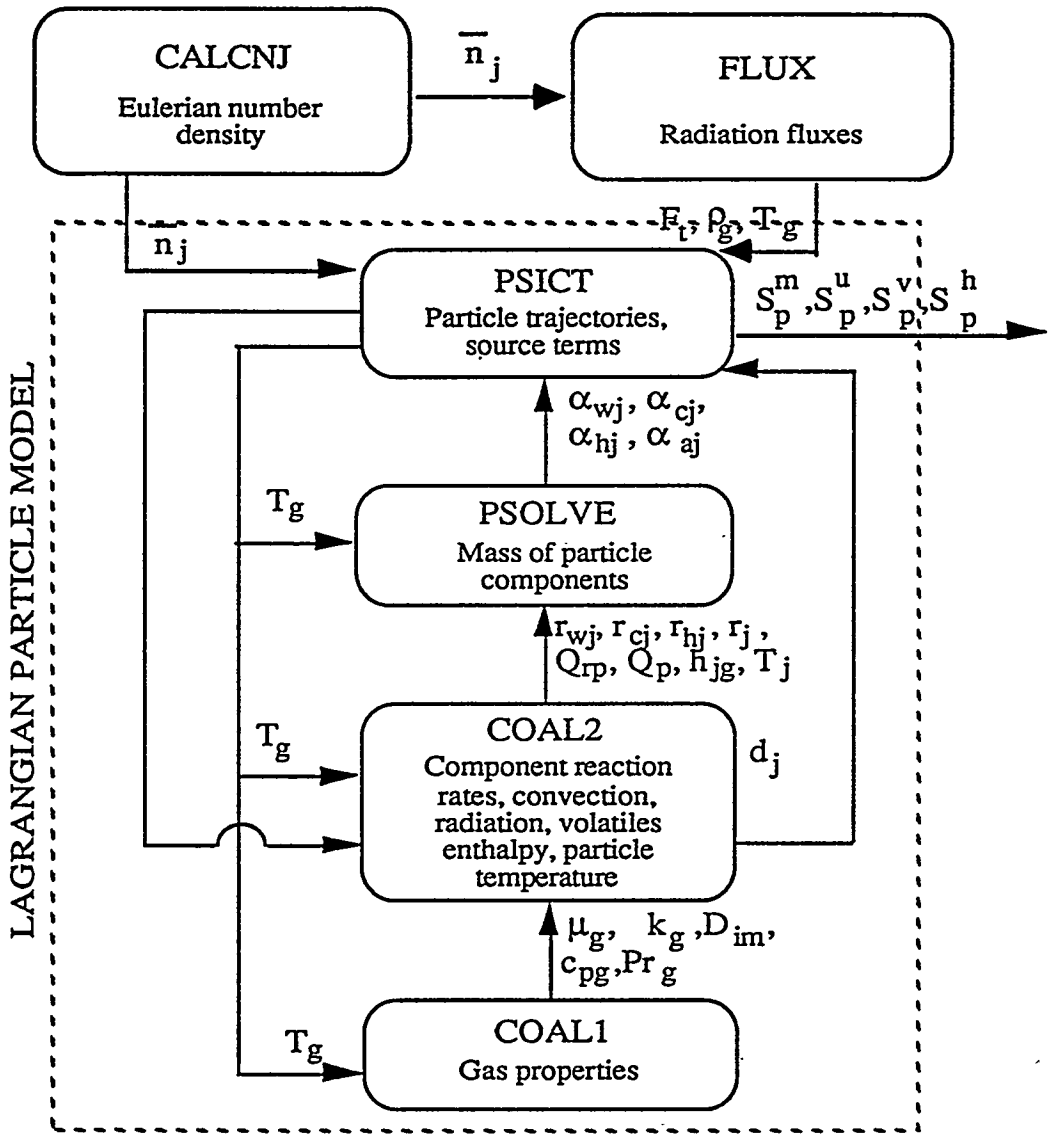

Fig. 3-20. Information flow diagram for mixed Eulerian-Lagrangian particle model.

submodel and the Lagrangian particle submodel for calculating turbulent particle dispersion. Four routines perform most of the calculations in the Lagrangian particle model. PSICT calculates the particle trajectories and gas-phase source terms. PSOLVE integrates the particle enthalpy and continuity equations. COAL2 calculates the coal and char reaction rates, rates of heat transfer to the particle, particle temperature, and coal volatiles enthalpy. COAL1 calculates the local gas properties needed by COAL2.

Particle Source Terms

The Eulerian gas phase equations are coupled to the Lagrangian particle phase equations through particle source terms $\left(S_p^m,\ S_p^u,\ S_p^v,\ S_p^h\right)$. The particle field is modeled as a set of discrete trajectories, where each trajectory represents a number of particles of uniform particle size and starting location in the primary jet. It is assumed that the particle number flow rate $\left(\dot{n}_{ij}\right)$ along a trajectory is constant, so that $\dot{n}_{ij}$ may be calculated from the initial mass flow rate of particles $\left(\dot{m}_{po}\right)$, the appropriate initial mass fractions representing particle size and location, and the initial particle mass $\left(\alpha_{jio}\right)$. The particle number flow rate of the i^{th} particle size and the j^{th} starting location is calculated from the input conditions as follows:

$$\dot{n}_{ij} = \frac{\dot{m}_{jo} X_{io} Y_{jo}}{\alpha_{jio}} \tag{3-264}$$

where X_{io} is the mass fraction of particles of the i^{th} particle size and Y_{jo} is the mass fraction of the j^{th} starting location.

The particle mass source (S_p^m) to the gas phase is the change in mass of all particles that traverse the particular cell of interest. For the k^{th} cell, this change is represented by:

$$\left(\Delta\dot{m}_{pij}\right)_{kcell} = \dot{n}_{ij}\left[\left(\alpha_{pij}\right)_{out} - \left(\alpha_{pij}\right)_{in}\right]_{kcell} \tag{3-265}$$

The mass source term is taken to be negative when the particle loses mass in order to fit the gas-phase sign convention. The mass source term is calculated from:

$$\left(S_p^m\right)_{kcell} = \left[\frac{\sum_i \sum_j \Delta \dot{m}_{pij}}{V}\right]_{kcell} \tag{3-266}$$

The particle momentum source term $\left(S_p^u\right)$ for the u component of momentum is similarly derived:

$$\left(S_p^u\right)_{kcell} = \left(\frac{1}{V}\sum_i \sum_j \dot{n}_{ij}\left[\left(u_{pij}\alpha_{pij}\right)_{out} - \left(u_{pij}\alpha_{pij}\right)_{in}\right]\right)_{kcell} \tag{3-267}$$

The equation for S_p^v is similar to that for S_p^u:

$$\left(S_p^v\right)_{kcell} = \left(\frac{1}{V}\sum_i \sum_j \dot{n}_{ij}\left[\left(v_{pij}\alpha_{pij}\right)_{out} - \left(v_{pij}\alpha_{pij}\right)_{in}\right]\right)_{kcell} \tag{3-268}$$

The particle energy source term $\left(S_p^h\right)$ represents the energy given to the gas-phase by the particles. The enthalpy of the solid phase changes by convection, reaction, and radiation. The change in solids enthalpy due to convection and reaction affects the enthalpy of the gas in the cell, but the change due to radiation does not. Therefore, S_p^h is calculated from the net change in solids enthalpy excluding the effects of radiation:

$$\left(S_p^h\right)_{kcell} = \left(\frac{1}{V}\sum_i \sum_j \dot{n}_{ij}\left[\left(h'_{pij}\alpha_{pij}\right)_{out} - \left(h'_{pij}\alpha_{pij}\right)_{in}\right]\right)_{kcell} \tag{3-269}$$

where h'_{pij} is a pseudo enthalpy for the particle that neglects the effects of radiation. It is calculated from Eqn. 2-97 with the radiation term removed:

$$\frac{d\left(\alpha_j h_j\right)}{dt} = Q_j - (1-\chi) r_j h_{jg} \tag{3-270}$$

It should be realized that Eqn. 3-368 includes the effects of chemical reaction.

It has been found that the particle mass source terms sometimes introduce instabilities into the program especially during the first few gas-phase iterations. Therefore, the source terms are under-relaxed according to Eqn. 3-202. A value of 0.5-0.7 is typically recommended for the under-relaxation factor.

Particle Number Density

The bulk particle number density couples the particle field with the gas field in two ways: turbulent particle dispersion, and radiation coupling between the phases. This is evident in Eqns. 2-33, 2-34, and 2-140. The equation for n_j is found in Chapter 2 (Eqn. 2-35). This equation does not fit the general form of the gas phase equations in Table 2-1 due to the missing density (ρ). As was noted in the earlier discussion of Eqn. 2-35, the u_j and v_j terms are replaced by u_g and v_g:

$$\frac{\partial}{\partial x}\left(r\bar{u}_g\bar{n}_j\right)+\frac{\partial}{\partial r}\left(r\bar{v}_g\bar{n}_j\right)-\frac{\partial}{\partial x}\left(r\Gamma_j\frac{\partial\bar{n}_j}{\partial x}\right)-\frac{\partial}{\partial r}\left(r\Gamma_j\frac{\partial\bar{n}_j}{\partial r}\right)=0 \qquad (3\text{-}271)$$

This equation is cast into finite difference form in a manner analogous to the other gas phase variables. Differences occur in the definition of the convection coefficients (C's) and in the two modifications. The resulting finite difference equation is shown in Table 3-4. This equation is solved using the TDMA.

In the calculation of Γ_j from Eqns. 2-28 through 2-32, the ratio α_j/d_j is required. In PCGC-2 this ratio is evaluated at the reactor inlet (α_{jo}/d_{jo}) and assumed constant. The boundary conditions for Eqn. 3-370 are shown in Table 3-5.

TABLE 3-4

FINITE DIFFERENCE EQUATION FOR $\theta=\bar{n}_j$

$$A_P\theta_P = A_E\theta_E + A_W\theta_W + A_N\theta_N + A_S\theta_S + S_U$$

where

$$A_P = A_E + A_W + A_N + A_S - S_P$$

TABLE 3-4 (continued)

$$A_E = D_E^* - \frac{1}{2}C_E$$

$$A_W = D_W^* + \frac{1}{2}C_W$$

$$A_N = D_N^* + \frac{1}{2}C_N$$

$$A_S = D_S^* + \frac{1}{2}C_S$$

$$D_d^* = max\left(D_d, \frac{-C_d}{2}, \frac{C_d}{2}\right) \text{ where } d = E, W, N, or\ S$$

$$D_E = \frac{\left(\Gamma_{\phi P} + \Gamma_{\phi E}\right)A_{ew}}{2\delta x_{PE}}$$

$$D_W = \frac{\left(\Gamma_{\phi P} + \Gamma_{\phi W}\right)A_{ew}}{2\delta x_{PW}}$$

$$D_N = \frac{\left(\Gamma_{\phi P} + \Gamma_{\phi N}\right)A_n}{2\delta x_{PN}}$$

$$D_S = \frac{\left(\Gamma_{\phi P} + \Gamma_{\phi S}\right)A_s}{2\delta x_{PS}}$$

$$C_E = A_{ew}u_E$$

TABLE 3-4 (continued)

$$C_W = A_{ew} u_P$$

$$C_N = A_n v_N$$

$$C_S = A_s v_P$$

$$S_U = -min\left[\left(C_E - C_W + C_N - C_S\right),\ 0\right]\phi_P^{old}$$

$$S_P = -max\left[\left(C_E - C_W + C_N - C_S\right),\ 0\right]$$

TABLE 3-5

BOUNDARY CONDITIONS FOR $\overline{n}_j$

Inlet:	primary:	$\overline{n}_j = \overline{n}_{jo}$
	secondary:	$\overline{n}_j = 0$
Side walls:		$\frac{d}{dx}\left(\overline{n}_j\right) = 0$
Top wall:		$\frac{d}{dr}\left(\overline{n}_j\right) = 0$
Symmetry Axis		$\frac{d}{dr}\left(n_j\right) = 0$
Outlet:		Quadratic upstream extrapolation

Nitrogen Pollutants Submodel

Algorithm

The equations in the NO_x model are similar in form to the Eulerian gas-phase equations, and use the same solution technique as described previously. The major difference in solution of the equations in the NO_x model is the calculation of the overall reaction rates in the species continuity equations for NO, HCN, and NH_3. The procedure and equations used to calculate these reaction rates in the NO_x model were described in Chapter 2.

The equations for the pollutant species are decoupled from the coal combustion model since small pollutant levels will not significantly affect the velocity, density, or temperature fields. However, the equations for the pollutant species are coupled with each other since the pollutant reaction rates are solved following convergence of the fuel oxidation calculations.

The solution algorithm of the NO model involves starting with a guess for the initial pollutant concentrations throughout the reactor. Fractional conversion variables are then calculated for each nitrogen pollutant species, O_2, and N_2. Next, integration of the instantaneous rates over the probability of fluctuating mixture fractions is made. The local instantaneous temperature is calculated by knowing unique values of f and η associated with each point in the Gaussian quadrature. Values of the instantaneous species are calculated by scaling the local instantaneous maximum or equilibrium concentrations by the appropriate local fractional conversion variable. Local instantaneous rates are next calculated for each reaction in the kinetic mechanism. The integrated rate expressions are then summed to obtain overall mean rates for each nitrogen pollutant species. Species continuity is then solved for HCN, NH_3, and NO using the routines available in PCGC-2. O_2, OH, and N_2 mass fractions are calculated by performing atom balances. The updated mass fractions are then used to re-calculate the reaction progress variables. Thus, the solution is iterative, converging on the concentration fields for HCN, NH_3, and NO. Figures 3-21 and 3-22 show a flow chart of this procedure.

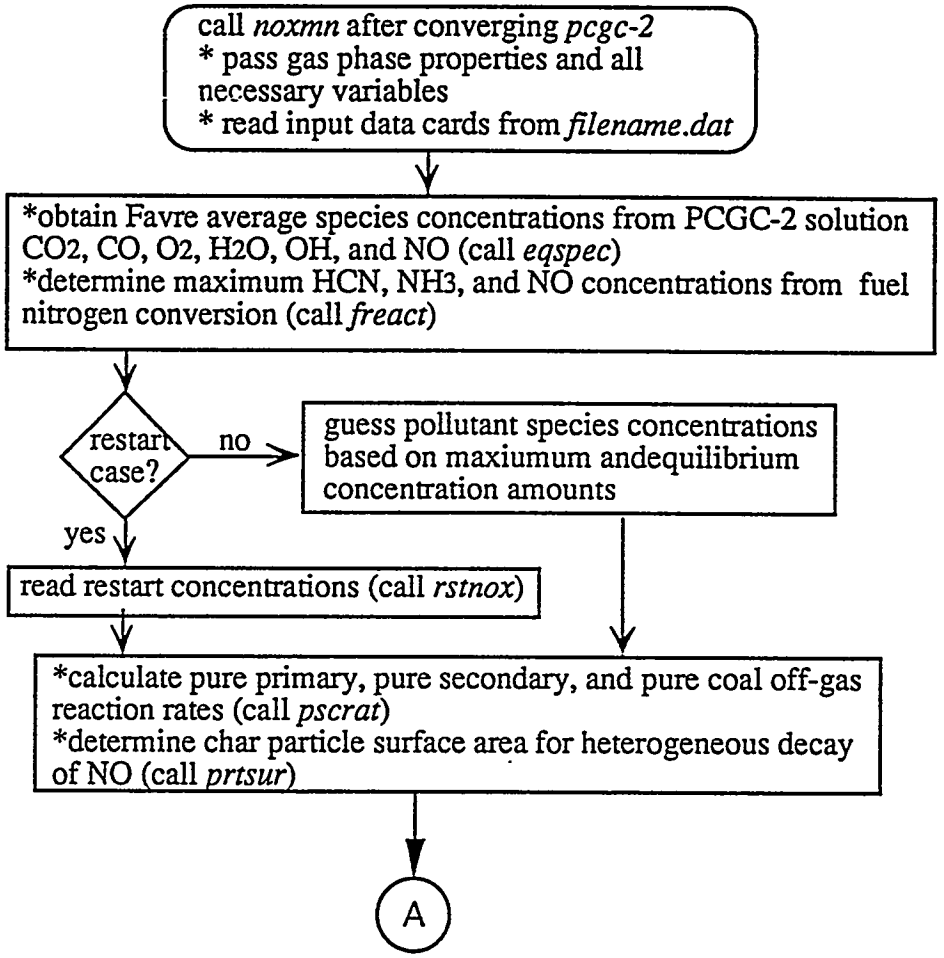
call *noxmn* after converging *pcgc-2*
* pass gas phase properties and all necessary variables
* read input data cards from *filename.dat*
*obtain Favre average species concentrations from PCGC-2 solution CO2, CO, O2, H2O, OH, and NO (call *eqspec*)
*determine maximum HCN, NH3, and NO concentrations from fuel nitrogen conversion (call *freact*)
restart case?
no
guess pollutant species concentrations based on maxiumum andequilibrium concentration amounts
yes
read restart concentrations (call *rstnox*)
*calculate pure primary, pure secondary, and pure coal off-gas reaction rates (call *pscrat*)
*determine char particle surface area for heterogeneous decay of NO (call *prtsur*)
A

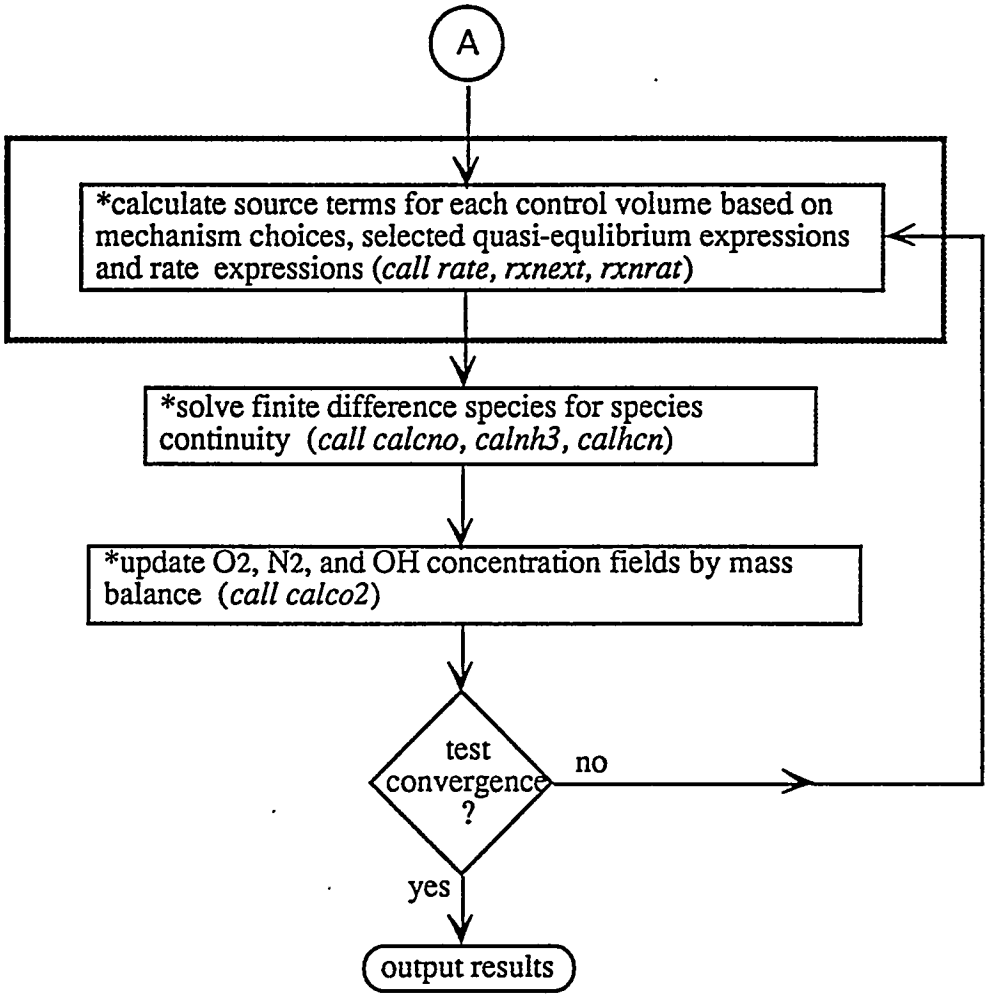

Fig. 3-21. NO_x model logical sequencing. Shaded box is expanded in Figure 3-22.

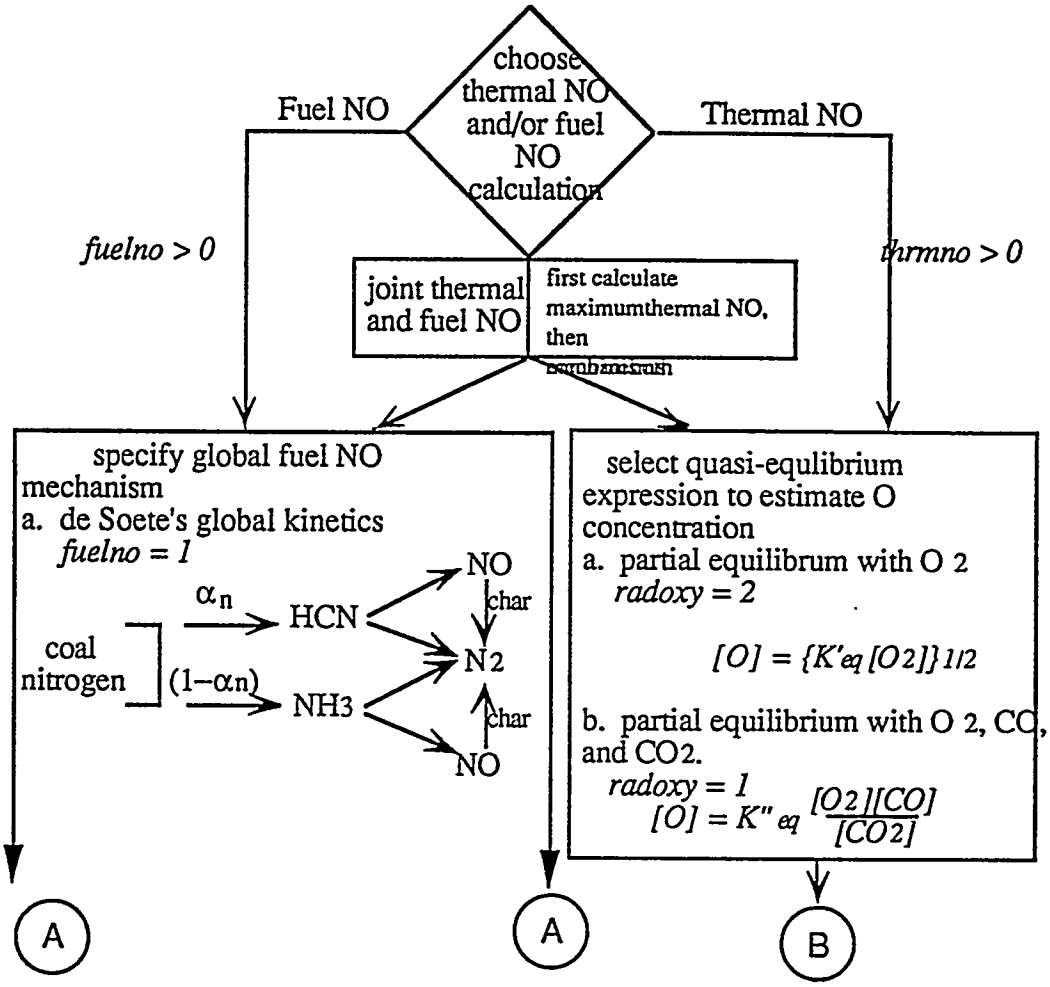
choose thermal NO and/or fuel NO calculation
Fuel NO
Thermal NO
fuelno > 0
thrmno > 0
joint thermal and fuel NO
first calculate maximumthermal NO, then
specify global fuel NO mechanism
a. de Soete's global kinetics
fuelno = 1
αn
HCN
NO
char
coal nitrogen
(1−αn)
N2
NH3
char
NO
select quasi-equlibrium expression to estimate O concentration
a. partial equilibrum with O 2
radoxy = 2
[O] = {K'eq [O2]} 1/2
b. partial equilibrium with O 2, CO, and CO2.
radoxy = 1
[O] = K" eq [O2][CO] / [CO2]
A
A
B

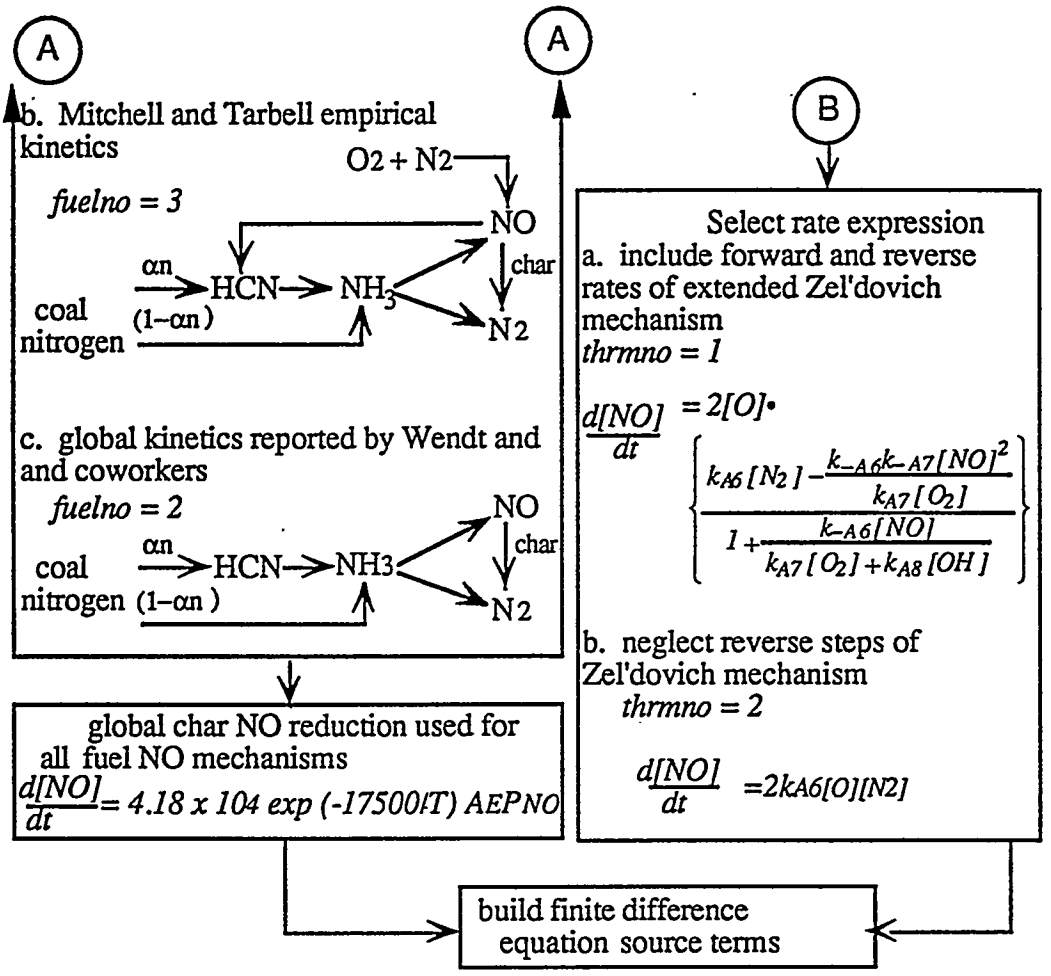

Fig. 3-22. Expansion of shaded box in Fig. 3-21. showing the alternative mechanisms and options available in the revised NO_x model. Input flags and values are discussed in the Chapter 5.

Sulfur Pollutants and Sorbent Reactions Submodel

The sulfur reactions submodel is also implemented as a post-processor to the comprehensive particle-gas flame calculations. An information flow diagram is shown in Fig. 3-23. After converging the reacting gas and particle flowfield, the sorbent model is called, and Eulerian gas properties are passed to it. Eulerian equations are then solved for sorbent particle number density, in a manner similar to the coal particles. Lagrangian trajectories representing ensembles of sorbent particles are then calculated, also in similar manner to the coal particles. The sorbent particles are allowed to react with either SO_2 or H_2S, providing source (sink) terms for the selected sulfur species. After calculating the sorbent particle trajectories and SO_2 or H_2S source (sink) terms, a continuity equation is solved for either SO_2 or H_2S, to distribute the effects of the capture throughout the flowfield. This provides a new concentration field for the sulfur species, and the sorbent particle trajectories and reactions are calculated again, providing new source terms, which are used to calculate a new sulfur species concentration field. This procedure is repeated until converged.

When calculating the new sulfur species concentration field, it is assumed that sulfur evolving from the coal forms SO_2 and H_2S in a ratio equal to that predicted for the reactor effluent gas at the conclusion of Step 1. Since there is no homogeneous chemistry considered in the submodel, there is no interconversion between SO_2 and H_2S, once formed. This leads to error in the prediction of sulfur species concentration in the fuel-rich region of a fuel-lean flame and in the fuel-lean region of a fuel-rich flame, but these regions are fairly small compared to the overall size of the combustor, and most sulfur capture occurs in the post-flame region. In fact, sorbent is often injected in the post-flame region in order to avoid the high flame temperatures that might cause sintering and loss of effectiveness.

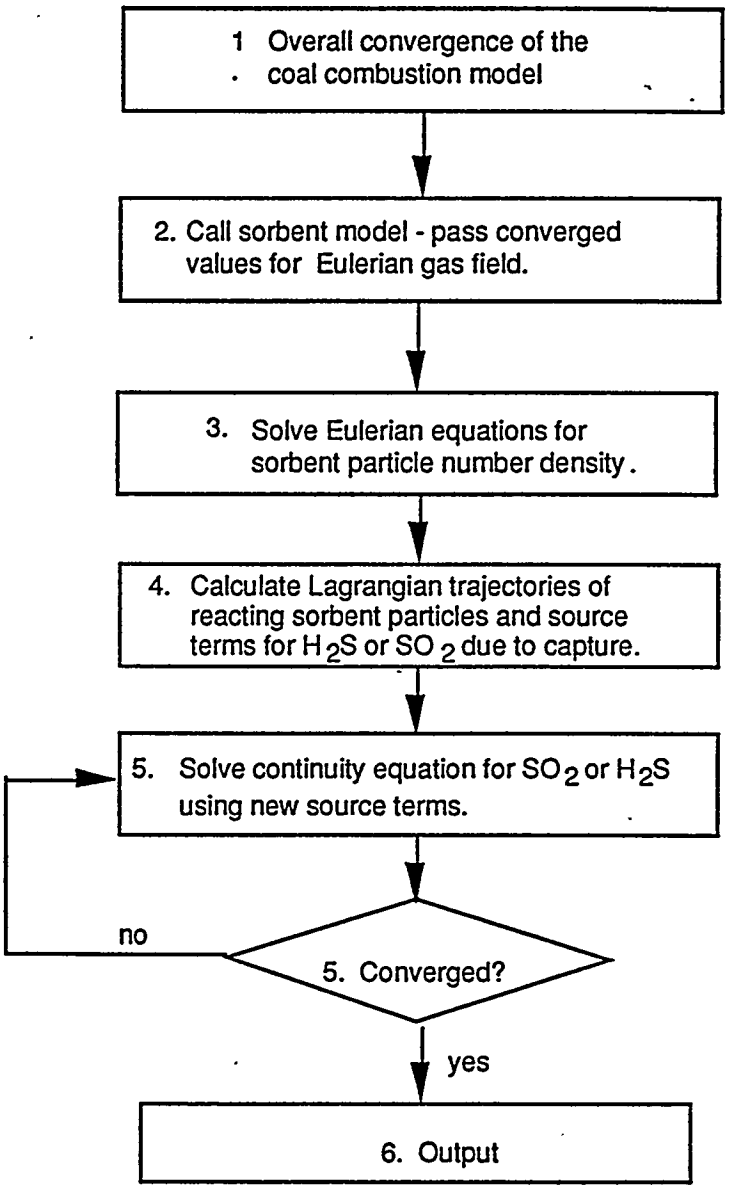

Fig. 3-23. Information flow diagram for the sorbent/sulfur capture submodel.

Chapter Four

Generalized Particle Reactions

This chapter presents a general description of FG-DVC, the model which simulates the coal thermal decomposition in the absence of oxygen, with its three submodels: coal viscosity, coal particle swelling and sulfur and nitrogen devolatilization. The coal reactivity model is discussed in this chapter as well. The nomenclature of all the variables in the equations of this chapter is given in Table 4-1.

FG-DVC Model Basis

FG-DVC is a general model for coal pyrolysis which predicts the coal's decomposition into tar, char, and gas, given the ambient pressure and the temperature history of an homogeneous coal particle. The model predicts the amount, functional group composition, elemental composition, and molecular weight distribution of tar and char and the amount and composition of the gas. The model is described in more detail in Appendices J-O.

The letters FG stand for Functional Group, and DVC for Depolymerization, Vaporization and Crosslinking. The FG model considers certain functional groups in the coal which decompose to form the light gas

species. At the same time, the DVC model describes the overall depolymerization of the macromolecular network which combines bridge breaking and crosslinking to produce fragments of the coal macromolecule. These fragments are then subjected to transport behavior, specifically the vaporization of the lightest fragments to form tar. The tar fragmentation process provides a second mechanism for the removal of functional groups from the coal. The model, whose parameters are determined in the laboratory at moderate temperatures and one atmosphere, can then be used to extrapolate away from the laboratory conditions to predict pyrolysis and combustion in high temperature reactions, or liquefaction at high pressure.

The model for coal thermal decomposition has six basic concepts.

- Functional Groups (decompose to produce light gases)
- Macromolecular Network (decomposes to produce tar and metaplast)
- Network Coordination Number (possible number of attachments per cluster)
- Bridge Breaking (limited by hydrogen availability)
- Crosslinking (related to gas evolution)
- Mass Transport of Tar (evaporation of light network fragments into light gases)

The first concept is that light gases are formed by the decomposition of certain functional groups in the coal. For example, methyl groups can lead to the formation of methane, carboxyl groups can lead to the formation of CO_2, etc. The second concept is that coal consists of a macromolecular network. This network is made up of fused aromatic ring clusters (which are described by their molecular weight) linked by bridges, some of which are relatively weak. There are some unattached parts of the network which can be extracted. Sometimes, there is also a second component of high polymethylene content. When heated, this network decomposes to produce smaller fragments. The lightest of the fragments evaporate to produce tar and the heavier fragments form the metaplast. These heavier molecules are the primary liquid fragments in liquefaction or the fragments that make coal fluid.

The third concept is that one of the most important properties of the network is its coordination number. The coordination number describes the geometry of the network, and specifies how many possible attachments there are per aromatic ring cluster. For example, a linear polymer chain has a coordination number of 2, because each fused aromatic ring has two possible attachments to link it in the chain. On the other hand, a square "fish net" has a coordination number of 4, because there are four possible attachments at each ring cluster. The coordination number controls the molecular weight distribution of the network fragments at a given extent of decomposition. The extent of decomposition is specified by the probability that the possible attachments are made. For example, for 20% of broken bridges, a linear chain is totally fragmented, while a "fish net" will have some holes but is almost totally connected. In describing the network, a crosslink is defined to occur at a branch point where there are more than two attachments on a ring cluster. The coordination number is thus related to the crosslink density. With no possible crosslinks, the coordination number is two. With increasing crosslink density the coordination number increases.

The second important property of the network is the fraction of possible attachments, p, which are actually present. During thermal decomposition, this fraction is determined by the rates of bridge breaking. The factors which control how many of the weak links can break are the rate constant and the amount of hydrogen that can be donated from the coal to stabilize the free radicals which form when the links break.

A competitive process with the bond breaking is the retrogressive process of crosslinking. Crosslinking reactions appear to be related to the evolution of certain gases. Specifically, for low rank coals, crosslinking at low temperature (prior to bridge breaking) seems to be related to the evolution of carbon dioxide. For coals of all rank, a higher temperature crosslinking event (following bridge breaking) seems to be related to the evolution of methane. At high temperatures, the evolution of hydrogen is also related to crosslinking.

The final concept is that the tar evolution is controlled by mass transport. Bridge breaking and crosslinking produce a set of fragments with a molecular weight distribution. The lightest fragments can leave the coal melt by evaporation

into the light gas species. The heavier fragments remain, forming the metaplast which controls the coal's fluidity. In the following sections, the descriptions of DVC and FG, and other coal chemistry submodels: viscosity, particle swelling, sulfer and nitrogen, and reactivity, are given. More details can be found in Appendices J and K for FG-DVC.

Depolymerization-Vaporization-Crosslinking (DVC) Formulation

The DVC model predicts the yield and molecular weight distribution of the tar, and the yield and molecular weight distribution, extract yield, and the crosslink density of the char. The theory describes the combined effects of: 1) **depolymerization and hydrogen consumption**; 2) **cross-linking**; and 3) **transport.** These processes, which are described below, are incorporated into a computer code which employs a percolation theory method for performing the statistical analysis(see Appendix L).

Process 1. Depolymerization and Hydrogen Consumption. Bond cleavage in coal is likely to be very complicated, including homolytic cleavage, ipso substitution, and hydrogen-transfer-induced bond-scission reactions for a variety of bond types. However, it has been observed that tar evolution is consistent with a narrow distribution of activation energies which allows consideration in the model of a single representative bridge (while acknowledging that other types may be present). Also, the rate for tar formation from coal, k_{tar}, is in good agreement with the rate determined for the breaking of ethylene bridges between naphthalene rings, k_B. This kinetic rate, k_B, employs an activation energy which is in agreement with resonance-stabilization calculations and an overall rate which agrees with previous measurements on model compounds. In view of these observations, a single type of bond (ethylene) undergoing homolytic cleavage is assumed for coal as a simple approximation of a complex behavior.

Bond cleavage is accompanied by the consumption of donatable hydrogens, H(al), to cap free radicals, along with corresponding carbon-carbon double bond formation at the donor site. For simplicity, the DVC model assumes all the coal's

donatable hydrogens, whether in bridges or in hydroaromatic rings, are in bridges, i.e., H(al) = (2/28)W_B, where H(al) is the weight fraction of donatable hydrogen and W_B is the weight fraction of labile bridges. This approximation will produce some error in tar yield since a broken bond in a hydroaromatic ring will not be as effective as a broken bond in a bridge in fragmenting the coal. But this effect will be compensated for, since H(al) is a parameter which is determined for each coal from a selected pyrolysis experiment. H(al) could, in principle, be determined by FT-IR or NMR, but not with sufficient accuracy.

The equation describing the disappearance of labile bridges in the char, W_B (char), due to bridge breaking and hydrogen donation is,

$$dW_B/dt = -2k_B W_B \qquad (4\text{-}1)$$

The value for k_B is the same as for tar formation, k_{tar} . The rate of decrease of labile bridges is twice the rate of bridge breaking since for each broken bridge, an additional labile bridge is converted to a non-labile bridge with the donation of hydrogen. By assuming that all the donatable hydrogens are in the labile bridges, the consumption of labile bridges and donatable hydrogens occurs simultaneously. The redistribution of hydrogen creates source and loss terms, dW_i(DVC)/dt, in the equations for the char functional groups W_i(char), as will be discussed with the FG part of the model (see Eq. 4-13).

Equation 4-1 only describes the loss due to bridge breaking and hydrogen donation. The loss of labile bridges due to evolution with the tar is computed by using the transport equations (Eqs. 4-3 and 4-7) discussed below.

Process 2. Crosslinking. Crosslinking reactions are important in describing the rank and heating rate dependence of the tar molecular weight distributions and yields. It appears that a correlation exists between gas evolution and crosslinking, which permits the rates for crosslinking and the number of crosslink sites to be related to rates and yields for gas evolution. The model assumes the following expression for the rate of increase of the number of crosslinks, per gram of coal, m

$$\frac{dm}{dt} = N_0 \left[\left| \frac{dW_{CO_2}(gas) \,/\, dt}{44} \right| + \left| \frac{dW_{CH4}(gas) \,/\, dt}{16} \right| \right] \quad (4\text{-}2)$$

where the rates, dW_i/dt, of evolution per gram of coal of CO_2 and CH_4 are calculated in the FG subroutine. N_0 is Avogadro's number.

Again, caution should be added that the reactions which have been assumed must be a gross simplification of a very complicated set of chemical reactions. This is especially true for the crosslinks occurring during methane formation, during which time there is extensive bond breaking and crosslinking accompanying tar formation.

Process 3. Transport. The external transport of tars from the particle surface to the bulk gas by vaporization and diffusion through a gas boundary layer is described with the model of Unger and Suuberg (Unger and Suuberg, 1981). The rate of evolution per gram of coal, $(dn_j/dt)_{ET}$, of oligomers of molecular weight M_j is given by

$$(dn_j \,/\, dt)_{ET} = (3/r_0^3 \rho) r D_j \chi_j^s \, (P_j \,/\, RT) \quad (4\text{-}3)$$

where r is the particle radius assumed to shrink with the cubic root of its mass and r_o is the initial particle radius, ρ is the particle density, χ^s_j is the mole fraction of species of molecular weight M_j in the metaplast at the surface of the particle, P_j is the vapor pressure for oligomers of molecular weight M_j (Fletcher et al., 1992),

$$P_j = 87{,}060 \exp\left(-299 \, M_j^{0.59}/T\right) \quad (4\text{-}4)$$

D_j is the gas-phase diffusivity of species of molecular weight M_j , R is the gas constant and T is the particle temperature.

For softening coals, the internal transport mechanisms include: i) the transport of tar molecules through the liquid to the surface; ii) the transit of bubbles containing tar from the interior of the particle to the surface; iii) the transport of tars within the liquid to the bubbles; and iv) the stirring action of the bubble evolution. For non-softening coals, transport occurs by v) convection and diffusion within the pores.

A common feature of mechanisms iii and v is that tars are transported out of the particle with the light devolatilization products which exit the coal via bubbles or pores. In the DVC model, we assume the upper limit for this process. This limit, which occurs when the tars achieve their equilibrium vapor pressure in the evolving gases, can be computed with few assumptions. In this case, the rate of transport, per gram of coal $(dn_j/dt)_{IT}$, for tar component j is proportional to the volume of gases evolved, dV/dt. That is

$$(dn_j/dt)_{IT} = P_j \chi_j^b \, (dV/dt) \, (1/RT) \qquad (4\text{-}5)$$

The volume of gases is proportional to the number of gas molecules and the temperature. It is inversely proportional to the pressure within the particle, $P_0 + \Delta P$ where P_0 is the ambient pressure and ΔP is the average pressure difference between the surface and the particle's interior. Then

$$dV/dt = \sum_i (dn_i/dt)_{gas} \left(\frac{RT}{P_0 + \Delta P} \right) \qquad (4\text{-}6)$$

where $\Sigma_i \, (dn_i/dt)_{gas}$ is the rate of production per gram of coal of gas components i summed over all gas and light tar species. For gas molecules, dn_i/dt is taken as the rate of production given by the FG model. For light tar molecules dn_i/dt is taken as the total amount transported out of the particle as tar computed in the previous time step. For computational efficiency, the sum has been limited to molecular weights less than 300 amu, since this accounts for over 90% of the volume. Combining the two equations with this approximation gives,

$$(dn_j/dt)_{IT} = P_j \chi_j^b \sum_{i<300} (dn_i/dt)_{gas} \left[\frac{1}{P_0 + \Delta P}\right] \qquad (4\text{-}7)$$

ΔP is used as an adjustable parameter which varies with the coal and experimental conditions. For the highly fluid Pittsburgh Seam bituminous coal, in cases where P_0 is one atmosphere or greater, we have considered the upper limit to this rate where $P_0 >> \Delta P$. Then all the terms in Eq. 4-7 can be determined by the combined FG-DVC model.

While $\Delta P = 0$ appears to be a good approximation for fluid coals at one atmosphere or more, $\Delta P > 0$ is expected for some coals and situations. ΔP is proportional to the coal's viscosity and so, will become important for less fluid coals. ΔP is also important when P_0 is small, for large particles and when the heating rates are very high. For non fluid coals, ΔP is very large due to the limited gas transport ability of these coals, while the highly fluid coals have a small ΔP. In the model, ΔP is 20 atm for non fluid coals and 0.2 atm for fluid coals.

Since we do not have a good method to determine χ^s_j, calculations are made assuming that the external-transport term can be neglected i.e.,

$$(dn_i/dt)_{tot} = (dn_i/dt)_{IT} \qquad (4\text{-}8)$$

This provides an excellent fit to the data for 50 μm diameter particles. It is likely that the external transport term will be increasingly important for smaller particles, but this will require better knowledge of the liquid phase diffusion coefficient, (mechanism i) and the stirring action of bubbles (mechanism iv).

The quantity needed for the FG part of the model [X] is given as:

$$dX/dt = -\sum_J (dn_j/dt)_{Tot} \bullet M_j/M \qquad (4\text{-}9)$$

where n_j is the number of molecules of molecular weight M_j in the tar, and M is the weight of the molecule being computed.

Functional Group (FG) Model Formulation

The Functional Group (FG) model permits the detailed prediction of the composition of volatile species (gas yield, tar yield and tar functional group and elemental composition) and of char (elemental and functional group composition). It employs coal dependent rates for the decomposition of individual assumed functional groups in the coal and char to produce gas species. The ultimate yields of each gas species are related to the coal's functional group composition. Tar evolution is a parallel process which competes for all the functional groups in the coal. There are three additional processes in the FG part.

Process 4. Gas Formation. The evolution of each gas species is assumed to be a first order reaction,

$$dW_i\ (gas)\ /dt \ = \ k_i\ W_i\ (char) \ = \ k_i\ XY_i \qquad (4\text{-}10)$$

where, $dW_i(gas)/dt$ is the rate of evolution of species i into the gas phase, k_i is a distributed rate for species i, and $W_i(char)$ is the functional group source remaining in the char. X is an arbitrary coordinate representing the extent of pyrolysis and is defined as the weight fraction of the char. It equals 1.0 at time zero(the beginning of the pyrolysis) and will reduce to a value between 1.0 and 0 at the end of the pyrolysis. Y_i is the weight fraction of i^{th} species in the char. This representation of pyrolysis can be well explained with Figure 4 in Appendix J.

We employ the concept of the distributed rate where k_i is given by an Arrhenius expression $k_i = k^0_i \exp(-(E_i \pm \sigma_i)/RT)$, where $\pm\ \sigma_i$ indicates that a Gaussian distribution is employed to describe the product sources, $W_i(E_i)$, as a function of the activation energies E_i.

$$W_i(E_i) = \frac{W^0{}_i}{(2\pi)^{1/2}\sigma_i} \exp(-\frac{(E_i-E^0{}_i)^2}{2\sigma_i^2}) \qquad (4\text{-}11)$$

E^0_i is the average activation energy and σ_i is the standard deviation of the Gaussian distribution.

Process 5. Tar Formation. The tar composition is tracked by summing the functional group contributions evolved with the tar. The rate of evolution of each contribution is:

$$dW_i\ (tar)\ /dt = (dX/dt)Y_i \qquad (4\text{-}12)$$

where $dW_i(tar)/dt$ is the rate of evolution of each functional group component with the tar.

Process 6. Char Formation. The change in the i^{th} char pool, $W_i(char)$, is computed by summing the losses to the gas and tar, and the redistributions determined in the DVC subroutine,

$$dW_i\ (char)/dt = -dW_i\ (gas)/dt - dW_i\ (tar)/d + dW_i\ (DVC)/dt \qquad (4\text{-}13)$$

where $dW_i\,(DVC)/dt$ includes the source and loss terms from the DVC model, given by $(30/28)k_BW_B$, $(2/28)k_BW_B$, $(24/28)k_BW_B$ and $-2k_BW_B$ for methyl, aromatic H, aromatic C, and labile bridge functional groups, respectively.

Percolation Theory

The coal macromolecular network can be represented using several

methods. This model uses the percolation theory, which predicts analytically the probability of a bond to be occupied given the coordination number and the starting bond occupation probability(Appendix L).

The DVC model predicts, and experiments confirm, that there are more than one kind of bond bridges and crosslinks which have different coordination numbers, and independent probabilities of being broken. To take advantage of the benefits of percolation theory, we have extended percolation theory on a Bethe lattice (one with no loops) to use two independent sub-networks, as illustrated in Figure 4-1. In the figure, double lines represent one of the bond types, while single lines represent the other. As can be seen by comparing Figure 4-1a and 4-1b, this lattice has the desired feature of modeling a transition from chain-like structures (a) to fishnet structures (b). The mathematics of this two-bond percolation theory follows closely that of the standard theory. The mathematics are presented in Appendix L.

There are four parameters describing the network: p, q, σ_1 and σ_2. p and q are the occupation probabilities of bridges and crosslinks, respectively, while σ_1+1 and σ_2+1 are the coordination numbers for bridge linkage and crosslink linkage, respectively. σ_1 and σ_2 are model constants. p and q, are the state variables computed at each time step, and are set equal to the input parameters p_o, q_o, at time equal 0. p_o, q_o vary with each coal.

Coal Viscosity Model

The coal fluidity model is based on the decomposition and condensation of the macromolecular network under the influence of bridge breaking and crosslinking reactions(Appendix M). The fluidity is dependent on the relative amounts of the liquid, (molecules detached from the network) and solid (the remaining network) and on the fluidity of the liquid component. The fluidity of the liquid component depends on the average molecular weights of the liquid and on the temperature.

The viscosity model used here has terms that depend on the coal liquid

temperature, and the volume fraction of solids, with an inhomogeneous gel-point. It is the last two factors which are the most important. In common with previous studies of coal viscosity, a two-phase model is used. The particular equation chosen is as follows:

$$\ln (\eta/\eta_{liq}) = \left[\frac{k_E\phi_s}{1 - \phi_s / \phi_c}\right] \qquad (4\text{-}14)$$

where η is the viscosity of the suspension, η_{liq} is the viscosity of the liquid, k_E is the Einstein coefficient, and ϕ_s is the volume fraction of solids, having a critical value ϕ_c at which η goes to infinity.

The viscosity of the liquid phase is given by the Andrade equation

$$\eta_{liq} = C \exp(E_\eta / RT^*) \qquad (4\text{-}15)$$

which on combining with Eq. 4-14 leads to:

$$\eta = C \exp (E_\eta /RT^*) \left[\exp \frac{k_E\phi_s}{1 - \phi_s / \phi_c}\right] \qquad (4\text{-}16)$$

The constants used in the viscosity theory are as follows:

k_E: Einstein coefficient, $k_E = 5.0$

ϕ_c: Volume fraction of the solid phase at the gel-point, $\phi_c = 0.65$

η_{liq}: viscosity of the liquid phase

$\eta_{liq} = C_1 \exp(E_{\eta 1}/RT^*) = 5.0 \times 10^{-30} \exp(100{,}000/RT^*)$ for $T \leq 708$ K

$\eta_{liq} = C_2 \exp(E_{\eta 2}/RT^*) = 1.082 \times 10^{-14} \exp(50{,}000/RT^*)$ for $T \geq 708$ K

T^*: Absolute temperature, cut-off at $T^c = 750$ K

i.e., $T^* = T$ for $T \leq T^c$ K: $T^* = T^c$ for $T > T^c$ K

R: Gas constant, R = 1.98 cal $mole^{-1}$ K^{-1}

The value of $k_E = 5$ was arrived at empirically, i.e., to fit the data. This value, however, matches the situation in which liquid is entrapped within large agglomerates of solid. The value of the activation energies for coal was chosen based on measured liquid viscosities (from 50 to 100 kcal/mole).

Coal Swelling Model

Under certain conditions, coals which become fluid when heated also swell, due to the internal pressure of trapped, evolved gases. Experimental observations of the swelling are made both on single particles which have swollen in essential isolation, and on agglomerates, as in a measurement of the free-swelling index. Although the same basic phenomena are involved in both cases, only the swelling of individual particles of pulverized coal (radius < 100 μm, say) has been modeled to date.

When microscopic observations of swollen coal particles are made it becomes apparent that the particles do not behave in an identical fashion. At average heating rates, between 10^2 and 10^4 K s^{-1}, the swollen particles of a typical swelling coal, Pittsburgh No. 8, can be categorized into one of three types: a small fraction ($\sim$ 10%) which shows virtually no sign of fluidity, and hence no swelling; the majority ($\sim$ 80%) which experience swelling of about the same magnitude; and another small fraction ($\sim$ 10%) which exhibits behavior that can be associated with a much higher fluidity (lower viscosity) than the majority. We have associated the three behaviors with the three main maceral types of the coal; inertinite, vitrinite, and exinite, respectively. In the model the properties only of average particles are described, and this must be recognized when comparing predictions with microscopic observations.

The range of "swelling" behaviors encompassed by our model includes the swelling which is observed for moderate heating, but also the behaviors at the extremes of heating rate. At very low heating rates ($\leq$ 10 K s^{-1}) there is

virtually no swelling. At extremely high rates ($\geq 5 \times 10^4$ K s^{-1}), the liquid walls surrounding the gas-filled internal voids rupture, allowing the gas to escape. Minimal swelling is observed in this case. Microscopic observations of particles which have ruptured in this way reveal a variety of images. For some coals the shapes are not unlike fairly smooth skinned potatoes, but with many holes over the surface. For others the surfaces are still pitted with holes, but with a more angular morphology indicative of low flow.

The starting point for our model is the equation described by (Chiou and Levine, 1981), who considered the swelling rate of a pulverized coal particle of external radius r_2, with a single void of radius r_1, with spherical symmetry. The swelling they depict is due to the pressure, ΔP_t, of trapped evolved gases, doing work against viscous forces (viscosity = η). Their equation was further modified to take account of the pyrolysis weight loss.

For this single bubble model, the equation for the velocity of the outer wall is given by

$$\frac{dr_2}{dt} = \frac{r_1^3 r_2 \, \Delta P_t}{4\eta(r_2^3 - r_1^3)} + \frac{r_2}{3(r_2^3 - r_1^3)} \frac{d(r^3)}{dt} \qquad (4\text{-}17)$$

Where r_1 and r_2 are the radius of the inner bubble and the coal particle with one bubble, respectively; $4\pi/3 \; r^3$ is the coal volume in this particle.

In our model, the temperature-dependent viscosity is supplied by the viscosity model. The accounting of excess internal pressure begins at t = 0, considering the gas gain from trapped, evolved gas, and loss due to out-diffusion. The number of moles of gas, n_g, evolved in one second, by the particle walls of volume, Δv, is obtained from the FG-DVC model, Δv being updated to account for pyrolysis. Of the evolved gas, a fraction $r_1^2 / (r_1^2 + r_2^2)$ is captured within

the void, so that the captured gas is given by

$$dn_c = n_g \, r_1^2 \, / \, (r_1^2 + r_2^2) \bullet dt \qquad \textbf{(4-18)}$$

In this same period an amount of gas diffuses out:

$$dn_d = \frac{4\pi D_l \, c_1 dt}{(1/r_1 - 1/r_2)} \qquad \textbf{(4-19)}$$

where D_l is the diffusivity of the gas in the coal liquid, $c_1 = 3 \, n_t \, / \, 4\pi \, r_1^3$, and the total gas within the cenosphere, n_t, is the "sum" of Eqs. 4-18 and 4-19

$$\frac{dn_t}{dt} = \frac{dn_c}{dt} - \frac{dn_d}{dt} \qquad \textbf{(4-20)}$$

The excess of internal over external pressure, ΔP_g, due to the trapped gas is given by

$$\Delta P_g = \frac{3 \, n_t \, RT}{4\pi \, r_1^3} \qquad \textbf{(4-21)}$$

The calculation of the amount of the trapped ambient gas n_a follows the similar argument in Eq. 4-19 and 4-20:

$$\frac{dn_a}{dt} = \frac{4\pi\ D_a}{1/r_1 - 1/r_2}\left[\frac{P_0}{RT} - \frac{n_a}{4\pi\ r_1^3/3}\right] \qquad (4\text{-}22)$$

where P_0 is the ambient pressure and D_a the diffusivity of ambient gas. The pressure difference is then

$$\Delta P'_t = \frac{3\ (n_t + n_a)KT}{4\pi r_1^3} - P_0 \qquad (4\text{-}23)$$

But this is reduced by the effective negative pressure due to the surface tension, σ; so that the total outward pressure differential, ΔP_t, is

$$\Delta P_t = \frac{3\ (n_t + n_a)\ RT}{4\pi\ r_1^3} - \sigma\ (\frac{1}{r_1} + \frac{1}{r_2}) - P_0 \qquad (4\text{-}24)$$

This is the pressure difference used in Eq. 4-17, to calculate swelling.

If $\Delta P'_t$ is sufficiently large, the stress of the wall will exceed the strength of the wall S_c. Cell rupture is defined to occur when

$$S_c \leq -P_0 + \frac{1.5\ r_1^3\ \Delta P'_t}{(r_2^3 - r_1^3)} \qquad (4\text{-}25)$$

The parameters of the model are: D_l, D_a, σ, and S_c, which are listed in Table 4-2.

Large particles are expected to contain more than one bubble. The value of r_2, the radius of a particle with only one bubble, is found to be 20μm to fit the data of most of the coals. The extrapolation of this single bubble model to large particles needs to be further investigated. The current model assumes that the number of bubbles in a particle of radius R is $(R/r_2)^3$.

Char Reactivity Model

As previously mentioned in section II-G(PCGC-2 1988 version), three rate-limiting steps are considered for this process: 1) gas phase diffusion, 2) heterogeneous reaction, 3) heterogeneous reaction + pore diffusion. This section considers both the determination of the intrinsic rate coefficient and the incorporation of the effect of particle diffusion limitations. In order to obtain the intrinsic rate coefficient, the model uses correlations with chemical properties such as the char hydrogen content and the coal oxygen and mineral contents. In the diffusion regime, the model determines the value of the reaction rate as a function of the intrinsic reaction rate coefficient and char structural properties such as porosity, tortuosity and mean pore radius. Specifically, it calculates the effectiveness factor (i.e. the ratio of the actual rate over the rate without diffusion limitations) using the Thiele modulus. In the pore diffusion regime when high Thiele modulus values are assumed (i.e. reaction is thought to occur mostly on the external surface of the particle), the model predicts that the activation energy is approximately half the intrinsic activation energy. A first order equation is used for the intrinsic reaction. The overall reaction rate (including gas phase diffusion) r_{hjl} is calculated following equation 114 (PCGC-2, 1988 version) :

$$r_{hjl} = \frac{A_j^{\prime} M_{hj} M_g \phi_l k_{cjl} k_{jl} \xi_j C_{olg} C_g}{M_g A_j C_g ({}^{\prime}\xi_j k_{jl} + k_{cjl}) + r_j} \qquad (4\text{-}26)$$

If mass transfer is neglected, the equation for the particle reaction rate becomes :

$$r_{hjl} = A_j M_{hj} \phi_l k_{jl} \xi_j C_{olg} \quad with \quad \xi_j = \eta \; surf \,/\, surfe \qquad (4\text{-}27)$$

where A_j is the external surface area, M_{hj} is the molecular weight of carbon, ϕ_l is a stochiometic factor, k_{jl} is the intrinsic rate coefficient, ξ is a surface coefficient, C_{olg} is the oxidant concentration, η is the effectiveness factor, and surf and surfe are the internal and external surface areas respectively (both in m^2/g-available char).

The value of the intrinsic reaction rate coefficient k_{jl} has been experimentally found to be well represented by the equation :

$$k_{jl} = A1_{jl}\, T_j \exp(-\frac{E1_{jl}}{R\, T_j}) \qquad (4\text{-}28)$$

where T_j is the particle temperature, $E1_{jl}$ is the activation energy in the kinetic regime (32000 cal/mol), and $A1_{jl}$ is the pre-exponential factor which depends on the starting coal and the pyrolysis conditions. For reaction with oxygen, $A1_{jl}$ is defined, for high rank coals (oxygen content lower than 13 %), as :

$$A1_{jl} = 4.75 \times 10^{-4} \exp(1.49\, H_{char}) \exp(0.28\, O_{coal}) \qquad (4\text{-}29)$$

where H_{char} is the char hydrogen content, and O_{coal} the coal oxygen content. For low rank coals (oxygen content higher than 13 %) $A1_{jl}$ becomes :

$$A1_{jl} = 5.33 \times 10^{-2} \exp(1.49\, H_{char}) \exp(1.65 \text{ min}) \qquad (4\text{-}30)$$

where min represents the "effective" coal dispersed mineral content. At low

temperature, min is equal to the measured dispersed mineral content min0, while at high temperature, min is calculated using a deactivation function as follows:

$$\text{min} = min0 \exp\left(-\frac{Em_{jl}}{R} x \left(\frac{1}{Tm} - \frac{1}{T_j}\right)\right) \qquad (4\text{-}31)$$

where Em_{jl} is the deactivation energy, and Tm is an adjustable temperature.

The effectiveness factor η (and as a result, the surface coefficient ξ_i) is calculated using the Thiele modulus Φ_s:

$$\eta = \frac{3}{\Phi_s}\left[\frac{1}{\tanh\Phi_s} - \frac{1}{\Phi_s}\right] \qquad (4\text{-}32)$$

where Φ_s is given by :

$$\Phi_s = \frac{d}{2}\left(\frac{M_g\, surf\, sigma}{D_{eff}\, \phi_l\, M_{hj}}\, k_{jl}\right)^{0.5} \qquad (4\text{-}33)$$

where Deff is the effective diffusivity, and sigma is the particle density. The effective diffusivity Deff is dependent on the mean pore radius radp (needed to calculate the Knudsen diffusivity), the porosity eps and the tortuosity tau, and is given by :

$$Deff = 9.7 \times 10^{1}\, radp \left(\frac{T_j}{M_g}\right)^{0.5} \frac{eps}{tau} \qquad (4\text{-}34)$$

At this point, the model contains numerical parameters for the O_2-char reaction

only. However the same approach can be used for other gas-char reactions.

Coal Sulfur and Nitrogen Devolatilization Model

The phenomenon of coal sulfur decompositions is complicated by the various forms of sulfur existing in the coal structure on one hand and the various gas species produced by the decompositions on the other. The weak absorbance of H_2S, which is a major product of sulfur pyrolysis evolution, from FTIR spectra makes the understanding of the physical and chemical nature of this process more difficult. The lack of measures to distinguish the origins of sulfur products in the spectra is the major obstacle in our investigation. Efforts have been made in analyzing the data of the post oxidized runs at AFR (Bassilakis, 1992) and those of COS and SO_2 of the ordinary pyrolysis. A preliminary understanding of this phenomenon has been reached and forms the basis of the sulfur model in the current code.

Sulfur exists in coals in three forms: organic sulfur, pyritic sulfur, and sulfates. Organic sulfur is in the coal structure, either in aromatic rings or in the aliphatic portion. Pyrite exists in coal as dispersed particles, but interactions with the coal structure to a certain extend are expected. Sulfates are only a very small part of the total sulfur in most coals, especially coals from Argonne Coal collection (Vorres, 1989), and therefore, are ignored in the current model.

During devolatilization, sulfur in various forms decomposes into gas species, including H_2S, COS, SO_2 and CS_2, and a large amount of it remains in char and then decomposes in the combustion cycle. Some amount of the sulfur is entrained by tar as other gas pools, and it does not constitute a modeling problem here. Pyrite FeS_2 is believed to decompose mainly as $FeS_2 \rightarrow FeS + S$, and the further reaction of FeS is slow during pyrolysis. Alternative pyrite reactions with coal gases are possible, but they may be less significant. S from FeS_2 decomposition reacts with coal structure forming all possible sulfur gas species listed above. Among all the gases, H_2S is the major species of sulfur evolution, and other gases are just the background under the H_2S peaks. Therefore, efforts have only been made to predict the overall sulfur evolution with H_2S. For all

coals, a part of the organic sulfur is retained in char and the percentage of the retention is coal rank dependent.

As shown by Bassilakis (Bassilakis, 1992), SO_2 evolution in a post oxidized run has three peaks during pyrolysis. The first peak at low temperature is attributed mainly to the aliphatic organic sulfur, but for low rank coals it has part of the sulfur from the pyrite as the product of its low temperature decomposition. The second peak is sharp and coincides with the pure pyrite decomposition temperature, so it is believed mainly due to pyrite devolatilization. The third peak at high temperature is much broader than the two previous peaks and is actually a shoulder of the second peak. This peak consists of the products from the high temperature evolution of organic sulfur and pyritic sulfur. A schematic representation of above discussion is given in Figure 4-3.

In FG-DVC, the organic sulfur is distributed into two H_2S(loose and tight), one SO_2, one COS, one CS_2 and one char S pools. The pyritic sulfur decomposes at two temperatures. The low temperature decomposition is the result of the coal+pyrite reaction, which produces H_2S. The high temperature decomposition releases H_2S, SO_2, COS, and CS_2 gases. Some sulfur released from this reaction remains in the coal structure and evolves at higher temperature as H_2S. Another part of it could remain in the char. The product distribution discussed above is depicted in Table 4-3.

Under oxidized conditions, the decompositions of both organic and pyritic sulfur are 100%. The biggest change is the release of FeS and the organic char sulfur which are stable in absence of oxygen. However, the positions of these additional peaks are tentatively assigned and more work needs to be done. In FG-DVC, the FeS evolution is invoked only when the inlet gas is oxidized. The FeS peak is placed at temperature slightly high than the FeS_2 intrinsic sharp peak, and the organic char sulfur oxidation peak is in between the first peak and the second peak. This overall evolution profile is consistent with the result by LaCount (LaCount, 1991), but our peak assignment(Figure 4-3) is different.

All the devolatilizations follow the standard description of gas evolutions in Eq. (4-10).

The forms of the coal nitrogen are much simple comparing to sulfur. Most of the coal nitrogen is in pyrrole and pyridine structures, which are both aromatic. There is only a very small amount of amine in lignite. The main evolution gases are HCN and NH_3. What makes the nitrogen evolution difficult to be modeled is the heating rate dependency (Bassilakis, 1992). At 30°C/min, NH_3 was the major product of nitrogen evolution in pyrolysis, and there was only less than 5% of the volatile nitrogen in HCN. While in an entrained flow reactor of furnace temperature at 1100°C, HCN evolution was strongly enhanced and the amount of NH_3 became too low to be detected.

The modeling scheme used in this version is outlined in Figure 4-4. HCN evolves directly from its pool precursors. NH_3 gas comes from two sources: the direct evolution from coal nitrogen(pools) and the secondary conversion from evolved gaseous HCN to NH_3. The former contributes only a small amount, while the later is the major reaction pathway. The conversion is assumed via the reaction of the gaseous HCN with the coal hydrogen in the pore structure of coals when HCN is making its way out of the coal particles. The completeness of this reaction is obviously dependant upon the comparison of the gas residence time in the pore structure to the coal reaction residence time in reactors. Since nitrogen evolves at higher temperature than other gases, the gas residence time depends on the char structure instead of the coal structure. The precise determination of the gas residence time is difficult. It can be more complicated if pyrolysis of large coal chunks is to be modeled, in which case bed conditions can affect the gas release.

This model uses a simplified single cell structure to estimate the gas residence time. Consider a spherical char particle with an original radius r_0. The radius changes to r_2 in the pyrolysis due to the weight loss and swelling. The particle has a single inner bubble of radius r_1. During pyrolysis, the evolution gas flux in this particle is always positively outward. We assume that the gas starts to transport outward immediately after it evolves, so the gas residence time is defined as the time elapse of its traveling from the sphere origin to the particle surface. It is obvious that if the coal particles are packed the residence time will be longer than we estimate here.

With this single cell particle model, for the gas that evolves at a point inside this particle of distance r from the center of the sphere, the residence time, Δt_n, of the evolution gas before leaving the particle is

$$\Delta t_n(r)=\Delta t_{n0}\ln\frac{r_2}{r} \tag{4-35}$$

and

$$\Delta t_{n0}=\frac{3P^*\phi_v}{\rho n_{tot}RT} \tag{4-36}$$

where P* is the gas pressure in the coal pores, n_{tot} is the total gas evolution rate per unit weight coal, R is the gas constant, T is the temperature, ρ is the coal solid density, and ϕ_v is the volume swelling ratio that can be calculated by swelling model. The HCN gas that is generated within the shell $4\pi r^2 dr$ has a time period of Δt_n to react to NH_3. The modified HCN evolution rate is then

$$\frac{dW^*_{HCN}(gas)}{dt}\Big|_r=\frac{dW_{HCN}(gas)}{dt}e^{(-k_n\Delta t_{n0}\ln(\frac{r_2}{r}))} \tag{4-37}$$

where k_n is the reaction constant of HCN to NH_3 conversion, and $dW_{HCN}(gas)/dt$ is the HCN evolution rate given by Eq. (4-10). Averaging over the whole particle leads to

$$\frac{dW^*_{HCN}(gas)}{dt}=f_n\frac{dW_{HCN}(gas)}{dt} \tag{4-38}$$

where

$$f_n=(1-f_{n0})\frac{1-e^{(-k_n\Delta t_{n0}\ln(\frac{r_2}{r_1}))}(r_1/r_2)^3}{(1-(r_1/r_2)^3)(1+k_n\Delta t_{n0}/3)}+f_{n0} \qquad (4\text{-}39)$$

where f_{n0} is a non-zero residue fraction of HCN rate. $(1-f_n)$ is the HCN to NH_3 conversion factor. And

$$\frac{dW^*_{NH_3}(gas)}{dt}=\frac{M_{NH_3}}{M_{HCN}}(1-f_n)\frac{dW_{HCN}(gas)}{dt} \qquad (4\text{-}40)$$

where M_{HCN} and M_{NH_3} are the molecular weights of HCN and NH_3, respectively.

To extend this single cell structure model to the generally heterogeneous coal/char structure, the residue HCN rate fraction f_{n0}, the coal volume swelling ratio, ϕ_v, and coal particle-bubble radius ratio, r_1/r_2, are the model parameters.

A non zero f_{n0} is to retain a small fraction of HCN after the most of it has been converted to NH_3, even at very low heating rate (Bassilakis, 1992). f_{n0} is affected by the char particle size and the char structure, which in turn are affected by the heating rate. f_{n0} is also a function of reaction bed conditions that could alter Δt_n evaluated above. The model suggested f_{n0} value is 0.1. It is only important for low heating rate, while for very high heating rate cases in which the conversion has no time to complete, f_{n0} is not important.

Although the char volume swelling ratio, ϕ_v, and the ratio of the inner bubble size to the char particle size, r_1/r_2, can be calculated directly from the swelling model, we would rather treat them as model parameters, because the single cell swelling model is too primitive to describe the heterogeneity of the char structure. For most of the combustion cases that PCGC-2 is to apply, swelling is not significant due to the very high heating rate and the presence of oxygen. Therefore, ϕ_v is set to 4 and r_1/r_2 to 0.8. P* is also related to the

swelling computation, since it is the gas pressure in the coal pores. But because nitrogen evolves at higher temperature than most of the gases and after the swelling, at the time nitrogen starts to evolve, P is almost at equilibrium with the ambient gas pressure. So P* is set to equal to the ambient pressure in nitrogen computation.

In the current version these model parameters are not adjustable by users.

Solution Technique

FG-DVC calculations are performed at each time step along the particle trajectory calculation of every particle. At each time step, the time increment, the current particle temperature and the local pressure are passed to FG-DVC subroutines. The coupled equations in FG-DVC are integrated for this time increment to get the updated particle elemental composition, the weight loss due to devolatilization, and the new particle size due to swelling for PCGC2.

The coupled Eqs. 4-10, 4-12, and 4-13 in FG part are integrated by using a basic Euler method. The size of the sub-time step is controlled by the quickest evolving species at the time so that the evolved amount of this gas pool at this time step must be less than a few percent of its original amount in the coal. This scheme is proven to be accurate enough for the current problem. Integrations start with initial gas pool composition read from FG-DVC input coal data file for the coal in the calculation. Gas evolution kinetic data are read from FG-DVC kinetic file which is also coal dependent.

In the DVC part, the network parameters p and q are updated using the bond breaking rate and crosslinking rate passed from FG part(Eq. 4-2), so that an updated network oligomer weight distribution can be obtained, and is used to calculated liquid/solid fractions of the coal. The oligomers with molecular weight less than 300 amu are the candidates for tar formation. Tar vaporization is determined by Eq. 4-7, an internal transport limit process, where higher pressure will reduce tar formation rate. The FG-DVC predicted pressure effect on pyrolysis agrees with experimental data very well. The initial molecular

distribution and network parameters p_0 and q_0 are read from FG-DVC coal dependent polymer file.

The coal viscosity at one time step is calculated directly from Eq. 4-16 following the FG-DVC calculation.

The particle swelling calculation proceeds by integrating Eqs. 4-17, 4-20, and 4-22. n_g in Eq. 4-18 is the sum of all gas evolution rates per particle from FG-DVC. The viscosity η in Eq. 4-17 is from viscosity model. At time equal to zero,

$$n_t=0 \tag{4-41}$$

and

$$n_a=\frac{4\pi r_1^3 P_0}{3RT} \tag{4-42}$$

where P_0 should be the local pressure at the place the particle trajectory starts. Before integrating Eq. 4-17, it is transformed to

$$\frac{d(r_2-r_1)}{dt} = -\frac{(r_2-r_1)(r_2+r_1)r_2}{r_1^2 r^3}\left[\frac{r_1^3\Delta P}{4\eta}+\frac{1}{3}\frac{d(r^3)}{dt}\right] + \frac{1}{3r_1^2}\frac{d(r^3)}{dt} \tag{4-43}$$

where $4\pi r^3/3$ is the current volume of the particle, and $4\pi/3d(r^3)/dt$ is the rate of volume loss due to combustion and pyrolysis. The relationship

$$r_2^3=r_1^3+r^3 \qquad (4\text{-}44)$$

is used to derive Eq. 4-43. Defining a new variable $w=r_2-r_1$, Eq. 4-43 is integrated instead of Eq. 4-17. Because the bubble shell thickness r_2-r_1 will be in the order of $10^{-3} \times r_2$ after the particle starts to swell, the very small time step required in integrating Eq. 4-17 to insure the accuracy of r_2-r_1 makes the calculation very inefficient. Using Eq. 4-43 to replace Eq. 4-17 solves this problem.

Numerical difficulties in this submodel originate from the abrupt nature of swelling at high heating rates and the subtle pressure balance to be maintained across the bubble shell. An error control Runge-Kutta-Fehlberg method is used in the integration. This variable step size method allows using large step sizes at the time the particle does not swell and small step sizes when the particle does swell.

This set of coupled equations becomes numerically stiff, when the particle heating rate is low or the particle residence time is large(>3 second). The diffusion equations of Eqs. 4-20 and 4-22 are the origin of the stiffness. This was resolved partially by analytically integrating Eqs. 4-20 and 4-22 in one sub time increment Δt to yield

$$n_t^{new}=\frac{-B+(An_t+B)_{\Delta t=0}\exp(A\Delta t)}{A} \qquad (4\text{-}45)$$

and

$$n_a^{new}=\frac{-C+(A_a n_t+C)_{\Delta t=0}\exp(A_a\Delta t)}{A} \qquad (4\text{-}46)$$

where

$$A=-\left[\frac{3D_i r_2}{(r_2-r_1)r_1^2}\right]_{\Delta t=0} \tag{4-47}$$

$$B=\left[\frac{r_2^2}{r_1^2+r_2^2}n_g\right]_{\Delta t=0} \tag{4-48}$$

$$C=\left[\frac{4\pi D_i P r_1 r_2}{RT(r_2-r_1)}\right]_{\Delta t=0} \tag{4-49}$$

$$A_a=-\left[\frac{3D_a r_2}{(r_2-r_1)r_1^2}\right]_{\Delta t=0} \tag{4-50}$$

P is the local pressure; T is the particle temperature; D_i and D_a are the apparent diffusivities of evolved gas and ambient gas, respectively.

In the reactivity model, the calculation of the mass loss rate due to heterogeneous reactions is performed through iterations with temperature. k_{jl} and ξ are calculated at each call of the subroutine KLCALC and are passed onto COAL2.

Model Parameters

In parallel with the model development of FG-DVC, much work has been done to obtain the coal dependent pyrolysis gas evolution kinetic rates, coal functional group compositions, coal polymer network parameters, and other model parameters in the viscosity and swelling models to fit experimental data. Table 4-4 lists the elemental compositions of the eight Argonne Premium Coals and three PSOC coals, for which coal data have been derived experimentally. The kinetic data of major gas pools of the Argonne coals are listed in Table 4-5. The elemental and functional group compositions, kinetic rates, and coal polymer network parameters of each Argonne coal are collected in three FG-DVC coal data input files

composition file	coal.arN.7
kinetics file	kin.arN.7
network parameter file	polymr.arN.7

respectively. The letter N will be the coal serial number defined in Table 4-4. For instance, the coal composition file for N. D. zap-lignite is 'coal.ar1.7'. Only files of Argonne coals are provide with the PCGC2 package. To select a coal for a PCGC-2 run, it is necessary to specify the correct coal data file names for this coal in PCGC-2 input file. The description of these files are given in User's Guide part of the manual.

If the coal in use is not one of the Argonne coals, a new set of the above three coal data files has to be created. It is not simple for users to do this, because getting these data requires special instruments, understandings of FG-DVC, and a stand-alone FG-DVC program. A utility program COALS was therefore written to assist users in maintaining and creating the FG-DVC coal data

files. The full functions of COALS have been incorporated into PCG2-2 pre-processing program PREC. For the usage of PREC, read Chapter 6.

References

Fletcher, T. H., Kerstein, A. R., Pugmire, R. J., Solum, M. S., and Grant, D. M., "*Chemical Percolation Model for Devolatilization. 3. Direct Use of ^{13}C NMR Data to Predict Effects of Coal Type*", Energy & Fuels, 1992, 6, 414.

Fong, W. S., Peters, W. A., Howard, J. B.," *Plastic Behaviour of Coal under Rapid-Heating High-Temperature Conditions*", Fuel 1986, 65, 195

Chiou, M. J., and Levine, H. B.," *Investigation of Structure Deformation of Coal Particles in Pyrolysis*", Internal Report, JAYCOR, 1981.

Bassilakis, R., Serio, M. A., and Solomon, P. R., "*Sulfur and Nitrogen Evolution in the Argonne Coals*", Prep. Papers Am. Chem. Soc. Div. Fuel Chem., 1992, 37(4), 1712.

Vorres, K., (prepared),"*Users Handbook for the Argonne Premium Coal Sample Program*", October, 1989, Argonne National Laboratory.

LaCount, R. B., Kern, D. G., King, W. P., LaCount Jr., R. B., Miltz Jr., D. J., Stewart, A. L., Trulli, T. K., Walker, D. K., and Wicker, R. K., "*Advances in Coal Characterization by Programmed-Temperature Oxidation*", Prep. Papers Am. Chem. Soc. Div. Fuel Chem., 1991, 36(3), 1217.

Unger, P.E. and Suuberg, E.M., "*Modeling the Devolatilization Behavior of a Softening Bituminous Coal*", 8th Symp. (Int'l) on Combust., 1203, 1981.

Table 4-1 Nomenclature of the Varibles in Chapter 4

Symbol	Definition
$A1_{jl}$	Pre-exponential factor, kinetic regime, reactivity model, m/sK
A_j	External surface area, m^2
C_{olg}	Oxidant concentration, $kmol/m^3$
D_a	Apparent ambient gas diffusivity in coal liquid, cm^2/s
Deff	Effective diffusivity, reactivity model, m^2/s
D_j	Tar vapor diffusivity of species of molecular weight M_j
D_l	Apparent evolution gas diffusivity in coal liquid, cm^2/s
d	Particle diameter, m
E_i	Activation energy for k_i, K
E_η	Activation energy for coal liquid viscosity
$E1_{jl}$	Activation energy for kinetic regime, reactivity model, cal/mol
Em_{jl}	Minerals deactivation energy, reactivity model, cal/mol
eps	Porosity, reactivity model
f_n	$1-f_n$ is the HCN to NH_3 conversion fraction
f_{no}	HCN to NH_3 residue fraction

Table 4-1 Nomenclature of the Varibles in Chapter 4 - cont.

Symbol	Definition
h_{char}	Char hydrogen content, reactivity model, wt %
k_E	Einstein coefficient, viscosity model
k_i	Rate constant of gas species i, 1/s
k_{jl}	Intrinsic reaction rate coefficient, reactivity model, m/s
k_n	HCN to NH3 reaction rate constant, 1/s
M_{olg}	Molecular weight of oxidant gas, reactivity model, g/mole
M_{hj}	Molecular weight of material, reactivity model, g/mol
M_j	Molecular weight of j^{th} tar species
min	Effective mineral content, reactivity model, wt%
min0	Measured dispersed mineral content, reactivity model, wt%
n_a	Mole of ambient gas trapped in the coal bubble, swelling model
n_i	Mole of gas species i per gram raw coal
n_j	Tar species of molecular weight M_j, mole per gram coal
n_c	Mole of evolved gas trapped in the coal bubble, swelling model
dn_d/dt	Rate of gas diffusing out the bubble, swelling model, mole/s

Table 4-1 Nomenclature of the Varibles in Chapter 4 - cont.

Symbol	Definition
n_g	Rate of gas evolution of the coal particle, swelling model, mole/s
n_t	Amount of evolution gas trapped in the bubble, swelling model, mole
n_{tot}	Total gas evolution rate, moles per gram DAF coal per second
Ocoal	Coal oxygen content, reactivity model, wt %
P_j	Vapor pressure of the oligomer of molecular weight M_j
P_0	Ambient pressure, atm
ΔP	Pressure drop from coal inner pores to outside, atm
ΔP	Effective pressure difference across the coal bubble wall, outward positive, atm
r	Particle radius
r_0	Initial particle radius, cm
r_1	Inner bubble radius, swelling model, cm
r_2	Particle radius, swelling model, cm
r_{hjl}	Overall reaction rate, reactivity model, kg/s
radp	Mean pore radius, reactivity model, m
S_c	Strength of coal bubble wall, swelling model, atm
sigma	Particle density, reactivity model, kg/m^3

Table 4-1	Nomenclature of the Varibles in Chapter 4 - cont.
Symbol	Definition
surf	Internal surface area, reactivity model, m^2/g
surfe	External surface area, reactivity model, m^2/g
tau	Tortuosity, reactivity model
T_m	Deactivation temperature I, reactivity model, K
T_j	Temperature of j^{th} particle classification, reactivity model, K
Δt_n	HCN residence time in coal particle
Δt_{no}	HCN residence time constant
V	Mole volume of evolved gas per gram raw coal
W_i, i=gas species	Amount of gas species i, gram per gram raw coal
ξ_j	Surface area factor, reactivity model
η	Coal viscosity, pascal*second
η	Effectiveness factor, reactivity model
ρ	Coal density, g/cm^3
σ	Surface tension of coal liquid, $dynes/cm^2$
σ_i	Standard deviation of distributed evolution rate of gas species i
ϕ_1	stochiometric factor, reactivity model

Table 4-1 Nomenclature of the Varibles in Chapter 4 - cont.

Symbol	Definition
ϕ_{liq}	Volume fraction of the liquid phase in the coal particle, viscosity model
ϕ_s	Volume fraction of the solid phase in the coal particle , viscosity model
ϕ_c	Volume fraction of the solid phase at the gel-point, viscosity model
ϕ_v	Volume swelling ratio
χ_j^b	Mole fraction of species of molecular weight M_j in the metaplast in the bulk of the particle
χ_j^s	Mole fraction of species of molecular weight M_j in the metaplast at the surface of the particle

Table 4-2 Swelling model parameters.

Calculation Particle Radius, cm	0.002
Bubble Radius, cm	0.0008
Apparent Pyrolysis Gas Diffusivity, cm^2/sec	$7.5e\text{-}5(T/773)^{1.8}$
Apparent Ambient Gas Diffusivity, cm^2/sec	7.5e-4
Critical Bubble Wall Stress, atm	1.0
Coal Liquid Surface Tension, $dynes/cm^2$	30.0

Table 4-3 Sulfur devolatilization: correspondence between pools and gases.

Peak 1	Organic Sulfur	16 - SO_2
		17 - COS
		18 - CS_2
		20 - H_2S Loose
	Pyritic Sulfur	58 - H_2S
Peak 2	Pyritic Sulfur	51 - SO_2
		52 - COS
		53 - CS_2
		55 - H_2S Loose
		57 - H_2S Gas
Peak 3	Organic Sulfur	19 - H_2S Tight
	Pyritic Sulfur	54 - H_2S Tight

Table 4-4 Elemental Compositions of the Eight Argonne Coals and the Three PSOC Coals. Pyrite sulfur contents are given in grams per 100 grams DAF coal.

Coal #	Coals	Elemental Composition, wt%(DAF) C	H	O	N	S	S (pyrite)
1	Beulah-Zap	72.97	4.83	20.35	1.15	0.7	0.155
2	Wyodak-Anderson	75.03	5.34	18.04	1.12	0.47	0.186
3	Illinois #6	77.72	5.00	13.53	1.37	2.38	3.32
4	Blind Canyon, UT	80.71	5.76	11.59	1.57	0.37	0.251
5	Lewis-Stockton WV	82.69	5.26	9.84	1.56	0.65	0.200
6	Pittsburgh Seam	83.30	5.33	8.84	1.64	0.89	1.50
7	Upper Freeport PA	85.50	4.70	7.51	1.55	0.74	2.04
8	Pocahontas #3 VA	91.23	4.45	2.49	1.33	0.50	0.158
9	PSOC 1448	84.08	6.04	7.52	1.84	0.52	0.05
10	PSOC 1521	87.00	5.13	5.08	1.87	0.92	0.52
11	PSOC 1522	89.09	4.56	3.47	1.89	0.90	0.02

Table 4-5 Kinetic Data of Major Functional Group Pools. R is the Gas Constant, A is in 1/sec., E/R and σ/R are in K

Kinetic Rate Parameters for Argonne Coals

	ZAP	WYO	ILL	UTA	STK	PIT	UPF	POC
CO_2-XL	A=5.00e+12							
E/R	18000.	18000.	20500.	21000.	21250.	21500.	22000.	23000.
σ/R	1500.0	1500.0	3000.0	4000.0	3500.0	3600.0	2000.0	2500.0
CO_2-L	A=5.00E+12							
E/R	23500.	24000.	24750.	25500.	26000.	26500.	27000.	28000.
σ/R	2000.0	2500.0	1750.0	2000.0	3000.0	3000.0	3000.0	2500.0
CO_2-T	A=7.500E+12							
E/R	31000.	32000.	32000.	32000.	32000.	32000.	32000.	33500.
σ/R	3000.0	2800.0	2750.0	3000.0	3200.0	3000.0	2500.0	2700.0
CO-L	A=5.00E+12							
E/R	24500.	24750.	25000.	25000.	25500.	26000.	28000.	29000.
σ/R	3000.0	2500.0	1000.0	1250.0	1100.0	1250.0	750.0	1250.0
CO-T	A=5.00E+12							
E/R	30000.	30250.0	30500.	30500.	30500.	30750.	31500.	32000.
σ/R	3000.0	3000.0	2000.0	2000.0	1600.0	1900.0	1400.0	1500.0
CO-XT	A=2.00E+14							
E/R	39000.	39750.	40000.	40000.	40000.	40000.	40000.	40000.
σ/R	2500.0	2500.0	3000.0	2500.0	3000.0	2800.0	2250.0	3200.0
CH_4-L	A=3.00E+13							
E/R	28000.	28000.	28000.	28300.	28000.	28000.	28750.	29500.
σ/R	2500.0	2250.0	1800.0	1800.0	1200.0	1300.0	800.0	750.0
CH_4-T	A=6.00E+13							
E/R	32000.	32000.	32000.	31500.	32000.	32000.	32000.	33000.
σ/R	2200.0	2500.0	2200.0	2200.0	2200.0	2200.0	2000.0	1700.0
H_2O-XL	A=5.000E+12							
E/R	16500.	17000.	18000.	—	—	—	—	—
σ/R	1500.0	1500.0	1800.0	—	—	—	—	—
H_2O-L	A=5.000E+12							
E/R	23000.	24250.	25000.	25000.	25500.	26000.	27500.	28000.
σ/R	2700.0	2500.0	1500.0	1250.0	1250.0	1250.0	1250.0	1250.0
H_2O-T	A=2.000E+14							
E/R	31000.	31000.	32000.	32000.	32000.	32000.	34000.	35000.
σ/R	3500.0	3500.0	2800.0	2500.0	2500.0	2500.0	2000.0	2500.0
Tar-BB	A=1.000E+14							
E/R	26000.	26000.	26000.	27000.	27250.	27500.	28250.	29000.
σ/R	1000.0	1000.0	750.0	1250.0	1000.0	1250.0	1250.0	750.0

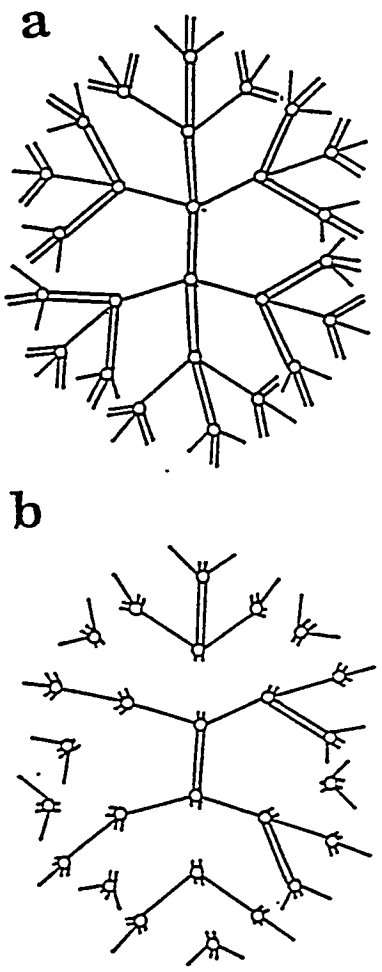

Figure 4-1 Bethe Lattice for Two-σ Model with $\sigma_1 = \sigma_2 = 1$ (shown as single bonds). a) Fully Linked Case (p=q=1) is like One-σ Model with σ=3. b) With Most Double Bonds Representing the Crosslinks not yet Formed to Represent the Starting Coal. The Lattice is Like One-σ Model with σ=1, Linear Chains.

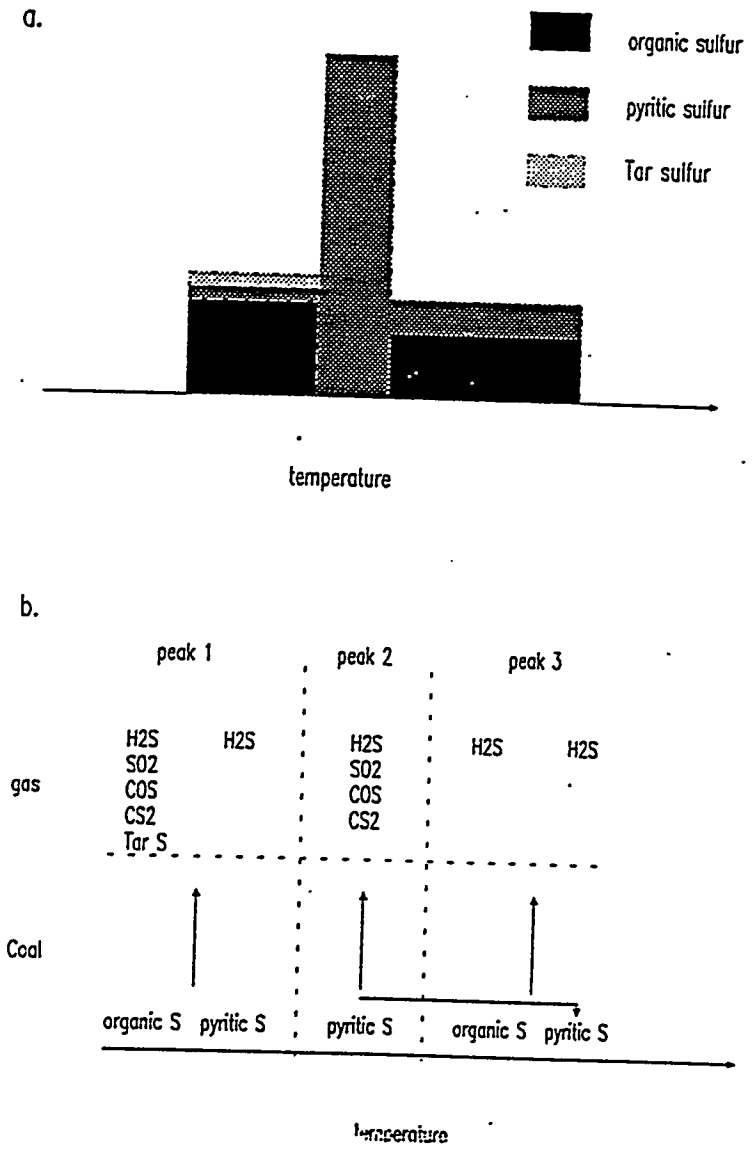

Figure 4-2 Schematic diagrams of sulfur devolatilization: a. the three peak framework. b. sulfur gas distribution.

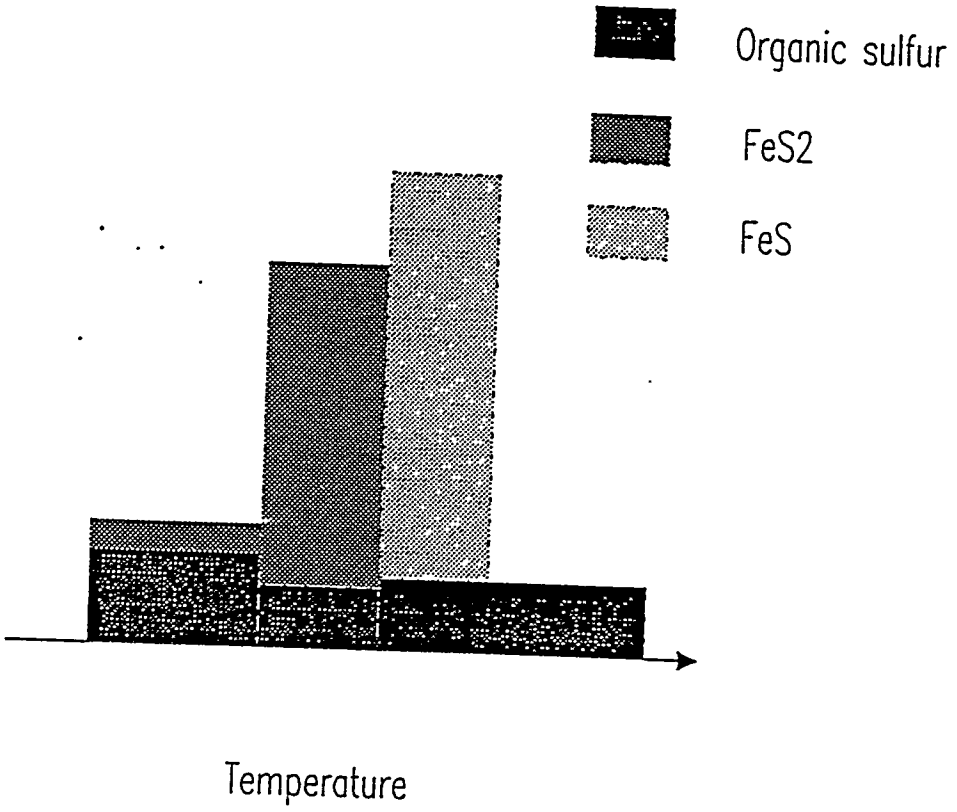

Figure 4-3 A schematic diagram of sulfur devolatilization in oxidation conditions.

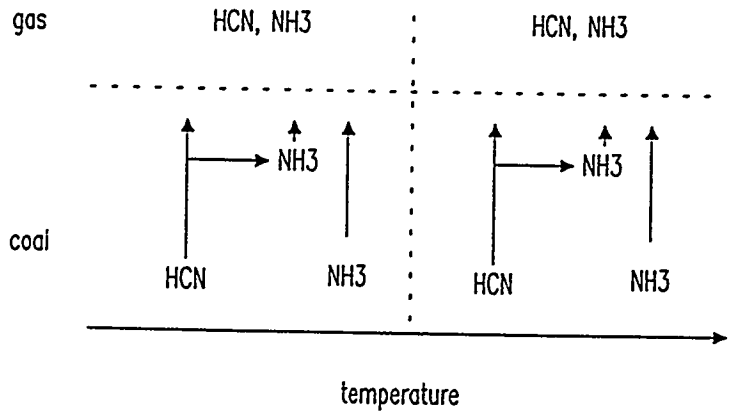

Figure 4-4 A schematic diagram of nitrogen gas distribution.

Chapter Five

User's Guide

General Description

PCGC-2 was originally developed on a VAX/11-750 computer with VMS FORTRAN. Recent development has been done on UNIX machines, adhering to the FORTRAN 77 standard. Plotting or graphics routines are not distributed with the code, but are available separately. Graphics is very important for understanding the code's voluminous output of data, and graphics is discussed in a section below. Intermediate computational values of all variables can be saved for restarting, so that computations need not start from scratch each time. Approximately 1.5 megabytes of disk space are required for the FORTRAN listing. At least two megabytes of real memory are required for running the code.

All input data to PCGC-2 are in SI units with the exception of angles, which are in degrees. The essential input is summarized in Table 5-1. All working variables within the program are either dimensionless or in SI units. Units associated with all variables are given in the nomenclature.

CPU run time varies widely according to the particular simulation and the machine. Ten CPU-hours is typical for simulation of simple pulverized-coal combustion with a Sun SPARC II workstation.

TABLE 5-1
SUMMARY OF INPUT FOR PCGC-2

Geometry
Primary tube diameter (m)
Secondary tube diameter (m)
Chamber diameter (m)
Chamber length (m)
Additional[1] inlets, location and sizes

Feed Rates
Primary gas (kg/s)
Secondary gas (kg/s)
Additional inlet #1 (kg/s)
Additional inlet #2 (kg/s), etc.
Coal particle loading in each inlet
Sorbent particle loading in each inlet

Inlet Gas Properties
Primary swirl number
Primary turbulence intensity (% or m/s)
Primary temperature (K)
Primary mole fractions of all species
Secondary swirl number
Secondary turbulence intensity (% or m/s)
Secondary temperature (K)
Secondary mole fractions of all species
Turbulence intensity, temperature and composition for additional inlets[2]

Reactor Parameters
Reactor pressure (N/sq m)
Wall temperatures (K)

Particle Parameters
Particle solid density (kg/cu m)
Mass mean particle diameter and distribution of particle sizes (m)

[1]Up to 3 additional inlets are allowed
[2]Some restrictions apply to temperature and composition of additional inlets.

TABLE 5-1 (continued)

Coal composition (≠ proximate analysis) (%)
- raw coal
- char
- ash
- water

Coal type

Description of Subroutines

A complete description of the routines is given in Appendix B. A brief description is given below.

The main program is PCGC-2. INFLOW reads the input data for the inlet streams. GRID generates the numerical grid. GRMAP modifies the numerical grid if a grid data file is being used and writes a new grid data file. GRDGRF writes a schematic showing the grid locations in the output file. CREEO reads the reactant composition data and thermochemical data file. INIT initializes arrays used in the code.

PSICTO, COALO, FLUXO, and NOXMNO read input data and perform initial calculations for the particle trajectory calculations, particle reaction scheme, radiation submodel, and nitrogen pollutants submodel, respectively. Other input data are read primarily by the main program and by the driver program for the nitrogen oxide submodel (NOXMN).

TABLE is the driver program for generating the table of equilibrium gas properties for lookup. TBLF, TBLFE, TBLFEH, and TBLFH generate tables of equilibrium properties as functions of f only; both f and h, f, h, and h_r; and both f and h_r; respectively. These four tables correspond to adiabatic, gas only; adiabatic, gas and reacting particles; non-adiabatic, gas and reacting particles; and non-adiabatic, gas only; respectively. All four table generators call CREE to calculate the equilibrium properties. TBLFE and TBLFEH provide for table restart (TBLRSTFE and TBLRSTFEH).

PROFIL reads input data and sets the boundary values for the gas inlet streams. PRINT is a routine that is called frequently to print values of field variables to the output file. RESRT reads and writes gas-phase restart files. Particle phase restart files are read and written by the main program. FLINT initializes the flow field variables and calculates the gas density field. EULINT is an entry in PSICTO that calculates the particle number flowrate for each particle trajectory.

PROPS calculates the time-mean gas properties, incorporating the effects of turbulence. FGTABL is a routine that provides the upper and lower limits of the clipped Gaussian probability density function from a table of precalculated values. CREE may be utilized to calculate equilibrium gas properties when residual enthalpy falls outside the table limits. UPDATE is an entry point in TABLE that calls the appropriate entry point in TBLF, TBLFE, TBLFEH or TBLFH, to retrieve the needed gas properties.

STREAM calculates the velocity streamlines for plotting. PLTWRT writes plotting files.

The CALC routines calculate the flowfield variables such as velocities, turbulence properties, mixture fractions, and pressure, at each node throughout the flow field (Step 2 of Fig. 3-1). Each CALC routine calls an entry point in PROMOD or a separate "MOD" routine to modify the coefficients and source terms in the appropriate finite difference equation in order to account for the boundary conditions as described in Chapter 3. LISOLV is the solver that performs the operations of the TDMA algorithm to solve the finite difference equations.

PROG monitors the progress of the calculation toward convergence by recording the values of the variables at a specified location for each iteration.

EOLP is the driver program for the particle calculations. CALCNJ solves the Eulerian particle density equation using the TDMA (LISOLV). CALACJ, CALAHJ, and PSOLVP solve the Eulerian particle calculations. Although the pure Eulerian approach for solving the particle phase has been programmed into PCGC-2, it is not operational. FLUX is the driver program for the radiation submodel. BVALIN is an entry point in BPROPS that inserts reasonable values into boundary intrusions in order to allow for 2-D interpolation of gas properties. PSICT solves the particle trajectories using the Particle-Source-In-Cell of Crowe and coworkers (1977) and calculates the particle source terms. COAL1 calculates the gas properties. COAL2 calculates the particle reaction rates, and PSOLVE solves the particle continuity equations. PSOLVS is a special solver that is used when the particle enthalpy equation goes stiff (after burnout it is essentially complete). BVALOUT is an entry in BPROPS that substitutes the original values of properties back into the boundary intrusions after particle trajectory calculations are complete.

An information flow diagram for the combined Eulerian-Lagrangian particle model is shown in Figure 5-1. CALCNJ first calculates the Eulerian number density field for each particle size. The Eulerian number density is needed by the FLUX routines for calculating the radiation fluxes and by the PSI-CELL routine for calculating the turbulent diffusion component of particle velocity as given by Eqn. 2-34. PSICT solves the particle momentum equations for each trajectory, keeps track of particle position and properties as a function of time, and calculates the appropriate source terms for each cell. PSICT also interpolates Eulerian properties

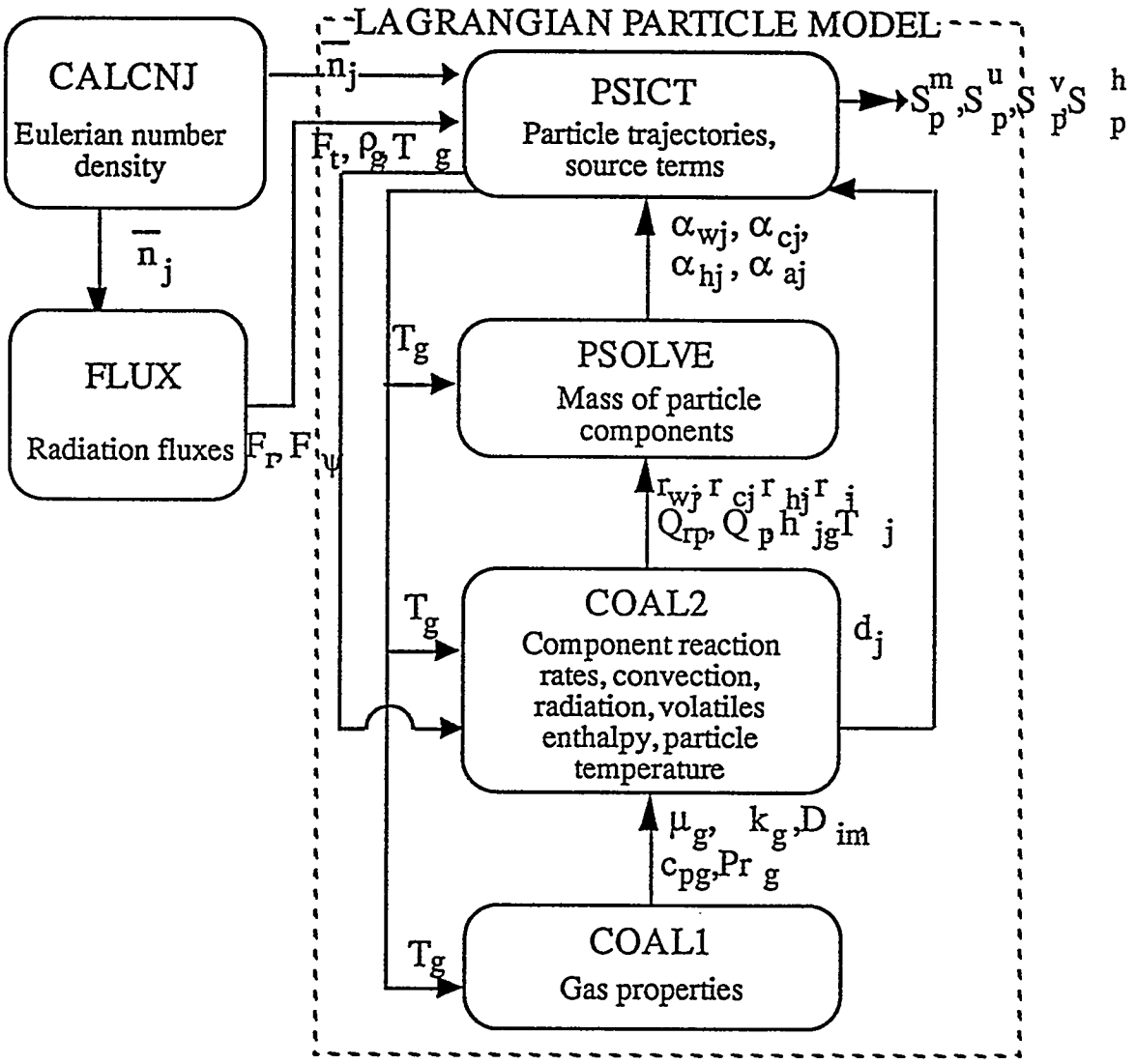

Fig. 5-1. Information flow diagram for combined Eulerian-Lagrangian particle model.

(total radiation flux, gas density, and gas temperature) across cells to be used in the particle calculations. COAL1 uses the local gas temperature to calculate gas viscosity, gas thermal conductivity, species diffusivities, gas thermal heat capacity, and Prandtl number. COAL2 uses this information to calculate the component reaction rates, convection and radiation heat transfer rates, volatiles enthalpy, and particle temperature. Particle diameter is also calculated by COAL2 and used by PSICT in solving the momentum equations. PSOLVE uses the particle reaction rates, heat transfer rates, particle temperature, and volatiles enthalpy to solve the particle continuity equations and provide the mass of each particle component at each time step. The final product of the particle model is the source terms which are returned to the gas phase.

RADCOF calculates the gas emissivity and absorption and scattering coefficients for either the VARMA six-flux (VFM) or discrete ordinates (DOM) radiation model. EICO2 and EIH20 calculate the emissivity contributions for carbon dioxide and water vapor, respectively. DISORD solves the radiation equations using the DOM model. RESULT prints a summary of the results of the DOM calculations in the output file. SETUP calculates the coefficients for the VFM model. FLUXX, FLUXR, and FLUXT solve the VFM model equations for the axial, radial, and tangential directions, respectively. The equation for the tangential direction is algebraic due to the axial symmetry and does not utilize the TDMA solver (LISOLV).

NOXMN is the driver for the NO_x pollutant submodel. NOXMN reads input cards from the data file, controls the NO_x model logical sequence, tests for convergence, and prints out intermediate and final results. EQSPEC calculates Favre average equilibrium concentrations for gas species used to estimate atomic oxygen (O) and hydroxide (OH) concentrations. FREACT calculates the maximum possible concentrations of HCN, NH_3 and NO at each grid location for fuel nitrogen conversion. PSCRAT calculates the rate of homogeneous reactions for intermittent primary, secondary and coal off-gas. Mean reaction rates and species continuity source terms are calculated in RATE which calls RXNEXT to calculate reaction progress variables and RXNRAT to calculate the local instantaneous homogeneous chemical reaction rates for all mechanisms. RATE incorporates the time-mean effects of turbulence on the homogeneous reaction rates, analogous to the manner in which PROPS incorporates the effects of turbulence on the time-mean gas properties. The subroutine B is called to determine the power for oxygen concentrations from the auto-correlation given by de Soëte (1975) for HCN and NH_3 global oxidation reactions. PRTSUR calculates the surface area of char particles which is required for the heterogeneous NO decay reactions. CALCNO, CALHCN, and CALNH3 calculate the field values for NO, HCN, and NH_3 respectively, using LISOLV, analogous to the other CALC routines which

solve the field variables for the gas phase. CALCO2 adjusts the time-mean mass fractions of O_2, N_2, and OH throughout the flowfield following the pollutant reactions. Finally, INTGRT computes integrated average dry mole fraction at each axial node for final output while RSTNOX reads and writes to a restart file.

SORPAR is the driver for the SO_x/sorbent reactions submodel. SORPAR controls the sorbent reactions model logical sequence, tests for convergence, and prints out intermediate and final results. SORB0 reads the input files while CALCSJ calculates the Eulerian number density for the sorbent particles. SPSICT calculates the Lagrangian trajectories for the sorbent particles and calls SULFAT and SULFHS which calculate the progressive sulfation of the sorbents due to SO_2 and H_2S capture. Thus, SPSICT calculates the source terms for SO_2 and H_2S capture in each computational cell. SULFAT and SULFHS are based on the shrinking-core grain model. CALSO2 and CALH2S calculate the field values for SO_2 and H_2S respectively, using LISOLV, analogous to the other CALC routines which solve the field variables for the gas phase.

Program Input

At least three input files are required by PCGC-2: the main data file (PCGCIN), the thermodynamic properties data file (THERMO), and the inlet profile data file (INLET). Other data files may also be required. For example, if the individual grid locations are to be specified (INRDGD = T in the main data file) a grid data file (GRID) is needed. If the calculation is being restarted from the results of a previous calculation (INRST = T and/or INPRST = T in the main data file), restart files are needed for the gas (INOUT) and/or particles (PARSOU). If the FG-DVC submodel for devolatilization is being used, additional data files are needed.

The data contained in the three required input files are shown in Table 5-2 and are briefly described below. The data are given in the actual order in which they are read by the program, and are divided into seventeen groups according to function. Also shown in Table 5-2 are the calling routine and the required format. A detailed description of the input data is given in Appendix C.

Group 1 in Table 5-2 contains comment statements that are printed out as a header at the beginning of the main output (PCGCOT) and log files. Any number of comment statements may be included in the header.

Group 2 contains program control information, including which field variables are to be calculated, and numerical parameters for degree of under-relaxation, convergence criteria, etc. The reactor geometry, temperature bounds for

the physical properties table, reactor heat loss, wall temperatures, and gas viscosity and pressure are also specified in Group 2.

Group 3 describes the flowrate, composition (in terms of the reactant streams described below), swirl, turbulence intensity, coal particle loading, and sorbent particle loading of each of the gas inlet streams. Up to three additional inlets (in addition to the primary and secondary) may be included, but they must all be described in terms of the reactant streams specified below.

Data in Groups 1, 2, and 3 are all contained in the main input file, PCGCIN. For Groups 4 and 5, only the first data item, i.e. the keywords ELEM and THER, are contained in file PCGCIN. The remaining data in these groups are contained in the THERMO file. Group 4 gives the molecular weight and valence of each of the elements. The order in which the elements are listed is the order in which they are treated in the program calculations. Group 5 gives the elemental composition, heat of formation, temperature ranges, and heat capacity coefficients for each of the molecular species.

Group 6 describes the reactant streams that are used to specify the inlet stream compositions and temperatures. Only two reactant streams are allowed. The inlet streams are specified as a mixture of the two reactant streams. Usually, the first reactant stream is used to specify the primary gas, and the second reactant stream is used to specify the secondary and any additional inlets. However, any inlet may also be specified as any mixture of both reactant streams using the input variable FFLOW in Group 3.

TABLE 5-2

INPUT DATA

Group	Calling Routine	Data File[1]	Line	Data Items	Format
1	MAIN	PCGCIN	1	NSAY	*
			2	SAY (I) . . . SAY (18)	18A4
			•	• • •	•
			NSAY +1	SAY	•
2	MAIN	PCGCIN	1	INRST, INCALF, INCREK, INCALH, INCALG	8LF
			2	IPSICT, INPRST, INEACH, INCLET, INCLGE	•
			3	INCALN, INCURF, LEULP, INTFRZ, INSIMP	•

TABLE 5-2 (continued)

Group	Calling Routine	Data File[1]	Line	Data Items	Format
			4	INSMPC,INCLKE,LPOST	•
			5	INCNOX, POLLUT, INQRL, INCSWP, INCSWS	•
			6	INNOZZ, INFSOU, LTBUG, GRDOUT, INPROG	•
			7	INCFP, INRAD, INRDGD, INTRUS, MAGHJER	•
			8	INETA2,HTRACK,FGDVC,LAMINAR,LBUOY	•
			9	UPDOWN	*
			10	URFU, URFV, URFW, URFH	*
			11	URFE, URFK, URFF, URFG, URFVIS	*
			12	URFDEN, URFETA, URFGET, URFNJ, URFPP,URFP	*
			13	DIAP, DIAS, DIACH	*
			14	NDIA(REAL), THICK	*
			15	MAXIT, INDPRI, INDRST	*
			16	NJINP, NJINS, NIWOQ	*
			17	AL1, EPSX, NL, EPSI, EPSD	*
			18	TMIN, TMAX, HLOSS	*
			19	TLODEL, THIDEL	*
			20	NIINQ, QHA, QLX	*
			21	TBN, TBW, TBE	*
			22	VISCOS, PRES, IEUCK	*
			23	SORMAX, SORMIN	*
3	INFLOW	PCGCIN	1	STRING	A5
			2	FLOW(I), FFLOW(I), SWIRLN(I), TINFLO(I), PLOAD(I), PLOADS(I) I=primary, secondary [,1, . . . ,NINLET]	*
4	CREEØ	PCGCIN THERMO	1	ELEM	A4
			2	ATOMID(NLM), ATOM(1, NLM), ATOM(2,NLM) repeat the above card for each element (NLM total)	A2, 7X, 2F10.6
			3	BLANK LINE	A4
5	CREEØ	PCGCIN THERMO	1	THER	A4
			2	DATA(1), DATA(2), DATA(3)	3A4, 6X

TABLE 5-2 (continued)

Group	Calling Routine	Data File[1]	Line	Data Items	Format
				DT1, DT2, AT(1), B(1)	2A3, A2, F3.0
				AT(2), B(2), AT(3), B(3)	2(A2, F3.0)
				AT(4), B(4), PHASE	A2, F3.0, A1
				TLOW, THIGH	2F10.3
				IDON(1), IDON(2), IDON(3), IDON(4)	4I3
				NCD	I3
			3	Z(1, 1, NS), Z(2, 1, NS), Z(3, 1, NS)	3E15.8
				Z(4, 1, NS), Z(5, 1, NS), NCD	2E15.8, I5
			4	Z(6, 1, NS), Z(7, 1, NS), Z(1, 2, NS)	3E15.8
				Z(2, 2, NS), Z(3, 2, NS), NCD	2E15.8, I5
			5	Z(4, 2, NS), Z(5, 2, NS), Z(6, 2, NS)	3E15.8, I5
				repeat the above 4 cards for each chemical species (NS total)	
			6	BLANK LINE	A4
6	CREEØ	PCGCIN	1	REAC	A4
			2	TMP	*
			3	AT(1), B(1), . . . , AT(4),B(4),	4(A2, F7.5)
			3	ASUB(1), ASUB(2), PECWT,	2A4, 1X, F7.5
			3	MOLE, PHASE	A1, 9X, A1
				Repeat the above card for each species in the primary reactant stream	
			4	BLANK LINE	A4
				Repeat group 6 once for the secondary stream	
7	PSICTØ	PCGCIN	1	NSL, NPS	*
			2	PDEN	*
			3	XPS(ISL), YPS(ISL), SPRANG(ISL)	*
				Repeat previous line for a total of NSL times	

TABLE 5-2 (continued)

Group	Calling Routine	Data File[1]	Line	Data Items	Format
			18	Y0(5)	*
			19	Y0(6)	*
			20	Y0(8)	*
			21	Y0(9)	*
			22	Y0(10)	*
			23	Y0(11)	*
			24	Y0(12)	*
			25	Y0(13)	*
			26	Y0(14)	*
			27	Y0(16)	*
			28	Y0(17)	*
			29	Y0(18)	*
			30	Y0(19)	*
			31	Y0(20)	*
			32	Y0(21)	*
			33	Y0(22)	*
			34	Y0(23)	*
			35	Y0(27)	*
9	GETKIN	PCGCIN	1	STRING (kinetics file name)	A
		STRING	2	VERSN	*
			3-46	SIGMAA(I), I=1,44	*
			47	CS	*
			48	AA	*
			49	BA	*
			50	ATAR	*
			51	BTAR	*
			52	AM	*
			53	BM	*
			54	ASZ(1)	*
			55	BSZ(1)	*
			56	ASZ(2)	*
			57	BSZ(2)	*
			58	AOL	*
			59	BOL	*
			60	AAC	*
			61	BAC	*
			62	ASOOT	*
			63	BSOOT	*
10	NETIN	PCGCIN	1	STRING (polymer file name)	A
		STRING	2	VERSN	*

TABLE 5-2 (continued)

Group	Calling Routine	Data File[1]	Line	Data Items	Format
			3	OLIGST, MONO, FETHYL, FLINK, BEAD, XT0, CNST2, Q0, PH0	*
			4	MMASS(1), MNUMB(1)	*
			⋮	⋮	⋮
			MONO+3	MMASS(MONO), MNUMB(MONO)	*
			MONO+4	XEFF(J), J=1,35	*
			MONO+5	RADI0, DENSTY, PRESS, AMVSOL, AMWCOL, VSRCOL, VSRMIN	*
			MONO+6	MERS, DVG1, VISENG, DVG3, DVG4, VSTMAX, VISMAX, PHIMAX	*
			MONO+7	MERMAS(J), J=1,MERS	*
			MONO+8	MASSLM(J), J=1,2	*
			MONO+10	LJUNK1	*
			MONO+11	LJUNK2	*
			MONO+12	S1, S2	*
			MONO+13	SURF0	*
			MONO+14	EPS0	*
11	NETIN	mass_bin	1	AVEMW, JMAX	*
			2	DUMMY, PDIST(1,J), J=1,JMAX	7F10.3
			⋮	⋮	⋮
			NBINS+2	DUMMY, PDIST(NBINS,J), J=1,JMAX	7F10.3
12	COALØ	PCGCIN	1	NCARD	*
			2	COMENT(1,1), . . . , COMENT (1, 14) . . .	14A4
			2	COMENT(2, 1), . . . , COMENT(2,14) . . .	
			2	COMENT(NCARD, 1), . . . , COMMENT(NCARD, 14)	
13	COALØ	PCGCIN	1	INCOAL	L5
			2	URFPM, URFPH	*
			3	NCRXN, NHRXN, NPROP, KEQ, NSHRNK	*
			4	DELTPJ, DELRRJ, GAMMA	*

TABLE 5-2 (continued)

Group	Calling Routine	Data File[1]	Line	Data Items	Format
14	COALØ	PCGCIN	1	XI(1)	*
			2	QHC(1), HHO(1), HAO(1)	*
		. .	3	HWO(1), TNBP	*
			4	OMEGAC(1), OMEGAH(1), OMEGAA(1)	*
			5	OMEGAW(1)	*
			6	AMJ(1,1), EMJ(1,1), YY(1,1)	*
			7	HGV(1,1) Repeat previous two lines for each raw coal reaction up to a total of NCRXN	*
			8	OXYD(1), OXYD(2) . . . OXYD(NHRXN)	5A4
			9	PHIL(1), PHIL(2), . . . PHIL(NHRXN)	*
			10	AL(1,1), EL(1,1), EMM(1,1) Repeat the previous line for each char reaction up to a total of NHRXN	*
15	GETRCT0	PCGCIN STRING	1	STRING (reactivity input file name)	A
			2	SURF0, EPS0, TAU0, PSI, RADP, MIN0	*
			3	E1(JP,1), E2(JP,2), EM(JP,2)	*
			⋮	⋮	⋮
			NXN+2	E1(JP,NXN), E2(JP,NXN), EM(JP,NXN)	*
			NXN+3	THIELE	*
16	COAL0	PCGCIN	1	WIC(1,1), WIC(1,2), . . . WIC(1, NLM) Repeat the previous line enough times to specify values for NLM elements, 3 on a line Group 11 parameters are used for all particles	*
17	MAIN	THERMO	1	ASUB(1,J), J=1,3	3A4
			2	S(1), EK(1), DELTA(1),HFORM(1) Repeat the previous two lines for each species up to a total of NS	*

TABLE 5-2 (continued)

Group	Calling Routine	Data File[1]	Line	Data Items	Format
			4	UPLAG(IPS), IPS=1,NPS Repeat previous line enough times to specify values for NPS particle sizes, 5 on a line	*
			5	TLAG(IPS), IPS=1, NPS Repeat previous line enough times to specify values for NPS particle sizes, 5 on a line	*
			6	PD(IPS), IPS=1, NPS Repeat previous line enough times to specify values for NPS particle sizes, 3 on a line	*
			7	PMF(IPS), IPS=1, NPS Repeat previous line enough times to specify values for NPS particle sizes, 5 on a line	*
			8	LPBUG, LYPS, LPARTP, LPARTS, LPBOTH	5L5
			9	LSPM, LSPU, LSPV, LSPH	5L5
			10	YPSH, YPSL	*
			11	MAXITP, MINITP, IGASV	*
			12	PRK(IPS), IPS=1, NPS Repeat previous line enough times to specify values for NPS particle sizes, 5 on a line	*
8	GETCDF	PCGCIN	1	STRING (coal composition file name)	A
		STRING	2	TITLE	A
			3-5	Lines not used	
			6	CA	*
			7	CB	*
			8	XCO0	*
			9	XHO0	*
			10	XO0	*
			11	XNO0	*
			12	XSO0	*
			13	XSM0	*
			14	XOH	*
			15	Y0(1)	*
			16	Y0(2)	*
			17	Y0(3)	*

TABLE 5-2 (continued)

Group	Calling Routine	Data File[1]	Line	Data Items	Format
18	COALØ	PCGCIN	1	SLRCMP9I), I=1, 3	A4
			2	FBACK,LBACK	*
19	FLUXØ	PCGCIN	1	LDISO, LGASE, LEMCOR, MAXITR	3L5, 2X, I10
			2	EMW, TOUT	*
			3	AØ, AF	*
20	PROFIL	INLET	1	UPDAT, KOPUP, USDAT, KOPUS	2(1X, L1, 1X, I3)
			1	UPD(N), KOPY(N), N=1, NINLET	3(1X, L1, 1X, I3)
			2	VPDAT, KOPVP, VSDAT, KOPVS	2(1X, L1, 1X, I3)
			2	VPD(N), KOPV(N), N=1, NINLET	3(1X, L1, 1X, I3)
			3	WPDAT, KOPWP, WSDAT, KOPWS	2(1X, L1, 1X, I3)
			3	WPD(N), KOPW(N), N=1, NINLET	3(1X, L1, 1X, I3)
			4	TIPDAT, KOPTEP, TISDAT, KOPTES	2(1X, L1, 1X, I3)
			4	TIPD(N),KOPTE(N), N=1, NINLE	3(1X, L1, 1X, I3)
			5	EDPDAT, KOPEDP, EDSDAT, KOPED	2(1X, L1, 1X, I3)
			5	EDPD(N), KOPED(N), N=1, NINLET	3(1X, L1, 1X, I3)
21	PROFIL	INLET	1	PLS, SLS	*
			2	NSFORM, ALPHAO	*
			3	RP, RS1, RS2	*
			4	UIN(1), VIN(1), WIN(1), TURBIN(1)	*
			4	EDIN(1), RIN(1) Repeat line 4 for entire profile defined by an arbitrary number of radial locations	*
22	NOXMN	NOXIN	1	NSAYNX	*

TABLE 5-2 (continued)

Group	Calling Routine	Data File[1]	Line	Data Items	Format
			2	SAYNX(1), SAYNX(2),... SAYNX(18)	18A4
			•	• • •	
			NSAYNX+1	SAYNX(1), SAYNX(2),... SAYNX(18)	18A4
23	NOXMN	NOXIN	1	FUELNO	*
			2	THRMNO	*
			3	RADOXY, EQTEST, RADOH, OHADJS	*
			4	CHARNO	*
			5	PRNOX,PRHCN, PRNH3, FCTNO, FCTHCN,FCTNH3	*
			6	MXITNX, ITYNX, INDPNX, ICALCN	*
			7	XIANOX, ZEDA, FN2PRT, MAXRES	*
			8	IRSTNX, IPLTNX, INHTNX	3L5
24	SORB0	SOXIN	1	NSAYSX	*
			2	SAYSX(1), SAYSX(2),... SAYSX(18)	18A4
			⋮	⋮	
			NSAYSX+1	SAYSX(1), SAYSX(2),... SAYSX(18)	18A4
25	SORB0	SOXIN	1	NSTYPE	*
			2	NSLS, NPSS	*
			3	SPDEN	*
			4	BETSUR	*
			5	XPS(ISL), YPS(ISL), SPRANG(ISL) Repeat the above line for each sorbent particle starting location.	*
			6	PDS(IPS), IPS=1,3 Repeat the above line enough times to specify particle diameter for all sorbent particle sizes, 3 on a line.	*
			7	PMFS(IPS), IPS=1,5 Repeat the above line enough times to specify mass fractions for all particle sizes, 5 on a line.	*

TABLE 5-2 (continued)

Group	Calling Routine	Data File[1]	Line	Data Items	Format
			8	LSPBUG, LSYPS, LPARTP, LPARTS, LPBOTH	5L5
			9	LRBNDS	5L5
			10	YPSH, YPSL	*
			11	PRKS(IPS), IPS=1,5 Repeat the above line enough times to specify values for all particle sizes, 5 on a line.	*
			12	PRSO2	*
			13	MXITSX, MAXRES	*
			14	URFSO2	*

[1]Indicates data file where information is found.

[2]If case uses restart file for particles (INPRST = TRUE), it is read in prior to reading data group 6.

Group 7 gives information about the particles, including the number of particle starting locations (up to NUMSTR), number of particle sizes (up to NUMPAR), particle density, starting location of the trajectories, initial particle velocity and temperature, initial particle size distribution, particle Prandtl number, and information controlling the particle phase calculations, such as maximum number of particle iterations.

Groups 8 through 18 give information about the solids composition and reactions. Groups 8, 9, 10, and 11 contain input data for the FG-DVC submodel and are described in more detail in Chapter 6. Group 12 contains any number of comment cards which are reprinted in the output file. Group 13 specifies the number of reactions and numerical control parameters. Group 14 gives kinetic parameters for each of the devolatilization and char oxidation reactions (if FGDVC=F), as well as the oxidizing species and stoichiometry. Group 15 contains input data for the reactivity submodel that goes along with the FG-DVC devolatilization submodel. These data are explained in more detail in Chapter 6. Group 16 gives the elemental analysis of the "raw coal" portion of the particles. Group 17 gives the Lennard-Jones parameters for predicting the transport properties of the gas species. Group 18 specifies the slurry component and fraction of enthalpy from volatiles combustion that should be fed back directly to the particle.

Group 19 gives information for the radiation submodel, including the method of solving the governing equations (Varma six-flux or discrete ordinates),

whether to include gas emissivities sand corrections, and maximum number of iterations. Absorption and scattering cross-sections are calculated by the model, based on particle size.

Groups 20 and 21 contain data for calculating (theoretical) or reading (experimental) profile data for velocity, turbulence intensity, and eddy dissipation for the primary and secondary inlets. These data are contained in the inlet profile data file.

Groups 22 and 23 contain input data for the NO_x pollutant submodel. Group 22 contains comment statements. Group 23 contains the kinetic, numerical, and program control parameters.

Groups 24 and 25 contain input data for the sorbent reactions submodel.

As explained above, several optional data files may be included as input to PCGC-2. These include: 1) a file containing information which describes the grid geometry (assigned logical name GRIDS in the FORTRAN subroutine GRMAP), 2) files used as initial guesses based on previous calculations for the gas phase (assigned logical name INOUT in the FORTRAN subroutine RESTRT) and for the particle phase (assigned logical name PARSOU in the FORTRAN program PCGC2), and 3) a file consisting of the equilibrium table (assigned logical name TBLRST in the FORTRAN subroutines TBLRSTFE and TBLRSTFEH) used in calculating gas properties (temperature, density, etc.) as functions of the progress variables `f`, `h`, and `hr`.* Each of the data files are accessed in VAX/VMS FORTRAN using an OPEN statement. Some use the IOSTAT qualifier to insure proper operation. IOSTAT is assumed equal to 0 if the open command is successful.

* An option is provided (INCALH = F) for assuming a locally adiabatic reactor, in which case h is not independent of f and η.

Program Output

Program output is contained in the main output (PCGCOT) and log (for batch runs) files. The quantity of output in the main output file is controlled by the relative values of INDPRI and MAXIT ash shown in Table 5-3. Three options are available: Output can be a) turned completely off, b) restricted to the beginning and end of the calculation, or c) printed periodically during program execution. Option (a) is used most commonly, since the output file can \get rather large and cumbersome otherwise, and graphics are usually used to examine code results.

Table 5-4 presents an outline of the output file produced during a PCGC-2 computation. All of the input parameters (i.e. thermodynamic properties, flowrates, particle size information, coal reaction rate information, and radiation information) and many parameters calculated from them are written to the output file early during execution (Option b and c). Also, the initial values for each scalar field (i.e. gas temperature, velocities, pressure, etc.) used for initialization are written to the output file. During the iteration process, values of each critical field variable are printed for each node point in the computational grid (Options c). The y (or r) values of the grid are found at the right-hand side of the array, and the axial location (x) is found along the bottom of the grid printout. Since the sample grid is too long to be printed in one block, it is "wrapped around" in three segments. The index values for the node point (I and J) are also printed out. Other gas properties are printed only upon convergence or after other normal termination (Options b and c).

The particle trajectory information is printed out each 10 trajectory time steps as the calculations proceed. Among other things, the output shows the location of the particle (XP and YP), the time step of integration (DT), and the elapsed residence time along the particle trajectory (TIME), the particle and gas temperatures (TMP and TG), the mass of liquid, raw coal, char, ash, and total mass of the particle normalized by the original particle mass (WFRAC, CFRAC, HFRAC, AFRAC, TFRAC, respectively). This information is given for each of the particle trajectories (ISL = initial starting location, and IPS = initial particle size).

In addition to the main output file, several other files contain program results. These are summarized in Table 5-5. Standard FORTRAN 77 commands were used, where possible, to manipulate these files.

TABLE 5-3

PROGRAM OUTPUT CONTROL

INDPRI	Output
a) <0 or > MAXIT	None
b) = MAXIT	Input summary, initial values of field variables, final values of field variable.
c) > 0 and < MAXIT	Same as b) plus intermediate output of field variables every INDPRI iterations.

TABLE 5-4
OUTLINE OF OUTPUT FROM PCGC-2 CALCULATION

I. INPUT DATA FOR COMPUTATION
   a) Comment lines describing calculation
   b) Elements considered
   c) Thermodynamic data required to predict equilibrium properties
   d) Inlet stream information
   e) Particle property information
   f) Particle reaction information
   g) Radiation information
   h) Reactor parameters
   i) Computational grid information
   j) Initial scalar fields (i.e. velocity, mixture fraction, etc.)

II. GAS PHASE ITERATION INFORMATION (see note below)
   a) Normalized residual source sums

III. PARTICLE ITERATION INFORMATION
   a) Time/position information for Lagrangian particle trajectories
   b) Axial mixing-cup coal burnout

IV. FINAL OUTPUT
   a) All scalar fields
   b) Summary of CPU time requirements

Note: Residual terms are printed for either INDRST iterations or until gas phase convergence is obtained. On gas phase convergence, the field variables are printed and the computation proceeds in the particle phase until convergence. After each Lagrangian particle calculation is completed, computation returns to the gas phase at which time the field variables are computed with the updated particle source terms. If the difference between and the most recent calculated field variables and those calculated at the end of the last gas phase iteration is less than SORMIN the calculation is complete. Otherwise, computation continues in the gas phase after gas phase. If the gas phase converges in fewer than MINITP iterations, the calculation is considered complete. Otherwise, computation returns to the particle phase after gas phase convergence, and the process is repeated. On overall convergence, the field variables are written to the output file along with a summary of the time required.

TABLE 5-5

PCGC-2 OUTPUT FILES

Filename	Type	Description
GASPLT	Text	Eulerian gas properties and particle density for plotting
INOUT	Binary	Eulerian gas properties for plotting
output.fg	Text	FGDVC submodel results
PARSOU	Binary	Particle source terms for restart (INPRST = T)
PCGCOT	Text	Main output file
POLPLT	Binary	Pollutant data for plotting
PPLOT1	Text	Number of records for each trajectory in PPLOT2 and pointers to trajectories in PPLOT3
PPLOT2	Text	Particle coordinate residence time, and time increment for plotting. Also contains radially integrated burnout and centerline mixture fraction data
PPLOT3	Text	Particle coordinates, composition, temperature, and gas temperature for plotting
PRGRSS	Text	Residual source sums and gas properties at a selected point in the reactor for monitoring progress toward convergence
PSORB1, PSORB2, PSORB3	Text	Same as PPLOT1, PPLOT2, PPLOT3, except for sorbent particles
RSNXIO	Binary	NO_x pollutant data for restart (IRSTNX = T)
SORDN1	Text	Restart file for sorbent particle number density
TBLRST	Binary	Gas property data

TABLE 5-5 (continued)

Filename	Type	Description
TWODDBV	Binary	Gas plotting file for CEQUEL post-processor
YH2S1	Text	Restart file for H_2S concentration with sorbents
YSO21	Text	Restart file for SO_2 concentration with sorbents

Code Operation

PCGC-2 is a "user-specialist" code that requires familiarity with the theory and structure of the code in order to be used correctly and efficiently. This section gives several hints for new users. A thorough understanding of the problem physics and numerical assumptions is essential.

New Cases

When setting up a new problem for simulation, it is easiest to start by editing input files from a previous, similar, simulation, if one is available. If not, the pre-processor can be used as explained later in this chapter.

Restart

Unless the user has a converged or partially converged solution of a similar problem with identical geometry, he will probably want to start his problem from "scratch". To do so, the logical variables that will cause the code to try to "restart" from a guessed solution (INRST, INPRST, and IRSTNX) must be set equal to F in the main input file. This will not prevent the code from writing restart files for future restarts, since writing to restart files is automatic at a frequency specified by the variable INDRST. A value of 50 is recommended. Subsequent runs for the same case can be restarted from a previously converged solution by setting the above logical variables equal to T in the input file. The restart feature is useful

when small changes are made for the same case and geometry. If the changes are large or the geometry changes, the restart option should no be used.

Particle and Gas Iterations

The maximum number of particle iterations is controlled by the parameter MAXITP. It typically takes 5-15 particle iterations to converge a PCGC-2 calculation from scratch. The maximum number of gas iterations is controlled by the parameter MAXIT. A typical value of MAXIT is 1000.

Gas Convergence

The code has the capability of completely converging the gas phase for every calculation of the particle phase, which is the normal approach, or of calculating the particle phase every 5 iterations of the gas phase. The latter approach is used when INEACH is set to T. and may be useful in cases where the gas and particles are highly coupled. In all cases, convergence of the gas phase is controlled by the value of SORMAX. Overall convergence is controlled by SORMIN.

An efficient approach to obtaining a solution is as follows. Obtain an approximate solution by selecting large values for SORMAX and SORMIN, 1.0 and 2.5 respectively, for example. Systematically reduce both parameters, converging the case between each change. For example, after a case is converged with SORMAX = 1.0 and SORMIN = 2.5, change the parameters to 0.1 and 0.5, respectively. Then change them to 0.01 and 0.10, respectively. This is usually sufficient for most cases. If detailed analysis of trace species is desired, both may be reduced further. It is usually desirable to solve the NO_x and sorbent reactions submodels only after the main code is converged to the desired level.

Gaseous Combustion (No Particles)

For gaseous combustion (no particles), the following control variables should be turned off (set equal to F): INCLET, INCLGE, IPSICT, INPRST and INCALN. This will prevent the calculation of the coal gas mixture fraction and its variance, particle trajectories, and particle Eulerian density. In addition, the input data for the particle phase (data groups 7-13) should be removed.

Coal Particle Combustion

In most combustion simulations, both the primary and secondary gas streams are composed of air and are therefore identical in composition. If the gas streams were also identical in temperature, it would be unnecessary to calculate the gas mixture fraction (controlled by INCALF) or its variance (INCALG). However, the secondary stream is usually preheated, and in this case is may be important to calculate the gas mixture fraction. However, the turbulent fluctuations can often be ignored, even though there is a difference in temperature. Of course, the coal-gas mixture fraction (controlled by INCLET) and its variance (controlled by INCLGE) must always be calculated when reacting coal particles are present.

Energy Equation

If a locally adiabatic solution is desired, the calculation of enthalpy can be turned off with the logical INCALH. Otherwise, the energy equation is explicitly solved subject to the given temperature boundary conditions (TBN, TBW, and TBE).

If the energy equation is to be solved, upper (TMAX) and lower (TMIN) bounds for temperature must be given. These bounds are for the equilibrium table for gas properties. It is recommended that the table debug flag (LTBUG) be turned on when generating a new table. This will stop execution after table generation so that the results of the table generation calculations can be reviewed before the actual simulation begins. If failures in the equilibrium algorithm occur during table generation, messages will appear on the screen and in the output file (if one is being generated).

TMIN should be set equal to the lowest expected temperature in the simulation. This is usually the temperature of the coldest inlet stream. TMAX should be set equal to the highest expected temperature. This is usually 2500 K for combustion and 3500 K for oxygen-blown gasification. Sometimes, wider limits may be required. If so, the code will print a message to that effect during execution. It is desirable to keep the limits as narrow as possible in order to confine the table to the region of interest and maximize the accuracy of the table look-up and interpolation procedure. In order to further narrow the table limits and improve accuracy, two other parameters are required. TLODEL and THIDEL specify the maximum variation in temperature on the low side and on the high side compared with the adiabatic temperature at a given stoichiometry. IF TLODEL and THIDEL are large, TMIN and TMAX will always be limiting. If TLODEL and THIDEL are not large, they may be used to confine the region of the table closer to the adiabatic temperature. Again, if the code requires properties at temperatures outside the table

limits, it will print a message to that effect on the screen and tell the user which parameter to adjust and suggest a value to adjust it to.

Whenever table values are needed by the program outside the range of the table, the residual enthalpy is reset to the table limiting value for the particular values of f and η, and a counter (NCREE) is incremented. NCREE is printed in the log and output files, and therefore represents the number of times (for a given gas-phase iteration) the residual enthalpy was outside the table limits. For an unconstrained solution, NCREE should be equal to zero at the solution. The narrower the table limits, the fewer the number of table failures, but the larger the value of NCREE.

After successfully generating the table, LTBUG should be turned off to allow the combustion calculation to proceed using the table that was generated previously. A new table will then be generated only when a variable that affects the table generation is altered. If for some reason the user desires to regenerate the table, even though no variable affecting the table generation has been altered, he must delete the file containing the previous table (Runid.TBL or TBLRST).

There is a high degree of energy coupling between the particle and gas phases, and it may be necessary to reduce the under-relaxation factor for the particle source term for enthalpy (URFPH). A value of 0.5 is typically used, but values as low as 0.1 may be required. As the solution is approached, it should generally be possible to slowly increase URFPH.

Radiation

In the 1987 version of PCGC-2, the discrete ordinates method was first included as an option in the radiation submodel. This option can be chosen by setting the logical variable LDISO equal to true in the main data file. Gas-phase radiation is included if LGASE is set to true; otherwise only radiation due to the particulates (excluding soot) is considered. The gas phase radiation is calculated in two ways: if LEMCOR is set to true, the calculation includes the corrections in gas emissivities due to species partial pressures and spectral overlap of CO_2 an H_2O emissivities, using the Hottel chars (Hottel and Sarofim, 1967); otherwise, the overall emissivity of the gas is calculated using the Hadvig (1970) plot. 'QAB' and 'QSC' are the absorption and scattering efficiencies of the particulates based on Mie theory. These are calculated internally by the code, as a function of particle diameter.

The scattering phase function was changed to linearly anisotropic in the 1987 version of the code because it can be adjusted to account for either isotropic, or strongly forward- or backward-directed scatter. Since scatter by coal/char particles is known to be strongly forward-directed, the recommended value for a_o,

the asymmetry factor, is 1.0. The phase function used in earlier versions of PCGC-2 was that for ash particles (Hottel and Sarofim, 1967), which represented strongly backward-directed scatter.

Finally, the user can choose a value for the differencing factor, *f*, in extrapolating intensities across volume elements. This parameter is contained in the main data file. If a value of 1.0 (i.e., central differencing scheme) is chosen, and negative intensities are encountered, the radiation submodel will automatically adjust (reduce) the value of *f* until the negative intensities are all removed. This is expected to result in slightly more accurate predictions of the intensity field as compared with upwind differencing (i.e., f=0.0), but requires more computer time. It is therefore recommended that upwind differencing (f=0.0) be used.

Numerical Algorithm

Two choices of numerical algorithm for solving the gas phase are provided: SIMPLE and SIMPLER. In addition, either method may be used with the SIMPLEC approximation. SIMPLER (selected by INSIMP equals T) with SIMPLEC (INSMPC=T) is recommended in all cases because it is more efficient. The use of SIMPLE requires significantly lower under-relaxation parameters, as explained below.

Under-relaxation

When using SIMPLER, values of 0.7-0.9 are recommended for all under-relaxation factors for the independent gas field variables except URFPP and URFP (which should be 1.0) and URFDEN (which should be 0.5-0.7). When using SIMPLE, all factors should be substantially lower (0.3-0.6). A value of 0.9 is recommended for URFH for both algorithms. Of course, these factors are problem-dependent, and the convergence rate can be increased by increasing the under-relaxation factor of variables that seem to be controlling the convergence rate, as determined by monitoring the terminal-directed output from the code. The most efficient mode of operation is for each under-relaxation parameter to be as high as possible without causing the program to oscillate or diverge. However, optimizing the under-relaxation parameters is a difficult process and often takes more time than converging the code with non-optimum values. In addition to being problem-dependent, optimum values also change with level of convergence for a single problem, further complicating any optimum procedure. If desired, under-relaxation factors can be altered interactively every 25 iterations by setting INCURF equal to T.

A value of 0.5-1.0 is recommended for the particle phase under-relaxation (URFPM). This parameter is applied to all particle source terms except enthalpy. The latter uses URFPH, which often requires a much lower value (e.g. 0.1) to converge.

Maximum Number of Iterations and Generation of Output

A value of 1000 is recommended for the maximum number of iterations for the gas phase (MAXIT). The frequency of intermediate output is determined by INDPRI. A value of zero is recommended unless printed output is desired.

Grid Generation

The maximum number of nodes for both the axial and radial directions is determined by the values of NUMXPT and NUMYPT in the file PARAMETER.INC. Enough node points should be used to achieve grid-independence. In most cases, it is wise to use at least 40 node points in each direction. Many cases may require more node points.

Only the number of axial node points is specified directly in the input. This is done by the variables NIINQ (number of nodes inside the quarl region) and NIWOQ (number of nodes outside the quarl). The sum of these two variables is the total number of axial nodes (must be less than or equal to NUMXPT). The spacing of the nodes is determined by AL1, EPSX, and NL.

The number of radial nodes is specified indirectly by NJINP, NJINS, EPSI, EPSD, and INNOZ. The grid generation algorithm uses these parameters to generate a grid for specified reactor dimensions that spaces the grid points closely near the reactor centerline and near the walls, where gradients are expected to be large, and less closely in regions where the gradients are expected to be small. Trial and error is often required to generate an acceptable grid for new geometry.

The program also allows the user to specify the grid locations directly. In this case, another input file for the grid must be created, and the variable INRDGD in the input must be set equal to T. The recommended approach is to let PCGC-2 generate a grid file (GRDOUT equal to T and INRDGD equal to F) and then edit the resulting grid file that is generated. INRDGD can then be set equal to T.

Either grid point or cell face locations can be specified. If specifying grid point locations, the key word at the beginning of the GRIDS (.grd) file should be "NODE". If specifying cell face locations, the key word should be "FACE". It is easier to specify node locations, since faces are located midway between nodes. However, it is easier to model complicated geometry by specifying face locations. If the grid spacing is too non-uniform when specifying face locations, it may be

impossible to calculate the node locations such that the faces are located midway between adjacent nodes, unless the nodes are located outside of the cells. This condition is unacceptable. If it occurs, the cell face locations must be altered to achieve a more uniform grid, or more cells must be added.

The grid in the radial direction is configured based on either the secondary duct diameter (INNOZ = F) or both the primary and secondary duct diameters (INNOZ = T). The latter method was designed for modeling nozzles in slurry combustion. For dry (non-slurry) coal combustion, INNOZ is ordinarily set equal to false. In this case, NJINS represents the total number of nodes desired in the secondary duct and in the tube wall. The nodes in the secondary are all equally spaced. The equal node spacing in the secondary duct is also extended through the tube wall toward the primary duct. In the primary duct, the node spacing is decreased toward the centerline by the factor EPSD. It is possible, depending on the primary and secondary duct diameters and the values of NJINS and EPSD, to specify a condition where an infinite number of nodes would be required to reach the centerline. In this case, an error message will be printed in the log and output files. The remedy is to decrease NJINS, increase EPSD, or both. Alternatively, the nozzle configuring option (described below) may provide an acceptable grid in some cases (e.g. reactors with a large diameter relative to the primary stream).

To use the nozzle configuring option, INNOZ should be set equal to true. The grid will then be configured based on both NJINS and NJINP, the number of nodes specified in the secondary and primary ducts, respectively. In this case, the nodes are equally spaced in both the primary and secondary ducts, and the node spacing is incremented in the tube wall. This option puts the most closely spaced nodes in the primary duct.

Intrusions

The program can accommodate intrusions within the constraint of axisymmetric geometry. An intrusion is a boundary cell in the interior of the flowfield. To define intrusions, the grid structure must be read from an input file. Therefore, the easiest approach is to first generate a grid input file as described above, and then add intrusions at the appropriate locations by changing O's to X's. The logical variables INTRUS and INRDGD must both be equal to T to use this option.

Additional Inlets

Additional inlets are used in a manner similar to intrusions by altering a previously generated grid file. Up to three additional inlets may be specified by

changing X's to 1's, 2's or 3's at the appropriate boundary locations on the north or west walls. The flowrate, composition (in terms of the reactant streams), swirl number, and turbulence intensity must be specified in the input file for each additional inlet. In addition to modifying the grid file to show he location of the additional inlets, the inlet profile data file must be modified to give information for the velocity and turbulence properties profiles for the additional inlets. Currently, a flat profile is the only option for additional inlets.

Overall Code Convergence

Overall convergence of the code is assumed when the particle source terms do not change significantly between two consecutive particle iterations. Two criteria are used to determine this condition quantitatively, and these criteria are mutually independent. Satisfying either criterion causes the program to terminate with the assumption of overall convergence.

The convergence criteria are specified by two input parameters: SORMIN and MINITP. If the maximum residual source sum is less than SORMIN (typically 0.1) on the first iteration, then overall convergence is assumed. This is the first criterion. Since the gas phase is converged to the value of SORMAX (typically 0.01) each time, this means that if the maximum residual source sum increases from 0.01 to no more than 0.1 following a particle iteration, overall convergence is assumed. Overall convergence is also assumed if the gas phase can be reconverged to the value of SORMIN in less than MINITP (typically 25) iterations, regardless of the value of the maximum residual source sum on the first iteration after a particle iteration. This is the second, or alternative, convergence criterion. It is recommended that users attempt to converge their cases according to the first criterion because it puts a quantitative limit on the degree of mismatch between the particle and gas solutions.

The second criterion is intended primarily as a safeguard in case the user specifies values of SORMIN and SORMAX that make it impossible to satisfy the first criterion. For example, if the gas phase is not converged tightly enough (SORMIN too large), it may be impossible to satisfy the SORMIN criterion due to variations in the gas phase solution that feed to the particle phase and then back to the gas phase. This situation is usually typified by a solution that reaches a steady state and stops improving. The gas phase converges readily each time, but the maximum residual source sum on the first gas iteration after a particle iteration stops improving (decreasing). Tightening up (decreasing) the value of SORMAX causes the gas phase to be converged more tightly and may result in being able to satisfy the SORMIN criterion for overall convergence. This adjustment has been found to be particularly useful in cases without swirl. For example, if the swirl in the coal

combustion case in Appendix G is turned off, the case will not converge without tightening up the value of SORMAX from 0.01 to 0.005.

Particle Reaction Rate Parameters

The particle reaction rate parameters (AMJ, EMJ, YY, ALJ, EL, EMM, etc.) are coal-specific. Also, the code predictions are quite sensitive to these parameters, and they need to be chosen carefully, based on experimental data for the coal-type and conditions of interest (See Chapter 2).

NO_x/Sorbent Reactions Submodel

The NO_x and sorbent reactions submodels are decoupled from the main solution and can be executed separately, based on a previous solution of the main code. This is accomplished by setting `POLLUT` equal to T. The NO_x submodel is executed when `INCNOX` is set equal to `.TRUE.`. The sorbent reaction submodel is executed when `INSORB` is set equal to `.TRUE.`.

It was found that a value for `MAXRES`$\leq$0.001 was sufficient to obtain a converged solution for a natural gas flame simulated with 1600 nodes. If less nodes are used, `MAXRES` should be set lower since the error is summed for all nodes. In determining convergence for PCGC-2, the analogous convergence criteria for all gas phase equations (e.g. pressure, enthalpy, and mixture fractions) is typically set equal to 0.01. This value is also suggested as a minimum for `MAXRES` for any natural gas or coal combustion simulation.

Achieving converged NO model solutions is often not trivial and requires appropriate selection of under-relaxation factors. Some difficulties may be encountered in obtaining converged solutions when either the empirical kinetics of Mitchell and Tarbell (1982) or the global rate expressions of Wendt and coworkers (Bose et al., 1988) are used. This difficulty is attributed to the coupling between chemical reactions. In order to dampen oscillations in the solutions from iteration to iteration, several combinations of under-relaxation factors may be required. This dampening can best be accomplished by running the code in an interactive debugger to allow manipulation of the under-relaxation factors. Despite this level of user-interaction, some cases may still be difficult to converge. In order to improve convergence, the parameter `ICALCN` can be used to dampen coupled interactions between the HCN and NH_3 reactions. With `ICALCN` assigned a value of 10, both the NH_3 and NO species continuity equations are often effectively converged while at the same time slowly progressing the convergence of the HCN continuity equation.

Chemical Species

The chemical species considered in the equilibrium calculations are governed by the input in the THERMO file. Data for additional species not being considered can be stored by moving them to the end of the file (after the Leonard-Jones parameters).

Coal-Water Mixtures

Simulation of coal-water slurries is limited to cases where all inlet gas streams have the same composition and temperature. The gas mixture fraction variable is then used to track the evaporating slurry liquid from the droplets rather than the inlet gas mixing. In such cases, INFSOU should be set equal to T to include a source term in the *f* equation. The variable OMEGAW is used to specify the initial liquid content of the slurry. For ordinary combustion of pulverized coal, OMEGAW is set equal to zero, and the inherent moisture of the coal is incorporated directly in the input composition and flowrate of the primary gas.

The variable INNOZZ allows specification of the primary nodes for grid generation rather than the secondary nodes. This option is useful when primary diameters are small, such as when slurry nozzles are being modeled. The option can also be used to generate a grid for dry coal combustion, however, if the diameter of the reactor is large compared with the primary diameter.

Graphics

Pre-processor

The pre-processor generates input files for PCGC-2. It is a separately licensable product available from ACERC as described in Chapter 1. It is based on the CQUEL program developed by the Engineering Computer Graphics Laboratory at BYU. Its purpose is to allow the experienced or inexperienced user of PCGC-2 to quickly set up the input files for a new case from scratch without having to understand all of the details about the input data, formatting, etc. The program is designed to be used with X-windows terminals or workstations.

When the program is first started, a menu bar appears at the top of the screen as shown in Fig. 5-2. A help window is provided near the bottom of the screen (It is shown near the top in Fig. 5-2 for illustrative purposes).

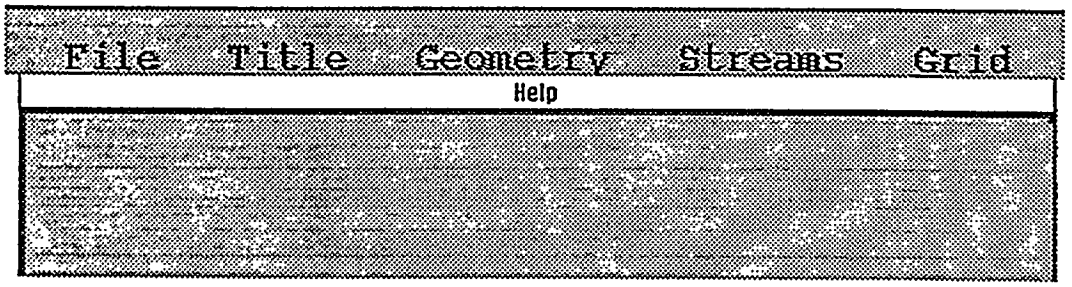

Fig. 5-2. Menu bar and help window.

Step 1: Load data files. The user first clicks on the word "File" in the main menu and selects either "New" or "Read" as shown in Fig. 5-3. "New" reads in default values from a set of files that the user can customize to his/her own particular needs. A standard set of default files are provided with the program. "Read" brings up a window where the user can type in the specific location and name of the files he/she wants to read into the pre-processor as shown in Fig. 5-4. Thus it is possible for the user to create a new case based on a previous case.

Fig. 5-3. Pull-down menu for reading and saving input files.

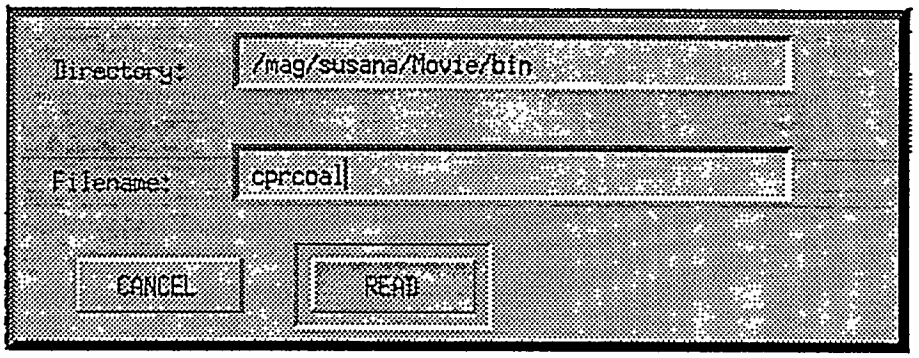

Fig. 5-4. Window for specifying filename for reading input files.

Step 2: Edit the title. The user then clicks on the word "Title" in the main menu and brings up the title window shown in Fig. 5-5. The title which appears is the one that was read in during Step 1. This can now be edited using standard mouse and keyboard entry techniques. After entering the title, the user clicks on the "SAVE" button to save his/her changes. Clicking on the "RESET" button changes the title back to what was originally read, and clicking on the "CANCEL" button gets rid of the window without saving any changes.

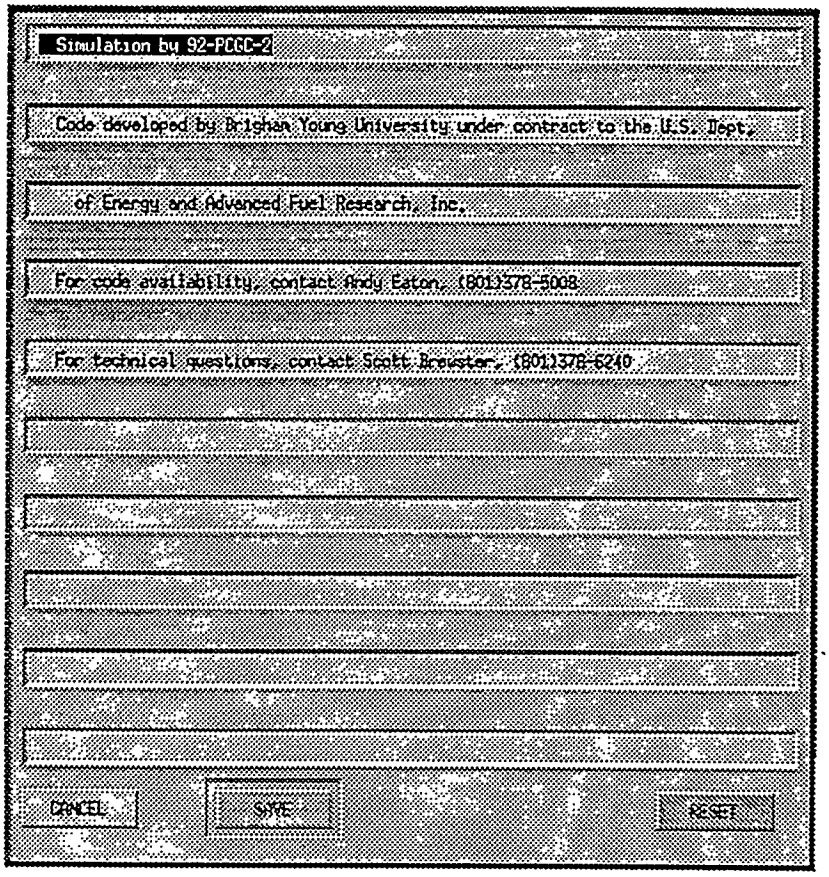

Fig. 5-5. Window for specifying simulation title.

Step 3: Enter the reactor geometry. The user then clicks on the word "Geometry" in the main menu and brings up the geometry window shown in Fig. 5-6. He/she edits the information shown, clicking on the desired units button for each data entry. He/she clicks on the desired configuration button, and then clicks on "DONE" to save the changes.

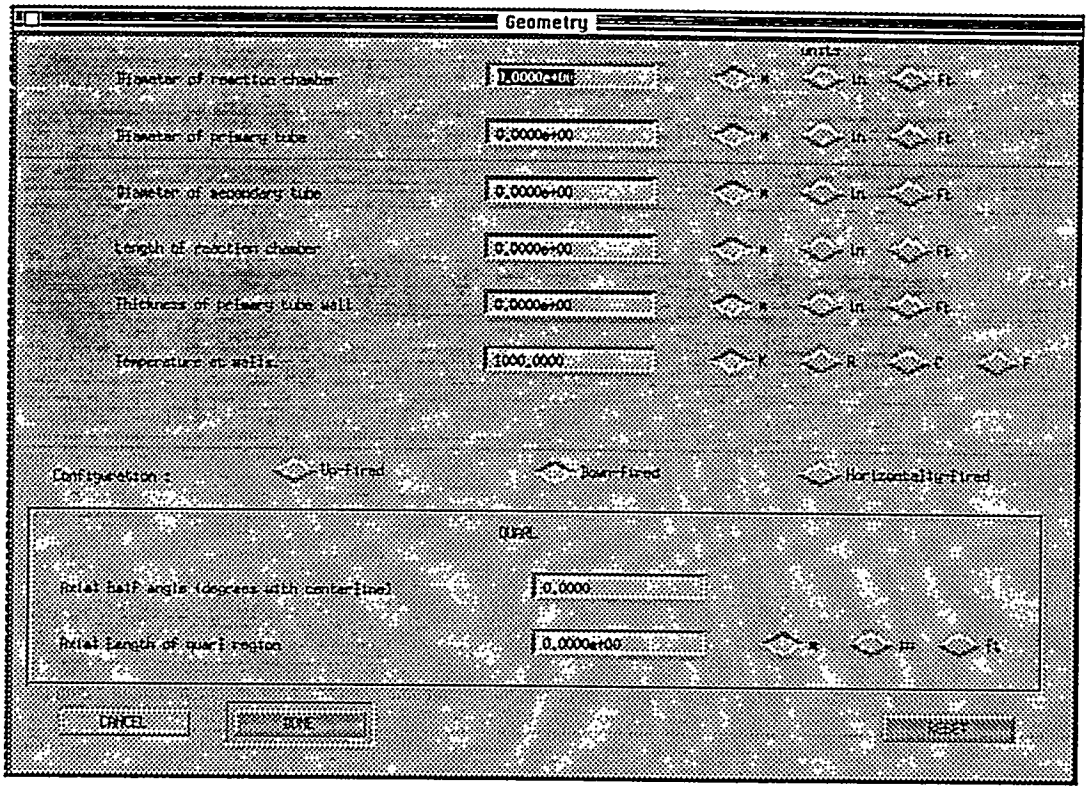

Fig. 5-6. Window for specifying reactor geometry.

Step 4: Specify the primary stream. The user then clicks on the word "Streams" in the main menu and selects the word "Primary," bringing up the primary stream window as shown in Fig. 5-7. Again, he/she edits the information shown using the mouse and keyboard. The "Other Species" button brings up a window with a scrollable list of species as shown in Fig. 5-8. To add one of these species to the primary stream, the user need merely select it and then click "DONE." The species gets entered automatically into the lower portion of the primary stream window. If the user knows beforehand what species are available and the library name of the species, it can entered directly into the primary stream window.

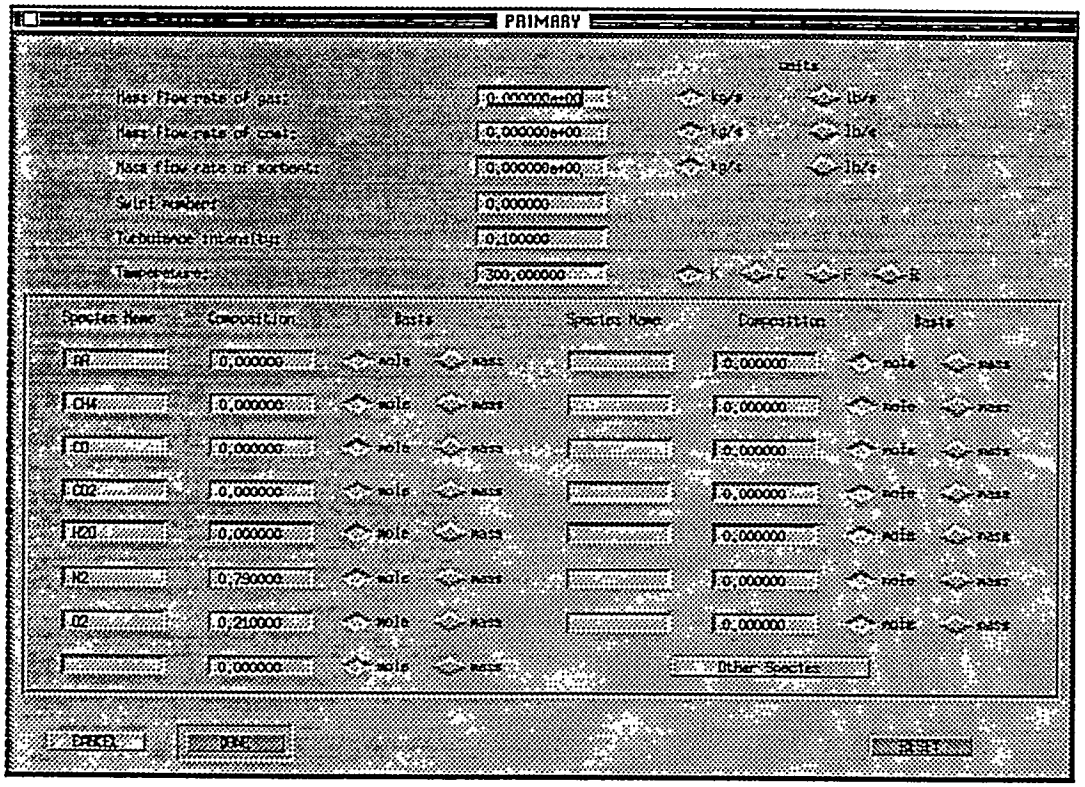

Fig. 5-7. Window for specifying primary inlet parameters.

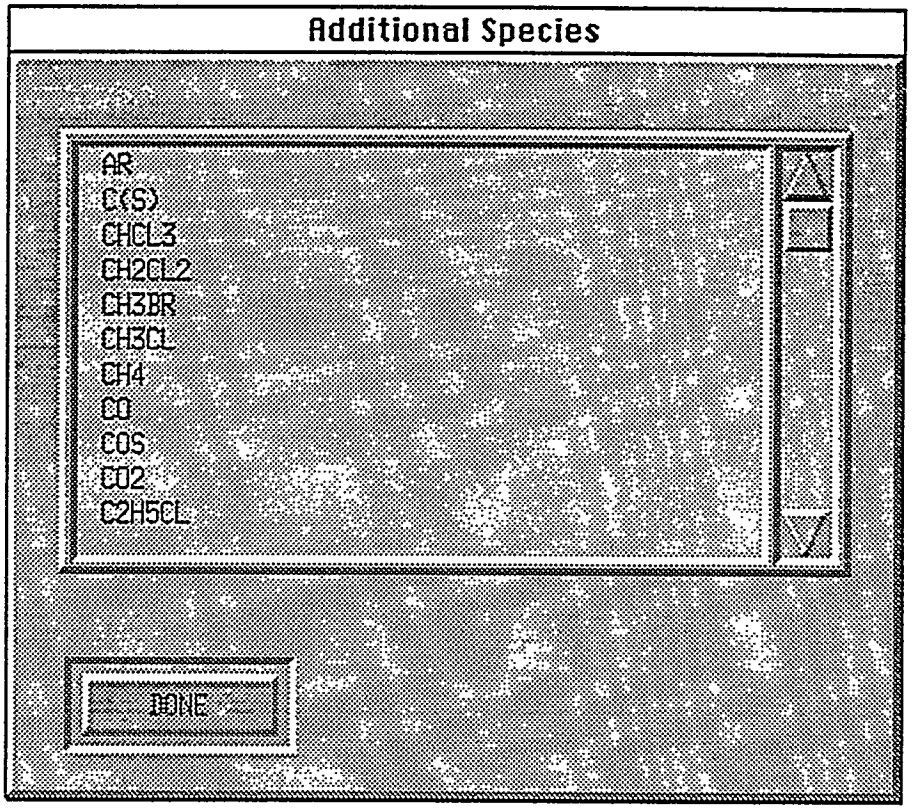

Fig. 5-8. Window for selecting chemical species to add.

Step 5: Specify the secondary stream. After specifying the primary stream, the user clicks again on the word "Streams" in the main menu and selects the word "Secondary," bringing up the secondary stream window. This window is identical to the primary stream window, and the user edits the data for the secondary stream just as was done for the primary stream.

Step 6: Generate the computational grid. This step may be performed any time after Step 3. To construct the computational grid, the user clicks on the word "Grid" in the main menu, thus bringing up the grid window shown in Fig. 5-9.

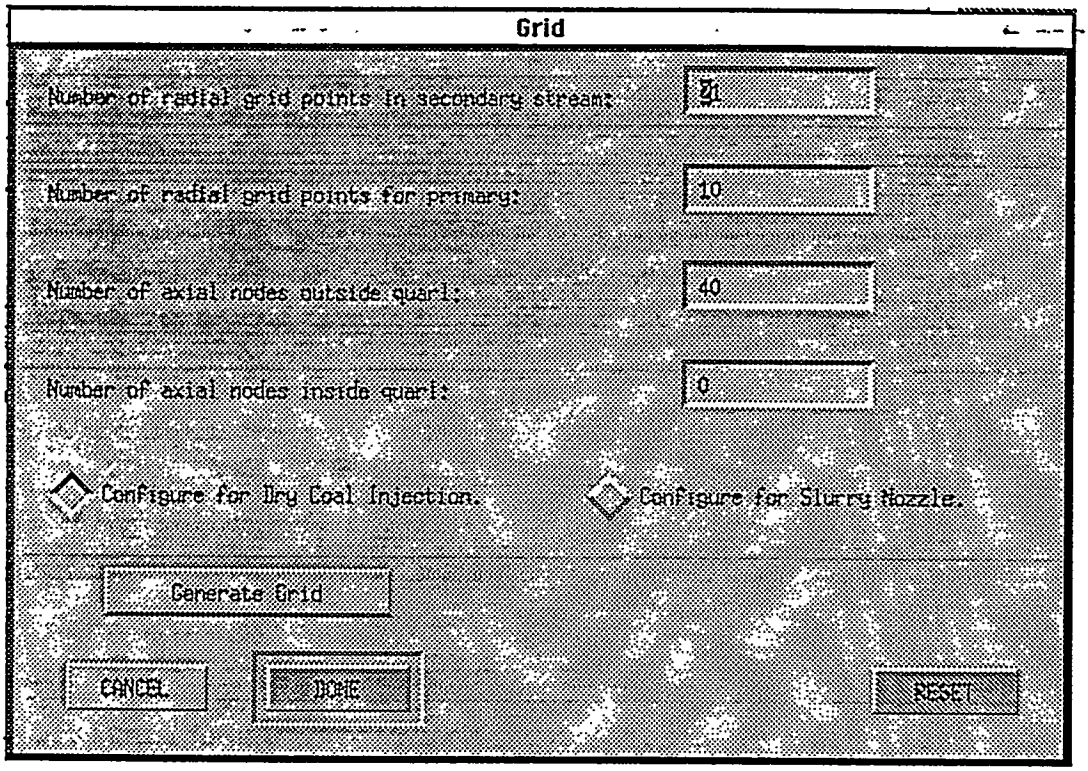

Fig. 5-9. Window for specifying grid generation parameters.

The user first enters an estimate for the number of radial grid points for the secondary duct. This is typically on the order of five. If the primary diameter is quite small relative to the secondary duct, he/she also enters an estimate for the number of grid points in the primary. The pulverized fuel combustion option is the one intended for most applications, for this case, a value of zero number for the radial grid points in the primary is used independently of the value inputted in the window. For slurry nozzles a non zero value for the radial grid points in the

primary must be given. Next the user enters the number of axial nodes desired for the quarl and outside-of-the-quarl regions. The total of these two numbers should be less than or equal to 100. After entering the required parameters, the grid can be generated by clicking the mouse on the "Generate Grid" button. A message will appear in the information window as shown in Fig. 5-10 giving the results. If the grid generation is successful, the number of radial grid points (NJ) will be printed. NJ must be less than or equal to 100. If the grid generation is unsuccessful, a diagnostic message will be printed.

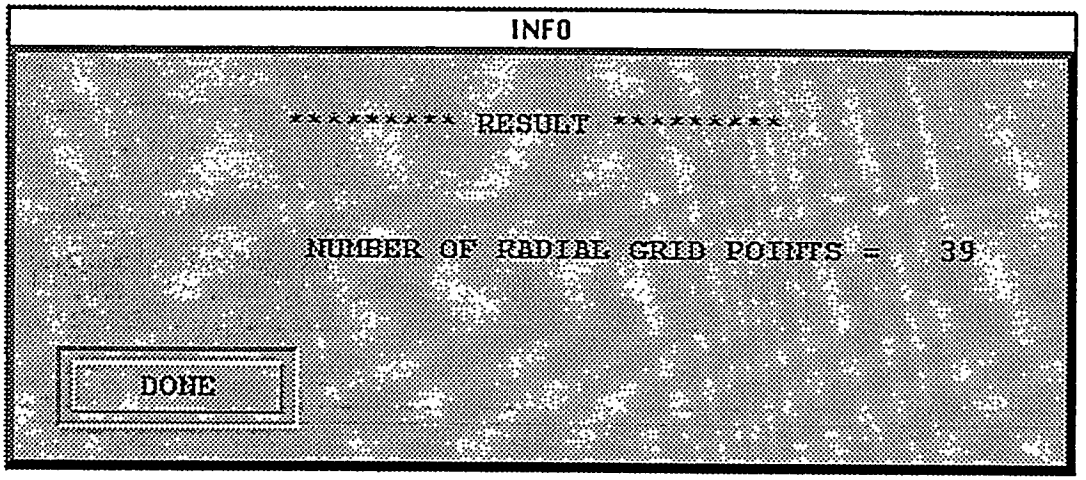

Fig. 5-10. Message window for generating the calculational grid.

Step 7: Enter the coal particle data. If coal particles are entrained in either the primary or secondary stream, the user can click on the word "Particles" in the main menu as shown in Fig. 5-11 and select the word "Coal."

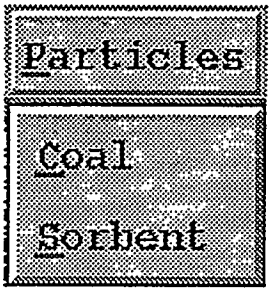

Fig. 5-11. Pull-down menu for selecting coal or sorbent particle properties.

The user will then enter the coal particle data in the coal window shown in Fig. 5-12. The pre-processor calculates the required input data for a flat particle size distribution based on the minimum and maximum particle sizes entered in this window. Any of the Argonne data bank coals can be selected by clicking on the appropriate box. The pre-processor assumes the user desires to use the FG-DVC devolatilization submodel. The desired oxidizers can also be selected by clicking with the mouse.

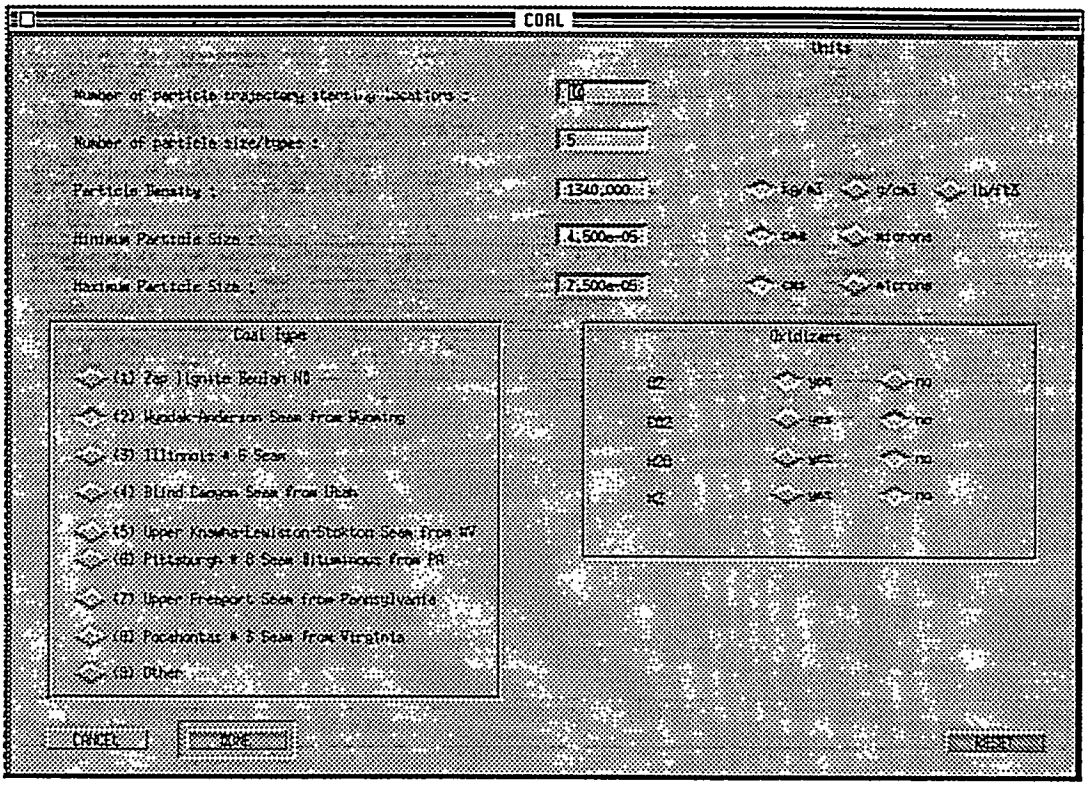

Fig. 5-12. Window for specifying coal particle input data.

If the user has a coal different from those of the Argonne data bank, the pre-processor can interpolate the Argonne data base to generate required data. This is done by clicking on the "other" button. The coal elemental composition is specified in the window shown in Fig. 5-13. After entering the required parameters, the coal data can be generated by clicking the mouse on the "Generate Coal Data File" button. A message will appear in the information window shown in Fig. 5-14 giving the results of the coal generation program. The user can also make changes to existing coal data files or the ones he/she just generated. To read existing data

files, the user must click on the "Data from Files" button. The Program will pop up a window so the user can specify the name of the files to be read.

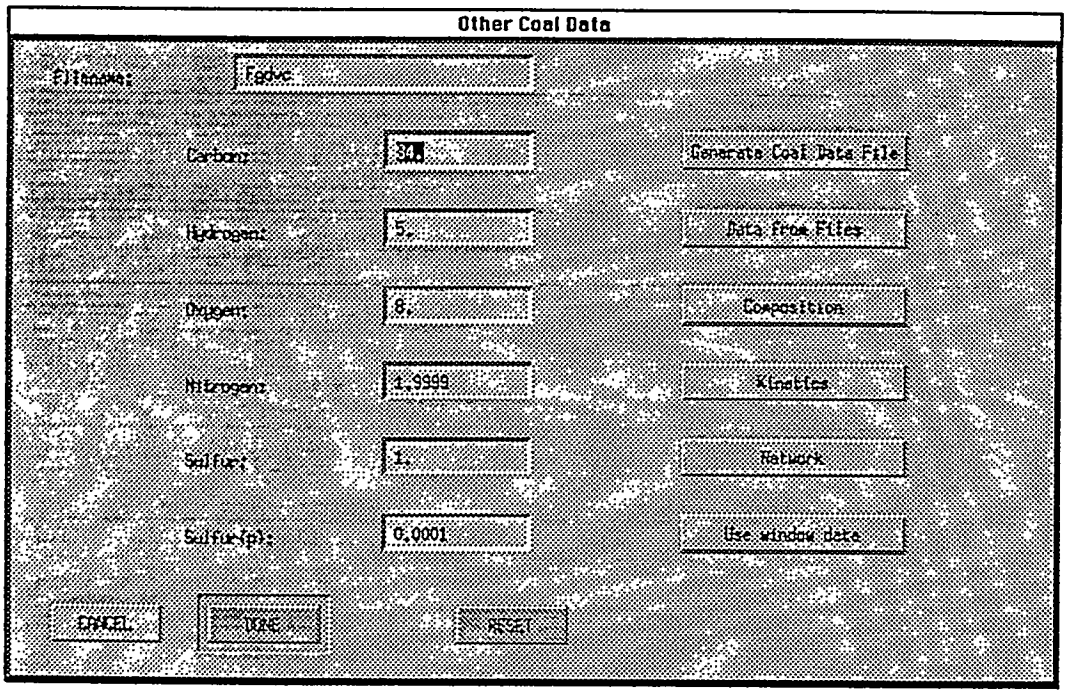

Fig. 5-13. Window for specifying elemental coal composition for coals not included in the Argonne data bank.

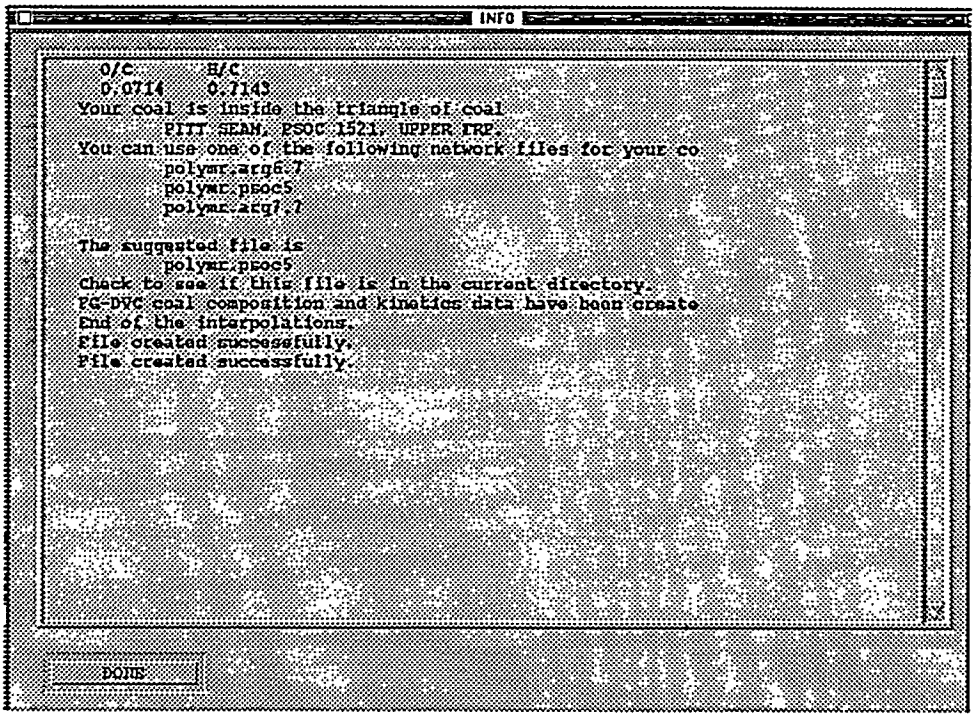

Fig. 5-14. Information window displaying results of coal data file generation program.

To make changes to the composition file, the user must click on the "Composition" button. This button will write the functional group composition of the coal in the information window, and will pop up a window, as shown in Fig. 5-15, where the user can make changes. Similarly, the kinetics data file can be modified as shown in Fig. 5-16.

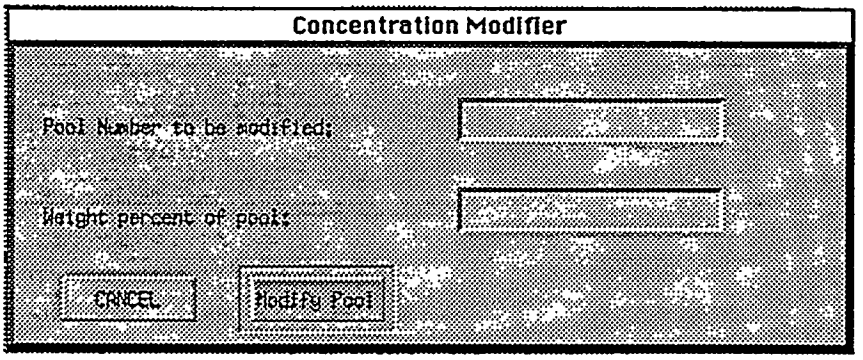

Fig. 5-15. Window for modifying coal composition data files.

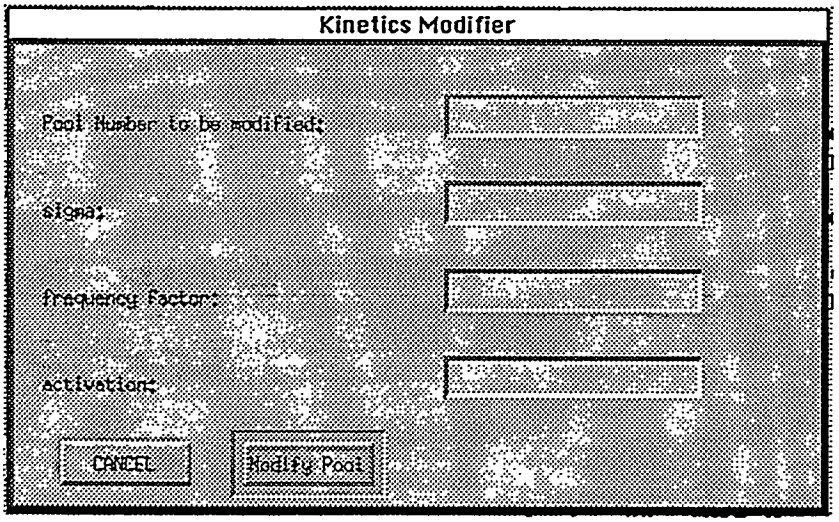

Fig. 5-16. Window for modifying coal kinetics data files.

The user can go back to the data in the window with the "Use window data" button. If an error occurs during any step, the program will pop up a different information window to help the user make the needed changes. The user can save the files by clicking on the "DONE" button. The program will save the files using the name indicated. If the files already exist, the program will ask for a different name to save the resulting data. For more information on the specifics of the coal data file generation program, the user can refer to Chapter 7.

Step 8: Enter the sorbent particle data. If sorbent particles are entrained in either the primary or secondary gas streams, the user clicks again on the word "Particles" in the main menu and selects the word "Sorbent." The sorbents window is shown in Fig. 5-17. As with the coal, a flat particle size distribution is assumed, based on the specified minimum and maximum particle sizes.

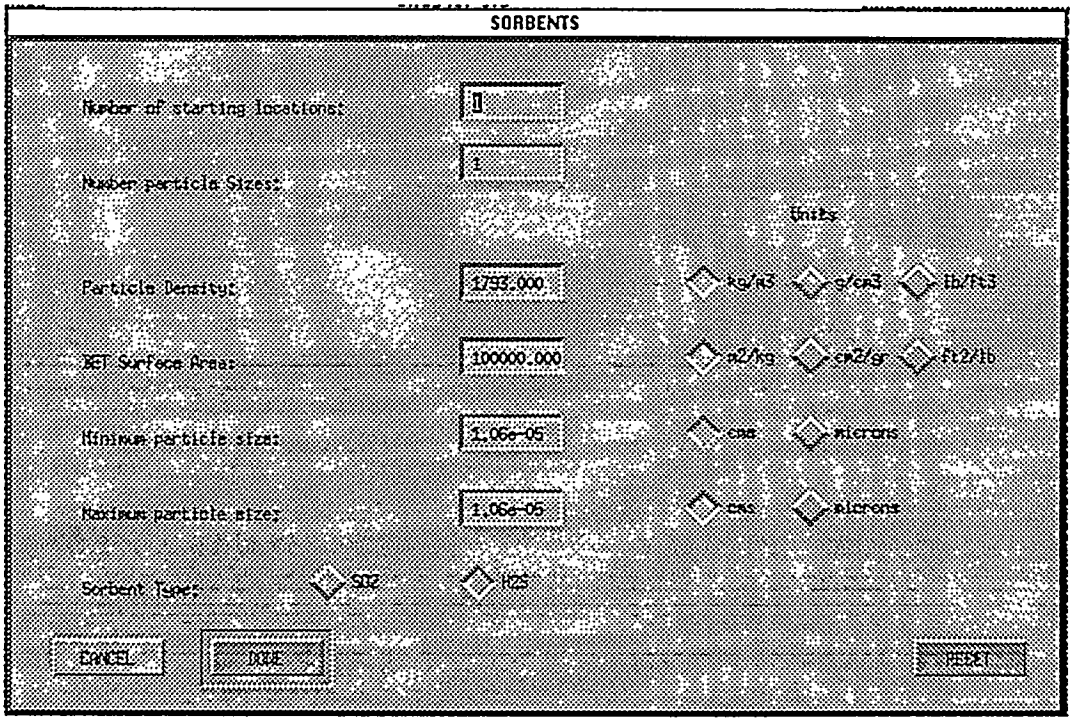

Fig. 5-17. Window for specifying sorbent particle input data.

Step 9: Save the new input files. After all of the data entries are completed and the grid has been successfully generated, the user clicks again on the word "File" in the main menu and selects the word "Save" or "Save As." "Save" saves the files under the same name they were opened under. "Save As" saves them under a new name which the user can specify in the window shown in Fig. 5-18. If the user tries to quit the program without saving the new data files, he/she is prompted with the window shown in Fig. 5-19.

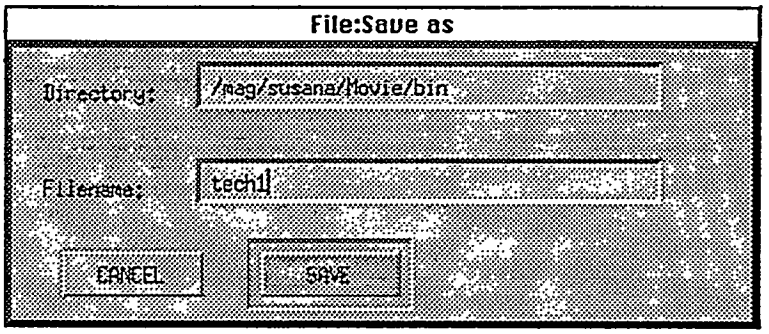

Fig. 5-18. Window for specifying filename to save input data.

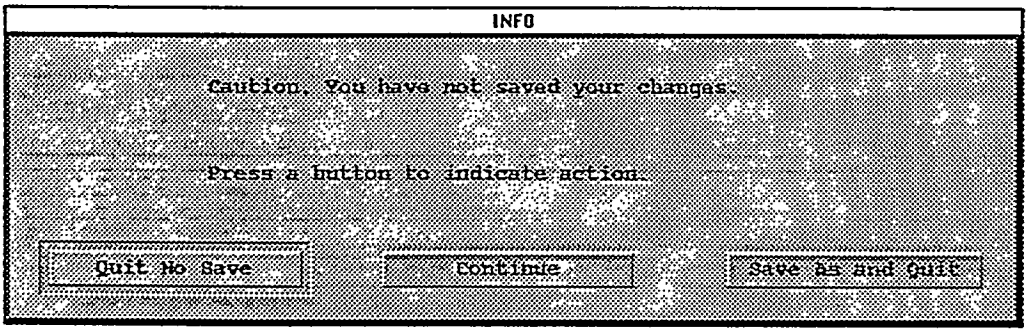

Fig. 5-19. Prompting window for saving data files.

DISSPLA Post-processor

PCPLOT is a menu-driven driver program for PCGC-2, used in conjunction with the DISSPLA[3] graphics package. It produces specially formatted meta-files that can be displayed on the screen or printed in hard-copy, depending on the user's system. PCPLOT reads the following plotting files from PCGC-2:

filename.gsp: gas properties
filename.grd: grid configuration
filename.pp1: coal particle
filename.pp2: coal particle
filename.pp3: coal particle
filename.ps1: sorbent particle
filename.ps2: sorbent particle
filename.ps3: sorbent particle
filename.nxp: NO_x
filename.sxp: SO_x

The initial menu displays the types of plots that can be produced with PCPLOT and the program options for modifying these plots :

```
1.  Gas Properties
2.  Coal Particle Properties
3.  Sorbent Particle Properties
4.  Experimental Comparisons
5.  SOx Pollutants
6.  NOx Pollutants
7.  Spreadsheet Format
8.  Velocity Vector Plots
9.  Zoom-in Plots
10. Plot Grid Setup
```

[3]Available from : Computer Associates International, Inc.
711 Stewart Avenue
Garden City, NY 11530-4787
tel 1-800-645-3042

```
11. Read New File Name
12. Omit Title
13. Normalize
14. Black and White
15. STOP
```

Gas Properties. Option 1 from the main menu, brings up a new menu . This menu shows the properties included in the .gsp file. For example:

```
0.  Complete Set of Plots
1.  Axial Velocity
2.  Radial Velocity
3.  Tangential Velocity
4.  Stream Function
5.  Gas Temperature
6.  Turbulent Kinetic Energy
7.  Dissipation of TKE
8.  Mixture Fraction
9.  Coal Gas Mixture Fraction
10. Residual Enthalpy
11. Particle Number Densities
12. Axial Radiation Flux
13. Radial Radiation Flux
14. Azimuthal Radiation  Flux
15. Sum of Radiation  Fluxes
16. Gas Species
17. Surface Plots
18. RETURN
19. STOP
```

All gas properties can be plotted either as surface plots or as contour plots. Option 17 produces four different rotations of the surface plots in addition to the contour plot. The user can choose to have one plot on each page or all four rotations on the same page. The first choice plots all the gaseous variables that PCGC-2 wrote in the .gsp file. Plotting all of these properties, however, will take a lot of time and a lot of space for the resulting meta-files. Option 11 will produce a menu telling the user how many particle diameters there are in the file and will ask him/her how many of these he/she wants to plot. If the user chooses Option 16, PCPLOT will list the names of all the species in the .gsp file, so he/she can choose

which ones to plot. Option 18 is used to go back to the main menu. Option 19 is used to clean-up and finish the resulting plots.

As an example, the following sequence was used to generate Fig. 5-20:

```
ENTER FILENAME

CPR

cpr.pop    IF FILE EXISTS, DO YOU WANT TO WRITE OVER ? (y/n)

Y

SELECT:

     1. Gas Properties
     2. Coal Particle Properties
     3. Sorbent Particle Properties
     4. Experimental Comparisons
     5. SOx Pollutants
     6. NOx Pollutants
     7. Spreadsheet Format
     8. Velocity Vectors plots
     9. Zoom-in plots
     10. Plot Grid Setup
     11. Read New File Name
     12. Omit Titles
     13. Normalize
     14. Black and White
     15. STOP


     1


     SELECT VARIABLE:

     0. Complete Set of Plots
     1. Axial Velocity
     2. Radial Velocity
```

```
3. Tangential Velocity
4. Stream Function
5. Gas Temperature
6. Turbulent Kinetic Energy
7. Dissipation of TKE
8. Mixture Fraction
9. Coal Gas Mixture Fraction
10. Residual Enthalpy
11 - 25. Particle Number Densities
26. Axial Radiation Flux
27. Radial Radiation Flux
28. Azimuthal Radiation  Flux
29. Sum of Radiation  Fluxes
30 - 50. Gas Species
51. Surface Plots
52. RETURN
53. STOP

51

SURFACES: 4 PER PAGE OR 1 PER PAGE? (4,1)

4

SELECT VARIABLE:

0. Complete Set of Plots
1. Axial Velocity
2. Radial Velocity
3. Tangential Velocity
4. Stream Function
5. Gas Temperature
6. Turbulent Kinetic Energy
7. Dissipation of TKE
8. Mixture Fraction
9. Coal Gas Mixture Fraction
10. Residual Enthalpy
```

```
11 - 25. Particle Number Densities
26. Axial Radiation Flux
27. Radial Radiation Flux
28. Azimuthal Radiation  Flux
29. Sum of Radiation  Fluxes
30 - 50. Gas Species
51. Surface Plots
52. RETURN
53. STOP
```

5

```
PLOTTING TEMPERATURE (K)

SELECT VARIABLE:

0. Complete Set of Plots
1. Axial Velocity
2. Radial Velocity
3. Tangential Velocity
4. Stream Function
5. Gas Temperature
6. Turbulent Kinetic Energy
7. Dissipation of TKE
8. Mixture Fraction
9. Coal Gas Mixture Fraction
10. Residual Enthalpy
11 - 25. Particle Number Densities
26. Axial Radiation Flux
27. Radial Radiation Flux
28. Azimuthal Radiation  Flux
29. Sum of Radiation  Fluxes
30 - 50. Gas Species
51. Surface Plots
52. RETURN
53. STOP
```

53

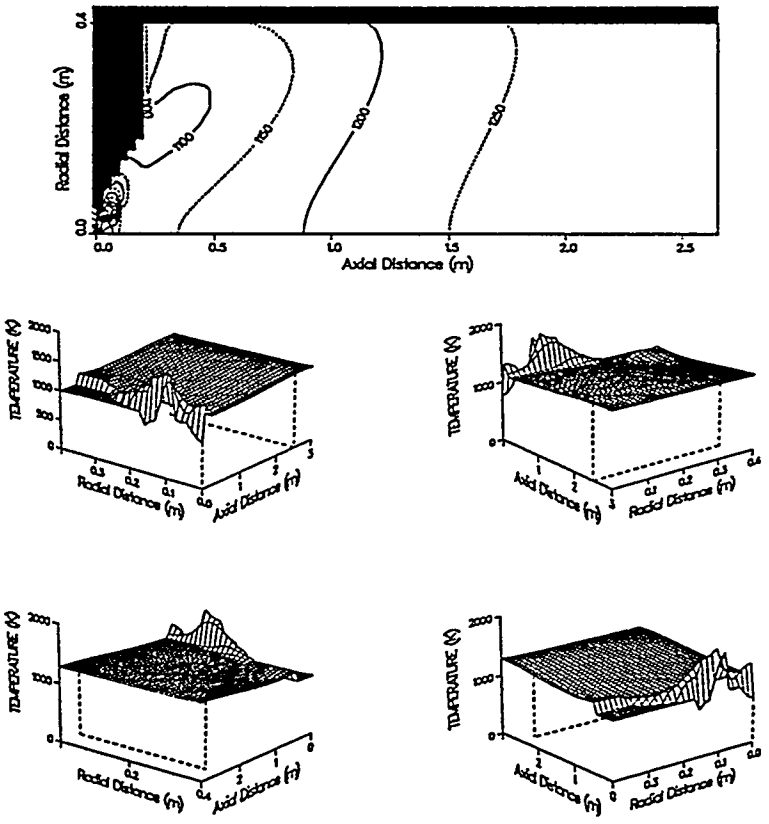

Fig. 5-20. Sample plot of gas temperature.

Coal and Sorbent Particle Properties. When the user chooses either Option 2 or Option 3 from the main menu, a new menu will appear. This menu shows the properties included in either the .pp1, .pp2, and .pp3 files for coal properties or the .ps1, .ps2, and .ps3 files for sorbent particles. For the coal, the user can choose from the following menu:

```
1. Plot all Particle Trajectories
2. Plot Specific Particle Trajectories
3. Plot Individual Particle Parameters
4. Plot Axial Burnout of Coal Particles
5. Plot Trajectories of Ignited Particles
6. Plot Specific Particle Trajectories
```

Option 3 will provide a menu telling the user how many particle diameters there are in the file, and will ask how many and which ones to plot. Similarly, when the user chooses Option 2, he/she will be able to choose which particle trajectories he/she wants to plot from the limits given. A similar menu appears when the user wants to plot sorbent particle properties.

Experimental Comparisons. PCPLOT compares data from the .gsp file with experimental data in the .exp file with the special format:

number of points (integer) radial position (real)

list of axial positions (real)

data values (real)

a final value of 0.0 that tells the program to stop reading data.

For example:

```
9 0.19
0.0 0.05 0.1 0.15 0.2 0.25 0.3 0.35 0.4
.0274 .0346 .0376 .0173 .013 .012 .0086 .012
0 0.
```

Usually the locations of the experimental data do not coincide with the grid used by PCGC-2. To obtain data in the same locations as the experimental data, PCPLOT performs a linear interpolation of the PCGC-2 data, in both the axial and radial directions. PCPLOT calculates the limits of the plots as the minimum and

maximum x positions and the smallest and biggest values of the variable to be plotted, from all the experimental and interpolated data. If the user wants to look only at the portion of the interpolated data close to his/her experimental points, he can change the initial and final value of the x positions.

SO_X and NO_X Pollutants. These plots are specific for the cases when SO_X and NO_X calculations have been performed. They use the `.nxp` and `.sxp` files. As with the other options, the user will get a menu showing the possible plots he/she can generate. For the NO_X data files, the menu is :

1. Mole fraction of NO_X (ppm)
2. Mole fraction of HCN (ppm)
3. Mole fraction of NH_3 (ppm)
4. Mole fraction of O_2 (ppm)
5. NO_X rate
6. HCN rate
7. NH_3 rate
8. RETURN
9. STOP

For the SO_X data files, the menu is :

1. Equilibrium SO_2
2. SO_2
3. Equilibrium H_2S
4. H_2S
5. RETURN
6. STOP

Spreadsheet Format. PCPLOT allows the user to generate a `.sp1` file in a text format that can be read by standard spreadsheet programs. The user can choose any variable he/she wants to write in this file. The main spreadsheet dialog is:

1. Gas Properties
2. Coal Particle Properties
2. Sorbent Particle Properties
4. Experimental comparisons

```
5. SOx Pollutants
6  NOx Pollutants
7. Close-up
8. Normalize
9. RETURN
10. STOP
```

Each of the menus works in exactly the same way as the corresponding menu of the DISSPLA graphics. For example, to generate a coal particle spreadsheet file with all the properties for a given particle, as shown in Table 5-5, the following sequence was used:

```
ENTER FILENAME

CPR

cpr.pop    IF FILE EXISTS, DO YOU WANT TO WRITE OVER ? (y/n)

Y

SELECT:

     1. Gas Properties
     2. Coal Particle Properties
     3. Sorbent Particle Properties
     4. Experimental Comparisons
     5. SOx Pollutants
     6. NOx Pollutants
     7. Spreadsheet Format
     8. Velocity Vectors plots
     9. Zoom-in plots
     10. Plot Grid Setup
     11. Read New File Name
     12. Omit Titles
     13. Normalize
     14. Black and White
     13. STOP

     7

SELECT:
```

```
1. Gas Properties
2. Coal Particle Properties
3. Sorbent Particle Properties
4. Experimental Comparisons
5. SOx Pollutants
6. NOx Pollutants
7  Close-up
8. Read New File Name
9. Normalize
10. ***RETURN***
11. ***STOP***

2

   READING CPR INPUT FILE (S)

     READING PARTICLE SIZE : 1 LOCATION : 1
           ...
           ...
           ...
        READING PARTICLE SIZE : 5 LOCATION : 5

READING OF PARTICLE INPUT IS COMPLETE



1. Plot All Particle Trajectories
2. Plot Specific Size Class Trajectories
3. Plot Individual Particle Trajectories
4. Plot Axial Burnout of Coal Particles
5. Plot Trajectories of Ignited Coal Particles
6. Plot Specific Starting Locations
7. RETURN
8. STOP

     CHOOSE A NUMBER (1-8)

3
```

```
          HOW MANY PARTICLES DO YOU WANT PLOTTED? (1-25)

          1


          INPUT THE STARTING LOC. AND SIZE CLASS DESIRED
FOR PLOT NUMBER 1 (i.e. ISL = 1, IPS = 2):

          1,3

          1. Plot All Particle Trajectories
          2. Plot Specific Size Class Trajectories
          3. Plot Individual Particle Trajectories
          4. Plot Axial Burnout of Coal Particles
          5. Plot Trajectories of Ignited Coal Particles
          6. Plot Specific Starting Locations
          7. RETURN
          8. STOP

               CHOOSE A NUMBER (1-8)

          8
```

TABLE 5-6
SPREADSHEET OUTPUT FROM PCPLOT

Starting Location 1 Particle Size 3

Axial location (m)	Radial location (m)	Total Fraction	Water Fract ...
9.010E-07	2.660E-04	1.000E+00	0.000E+00 ...
1.390E-02	2.750E-04	1.000E+00	0.000E+00 ...
4.390E-02	3.250E-04	1.000E+00	0.000E+00 ...
7.370E-02	3.770E-04	1.000E+00	0.000E+00 ...
1.040E-01	4.430E-04	1.000E+00	0.000E+00 ...
1.330E-01	5.760E-04	9.990E-01	0.000E+00 ...
1.410E-01	6.140E-04	9.910E-01	0.000E+00 ...
1.480E-01	6.520E-04	9.800E-01	0.000E+00 ...
1.630E-01	7.220E-04	9.250E-01	0.000E+00 ...
1.780E-01	7.860E-04	8.250E-01	0.000E+00 ...

TABLE 5-6 (continued)

1.930E-01	8.550E-04	7.800E-01	0.000E+00 ...
2.080E-01	9.580E-04	7.650E-01	0.000E+00 ...
2.360E-01	1.450E-03	7.590E-01	0.000E+00 ...
2.490E-01	2.100E-03	7.480E-01	0.000E+00 ...
2.540E-01	2.680E-03	6.780E-01	0.000E+00 ...
2.570E-01	3.310E-03	6.350E-01	0.000E+00 ...
2.580E-01	3.490E-03	6.300E-01	0.000E+00 ...
2.590E-01	3.770E-03	6.210E-01	0.000E+00 ...
2.600E-01	4.040E-03	6.150E-01	0.000E+00 ...
2.600E-01	4.350E-03	6.110E-01	0.000E+00 ...
2.610E-01	4.960E-03	6.040E-01	0.000E+00...
2.620E-01	5.570E-03	6.000E-01	0.000E+00 ...
2.630E-01	6.690E-03	5.960E-01	0.000E+00 ...
2.630E-01	7.940E-03	5.930E-01	0.000E+00 ...
2.630E-01	1.050E-02	5.890E-01	0.000E+00 ...
2.630E-01	1.560E-02	5.850E-01	0.000E+00 ...
2.600E-01	2.790E-02	5.760E-01	0.000E+00 ...
2.550E-01	4.000E-02	5.710E-01	0.000E+00 ...
2.470E-01	5.210E-02	5.650E-01	0.000E+00 ...
2.350E-01	6.660E-02	5.590E-01	0.000E+00 ...
2.120E-01	8.560E-02	5.480E-01	0.000E+00 ...
2.120E-01	1.120E-01	5.420E-01	0.000E+00 ...
2.520E-01	1.380E-01	5.330E-01	0.000E+00 ...
3.040E-01	1.630E-01	5.200E-01	0.000E+00 ...
3.730E-01	1.730E-01	5.140E-01	0.000E+00 ...
4.640E-01	1.600E-01	5.100E-01	0.000E+00 ...
5.850E-01	1.350E-01	5.060E-01	0.000E+00 ...
7.460E-01	1.390E-01	5.030E-01	0.000E+00 ...
9.610E-01	1.710E-01	4.990E-01	0.000E+00 ...
1.240E+00	1.960E-01	4.940E-01	0.000E+00 ...
1.620E+00	1.930E-01	4.870E-01	0.000E+00 ...
2.120E+00	1.870E-01	4.790E-01	0.000E+00 ...
2.710E+00	1.870E-01	4.730E-01	0.000E+00 ...

Velocity Vector Plots. With Option 8 the user can generate both velocity vector plots and superimposed plots of particle trajectories and velocity vectors. It plots the U-V velocities as vectors with a magnitude proportional to the velocity at a grid point. For this case, the menu is :

```
1. U-V Velocity Vectors
2. U-V Velocity Vectors and Coal Part. Trajs
3. U-V Velocity Vectors and Sorbent Part. Trajs.
4. Renormalize
5. Plot all vectors
6. Reduce number of vectors
7. RETURN
8. STOP

CHOOSE A NUMBER (1 - 8)
```

Note that the grid point corresponds to the originating end of the arrow. This does not mean that there is flow going into the wall but that the velocity at the grid point has the magnitude and direction shown in the plot. PCPLOT will automatically reduce the number of vectors plotted to eliminate confusing page blackening from overlapping vectors. The user can plot the vectors at all grid points with Option 5. The user can further reduce the number of plotted vectors with Option 6.

For example, to generate Fig. 5-21, the following sequence was used:

```
ENTER FILENAME

CPR

cpr.pop    IF FILE EXISTS, DO YOU WANT TO WRITE OVER ? (y/n)

Y

SELECT:

     1. Gas Properties
     2. Coal Particle Properties
     3. Sorbent Particle Properties
     4. Experimental Comparisons
     5. SOx Pollutants
     6. NOx Pollutants
     7. Spreadsheet Format
     8. Velocity Vectors plots
     9. Zoom-in plots
     10. Plot Grid Setup
     11. Read New File Name
```

```
      12. Omit Titles
      13. Normalize
      14. Black and White
      13. STOP

      8

   1. U-V Velocity Vectors
   2. U-V Velocity Vectors and Coal Part. Trajs
   3. U-V Velocity Vectors and Sorbent Part. Trajs.
   4. Renormalize
   5. Plot all vectors
   6. Reduce number of vectors
   7. RETURN
   8. STOP

CHOOSE A NUMBER (1 - 8)

         1

   DOING VECTOR PLOTS

   1. U-V Velocity Vectors
   2. U-V Velocity Vectors and Coal Part. Trajs
   3. U-V Velocity Vectors and Sorbent Part. Trajs.
   4. Renormalize
   5. Plot all vectors
   6. Reduce number of vectors
   7. RETURN
   8. STOP

CHOOSE A NUMBER (1 - 8)

         8
```

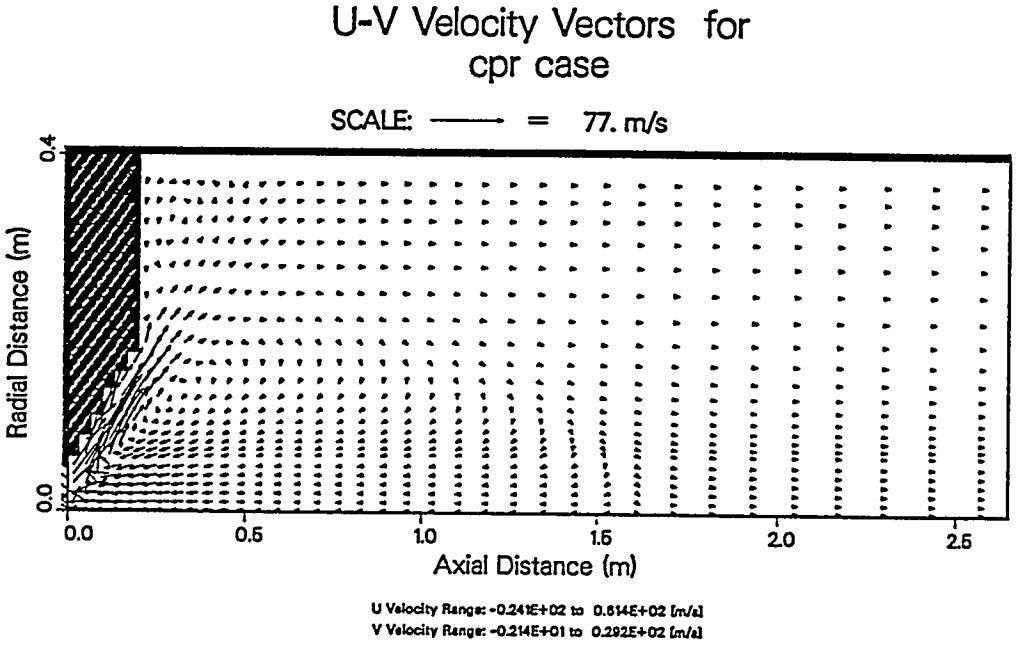

Fig. 5-21. Sample U-V velocity vector plot.

If the user selects combined particle and trajectories plots, PCPLOT will prompt the user to specify whether he/she wants all the particle trajectories or several specific ones.

There are special cases when the resulting vectors are too large, and the plot is unclear. The user can renormalize the vectors using Option 4 . The user can do one or two normalizations. When the user selects this option, PCPLOT will display the values used in previous plots and will ask if the user will use one or two normalizations. For one normalization the user will need to give only one normalization value.

For example, to generate both Figs. 5-22 and Fig. 5-23, the following sequence was used:

```
ENTER FILENAME

CPRCOAL

cprcoal.pop  IF FILE EXISTS, DO YOU WANT TO WRITE
OVER ? (y/n)

Y

SELECT:

     1. Gas Properties
     2. Coal Particle Properties
     3. Sorbent Particle Properties
     4. Experimental Comparisons
     5. SOx Pollutants
     6. NOx Pollutants
     7. Spreadsheet Format
     8. Velocity Vectors plots
     9. Zoom-in plots
     10. Plot Grid Setup
     11. Read New File Name
     12. Omit Titles
     13. Normalize
     14. Black and White
     15. STOP

     9

DO YOU WANT ONLY ZOOM-IN PLOTS?  (Y,N)

     Y

SELECT:

     1. Gas Properties
     2. Coal Particle Properties
```

```
   3. Sorbent Particle Properties
   4. Experimental Comparisons
   5. SOx Pollutants
   6. NOx Pollutants
   7. Spreadsheet Format
   8. Velocity Vectors plots
   9. Zoom-in plots
   10. Plot Grid Setup
   11. Read New File Name
   12. Omit Titles
   13. Normalize
   14. Black and White
   15. STOP

   8

  1. U-V Velocity Vectors
  2. U-V Velocity Vectors and Coal Part. Trajs
  3. U-V Velocity Vectors and Sorbent Part. Trajs.
  4. Renormalize
  5. Plot all vectors
  6. Reduce number of vectors
  7. RETURN
  8. STOP

CHOOSE A NUMBER (1 - 8)

        1
  Initial x value (0, 2.6)

        0.
  Final x value (0, 2.6)

        0.5
  Initial y value (0, 0.4)

        0.
  Final y value (0, 0.4)
```

```
      0.2

   DOING VELOCITY VECTORS PLOT


   1. U-V Velocity Vectors
   2. U-V Velocity Vectors and Coal Part. Trajs
   3. U-V Velocity Vectors and Sorbent Part. Trajs.
   4. Renormalize
   5. Plot all vectors
   6. Reduce number of vectors
   7. RETURN
   8. STOP

CHOOSE A NUMBER (1 - 8)

      4

   VHNORM AND VLNORM FOR LAST RUN   47.2743     0.
   ONE OR TWO VECTOR NORMALIZATIONS ?

      2

   GIVE VECTOR LOW AND HIGH NORMALIZATIONS

      47.3        94.6

   SMALL-TO-LARGE VECTOR DIVISION POINT

      8

   1. U-V Velocity Vectors
   2. U-V Velocity Vectors and Coal Part. Trajs
   3. U-V Velocity Vectors and Sorbent Part. Trajs.
   4. Renormalize
   5. Plot all vectors
   6. Reduce number of vectors
   7. RETURN
   8. STOP

CHOOSE A NUMBER (1 - 8)
```

```
      1

 DOING VECTOR PLOTS

 1. U-V Velocity Vectors
 2. U-V Velocity Vectors and Coal Part. Trajs
 3. U-V Velocity Vectors and Sorbing Part. Trajs.
 4. Renormalize
 5. Plot all vectors
 6. Reduce number of vectors
 7. RETURN
 8. STOP

CHOOSE A NUMBER (1 - 8)
      8
```

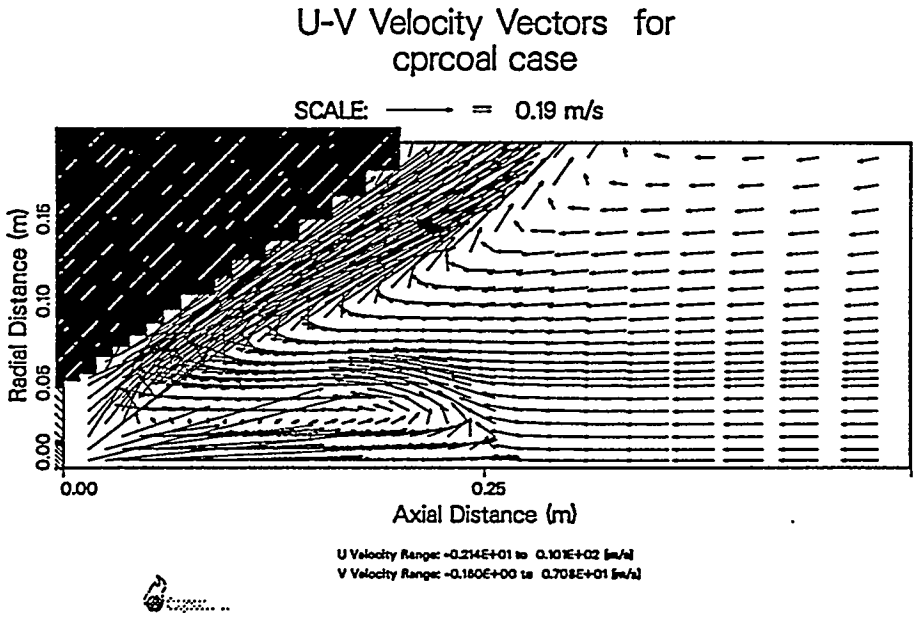

Fig. 5-22. Near-Burner U-V velocity vector plot.

The velocity plot in Fig. 5-22 is a zoom-in of the near-burner region of the reactor and has a normalization value was 47.3. If two normalizations are used, the resulting plot will have two type of vectors. In this case, the user will have to give values for both high and low normalization as well as small-to-large vector division point. The vector division point decides at what length large instead of small vectors will be plotted. It is usually set to approximately 6.0.

As shown, two normalization values were used: a high normalization value of 94.6 (twice the original normalization value) and low normalization value of 47.3. The division point value of 8 (~= 47.3/5.9) was used for normalizing only the vectors over 5.9 m/s with the higher normalization value, a different type of vector, and half their original size.

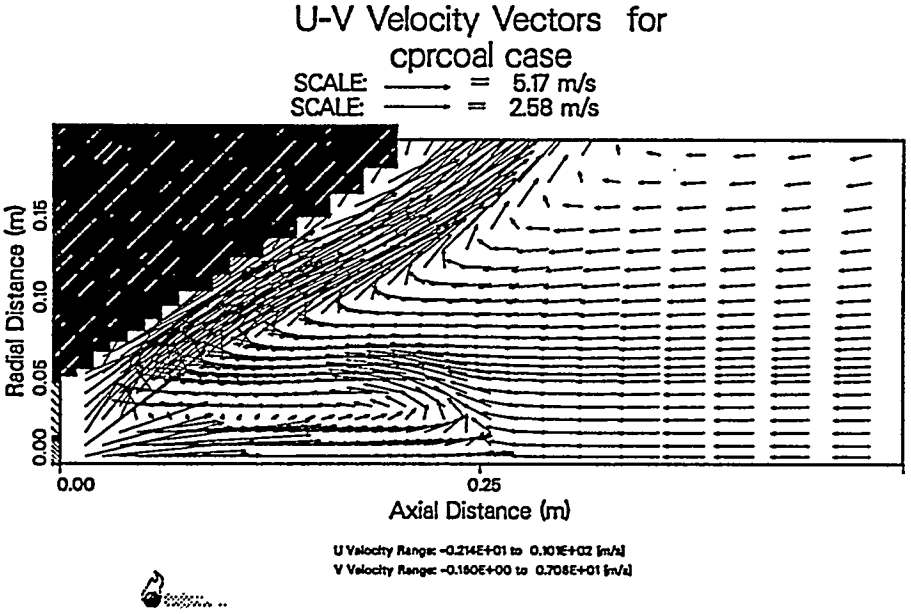

Fig. 5-23. Near-burner U-V velocity vector plot with two types of arrows representing two velocity scales.

Zoom-in Plots. Option 9 in the main menu can be used to zoom in at the details of one or all variables in a given region. If the user wants zoom-in plots, he/she must specify whether he/she wants only these plots, or both complete data plots and zoom-in plots. Once the user turns on this option, all the following plots will be generated using this option. The first time a zoom-in plot is produced, the user must specify the initial and final x and y positions for the plots. PCPLOT will ask him/her for the values:

`initial x value`	(x_0, x_{ni})
`final x value`	(x, x_{ni})
`initial y value`	(y_0, y_{nj})
`final y value`	(y, y_{nj})

where the allowed range for the input value is given in parentheses. X_0 is the original value at the origin of the x axis, y_0 is the original value of the origin of the y axis, x_{ni} is the original value at the extreme of the x axis, y_{nj} is the original value of the extreme of the y axis, and x,y are the values typed by the user. If the user types a value outside the range given in the parentheses, the program will indicate the value is outside the range and will ask for new values.

Plot Grid Setup. The grid setup used by PCGC-2 can be plotted with Option 10. The location and type of cells is read from the `.grd` file. The resulting plot shows the grid points as well as the cell boundaries.

Read New File Name. A new group of data files can be read without leaving PCPLOT using Option 11. Once the name of a data file is read, PCPLOT checks to see if a `.pop` metafile exists. If the metafile exists, PCPLOT will advise the user of its existence. He/she can now write over this file or give a new name for the resulting metafile.

Omit Titles. The user can omit the titles on the plots by using Option 12. He/she can toggle back to typing titles by using Option 12 which will now read `Print Titles`. Option 12 is useful when preparing figures for reports, publications, etc.

Normalize. If the user wants to normalize the axis values, he/she can do so with Option 13. This option toggles between using normalized scales and actual scales. Option 13 is useful when preparing figures for presentation when the exact dimensions of the reactor are proprietary and cannot be divulged.

Black and White. PCPLOT produces plots in black and white, or in color, according to the user's choice and his/her particular hardware. Initially the color is turned on. If the user selects Option 14 in the main menu, the color is turned off and the option will now read: `Colors`. The user can then toggle back to color plots again with this option.

Chapter Six

FG-DVC Submodel Descriptions

The coal dependent capability of PCGC-2 is provided by FG-DVC submodel. The physical background of this submodel is given in Chapter Four. FG-DVC has three coal description files, i. e., a coal composition file, a kinetic file, and a polymer file, to form a set of descriptions of a coal's chemical and physical properties needed in its computation. The reactivity submodel has its own input file. This section discusses the FG-DVC subroutines and explains the structures of these input files. A list of subroutines is given in Figure 6-1.

Eight sets of coal input files for the eight Argonne coals are provided with the PCGC-2 package. Three additional sets of input files for three PSOC coals are provided for the interpolation of FG-DVC input data. The elemental compositions(DAF) of these coals and three PSOC coals are listed in Table 4-4. When running PCGC-2 with an Argonne coal on this list, a user only needs to specify the file names of the files of this coal. When using a coal not on this list, the user needs to create a new set of files for the coal with PCGC-2 preprocessor PREC. All the FORTRAN variables of the input data are listed in Figure 6-2.

FG-DVC Subroutines

FG-DVC subroutines are called by PCGC-2 to compute the coal particle

devolatilization, if the FORTRAN variable FGDVC in the PCGC-2 data input file is set to be TRUE. FG-DVC calculations are done at each time-temperature step. The main PCGC-2/FG-DVC interface is in COAL2. A logical flow diagram of this part of the program is given in Figure 6-3. In each step THER15P is called first and the FG part of the calculations is executed for each of the function groups there, and later PERCVAP is called for the DVC part. TBLRTS calculates the kinetic rates of all functional group pools as well as the bond-breaking rate at a given temperature. In PERCVAP, the bond breaking and cross linking rates, which are being calculated in parallel with FG calculations, are used to update the macromolecular network parameters p and q. These two parameters are then used to calculated the new mass bin distribution and coal liquid fraction. The results are submitted to subroutine TARVAP to calculate the tar evaporation rate, in combination with coal dependent network properties such as the molecular weight distribution of ring clusters of coals. After returning to THER15P, appropriate function group redistributions are necessary due to the network change to further update the function group composition. COAL2 calls the other two subroutines VISCOSP and DWGOUT. VISCOSP calculates the coal viscosity, while DWGOUT calculates the total evolution rate and individual rates of all gas pools and calls SWESUB to invoke the coal particle swelling calculation. RK is called in SWESUB to perform Runge-Kutta integration at this time increment. SWEFUN, NGFUN, and WGFUN are the three functions used in the integration. FINFL1 is called to prepare the output.

In parallel to the FG-DVC calculations of the coal material, the pyrite decomposition is calculated by calling PYRITE1, PYDIST, and PYRITE2 at appropriate points in THER15P.

PER12 calculates the elemental compositions of char, tar, and gas phase. PER12P is the counterpart of PER12 for pyrite distribution.

GETCDF, GETKIN, and NETIN are three input subroutines to input the coal related data for FG-DVC routines. INITY0 and REINIT initialize the functional group compositions and the coal network parameters at the beginning of the particle trajectory calculations.

NTRGN2 is called from inside THER15P to compute the secondary nitrogenous gas reaction that converts HCN to NH_3.

The Coal Composition File

The coal composition file contains the elemental and functional group composition information of a coal. The structure of this file can be explained by an example in Figure 6-4. The first line of this file is the version number line. It must start with a version number in REAL format. Lines 2 through 6 are comment lines in which users can write anything they want. In this example, the second line gives the name of the coal. Line 7 is the fraction of the volatile pyrite sulfur that decomposes at low temperatures. Lines 8 through 12 contain the coal's elemental composition, while line 13 is the pyrite sulfur content, which should be given in grams per 100 grams DAF coal. Line 14 is not active. Lines 15 through 46 list the compositions of all the functional groups. Lines 47 through 52 are the fractions that determine how the pyrite decomposes into gases during the high temperature decomposition. Line 53 is the fraction of $-H_2C-CH_2-$ type bridges among total bridges, which affects the ultimate yield of CH_4.

Any data line users only the first value. Anything after one datum and a comma is considered as a comment. Merger of any two lines will cause severe problems.

The Kinetics File

The kinetics file contains kinetics that control the evolutions of all functional groups. An example is given in Figure 6-5. As in coal data files, the first line is the version line starting with a version number. Lines 2 through 40 are the σ values of all the functional groups. Line 41 is the σ for pyrite low temperature decomposition. After two inactive lines, lines 44 and 45 are the sigma values for pyrite FeS_2 and FeS. Lines 49 and 50 are the pre-exponential factor and activation energy for bond breaking. Lines 63 through 97 are the pre-exponential factors of all the functional groups, line 102 is for pyrite low

temperature decomposition, and lines 103 and 104 of pyrite FeS_2 and FeS. Lines 105 through 139 are the activation energies of all the functional groups. Line 144 is for pyrite low temperature decomposition, and lines 145 and 146 of pyrite FeS_2 and FeS. All the other lines are inactive but should not be modified.

Any data line uses only the first value. Anything after one datum and a comma is considered as comment. Merger of any two lines will cause severe problems.

The Polymer File

The polymer file contains coal macromolecular network parameters. Its structure is displayed in Figure 6-6.

Among the few adjustable parameters in polymer files are the last two numbers at the second line of the files, q_0 and p_{h0}. q_0 is the initial value of the occupation probability of crosslinks, q, and p_{h0} the initial value of the unbreakable bond fraction, p_h, (see Chapter 4 for the description of FG-DVC model). An increase of any of these two values will decrease the tar yield and the coal fluidity, with p_{h0} most effective for tar yield and q_0 for fluidity. Table 6-1 lists the q_0 and p_{h0} of the eight Argonne coals and they should be used as a reference in selecting these two values. In most of the cases users can use the polymer file of a coal on the list with H/C and O/C closest to those of the coal in use without any modification.

Another adjustable parameter in polymer files is xt0, which is the pyridine extractable yield in weight fraction of a coal measured at room temperature. In FG-DVC, it is a measure of the initial looseness of a coal material and is used to calculate the initial breakable bond fraction, p_0, with p_{h0}.

mbin is the option number for mass bin file selection, and should be 1 for Pocahontas #3 and 0 for all another Argonne coals. See Section Mass Bin Files.

The Mass Bin File

It is found that the weight distributions of oligomers in coals are invariant and independent of coal rank for almost all rank coals except very high rank coals like Pocahontas #3 of the Argonne coals. So only two mass bin files are supplied, mass_bin and mass_bi1. The former is for all Argonne coals except Pocahontas #3, and contains the oligomer weight distributions up to 6-mers. The latter is for Pocahontas #3 only.

The Reactivity Input File

Input parameters for the reactivity submodel are of two types : coal (and char) dependent parameters, and model dependent parameters. Parameters from the first type include : eps0, min0, psi, radp, surf0, while the parameters $E1_{jl}$, $E2_{jl}$, Em and tau0 are considered as model parameters, and are kept constant. The parameter "thiele" is a logical variable which, when set to "true", corresponds to the use of the Thiele modulus to calculate the rate in the pore diffusion regime.

The internal surface area surf0 is obtained by N_2 or CO_2 adsorption (with the char having at least 5 % burnoff), and is typically found in the range 50 to 1000 m^2/g. An average value which can be taken is 300 m^2/g. The porosity eps0 varies with the pyrolysis conditions (the higher the heating rate, the more porous the resulting char) and the starting coal type (chars from high rank coals have, in general, lower porosities then the ones from low rank coals). Chars from high rank coals usually give porosities between 0.1 and 0.3, while those from low rank coals show porosities in the range 0.5 to 0.8. The mean pore radius radp can be obtained experimentally from pore size distribution measurements using gas adsorption. For high heating rate chars (which is typical for pulverized coal conditions), a useful range for this parameter is 100-200 Å. The parameter min0 is coal dependent, is used in the case of low rank coals only, and represents the amount of dispersed minerals (in particular calcium), as measured by FTIR and SEM. As an example, in the case of a Zap lignite, a

typical value for this parameter is about 1 %, while for a Wyodak sub-bituminous coal the value is about 0.9 %. The parameter psi is used to represent the variations of internal surface area (in the kinetic regime, for high rank coals) as a function of burnoff, and is char dependent. Its value generally falls between 5 and 10.

Concerning the model parameters, tau0 represents the tortuosity of the char pore network, cannot be measured directly and is consequently kept to a constant value of 2. E1 is the intrinsic activation energy, which has been found to be relatively constant for different chars, and is equal to 30 kcal/mol. E2 represents the activation energy observed in the pore diffusion regime. This parameter is generally not used since, following the Thiele model, half the intrinsic activation energy is usually taken for the pore diffusion regime. Em represents the energy of "deactivation" (to account for sintering, etc..) of the minerals, and is in effect in the pore diffusion regime (i.e. at high temperature). "Thiele" is a flag which, when set to "true", allows the calculation to follow the Thiele model. In the case where "thiele" is set to "false", E2 is used for the activation energy in the pore diffusion regime.

FG-DVC Input Data Creation and Maintenance

The stand-along FG-DVC has a utility program COALS for creating coal input data files for a new coal and maintaining the existing coal data files. The full capability of COALS has been incorporated into PCGC-2's preprocessor PREC. When users click on a designated button in PREC's pull down menu, the appropriate functions of COALS will be invoked. If users elect to enter a new coal, the program enters the creation mode. If users type in some valid file names of existing FG-DVC coal data files, it is in the maintenance mode. This section discusses the basic concepts of COALS. For operational instructions of PREC, read appropriate sections in this manual.

In the creation mode, COALS interpolates the functional group composition and gas evolution kinetics of a new coal from the data of six of the

Argonne coals and three additional PSOC coals. The interpolation is based on a triangular finite element construction and uses H/C and O/C as two basic coordinates. The triangular finite element mesh in the H/C-O/C two dimensional plane is plotted in Figure 6-7. The nine nodal points correspond to the nine coals, while the two points not connected are Stockton and Pocahontas # 3 which are not selected for interpolations. Interpolations can be performed for coals with H/C an O/C inside this range only. Any coal with its elemental composition out of this range is not covered. In this mode, users need to give the elemental composition(DAF) of the new coal with the content of pyrite sulfur given in grams of sulfur in pyrite per 100 grams of DAF coal. Upon requests, COALS will display the functional group compositions and the pool kinetics created by the interpolation and enter the maintenance mode in which manual adjustments can be done.

COALS does not create FG-DVC coal polymer data, since the rank dependence of the coal network is more complicated and has not been fully studied. Based on the elemental compositions users entered, COALS recommends users to use one of the polymer files of the eight Argonne coals and the three PSOC coals. Modifications of the polymer files have to be done with a text editor, like UNIX *vi*.

In the maintenance mode, the interpolation step is skipped and users have choices to enter the composition or kinetics branch of the code.

Composition Branch

In the composition branch, the functional group composition of the coal is displayed and users have three options: 1) creating a new coal composition file, 2) modifying the composition manually, 3) exit to main selection. By choosing option 2, users can modify the FG composition according to their own knowledge of the coals. It is very important for users to understand that most of the pools cannot be adjusted without changing other pools because of the mass conservation. Oxygen is distributed in H_2O, CO, CO_2 and, in relatively small amount, SO_2 and COS. Altering any of these pools will cause other pool sizes to be changed. The same situation exists for the sulfur and nitrogen pools. In

other words, changes in one pool will cause reshuffling of other pools based on the mass conservation of O, S, and N. Internal rules in COALS in this respect are:

1) Total amount of H_2O, CO, or CO_2

Adjusting the size of any one of the above will cause one of the others to change size, according to the following rule:

$$H_2O \rightarrow \quad CO \rightarrow \quad CO_2 \rightarrow \quad H_2O$$

while maintaining the total oxygen content in these three pool groups unchanged.

2) Individual pool sizes of H_2O, CO and CO_2 pools

Adjusting the size of any one of the individual pools of one of the above pool groups will cause one of the other pools in the same group to change size, according to the following rule:

Extra Tight→Tight→Loose→Extra Loose→Extra Tight

while maintaining the total amount of this pool group unchanged. For instance. A reduction of CO loose pool size will lead to an increase in the CO extra loose pool size, and so on.

3) Individual pool sizes of the organic sulfur pools

Adjusting the size of any one pool in the sulfur pool group except H_2S tight will cause H_2S tight to change size to maintain the sulfur content. Changing the H_2S tight pool size can only be done indirectly by changing the other sulfur pool sizes.

Notice that the changes in SO_2 and COS pool sizes will alter oxygen content in H_2O, CO and CO_2 pools, and therefore modify these pool sizes.

4) Individual pool sizes of the organic nitrogen pools

Adjusting the size of any one pool in the nitrogen pool group except HCN tight will cause HCN tight to change size to maintain the nitrogen content. Changing the HCN tight pool size can only be done indirectly by changing the other nitrogen pool sizes.

5) Individual pool sizes of CH_4, Olefin and Paraffin, and the fraction of -CH_2CH_2- type bond, X_CH_4.

These pools can be modified independently. The CH_4 pool amounts will be altered in the FG-DVC subroutine REINIT according to source term redistribution rules. The additional CH_4 contribution from -CH_2-CH_2- bridge breaking, termed terminal CH_4, changes the ultimate CH_4 yield. Modifying X_CH_4 in coal data files changes the amount of this contribution.

X_CH_4 is assigned to pool number 61 in COALS only. It is not a gas pool in PCGC2/FG-DVC. It is the fraction of -CH_2CH_2- type bond that creates two terminal CH_3's when it breaks.

6) Pyrite pools

Pyrite in coals will decomposes into various sulfur gases and FeS during the pyrolysis. In FG-DVC, FeS is assumed stable in pyrolysis. The other half of the sulfur from the pyrite evolves into H_2S, SO_2, COS and CS_2. Part of it could stay in the coal structure as char sulfur. Users are allowed to specify the fractions of evolving pyritic sulfur into the above pools. Note that it is the fraction of evolving pyritic sulfur(half of the total pyritic sulfur) that is used.

Pyrite decomposes at two temperatures. The low temperature

decomposition produces H_2S only. Changing the size of this pool will change the pools in the high temperature decomposition group proportionally.

In the higher temperature group, all the pools except H_2S-GAS can be modified directly, but the H_2S-GAS pool size changes indirectly if any of those pools gets changed.

These pool numbers are valid in COALS only.

7) Other pools

All the other pools are not manually adjustable, but aliphatic C and H pools act like two reservoirs for C and H, respectively. They save all the remaining C and H after they are distributed into the other pools.

Increasing or reducing any pool too much will cause some component pool sizes to be negative, suggesting further adjustments.

Kinetics Branch

In kinetics branch, users can select a number of pools to modify their devolatilization kinetics, which include the sigma and the mean activation energy for the distributed activation energy model, and the pre exponential factor. The modifications are straight forward.

Coals not in the range

There will be cases in which users have coals with elemental compositions outside the H/C-O/C range covered by COALS. If that happens, follow the suggestions here to create the coal composition files:

Step 1. Take the coal composition file of a coal with the elemental composition closest to the new coal, and use a text editor to modify the file so that the composition of the new coal

is specified, referring to the section of Coal Composition File and Figure 6-4. Save the file.

Step 2. Use COALS to modify this file further.

To create a new kinetics file for this coal, compare the coal elemental composition with those of the eleven coals provided, select the kinetics file of one of these coals, which has its composition closest to that of the new coal, and modify it with PREC based on your own knowledge of the coal. After the kinetics of file an Argonne coal has been selected, the polymer file of the same coal should be used for the new coal.

FG-DVC Subroutines

AMNT	Real function for calculating the amount of change in a given functional group pool.
DECOD	Subroutine for reading the value of a variable from input files.
DWGOUT	Subroutine to calculate the time derivatives of gas species and to call the swelling subroutine.
ELBACK	Subroutine calculating at the end of particle trajectory the amount of coal species that reacted with pyrite.
FINFL1	Subroutine for preparing an output file (Part I). Calculates updated amounts and elemental compositions of char, tar, gases and their elemental compositions.
FINFL2	Subroutine for preparing an output file (Part II). Calculates the distribution of individual functional groups in char, tar, gases, and missing.
FKSU	Real Function to calculate the probability of a site belonging to an n-mer from a given combination of two oligmers.
FNPQ	Subroutine to obtain tar, extract, and liquid fractions using percolation theory. It uses or calls FKSU and FPQ.
FPQ	Subroutine to calculate the liquid fraction and the mean cluster size for a given Bethe lattice.

Figure 6-1 FG-DVC Subroutines

GETCDF	Subroutine to read a coal composition file (elemental composition and functional group composition of a specified coal).
GETKIN	Subroutine to read a kinetic file, including frequency factors, activation energies and their distribution parameters for all functional groups.
INITY0	Subroutine to initialize all functional groups in terms of weight fraction (daf basis).
KBAR	Real function for averaging kinetic rates for a given FG pool based on distributed activation energies.
MAKNAM	Subroutine for making a name in output for a specified time step.
NETIN	Subroutine to read the coal network/polymer file and to calculate the related network parameters.
NETOUT	Subroutine to write the computational results in DVC part into an output file.
NFCN	Real function for calculating new distribution functions for kinetic rates.
NGFUN	Real funtion for evaluating ambient gas diffusion function in swelling integration.
NTRGN2	Subroutine to compute the nitrogen gas evolutions.

Figure 6-1 FG-DVC Subroutines - continued

PER12	Subroutine to calculate the elemental composition in char, tar, and gas phase, etc.
PER12P	Subroutine to calculate the elemental contents in char, tar, and gas phase, contributed by pyrite.
PERCVAP	Driver routine to perform the DVC computations using percolation theory.
PYDIST	Subroutine to distribute pyrite decomposition products into gas pools.
PYRITE1	Subroutine to calculate pyrite thermo-decomposition, part 1.
PYRITE2	Subroutine to calculate pyrite thermo-decomposition, part 2.
REINIT	Subroutine to reinitialize variables to zero or their starting values.
RK	Subroutine to perform Runge-Kutta integration of swelling equations.
SWEFUN	Real function to evaluate the swelling function in swelling integration.
SWELLDATA	Block data subroutine for swelling parameters.
SWESUB	Driver subroutine to simulate swelling process based on the given viscosity values computed in subroutine VISCOS and total gas evolution rate.

Figure 6-1 FG-DVC Subroutines - continued

TARVAP	Subroutine to calculate tar vaporization and incorporate the results into the percolation computations.
TBLRTS	Subroutine for setting up kinetic rates for functional groups, performed at each time step.
THER13P	Driver routine to simulate pyrolysis using the FG-DVC model. Uses theory 13 and assumes that evolved tars are removed immediately or stay for a short residence time to further produce gases.
THER15P	Driver routine to simulate pyrolysis using the FG-DVC model. Uses theory 15 and assumes that evolved tar further reacts to produce gases the same way as char does.
VISCOSP	Real function for calculating viscosity of coal at a given temperature.
VOLSWL	Subroutine for calculating the volumetric swelling ratio from crosslink density.
WGFUN	Real funtion for evaluating devolati-lized gas diffusion function in swelling integration.
WRTOUT	Subroutine for writing the computational results of the FG part into an output file.

Figure 6-1 FG-DVC Subroutines - continued

Variables	Type	Unit	Description and Usual Symbol
A1 to A44	Real	Kelvin	Activation energy of pool devolatilizations, E_i for k_i in Eq. (4-10).
amvsol	Real	--	Molar volume of solvent (pyridine), not used in PCGC-2.
amwcol	Real	--	Start crosslinking density, not used in PCGC-2.
atar	Real	Kelvin	Activation energy of bond breaking, for k_B in Eq. (4-1).
B1 to B44	Real	s^{-1}	Pre-exponential factor of pool devolitilization k_i^0 for k_i in Eq. (4-10).
btar	Real	s^{-1}	Pre-exponential factor of bond breaking, for k_B in Eq. (4-10).
bead	Integer	--	Total number of monomers in network sample, not used.
cnst2	Real	atm	Gas pressure drop from outside to inner coal pores, ΔP in Eq. (4-6) AND (4-7).

Figure 6-2 A list of FORTRAN variables of the input data for FG-DVC.

Variables	Type	Unit	Description and Usual Symbol
density	Real	g/cm3	Coal density, not used PCGC-2.
dvg3	Real	--	Not used.
dvg4	Real	--	Not used.
dummy	Real	--	Dummy variable.
fethyl	Real	--	Initial number of hard (double) bonds, not used in PCGC-2.
flink	Real	--	Initial number of crosslinks in starting coal, not used in PCGC-2.
Idummy	Logical	--	Dummy variable.
masslm(i)	Real	--	Char bin parameters, not used.
mers	Integer	--	Number of mass bins for tar vaporization.
mermas(i)	Real	Dalton	Binned mass of oligmers for tar vaporization.
oligst	Real	--	Starting number of oligomers in the network, not used.

Figure 6-2 A list of FORTRAN variables of the input data for FG-DVC, (continued).

Variables	Type	Unit	Description and Usual Symbol
ph0	Real	--	Initial hard bond fraction of the coal network, used with xt0 to initialize p.
phimax	Real	--	Volume fraction of solid in coal at gel point for coal viscosity model, ϕ_c in Eq. (4-13) and (4-15).
q0	Real	--	Initial occupation probability of crosslinks, q_0.
radis0	Real	--	Coal particle radius, not used.
s1,s2	Integer	--	Coal network coordination numbers, σ_1 and σ_2.
sigma(i)	Real	Kelvin	Standard deviation of Gaussion, for distributed activation energies of pool deviations, σ_i for k_i in Eq. (4-10).
viseng	Real	Kelvin	Activation energy for coal viscosity, k_E in Eq. (4-13) and (4-15).
vismax	Real	pacal*sec	Maximum viscosity.
vsrcol	Real	--	Volumetric swelling ratio of raw coal, not used.

Figure 6-2 A list of FORTRAN variables of the input data for FG-DVC, (continued).

Variables	Type	Unit	Description and Usual Symbol
vsrmin	Real	--	Minimum volumetric swelling ratio of char, not used.
xeff(i)	Real	--	Crosslink coefficients of gas pools.
xt0	Real	--	Weight fraction of solvent extractables of starting coal at room temperature, use with ph0 to initialize p.
E1(j,I)	Real	--	Intrinsic activation energy for reactivity model, for particle size index j and reaction l, $E1_{jl}$.
E2(j,I)	Real	--	Activation energy in the pore diffusion regime, for particle size index j and reaction l, $E2_{jl}$, reactivity model.
Em(J,I)	Real	--	Activation energy for "deactivation" of the minerals (to account for sintering), for particle size index j and reaction l, Em_{jl}, reactivity model.
eps0	Real	--	Tortuosity of the char network. Since it cannot be measured, it is kept at a constant value of 2, eps0, reactivity model.

Figure 6-2 A list of FORTRAN variables of the input data for FG-DVC, (continued).

Variables	Type	Unit	Description and Usual Symbol
min0	Real	--	Dispersed minerals concentration (in %). Represents the amount of calcium as measured by FTIR and SEM, min0, reactivity model.
psi	Real	--	Structure parameter, to represent variations in internal surface area for the kinetic regime, for high rank coal. It's value usually falls between 5 and 10, Ψ, reactivity model.
radp	Real	--	Mean pore radius. Obtained from gas adsorption measurements, radp, reactivity model.
thiele	Logical	--	.true. means that the Theile model is used, i.e. that $E1_{ji}/2$ is the activation energy used in the pore diffusion regime. If. false., then $E2_{ji}$ is used, reactivity model.
surf0	Real	--	Internal surface area in m^2/g, obtained from gas adsorption, surf0, reactivity model.
tau0	Real	--	Tortuosity factor, taken as a value of 2, tau0, reactivity model.

Figure 6-2 A list of FORTRAN variables of the input data for FG-DVC, (continued).

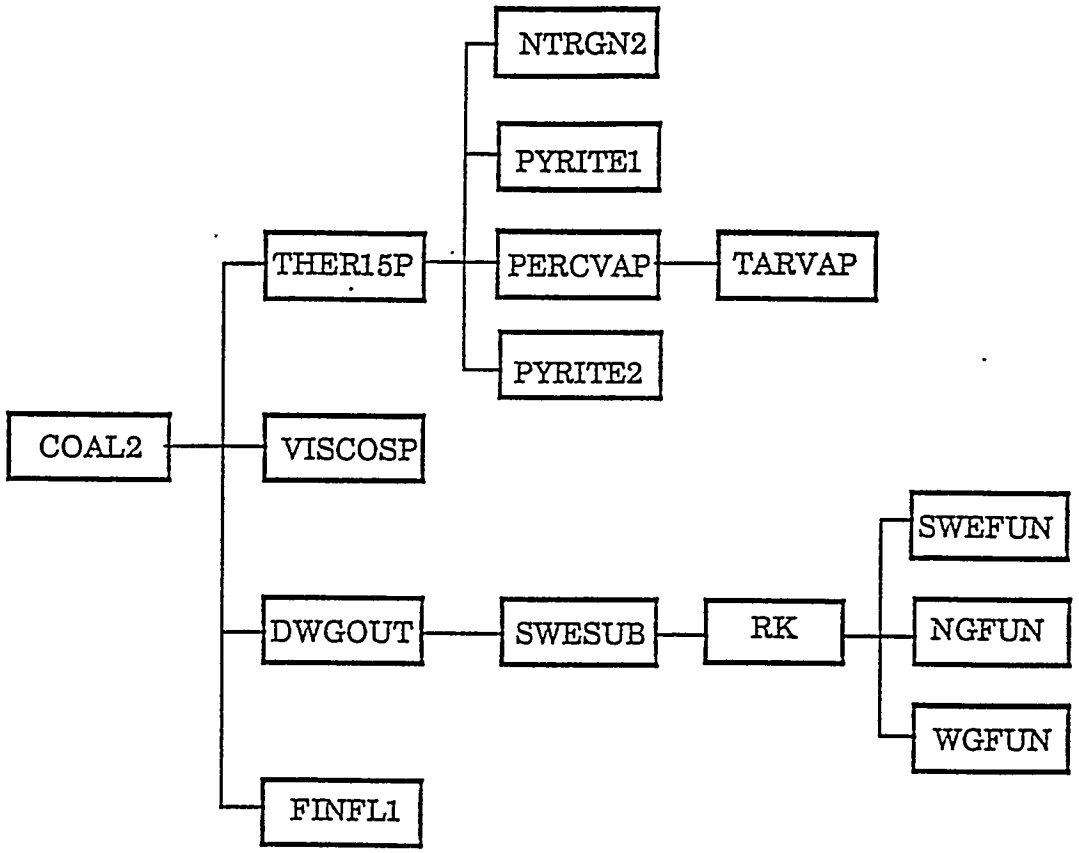

Figure 6-3 FG-DVC Subroutine Called from COAL2.

```
7.0, created by "coals"
Illnois #6, Argonne Coal
comment line
comment line
comment line
0.000000,  inactive
  0.1860,  Fraction of low temp. FeS2
 77.7200,  XC0
  5.0000,  XH0
 13.5300,  XO0
  1.3700,  XN0
  2.3800,  XS0
3.320000,  XSM0
0.000000,  inactive
0.109500,  XOH
0.011627,  1-CO2
0.001500,  2-NH3-loose
0.530000,  3-Fraction of CO2 tight
0.015711,  5-H-aromatic
0.009762,  6-HCN tight
0.000000,  7-HCN loose
0.600000,  8-Fraction of H2O tight
0.080000,  9-Fraction of H2O extra-loose
0.034401,  10-CO-extra-tight
0.931507,  11-Fraction of Water in OH
0.119996,  12-Fraction of CO2 extra-loose
0.003225,  13-CO-loose
0.000000,  14-Terminal CH4, not an input
0.000000,  15-CO-XX-tight
0.001000,  16-SO2
0.001000,  17-COS
0.000000,  18-CS2
0.004300,  19-H2S-tight
```

Figure 6-4 An example of the coal composition file.

```
0.011400,  21-Char S
0.000000,  22-Empty
0.000000,  24-NH3-tight
0.000000,  25-Empty
0.004000,  26-C2H4
0.000000,  27-C3H6
0.027000,  28-Olefins-C6H12
0.004000,  29-C2H6
0.000000,  30-C3H8
0.025000,  31-Paraffins-c6h14
0.030500,  32-CH3
0.622951,  33-Fraction of CH4 tight
0.550000,  37-Carbon
0.050000,  1-SO2-pyrite
0.050000,  2-COS-pyrite
0.000000,  3-CS2-pyrite
0.400000,  4-H2S-LOOSE-pyrite
0.000000,  5-H2S-TIGHT-pyrite
0.000000,  6-CHAR-S
1.000000,   -X_CH4-C-C-BRIDGE FRACTION
```

Figure 6-4 An example of the coal composition file (continued).

```
7.0, VERION #  /OCT., 1991/
1750., --> 1200.,  SIGMA1-CO2-LOOSE *** / ILLIN6 / ARGONNE /
OCTOBER 90 /
1500.,2000.,  SIGMA2-NH3
2750., --> 4500.,  SIGMA3-CO2-TIGHT
2000.,  SIGMA4-CO-TIGHT
6000.,  SIGMA5-HYDROGEN
3000.,4750.,  SIGMA6-HCN-TIGHT
3000.,1500.,  SIGMA7-HCN-LOOSE
2800.,  SIGMA8-H20-TIGHT
1800.,  SIGMA9-H2O-EX-LOOSE
3000.,  SIGMA10-CO-EX-T
1500.,  SIGMA11-H20-LOOSE
3000.,  SIGMA12-CO2-EXTRA-LOOSE
1000.,  SIGMA13-CO-LOOSE
2500.,  2000., SIGMA14-TERMINAL METHYL
1000.0,  SIGMA15-CO-XXT
1000.0,  SIGMA16-SO2
1000.0,  SIGMA17-COS
1000.0,  SIGMA18-CS2
2500.0,  SIGMA19-H2S-TIGHT
1000.0,  SIGMA20-H2S-LOOSE
2000.0,  SIGMA21-CHAR-S
1000.0,  SIGMA22-EMPTY
2000.0,  SIGMA23-CHAR-N
2500., 2000.0,  SIGMA24-NH3-TIGHT
3000.0,  SIGMA25-HCN-to-NH3
1500.,  SIGMA26-C2H4
1500.,  SIGMA27-C3H6
1500.,  SIGMA28-OLEFINS
1500.,  SIGMA29-C2H6
1500.,  SIGMA30-C3H8
1500.,  SIGMA31-PARAFFINS
```

Figure 6-5 An example of the kinetic file.

```
1800., --> 1650., SIGMA32-CH4-LOOSE
2500., 2200., --> 2000., SIGMA33-CH4-TIGHT
1500., SIGMA34-CAL
1500., SIGMA35-HAL
5000., SIGMA36-EMPTY
7000., SIGMA37-EMPTY
750., > > > 1250.SIGMA38
,      SIGMA39-
4000., SIGMA40-PYRITE-LOW-TEMPERATURE
1500., SIGMA41-NOT ACTIVE
1500., SIGMA42-NOT ACTIVE
100., SIGMA43-FES2
100., SIGMA44-FES
1.,    CS
,      AA
26400., BA
1.0E14, AX2-ATAR
26000., BX2-BTAR
,      AM-MISSING
26400., BM
7467., AS1
10173., BS1
44916, AS2
14523., BS2
1.5E11, AOL
27600., BOL
2.1E7, AAC-HIGH
22000., BAC
,      ASOOT
60000., BSOOT
5.0E12, A1-CO2-LOOSE
3.0E12, A2-NH3
```

Figure 6-5 An example of the kinetic file (continued).

```
7.5E12, A3-CO2-TIGHT
5.0E12, A4-CO-TIGHT
.25E15, A5-HYDROGEN
5E12, 17.3E12,A6-HCN-TIGHT
5E12,  4.2E13, A7-HCN-LOOSE
2.0E14, A8-WATER-TIGHT
5.0E12, A9-H20-EX-LOOSE
2.0E14, A10-CO-EX-TIGHT
5.0E12, A11-WATER-LOOSE
5.0E12, A12-CO2-EXTRA-LOOSE
5.0E12, A13-CO-LOOSE
6.0E13, A14-TERMINAL METHYL
0.00,  A15-CO-XXT
5.0E12,  A16-SO2
5.0E12,  A17-COS
0.0,     A18-CS2
5.0E12, A19-H2S-TIGHT
5.0E12, A20-H2S-LOOSE
0.00,  A21-CHAR-S
0.0,    A22-EMPTY
0.00,  A23-CHAR-N
5.0E12,  A24-NH3-TIGHT
5.0E13,  A25-HCN-to-NH3
5.0E12, A26-C2H4
5.0E12, A27-C3H6
5.0E12, A28-OLEFINS
5.0E12, A29-C2H6
5.0E12, A30-C3H8
5.0E12, A31-PARAFFINS
3.0E13, A32-CH4-LOOSE
6.0E13, A33-CH4-TIGHT
0.,     A34-CAL
0.,     A35-HAL
```

Figure 6-5 An example of the kinetic file (continued).

```
5E34,A36-EMPTY
5E17, 5E31,A37-EMPTY
2.5E11, A38-AAC-LOW
10,     A39,TEMP CROSSOVER ACET
5.0E12, 368.5,  A40-PYRITE-LOW-TEMPERATURE
5.0E12,  A43-FES2-PYRITE
5.0E12,  A44-FES
24750., --> 24500., B1-CO2-LOOSE
26000., 25500., 27300., B2-NH3
32000., B3-CO2-TIGHT
30500., B4-CO-TIGHT
40500., 40500., B5-HYDROGEN
34000., B6-HCN-TIGHT
33000., 23500., B7-HCN-LOOSE
32000., B8-H20-TIGHT
18000., B9-H20-EX-LOOSE
40000., B10-CO-EXTRA-TIGHT
25000., B11-WATER-LOOSE
20500., --> 20750., B12-CO2-EXTRA-LOOSE
25000., B13-CO-LOOSE
31500., 32000., B14-TERMINAL METHYL
0.00,  B15-CO-XXT
24000., 31000.,  B16-SO2
24000.,  B17-COS
24000., 0.00,  B18-CS2
29500.,   B19-H2S-TIGHT
24300.,  B20-H2S-LOOSE
0.00,  B21-CHAR-S
25500.,B22-NOT ACTIVE
0.00,  B23-CHAR-N
33000.,  B24-NH3-TIGHT
15000.,  B25-HCN-to-NH3
25000., B26-C2H4
```

Figure 6-5 An example of the kinetic file, (continued).

```
25000., B27-C3H6
25000., B28-OLEFINS
25000., B29-C2H6
25000., B30-C3H8
25000., B31-PARAFFINS
28000., B32-CH4-LOOSE
32000., B33-CH4-TIGHT
30000., B34-CAL
30000., B35-HAL
75000.,  B36-NOT ACTIVE
100000., B37-NOT ACTIVE
32500., B38-NOT ACTIVE
8408.,  B39-NOT ACTIVE
23500.,  B40-PYRITE-LOW-TEMPERATURE
28500.,  B43-FES2-PYRITE
30000.,  B44-FES
```

Figure 6-5 An example of the kinetic file, (continued).

```
oligst,mono,fthyl,flink,bead,xt0,cnst2,q0,ph0
nmass(1),mnumb(1)
nmass(2),mnumb(2)
nmass(3),mnumb(3)
nmass(4),mnumb(4)
nmass(5),mnumb(5)
nmass(6),mnumb(6)
nmass(7),mnumb(7)
xeff(i),i=1,17
xeff(i),i=18,35
radi0,density,dummy,amvsol,amwcol,vsrcol,vsrmin
mers,dvg1,viseng,dvg3,dvg4,vstmax,vismax,phimax
mermas(j),j=1,mers
masslm(1),masslm(2)
ldummy
ldummy
s1,s2
mbin
```

Figure 6-6 The data structure of the polymer file.

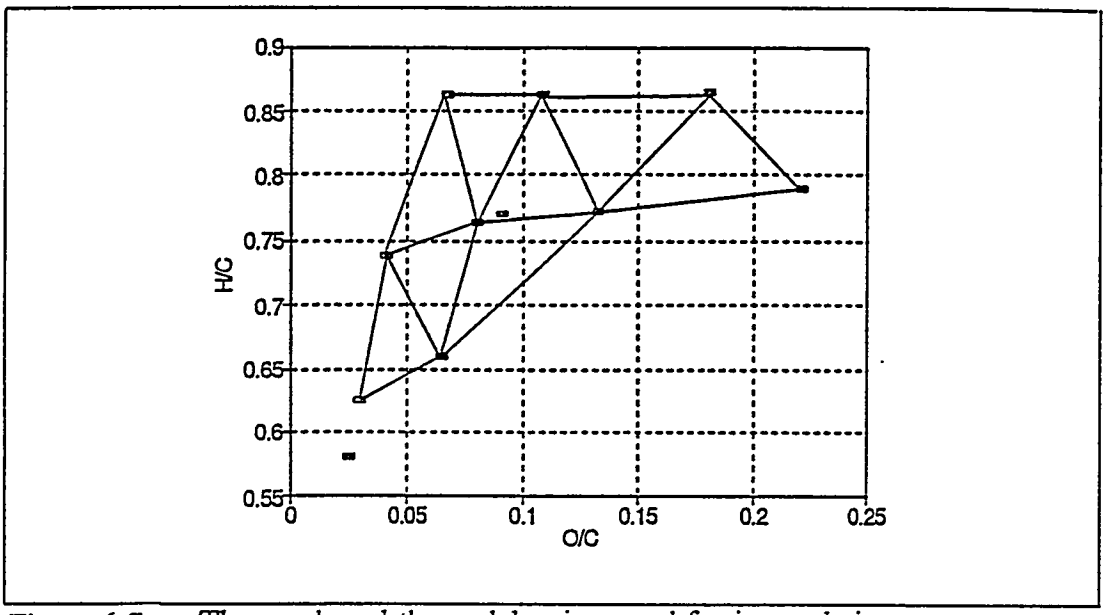

Figure 6-7. The mesh and the nodal points used for interpolations.

Table 6-1 q_0's and p_{b0}'s of the Eight Argonne Coals.

Argonne Coals	q_0	p_{b0}
1	0.35	0.06
2	0.2	0.045
3	0.06	0 .1
4	0.22	0.06
5	0	0.06
6	0	0.037
7	0.1	0.03
8	0.05	0.036

Chapter Seven

Implementation Guide

Code Files

This chapter discusses the implementation of PCGC-2 on UNIX operating systems. The concepts that are illustrated are applicable to other computer systems as well.

A typical simulation requires approximately 30 input and output files, and programmed procedures, such as script (command) files, are recommended to perform the file management task. Script files can also be used to automatically recompile subroutines that have been modified, relink the program, submit jobs to a batch queue, and prompt interactively for names of files or batch queues.

Typical script files are included in Appendix D. The operation of these files is as follows: First, filenames are specified. These filenames include the main data file (geometry and general flow conditions), inlet data file (inlet velocity flow conditions), thermo data file (thermodynamic parameters), output data files (formatted output file and files created specifically for graphics display), and restart data files (for both gas and particle phases). The script (command) file prompts interactively for the names of these five sets of files if they are not given on the command line. If only a single parameter is specified on the command line, all filenames are assumed identical except for the extensions.

After specifying the filenames for the particular run, links are created (logical variables are assigned) that correspond with the FORTRAN filenames used in PCGC-2. For example, the FORTRAN name for the main data file is PCGCIN. Creating a link called PCGCIN for the filename that was specified above for the main data file allows the data file to be opened by the program. The FORTRAN

filenames that are opened by PCGC-2 and a brief description of each are given in Table 7-1.

Filenames for the coal, kinetics, polymer, and char reactivity data files are specified in the main data file. The file name for the file containing the probability distribution of the mass bins (either MASS_BIN or MASS_BIN8) is determined by the program. After creating links for each of the filenames where required, PCGC-2 is compiled and linked using the most recent versions of each subroutine. This step is especially important if code development is being performed. The MAKE utility automates this step on UNIX systems. An example of a "Make" file is shown in Appendix E. After compiling and linking the program (if necessary), the program is executed. The script file may prompt for the name of the batch queue at this point. After the program has finished executing, the links are deleted.

TABLE 7-1

FILES OPENED BY PCGC-2

FORTRAN Filename	Filename Extension	Subroutine	Unit No.	Description
Character string	NA	GETCDF	10	Coal data file
Character string	NA	GETKIN	10	Kinetics data file
Character string	NA	GETRCT0	25	Char reactivity data file
Character string	NA	NETIN	10	Polymer data file
GASPLT	.gsp	PLTWRT	23	Gas plotting file
GRIDS	.grd	GRMAP	13	Grid data file
INLET	.inl	PROFIL	20	Inlet data file
INOUT	.rst	RESTRT	21	Gas restart file

TABLE 7-1 (continued

Fortran Filename	Filename Extension	Subroutine	Unit No.	Description
mass_bin8 or mass_bin	NA	NETIN	11	Probability distribution of mass bins
NOXIN	.nox	NOXMN	7	NO_x data file
PARSOU	.pso	EOLP, Main program	22	Coal particle restart file
PCGCIN	.dat	Main program	1	Main data file
PCGCOT	.out	Main program	3	Output file
POLPLT	.nxp	NOXMN	24	NO_x plotting file
PPLOT1	.pp1	PSICT	23	Coal particle plotting file
PPLOT2	.pp2	EOLP	15	Coal particle plotting file
PPLOT3	.pp3	PSICT	20	Coal particle plotting file
PRGRSS	.prg	PROG	14	Progress monitoring file
PSORB1	.ps1	SPSICT	23	Sorbent particle plotting file
PSORB2	.ps2	SPSICT	27	Sorbent particle plotting file
PSORB3	.ps3	SPSICT	20	Sorbent particle plotting file
RSNXIO	.rnx	RSTNOX	22	NO_x restart file
SORDN1	.sdn	SDNRST	27	Sorbent particle no. density restart file
SOXIN	.sox	SORB0	8	Sorbent reactions data file

TABLE 7-1 (continued

Fortran Filename	Filename Extension	Subroutine	Unit No.	Description
SOXPOL	.sxp	SORPAR	24	Sorbent reactions gas plotting file
TBLRST	.tbl	TBLRSFEH, TBLRSTFE	28	Table restart file
THERMO	.thm	Main program	21	Thermodynamic data file
TWODDBV	.dbv	OVENDB	110	CEQUIL post-processor plotting file
YH2S1	.h2s	SLFRST	27	H_2S restart file
YSO21	.so2	SLFRST	27	SO_2 restart file

FORTRAN and Machine Incompatibilities

PCGC-2 was originally developed on a VAX/VMS computer. Development and maintenance during the past six years has been on UNIX machines. The programming conforms to FORTRAN-77 standards. Therefore, the code should be easily portable to other systems with the following considerations:

1. Scripts for running the code have been developed for the C-shell under UNIX and will need to be converted to run under other UNIX shells or other operation systems.
2. Some variables may not be initialized. PCGC-2 assumes that all memory registers allocated for its use are initialized prior to execution. Most compilers do this automatically or have an option to do it. If the compiler being used cannot perform this initialization, modifications may be required in the code.
3 Direct-access files are used in some instances. The direct-access feature of these files is useful for post-processing of data for plotting. All of these files can be changed to sequential without changing the performance of the code, with the exception of the PRGRSS file. The purpose of this file is to

be accessible and provide information on the progress of the simulation during execution. This file is unnecessary for UNIX systems as all input and output files are accessible for viewing while the program is running. Machine-specific modifications of this file may be needed on other systems.

4. Before closing the restart, plotting, and other sequential files, it may be necessary to rewind them so they will be written from the beginning the next time they are opened. Otherwise, they may be appended, defeating their purpose and consuming large amounts of disk space.
5. PCGC-2 frequently calls a subroutine called CPUTIM, which uses a system-dependent utility to monitor the amount of CPU time used in various sections of the code. The CPUTIM and GETCPU subroutines may need to be modified for this function. Alternatively, the calls to CPUTIM may be commented out, or dummy variables may be passed back from CPUTIM to PCGC-2 .
6. PCGC-2 sometimes uses calls to FLUSH, a UNIX utility, for emptying the contents of output buffers in a timely fashion. These calls need to be replaced with calls to a similar utility applicable on the current machine. Alternatively, they may be removed, but removing these calls would make the progress of the calculation more difficult to monitor and increase the difficulty of debugging.

Chapter Eight

Sample Problems

Three sample problems are presented in this chapter: gaseous combustion, coal combustion, and coal gasification. Input data files for all cases are included in the appendices and are available on magnetic tape with the licensing of the program as explained in Chapter 1. The output files are too lengthy to include here, but are included on the tape.

Gaseous Combustion

This sample problem is the combustion of natural gas in air. Natural gas is fed at room temperature in the primary stream, and air is fed at room temperature in the secondary stream. Primary stream is not swirled. The secondary stream is swirled and enters the reactor at a swirl number of 1.45. The reactor is at a pressure slightly below atmospheric pressure. Important parameters for the problem are shown in Table 8-1, and the inlet files are contained in Appendix E.

Coal Combustion with NO_x Formation

This sample problem is the combustion of coal in air. Pulverized coal entrained in air is fed at room temperature in the primary stream. The secondary air is preheated and swirled. The reactor is at atmospheric pressure. The coal is a bituminous coal (Utah Blind Canyon). Other important parameters are shown in Table 8-2. The case uses ten chemical species and fifty particle trajectories. Input files are included in Appendix F. The inlet and thermo files are not included

TABLE 8-1

KEY INPUT DATA FOR NATURAL GAS COMBUSTION CASE

Geometry	
Primary tube diameter (m)	0.027
Secondary tube diameter (m)	0.098
Chamber diameter (m)	0.800
Chamber length (m)	2.650
Feed Rates	
Primary gas (kg/s)	2.611E-03
Secondary gas (kg/s)	0.150
Inlet Gas Properties	
Primary swirl number	0.000
Primary turbulent intensity	0.10
Primary temperature (K)	298.0
Primary mole fractions:	
CH_4	0.801
CO_2	0.016
C_2H_6	0.120
C_3H_8	0.054
N_2	0.009
Secondary swirl number	1.450
Secondary turbulent intensity	0.10
Secondary temperature (K)	298.0
Secondary mole fractions:	
O_2	0.233
N_2	0.767
Reactor Parameters	
Reactor pressure (N/sq m)	8.6E+04
Side wall temperature (K)	1000.0

TABLE 8-2

KEY INPUT DATA FOR PULVERIZED COAL COMBUSTION CASE

Geometry	
Primary tube diameter (m)	0.027
Secondary tube diameter (m)	0.098
Chamber diameter (m)	0.800
Chamber length (m)	2.650
Feed Rates	
Primary gas (kg/s)	4.170E-03
Secondary gas (kg/s)	0.035
Coal in primary (kg/s)	3.169E-03
Inlet Gas Properties	
Primary swirl number	0.000
Primary turbulent intensity	0.10
Primary temperature (K)	298.0
Primary mole fractions:	
H_2O	0.062
N_2	0.720
O_2	0.219
Secondary swirl number	1.400
Secondary turbulent intensity	0.10
Secondary temperature (K)	423.0
Secondary mole fractions:	
N_2	0.767
O_2	0.233
Reactor Parameters	
Reactor pressure (N/sq m)	1.013E+05
Side wall temperature (K)	1250.0
Particle Parameters	
Particle solid density (kg/cu m)	1340.0
Heat of formation, daf (J/kg)	
Mass mean particle diameter (m)*	4.50E-05

TABLE 8-2 (continued)

Initial analysis:	
raw coal	0.861
ash	0.139
Elemental analysis (daf):	
C	0.696
H	0.053
O	0.094
N	0.013
S	0.005

*Continuous distribution simulated with 5 discrete sizes.

because they are essentially the same as the ones shown in Appendix E. A grid file is shown, which can be used to alter the node locations, add nodes (up to a total of 100 in each direction), add intrusions, and/or add additional inlets (up to 3) as discussed in Chapters 3 and 5. The right-hand side of the bottom portion of the grid file is truncated because of space limitations on the printed page.

The log file for this case is also included in Appendix F. Information identifying the computation was first printed out, followed by a figure showing the important node locations. As shown, this problem used a 55 x 49 grid. After the figure, the names of the FG-DVC input files are printed out followed by a set of parametric values calculated when using the FG-DVC submodel. Next, a header was printed out for the gas phase solution. Next, the physical properties table was generated. Because the energy equation was solved in this case (INCALH is set to T in the main data files), the table is a function of three independent variables: gas mixture fraction (f), coal gas mixture fraction (η), and residual enthalpy (h_r).

After generating the table, the first gas phase iteration began. As shown, information was printed out for the first iteration and every 5 gas macro-iterations thereafter. This corresponds to Steps 2 and 3 in Fig. 3a-1. Residual source sums were printed out for the *u*-velocity, *v*-velocity, *w*-velocity, mass source term, pressure, enthalpy, mixture fraction, and coal-gas mixture fraction. The maximum of these source sums was printed to the left. At the far right, is shown the number of potential calls to CREE, or the number of times equilibrium properties were needed for a value of residual enthalpy that was outside the table limits. For this particular case there was no potential call to CREE.

After the gas phase was calculated, the gas properties were updated (Step 4, Fig. 3a-1) and then the Eulerian particle number density field was calculated (Step 5, Fig. 3a-1). The bulk velocity of the particles is assumed equal to that of the gas, with the particles diffusing according to the concentration gradient. This calculation is indicated in the log file by the brief header starting with "NJITER" shown following the gas phase. Residual source sums for each of the allowable five particle sizes are printed out in a manner similar to the source sums for the gas phase every five iterations. For this case, the number density calculation converged at between 5 and 10 iterations, after the first gas phase iteration.

After the particle density fields were calculated, the radiation field was solved (Step 6, Fig. 3a-1). In this case, the discrete ordinates method was used (LDISO = T in the main input file of Appendix F). As shown in the log file, the radiation model is solved alternately without (SCATTER ITER: 0) and with (SCATTER ITER: 1) radiation scattering by particles included. A total of six iterations were required the first time without scattering followed by four iterations to converge with scattering. Iteration continued until the change in total net wall flux fell below a prescribed level.

After solving the gas phase, particle density, and radiation fields, the Lagrangian particle calculation was performed (Steps 7-10, Fig. 3a-1). The assumption for this case was that all particles stick when they hit the wall. For each particle size and starting location, the terminating location, transit time, and number of iteration steps are shown. If the trajectory recirculated, it was so noted. After the particle trajectory information, a summary of the solid phase coupling was printed. This is the sum of the particle source terms for all of the gas cells for η, f, mass u-velocity, v-velocity, and enthalpy. Since this is a coal combustion case, the values for SSPE (η) and SSPM (mass) are identical, since the only source of mass to the gas phase is from the coal. For coal-water mixture combustion, the variable f is used to track the mixing of the moisture from the coal-water droplets, and both SSPE and SSPF would be non-zero, with SSPM being the sum of both. Finally, the cumulative particle burnout was printed for the outlet location of the reactor. After the particle phase was calculated, the gas phase was recalculated, using the new particle source terms.

This case was converged from restart in four particle iterations. The convergence criterion which finally terminated the calculation was the SORMIN criterion. After the third particle iteration, the maximum residual source sum for the gas phase during the first iteration was 0.09512, which is less than the value of 0.1 specified for SORMIN in the main data file. The gas phase was converged one more time, followed by one more particle iteration. For the final gas phase calculation, less than 15 macro-iterations were required.

After converging the particle-gas combustion model, the NO_x calculations are performed. In this case, only fuel NO_x was calculated. The NO_x iterations can be seen at the end of the log file.

Coal Gasification with Sidewall Sorbent Injection and Sulfur Capture

This sample problem is the gasification of Illinois No. 6 bituminous coal at 2 atm in the BYU gasifier (Huber, 1985). The primary stream consisted of coal transported by Argon. The secondary stream was oxygen. Sorbent was injected through the sidewall. Important parameters are shown in Table 8-3 and the input files are included in Appendix G.

TABLE 8-3

PARAMETERS FOR COAL GASIFICATION CASE

Geometry	
Primary tube diameter (m)	0.013
Secondary tube diameter (m)	0.029
Chamber diameter (m)	0.200
Chamber length (m)	2.000
Feed Rates	
Primary gas (kg/s)	0.0011
Secondary gas (kg/s)	0.0052
Tertiary (sidewall) gas (kg/s)	0.0013
Coal in primary (kg/s)	0.0083
Inlet Gas Properties	
Primary swirl number	0.000
Primary turbulence intensity	0.010
Primary temperature (K)	356.0
Primary mole fractions:	
Ar	1.000
Secondary swirl number	0.000

TABLE 8-3 (continued)

Secondary turbulence intensity	0.100
Secondary temperature (K)	589.0
Secondary mole fractions:	
O_2	1.000
Tertiary swirl number	0.000
Tertiary turbulence intensity	0.010
Tertiary temperature (K)	356.0
Tertiary mole fractions	
Ar	1.000
Reactor Parameters	
Reactor pressure (N/sq m)	1.84E+05
Side wall temperature (K)	1100.0
Coal Particle Parameters	
Particle solid density (kg/cu m)	1340
Particle mass fractions	
5 μm	0.200
13 μm	0.200
32 μm	0.200
50 μm	0.200
100 μm	0.200
Initial analysis:	
raw coal	0.941
ash	0.059
Elemental analysis (daf):	
C	0.777
H	0.050
O	0.137
N	0.014
S	0.022
Sorbent Particle Parameters	
Particle solid density (kg/cu m)	1793
Particle mass fractions	
10.6 μm	1.000
BET surface area (sq m/g)	1E+5

Nomenclature

Nomenclature for Chapters 4 and 6 are found at the end of those chapters. Nomenclature for all other chapters is found below.

Symbol	Units	Definition
$\dot{m}$, $\dot{M}$	kg s-1	Mass flow rate
$\bar{b}, \bar{f}, \bar{s}$	--	Backward-, forward- and side-scattered components
A	kg s^{-1}	Total coefficient (convection plus diffusion)
A	varies	Pre-exponential factor
a	--	Size parameter $\pi d/\gamma$
A, B	m^2	Area
A_E	m^2	Char surface area in NO_x submodel
a_o	--	Asymmetry factor

Symbol	Units	Definition
B	--	Blowing parameter
b	--	Coefficient on oxygen concentrations in NO_x submodel
b	--	Element mass fraction, back scatter
bcn	--	Weight fraction of nitrogen in coal in NO_x submodel
C	(VFM)	Pressure-correction factor, coefficients
C	kg m^{-3}	Concentration
C	kg s^{-1}	Convection coefficient
C	--	"Universal" constant
c	varies	Variable constant
C_d	--	Drag coefficient
C_p	J kg^{-1} K^{-1}	Heat capacity
D	kg s^{-1}	Numerical coefficient for diffusion
D	m^2 s^{-1}	Diffusivity
D, d	m	Diameter
E	cal $gmol^{-1}$ K^{-1}	Activation energy in NO_x submodel
E	J $kmol^{-1}$	Activation energy
E	kW/m^2	Emissive power
E	--	Constant in the law of the wall

Symbol	Units	Definition
F	J m^{-2} s^{-1}	Radiation flux
F	kW/m^2	Radiative flux-sum
F	--	Adjusted mixture fraction (in PDF)
f	N m^{-2}	Drag force
f	--	Differencing factor
f	--	Mixture fraction, interpolation factor, forward scatter
f_p	--	Mixture fraction corrected for h
G	kg m^{-2} s^{-1}	Mass flux
G	--	Adjusted variance
g	m s^{-2}	Gravitational acceleration
g	--	Mean square fluctuation (variance)
h	J kg^{-1}	Enthalpy
hg	J kg^{-1}	Enthalpy reaction
I	varies	Turbulence intensity, radiation intensity
i	--	Imaginary ($i^2 = -1$)
j	kg m^{-2} s^{-1}	Mass flux
K	--	Absorption coefficient
K	--	Chemical equilibrium constant in NO_x submodel

Symbol	Units	Definition
K	--	Scattering coefficient
k	J m^{-1} K^{-1} s^{-1}	Thermal conductivity
k	m^2 s^{-2}	Kinetic energy of turbulence
k	m^3 $kmol^{-1}$ s^{-1}	Arrhenius rate constant in NO_x submodel
k	varies	Constant, kinetic rate coefficient
k_a, k_s, k_t	m	Absorption, scattering and extinction coefficients
L	m	Length
L	--	Lower limit
L_e	m	Mean (effective) beam length
M	kg	Mass of fluid atoms
M	kg $kmol^{-1}$	Molecular weight
M, m	--	Mass fraction of species
MW	kg $kmol^{-1}$	Molecular weight in NO_x submodel
N	--	Total number of directions used
n	m^{-3}	Particle number density
n	s^{-1}	Particle number flow rate
n	--	Direction normal to boundary
n	--	Order of discrete ordinates approximation
Nu	--	Nusselt number

Symbol	Units	Definition
P	Pa	Pressure in NO_x submodel
P	--	Probability density function (PDF), phase function, P cell
P	--	Scattering phase function
p, P	N m^{-2}	Pressure
Pr	--	Prandtl number
Q	J s^{-1}	Heat flow
q	J m^{-2} s^{-1}	Heat flux
q	kW/m^2	Net flux
Q_a, Q_s	--	Absorption and scattering efficiency
Q_R	kW	Net radiative exchange for a single particle
q_R	kW/m^3	Net radiative exchange for a volume element
$q^{\pm}$	kW/m^2	Hemispherical flux
R	J $kmol^{-1}$ K^{-1}	Universal gas constant
R	m^3 Pa $kmol^{-1}$ K^{-1}	Universal gas constant in NO_x submodel
r	kg s-1	Reaction rate
r, R	M	Radius, radial direction
r, x	m	Distance along radial and axial directions
Re	--	Reynolds number

Symbol	Units	Definition
S	varies	Source term
s	--	Scattering factor, conserved scalar
Sc	--	Schmidt number
Sh	--	Sherwood number
T	K	Temperature
T, t	s	Time, time period
U	--	Upper limit
u	m s^{-1}	Axial velocity
V	m^3	Volume
v	m s^{-1}	Radial velocity, velocity vector
W	kg m^{-3} s^{-1}	Overall mean reaction rate or source term in NO_x submodel
W	kg m^{-3} s^{-1}	Overall species reaction rate
w	kmol m^{-3} s^{-1}	Individual reaction rate
w	m s^{-1}	Tangential velocity
w_m	sr	Angular quadrature weight
X	--	Mole mass fraction
X	--	Particle size function
x	m	Axial position

Symbol	Units	Definition
Y	--	Volatiles coefficient, particle starting location fraction
y	--	Species mole fraction, fluctuating mass fraction
Z	--	Arbitrary variable
$[\ ]$	gmol cm^{-3}	Concentration of enclosed species symbol (NO_x submodel)

Greek Symbols

Symbol	Units	Definition
$\underset{\sim}{\Omega}$, $\underset{\sim}{\Omega}'$	--	Outward and inward directions of radiation
α	kg	Mass
α	--	Intermittency factor
β	varies	Arbitrary property
β	--	Intermittency
χ	m	Wavelength of radiation
δ, Δ	--	Difference operator
ε	$m^2\ s^{-1}$	Dissipation rate of turbulence energy
ε	--	Emissivity

Symbol	Units	Definition
Φ	kg m^{-1} s^{-1}	Dissipation function
ϕ	varies	General variable
ϕ	--	Angle between incident and scattered intensities
Γ	varies	Exchange coefficient
γ	--	Heat loss factor
γ	--	Particle swelling coefficient
H	radians	Azimuthal direction
η	--	Coal gas mixture fraction
κ	--	Constant
λ	--	Under-relaxation factor; wavelength of radiation
μ	kg m^{-1} s^{-1}	Dynamic viscosity
μ, η, ξ	--	Direction cosines
ν	m^2 s^{-1}	Kinematic viscosity
π	--	Percentage perturbation
θ, ψ	--	Polar and azimuthal angles/directions
ρ	kg m^{-3}	Density

Symbol	Units	Definition
σ	--	Schmidt or Prandtl number
τ	$m^2\ s^{-2}$	Shear stress
Ω	--	Collision integral
Ω	--	Differencing scheme coefficient
ω	kmol $m^{-3}\ s^{-1}$	Reaction rate (NO_x submodel)
ω_o	--	Albedo for forward radiation scattering
ξ	s^{-1}	Vorticity
ξ	--	Dimensionless coordinate of integration
Ψ	$m^2\ s^{-1}$	Stream function
ζ	--	Constant in NO_x model
ζ	--	Fraction of heat of reaction given to particle phase
ζ	--	Pore diffusion adjustment factor
ζ	--	Reaction progress (extent of reaction or deviation from equilibrium factor) or fraction of nitrogen released from coal (NO_x submodel)
ζ	--	Surface area factor

Subscripts

Symbol	Definition
a	Absorptive, ash, arbitrary
b	Black-body, bulk, boundary, backward scattering
B	Boundary
c	Cell, pure coal off-gas, convective, raw coal
d	Direction, diffusive, drag
E, e	East direction, effective
eq	Equilibrium (NO_x submodel)
f	Mixture fraction, formation
f	Fuel NO mechanism reaction (NO_x submodel)
F	Radiation flux, furnace
g	Mean square fluctuations (variance), gas phase
g_1, g_2	Universal (found empirically)
h	Enthalpy, char
h	Heterogeneous reaction (NO_x submodel)
i	Gas species index, summation index
i, ,	Species or reaction index (NO_x submodel)
i, j	Area indices in the radial and axial directions, j^{th} particle size

Symbol	Definition
I	Pure inlet gas
j	Particle size, gas species index
k	Turbulent kinetic energy, element
k	Species or reaction index (NO_x submodel)
l	Char reaction index
m	Devolatilization reaction index, mass, mixture
m, m'	Directions of the discrete ordinates
n	Number density, nitrogen (NO_x submodel)
N, n	North direction
N	Nitrogen
o	Initial, oxidizer
P, p	Primary stream, particle, P-cell
ref	Reference
r	Reactor, radial, radiation
r	Non-chemical sources (NO_x submodel)
s	Secondary stream, scattering, south direction
S	South direction, source
t	Turbulence
t	Thermal NO mechanism reaction constant (NO_x submodel)
T	Temperature

Symbol	Definition
T	Total (NO_x submodel)
u	Axial velocity, u cell
U	Non-proportional part of source term
v	Radial velocity, v cell, volatiles, devolatilization
w	Wall
$W,\ w$	West direction
$x,\ z$	Axial direction
Y	Gas phase species (NO_x submodel)
ε	Dissipation rate
η	Coal gas mixture fraction
θ	Azimuthal direction
μ	Viscosity
σ	Solid
ϕ	General variable
λ	Coal component
0	Initial value

Superscripts

Superscripts	Definition
~	Favre mean
'	Fluctuation, flux
', '', '''	Used to distinguish different reaction rate constants (NO_x submodel)
*	Guessed
=	Tensor
$\rightarrow$	Vector
c	Corrected
ε	Dissipation of turbulent kinetic energy
eq	equilibrium species value (NO_x submodel)
ϕ	Arbitrary variable
f	f mixture fraction
f	Frozen
f	Full conversion of volatile fuel nitrogen to species (NO_x submodel)
fuel	Related to fuel NO mechanism (NO_x submodel)
η	Coal gas mixture fraction

Symbol	Definition
h	Enthalpy
k	Turbulent kinetic energy
ℓ	Laminar
m	Mass
μ	Viscosity
max	Maximum species value attainable by limiting reactants (NO_x submodel)
min	Minimum species value attainable by limiting reactants (NO_x submodel)
n	Temperature
o	Standard or reference
p	P cell
ρ	Density
r	Radial direction
T	Temperature
t	Turbulent
thermal	Related to thermal NO mechanism (NO_x submodel)
u	Axial velocity, u cell
v	Radial velocity, v cell
x	Axial direction

Symbol	Definition
^{o}	Initial (NO_x submodel)
$\pm$	Positive and negative directions of propagation
$-$	Reynolds mean

References

References for Chapters 4 and 6 are found at the end of those chapters. References for all other chapters are found below.

Abramowitz, M. and Stegun, A. S., Handbook of mathematical functions, Dover Publications, New York, NY (1972).

Anson, D., Moles, F. D. and Street, P. J., "Structure and surface area of pulverized coal during combustion," Combust. Flame, 16, 265 (1971).

Anthony, D. B., Howard, J. B., Hottel, H. C. and Meissner, H. P., "Rapid devolatilization and hydrogasification of bituminous coal," Fuel, 55, 121 (1976).

Argarwal, R. K., A third-order-accurate upwind scheme for Navier-Stokes solutions at high Reynolds numbers, St. Louis, MO, AIAA 19th Aerospace Sciences Meeting, January, St. Louis, MO (1981).

Badzioch, S. and Hawksley, P. G. W., "Kinetics of thermal decomposition of pulverized coal particles," IEC Proc. Des. Dev., 9, 521-30 (1970).

Bailey, G. H., Slater, I. W. and Eisenklam, P., "Dynamic equations and solutions for particles undergoing mass transfer," Brit. Chem. Eng., 15, 912-16 (1970).

Baxter, L. L., Fletcher, T. H. and Ottesen, D. K., "Spectral emittance measurements of coal particles," Energy & Fuels, 2, 423-430 (1988).

FORTRAN Variable	FORTRAN Dimensions	FORTRAN Common Block or Routine	User's Manual Nomenclature	Units	User's Manual Eq. Nos.	Definition
spupold	numxpt,numypt	COMMON under				Old values of spup
spuu	numxpt,numypt	COMMON cpsou				Particle momentum source term for u velocity
spuuold	numxpt,numypt	COMMON under				Old values of spuu
spv	numxpt,numypt	COMMON cpsou				Particle momentum source term for v velocity
spvold	numxpt,numypt	COMMON under				Old values of spv
spw	numxpt,numypt	COMMON cpsou				Particle momentum source term for w velocity
SRHVJM	--	COAL2	$\sum(\dot{m}_{vjm} h_{vjm})$		2-125	Total enthalpy of volatiles produced by all devolatilization reactions for the j^{th} particle classification.
sspe	--	COMMON ssum		--		Sum of particle coal gas mixture fraction source terms
sspf	--	COMMON ssum		--		Sum of particle mixture fraction source terms
ssph	--	COMMON ssum		--		Sum of particle enthalpy source terms

FORTRAN Variable	FORTRAN Dimensions	FORTRAN Common Block or Routine	User's Manual Nomenclature	Units	User's Manual Eq. Nos.	Definition
sspm	--	COMMON ssum		--		Sum of particle mass source terms
sspu	--	COMMON ssum		--		Sum of particle u-momentum source terms
sspv	--	COMMON ssum		--		Sum of particle v-momentum source terms
sspw	--	COMMON ssum		--		Sum of particle w-momentum source terms
su	numxpt, numypt	COMMON coef	S_U		3-70	Source coefficient
su	numxpt,numypt	COMMON coef	S_U		3-70	Source term
sukd, spkd	numxpt,numypt	COMMON susp				Linearized source term for turbulent kinetic energy
suu	numxpt, numypt	COMMON flupr2		--		Source term in u equation
svu	numxpt, numypt	COMMON flupr2		--		Source term in v equation
swirlp	--	COMMON swrl		--		Primary swirl no..
swirls	--	COMMON swrl		--		Secondary swirl no.
swrlin	numlet	COMMON adflo				Swirl no. for each additional inlet
t	numxpt, numypt	COMMON fluc		K		Gas temperature

FORTRAN Variable	FORTRAN Dimensions	FORTRAN Common Block or Routine	User's Manual Nomenclature	Units	User's Manual Eq. Nos.	Definition
taurx, taurth, tauxr, tauxth	numxpt,numypt	COMMON shear				Components of shear stress
tbe	--	COMMON sherx		K		Temperature of east wall boundary
tbn	--	COMMON kaset1		K		Temp. of north wall boundaries
tboil	--	COMMON hcap		K		Normal boiling pt. for slurry liquid
tbw	--	COMMON kaset1		K		Temp. of west wall boundaries
TCT	--	PROPS	T_c		2-80, where β=T	Temperature of pure coal offgas
tct	--	COMMON pvar		kg $kmol^{-1}$		Coal offgas adiabatic temperature
te	numxpt,numypt	COMMON var				Turbulent kinetic energy
tf0	--	COMMON flaf0		K		Temperature of f=0 stream
tf1	--	COMMON flaf0		K		Temperature of f=1 stream
tflof0	--	COMMON tflof10		kg s^{-1}		Total flow of f=0 stream
tflof1	--	COMMON tflof10		kg s^{-1}		Total flow of f=1 stream
tflux	--	COMMON timer		s		Total cpu time spent in flux

FORTRAN Variable	FORTRAN Dimensions	FORTRAN Common Block or Routine	User's Manual Nomenclature	Units	User's Manual Eq. Nos.	Definition
tg	--	COMMON traj		K		Gas temperature
thermno	--	COMMON ratpar		--		.TRUE. causes thermal NO to be calculated
thiact	--	COMMON pdim		m		Actual thickness of primary tube wall
thick	--	COMMON grid1		m		Thickness of primary tube wall
thigh	--	COMMON spece		K		Upper temperature for JANAF correlations
time	--	COMMON cpart		s		Time along a particle trajectory
tinlet	numlet	COMMON adflo		K		Temperature for additional inlet
tinlt	numlet	COMMON adflo				Turbulence intensity for additional inlet
tinp	--	COMMON pdim		--		Primary stream turbulence intensity
tins	--	COMMON pdim		--		Secondary stream turbulence intensity
tions	numspe	COMMON lution		--		Map of species to solutions in equilibrium algorithm
tk	--	COMMON cparam		K		Temperature
tkinv	--	COMMON cchemi		K^{-1}		Inverse of tk

FORTRAN Variable	FORTRAN Dimensions	FORTRAN Common Block or Routine	User's Manual Nomenclature	Units	User's Manual Eq. Nos.	Definition
tlag	numpar	COMMON cpart		--		Ratio of particle temperature to gas temperature at starting location
tlis	--	COMMON timer		s		Total cpu time spent in lisolv
tlow	--	COMMON spece		K		Minimum temperature for JANAF correlations
tmh	--	COMMON magnusse n		K		Temperature of product stream (Magnussen-Hjertager method)
tmid	--	COMMON spece		K		Dividing tempeature for JANAF temperature ranges
tmp	--	COMMON traj		K		Particle temperature
tnbp	--	COMMON ctnbp		K		Normal boiling point of slurry liquid
tomit	--	PARAMETE R		--		Flag indicating that a species or solution is not active in the equilibrium system
totflo	--	COMMON tflof10		kg s^{-1}		Total flow of gas into reactor
tout	--	COMMON diso		K		Outlet temperature for radiation calculations
tp	--	COMMON pands		K		Primary stream temperature

FORTRAN Variable	FORTRAN Dimensions	FORTRAN Common Block or Routine	User's Manual Nomenclature	Units	User's Manual Eq. Nos.	Definition
tprom	--	COMMON timer		s		Total cpu time spent in promod and mod* subroutines
tprops	--	COMMON timer		s		Total cpu time spent in props
trace	--	COMMON bug				.TRUE. turns on tracing messages for entering and leaving props subroutine
trange	nrange+1,numspe	COMMON spece				Temperature ranges for least squares fit
ts	--	COMMON pands		K		Secondary stream temperature
tup	--	COMMON timer		s		Total cpu time spent in table lookup
u	numxpt,numypt	COMMON var		$m\ s^{-1}$		Axial velocity
udpdxt	--	COMMON enth		$J\ s^{-1}$		Total enthalpy gained from PV work in axial direction
updwn	--	COMMON direct		--		1.0 = down-fired -1.0 = up-fired 0.0 = horizontally fired
uplag	numpar	COMMON cpart		--		Ratio of particle velocity to gas velocity at starting location
uprim	--	COMMON flin		$m\ s^{-1}$		The average primary velocity

FORTRAN Variable	FORTRAN Dimensions	FORTRAN Common Block or Routine	User's Manual Nomenclature	Units	User's Manual Eq. Nos.	Definition
urfden	--	COMMON fluc	--			Under-relaxation factor for den
urfe	--	COMMON tdis	--			Under-relaxation factor for ed
urfeta	--	COMMON cgasmf	--			Under-relaxation factor for eta
urff	--	COMMON mixfr	--			Under-relaxation factor for f
urfg	--	COMMON fluc	--			Under-relaxation factor for g_f
urfget	--	COMMON cgasmf	--			Under-relaxation factor for geta
urfh	--	COMMON enth	--			Under-relaxation factor for gas enthalpy
urfh2s	--	COMMON ratesx	--			Under-relaxation factor for H_2S
urfhcn	--	COMMON calcyi	--			Under-relaxation factor for HCN
urfk	--	COMMON ten	--			Under-relaxation factor for te
urfnh3	--	COMMON calcyi	--			Under-relaxation factor for NH_3
urfnj	--	COMMON pard	--			Under-relaxation factor for parden
urfnox	--	COMMON calcyi	--			Under-relaxation factor for NO_x
urfp	--	COMMON pcor	--			Under-relaxation factor for p

FORTRAN Variable	FORTRAN Dimensions	FORTRAN Common Block or Routine	User's Manual Nomenclature	Units	User's Manual Eq. Nos.	Definition
urfph	--	COMMON under		--		Under-relaxation factor for particle enthalpy source terms
urfpm	--	COMMON under		--		Under-relaxation factor for particle mass source terms
urfpp	--	COMMON pcor		--		Under-relaxation factor for pressure
urfso2	--	COMMON ratesx		--		Under-relaxation factor for SO_2
urfu	--	COMMON uvel		--		Under-relaxation factor for u velocity
urfv	--	COMMON vvel		--		Under-relaxation factor for v velocity
urfvis	--	COMMON fluc		--		Under-relaxation factor for vis
urfw	--	COMMON wvel		--		Under-relaxation factor for w velocity
use	numspe	COMMON cparam		--		use(j)=0 --> species j in solution use(j)<0 --> species j is pure phase and not included use(j)>0 --> species j is pure phase and included
v	numxpt,numypt	COMMON var		m s^{-1}		Radial velocity

FORTRAN Variable	FORTRAN Dimensions	FORTRAN Common Block or Routine	User's Manual Nomenclature	Units	User's Manual Eq. Nos.	Definition
vdpdrt	--	COMMON enth		J s^{-1}		Total enthalpy gained from PV work in radial direction
vellaq	--	COMMON traj		m s^{-1}		Slip velocity between particle and gas
vinlt	numlet	COMMON adflo				Radial velocity false boundary for north wall inlets
vis	numxpt, numypt	COMMON fluc		kg m^{-1} s^{-1}		Total viscosity
viscos	--	COMMON fluc		kg m^{-1} s^{-1}		Laminar viscosity
visl	numxpt, numypt	COMMON fluc		kg m^{-1} s^{-1}		Laminar viscosity
vislf0	--	COMMON flaf0		kg m^{-1} s^{-1}		Laminar viscosity for f=0 stream
vislf1	--	COMMON flaf0		kg m^{-1} s^{-1}		Laminar viscosity for f=1 stream
vislinlet	numlet	COMMON adflo		kg m^{-1} s^{-1}		Laminar viscosity for additional inlet
vislp	--	COMMON pands		kg m^{-1} s^{-1}		Primary stream laminar viscosity
visls	--	COMMON pands		kg m^{-1} s^{-1}		Secondary stream laminar viscosity
vislsct	--	COMMON pvar		kg $kmol^{-1}$		Coal offgas laminar viscosity

FORTRAN Variable	FORTRAN Dimensions	FORTRAN Common Block or Routine	User's Manual Nomenclature	Units	User's Manual Eq. Nos.	Definition
w	numxpt,numypt	COMMON var		m s^{-1}		Tangential velocity
wfac	numxpt	COMMON geom		--		Geometric factor
wfinit	--	COMMON cwater		--		Initial overall fraction of water in particles
wmin	--	COMMON cwater		kg s^{-1}		Total mass flow rate of water into reactor
wq	4,5	COMMON diso	w_m	--	2-142	Angular quadrature weight
wtm	numxpt, numypt	COMMON molwt		kmol kg^{-1}		Inverse of mixture mol. wt.
x	numspe+2	COMMON cmatri				Solution to Gauss matrix
x	numspe+2	COMMON cmatri				Solution to Gauss matrix
x	numxpt	COMMON geom		m		Location of axial nodes
XFRAC	NUMSPE	Common TRAJ		kmol i kg^{-1}		Species mole number
xfrac	numspe	COMMON traj		--		Gas mole fractions
xh2s	numxpt, numypt	COMMON ratesx		--		H_2S mole fraction
XI	NUMPAR	Common PFAC	ζ	--	2-131	Surface area factor.

FORTRAN Variable	FORTRAN Dimensions	FORTRAN Common Block or Routine	User's Manual Nomenclature	Units	User's Manual Eq. Nos.	Definition
xi	numpar	COMMON pecor		--		Ratio of total active surface area for oxidation to surface area of a sphere
xianox	--	COMMON ratpar		--		Fractional change in external char area used in NO model as a result of swelling and fracturing
xico	numxpt, numypt	COMMON ratecm				
xico2	numxpt, numypt	COMMON ratecm				
xinc	--	COMMON upnx				Increment in residual enthalpy in physical properties table
xln	numypt	COMMON cpart		m		Axial location of the front wall for each j-node
xlp	--	COMMON cpart		m		Axial location of reactor exit plane
xps	numstr	COMMON cpart		m		Axial coordinate of particle starting locations
xso2	numxpt, numypt	COMMON ratesx		--		SO_2 mole fraction
xu	numxpt	COMMON geom		m		Axial location of west face of p-cell

FORTRAN Variable	FORTRAN Dimensions	FORTRAN Common Block or Routine	User's Manual Nomenclature	Units	User's Manual Eq. Nos.	Definition
y	numspe+2	COMMON cmatri				Natural log of moles of each species
y	numspe+2	COMMON cmatri				Natural log of moles of each species
y	numypt	COMMON geom		m		Location of radial nodes
yco2eq	numxpt, numypt	COMMON ratecm		--		Equilibrium CO_2 field
ycoeq	numxpt, numypt	COMMON ratecm		--		Equilibrium CO field
yf	--	COMMON ctable				
yfh2eq	numxpt, numypt	COMMON ratecm		--		Equilibrium H_2 field
yfu	numxpt, numypt	COMMON magnusse n		--		Mass fraction of fuel (used in Magnussen-Hjertager method)
yh2oeq	numxpt, numypt	COMMON ratecm		--		Equilibrium CO field
yh2s	numxpt, numypt	COMMON ratesx		--		H_2S field
yh2seq	numxpt, numypt	COMMON ratesx		--		Equilibrium H_2S
yhcn	numxpt, numypt	COMMON calcyi		kg HCN kg^{-1}		HCN mass fraction
yhcnf	numxpt, numypt	COMMON ratecm		--		Total nitrogen evolved from the coal

FORTRAN Variable	FORTRAN Dimensions	FORTRAN Common Block or Routine	User's Manual Nomenclature	Units	User's Manual Eq. Nos.	Definition
yhcnpr	--	COMMON intrat				Initial guess for hcn fraction in primary
yhcnpr	--	COMMON psccom		--		Initial guess fraction of HCN in primary stream
yhcns	--	COMMON intrat				Initial gues for hcn fraction in secondary
yhcns	--	COMMON psccom		--		Initial guess fraction of HCN in secondary stream
yln	--	COMMON cpart		m		Radial location of reactor centerline (i.e. zero)
ylp	numxpt	COMMON cpart		m		Radial location of reactor wall at each i-node
yn2	numxpt, numypt	COMMON calcyi		kg N_2 kg^{-1}		Nitrogen mass fraction
yn2eq	numxpt, numypt	COMMON ratecm		--		Equilbrium N_2 field
ynh3	numxpt, numypt	COMMON calcyi		kg NH_3 kg^{-1}		NH_3 mass fraction
ynh3eq	numxpt, numypt	COMMON ratecm		--		Equilibrium NH_3 field
ynh3f	numxpt, numypt	COMMON ratecm		--		NH_3 field
ynh3pr	--	COMMON psccom		--		Initial guess fraction of NH_3 in primary stream

FORTRAN Variable	FORTRAN Dimensions	FORTRAN Common Block or Routine	User's Manual Nomenclature	Units	User's Manual Eq. Nos.	Definition
ynh3s	--	COMMON psccom		--		Initial guess fraction of NH_3 in secondary stream
ynoeq	numxpt, numypt	COMMON ratecm		--		Equilibrium NO field
ynox	numxpt, numypt	COMMON calcyi		kg NO_x kg^{-1}		NO_x mass fraction
ynoxf	numxpt, numypt	COMMON ratecm		--		The amount of nitrogen available from the coal plus the maximum amount of thermal NO that can be formed when joint thermal NO and fuel NO calculations are made
yo2	numxpt, numypt	COMMON calcyi		kg O_2 kg^{-1}		Oxygen mass fraction
yo2eq	numxpt, numypt	COMMON ratecm		--		Equilibrium O_2 field
yoh	numxpt, numypt	COMMON ratecm		--		OH field
yoheq	numxpt, numypt	COMMON ratecm		--		Equilibrium OH field
yox	numxpt, numypt	COMMON magnusse n		--		Mass fraction of oxygen (Magnussen-Hjertager method)

FORTRAN Variable	FORTRAN Dimensions	FORTRAN Common Block or Routine	User's Manual Nomenclature	Units	User's Manual Eq. Nos.	Definition
ypr	numxpt, numypt	COMMON magnusse n		--		Mass fraction of product (Magnussen-Hjertager method)
yps	numstr	COMMON cpart		m		Radial coordinate of particle starting locations
ypsh	--	COMMON cpart		--		Upper found (fractional distance) for location of particles in a duct
yso2	numxpt, numypt	COMMON ratesx		--		SO_2 field after sorbent capture
yso2eq	numxpt, numypt	COMMON ratesx		--		Equilibrium SO_2 field
yv	numypt	COMMON geom		m		Radial location of south face of p-cell
yy	numpar,n umdev	COMMON rrat		--		Volatiles fraction for coal reaction
zeda	--	COMMON ratpar		--		Fractional conversion of devolatilized nitrogen to HCN in the gas phase
zinc	--	COMMON upnx				Increment in mixture fraction in physical properties table
zzz	mxcoef,n range,nu mspe	COMMON spece				Coefficients to least squares fit to JANAF data

Appendix I

Sample Calculations

Char Oxidation Parameters

Table 2-8 reports a value of 300 $\frac{\text{m}}{\text{s K}}$ for A_{jl} for the data of Field et al. (1967) for char/O_2 reaction. This value is derived from the value reported by Field et al.(8710 $\frac{\text{g}}{\text{cm}^2\ \text{s atm}}$) as follows:

The oxidizer-char reaction rate is given by Eqn. 2-131, which takes into account the effect of mass transfer on the reaction rate. If mass transfer is neglected, Eqn. 2-131 becomes

$$r_{hjl} = A_j M_{hj} \phi_l k_{jl} \zeta_j C_{olg} \qquad \text{(I-1)}$$

where r_{hjl} is kg char/s reacting for the j^{th} particle classification and the l^{th} char reaction. A_j is the particle surface area (m^2), M_{hj} is the char molecular weight, ϕ_l is the stoichiometric factor (moles char required per mole of oxidizer), ζ_j is a particle surface area factor, and C_{olg} is bulk concentration of oxidizer (kmol oxidizer/m^3). The rate coefficient k_{jl} (m/s) is given by Eqn. 2-132, using the parameters in Table 2-8. The units of Eqn. (I-1) are thus

$$\left(\frac{\text{kg char}}{\text{s}}\right)=\left(\text{m}^2\right)\left(\frac{\text{kg char}}{\text{kmol char}}\right)\left(\frac{\text{kmol char}}{\text{kmol oxidizer}}\right)\left(\frac{\text{m}}{\text{s}}\right)\left(\frac{\text{m}^2}{\text{m}^2}\right)\left(\frac{\text{kmol oxidizer}}{\text{m}^3}\right) \quad \text{(I-2)}$$

Using the reaction rate of Field et al. (1967), r_{hjl} is given by:

$$r_{hjl} = A_j k_{jlf} \zeta_j P_{olg} \quad \text{(I-3)}$$

where the subscript "*f*" has been added to k_{jl} to indicate that this is the rate constant for Field et al. The rate coefficient k_{jl} is given by

$$k_{jl} = A_{jlf} \exp\left(\frac{-E_{jl}}{RT_j}\right) \quad \text{(I-4)}$$

where the subscript "*f*" on A_{jlf} indicates the Field et al. value. The units of Eqn. (I-3) are given by

$$\left(\frac{\text{kg char}}{\text{s}}\right)=\left(\text{m}^2\right)\left(\frac{\text{kg char}}{\text{m}^2\ \text{s Pa}}\right)\left(\frac{\text{m}^2}{\text{m}^2}\right)(\text{Pa}) \quad \text{(I-5)}$$

Equating (I-1) and (I-3), one obtains

$$k_{jl} = \frac{k_{jlf} P_{olg}}{M_{hj} \phi_l C_{olg}} \quad \text{(I-6)}$$

The relationship between A_{jl} and A_{jlf} can be obtained by substituting Eqn. 2-132 with n equal to unity and (I-4) into (I-6), and by using the ideal gas law to replace the ratio of P_{olg} and C_{olg} with RT_j to obtain

$$A_{jl} = A_{jlf}\left(\frac{R}{M_{hj}\phi_l}\right) \quad \text{(I-7)}$$

The value of A_{jl} reported in Table 2-8 for Field et al. is thus obtained as follows:

$$A_{jl} = \left(8710 \frac{\text{g-char}}{\text{cm}^2 \text{ s atm}}\right) \left[\frac{82.05 \frac{\text{cm}^3 \text{ atm}}{\text{mol-O}_2 \text{ K}}}{\left(\frac{12 \text{ g-char}}{\text{mol-char}}\right)\left(\frac{2 \text{ mol-char}}{\text{mol-O}_2}\right)}\right] \left(\frac{\text{m}}{100 \text{ cm}}\right) = 300 \frac{\text{m}}{\text{s K}} \quad \text{(I-8)}$$

Appendix J

General Model of Coal Devolatilization

Reprinted from Journal of ENERGY & FUELS, 1988, 2, 405.

General Model of Coal Devolatilization†

P. R. Solomon,* D. G. Hamblen, R. M. Carangelo, M. A. Serio, and G. V. Deshpande

Advanced Fuel Research, Inc., 87 Church Street, East Hartford, Connecticut 06108

Received December 21, 1987. Revised Manuscript Received April 21, 1988

A general model for coal devolatilization, which combines a functional group model for gas evolution and a statistical model for tar formation, has been presented. The tar formation model includes depolymerization, cross-linking, external transport, and internal transport. The cross-linking is related to the evolutions of CO_2 and CH_4, with one cross-link formed per molecule evolved. The model predictions compare favorably with a variety of data for the devolatilization of Pittsburgh Seam coal and North Dakota (Beulah) lignite, including volatile yields, extract yields, cross-link densities, and tar molecular weight distributions. The variations with pressure, devolatilization temperature, rank, and heating rate were accurately predicted. Comparison of the model with several sets of data employing alternative assumptions on transport suggests that assuming that the particle is well mixed (i.e. the surface concentration of tar molecules is the same as the bulk) overpredicts the transport rate. For 50-μm particles, assuming that the internal-transport limitation dominates (i.e. neglecting the external transport) provides a good fit to the data. The rank dependence of tar formation, extract yields, cross-linking, and viscosity appears to be explained by the rank dependence of CO_2 yields and its associated cross-linking. High CO_2 yields in low-rank coals produce rapid cross-linking at low temperatures and hence thermosetting behavior, low tar yields, low extract yields, loss of solvent-swelling properties, and high viscosities. The relative importance of cross-linking compared to bond breaking is, however, sensitive to heating rate, and this effect is predicted by the model. Areas for improving the model include (1) refinement of the internal and external transport assumptions, (2) accounting for hydroaromatic structures and bridge structures besides ethylene, and (3) including polymethylene "guest" molecules.

Introduction

Coal devolatilization is a process in which coal is transformed at elevated temperatures to produce gases, tar, and char. (Tar is defined as the room-temperature condensibles formed during coal devolatilization.) The combined chemical and physical processes in devolatilization have been reviewed by a number of investigators.[1-6] Gas formation can often be related to the thermal decomposition of specific functional groups in the coal and can be predicted with reasonable accuracy by models employing first-order reactions with ultimate yields.[5-15] On the other hand, tar and char formation are more complicated, and success in mechanistic modeling of tar formation has been more limited.

Predicting tar formation is, however, important for several reasons. Tar is a major volatile product (up to 40% of the DAF coal weight for some bituminous coals). Tar yields vary substantially depending on reactor conditions

*To whom correspondence is to be addressed

†Presented at the Symposium on Coal Pyrolysis: Mechanisms and Modeling, 194th National Meeting of the American Chemical Society, New Orleans, LA, August 31–September 4, 1987.

(1) Howard, J. B.; Peters, W. A.; Serio, M. A. "Coal Devolatilization Information for Reactor Modeling"; Final Report on EPRI Project No. 986-5, 1981.
(2) Howard, J. B. In *Chemistry of Coal Utilization*; Elliott, M. A., Ed.; Wiley: New York, 1981; Chapter 12, p 665.
(3) Gavalas, G. R. *Coal Pyrolysis*; Elsevier: Amsterdam, The Netherlands, 1981.
(4) Suuberg, E. M. In *Chemistry of Coal Conversion*; Schlosberg, R. H., Ed.; Plenum: New York, 1985; Chapter 4.
(5) Solomon, P. R.; Hamblen, D. G. In *Chemistry of Coal Conversion*; Schlosberg, R. H., Ed.; Plenum: New York, 1985; Chapter 5, p 121.
(6) Serio, M. A.; Hamblen, D. G.; Markham, J. R.; Solomon, P. R. *Energy Fuels* 1987, *1*, 138.
(7) Suuberg, E. M.; Peters, W. A.; Howard, J. B. *Seventeenth Symposium (International) on Combustion*; The Combustion Institute: Pittsburgh, PA, 1979; p 117.
(8) Juntgen, H.; van Heek, K. H. *Fuel Process. Technol.* 1979, *2*, 261.
(9) Weimer, R. F.; Ngan, D. Y. *Prepr. Pap.—Am. Chem. Soc., Div. Fuel Chem.* 1979, *24*(3), 129.
(10) Campbell, J. H. *Fuel* 1978, *57*, 217.
(11) Solomon, P. R.; Colket, M. B. *Seventeenth Symposium (International) on Combustion*; The Combustion Institute: Pittsburgh, PA, 1979; p 131.

0887-0624/88/2502-0405$01.50/0

(pressure, heating rate, final temperature, bed geometry, particle size, etc.). In combustion or gasification, tar is often the volatile product of highest initial yield and thus controls ignition and flame stability. It is a precursor to soot, which is important to radiative heat transfer. The process of tar formation is linked to the char viscosity[16-19] and the subsequent physical and chemical structure of the char and so is important to char swelling and reactivity. Also, because tar molecules are sometimes minimally disturbed coal molecular fragments, primary tars provide important clues to the structure of the parent coal.[5,6,20]

It is generally agreed that the tar formation includes the following steps: (1) depolymerization by rupture of weaker bridges in the coal macromolecule to release smaller fragments that make up the "metaplast";[3,5,7,16,21-33] (2) repolymerization (cross-linking) of metaplast molecules;[3,5,7,16,21-33] (3) transport of lighter molecules away from the surface of the coal particles by combined vaporization and gas phase diffusion;[23,32] (4) internal transport of lighter molecules to the surface of the coal particles by convection and diffusion in the pores of nonsoftening coals[24,27,34,35] and liquid-phase or bubble transport in softening coals.[17,36-38] Char is formed from the unreleased or recondensed fragments. Varying amounts of loosely bound "guest" molecules, usually associated with the extractable material, are also released in devolatilization.

The complexity of proposed devolatilization models varies substantially. They can be divided into four categories. The simplest are the "weight loss models" employing a single rate,[5,22,39-42] two rates,[39,43] multiple parallel rates, or distributed rates.[9,22] These models do not account for the variations in tar yield with reaction conditions, and a number of "tar formation models" incorporating retrogressive char-forming reactions and mass transport have been proposed that account for such variations.[16,21-33,37,44-49] A recent innovation has been the description of the decomposition and repolymerization of the macromolecular network by using statistical methods.[28,29,44-46,50,51]

Most of the above models do not consider the evolution of gas species, which have been treated in a number of "species evolution/functional group models" as parallel first-order reactions.[5-13] More complicated "comprehensive chemical models" also describe the composition of the char and tar.[3,5,6,11-13,33,48,49,51]

The level of detail required in a model depends on its application. In the modeling of combustion and gasification, the simple "weight loss models" have often been employed. However, to predict the variations in yield with reactor conditions, the more complicated "tar formation models" must be used. A case can also be made for employing "species evolution/functional group models" or "comprehensive chemical models". For example, in predicting the energy released from combustion of the volatiles, it is important to know that for low-rank coals a high percentage of the volatiles may be noncombustible H_2O and CO_2. For a North Dakota lignite, the total of these two components can be as high as 35% of the rapidly released volatiles which are important for ignition.[6] In addition, the swelling, particle agglomeration properties, char reactivity, and char fragmentation are functions of the char composition. Soot formation (which can dominate radiative energy transport) is controlled by the tar amount.

In the modeling of liquefaction and mild gasification, knowledge of the chemical makeup and molecular weight distribution of the soluble and volatile products is essential, requiring the more complete "comprehensive chemical models".

This paper presents a "comprehensive chemical model" for coal devolatilization that considers the evolution of gas, tar, char, and guest molecules. The model is general in its applicability to bituminous coals, subbituminous coals,

(12) Solomon, P. R.; Hamblen, D. G.; Carangelo, R. M.; Krause, J. L. *Nineteenth Symposium (International) on Combustion*; The Combustion Institute: Pittsburgh, PA, 1982; p 1139.
(13) Solomon, P. R.; Serio, M. A.; Carangelo, R. M.; Markham, J. R. *Fuel* 1986, *65*, 182.
(14) Xu, W.-C.; Tomita, A. *Fuel* 1987, *66*, 627.
(15) Juntgen, H. *Fuel* 1984, *63*, 731.
(16) Fong, W. S.; Peters, W. A.; Howard, J. B. *Fuel* 1986, *65*, 251.
(17) Oh, M. S.; Peters, W. A.; Howard, J. B. *Proceedings of the 1983 International Conference on Coal Science*; Center for Conference Management: Pittsburgh, PA, 1983; p 483.
(18) Fong, W. S.; Khalil, Y. F.; Peters, W. A.; Howard, J. B. *Fuel* 1986, *65*, 195.
(19) Van Krevelen, D. W. *Properties of Polymers*; Elsevier: Amsterdam, 1976.
(20) Solomon, P. R. *New Approaches in Coal Chemistry*; ACS Symposium Series 169; American Chemical Society: Washington, DC, 1981; pp 61–71.
(21) van Krevelen, D. W.; Schuyer, J. *Coal Science*; Elsevier: Amsterdam, 1957.
(22) Anthony, D. B.; Howard, J. B.; Hottel, H. C.; Meissner, H. P. *Fifteenth Symposium (International) on Combustion*; The Combustion Institute: Pittsburgh, PA, 1974; p 1303.
(23) Unger, P. E.; Suuberg, E. M. *Eighteenth Symposium (International) on Combustion*; The Combustion Institute: Pittsburgh, PA, 1981; p 1203.
(24) Russel, W. B.; Saville, D. A.; Greene, M. I. *AIChE J.* 1979, *25*, 65.
(25) James, R. K.; Mills, A. F. *Lett. Heat Mass Transfer* 1976, *3*, 1.
(26) Lewellen, P. C. S.M. Thesis, Department of Chemical Engineering, MIT, 1975.
(27) Chen, L. W.; Wen, C. Y. *Prepr. Pap.—Am. Chem. Soc., Div. Fuel Chem.* 1979, *24*(3), p 141.
(28) Niksa, S.; Kerstein, A. R. *Combust. Flame* 1986, *66*, 95.
(29) Niksa, S. *Combust. Flame* 1986, *66*, 111.
(30) Solomon, P. R.; Squire, K. R.; Carangelo, R. M. *Proceedings of the International Conference on Coal Science*; Pergamon: Sydney, Australia, 1985; p 945.
(31) Solomon, P. R.; Squire, K. R. *Prepr. Pap.—Am. Chem. Soc., Div. Fuel Chem.* 1985, *30*(4), 347.
(32) Suuberg, E. M.; Unger, P. E.; Lilly, W. D. *Fuel* 1985, *64*, 956.
(33) Solomon, P. R.; Hamblen, D. G.; Carangelo, R. M.; Serio, M. A.; Deshpande, G. V. *Prepr. Pap.—Am. Chem. Soc., Div. Fuel Chem.* 1987, *32*(3), 83.
(34) Gavalas, G. R.; Wilks, K. A. *AIChE J.* 1980, *26*, 201.
(35) Simons, G. A. *Prog. Energy Combust. Sci.* 1983, *9*, 269.
(36) Suuberg, E. M.; Sezen, Y. *Proceedings of the International Conference on Coal Science*; Pergamon: Sydney, Australia, 1985; p 913.
(37) Melia, P. F.; Bowman, C. T. *Combust. Sci. Technol.* 1983, *31*, 195; Paper presented at the Western States Section of the Combustion Institute, Salt Lake City, UT, 1982.
(38) Oh, M. S. Sc.D. Thesis, Department of Chemical Engineering, MIT, Cambridge, MA, 1985.
(39) Kobayashi, H.; Howard, J. B.; Sarofim, A. F. *Sixteenth Symposium (International) on Combustion*; The Combustion Institute: Pittsburgh, PA, 1977; p 411. Kobayashi, H. Ph.D. Thesis, Department of Mechanical Engineering, MIT, Cambridge, MA. 1976.
(40) Niksa, S.; Heyd, L. E.; Russel, W. B.; Saville, D. A. *Twentieth Symposium (International) on Combustion*; The Combustion Institute: Pittsburgh, PA, 1984; p 1445.
(41) Badzioch, S.; Hawksley, P. G. W. *Ind. Eng. Chem. Process Des. Dev.* 1970, *9*, 521.
(42) Maloney, D. J.; Jenkins, R. G. *Twentieth Symposium (International) on Combustion*; The Combustion Institute: Pittsburgh, PA, 1984; p 1435.
(43) Witte, A. B.; Gat, N. Presented at the DOE Direct Utilization AR&TD Contractor's Meeting, Pittsburgh, PA, 1983.
(44) Solomon, P. R.; King, H. H. *Fuel* 1984, *63*, 1302.
(45) Solomon, P. R.; Squire, K. R.; Carangelo, R. M. *Prepr. Pap.—Am. Chem. Soc., Div. Fuel Chem.* 1984, *29*(1), 10.
(46) Squire, K. R.; Solomon, P. R.; Carangelo, R. M.; DiTaranto, M. B. *Fuel* 1986, *65*, 833.
(47) Squire, K. R.; Solomon, P. R.; DiTaranto, M. B.; Carangelo, R. M. *Prepr. Pap.—Am. Chem. Soc., Div. Fuel Chem.* 1985, *30*(1), 386.
(48) Gavalas, G. R.; Cheong, P. H.; Jain, R. *Ind. Eng. Chem. Fundam.* 1981, *20*, 113.
(49) Gavalas, G. R.; Cheong, P. H.; Jain, R. *Ind. Eng. Chem. Fundam.* 1981, *20*, 122.
(50) Solomon, P. R.; Hamblen, D. G.; Carangelo, R. M.; Serio, M. A.; Deshpande, G. V. *Combust. Flame* 1988, *71*, 137.
(51) Solomon, P. R.; Hamblen, D. G.; Deshpande, G. V.; Serio, M. A. *Coal Sci. Technol.* 1987, *11*, 601.

and lignites (employing rank-independent kinetic parameters), in its application to reactors of widely differing heating rates (0.05 to 20 000 °C/s), and in its ability to predict the variations in tar yield with reactor conditions.

Two previously developed models, a functional group (FG) model[5,6,11-13] (a "species evolution/functional group model") and a depolymerization–vaporization–cross-linking (DVC) model[30,31,44-47] (a "tar formation model") have been combined as subroutines of what is now called the "FG–DVC" model.[33,50,51] The DVC subroutine is employed to determine the yield of tar and the molecular weight distribution of the tar and char. The FG subroutine is used to describe the gas evolution and the elemental and functional group compositions of the tar and char. Cross-linking in the DVC subroutine is computed by assuming that this event is correlated with CO_2 and CH_4 evolutions predicted in the FG subroutine. The dependence of the yield of rapidly released CO_2 (which is related to coal rank or weathering) is the factor that controls the thermosetting or thermoplastic behavior of coals.

The combined FG–DVC model was described in two previous publications,[50,51] and comparisons were made to a limited set of data. In this paper, a description of internal transport has been added to the model. The model equations are presented, and comparisons are made to a wider set of data. The paper also includes a discussion of the assumptions, approximations, and exceptions to the model and a sensitivity analysis for the parameters of the DVC subroutine. The model describes the processes of (1) depolymerization and hydrogen consumption, (2) cross-linking, (3) external transport, (4) internal transport, (5) gas formation for all principal species, (6) tar composition, and (7) char composition.

The work presented here is limited to dilute phase reactions of small coal particles where internal temperature gradients can be neglected. Secondary gas phase reactions have been discussed elsewhere,[6] and reactions of pyrolysis products with a char bed and large particle effects have not yet been included. Only reactions involving C, H, and O are discussed here.

A number of coal composition parameters and reactor parameters (pressure, particle time–temperature profile) are required to predict the pyrolysis behavior. A substantial reduction in the number of parameters that must be measured for each coal is made by the use of rank-independent kinetic rates. These parameters have already been determined for a wide variety of coals and reactors. This simplification is a good first approximation to describe the kinetics of individual evolved species and the functional group decompositions.[5,6,49,52-55] The properties predicted as a function of time, include the following: for tar, molecular weight distribution, elemental and functional group composition, and yield; for char, molecular weight distribution, elemental and functional group composition, yield, cross-link density, and extract yield; for gas, yields of individual light gas species. Results are presented for a Pittsburgh Seam bituminous coal and a North Dakota lignite.

Experimental Section

Coals Examined. The two coals described in this paper are a Pittsburgh Seam bituminous coal and a North Dakota (Beulah, Zap) lignite. Samples of the Pittsburgh Seam coal were obtained from the Pittsburgh Energy Technology Center and the Argonne National Laboratory premium coal sample collection. Samples of the North Dakota (Beulah, Zap) lignite were obtained from the University of North Dakota Energy Research Center and the Argonne National Laboratory premium coal sample collection. Data on the premium samples are presented in ref 56, and data on the other two samples, in ref. 6. The FG–DVC model was also compared to data on Pittsburgh coal samples from ref 7, 16, and 22, and characterizations of these samples are presented therein.

Coal Characterization. The cross-link density was estimated by using the volumetric swelling technique developed by Larsen and co-workers.[57-59] Pyridine extract yields were obtained by using a Soxhlet apparatus. Molecular weight distributions of tars were obtained at SRI International on the field-ionization mass spectrometry (FIMS) apparatus described by St. John et al.[60] Tar samples were collected from the pyrolysis apparatus and vaporized from a heated probe into the FIMS apparatus. In addition, coal samples were pyrolyzed directly in the FIMS apparatus.

Apparatus. Pyrolysis experiments were performed in several apparatuses that have been described previously including a heated-grid pyrolyzer,[5,12] a heated-tube reactor,[6,13] and a thermogravimetric analyzer with analysis of evolved products by Fourier transform infrared (FT-IR) spectroscopy (TG-FTIR).[6,61]

General Model

Any general model of a process as complicated as coal devolatilization must of course be a gross approximation. However, there are many general trends that have been observed in devolatilization. The trick in developing a model is to pick a set of first approximations that best match the majority of these trends. There will of course be exceptions to the trends. These exceptions can be treated as perturbations to the first-order approximation. Differences in models occur because of the subjective choice of what is a general trend and what is an exception. The following discussion presents the authors' view of the general trends and the exceptions.

General Trends in Devolatilization. The general model of coal pyrolysis is based on a number of observations that have been previously made concerning coal pyrolysis. These are as follows: (i) Pyrolysis species kinetics are insensitive to rank.[5,6,11-13,52-55] (ii) Species amounts vary with coal rank and can be correlated with the coal's functional group compositions.[5,6,14,15,48,49,52] The evolution of each species can be correlated with the change in the corresponding functional group composition in the char.[5,6,52] (iii) The primary tar composition is similar (except for a higher concentration of methyl groups) to that of the parent coal for bituminous coals and rapidly heated low-rank coal.[5,20,45,62-64] (iv) Tar yields are controlled by the amount of donatable hydrogen and how efficiently it is used.[5,6,20,46] (v) Cross-linking correlates with CO_2 and CH_4 evolution.[50,51]

The general outline of devolatilization based on these observations was presented by Solomon and Hamblen[5] and Serio et al.[6] Figure 1 (adapted from ref 6) presents a hypothetical picture of the coal's or char's organic structure at successive stages of devolatilization. The figure represents (a) the raw coal, (b) the formation of tar and light

(52) Solomon, P. R.; Hamblen, D. G. *Prog. Energy Combust. Sci.* 1983, *9*, 323.
(53) Xu, W. C.; Tomita, A. *Fuel* 1987, *66*, 632.
(54) Agarwal, P. K. *Fuel* 1985, *64*, 870.
(55) Agarwal, P. K.; Agnew, J. B.; Ravindran, N.; Weimann, R. *Fuel* 1987, *66*, 1097.
(56) Vorres, K. S. *Prepr. Pap.-Am. Chem. Soc., Div. Fuel Chem.* 1987, *32*(4), 221.
(57) Green, T. K.; Kovac, J.; Larsen, J. W. *Fuel* 1984, *63*, 935.
(58) Green, T. K.; Kovac, J.; Larsen, J. W. In *Coal Structure*; Meyers, R. A., Ed.; Academic: New York, 1982.
(59) Suuberg, E. M.; Lee, D.; Larsen, J. W. *Fuel* 1985, *64*, 1668.
(60) St. John, G. A.; Butrill, S. E., Jr.; Anbar, M. *ACS Symp. Ser.* 1978, *No. 71*, 223.
(61) Carangelo, R. M.; Solomon, P. R.; Gerson, D. J. *Fuel* 1987, *66*, 960.
(62) Solomon, P. R.; Colket, M. B. *Fuel* 1978, *57*, 748.
(63) Brown, J. K.; Dryden, I. G. C.; Dunevein, D. H.; Joy, W. K.; Pankhurst, K. S. *J. Inst. Fuel* 1958, *31*, 259.
(64) Orning, A. A.; Greifer, B. *Fuel* 1956, *35*, 318.

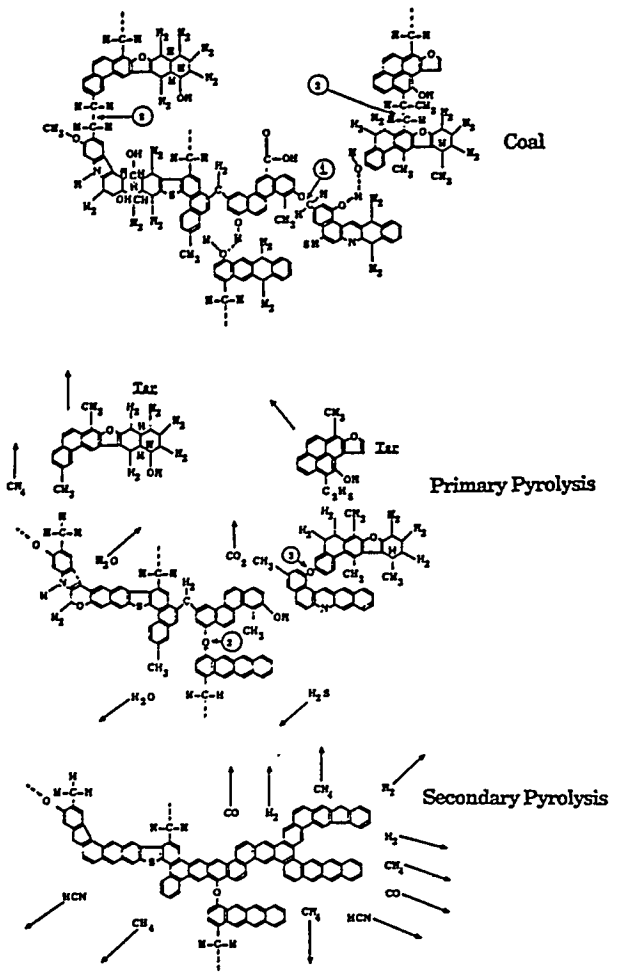

Figure 1. Hypothetical coal molecule during stages of pyrolysis. Adapted from ref 6.

hydrocarbons during primary pyrolysis, and (c) char condensation and cross-linking during secondary pyrolysis. The hypothetical structure in Figure 1a represents the chemical and functional group compositions for a Pittsburgh Seam bituminous coal as discussed by Solomon.[20] It consists of aromatic and hydroaromatic clusters linked by aliphatic bridges. During pyrolysis, the weakest bridges, labeled 1 and 2 in Figure 1a, can break producing molecular fragments (depolymerization). The fragments abstract hydrogen from the hydroaromatics or aliphatics, thus increasing the aromatic hydrogen concentration. These fragments will be released as tar if they are small enough to vaporize under typical pyrolysis conditions and do not undergo retrograde reactions before escaping from the particle. The two lightest fragments are labeled tar. The other two fragments are shown to have repolymerized, producing a molecule that is too large to vaporize.

The other events during primary pyrolysis are the decomposition of functional groups to release CO_2, light aliphatic gases, and some CH_4 and H_2O. The release of CH_4, CO_2, and H_2O may produce cross-linking, CH_4 by a substitution reaction in which the attachment of a larger molecule releases the methyl group, CO_2 by condensation after a radical is formed on the ring when a carboxyl is removed, and H_2O by the condensation of two OH groups to produce an ether link (labeled 3 in Figure 1b). The cross-linking is important to determine the release of tar and the viscoelastic properties of the char.

The end of primary pyrolysis occurs when the donatable hydrogens from hydroaromatic or aliphatic portion of the coal are depleted. During secondary pyrolysis (Figure 1c) there is additional methane evolution (from methyl groups), HCN from ring nitrogen compounds, CO from ether links, and H_2 from ring condensation. These general concepts are incorporated into the combined FG–DVC model.

Exceptions to the General Trends. a. Polymethylene. The major exception to the trends described above is the presence of varying amounts (typically 0–9%, but in some cases as high as 18%) of long-chain aliphatics (polymethylenes). These have recently been reported in pyrolysis products by Nelson[65] and by Calkins and coworkers[66–69] and references quoted therein. The chains appear alone and attached to aromatic nucleii.[65] During devolatilization, the smaller molecules may be released without bond breaking and the heavier molecules with bond breaking to contribute to the tar. The presence of these polymethylenes makes the tar more aliphatic than the parent coal. Further cracking of this material under more severe devolatilization conditions produces ethylene, propylene, and butadiene from which the concentration of polymethylenes may be determined.[68] Presently, the polymethylenes are included in the FG model as part of the aliphatic functional group pool, which is assumed to decompose to produce gas products, not tar. If the amount of heavy polymethylenes is determined, these can be computed as a separate functional group pool with an appropriate release rate and added to the tar. The modeling of polymethylene evolution will be the subject of a subsequent publication.

b. Tar/Coal Similarities. The general model assumed, as a first approximation, that tar is derived from material of the same average composition as that of the parent coal. The model predicts that the tar is richer than the parent coal in methyl groups (due to hydrogen stabilization) and poorer in the rapidly removed functional groups. Evidence for this assumption is the similarities in elemental composition, infrared spectra and NMR spectra[5,20,45,62–64] between the primary tar and parent coal observed for bituminous coals. It was, however, noted[5,45,70] that the infrared spectrum for a lignite tar was significantly different from that of the parent coal. The tar is much richer in aliphatic groups and poorer in oxygen functional groups. Freihaut et al. have recently reported a systematic increase in the tar hydrogen concentration with decreasing rank that suggests a similar trend.[71]

There are at least two reasons for this variation with rank. One reason is the influence of the polymethylene groups. As noted by Calkins,[68] the concentration of polymethylenes increases with decreasing rank (~4% for high volatile bituminous coals compared to ~8% for lignites). In addition, the tar yield decreases with decreasing rank (~6% for the North Dakota lignite compared to 30% for the Pittsburgh Seam bituminous coal). The relative contribution of the polymethylenes to the tar is therefore increased with decreasing rank. This will lead to a higher aliphatic content and lower oxygen content for the low-rank coal tar. This effect can be treated in the FG–DVC model by the addition of polymethylenes to the tar as discussed above.

(65) Nelson, P. F. *Fuel* 1987, *66*, 1264.
(66) Calkins, W. H.; Hagaman, E.; Zeldes, H. *Fuel* 1984, *63*, 1113.
(67) Calkins, W. H.; Tyler, R. J. *Fuel* 1984, *63*, 1119.
(68) Calkins, W. H. *Fuel* 1985, *63*, 1125.
(69) Calkins, W. H.; Hovsepian, B. K.; Drykacz, G. R.; Bloomquist, C. A. A.; Ruscic, L. *Fuel* 1984, *63*, 1226.
(70) Solomon, P. R. *Coal Structure*; Advances in Chemistry Series 192; American Chemical Society: Washington, DC, 1981; p 7.
(71) Freihaut, J. D.; Proscia, W. M.; Seery, D. J. Presented at the 194th National Meeting of the American Chemical Society, New Orleans, LA, Aug 31–Sept 4, 1987.

A second reason for differences in structure between the tar and parent coal is that the extensive cross-linking in low-rank coals is related to the carboxyl group concentration, which increases with decreasing rank. This cross-linking will thus selectively repolymerize the fragments rich in oxygen, while those poorer in oxygen are more likely to be released as tar. This effect has not as yet been included in the model.

It is interesting to note an exception to the above observations. At very high heating rates, the North Dakota (Beulah, Zap) lignite is observed to melt and swell and produce a higher yield of tar that resembles the parent coal.[13,30,31] The high heating rate appears to reduce the effect of cross-linking, leading to higher oxygen concentrations in the tar and to increase yields. Both effects enhance the resemblance to the parent coal.

c. Variations of Kinetic Rates with Rank. While the model assumes rank-independent kinetic rates, there is a systematic variation of rate with rank. As reported by Solomon and Hamblen,[52] the variation between a lignite and bituminous coal results in a 50–75 °C difference in the peak evolution temperature for most species (at a heating rate of 30 K/min). Systematic rank variations in the rate constants can be added to the model if increased accuracy is desired.

d. Macerals. Individual macerals are not considered in this model. The influence of the maceral concentration is assumed to occur through its effect on the average elemental and functional group composition. If details on macerals are desired, then each maceral must be treated as a distinct molecular population with its own functional group composition and molecular weight distribution.

e. Physical Properties of Molecular Fragments. The general model has assumed that the vaporization and solubility of the molecular fragments are functions of molecular weight alone. Both properties are expected to depend on functional group composition. Such effects can be included as corrections to the vaporization law and solubility assumptions.

Depolymerization–Vaporization–Cross-Linking (DVC) Subroutine Formulation. The DVC model has been described in a number of publications.[30,31,44-47,50,51] It predicts the tar yield, the tar molecular weight distribution, the char yield, the char molecular weight distribution, the extract yield, and the cross-link density. The model had its beginning in a study of polymers representative of structural features found in coal.[44] The objective of that study was to develop an understanding of coal pyrolysis by studying a simpler, more easily interpretable system. The polymers were studied in a series of pyrolysis experiments in which tar amounts and molecular weights were measured. The theory which was developed describes the combined effects of (1) *depolymerization and hydrogen consumption*, (2) cross-linking, and (3) *external transport*. Recently, an expression to describe (4) *internal transport* has been added to the model.[33] These processes, which are described below, are incorporated into a computer code that employs a Monte Carlo method for performing the statistical analysis.

Process 1. Depolymerization and Hydrogen Consumption. Bond cleavage in coal is likely to be very complicated, including homolytic cleavage, ipso substitution,[46] and hydrogen-transfer-induced bond-scission reactions[72] for a variety of bond types. However, it has been observed that tar evolution is consistent with a narrow distribution of activation energies,[5,6,12] which allows consideration in the model of a single type of bridge (while acknowledging that other types may be present). Also, the rate for tar formation from coal, k_{tar},[6,13] is in good agreement with the rate determined for the breaking of ethylene bridges between naphthalene rings, k_B. This kinetic rate, k_B,[46] employs an activation energy that is in agreement with resonance-stabilization calculations[73,74] and an overall rate that agrees with previous measurements on model compounds.[75] In view of these observations, a single type of bond (ethylene) undergoing homolytic cleavage is assumed for coal as a simple approximation of the complicated behavior.

Bond cleavage is accompanied by the consumption of donatable hydrogens, H(al), to cap free radicals, along with corresponding carbon–carbon double-bond formation at the donor site. In the polymers that were studied, the ethylene bridges were identified as a source of donatable hydrogen with the formation of a double bond between the bridge carbons.[46,47] The double-bond formation was assumed to remove a breakable bond. It should be noted that hydroaromatic groups are also a source of donatable hydrogen with aromatization of the ring. However, for simplicity, the DVC model assumes all the coal's donatable hydrogens, whether in bridges or in hydroaromatic rings, are in bridges, i.e., $H(\text{al}) = (2/28)W_B$. This approximation will produce some error in tar yield since a broken bond in a hydroaromatic ring will not be as effective as a broken bond in a bridge in fragmentating the coal. But this effect will be compensated for, since H(al) is a parameter that is determined for each coal from a selected pyrolysis experiment. H(al) could, in principle, be determined by FT-IR or NMR, but not with sufficient accuracy.

The equation describing the disappearance of labile bridges in the char, W_B (char), due to bond breaking and hydrogen donation is

$$dW_B/dt = -2k_B W_B \quad (1)$$

The value for k_B is taken as the previously determined k_{tar}.[6] The rate of decrease of labile bridges is twice the rate of bond breaking since for each broken bond, an additional labile bridge is converted to a nonlabile bridge with the donation of hydrogen. By assuming that all the donatable hydrogens are in the labile bridges, the consumption of labile bridges and donatable hydrogens occur simultaneously. The redistribution of hydrogen creates source and loss terms, $dW_i(\text{DVC})/dt$, in the equations for the char functional groups W_i(char), as will be discussed with the FG part of the model (see eq 7).

Equation 1 only describes the loss due to bond breaking and hydrogen donation. The loss of labile bridges due to evolution with the tar is computed in the Monte Carlo calculation by using the transport equations (eq 3 and 4) discussed below.

Process 2. Cross-Linking. Cross-linking reactions are important in describing the rank and heating rate dependence of the tar molecular weight distributions and yields. While cross-linking reactions were originally included in the DVC model, using adjustable parameters for the rate and amount,[30,31,46] work has recently been performed to define the reactions that cause cross-linking.[33,50,51] Under the assumption that the cross-linking reactions may also

(72) McMillen, D. F.; Malhotra, R.; Hum, G. P.; Chang, S. J. *Energy Fuels* 1987, *1*, 193.

(73) Stein, S. E. *New Approaches in Coal Chemistry*; Blaustein, B. D., Bockrath, B. C., Friedman, S., Eds.; ACS Symposium Series 169; American Chemical Society: Washingtin, DC, 1981; p 208.

(74) Stein, S. E. "Multistep Bond Breaking and Making Processes of Relevance to Thermal Coal Chemistry"; Annual Report for GRI Contract No. 5081-261-0556; Accession No. GRI-81/0147, 1983.

(75) Stein, S. E.; Robauch, D. A.; Alfieri, A. D.; Miller, R. E. *J. Am. Chem. Soc.* 1982, *104*, 6567.

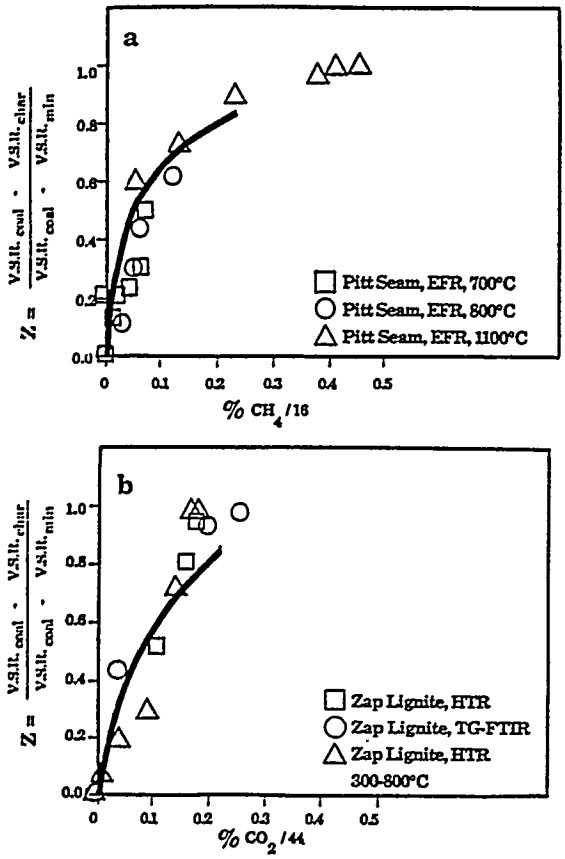

Figure 2. Measured and calculated normalized volumetric swelling ratio (VSR) for coal and chars: (a) Pittsburgh Seam bituminous coal plotted against the methane yield; (b) Zap North Dakota lignite plotted against the CO_2 yield. VSR_{min} is the value achieved when crosslinking is complete. The chars were prepared in an entrained-flow reactor (EFR), a heated-tube reactor (HTR), and a thermogravimetric analyzer with evolved product analysis by FT-IR (TG-FTIR) as described in ref 61.

release gas species, the molecular weight between cross-links (or cross-link density) measured by solvent swelling was correlated with the observed evolution of all the major gas species during pyrolysis. Likely candidates were CO_2 formation from carboxyl groups or methane formation from methyl groups. Suuberg et al.[59] also noted that cross-linking in low-rank coals is correlated with CO_2 evolution. Both CO_2- and CH_4-forming reactions may leave behind free radicals that can be stabilized by cross-linking. Condensation of hydroxyl groups to form water and an ether link is also a possible reaction.

For a series of chars, the reduction in the volumetric swelling ratio in pyridine was compared with CO_2 evolution for a North Dakota (Beulah) lignite and CH_4 evolution for a Pittsburgh Seam bituminous coal.[50] The results are presented in Figure 2. The abscissa (parameter Z), which is the change in the volumetric swelling ratio (VSR) between coal and char divided by the maximum change, is given by

$$Z = (VSR_{coal} - VSR_{char})/(VSR_{coal} - VSR_{min})$$

Z is 0 for coal and 1 for fully cross-linked char. Since the lignite reaches maximum cross-linking before the start of methane evolution and the Pittsburgh Seam bituminous coal evolves little CO_2, correlations can be made separately between cross-linking and CO_2 evolution in the lignite and cross-linking and CH_4 evolution in the Pittsburgh seam bituminous coal. On a molar basis, the evolution of CO_2 from the lignite and the evolution of CH_4 from the bituminous coal appear to have similar effects on the volumetric swelling ratio. The results suggest that one cross-link is formed for each CO_2 or CH_4 molecule evolved. No correlation was observed between the volumetric swelling ratio and tar yield for either coal. A correlation with water yield appears valid for the North Dakota (Beulah) lignite but not for the Pittsburgh Seam bituminous coal.

It therefore appears that a correlation exists between gas evolution and cross-linking which permits the rates for cross-linking and the number of cross-link sites to be related to rates and yields for gas evolution. The model assumes the following expression for the rate of increase of the number of cross-links per gram of coal, m

$$\frac{dm}{dt} = N_0\left[\frac{dW_{CO_2}(gas)/dt}{44} + \frac{dW_{CH_4}(gas)/dt}{16}\right] \quad (2)$$

where the rates, dW_i/dt, of evolution per gram of coal of CO_2 and CH_4 are calculated in the FG subroutine. N_0 is Avogadro's number.

Again, a caution should be added that the reactions which have been assumed must be a gross simplification of a very complicated set of chemical reactions. This is especially true for the cross-links occurring during methane formation, during which time there is extensive bond breaking and cross-linking accompanying tar formation. The inaccuracy in the description of this higher temperature cross-linking event is one of the present weaknesses in the model.

Process 3. External Transport. The external transport of tars from the particle surface to the bulk gas by vaporization and diffusion through a gas boundary layer as in the original DVC model[44-47,50,51] is described with the model of Unger and Suuberg.[23] However, in the current paper, the modified expression for the vapor pressure law of Suuberg et al.[32] is now used to replace that in the model of Unger and Suuberg. The rate of evolution per gram of coal, $(dn_j/dt)_{ET}$, of oligomers of molecular weight M_j is given by

$$(dn_j/dt)_{ET} = (3/r_0^3\rho)rD_j\mathcal{X}^s_j\,(P_j/RT) \quad (3)$$

where r is the particle radius assumed to shrink with the cubic root of its mass r_0 is the initial particle radius, ρ is the particle density, $\mathcal{X}^s_j$ is the mole fraction of species of molecular weight M_j in the metaplast at the surface of the particle, P_j is the vapor pressure for oligomers of molecular weight M_j (given by Suuberg et al.[32]), D_j is the gas-phase diffusivity of species of molecular weight M_j,[38] R is the gas constant, and T is the particle temperature.

In the previous work, it was assumed that the surface mole fraction, $\mathcal{X}^s_j$, was the same as that in the bulk, $\mathcal{X}^b_j$. That is, mass transport to the surface was not a limiting factor.

Process 4. Internal Transport. When comparing the predictions of the model to available data assuming $\mathcal{X}^s_j = \mathcal{X}^b_j$ it was found that tar yields were overpredicted when devolatilization occurred at low temperatures. This was observed for either low-heating-rate experiments[6] or experiments with rapid heating to relatively low temperatures.[16] As discussed in the Results, it appears that the lower yields were the result of the additional transport limitations within the particle.

For softening coals, the internal transport mechanisms include (i) the transport of tar molecules through the liquid to the surface, (ii) the transit of bubbles containing tar from the interior of the particle to the surface, (iii) the transport of tars within the liquid to the bubbles, and (iv)

the stirring action of the bubble evolution. For nonsoftening coals, transport occurs by (v) convection and diffusion within the pores.

Mechanism i was treated by Suuberg and Sezen.[36] The unknown factor is the diffusion coefficient of the tar molecules in the liquid. The detailed modeling of mechanisms ii and iii has been undertaken by several investigators.[4,26,37,38] Calculations for mechanism v have also been published.[24,25,34,35] The models are complicated and require many assumptions. A common feature of mechanisms iii and v is that tars are transported out of the particle with the light devolatilization products that exit the coal via bubbles or pores. In ref 33, the upper limit for this process was calculated. This limit, which occurs when the tars achieve their equilibrium vapor pressure in the evolving gases, can be computed with few assumptions. In this case, the rate of transport per gram of coal, $(dn_j/dt)_{IT}$, for tar component j is proportional to the volume of gases evolved, dV/dt. That is

$$(dn_j/dt) = P_j \mathcal{X}^b_j (dV/dt)(1/RT)$$

The volume of gases is proportional to the number of gas molecules and the temperature. It is inversely proportional to the pressure within the particle, $P_0 + \Delta P$ where P_0 is the ambient pressure and ΔP is the average pressure difference between the surface and the particle's interior. Then

$$dV/dt = \sum_i (dn_i/dt)_{gas} \left(\frac{RT}{P_0 + \Delta P} \right)$$

where $\sum_i (dn_i/dt)_{gas}$ is the rate of production per gram of coal of gas components i summed over all gas and light tar species. For gas molecules, dn_j/dt is taken as the rate of production given by the FG model. For light tar molecules, dn_j/dt is taken as the total amount transported out of the particle as tar computed in the previous time step. For computational efficiency, the sum has been limited to molecular weights less than 300 amu, since this accounts for over 90% of the volume. Combining the two equations with this approximation gives

$$(dn_j/dt)_{IT} = P_j \mathcal{X}^b_j \sum_{i<300} (dn_i/dt)_{gas} \left[\frac{1}{P_0 + \Delta P} \right] \quad (4)$$

ΔP is used as an adjustable parameter that varies with the coal and experimental conditions. For the highly fluid Pittsburgh Seam bituminous coal, in cases where P_0 is 1 atm or greater, we have considered the upper limit to this rate where $P_0 \gg \Delta P$. Then all the terms in eq 4 can be determined by the combined FG–DVC model. This limit coincides with assumptions recently used by Niksa in his FLASHKIN model for Pittsburgh Seam bituminous coal.[76]

While $\Delta P = 0$ appears to be a good approximation for fluid coals at one atmosphere or more, $\Delta P > 0$ is expected for some coals and situations. ΔP is proportional to the coal's viscosity and so will become important for less fluid coals. ΔP is also important when P_0 is small, when particles are large, and when the heating rates are very high.

Two possibilities have been considered for combining the internal and external transportation. In an earlier publication,[33] the internal-transport term and external-transport term (with $\mathcal{X}^s_j = \mathcal{X}^b_j$) were assumed to be in series. Then the transport was controlled by the smaller term. The internal-transport term was the smaller for all pyrolysis cases that were considered and so it dominated. *In fact, calculations performed by neglecting the external transport limitation where almost identical with those made by assuming the two terms to be in series.*

Alternatively, a case can be made that the total transport should be the sum of eq 3 and 4. The reasoning is that internal transport assumes the tars to be in equilibrium with the escaping light gases. It is more likely that this mechanism will transport the tars to the ambient gas than to the surface. In this case, the mechanism considered in eq 4 transports the tars away from the surface in parallel with the surface vaporization and gas diffusion considered in eq 3.

If the two terms are taken in parallel, it is again obvious that $\mathcal{X}^s_j = \mathcal{X}^b_j$ is a bad assumption. Since we did not have a good method to determine $\mathcal{X}^s_j$, calculations were made by assuming that the external-transport term can be neglected, i.e.

$$(dn_i/dt)_{tot} = (dn_i/dt)_{IT}$$

This provides an excellent fit to the data for 50-μm-diameter particles.

Therefore, for either parallel or series combinations of the transport terms, it appears best to neglect the external transport. It is likely that the external transport term will be increasingly important for smaller particles, but this will require better knowledge of the liquid-phase diffusion coefficient (mechanism i), and the stirring action of bubbles (mechanism iv). The relative importance of the various internal- and external-transport mechanisms is the subject of ongoing research.

Schematic Representation of DVC Model. In the current DVC model, the parent coal is represented as a two-dimensional network of monomers (condensed ring clusters) linked by strong and weak bridges as shown in Figure 3a. The monomers are linked to form unbranched oligomers of length "l" by breakable and nonbreakable bridges (shown as horizontal single or double lines, respectively, in Figure 3a). The monomers are represented by circles with molecular weights shown in each circle. The molecular weight distribution of the monomers is assumed to be Gaussian and is described by two parameters, M_{av} (mean) and σ (standard deviation). The breakable bridges (assumed to be ethylene) are represented by single lines, the unbreakable bridges by double lines. "m_0" cross-links per monomer are added (as vertical double lines in Figure 3a) to connect the oligomers of length l so that the molecular weight between cross-links, M_c, corresponds to the value reported in the literature[77] for coals of similar rank. The cross-links form the branch points in the macromolecule. Unconnected "guest" molecules (the extract yield) are obtained by choosing the value of l. A large value of l will mean that a completely connected macromolecule will be formed when even a small number of cross-links are added, leaving no extractable material. For smaller values of l some of the oligomers will be unattached after the cross-links are added, and these are the guest molecules. The number of ethylene bridges, W_B, (two donatable hydrogens per bridge) is chosen to obtain the appropriate value for total donatable hydrogen (i.e., to fit a selected laboratory pyrolysis experiment). The remainder are nonbreakable bridges whose carbons are counted with the aromatic carbons.

The parameters M_c, l, M_{av}, and σ determine the molecular weight distribution of oligomers in the starting coal molecule. A histogram showing the distribution created

(76) Niksa, S. Presented at the Western States Section/The Combustion Institute, Spring Meeting, Salt Lake City, UT, March 1988; Paper 88-4.

(77) Nelson, J. R. *Fuel* 1983, *62*, 112.

Table I. Coal Structure Parameters for DVC Subroutine

parameter	symbol	parameter determination: fixed	coal specific, determined	adjustable	dependent[b]	parameter values: Pittsburgh Seam	Zap lignite
			Concentrations				
wt fraction of labile bridges	W_B		from tar yield in a pyrolysis expt			0.094	0.082
wt fraction of nuclei (ring clusters)[a]	W_N		from FG model			0.562	0.440
wt fraction of peripheral groups (sources of gases)[b]	W_P				by difference	0.344	0.478
total						1.000	1.000
			Structure Parameters				
wt fraction of donatable hydrogens[b]	H(al)				$(2/28)W_B$	0.0067	0.0059
oligomer length (no. of monomers/oligomer)	l		from extract yield			7	10
molecular wt between cross-links	M_c		from solvent swelling (lit. values)			2900	1400
no. of initial cross-link sites per monomer[b]	m_0				M_{av}/M_c	0.088	0.183
no. of potential CO_2 cross-link sites per monomer	$m(CO_2)$		from FG model			0.070	0.582
no. of potential CH_4 cross-link sites per monomer	$m(CH_4)$		from FG model			1.063	0.875
			Molecular Weights				
mol wt of labile bridges	M_L	28				28	28
mol wt of monomers	M_{av} (σ)		from FIMS or NMR			256 (250)	256 (250)
mol wt of nonlabile bridges	M_{NL}	26				26	26
mol wt of pyridine solubles	M_{PS}	3000				3000	3000
			Other				
internal pressure, atm	ΔP			for each coal, particle, size, and reaction rate		0–0.2	1–10

[a] Carbon in aromatic rings plus nonlabile bridges. [b] Dependent parameters are calculated from the independent parameters.

by randomly picking monomers to form oligomers of length l and randomly cross-linking them to achieve an average molecular weight between cross-links, M_c, is presented at the right of Figure 3a. The distribution is divided into a pyridine-soluble portion below 3000 amu (light shading) and a pyridine-insoluble portion above 3000 amu (dark shading).

Figure 3b shows the molecule during pyrolysis. The rates for bond breaking and cross-linking are from the FG model and are the same for all coals and all experiments. Some bonds have broken, other bonds have been converted to unbreakable bonds by the abstraction of hydrogen to stabilize the free radicals, and new cross-links have been formed. To determine the change of state of the computer molecules during a time step, the number of cross-links formed is determined by using the FG subroutine and passed to the DVC subroutine. These cross-links are distributed randomly throughout the char, assuming that the cross-linking probability is proportional to the molecular weight of the monomer. Then the DVC subroutine breaks the appropriate number of bridging bonds and calculates the quantity of tar evolved for this time step by using the internal and external transport equations. The result is the coal molecule representation and the molecular weight distributions shown in Figure 3b. The lighter "tar molecules", which leave the particle according to the transport equations, are shown as crosshatched. A fraction of the donatable hydrogen is used to stabilize the free radicals formed by bridge breaking, creating two new methyl groups per bridge and the same fraction of breakable bridges is converted into (unbreakable) double bonds.

Figure 3c shows the final char, which is highly cross-linked with unbreakable bonds and has no remaining donatable hydrogen. The histogram now shows only tar and pyridine-insoluble fractions. The extractables have been eliminated by tar formation and cross-linking.

The output of the DVC subroutine is the molecular weight distribution in the coal, its time-dependent transformation during devolatilization, and the evolution of tar determined by the transport of the lighter components.

Selection of DVC Parameters. The DVC composition parameters employed for a Pittsburgh Seam coal and North Dakota lignite are summarized in Table I. The FG composition parameters and the kinetic parameters, which are fixed for all coals and experiments, are presented in Table II. In Table I, there are 11 independent composition parameters. Three parameters are fixed, the molecular weight of the labile bridges, M_L, the nonlabile bridges, M_{NL}, and the pyridine-extractable limit, M_{PS}.

Eight parameters are coal specific (i.e., fixed for each coal, for all conditions) and must be determined by some measurement. M_c and l are determined experimentally for each coal by the measured molecular weight between cross-links and the pyridine extract yield, respectively. The weight fraction of carbon in nucleii and nonbreakable bridges, W_N, is obtained from the FG model and is equal to the amount of nonvolatile carbon. This value is, in

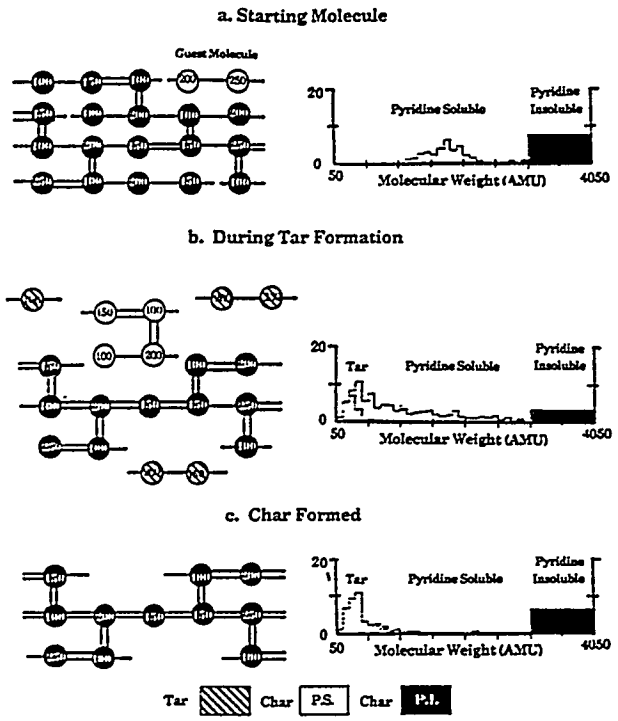

Figure 3. Representation of coal molecule in the DVC simulation and corresponding molecular weight distribution. In the molecule, the circles represent monomers (ring clusters and peripheral groups). The molecular weight shown by the numbers is the molecular weight of the monomer including the attached bridges. The single-line bridges are breakable and can donate hydrogen. The Double-line bridges are unbreakable and do not donate hydrogen. The molecular weight distribution of the coal. tar, and chars are shown as a histogram at the right. The histogram is divided into tar and char with pyridine-soluble and pyridine-insoluble fractions. The area under the histogram corresponds to the weight percent of the oligomers.

principle, determined for each coal for a single pyrolysis experiment. In practice, several experiments are performed. The number of potential cross-link sites, $m(CO_2)$ and $m(CH_4)$, are proportional to the total yield of CO_2 and the total yield of CH_4, respectively. W_B, M_{av}, and σ are determined by using the model to fit selected pyrolysis experiments. The value of W_B is adjustable to fit the tar yield or total volatile yield from one or two selected experiments. In principle, W_B could be measured by FT-IR or NMR but not with sufficient accuracy for this highly sensitive parameter. The values of M_{av} and σ are chosen based on FIMS analysis of the coal. M_{av} can be determined from the average cluster size determined by NMR.[78,79] The value of 256 chosen for both the lignite and bituminous coal is in reasonable agreement with these reported by Solum, et al.,[79] 290 for Zap and 300 for the Pittsburgh Seam coal.

One parameter, ΔP, is adjustable and can vary with each type of experiment. For fluid coals at pressures above one atmosphere, $\Delta P \approx 0$. For low external pressures, less fluid coals, large particles, or high heating rates, $\Delta P > 0$.

There are three dependent parameters that are computed from the other parameters: the weight fraction of peripheral groups, W_p; the donatable hydrogen, H(al); and the number of initial cross-link sites per monomer, m_0.

Functional Group (FG) Model Formulation. The Functional Group (FG) model has been described in a number of publications.[5,6,11-13] It permits the detailed prediction of the composition of volatile species (gas yield, tar yield, and tar functional group and elemental composition) and of char (elemental and functional group composition). It employs coal-independent rates for the decomposition of individual assumed functional groups in the coal and char to produce gas species. The ultimate yields of each gas species are related to the coal's functional group composition. Tar evolution is a parallel process which competes for all the functional groups in the coal. In the original FG model, the potential tar forming fraction of the coal, X^0, was an input parameter that was adjusted for each coal and type of experiment. In the combined FG–DVC model, the DVC subroutine provides this parameter.

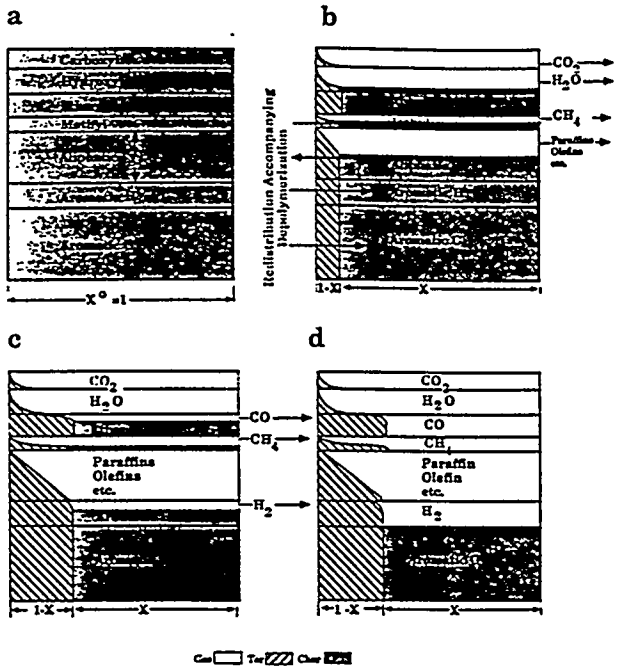

Figure 4. Schematic representation of functional group (FG) model: (a) Initial Coal Composition; (b) composition during tar formation; (c) composition after completion of tar formation; (d) composition after completion of devolatilization.

Schematic Representation of FG Model. The mathematical description of the functional group pyrolysis model has been presented previously.[5,6,11-13] The evolution of tar and light-gas species provides two competing mechanisms for removal of a functional group from the coal: evolution as a part of a tar molecule and evolution as a distinct gas species. This process is shown schematically in Figure 4. To model these two paths, with one path yielding a product that is similar in composition to the parent coal, the coal is represented as a rectangular area with X and Y dimensions. As shown in Figure 4a, the Y dimension is divided into fractions according to the chemical composition of the coal. Y_i^0 represents the initial fraction of a particular component (carboxyl, aromatic hydrogen, etc.), and the sum of the Y_i^0's equal 1. The evolution of each component into the gas (carboxyl into CO_2, aromatic hydrogen into H_2, etc.) is represented by the first-order diminishing of the Y_i dimension, $dY_i/dt = -k_iY_i$.

The X dimension is divided into char, X, and tar, $(1 - X)$; initially $X = 1$. The evolution of the tar is represented by the decreasing of the X dimension, dX/dt, computed in the DVC subroutine as

$$dX/dt = -\sum_j (dn_j/dt)_{tot} M_j$$

(78) Gerstein, B. C.; Murphy, P. D.; Ryan, L. M. *Coal Structure*; Meyers, R. A., Ed.; Academic Press: New York, 1982; Chapter 4.
(79) Solum, M. A.; Pugmire, R. J.; Grant, D. M.; Wolfenden, W. R., submitted for publication in *Energy Fuels*.

Table II. Kinetic Rate Coefficients and Species Composition Parameters for FG Subroutine

composition params	gas	primary functional group source	rate eq[a]	Pittsburgh No. 8 bituminous coal	North Dakota Zap lignite
C				0.821	0.665
H				0.056	0.048
N				0.017	0.011
S(org)				0.024	0.011
O				0.082	0.265
total				1.000	1.000
Y_1^0	CO_2 extra loose	carboxyl	$k_1 = 0.81E+13 \exp(-(22500 \pm 1500)/T)$	0.000	0.065
Y_2^0	CO_2 loose	carboxyl	$k_2 = 0.65E+17 \exp(-(33850 \pm 1500)/T)$	0.007	0.030
Y_3^0	CO_2 tight		$k_3 = 0.11E+16 \exp(-(38315 \pm 2000)/T)$	0.005	0.005
Y_4^0	H_2O loose	hydroxyl	$k_4 = 0.22E+19 \exp(-(30000 \pm 1500)/T)$	0.012	0.062
Y_5^0	H_2O tight	hydroxyl	$k_5 = 0.17E+14 \exp(-(32700 \pm 1500)/T)$	0.012	0.033
Y_6^0	CO ether loose		$k_6 = 0.14E+19 \exp(-(40000 \pm 6000)/T)$	0.050	0.060
Y_7^0	CO ether tight	ether O	$k_7 = 0.15E+16 \exp(-(40500 \pm 1500)/T)$	0.021	0.038
Y_8^0	HCN loose		$k_8 = 0.17E+14 \exp(-(30000 \pm 1500)/T)$	0.009	0.007
Y_9^0	HCN tight		$k_9 = 0.69E+13 \exp(-(42500 \pm 4750)/T)$	0.023	0.013
Y_{10}^0	NH_3		$k_{10} = 0.12E+13 \exp(-(27300 \pm 3000)/T)$	0.000	0.001
Y_{11}^0	CH_x aliphatic	H(al)	$k_{11} = 0.84E+15 \exp(-(30000 \pm 1500)/T)$	0.207	0.102
Y_{12}^0	methane extra loose	methoxy	$k_{12} = 0.84E+15 \exp(-(30000 \pm 1500)/T)$	0.000	0.000
Y_{13}^0	methane loose	methyl	$k_{13} = 0.75E+14 \exp(-(30000 \pm 2000)/T)$	0.020	0.017
Y_{14}^0	methane tight	methyl	$k_{14} = 0.34E+12 \exp(-(30000 \pm 2000)/T)$	0.015	0.009
Y_{15}^0	H aromatic	H(ar)	$k_{15} = 0.10E+15 \exp(-(40500 \pm 6000)/T)$	0.013	0.017
Y_{16}^0	methanol		$k_{16} = 0$	0.000	0.000
Y_{17}^0	CO extra tight	ether O	$k_{17} = 0.20E+14 \exp(-(45500 \pm 1500)/T)$	0.020	0.090
Y_{18}^0	C nonvolatile	C(ar)	$k_{18} = 0$	0.562	0.440
Y_{19}^0	S organic			0.024	0.011
total				1.000	1.000
X^0	tar		$k_B = k_T = 0.86E+15 \exp(-(27700 \pm 1500)/T)$		

[a] The rate equation is of the form $k_n = k_0 \exp(-(E/R \pm \sigma/R)/T)$, with k_0 in s^{-1}, E/R in K, and σ/R in K. σ designates the spread in activation energies in a Gaussian distribution. The notation for k_0 is defined as follows: 0.81E+13 is equivalent to 0.81×10^{13} etc.

The fractional amount of a particular functional group component in the char is

$$W_i(\text{char}) = XY_i$$

and the amounts in the gas and tar may be obtained by integration with respect to time starting from $t = 0$.

Secondary reactions such as further decomposition of aliphatic species to form olefins, acetylene, and soot modify the basic equations. Some of these have been described elsewhere.[6] These types of secondary reactions are not considered in the current paper.

Figure 4a shows the initial state of the coal. Values for Y_i^0 are obtained from elemental analysis and FT-IR analysis of the raw coal or from analysis of the products of one or two selected pyrolysis experiments. Figure 4b shows the initial stage of devolatilization, during which the most volatile components, H_2O, CO (loose), and CO_2 evolve from the hydroxyl, ether-loose, and carboxyl groups, respectively, along with aliphatics and tar. At a later stage (Figure 4c) CO (tight), HCN and H_2 are evolved from the ether-tight, ring nitrogen, and aromatic hydrogen groups. Figure 4d shows the final state of the char, tar, and gas.

The evolution of gas and the composition of the char and tar are then described mathematically as follows.

Process 5. Gas Formation. The evolution of each gas species is assumed to be a first-order reaction

$$dW_i(\text{gas})/dt = k_i W_i(\text{char}) = k_i X Y_i \qquad (5)$$

where, $dW_i(\text{gas})/dt$ is the rate of evolution of speices i into the gas phase, k_i is a distributed rate for species i and W_i(char) is the functional group source remaining in the char. The concept of the distributed rate was introduced by Pitt[80] and subsequently employed by Rennhack[81] and Anthony et al.[22] to describe weight loss. Hanbaba et al.,[82] van Heek et al.,[83] Weimer and Ngan,[9] and Solomon et al.[12] employed distributed rates for individual species. In the FG subroutine, k_i is given by an Arrhenius expression $k_i = k_i^0 \exp(-(E_i \pm \sigma_i)/RT)$, where $\pm\sigma_i$ indicates that a Gaussian distribution is employed to describe the product sources, $W_i(E_i)$, as a function of the activation energies E_i.[5,9,12,22] $W_i(E_i) = (W_i^0/\sigma_i(2\pi)^{1/2}) \exp(-(E_i - E_i^0)^2/2\sigma_i^2)$. E_i^0 is the average activation energy, and σ_i is the width of the Gaussian distribution.

Note that W_i(char) also is decreased by its evolution with the tar.

Process 6. Tar Formation. The tar composition is tracked by summing the functional group contributions evolved with the tar. The rate of evolution of each contribution is

$$dW_i(\text{tar})/dt = -(dX/dt)Y_i \qquad (6)$$

where $dW_i(\text{tar})/dt$ is the rate of evolution of each functional group component with the tar.

Process 7. Char Formation. The change in the ith char pool, W_i(char), is computed by summing the losses to the gas and tar and the redistributions determined in the DVC subroutine

$$dW_i(\text{char})/dt = -dW_i(\text{gas})/dt - dW_i(\text{tar})/dt + dW_i(\text{DVC})/dt \qquad (7)$$

where $dW_i(\text{DVC})/dt$ includes the source and loss terms from the DVC model, given by $(30/28)k_B W_B$, $(2/28)k_B W_B$,

(80) Pitt, G. J. *Fuel* 1962, *41*, 267.

(81) Rennhack, R. *Brennst.-Chem.* 1964, *45*, 300.

(82) Hanbaba, P.; Juntgen, H.; Peters, W. *Brennst.-Chem.* 1968, *49*, 368.

(83) Van Heek, K. H.; Juntgen, H.; Peters, W. *Ber. Bunsen-Ges. Phys. Chem.* 1967, *71*, 113.

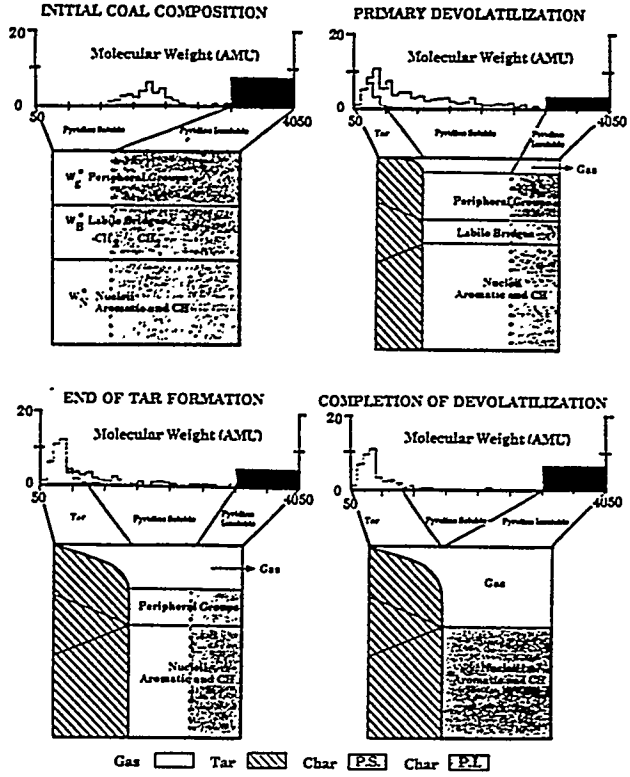

Figure 5. Schematic representation of the FG–DVC model combining the DVC and FG subroutines. The FG subroutine is illustrated for a single gas species only. The area under the histogram corresponds to the weight percent of the oligomers.

$(24/28)k_B W_B$, and $-2k_B W_B$ for methyl, aromatic H, aromatic C, and labile bridge functional groups, respectively.

The general rates and specific composition parameters for Pittsburgh Seam coal and North Dakota lignite are presented in Table II.

Schematic and Execution of FG–DVC Model. Figure 5 presents a schematic of the linked model for a simple case of only one gas species. The combined model connects the upper (DVC portion) and lower (FG portion) parts of Figure 5a–d. The model is initiated by specifying the functional group composition parameters (W_B, W_N, and, in this case, only one gas species parameter, W_p) and the coal structure parameters (starting oligomer length, l, number of added cross-links per monomer, m_0, and the monomer molecular weight distribution parameters, M_{av} and σ). The starting molecular weight distribution of oligomers is presented at the top of Figure 5a. The monomers are assumed to have the average elemental and functional group composition given by the FG parameters. The functional groups are divided into pyridine-soluble and pyridine-insoluble parts. Each computer simulation considers coal to consist of a network made from 2100–2400 monomers.

Once the starting distribution of oligomers in the coal is established, it is then subjected to a time–temperature profile made up of a series of isothermal time steps. Each time step is chosen so the temperature rise in each step does not exceed a fixed maximum. During each step, the gas yields, elemental composition, and functional group composition are computed by using the FG subroutine. The CO_2 and CH_4 yields are used to determine the number of new cross-links to be randomly added to the molecule. The molecular weight distribution, the escape of tar molecules, and the redistribution of hydrogens and carbons from the labile groups is computed with the DVC subroutine. Figure 5b illustrates tar formation simultaneous with gas formation. The labile bridges are either evolved with the tar, converted to methyl groups (and thus added to the peripheral groups), or converted to unbreakable bridges (and thus added to aromatic C and H groups). Tar formation is complete (Figure 5c) when all the labile bridges are consumed. Devolatilization is completed (Figure 5d) when all volatile functional groups (in this case the single gas species represented as peripheral groups) are removed from the char.

The model has been programmed in Fortran 77 and runs on the Sun Microsystems 3/260 and 3/50 computers. Run times on a Sun 3/260 are between 83 and 550 s/simulation for 2100–2400 monomers. A streamlined version of the code designed to run as a subroutine in a comprehensive combustion or gasification reactor simulation employs from 400 to 800 monomers and requires approximately 10 s/simulation for the pyrolysis of a single particle.

Summary of FG Subroutine Assumptions. (a) Light-gas species are formed from the decomposition of specific functional groups with rate coefficients that depend on the functional group but are independent of coal rank. The evolution rate is first order in the remaining functional group concentration in the char. The rates follow an Arrhenius expression with a Gaussian distribution of activation energies.[5,12,22]

(b) Simultaneous with the production of light-gas species is the thermal cleavage of bridge structures in the coal to release molecular fragments of the coal, which consist of a representative sampling of the functional group ensemble. These fragments may be transported out of the coal particle to form tar. The instantaneous tar yield is given by the DVC subroutine.

(c) Under conditions where pyrolysis products remain hot (such as an entrained-flow reactor), pyrolysis of the functional groups in the tar continues at the same rates used for functional groups in the char (e.g., the rate for methane formation from methyl groups in tar is the same as from methyl groups in the char).

Summary of DVC Subroutine Assumptions. (d) The oligomer length, l, the number of cross-links per monomer, m_0, and the fraction of labile bridges, W_B, are parameters of the model, chosen to be consistent with the coal's measured extract yield, cross-link density, and volatile yield in selected calibration experiments.

(e) The molecular weight distribution is adjusted so that the model predictions fit the observed molecular weight distribution for that coal, measured by pyrolysis of the coal (in vacuum at 3 °C/min to 500 °C) in a FIMS apparatus.[60] Molecular weights 106, 156, 206, 256, 306, 356, and 406 (which are aromatic one-ring through seven-ring compounds with two methyl substituents) are considered as representative of typical monomer molecular weights.

(f) During pyrolysis, the breakable bonds are assumed to rupture randomly at a rate $k_B = k_{tar}$, described by an Arrhenius expression with a Gaussian distribution of sources as a function of activation energies. Each rupture creates two free radicals that consume two donatable hydrogens to form two new methyl groups and convert two more donatable hydrogens to two aromatic CH groups. Oxymethylene bridges, which may be important for low-rank coals, have not been modeled although a second class of labile bridges could easily be added.

(g) All the donatable hydrogens are assumed to be located in the labile bridges. Two donatable hydrogens are available at each bridge. The consumption of the donatable hydrogen converts the bridge into an unbreakable bridge by the formation of a double bond. The unbreakable bridges are included in the aromatic hydrogen and

aromatic carbon functional groups.

(h) Tar formation continues until all the donatable hydrogens are consumed.

(i) During pyrolysis, additional unbreakable cross-links are added at a rate determined by the evolution of CH_4 and CO_2. One cross-link is created for each evolved molecule. The rates of CH_4 and CO_2 evolution are given by the FG subroutine.

(j) The cross-links are distributed randomly, with the probability of attachment on any one monomer being proportional to the molecular weight of the monomer.

(k) Tar molecules are assumed to vaporize from the surface of the coal particle (or into bubbles) with a molecular weight and temperature dependence based on the vapor pressure correlation of Suuberg et al.[32] The external-transport model is based on the surface-evaporation model of Unger and Suuberg.[23]

(l) To describe internal transport, a simple empirical expression (eq 4) is used to describe both bubble transport in softening coals and convective transport through pores in nonsoftening coals. The tar is assumed to be transported at its equilibrium vapor pressure in the light-gas species. The pressure increase that drives the transport within the particle, ΔP, is between 0 and 0.2 atm for the bituminous coal and between 0 and 10 atm for the lignite, depending on the experimental conditions.

(m) Extractable material (in boiling pyridine) in the char is assumed to consist of all molecules less than 3000 amu. This limit can be adjusted depending on the solvent and extraction conditions.

(n) The molecular weight between cross-links, M_c, is computed to be the total molecular weight of the computer molecule divided by the total number of cross-links. This assumption will underestimate M_c since broken bridges are not considered.

Results

The model predictions have been compared to the results obtained from a number of experiments on the pyrolysis of a Pittsburgh Seam coal[6,7,16,22] and a North Dakota (Beulah, Zap) lignite.[6,51] The coal composition and kinetic parameters are presented in Tables I and II. It should be noted that different samples of Pittsburgh seam coal from different sources were employed. While the elemental compositions were similar, extract yields varied depending on the sample source. The oligomer length in Table I was chosen to fit an extract yield of 30% for the Pittsburgh Seam coal and 1% for the lignite. Comparisons are considered for gas yields, tar yields, tar molecular weight distributions, extract yields, and volumetric swelling ratios.

Volatile Yields. Extensive comparisons of the FG model with gas yields have been presented previously for high- and low-heating-rate devolatilization experiments.[5,6,11-13] The evolution of gases for the combined model is similar to results of the FG model and will not be repeated here. There is good agreement between the measured and predicted results. The functional group parameters and the kinetic rates used for this work for the Pittsburgh Seam coal and North Dakota (Zap) lignite are principally those determined previously and published in ref 6. The methane parameters for the Pittsburgh Seam coal were, however, adjusted (methane X-L = 0.0, methane-L = 0.02, methane-T = 0.015, unchanged) to better match yields of refs. 5–7 (see Figure 20c in ref 6). Also note that the CH_x– aliphatic rate in ref 6 applies to the observed gas species (paraffins, olefins, C_2H_6, C_2H_4) only. The aliphatic material in the labile bridge part of the aliphatic groups is assumed to be made up of bridges that volatilize only when attached to a tar molecule (i.e., $k_i = 0$). Also,

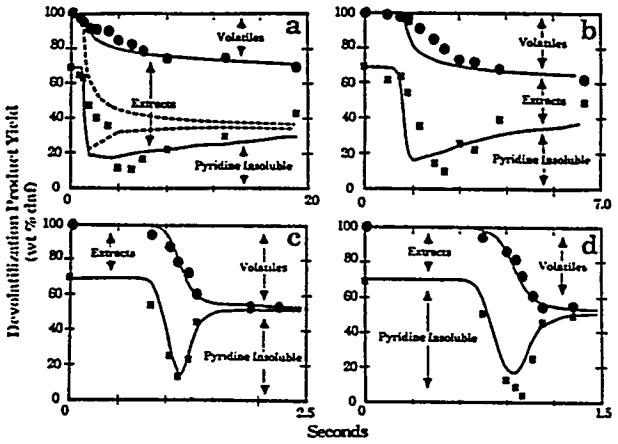

Figure 6. Comparison of FG–DVC model predictions with the data of Fong et al.[16] (symbols) for Pittsburgh Seam coal: (a) 813 K at 470 K/s; (b) 858 K at 446 K/s; (c) 992 K at 514 K/s; (d) 1018 K at 640 K/s. P = 0.85 atm. The solid line assumes transport by eq 4 (ΔP = 0 atm) and no external transport. The dashed line in part a shows the predicted yield assuming $\mathcal{X}^s_j = \mathcal{X}^b_j$ in eq 3 and no internal-transport limitations.

the rate for CO_2(loose) has been adjusted to improve the predictions of the change in tar molecular weight distributions and yield with heating rate. The predictions of gas yield due to this change have not been changed noticeably. The predicted values of X^0 from the DVC subroutine vary with heating rate and final temperature and are in good agreement with the values of X^0 used in the original FG model.

Extract Yields. Figure 6 compares the FG–DVC predictions to the data of Fong et al.[16] on total volatile yield and extract yield as a function of temperature in pyrolysis at 0.85 atm. The experiments were performed in a heated-grid apparatus at heating rates of approximately 500 °C/s, with variable holding times and rapid cooldown. The predictions at the two higher temperatures (Figures 6c,d) are in excellent agreement with the data.

The initial predictions for the two lower temperature cases, which neglected interal-transport limitations, were not good. The dashed line in Figure 6a shows the predicted yield in the absence of internal transport limitations (i.e., $(dn_j/dt)_{IT} = 0$ and with $\mathcal{X}^s_j = \mathcal{X}^b_j$ in eq 3). The predicted ultimate yield is clearly too high. The data suggest that the low yields are not a result of unbroken bonds (which would result from a lower bond breaking rate, k_B), since the extract yields at low temperatures are equivalent to those at the higher temperatures. The coal molecule thus appears to be well decomposed, the low yields resulting from poor transport out of the coal. This suggested an additional transport limitation in getting molecules to the surface, so $\mathcal{X}^s_j = \mathcal{X}^b_j$ appears to be a bad assumption.

Equation 4 was employed for the internal-transport rate, and surface evaporation by eq 3 was assumed to be unimportant ($\mathcal{X}^s_j = 0$). Then, W_B had to be slightly readjusted from 0.096 in ref 50 to 0.094 to match the 1018 K case. This new value of W_B was used for subsequent cases. The predictions with this assumption are the solid lines in Figure 6. The internal-transport limitation is most important when pyrolysis occurs at low temperatures and $\sum_{light} dn_i/dt$ in eq 4 is small.

There still is a discrepancy between the prediction and the data at early times for the two lower temperature cases (Figure 6a,b). While it is possible that the rate k_b for bond breaking is too high, adjustment of this rate alone would significantly lower the extractable yield, since the lower depolymerization rate is closer to the methane cross-linking

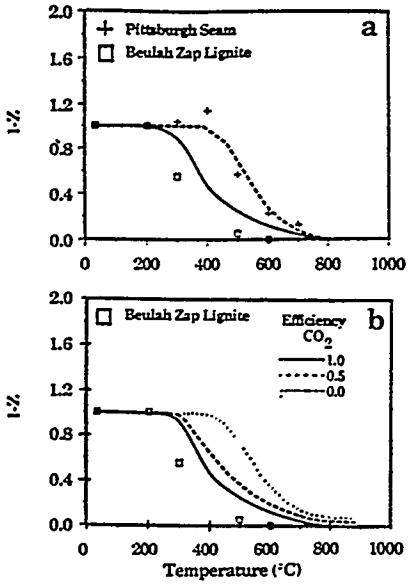

Figure 7. (a) Comparison of measured and predicted normalized volumetric swelling ratio as a function of temperature. The solid line is the prediction of Beulah lignite; the dashed line is for Pittsburgh Seam coal. The cross-link efficiency of CO_2 is 1.0. (b) Effect of cross-link efficiency of CO_2 on the normalized volumetric swelling ratio profile with temperature. For parts a and b the heating rate is 0.5 °C/s. $\Delta P = 0$ atm.

rate. In addition, both the methane and depolymerization rates appear to be in good agreement with the data at even lower temperatures.[6] Another possibility is that the coal particles heat more slowly than the nominal temperatures given by Fong et al.[16] Such an effect could be caused by having some clumps of particle that would heat more slowly than isolated particles, by reduction in the convective heat transfer due to the volatile evolution (blowing effect) or by endothermic tar forming reactions. A firm conclusion as to the source of this remaining discrepancy cannot be drawn without further investigation.

It is also seen in Figure 6a,b that the cross-linking rate is higher than predicted. This can be due to other crosslinking events not considered. These possibilities are currently under investigation.

Cross-Link Density. To examine the effect of coal rank on cross-linking, the volumetric swelling ratios (VSR) for North Dakota (Beulah, Zap) lignite and Pittsburgh Seam bituminous coal were measured as a function of temperature at 0.5 °C/s. The VSR can be related to the cross-link density.[77] The swelling data are plotted in Figure 7a as $1 - Z$, where Z is the change in VSR between coal and char normalized by the maximum change. For coal, Z is 0 and for completely cross-linked char, Z is 1. While the weight loss profiles of the two samples look similar at 0.5 °C/s, the swelling behaviors in Figure 7a are quite different. The Pittsburgh Seam coal starts to cross-link during tar evolution, and the Beulah lignite cross-links well before tar evolution. Similar results have been reported by Suuberg et al.,[59] who also suggested a correlation between cross-linking in lignites and CO_2 evolution. The coals that undergo early cross-linking are less fluid, produce less tar, and produce lower molecular weight tar compared with coals that do not experience early cross-linking.[30,31,44]

As discussed previously, under the assumption that the cross-linking reactions may also release gas species, the VSR was correlated with the observed evolution of gas species during pyrolysis. Correlations presented in Figure 2 show that on a molar basis, the evolution of CO_2 from the lignite and CH_4 from the bituminous coal appear to have similar effects on the VSR. Reactions that form these gases, leave behind free radicals that can be stabilized by cross-linking.

Assuming that one cross-link is formed for each CO_2 or CH_4 evolved from the char, the FG–DVC model predictions are presented as the lines in Figures 2 and 7a. The agreement between theory and experiment is good except that the increase in $1 - Z$ for the Pittsburgh Seam coal in Figure 7a is not predicted. This may be related to the restrictions of assumption n (see summary of DVC subroutine assumptions). The predictions in Figure 2a are different from those originally presented in ref 50. In ref 50, the value used for VSR_{min} was not appropriate for the fully cross-linked molecule. This error has now been corrected.

In Figure 7b, the effect of varying the CO_2 cross-linking efficiency is considered. The figure shows cases calculated for the lignite assuming 0, 0.5, and 1.0 cross-links are formed per CO_2 evolved. Varying this assumption has a major effect on the early cross-linking of the lignite. Assuming that the cross-linking efficiency per CO_2 is 1.0 gives the best agreement with the data.

The difference in crosslinking behavior between the two coals is manifested in several areas. At low heating rates, the Pittsburgh Seam chars soften; the Beulah, Zap chars do not. This is in agreement with the high predicted maximum extract yields in the Pittsburgh char (70%) compared to the low extract yields in the Beulah, Zap lignite (7%). The measured values are 71%[16] and ~6%, respectively. The predicted yield of tar plus aliphatic gases at 1 atm, 0.5 °C/s to 900 °C, of 26% is in good agreement with the measured value of 28% for the Pittsburgh Seam coal. The predicted value of 11% (for $\Delta P = 10$ atm) is in good agreement with the measured value of 10% for the Beulah, Zap lignite.

Molecular Weight Distribution. A sensitive test of the general model is the ability to predict the tar molecular weight distribution and its variations with rank, pressure, and heating rate. The input to the model is the distribution of monomer molecular weights. The tar, which consists of oligomers, has a different distribution from the monomer distribution and is controlled by the relative effects of bond breaking, cross-linking, and transport. The tar molecular weight distribution is not highly sensitive to the choice of M_{av} and σ. For Pittsburgh Seam coal, the average monomer was assumed to be a three-ring compound ($M_{av} = 256$) and a fairly broad distribution ($\sigma = 250$) was chosen. The same values appeared to work for the lignite. These are in reasonable agreement with the measured values of ~300 reported by Solum et al.[79] for both coals.

Figure 8c,d show results for the Pittsburgh Seam bituminous coal and the Beulah, Zap lignite pyrolyzed in the FIMS apparatus. The data have been summed over 50 amu intervals. While the Pittsburgh bituminous coal shows a peak intensity at about 400 amu, the lignite peak is at 100 amu. The predicted average tar molecular weight distributions are in good agreement with FIMS data as shown in Figure 8a,b. Since both tar distributions are from the same monomer distribution, the enhanced drop off in amplitude with increased molecular weight for the lignite compared to the bituminous coal must be due to early cross-linking and transport effects in the lignite.

Pressure Effects. The predicted effect of pressure on the tar molecular weight distribution is illustrated in Figure 9a,b. Pressure enters the model through the transport eq 3 and 4. The internal-transport rate (eq 4), which is assumed to dominate, is inversely proportional to the am-

Table III. Comparison of Measured and Predicted Yields for Pittsburgh Seam Bituminous Coal (ΔP = 0 atm)

experiment	heating rate, °C/s	P_0, atm	final temp, °C	max yield of tar + aliphatic gases, % measd	max yield of tar + aliphatic gases, % predicted	total max volatiles, wt % measd	total max volatiles, wt % predicted
TG-FTIR	0.5	1.0	600	25	29	35	37
entrained flow	5000	1.0	700	36	37	43	43
heated grid	640	0.85	745		40	47	47

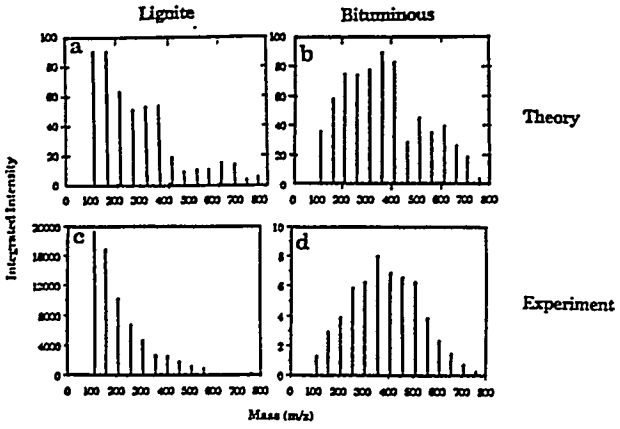

Figure 8. Comparison of measured and predicted tar molecular weight distributions for lignite and bituminous coals. The experiments are performed by pyrolysis of coal samples in a FIMS apparatus. Intensities have been summed over 50 amu intervals. For part a ΔP = 10 atm, and for part b ΔP = 0.0 atm.

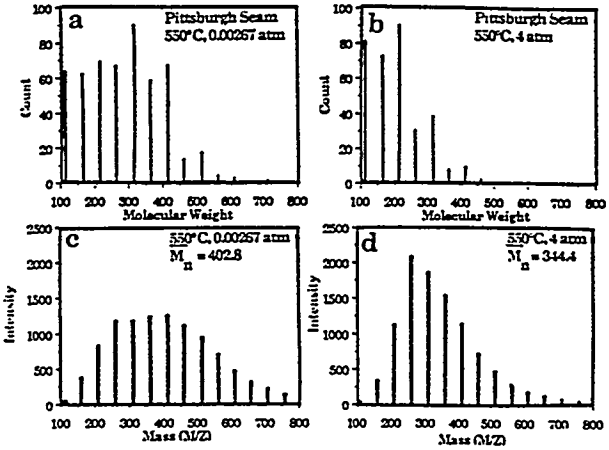

Figure 9. Comparison of predicted (a and b) and measured (c and d) tar molecular weight distribution for pyrolysis of a Pittsburgh Seam coal in a heat-grid apparatus at a heating rate of 500 °C/s to 550 °C. Parts a and c compare the prediction and the measurement at 0.00267 atm. Parts b and d compare the prediction and measurement at 4.0 atm. ΔP = 0.2 atm.

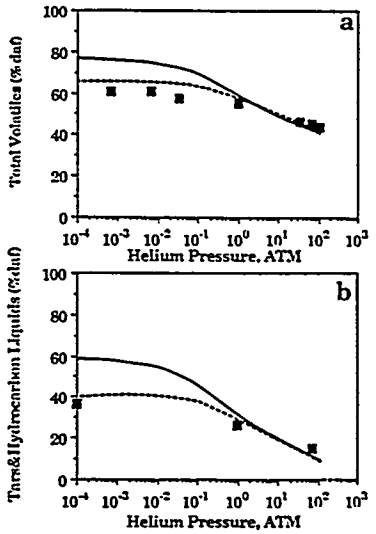

Figure 10. Comparison of measured and predicted volatile yield for a Pittsburgh Seam bituminous coal; (a) total volatiles, data of Anthony et al.;[22] (b) tars and hydrocarbon liquids, data of Suuberg et al.[7] The solid line assumes ΔP = 0 atm; the dashed line assumes ΔP = 0.2 atm.

bient pressure P_0. The reduced transport rate reduces the evolution rate of the heavier molecules. Therefore, the average molecular weight and vaporization "cutoff" decrease with increasing pressure. The trends are in agreement with observed tar molecular weight distributions shown in Figure 9c,d. The spectra are for previously formed tar that has been collected and analyzed in a FIMS apparatus.[60] The low values of intensity between 100 and 200 mass units are believed to be due to loss of these components due to their higher volatility.

Pressure effects on yields have also been examined. Figure 10 compares the predicted and measured pressure dependence on yield for a Pittsburgh Seam coal. Figure 10a compares the prediction to the total volatile yield data of Anthony et al.[22] while Figure 10b compares the prediction to the tar plus liquids data of Suuberg et al.[7] The agreement between theory and experiment is good at 1 atm and above, but the theory with ΔP = 0 (solid line) overpredicts the yields at low pressure. Below 1 atm, it is expected that ΔP within the particle will become important compared to the ambient pressure, P_0. The dashed lines, which agree with the data, were obtained by assuming ΔP = 0.2 atm, which is physically reasonable.

Heating-Rate Effects. It is well-known that the heating rate can affect the amount of volatiles produced.[29,76,84-86] Heating rate can also affect the melting and swelling behavior of low-rank coals.[13] Considering the mechanisms proposed for pyrolysis (including those in this paper), it is the relative rates of competing processes for tar formation (e.g., bond breaking, cross-linking, and mass transport) that provide the heating-rate effects. The relative rates of these processes change with temperature, and it is the heating rate that determines the temperature at which the controlling reactions occur. So it is really the temperature of tar formation and not the heating rate per se which is important.

Consider first the effects of heating rate on the yields of a Pittsburgh Seam bituminous coal. Table III summarizes the results for three experiments[16,87,88] in which the heating rate varied from 0.5 to 5000 °C/s and in which the final temperature reached is sufficiently high for tar

(84) Gibbins-Matham, J.; Kandiyoti, R. *Prepr. Pap.—Am. Chem. Soc., Div. Fuel Chem.* 1987, *32*(4), 318.
(85) Freihaut, J. D.; Seery, D. J. *Prepr. Pap.—Am. Chem. Soc., Div. Fuel Chem.* 1983, *28*(4), 265.
(86) Serio, M. A.; Peters, W. A.; Sawada, K.; Howard, J. B. *Prepr. Pap.—Am. Chem. Soc., Div. Fuel Chem.* 1984, *29*(2), 65.
(87) Serio, M. A.; Solomon, P. R.; Carangelo, R. M. *Prepr. Pap.—Am. Chem. Soc., Div. Fuel Chem.* 1988, *33*(2), 295.
(88) Solomon, P. R.; Hamblen, D. G.; Serio, M. A.; Smoot, L. D.; Brewster, S. "Measurement and Modeling of Advanced Coal Conversion"; First Annual Report for U.S. METC Contract No. DE-AC21-86MC23075, 1987.

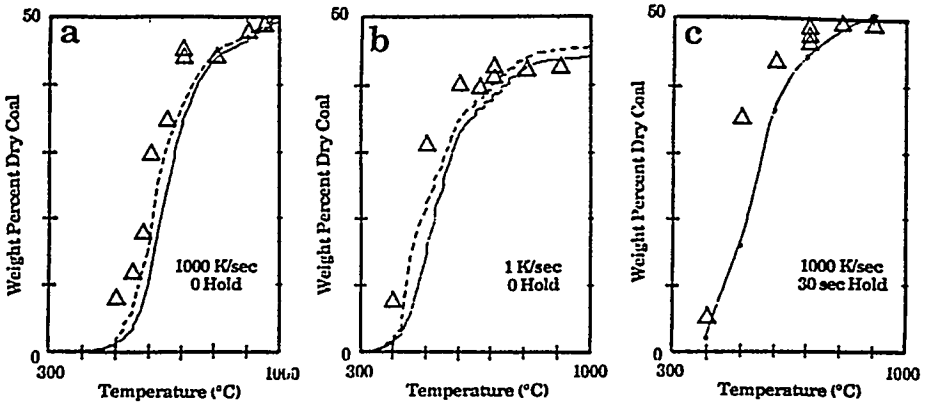

Figure 11. Comparison of FG–DVC model predictions with the data of Gibbins-Matham and Kandiyoti[83] (symbols) for Pittsburgh Seam coal: (a) 1000 K/s, zero hold; (b) 1 K/s, zero hold; (c) 1000 K/s, 30-s hold. P = 1.18 atm. Transport is by eq 4 ($\Delta P = 0$) and no external-transport limitation. The dashed line assumes no transport limitations for molecules whose vapor pressure exceeds $P_0 + \Delta P$.

formation to be completed during the heating period. As can be seen, the predicted and measured volatile yields increased by about 10% from low to high heating rates. As can also be seen, the increase in yield results from the increase in tar plus aliphatic gases. Examination of the rates in the model shows that the major contribution to the variation in yield is the internal-transport rate relative to the bond-breaking rate. At low temperatures, internal transport severely limits the evolution of the heavier molecules, resulting in smaller tar molecules and inefficient use of the donatable hydrogens.

A set of data showing the effect of heating rate on yield for the Argonne Pittsburgh Seam coal was recently reported by Gibbins-Matham and Kandiyoti.[84] Data were obtained in a wire-grid apparatus at 1 and 1000 °C/s with no holding time and at 1000 °C/s with a 30-s hold. These data (triangles) are compared to predictions of the model in Figure 11. For all three cases, the theory predicts the correct pyrolysis final yields, the correct yield variation with heating rate, and the correct temperature shift with heating rate.

The predicted yields, however, occur at temperatures from 20 to 80 °C higher than the comparable experimental yields. At this time, the reason for the discrepancy is not clear. One possible reason is the assumptions used for the internal transport limitations. Calculations were made assuming that molecules for which $P_j \geq P_0 + \Delta P$ evolve as they are produced, while only heavier molecules evolve as described in eq 4. The predicted curves (dashed lines in Figure 11) are 20–40 °C lower than in the original calculation. Alternatively, the vapor pressure may not be accurately described by the expression of Suuberg et al.[32] Oh[38] compared a number of correlations for the tar vapor pressure. At 1000 °C, the expression of Suuberg et al.[32] gave vapor pressures from 1–2 orders of magnitude lower than other published expression.[89,90] Calculations using the expression for aliphatic molecules of Maiorella[89] gave predictions at about 40 °C lower temperatures, in better agreement with the data of Gibbons-Matham and Kandiyoti. The simulation, however, required a lower value of W_B (0.060) to compensate for the higher volatility. Predictions using the same assumptions failed to match those of Fong et al.[16] in Figure 6 with regard to the temperature of evolution and the amount of extract produced. Possible refinements of the internal-transport model are being considered.

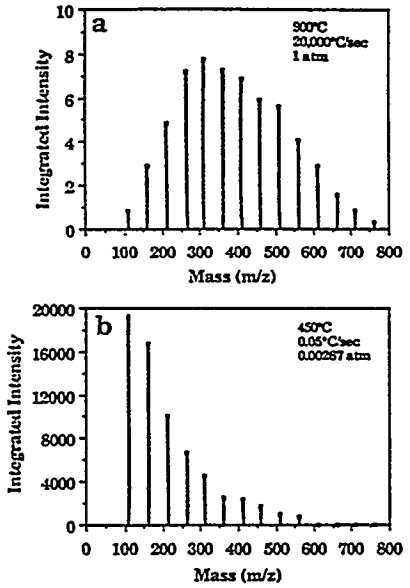

Figure 12. Comparison of FIMS spectra of tars of Beulah Zap lignite formed at (a) high heating rate (20000 °C/s) and (b) low heating rate (0.05 °C/s).

Another possible explanation for the discrepancy is the accuracy of the reported pyrolysis temperature, which has been notoriously variable among investigators. Other Pittsburgh Seam coal data (not shown) for Niksa et al.[40] under the same conditions as Figure 11c (1000 °C/s, 30-s hold) and from Oh[38] and Suuberg et al.[7] for the same conditions as Figure 11a (1000 °C/s, zero hold) show substantial variations in temperature compared to the results of Gibbons-Matham and Kandiyoti.[84] The theoretical predictions would lie within the scatter of the several data sets. Work is in progress to resolve this question.

Low-rank coals also exhibit heating-rates effects. It has been found that Beulah lignite chars soften and exhibit bubble formation at high heating rates (~20000 °C/s).[13] Under these conditions, molecular weight distribution of tars of Beulah lignite look like that of a bituminous coal.[30,31] The infrared spectrum of the tar is also closer in appearance to that of the parent coal.[31] The mass spectra of the tars formed at high heating rate (20000 °C/s) and low heating rate (0.05 °C/s) are shown in parts a and b of Figure 12, respectively. The low values of intensity between 100 and 200 mass units in Figure 12b are believed

(89) Maiorella, B. L. B.S. Thesis, Department of Chemical Engineering, MIT, Cambridge, MA, 1975.
(90) Grey, J. A.; Brady, A. J.; Cunningham, J. R.; Freeman, J. R.; Wilson, G. M. *Ind. Eng. Chem. Process Des. Dev.* 1983, 22, 410.

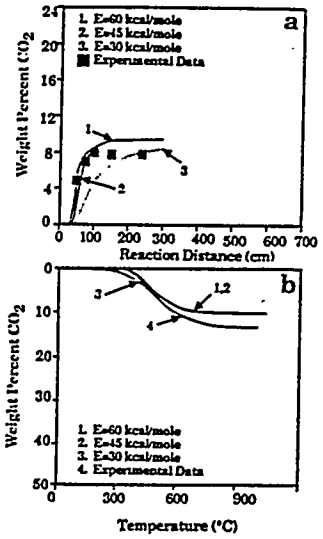

Figure 13. Comparison of CO_2 evolution data from North Dakota lignite for low-heating-rate (0.5 °C/s) and high-heating-rate (20000 °C/s) experiments with model predictions for different values of activation energy for CO_2 (extra loose) in the FG–DVC Model: (a) heated-tube-reactor experiments;[6] (b) TG-FTIR experiments.[6]

to be due to loss of these components due to their high volatility. The molecular weight distribution of the tars is very sensitive to the heating rate. The effect is attributed to the higher rate of depolymerization reactions relative to cross-linking reactions at high temperatures, as discussed in the sensitivity section.

The FG–DVC model, assuming the internal-mass-transport limitations, was used to simulate the low heating rate (0.05 °C/s) and high heating rate (20000 °C/s) pyrolysis of Beulah lignite. The activation energy for CO_2 (extra loose) in the FG subroutine was reduced from 60 to 45 kcal/mol in order to make it lower than the activation energy for bond breaking (55 kcal/mol). This was done since measurements of the rate of cross-linking at high heating rates suggested that the relative rate of bond-breaking and cross-linking reactions associated with CO_2 evolution is increased with increasing temperature.[91] This change in the activation energy makes only a slight change in the CO_2 evolution profiles for high-heating-rate (20000 °C/s) and low-heating rate (0.5 °C/s) predictions. The CO_2 gas evolution profiles are compared to the data in Figure 13a,b for high-heating-rate (20000 °C/s) and low-heating-rate (0.5 °C/s) experiments with Beulah lignite using activation energies of 60, 45, and 30 kcal/mol. When the activation energy for CO_2 (extra loose) evolution was reduced to 45 kcal/mol, acceptable fits to the gas evolution data were still obtained. However, at 30 kcal/mol, the high-heating-rate CO_2 evolution profile was quite different and did not agree with the experimental data.

The model, with internal-mass-transport limitations included, was used to simulate the tar molecular weight distributions with $\Delta P = 0$ atm for Beulah lignite for high heating rate (20000 °C/s) in Figure 14a,b. The simulations were done for both the original activation energy (60 kcal/mol) and altered activation energy (45 kcal/mol) for CO_2 (extra loose) evolution. The tar molecular weight distributions (for $\Delta P = 0$ atm) at high heating rates (Figure 14a,b) show the observed high values of the tar molecular weight at high heating rate (Figure 12a). The lower activation energy case (Figure 14a) exhibits more high molecular weight molecules and gives a higher tar yield (10%)

(91) Deshpande, G. V.; Solomon, P. R.; Serio, M. A. *Prepr. Pap.—Am. Chem. Soc., Div. Fuel Chem.* 1988, *33*(2), 310.

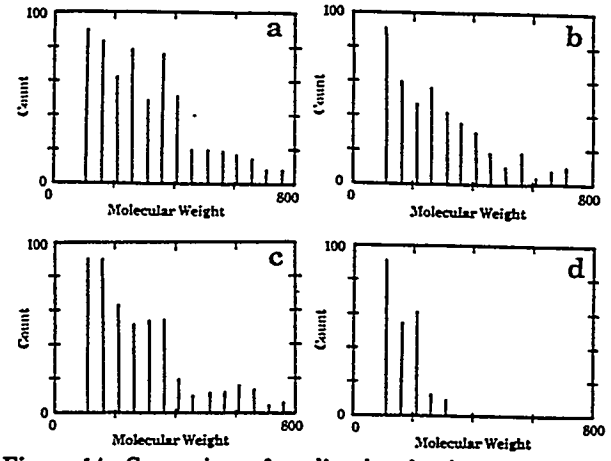

Figure 14. Comparison of predicted molecular weight distribution of tars of Beulah lignite for (a and b) high heating rate (20000 °C/s) and (c and d) low heating rate (0.05 °C/s). In parts a, c, and d the CO_2 activation energy is 45 kcal/mol and in part b it is 60 kcal/mol. In parts a–c $\Delta P = 0$ atm, and in part d ΔP = 10 atm.

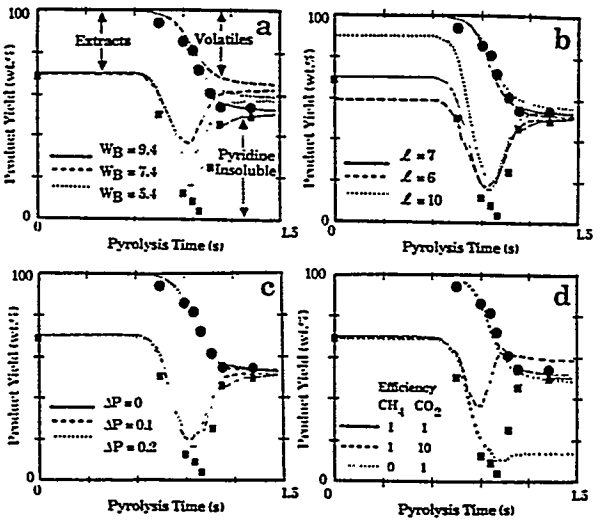

Figure 15. Effect on product yields of (a) fraction of labile bridges, W_B, (b) oligomer length, l, (c) internal pressure difference, ΔP, and (d) cross-linking efficiency. Data were taken from Fong et al.[16] for Pittsburgh Seam bituminous coal (1018 K at 640 K/s, P = 0.85 atm); $\Delta P = 0$ atm.

than the high activation energy case (8%) (Figure 14b). The low-heating-rate (0.05 °C/s) case ($\Delta P = 0$) (Figure 14c) exhibits lower molecular weights consistent with Figure 12b. At high heating rates, where cross-linking reactions are curbed and the lignite melts, ΔP is likely to be low. At low heating rate, due to the higher extent of cross-linking before tar evolution, the coal is less fluid, and hence ΔP (which is related to viscosity of the solid/liquid mixture) is likely to be higher. A simulation for the slow-heating-rate case with $\Delta P = 10$ atm is shown in Figure 14d. The measured molecular weight distribution in Figure 12b appears to be intermediate between the $\Delta P = 0$ and ΔP = 10 atm cases.

Sensitivity Analysis. This section considers the sensitivity of the FG–DVC model to variations in the DVC parameters. The FG parameter sensitivities have been considered elsewhere.[52]

(a) Variations in W_B. The number of labile bridges is the most important parameter in determining tar yield. The value of W_B for the Pittsburgh Seam coal was reduced from its value of 9.4 to 7.4 and 5.4. The results in Figure 15a were calculated for the case considered in Figure 6d.

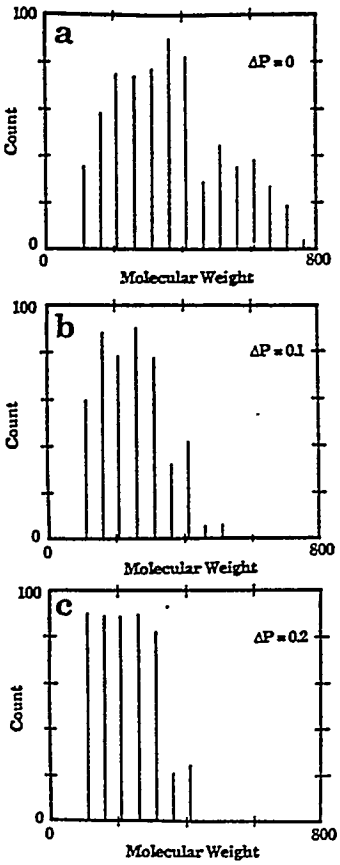

Figure 16. Effect of ΔP on tar molecular weight distribution for Pittsburgh Seam bituminous coal heated to 723 K at 0.05 K/s. P = 0.00267 atm.

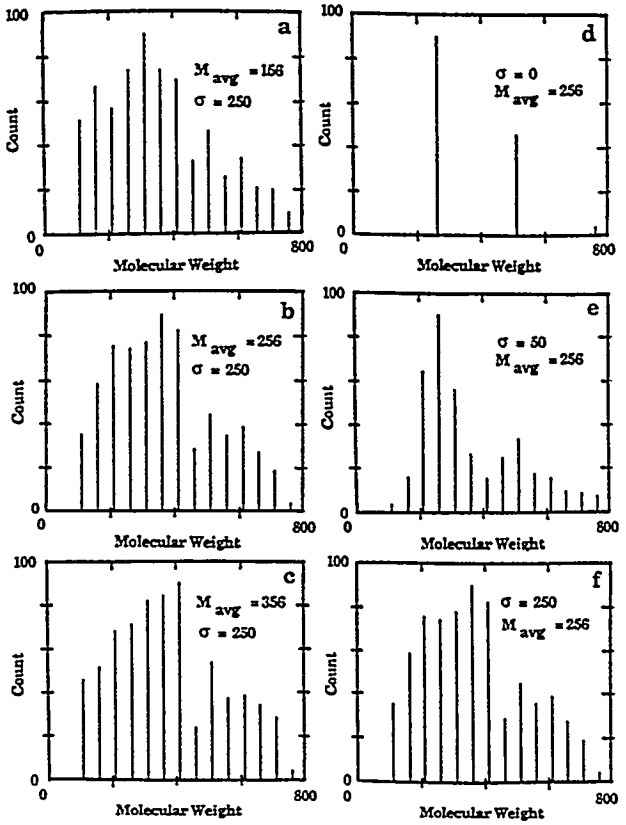

Figure 17. (a–c) Effect of M_{av} on the shape of the tar spectrum and (d–f) effect of σ on the shape of the tar spectrum. The heating rate is 0.05 °C/s to 450 °C, P = 0.00267 atm, and ΔP = 0 atm.

The reduction in W_B reduces the tar yield, the total volatile yield, and the extract yield. Higher values of W_B could not be considered because the molecule already contained the maximum number of labile bridges. This is a limitation in the model as it is currently formulated since all the donatable hydrogens are assumed to be in bridges.

(b) Variations in l. The parameter l affects mainly the extract yield in the raw coal. Figure 15b demonstrates variations in l from 6 to 10 around the base value of 7. The initial extract yield varies substantially while there is only a minor effect on the tar yield, total volatile yield, and extract yield at elevated temperature.

(c) Variations in ΔP. The effect of variations in ΔP on the overall yield are considered in Figure 10. There is no effect at 1 atm pressure and above but a strong effect at lower ambient pressures. Figure 15c confirms that ΔP has little effect on the tar yield or the total volatile yield for pyrolysis at 1 atm pressure. Only the extract yield is slightly affected.

Figure 16 illustrates the effect on the molecular weight distribution for three values of ΔP for pyrolysis in vacuum ($P_0 = 0$). The yield of higher molecular weight tars present for $\Delta P = 0$ is lower for $\Delta P = 0.1$ atm and eliminated for $\Delta P = 0.2$ atm. The total tar yields are 39%, 21%, and 17% for $\Delta P = 0$, 0.1, and 0.2 atm respectively. The tar molecular weight distribution for $\Delta P = 0$ atm gives the best match to Figure 9c, but ΔP = 0.1–0.2 atm provides the best match to the yield.

The variation of ΔP in the tar molecular weight distribution for lignite is discussed with reference to Figure 13.

(d) Variations in $m(CO_2)$ and $m(CH_4)$. Variations in $m(CO_2)$ were considered for the lignite in the discussion accompanying Figure 7. Variations in both $m(CO_2)$ and $m(CH_4)$ are considered in Figure 15d. These have a major effect on the yields. Increasing $m(CO_2)$ from 1 to 10 reduces the extract and volatile yields while reducing $m(CH_4)$ from 1 to 0 prevents the repolymerization of the extract.

(e) Variations in M_c. Variations in the M_c values were made. These chiefly affect the extract yield, requiring an adjustment in l. They have little effect on the subsequent cross-linking in the coal. The reason for this can be seen in Table I. The initial value of M_c consistent with the literature required only 0.09 and 0.18 cross-link/monomer for the bituminous coal and lignite, respectively. The total number of cross-links added during pyrolysis are 0.49 and 0.89, respectively. The added number of cross-links is thus much larger than that in the raw coal and, consequently, dominates the char's behavior.

(f) Variations in M_{av} and σ. Figure 17a–c illustrates the effects of variations in M_{av}. Varying M_{av} changes the shape of the tar spectrum, but not drastically. The shape is still dominated by the transport properties (e.g., see Figure 16). The effect on the tar yield is also modest, giving values of 45%, 44%, and 42% for M_{av} values of 156, 256, and 356, respectively.

A similar lack of sensitivity of the molecular weight distribution to M_{av} was exhibited for the lignite for both high-heating-rate (~20000 °C/s) and low-heating-rate (0.05 °C/s) cases (not shown).

The effect of variations in σ is illustrated in Figure 17d–f. σ = 250 fills in the spectrum in a more realistic fashion and is more aesthetically pleasing than the two smaller values of σ. The effect on the total tar yield is minor with yields of 41%, 46%, and 45% for σ = 0, 50, and 250, respectively.

(g) Variations in W_N. This parameter, which is taken from the FG model, controls the split between tar, char, and gas.

Table IV. Summary of Sensitivity Analysis[a]

	W_N	W_B	l	M_c	$m(CO_2)$	$m(CH_4)$	M_{av}	σ	ΔP
tar molecular weight	W	W	W	W	S	W	M	M	S
tar yield	S	S	W	W	S	M	W	W	S
char extract yield	W	S	W	W	S	S	W	W	M
coal extract yield	W	W	S	M	W	W	W	W	W
char solvent-swelling ratio	W	W	W	S	S	S	W	W	W
coal solvent-swelling ratio	W	W	W	W	W	W	W	W	W

[a] Key: W = weak or none; M = moderate; S = strong.

(h) Vaporization Law. The results are sensitive to the choice of the tar vapor pressure correlation. Higher vapor pressures result in faster tar evolution and higher yields as discussed in reference to Figure 11.

A summary of the sensitivity analysis is presented in Table IV. The concentration of labile bridges W_B and the CO_2 cross-linking parameter $m(CO_2)$ are the most important parameters in determining yields.

Conclusions

A general FG–DVC model for coal devolatilization, which combines a functional group model for gas evolution and a statistical model for tar formation, has been presented. The tar formation model includes depolymerization, cross-linking, external transport and internal transport. The cross-linking is related to the evolutions of CO_2 and CH_4, with one cross-link formed per molecule evolved. The predictions of the tar formation model are made by using Monte Carlo calculation methods. Predictions take between 10 s and 10 min (depending on coal rank, experimental conditions, and accuracy required) on a Sun 3/260 computer.

The FG–DVC model predictions compare favorably with a variety of data for the devolatilization of Pittsburgh Seam coal and North Dakota (Beulah) lignite, including volatile yields, extract yields, cross-link densities, and tar molecular weight distributions. The variations with pressure, devolatilization temperature, rank, and heating rate were accurately predicted. Comparison of the model with several sets of data employing alternative assumptions on transport suggests assuming that the particle is well mixed (i.e. the surface concentration of tar molecules is the same as the bulk) overpredicts the transport rate. For 50-μm particles, assuming that the internal-transport limitation dominates (i.e. neglecting the external transport) provides a good fit to the data. This is consistent with assuming (a) that the internal- and external-transport mechanisms act in series or (b) that they act in parallel but liquid-phase diffusion of tar molecules to the surface is very small and so the external transport term can be neglected.

The rank dependence of tar formation, extract yields, cross-linking, and viscosity appears to be explained by the rank dependence of CO_2 yields. The high CO_2 yields in low-rank coals produce rapid cross-linking at low temperatures and hence low tar yields, low extract yields, loss of solvent-swelling properties, and high viscosities. The relative importance of cross-linking compared to bond breaking is, however, sensitive to heating rate, and this effect is predicted by the FG–DVC model. The predicted cross-linking associated with methane evolution appears to match the observed cross-linking in high-rank coals (which evolve little CO_2).

The model has eight coal structure parameters that must be determined for each coal from selected laboratory experiments. Once determined, these remain fixed for all experiments. The model also contains one adjustable parameter, ΔP, the internal pressure difference that drives the volatiles out of the particle. A sensitivity analysis shows that the volatile yield is most sensitive to the fraction of labile bridges, W_B, the cross-linking parameters $m(CO_2)$ and $m(CH_4)$, and, in some cases (low-rank coals, low pressure), to ΔP. The monomer molecular weight distribution parameters, M_{av} and σ, have only a weak effect on yields and tar molecular weight distributions. The initial molecular weight between cross-links, M_c, and the initial oligomer length, l, affect the coal's solvent-swelling ratio and extract yield but have little effect on the subsequent pyrolysis behavior.

The model currently has several deficiencies. There is no model for estimating liquid-phase diffusion of tar molecules, which may be important for very small particles. The calculation of the average molecular weight between cross-links neglects the effect of labile bridge rupture. The assumption that all the donatable hydrogen is in bridges may be restrictive for some high hydrogen coals. The model presented here has neglected polymethylene in coal and the effect of other types of weak bonds besides ethylene bridges. There are some discrepancies between the predictions and reported temperatures of pyrolysis experiments. It is unclear at this time whether this is due to errors in the reported temperatures or in the transport predictions. Many of these deficiencies require only minor modifications to the model and are currently being addressed.

Acknowledgment. This work was supported under DOE Contracts DE-AC21-85MC22050, DE-AC21-84MC21004, DE-AC21-86MC23075, and DE-FG22-85PC80910. We express our thanks to Professor Eric Suuberg for many helpful discussions on transport properties and to Dr. Zhen Zhong Yu for assistance with the model calculations.

Appendix K

Can Coal Science Be Predictive

CAN COAL SCIENCE BE PREDICTIVE

Peter R. Solomon, David G. Hamblen, Michael A. Serio, Zhen-Zhong Yu, and Sylvie Charpenay
Advanced Fuel Research Inc., 87 Church Street, East Hartford, CT 06108

KEY WORDS: Coal, Pyrolysis, Network

ABSTRACT

This paper considers the development of a predictive macromolecular network decomposition model for coal conversion which is based on experimental results from a variety of modern analytical techniques. Six concepts which are the foundation of the Functional Group, Depolymerization, Vaporization, Crosslinking (FG-DVC) model are considered: 1) The decomposition of functional group sources in the coal yield the light gas species in thermal decomposition. The amount and evolution kinetics can be measured by TG-FTIR, the functional group changes by FT-IR and NMR. 2) The decomposition of a macromolecular network yields tar and metaplast. The amount and kinetics of the tar evolution can be measured by TG-FTIR and the molecular weight by FIMS. The kinetics of metaplast formation and destruction can be measured by solvent extraction, by Geissler plastometer and by proton magnetic resonance thermal analysis (PMRTA). 3) The molecular weight distribution of the metaplast depends on the network coordination number (average number of attachments on aromatic ring clusters). The coordination number can be determined by solvent swelling and NMR. 4) The network decomposition is controlled by bridge breaking. The number of bridges broken is limited by the available donatable hydrogen. 5) The network solidification is controlled by crosslinking. The changing crosslink density can be measured by solvent swelling and NMR. Crosslinking appears to occur with evolution of both CO_2 (prior to bridge breaking) and CH_4 after bridge breaking. Thus, low rank coals (which form a lot of CO_2) crosslink prior to bridge breaking and are thus thermosetting. High volatile bituminous coals (which form little CO_2) undergo significant bridge breaking prior to crosslinking and become highly fluid. Weathering, which increases the CO_2 yield, causes increased crosslinking and lowers fluidity. 6) The evolution of tar is controlled by mass transport in which the tar molecules evaporate into the light gas species and are carried out of the coal at rates proportion to their vapor pressure and the volume of light gases. High pressures reduce the volume of light gases and hence reduces the yield of heavy molecules with low vapor pressures. These changes can be studied with FIMS.

The paper describes how the coal kinetic and composition parameters are obtained by TG-FTIR, solvent swelling, solvent extraction, and Geissler plastometer data. The model is compared to a variety of experimental data in which heating rate, temperature, and pressure are all varied. There is good agreement with theory for most of the data available from our laboratory and in the literature.

INTRODUCTION

The question addressed by this paper is, can coal science be predictive? More specifically, is it possible, to accurately predict the way a coal behaves in a coal conversion process, given coal characteristics which can be measured in the laboratory. For example, Fig. 1 illustrates the behavior of coal in combustion. The left hand side of the figure shows a picture of a coal burning in a reactor where the coal is injected into the center of a hot air stream. The processes that occur are illustrated on the right hand side. Starting from the bottom, the figure represents the heating of the coal, coal softening, devolatilization, swelling, the ignition of the volatiles, the formation of soot, the burning of the volatiles, the ignition of the char, the combustion of the char, and finally the fragmentation of the char which determine the ultimate distribution of the ash particles. Can one qualitatively predict pyrolysis yields, swelling, soot formation, char reactivity, etc.?

As a second example, consider coal in a liquefaction process. The important step is the fragmentation of the coal macromolecule into small pieces. As shown in Fig. 2, that fragmentation takes place very quickly for a bituminous coal. The coal dissolves into the solvent, and the subsequent reactions between the solvent and the coal are all liquid-liquid phase interactions, which can occur very rapidly. In a lignite, this fragmentation process is prevented by low temperature crosslinking. The result is that

there is no quick solubilization of the coal, and most of the reaction takes place between the solvent and a solid crosslinked residue. Can one predict macromolecular fragmentation and crosslinking?

The research conducted during the last ten years suggests that many of the steps discussed above can be accurately predicted. Figure 3 shows the concept employed in our laboratory for developing predictive capabilities. We start with a set of laboratory characterization procedures that allow the appropriate kinetic and composition parameters for coal to be determined. Five kinds of experiments allow us to define the parameters for our model. The most important is the TG-FTIR, a thermogravimetric (TG) analyzer with the analysis of the evolved product by Fourier Transform Infrared (FT-IR) spectroscopy (1). This instrument allows us to determine the amount of the volatiles, their composition, the kinetics for their evolution, the reactivity of the char, and also the moisture and ash content of the coal. We also measure the solvent swelling ratio (2,3), the extract yield, and the fluidity in a Geissler plastometer (4), and employ nuclear magnetic resonance (NMR) (5), and Field Ionization Mass spectrometry (FIMS) data (6). These experiments determine the macromolecular network parameters for the model.

The model is the FG-DVC model (7,8). The letters FG stand for Functional Group, and DVC for Depolymerization, Vaporization and Crosslinking. The FG model considers certain functional groups in the coal which decompose to form the light gas species (9-12). At the same time, the DVC model describes the overall depolymerization of the macromolecular network which combines bridge breaking and crosslinking to produce fragments of the coal macromolecular (13-15). These fragments are then subjected to transport behavior, specifically the vaporization of the lightest fragments to form tar. The fragmentation process provides a second mechanism for the removal of functional groups from the coal. The model, whose parameters are determined in the laboratory at moderate temperatures and one atmosphere, can then be used to extrapolate away from the laboratory conditions to predict pyrolysis and combustion in high temperature reactions, or liquefaction at high pressure. Recently, we have explored extrapolation of the kinetics and reactions to low temperature geological transformations in coal beds (16).

The model for coal thermal decomposition has six basic concepts:

- Functional Groups (decompose to produce light gases)
- Macromolecular Network (decomposes to produce tar and metaplast)
- Network Coordination Number (determines fragment molecular weights)
- Bridge Breaking (limited by hydrogen availability)
- Crosslinking (related to gas evolution)
- Mass Transport of Tar (evaporation of light network fragments into light gases)

The first concept is that light gases are formed by the decomposition of certain functional groups in the coal. For example, methyl groups can decompose to form methane, carboxyl groups can decompose to form CO_2, etc. (9-12, 17-20). The second concept is that coal consists of a macromolecular network (2,3,7,13-15,21-36). This network is made up of fused aromatic ring clusters (which are described by their molecular weight) linked by bridges, some of which are relatively weak. There are some unattached parts of the network which can be extracted. Sometimes, there is also a second polymethylene component (37-41). When heated, this network decomposes to produce smaller fragments. The lightest of the fragments evaporate to produce tar (7,42), and the heavier fragments form the metaplast. These heavier molecules are the primary liquid fragments in liquefaction or the fragments that make coal fluid (8,43).

The third concept is that one of the most important properties of the network is its coordination number. The coordination number describes the geometry of the network by specifying how many possible attachments there are per aromatic ring cluster (node) (31-36). For example, a linear polymer chain has a coordination number of 2, because each fused aromatic ring has two possible attachments to link it in the chain. On the other hand, a "fish net" has a coordination number of 4, because there are four possible attachments at each node. The coordination number controls the molecular weight distribution of the network fragments at a given extent of decomposition. The extent of decomposition is specified by the probability that the possible attachments are made. For example, for 20% of broken

bridges, a linear chain is totally fragmented, while a "fish net" will have some holes but is almost totally connected. In describing the network, a crosslink is defined to occur at a node where there are more than two attachments. The coordination number is thus, related to the crosslink density. With no possible crosslinks, the coordination number is two. With increasing crosslink density the coordination number increases.

The second important property of the network is the fraction of possible attachments which are actually made. During thermal decomposition, this fraction is determined by the rates of bond breaking and crosslinking (7,15,44-47). The factors which control how many of the weak links can break are the rate constant and the amount of hydrogen that can be donated from the coal to stabilize the free radicals which form when the links break (10).

A competitive process with the bond breaking is the retrogressive process of crosslinking. Crosslinking reactions appear to be related to the evolution of certain gases (7,15,44,47). Specifically, for low rank coals, crosslinking at low temperature (prior to bridge breaking) seems to be related to the evolution of carbon dioxide (or possibly water). For coals of all rank, a higher temperature crosslinking event (following bridge breaking) seems to be related to the evolution of methane. At high temperatures, the evolution of hydrogen is also related to crosslinking.

The final concept is that the tar evolution is controlled by mass transport. Bridge breaking and crosslinking produce fragments with a molecular weight distribution. The lightest fragments can leave the coal melt by evaporation into the light gas species (7,42). The heavier fragments remain, forming the metaplast which controls the coal's fluidity.

The remainder of the paper describes how these concepts are incorporated into a practical predictive model. Section II considers the FG-DVC model in detail. It discusses each of the six concepts and the evidence for each assumption. Section III considers the experiments employed to obtain the model parameters, and Section IV compares predictions of the model with a variety of experimental data. Section V is the summary.

COAL PYROLYSIS MODEL

Functional Group Decomposition Model

Figure 4 illustrates the phenomena in coal thermal decomposition considered in the functional group model. The figure is not meant to describe the exact structure of coal or the exact chemistry which occurs in pyrolysis. It is meant to illustrate the kinds of structures that are being considered and the classes of phenomena that can occur. The important processes are the decomposition of the individual functional group to form the light gases and the competitive decomposition of the macromolecular network to form fragments, the lightest of which can evaporate as tar.

Figure 4a shows a representative piece of a Pittsburgh Seam coal macromolecule. The structure is based on measurements of the aromatic ring cluster size, the functional group composition and the elemental composition (48). The molecule consists of several fused aromatic ring clusters linked by labile bridges. The ring clusters have various functional groups attached to them. When the coal is heated, two things happen to the functional groups. The first is that certain functional groups can decompose to form light gases. The second is that fragmentation of the network, and removal of light fragments as tar, can cause the same type of functional group to be removed as part of the tar. So, there are two parallel processes for the volatilization of the functional groups.

The way the coal behaves during pyrolysis is illustrated in Fig. 4b. The carbon-carbon aliphatic bridge in the upper left hand corner of the molecule (labeled 2) broke and picked up hydrogen to form two methyl groups. This process creates a fragment which is light enough to evolve as tar. There is also independent decomposition of functional groups to form light gases. The carboxyl group that was shown in the middle of Fig. 4a is shown as a carbon dioxide evolving in Fig. 4b. Methyl groups have decomposed to form methane, there has been a condensation of hydroxyl groups to form water and an ether link (labeled 3), mercaptans decompose to form H_2S, etc.

The evidence for this description is as follows: 1) for bituminous coals and low rank coals heated rapidly, the tar is strikingly similar in elemental and functional group composition to the parent coal (9,10,48-50). The tar appears to consist of representative fragments of the parent coal macromolecule; 2) there is a correlation between the decrease in the functional group sources in the char and the evolution of specific gases (9-12); 3) there is a systematic variation in functional group composition with rank, and this variation is correlated with the evolved gas composition.

While there is good evidence for the above description, the details of the chemistry are not yet well understood. Also, tar produced from low rank coals at low heating rates appears to be significantly different in composition from the coal (51) and is probably dominated by polymethylenes.

Macromolecular Network Decomposition Model

The concept of a macromolecular network decomposition model, is illustrated in Fig. 5, which recently appeared in a paper by Grant and coworkers (36). The figure represents aromatic ring clusters with four possible attachments to their neighbors, arranged in a "fish net" type network, (a network with a coordination number of 4). Figure 5a illustrates what happens when 20% of the possible attachments are broken. As can be seen, there are only three fragments which are created, shown by the clusters with boxes around them. The breaking of 20% of the bridges produces very little fragmentation of the network. On the other hand, consider in Fig. 5b what happens when 45% of the bridges are broken. Now, there is a much higher concentration of fragments and the fragments have a molecular weight distribution from monomers up to 7-mers (consisting of 7 fused ring clusters linked together). The lightest of these fragments, monomers, dimers, and trimers can evaporate into the light gas species and are removed from the coal particles as tar. The heavier fragments make up the metaplast. The lightest of these can be extracted using solvent, while others are too heavy to be extracted. The presence of a sufficiently large fraction of these fragments are what makes these materials fluid.

Network Coordination Number

The importance of the network coordination number is illustrated in Figs. 5 and 6. In Fig. 5a with 20% of the bridges broken in a "fish net", only a small number of fragments are produced, and they are all monomers. On the other hand, if 20% of the bridges in the linear chain are broken, 100% of the material becomes fragments and there will be many dimers, trimers, etc. Thus, the molecular weight distribution of the fragments depends very strongly on the coordination number.

In Fig. 5, the molecular distribution was computed using Monte Carlo calculations in which a representative network is set up in computer memory and the fragment molecular weight distribution is calculated after the broken bridges are randomly distributed. Alternatively, a technique called percolation theory allows a closed form analytical solution of the molecular weight distribution as a function of the number of actual attachments per ring cluster.

Figure 6 shows percolation theory calculations for networks with two different coordination numbers: Fig. 6a is for a coordination number of 2.2 and Fig. 6b is for 4.6. The variable σ is one less than the coordination number. The figure shows the calculated distributions of: i) monomers, ii) up to trimers (i.e., monomer, dimer, trimer) representative of what might be evolved as tar for a ring cluster size of 300 Daltons, iii) the yields of all n-mer up to ten representative of extractable material, and 4) the yield of all n-mers. These are plotted as a function of α, which is the average number of bridges per fused aromatic rings. This term α is equal to the probability, p, that a bridge is occupied times the coordination number of the network divided by two, $\alpha = p(\sigma + 1)/2$. As can be seen, there is a very different distribution of fragments depending on the coordination number. For example, at a value of $\alpha = 0.9$, the network with coordination number 4.6 has most of the fragments in the tar, with only a small number of n-mers between 3 and 10 and almost no n-mers above 10. On the other hand, for a network with a coordination number of 2.2 at $\alpha = 0.9$, there is a smaller number of monomers, a somewhat smaller concentration of tar, but a much higher concentration of n-mers up to 10 and a 100% yield of all n-mers. In other words, for 0.9 bridges per cluster, most of the molecules had decomposed to produce fragments of one size or another.

The DVC model was originally implemented using a Monte Carlo solution method, which allows an arbitrary network geometry. Percolation theory, however, offers significant benefits in computational speed and reproducibility, at the cost of restricting the network geometries.

As we shall see below, in the Monte Carlo version of the model, the starting network is represented by linear chains of monomers (6-12 aromatic clusters) with some amount of crosslinking which tie the chains together. Thus the starting network has a coordination number between 2 (straight chains) and three or more (fully cross linked). As pyrolysis proceeds, the linear chain bonds (bridges) are broken, and crosslinks (the side bonds) are formed. Thus, the coordination number, or degree of branching, increases with extent of pyrolysis. The conventional percolation theory models of coal decomposition do not model this feature. With conventional percolation theory, one can make any identification of the various chemical bonds with the percolation lattice bonds, so that the probability of a bond being occupied tracks the chemistry; but the occupied bonds must be randomly distributed within the lattice. The structure cannot be converted from "chain-like" to "fishnet-like".

The DVC model predicts, and experiments confirm, that there are more than one kind of bond (bridges and crosslinks) which have different coordination numbers, and independent probabilities of being broken. To take advantage of the benefits of percolation theory, we have extended percolation theory on a Bethe lattice (one with no loops) to use two independent sub-networks, as illustrated in Figure 7 (32). In the Figure, double lines represent one of the bond types, while single lines represent the other. As can be seen by comparing Fig 7a and 7b, this lattice has the desired feature of modeling a transition from chain-like structures (a) to fishnet structures (b). The mathematics of this 2-bond percolation theory follows closely that of the standard theory (32). A comparison of the results obtained from the 2-bond percolation theory agree well with those obtained from the original Monte Carlo calculations, as will be discussed in the Results Section.

Bridge Breaking and Hydrogen Utilization

There are two questions with respect to bridge breaking: what is the bridge breaking rate and how many bridges break. Pyrolysis rates have been reviewed by a number of authors (10,52-54). One of the problems in pyrolysis over the last two decades is a very wide variation in the reported rates for either weight loss or tar evolution in pyrolysis.

Figure 8a presents several of the extremes in rates reported prior to 1985 for high heating rate experiments (10,55-58). At 800°C there is almost a four order of magnitude variation in the rate constant which has been reported. An analysis of the data shows that one can not ascribe this sort of variation in kinetics to variations in the coal type, because investigators who measured more than one coal type found that the variations in kinetics rates among coals are typically within a factor of 10. So there has to be another explanation for why there is such a wide variety of reported rates. The answer appears to be the knowledge of the coal particle temperatures (53,54,59-62). Almost none of the experiments are done with direct measurements of the coal particle temperature. For entrained flow reactor experiments, the temperature is usually calculated and the calculations depend critically on the rate of mixing of the preheated gases with the coal stream. A factor of two error in the heating rate can lead to errors of hundreds of degrees celsius in the particle temperature during pyrolysis. For heated grid experiments, temperature measurements are made with a thermocouple and the inference is made that the thermocouple temperature is the same as the coal particle temperature. Recent reviews of experiments for Pittsburgh Seam coal heated at 1000°C/sec show a wide variation in pyrolysis temperatures, suggesting that this is just not a good assumption (60,63).

Since 1985, several experiments have been performed in which coal particle temperatures were measured during pyrolysis (12,53,61,62,64). Careful experiments have also been performed at several low heating rates where the thermocouple temperature is a good measure of the coal particle temperature (65,66). As can be seen from Fig. 8b, the data are much more tightly grouped. There is a systematic variation with the rank of the coal and the kinetic rate constants appear to have an activation energy between 45 and 55 Kcal. This is the magnitude one would expect for the kind of labile bridges depicted in Fig. 4 (14,67).

Besides the kinetic rate for bridge breaking, one needs to know the number of bridges that can be broken. The number depends upon the amount of hydrogen that is available to stabilize the free radicals formed when bridges break. How the hydrogen utilization controls the amount of tar and its hydrogen concentration is illustrated in Fig. 9. The figure is based on the following consideration: every time a bridge is broken, the available hydrogen is used to stabilize the free radicals. Two radicals are assumed to be stabilized per tar molecule. If the tar is made up of large fragments, the utilization of hydrogen per unit weight of tar is very efficient. On the other hand, if the tar consists of small molecules, the utilization of hydrogen is much less efficient. The figure shows the results for 0.3% hydrogen in the coal available for donation to the tar. The figure presents the yield of tar and the percent of additional hydrogen in the tar as a function of the average molecular weight in the tar. For an average molecular weight of 100 Daltons, 15% tar is produced. The amount of additional hydrogen in the tar is 2%. On the other hand, at an average molecular weight of 300 Daltons the yield is up to 45%, while the weight percent of additional hydrogen per unit mass is only 0.7%. The average molecular weight of the tar is affected by crosslinking, pressure, heating rate, and bed geometry.

Crosslinking

During pyrolysis, another important process occurs besides bridge breaking. It is the process of crosslinking, where new bonds are formed between the fused aromatic ring clusters. One of the ways of measuring the crosslink density is through solvent swelling (2,3), in which a solvent (e.g., pyridine) is used to swell the char or coal (7,15,44-47). To understand how solvent swelling indicates the crosslink density, consider the analogy of an air mattress. An air mattress is stitched in long rows along the length of the mattress. When the mattress is inflated there are several connected small tubes, instead of one big round tube. The small tubes have a smaller volume than one large tube and the volume can be used to infer the limiting circumference of the tubes. In a similar manner, the addition of the solvent to a coal indicates the circumference of linked molecules that make a loop to limit the swelling. Since it is crosslinks (more than two attachments per cluster) that allow loops to be formed, the amount of swelling indicates the average molecular weight between crosslinks.

Figure 10 shows the behavior of the solvent swelling ratio as a function of the char temperature for coals of several ranks. Chars are produced by heating up to the indicated temperatures at 30°C/min in an inert atmosphere and then cooling. These chars are subjected to solvent swelling experiments which determines the volume of swollen coal divided by the unswollen volume. Coals have solvent swelling ratios as high as 2.7. As char is formed, new crosslinks reduce the swelling ratio to unity. The solvent swelling ratio in Fig. 10 is normalized. The parameter x is the difference in solvent swelling ratio between the coal and the char divided by the maximum differences that can be achieved. This normalization allows us to compare different coals with different starting solvent swelling ratios in a convenient manner. Figure 10 presents 1 - x as a function of the char temperature. If x = 0, we have a material that swells the same as coal and if x = 1 we have a fully crosslinked char.

There is a wide variation in behavior depending upon rank. This rank dependence of the crosslinking behavior was first noted by Suuberg and coworkers (44) who measured a lignite and a bituminous coal and found the same sort of difference that has been exhibited here. The lowest rank coal, Zap lignite, is shown by the open squares. At temperatures as low as 200°C, the char starts to undergo crosslinking, loosing most of its solvent swelling properties by a temperature of 400°C. It is between 400 and 500°C that most of the pyrolysis weight loss is occurring for this material. Thus, for a low rank coal, the crosslinking occurs well in advance of the bridge breaking.

For higher rank coals, the crosslinking event is delayed relative to bridge breaking. For a highly softening bituminous coal like Pittsburgh Seam coal, or Kentucky No. 9, we find the material swells even more as it is heated into the region of pyrolysis, and only looses its solvent swelling properties after most of the weight loss has occurred in pyrolysis. There is, thus, a very strong rank dependence of the crosslinking behavior. Low rank coals crosslink early, prior to bridge breaking, while high rank coals undergo crosslinking after most of the bridge breaking has taken place.

The results of solvent swelling experiments are not unambiguous because the solvent swelling ratio depends on two things: 1) the crosslink density and 2) the solvent interaction parameter. This

parameter can change with the functional group composition of the coal. Since the functional group composition will change as the coal pyrolyzes, the change in solvent swelling ratio could be due to the change in the functional group composition, not crosslinking. However, an analysis of how much the solvent swelling ratio may change with the functional group composition indicates that the kind of drastic change from a solvent swelling ratio of 2.7, typical for coal, down to 1 for char is not likely to occur for the small changes in the functional group composition with low temperature pyrolysis (47).

Another way of investigating the crosslink density is by experiments done using nuclear magnetic resonance (NMR). The work was performed at the University of Utah in collaboration with Solum and coworkers (68). Results of the NMR experiments are shown in Fig. 11. The NMR experiments employ cross polarization with magic angle spinning and dipolar dephasing (5). Dipolar dephasing allows the determination of the functional group form of the carbons that are being studied. When all the different kinds of bonds are considered, it is possible to determine an average molecular weight for the ring clusters and also the average number of attachments per ring cluster. In Fig. 11, the average number of attachments are compared to the solvent swelling data for Pittsburgh Seam bituminous coal and a North Dakota lignite. The average number of attachments determined by the NMR are also normalized to determine an NMR index which can be compared to 1 - x. Figure 11a compares the results for the lignite. The change in crosslink density determined by NMR is in reasonable agreement with that determined by the solvent swelling ratio. As can be seen, the material starts to crosslink at a reasonably low temperature and is almost completely crosslinked by a temperature of about 700 K (427°C), prior to significant bond breaking. For the Pittsburgh Seam coal shown in Fig. 11b the NMR index is in reasonable agreement with the solvent swelling ratio, and in this case both indices show that the char has not undergone appreciable crosslinking by a temperature of 700.

To develop an understanding of the chemistry of crosslinking, we attempted to determine whether the addition of crosslinks could be correlated with any other observation, specifically, the evolution of gases. In the initial work of Suuberg and coworkers (44), they noted that the one gas species which correlated with the early creation of crosslinking in the lignite was carbon dioxide.

Figure 12 shows the results obtained in our laboratory. Figure 12a presents the parameter x as a function of the carbon dioxide yield divided by 44 so that it is on a molecular basis. In Fig. 12 we have plotted x rather than 1 - x which was plotted in Figs. 10 and 11. For a wide variety of experiments (some at high heating rates and some at low heating rates) there is an very reasonable correlation between the loss of swelling and the appearance of carbon dioxide in pyrolysis. For all the low rank coals studied, there appears to be a good correlation between the appearance of crosslinks and the appearance of carbon dioxide. The line shown in Fig. 12a is from our FG-DVC model, where one crosslink is assumed for each carbon dioxide evolved.

For a higher rank coal, which does not produce significant yields of CO_2, a different correlation is observed. Figure 12b compares the normalized solvent swelling ratio for a Pittsburgh Seam coal with the evolution of methane divided by 16. There is a good correlation between these two parameters for chars created at a number of different temperatures at high heating rates. The line in Fig. 12b is from the FG-DVC model, where it is assumed that one crosslink is formed for each methane evolved.

We examined the correlation of the loss of swelling with other parameters and found the correlation between carbon dioxide and methane to be the best. There is a correlation for low rank coals between the formation of crosslinks and the water evolution, but not quite as good as for CO_2. There was no good correlation for high rank coals between crosslinking and tar evolution.

Three experiments which exhibit the phenomena of bridge breaking and crosslinking are presented in Fig. 13. Figure 13a presents the proton magnetic resonance thermal analysis (PMRTA) experiment done at CSIRO by Lynch, Sakurovs and coworkers (69-71). This experiment, which measures the relaxation time for protons, can distinguish between protons attached to mobile molecules (which are free to rotate) and those attached to a ridged lattice. The higher the concentration of mobile protons, the lower the values of the parameter M_{2T}. The data taken at 4°C/sec was provided by Dr. Sakurovs (72). The decrease in M_{2T} at low temperatures appears to be associated with melting, the sharp drop

in M_{2T} above 400°C is due to bridge breaking and the sharp increase of M_{2T} above 440°C is due to the crosslinking.

Figure 13b shows fluidity data measured with a Geissler plastometer for the same coal at a similar heating rate (3°C/sec) (4). While the fluidity below 400°C is probably due to melting, above 400°C bond breaking becomes important, while above 440°C crosslinking resolidifies the network.

Figure 13c presents data of Fong (73) on the extract yield in chars produced at a high heating rate of 640°C/sec. The maximum extract yield occurs at a much higher temperature than for the other two experiments due to the high heating rate. The increase in extract yield is due to bridge breaking and the decrease to crosslinking.

Transport

The above discussion shows how bridge breaking and crosslinking, can fragment the macromolecular network and allow small pieces to be formed. The evolution of tar is controlled by the formation of these small fragments and their transport out of the metaplast. In our FG-DVC model, we've assumed a very simple transport process. The assumption is that the fragments reach their equilibrium vapor pressure in the light gas species and are removed from the metaplast by convective transport in the light gas species (7). In a highly fluid coal, the expulsion of the light gases occurs by bubble transport. In a low rank thermosetting coal the transport of the light gas species is through the pores. In either case, the degree to which the tar molecules are transported depends upon the volume of light species that evolve and the vapor pressure of the molecule. The low macromolecular weight species that have high vapor pressure are therefore easily transported while heavy molecular weight species are not. The result is that the tar for a bituminous coal pyrolyzed at 1 atmosphere or below consists of molecules up to about 800 Daltons. As the pressure is increased the volume of the light gases is reduced and those marginal heavy products, which were previously transported at one atmosphere, can no longer be transported. Thus, as pressure is increased, the average molecular weight of the tar is reduced. The amount of tar is also reduced because of the reduced efficiency of hydrogen utilization.

For low rank coals, low temperature crosslinking increases the effective coordination number of the network and only small molecules are produced. The yields are low and pressure has little influence on the yield or molecular weight distribution.

Summary of FG-DVC Model

Figure 14 summarizes the FG-DVC model. In Fig. 14a we start with an assumed macromolecular network. In the Monte Carlo version of the model, each piece of this network is actually described in the computer memory. The description of the network contains the molecular weight of the aromatic ring clusters (shown as the number in the circles), and the crosslinking density (shown by the vertical double line). The potential number of labile bridges (related to the donatable hydrogen) are indicated by the single horizontal lines. The starting molecule is constructed from linear chains of a certain length (typically between 6 and 12 aromatic ring clusters) connected by the appropriate number of crosslinks. When this is done a certain number of the chains may be unattached to the rest of the macromolecular network. These are the guest molecules whose molecular weight is less than 3000 Daltons and would be pyridine soluble. The length of the chains is adjusted to obtain the proper pyridine solubles. The number of crosslinks is picked to get a coordination number which yields the right ratio of tar to heavier fragments (e.g., extracts) in the metaplast. The number of labile bridges (amount of donatable hydrogen) is picked to get the proper tar yield in the TG-FTIR experiments.

Figure 14b considers what happens during pyrolysis. As the temperature increases, some of the weak bridges (which are the single horizontal lines), can break according to the bridge breaking rate. The hydrogen limitation is accomplished by requiring that for each bridge that is broken, another one of the labile bridges becomes an unbreakable bridge as its hydrogen is used to stabilize the free radicals caused by the broken bridges. Thus, for each broken bridge, two of the labile bridges are consumed. The broken bridges and new unbreakable bridges are distributed randomly.

In the model, the crosslinking is assumed to correlate with the CO_2 and methane evolution. The evolution of these species is determined from the functional group part of the model and one crosslink is inserted randomly for each carbon dioxide and each methane group which is evolved. If bridge breaking dominates over crosslinking, the macromolecular network is broken up into smaller fragments. On the right hand side of the figure, the molecular weight distribution which results from the bridge breaking and crosslinking events is shown. Molecules below 3000 Daltons are increased, the lightest molecules escape as tar, and the rest of the network is described as pyridine insoluble.

Figure 14c shows the network at the conclusion of the pyrolysis process. When all the labile bridges are consumed, the decomposition of the network is complete. All of the network is completely connected by unbreakable bridges, and is highly crosslinking. All the previously loose fragments have been incorporated into the network by crosslinking or have escaped as tar.

ANALYSIS OF COMPOSITION AND KINETIC PARAMETERS

In this section, the laboratory characterization to determine the model parameters is considered. An analysis by TG-FTIR is employed to determine kinetic rates and functional group compositions. Solvent swelling, solvent extraction, and fluidity measurements in a Geissler plastometer are employed to obtain information on the molecular weight distribution of the metaplast and hence determine the network parameters. NMR and FIMS are used to determine the molecular weight of the ring clusters. These measurements are considered below.

TG-FTIR

Apparatus - As indicated in Fig. 3, TG-FTIR analysis of coal is employed to obtain the composition and kinetic parameter for the model. A schematic of the instrument is presented in Fig. 15. Its components are as follows: a DuPont™ 951 TGA; a hardware interface (including a furnace power supply); an Infrared Analysis 16 pass gas cell with transfer optics; a MICHELSON MB Series FT-IR; (Resolution: 4 cm^{-1}, Detector: MCT); and a PC-AT compatible computer. The cell is connected without restrictions to the sample area and a helium sweep gas is employed to bring evolved products from the TGA directly into the gas cell. This instrument is now available as the TG/plus from Bomem, Inc.

The most difficult volatiles to analyze are the tars which condense at room temperature. In the TG/plus, the rapid cooling from the high thermal conductivity helium sweep gas causes these products to form an aerosol which is fine enough to follow the gas through the analysis cell. The aerosol is also fine enough that there is little scattering of the infrared beam and it thus appears as though the tar was in the gas phase.

As an example of the analysis procedure, the pyrolysis and oxidation of a bituminous coal is described. More detail can be found in Ref. 1. Figure 16a illustrates the weight loss from this sample and the temperature history. A 25 mg sample of Pittsburgh Seam coal, loaded in the sample basket of the DuPont™ 951, is taken on a 30°C/min temperature excursion in the helium sweep gas, first to 150°C to dry, then to 900°C for pyrolysis. After cooling, a small flow of O_2 is added to the furnace at the 57 minute mark and the temperature is ramped to 900°C for oxidation.

During this excursion, infrared spectra are obtained once every forty seconds. As discussed previously (1) the spectra show absorption bands for CO, CO_2, CH_4, H_2O, SO_2, COS, C_2H_4, HCl, and NH_3. The spectra above 400°C also show aliphatic, aromatic, hydroxyl, carbonyl and ether bands from tar. The evolution of gases derived from the IR absorbance spectra are obtained by a quantitative analysis program which employs a database of calibration spectra for different compounds. The routine decides which regions of each calibration spectrum to use for best quantitation with the least interferences. A correlation between the sample spectrum and the reference spectrum is performed to determine gas amounts. A database of integration windows is also available for tracking functional groups absorptions. Tar quantitation is discussed in Ref. 1. The routine is fast enough so that the product analysis can be performed and displayed every 40 seconds during the actual experiment.

Figure 16b illustrates the integral of the evolution curves to obtain cumulative evolved product amounts. Because the data are quantitative, the sum of these curves match the weight loss as determined by the TGA balance. Discrepancies occur because of components such as H_2 which cannot be seen by IR. When O_2 is introduced, the balance shows a net gain in weight due to O_2 chemisorption.

Determination of FG-DVC Model Parameters - The kinetic and composition parameters for the FG-DVC model are obtained from the TG/plus pyrolysis cycle. The pyrolysis cycle for Illinois No. 6 coal (Argonne premium sample) is presented in Fig. 17. Figure 17a presents the weight loss and temperature profile. Also presented (dashed line) is the sum of species (tar, CH_4, H_2O, CO_2, CO, SO_2 NH_3, C_2H_4, and COS). The sum of species is within a few percent of the weight loss.

The water evolution (Fig. 17b) consists of a low temperature moisture peak followed by a pyrolysis peak. To fit the wide pyrolysis peak by the FG submodel, three sources are used for H_2O. Each source evolves according to

$$dW_i/dt = k_i W_i(char) \quad (1)$$

were W_i is the gas species and $W_i(char)$ is the amount of the functional group source remaining in the char. The rate constant, k_i is given by an Arrhenius expression of the form

$$k_i = A_i \exp((-E_i \pm \sigma_i)/RT) \quad (2)$$

where A_i is the frequency factor, E_i the activation energy and σ_i the distribution in activation energies. Two sources are employed for CH_4, and three sources for CO and CO_2. Note the elimination of the calcite CO_2 evolution peak (Fig. 17d) and the increase in tar (Fig. 17c) for the demineralized coal.

To obtain the model parameters, the model is fit to the TG/plus data at three heating rates (3, 30, and 100°C/min). When there are multiple sources for a given species and the sources have overlapping peaks, the determination of parameters is not unique and some rules must be assumed. Based on chemical arguments, A is restricted between 10^{12} and 10^{15} sec^{-1}. Also, the preexponential for a given species pool is assumed rank invariant based on the observed rank variation of the evolution curves. As the coal is increased in rank, the leading edges and the early peaks (Extra Loose or Loose pools) shift to higher temperatures while the trailing edge (Tight or Extra Tight pools) remain at the same temperature. An example of this is shown for water for five coals in Fig. 18a (16). From this figure it appears that the shift in the evolution curve with rank can be explained by the geological aging process. With increasing aging temperature and time, the maturation process gradually evolve the loosely bounded functional groups and leaves the tightly bounded groups intact.

The shift can be simulated by pyrolyzing a species described by a distribution of activation energies (Eq. 2) up to different bed temperatures. An example is shown in Fig. 18b. Starting with the evolution profile for Zap lignite, the coal is assumed to pyrolyze at 10°C/million years up to temperatures of (60, 120, 150, and 180°C). The resulting geologically aged samples is simulated using the TG/plus temperature profile and the predicted results are plotted. The curves for geological aging at 120, 150, and 180°C are similar to the actual TG/plus evolution curves shown in Fig. 18a for Illinois No. 6, Pittsburgh, No. 8, and Upper Freeport, respectively. Thus, the frequency factor is assumed to be constant as the rank increases, and the activation energy of the pool increased with increasing coal rank to fit the data. We find that the activation energy of tight pools generally change with rank much less than do the loose pools.

A typical comparison of theory and TG-FTIR experiments is shown in Fig. 19 for the Pittsburgh Seam coal for one heating rate. The amounts of the functional group pools are obtained from this procedure. The resolution of the hydrocarbon evolution into paraffins, olefins, ethane, ethylene, propane, and propylene is done in other experiments if required. Figure 20 compares the theory and experiment for three heating rates for weight loss, tar evolution, and methane evolution. The kinetic parameters are derived from these experiments. The agreement between the theory and experiment is quite good.

We have applied these curve fitting procedures for the eight Argonne coals according to the rules cited above (i.e., frequency factor between 10^{12} and 10^{15}/sec and constant for a given gas species pool independent of coal rank). Results for the rates for bond breaking, the evolution of methane (two pools), CO (three pools), CO_2 (three pools) and H_2O (three pools) are presented as a function of the coal's oxygen concentration in Fig. 21. As can be seen, there is a systematic increase in activation energy with increasing rank. The variation in activation energy is maximum for the loose pool and reduces as the activation energy increases. The amounts for these pools are presented in Fig. 22. There is a systematic variation in the amounts with rank.

Solvent Swelling, Extraction and NMR

Solvent swelling and extraction data for the Argonne coals are presented in Table 1. As discussed above, the extract yield is employed to determine the length of the chains (Monte Carlo) or the starting bond probabilities (percolation) used in the model. There appears to be some problem in employing this approach for the highest rank coals (Pocahontas and Upper Freeport). The swelling and extract yields for these coals in pyridine appears to be limited by weak crosslinking (other than hydrogen bonding) forces which are not eliminated by pyridine.

The solvent swelling ratio has been employed to determine the crosslink density (2,3,24-29). The various theories and values for the solvent interaction parameter (24-29) suggest that there are between 4 and 8 ring clusters between crosslinks, indicating a value of $\sigma + 1$ between 2.13 and 2.25 (32). NMR results of Solum et al. (5) for the number of bridges and loops suggest a value of $\sigma + 1$ of between 2 and 3, so a value in the neighborhood of 2.5 seems reasonable. However, the uncertainty of these determinations is too large to employ them in the model. The crosslink density is instead considered an adjustable parameter employed to fit the fluidity data.

Geissler Fluidity

As discussed above, the crosslink density controls the effective coordination number of the network, and hence the molecular weight distribution and amount of the fragments. For bituminous coals, it is the initial crosslink density which is important, since few new crosslinks are formed prior to pyrolysis. A recent theory for fluidity was developed based on the liquid fraction in the coal computed by the FG-DVC model (8,43). Measurements of the tar and the fluidity thus provide a constraint on the molecular distribution of the fragments and hence on the crosslink density.

Figure 23 presents a comparison of theory and experiment for four of the Argonne coals with the kinetic parameters fit from TG-FTIR data. The fitting procedure for fluidity and tar determines a unique combination of the crosslink density and donatable hydrogen.

Monomer Molecular Weight Distribution

The molecular weight distribution of the monomers is chosen based on the ring cluster size determined by NMR (5) and the results of the model checked with FIMS data (6).

RESULTS

Volatiles Evolution

A good test of the validity of using the TG-FTIR method over a range of low heating rates to obtain kinetic parameters is the ability to use the kinetic parameters to extrapolate to high heating rate conditions. Figure 24 presents results for Illinois No. 6 coal (obtained from Combustion Engineering) using the complete FG-DVC model and the most recent kinetic and composition parameters derived from the TG/plus (65). The predicted rates of evolution for each species are in good agreement with the observed rates except for water where moisture sometimes creates measurement errors. The data were obtained in the heated tube reactor where FT-IR emission and transmission measurements of coal particle temperatures determined the heating rate to be over 20,000 K/sec.

Char

A number of char characteristics can be measured and compared with the model. These include fluidity (already discussed in Section III), functional group composition, crosslink density, PMRTA, and extract yield. These are discussed below.

- Functional Group Composition - The functional group composition can be determined by FT-IR (74-77) or NMR CP-MS with dipolar dephasing (5). A set of chars was prepared by heating Pittsburgh Seam coal up to temperatures of 200, 300, 400, 500, and 600°C at 30°C/sec and the chars were characterized (68). Figure 25 compares the theory with NMR and FT-IR measurements. The fractions of aliphatic and aromatic carbons are compared in Fig. 25a, and aliphatic, aromatic, methyl, and hydroxyl hydrogens in Fig. 25b. Figures 25c and 25d compare the theory and FT-IR measurements for the same quantities (except methyl and aliphatic hydrogen are lumped together). The tar yield (Fig. 26a), and methane yield (Fig. 26b) are presented for comparison. The model predictions are in excellent agreement with the data.

Crosslink Density - The application of the volumetric swelling ratio to obtain the changing crosslink density in the char was discussed in Section II. Comparison with theory was discussed in Ref. 7. Figure 26c compares the theory and experiment for the set of chars in Figs. 25 and 26. The agreement is good. Figure 27 compares the theory and experiment for two coals (Zap lignite and Pittsburgh Seam). The theory predicts the early crosslinking in Zap lignite (related to CO_2 evolution) not seen for the bituminous coal. The agreement between theory and experiment is good except that the increase in 1 - x for the Pittsburgh Seam coal in Fig. 27 is not predicted.

The NMR data also provide a direct measurement of the number of attachments per cluster (5). Figure 28 presents data (68) for total number of attachments (which includes peripheral groups, bridges, and loops), and just bridges and loops (B & L) as a function of final temperature for Pittsburgh Seam coal heated at 30°C/min to the indicated temperature. The FG-DVC model predicts the number of B & L. This quantity (near 2 for coal) is the coordination number, suggesting that coal is quite chain-like. There is little change in B & L up to 400°C. B&L increased at 500°C and above where crosslinking related to methane evolution is believed to occur.

Notice that the total number of attachments changes very little. This would be reasonable if the methane peripheral groups were replaced by bridges in substitution reactions. This is believed to be the reason for the correlation between methane evolution and crosslinking.

PMRTA - Proton magnetic resonance thermal analysis (PMRTA) is employed at CSIRO as an alternative to fluidity measurements. The measurement of proton mobility can distinguish protons on molecules free to rotate from protons on a rigid lattice. The molecules ability to rotate depends on its freedom from the network (i.e., it must be unattached or attached at only one place) and on the mobility of free molecules to rotate (which depends on the temperature). From the measured M_{2T} values, a "mobile" liquid fraction can be defined by the expression (72)

$$\text{Liquid Fraction} = \frac{M_{2T}\,(\text{room temperature}) - M_{2T}(T)}{M_{2T}\,(\text{room temperature})}$$

At sufficiently high temperature, when the free molecules have sufficient energy to rotate, this quantity should be equal to the FG-DVC liquid fraction. Figures 29a and 29d, compare the measured and predicted liquid fraction using both the Monte Carlo and percolation models. As expected, the theory and experiment do not agree at low temperature, but there is good agreement on the softening temperature, peak fluidity temperature, and solidification temperature. The liquid amounts in the two theories are defined differently and so the absolute amounts do not agree. Also shown for comparison are the fluidity and tar evolution curves for the same coal at a similar heating rate. The agreement between the data and both theories is good.

Extract Yields - Figure 30 compares the FG-DVC predictions to the data of Fong et al. (73) on total volatile yield and extract yield as a function of temperature in pyrolysis at 0.85 atm. The experiment was performed in a heated grid apparatus at heating rates of 640°C to 1018 K, with variable holding times and rapid cooldown. The predictions in Fig. 30 are in reasonable agreement with the data. The predicted extract yields are not as high as the measured yields. However, such high yields of extracts have not been duplicated by others, and there is some possibility that the extracted fraction also contains some colloidal material.

Weathering - Oxidation of a Pittsburgh Seam coal in our laboratory was performed at 80°C for 10, 20, and 62 days. In our model, the loss of fluidity with increasing oxygen concentration is related to the increase in CO_2 evolution and hence increases in low temperature crosslinking. To determine the CO_2 evolution, measurements were made in the TG-FTIR (78). The data in Fig. 31a shows that the low temperature CO_2 evolution was significantly increased after 10 days of oxidation, becoming comparable to that for Illinois No. 6. After 20 days, the early CO_2 evolution was larger than that for the Utah bituminous coal. After three months at 110°C the CO_2 evolution was comparable to that of a lignite. When these increased CO_2 yields were incorporated in the simulation for the oxidized Pittsburgh Seam coal's fluidity, the maximum fluidity was reduced. We compare our predicted maximum fluidity with the measurement of Wu et al. (79) for comparable coal and oxidation treatment in Fig. 31b. The agreement is quite reasonable.

Predicted Molecular Weight Distribution in Char - The dominant event in determining the char's properties is the starting and low temperature crosslinking behavior. Figures 32a and 32b compare the predicted molecular weight distributions in the char for Zap lignite and a Pittsburgh Seam bituminous coal. The bituminous coal (Fig. 32a) exhibits substantial fragmentation of tar precursors (n-mers 1-3), extracts (n-mers 4-10), and liquids (n-mers 11-100). On the other hand, the initial crosslink density in the lignite, and the subsequent increase due to CO_2 related crosslinking, allows almost no n-mers except monomers, dimers, and trimers to be formed (Fig. 32b). These predictions of the model are related to the extract yields, PMRTA analysis fluidity, and tar yields.

Tar

Molecular Weight Distribution - The tar is evolved from the lightest fractions of the metaplast and depends on the metaplast distribution and the transport. This is illustrated in Fig. 32c and 32d, which are the predicted tar distribution for a bituminous coal and a lignite (two cases discussed above). For the bituminous coal, the upper molecular weight is limited only by the vapor pressure for the large molecules. For the lignite, the metaplast distribution limits the amount and molecular weight distribution.

Figures 33c, and 33d show measurements for the Pittsburgh Seam bituminous coal and the Beulah, Zap lignite pyrolyzed in the FIMS apparatus. The data have been summed over 50 amu intervals. While the Pittsburgh bituminous coal shows a peak intensity at about 400 Daltons, the lignite peak is at 100 Daltons. The predicted average tar molecular weight distributions are in good agreement with FIMS data as shown in Figs. 33a and 33b. Since both tar distributions are from the same monomer distribution, the enhanced drop off in amplitude with increased molecular weight for the lignite compared to the bituminous coal must be due to early crosslinking and transport effects in the lignite.

Pressure Effects - The prediction effect of pressure on the tar molecular weight distribution is illustrated in Figs. 34a and 34b. Pressure enters the model through the transport assumption. The internal transport rate is inversely proportional to the ambient pressure. The reduced transport rate reduces the evolution rate of the heavier molecules. Therefore, the average molecular weight and vaporization "cutoff" decrease with increasing pressure. The trends are in agreement with observed tar molecular weight distributions shown in Figs. 34c and 34d. The spectra are for previously formed tars that have been collected and analyzed in a FIMS apparatus (6). The low values of intensity between 100 and 200 Daltons are believed to be due to loss of these components due to their higher volatility.

Yield - The tar yields are measured in the TG-FTIR. Figure 35 compares the measured and predicted yield as a function of temperature. The agreement is good except for the low temperature evolution

of guest molecules, which is not well predicted in the standard model. Improvements to predict this early peak have been made (8).

Network Parameters

Figure 36 presents the adjustable network parameters which have been chosen to fit the tar evolution and fluidity data as functions of the oxygen concentration. The oligomer length and the molecular weight between crosslinks increase smoothly with rank. The concentration of available hydrogen for ring stabilization has a maximum for the high volatile bituminous coals.

In Fig. 37, we compare the predicted and measured extract yield and the predicted and estimated molecular weight between crosslinks. The crosslink density for the bituminous coals is within the range of measured values. The model, however, requires a high molecular weight between crosslinks, M_c, for Pocahontas and Upper Freeport, while the solvent swelling ratios would indicate a low M_c value. The model also requires a high extract yield for Upper Freeport while the measured yields are low. There may be an additional kind of weak crosslink for high rank coals, possibly associated with the aromatic-aromatic interactions suggested by Larsen (80). When the Upper Freeport coal is heated to 300°C and then cooled the solvent swelling ratio increases from 1.32 to 2.13 and the extract yield from 10.4 to 21%, suggesting that this treatment may loosen some of these weak bonds non-reversibly.

SUMMARY AND CONCLUSIONS

The paper poses the question, can coal science be predictive? The answer is yes for coal thermal decomposition in particles small enough to be isothermal. It is possible to construct a model based on reasonable assumptions to predict almost all of the observed behavior. The model has only one parameter which is adjusted for the process conditions. This is the internal pressure in the transport submodel. All other model parameters of the coal are fixed for each coal. The model has composition and kinetic parameters to describe the evolution of each individual gas species. These can be determined in TG-FTIR experiments and exhibit a systematic variation with rank. There are three network parameters in the Monte Carlo version of the model, the chain length, the crosslink density, and the available donatable hydrogen. A similar set of network parameters is used in the percolation theory. These are adjusted to fit the TG-FTIR, tar yields, extract yields, and fluidity. These also exhibit a systematic variation with rank.

The paper explores the six concepts which are the foundation of the FG-DVC model:

1) **The decomposition of functional group sources in the coal yield the light gas species in thermal decomposition.** The amount and evolution kinetics can be measured by TG-FTIR, the functional group changes by FT-IR and NMR. There is good agreement between the model and NMR, FT-IR, and TG-FTIR measurements on a Pittsburgh Seam coal heated at 30°C/min and for gas evolution for a lignite and an Illinois No. 6 bituminous coal at 30°C/min and 20,000°C/sec.

2) **The decomposition of a macromolecular network yields tar and metaplast.** The amount and kinetics of the tar evolution can be measured by TG-FTIR and the molecular weight by FIMS. The kinetics of metaplast formation and destruction can be measured by solvent extraction, by Geissler plastometer and proton magnetic resonance thermal analysis (PMRTA). Reasonable agreement has been demonstrated for solvent extract of a Pittsburgh Seam coal pyrolyzed at 30°C/min and 640°C/sec. Good agreement was shown for four of the Argonne coal samples for fluidity by Geissler plastometer, and for one coal by PMTRA.

3) **The molecular weight distribution of the metaplast depend on the network coordination number.** The coordination number can be determined by solvent swelling and NMR.

4) **The network decomposition is controlled by bridge breaking and the amount of bridge breaking is limited by the available donatable hydrogen.**

5) **The network solidification is controlled by crosslinking.** The changing crosslink density can be measured by solvent swelling and NMR. Crosslinking appears to occur with evolution of both CO_2 (prior to bridge breaking) and CH_4 after bridge breaking. Thus, low rank coals (which form a lot of CO_2) crosslink prior to bridge breaking and are thus thermosetting. High volatile bituminous coals (which form little CO_2) undergo significant bridge breaking prior to crosslinking and become highly fluid. Weathering, which increases the CO_2 yield, causes increased crosslinking and lowers fluidity. There is good agreement between the predicted and measured crosslink densities and fluidities in the FG-DVC model in which crosslinks are correlated with CO_2 and CH_4 gas evolution.

6) **The evolution of tar is controlled by mass transport in which the tar molecules evaporate into the light gas species and are carried out of the coal at rates proportion to their vapor pressure and the volume of light gases.** High pressures reduces the volume of light gases and hence reduces the yield of heavy molecules with low vapor pressure. These changes can be studied with FIMS. The changes in tar yield and molecular weight distribution with pressure have been accurately predicted using the vapor pressure law, of Suuberg and coworkers.

The paper describes how the coal kinetics and composition parameters are obtained by TG-FTIR, solvent swelling, solvent extraction, Geissler plastometer data, NMR data and FIMS data. The model is compared to a variety of experimental data in which heating rate (0.05 to 20,000°C/sec), temperature (100 to 1600°C), and pressure (vacuum to 100 atm) are all varied. There is good agreement with theory (both Monte Carlo and percolation) and most of the data available from our laboratory and in the literature.

The network parameters employed in the model have been presented. The results suggest that there is some form of weak crosslinks for Pocahontas and Upper Freeport coal.

While the experimental results and the model are consistent with the suggested processes, the chemical reactions for bridge breaking, crosslinking, and functional group decomposition are not defined in detail. Also, there is only sparse data to validate the transport assumption and the internal pressure in the particle is an adjustable parameter of the model.

ACKNOWLEDGEMENTS

The authors wish to acknowledge the following organizations for their support over the last ten years: U.S. Department of Energy, Morgantown Energy Technology Center, U.S. Department of Energy, Pittsburgh Energy Technology Center, National Science Foundation, and Gas Research Institute. The authors also wish to acknowledge the extensive contribution from many coauthors who have collaborated on the various aspects of this work: Robert Carangelo, James Markham, Philip Best, Erik Kroo, Yan Ping Zhang, Rosemary Bassilakis, Marie DiTaranto, Girish Deshpande, Po-Liang Chien, H.H. King, Tom Squires, and Kevin Squire who worked at Advanced Fuel Research, Inc., Meredith Colket from United Technologies Research Center, Douglas Smoot and Scott Brewster from Brigham Young University, Eric Suuberg from Brown University, Ronald Pugmire, David Grant, and Mark Solum from the University of Utah, Donald McMillen and Ripudaman Malhotra from SRI International, Rashid Khan from Texaco, Tom Fletcher from Sandia National Laboratory, Leo Lynch and Richard Sakurovs from CSIRO, Bernie Gerstein from Iowa State University, Jean Whelan from Woods Hole Oceanographic Institute, Harold Schobert and Caroline Burgess at Penn State University, Garry Vail, Fred Baudais, Michel Baillargeon, Daniel Gravel from Bomem, Inc. and Dennis Gerson from IBM Instruments.

REFERENCES

1. Solomon, P.R., Serio, M.A., Carangelo, R.M., Bassilakis, R., Gravel, D., Baillargeon, M., Baudais, F., and Vail, G., *Energy and Fuels*, 1990, *4*(3), 319.
2. Green, T.K., Kovac, J., and Larsen, J.W., *Fuel*, 1984, *63*, 935.
3. Green, T.K., Kovac, J., and Larsen, J.W., Coal Structure, R.A. Meyers, Ed., Academic, NY, 1982, p. 199.
4. The Geissler Plastometer data was supplied by Mr. George Engelke from Commercial Testing

and Engineering Company.
5. Solum, M.A., Pugmire, R.J., and Grant, D.M., *Energy & Fuels*, 1989, *3*, 187.
6. St. John, G.A., Butrill, S.E., Jr., and Anbar, M., ACS Symposium Series 71, American Chemical Society, Washington, DC, 1978, p. 223.
7. Solomon, P.R., Hamblen, D.G., Carangelo, R.M., Serio, M.A., and Deshpande, G.V., *Energy and Fuel*, 1988, *2*, 405.
8. Solomon, P.R., Serio, M.A., Hamblen, D.G., Yu, Z.Z., and Charpenay, S., *ACS Div. of Fuel Chem. Preprints*, 1990, *35*(2), 479.
9. Solomon, P.R., in Coal Structure, Advances in Chemistry Series, 1981, *192*, 95.
10. Solomon, P.R. and Hamblen, D.G., "Pyrolysis", in Chemistry of Coal Conversion, (R.H. Schlosberg, Editor), Plenum, New York, NY, 1985, pg. 121-251.
11. Solomon, P.R., Hamblen, D.G., Carangelo, R.M., and Krause, J.L., *Nineteenth Symposium (Int) on Combustion*, 1139, The Combustion Institute, Pittsburgh, PA, 1982, 1139.
12. Serio, M.A., Hamblen, D.G., Markham, J.R., Solomon, P.R., *Energy and Fuel*, 1987, *1*, 138.
13. Solomon, P.R. and King, H.H., *Fuel*, 1984, *63*, 1302.
14. Squire, K.R., Carangelo, R.M., DiTaranto, M.B., and Solomon, P.R., *Fuel*, 1986, *65*, 833.
15. Solomon, P.R., Hamblen, D.G., Carangelo, R.M., Serio, M.A. and Deshpande, G.V., *Combustion and Flame*, 1988, *71*, 137.
16. Solomon, P.R., Serio, M.A., Carangelo, R.M., Bassilakis, R., Yu, Z.Z., Charpenay, S., and Whelan, J., "Analysis of Coal by TG-FTIR and Pyrolysis Modeling", presented at the Pyrolysis '90 Meeting in Holland, June 1990, to be published in Journal of Analytical and Applied Pyrolysis.
17. Suuberg, E.M., Peters, W.A., and Howard, J.B., *Seventeenth Symposium (Int) on Combustion*, The Combustion Institute, Pittsburgh, PA 1979, 117.
18. Gavalas, G.R., Cheong, P.H., and Jain, R., *Ind. Eng. Chem. Fundam.*, 1981, *20*, 113.
19. Gavalas, G.R., Cheong, P.H., and Jain, R., *Ind. Eng. Chem. Fundam.*, 1981, *20*, 122.
20. Xu, W.C. and Tomita, A., *Fuel*, 1987, 66, 627.
21. van Krevelen, D.W., Coal, Elsevier, Amsterdam, 1961.
22. Solomon, P.R., Squire, K.R., and Carangelo, R.M., Int. Conf. on Coal Science, Pergamon, Sydney, Australia, 1985, p. 945.
23. Brenner, D., *Fuel*, 1985, *64*, 167.
24. Lucht, L.M. and Peppas, N.A., *Fuel*, 1987, *66*, 803.
25. Lucht, L.M., Larsen, J.M., and Peppas, N.A., *Energy & Fuels*, 1987, *1*, 56.
26. Larsen, J.W., *ACS Fuel Chem. Div. Preprints*, 1985, *30*(4), 444.
27. Green, T., Kovac, J., Brenner, D., and Larsen, J., Coal Structure, (R.A. Meyers, Ed.), Academic, NY, 1982, p 199.
28. Hall, P.J., Marsh, H., and Thomas, K.M., *Fuel*, 1988, *67*, 863.
29. Sanada, Y. and Honda, H., *Fuel*, 1966, *45*, 295.
30. Suuberg, E.M., Yoshi, O., and Deevo. S., *ACS Div. Fuel Chem. Prepr.*, 1988, *33*(1), 387.
31. Gavalas, G.R., Coal Pyrolysis, Elsevier, NY, 1982 p. 51
32. Solomon, P.R., Hamblen, D.G., Yu, Z.Z., and Serio, M.A., *Fuel*, 1990, *69*, 754.
33. Niksa, S., and Kerstein, A.R., *Combustion and Flame*, 1986, *66*, 95.
34. Niksa, S., *Combustion and Flame*, 1986, *66* 111.
35. Niksa, S. and Kerstein, A.R., *Fuel*, 1987, *66*, 1389.
36. Grant, D.M., Pugmire, R.J., Fletcher, T.H., and Kerstein, A.R., *Energy & Fuels*, 1989, *3*, 175.
37. Nelson, P.F., *Fuel*, 1987, *66*, 1264.
38. Calkins, W.H., Hagaman, E., and Zeldes, H., *Fuel*, 1984, 63, 1113.
39. Calkins, W.H., and Tyler, R.J., *Fuel*, 1984, *63*, 1119.
40. Calkins, W.H., *Fuel*, 1985, *64*, 1125.
41. Calkins, W.H., Hovsepian, B.K., Drykacz, G.R., Bloomquist, C.A.A., and Ruscic, L., *Fuel*, 1984, *63*, 1226.
42. Niksa, S., *AIChE J.*, 1988, *34*, 790.
43. Solomon, P.R., Best, P.E., Yu, Z.Z., and Deshpande, G.V., *ACS Div. of Fuel Chem. Preprints*, 1989, *34*(3), 895.
44. Suuberg, E.M., Lee, D., and Larsen, J.W., *Fuel*, 1985, *64*, 1668.
45. Suuberg, E.M., Unger, P.E., and Larsen, J.W., *Energy and Fuels*, 1987, *1*, 305.
46. Bockrath, B.C., Illig, E.G., and Eassell-Bridger, W.D., *Energy & Fuels*, 1987, *1*, 227.
47. Solomon, P.R., Serio, M.A., Deshpande, G.V., and Kroo, E., *Energy & Fuels*, 1990, *4*(1), 42.

48. Solomon, P.R., "Coal Structure and Thermal Decomposition", in New Approaches in Coal Chemistry, ACS Symposium Series 169, 1981, 61.
49. Brown, J.K., Dryden, I.G.C., Dunevein, D.H., Joy, W.K., and Pankhurst, K.S., *Inst. Fuel*, 1958, *31*, 259.
50. Orning, A.A. and Greifer, B., *Fuel*, 1956, *35*, 318.
51. Freihaut, J.D., Proscia, W.M., and Seery, D.J., *Energy & Fuels*, 1989, *3*, 692.
52. Anthony, D.B. and Howard, J.B., *AIChE J.*, 1976, *22*, 625.
53. Solomon, P.R., Serio, M.A., Carangelo, R.M., and Markham, J.R., *Fuel*, 1986, *65*, 182.
54. Solomon, P.R. and Serio, M.A., "Evaluation of Coal Pyrolysis Kinetics", in Fundamentals of the Physical-Chemistry of Pulverized Coal Combustion, J. Lahaye and G. Prado, Eds.), Martinus Nijhoff, 1987, 126.
55. Kobayashi, H., Howard, J.B., and Sarofim, A.F., *Sixteenth Symposium (Int) on Combustion*, The Combustion Institute, Pittsburgh, PA, 1977, 411.
56. Solomon, P.R., and Colket, M.B., *Seventeenth Symposium (Int) on Combustion*, The Combustion Institute, Pittsburgh, PA, 1979, 131.
57. Anthony, D.B., Howard, J.B., Hottel, H.C., and Meissner, H.P., *Fifteenth Symposium (Int) on Combustion*, The Combustion Institute, Pittsburgh, PA, 1974, 1303.
58. Badzioch, S., and Hawksley, P.G., *Ind. Eng. Chem. Proc. Des., Dev.*, 1970, 9, 521.
59. Solomon, P.R., Fletcher, T.H., and Pugmire, R.J., Progress in Coal Pyrolysis, Pittsburgh Coal Conference, (Sept. 10-14, 1990).
60. Solomon, P.R., Serio, M.A., and Suuberg, E.M., Review of Coal Pyrolysis: Experiments, Kinetic Rates, and Mechanisms, Progress in Energy and Combustion Science, submitted (1990).
61. Fletcher, T.H., *Combustion and Flame*, 1989, *78*, 223.
62. Fletcher, T.H., *Combust. Sci. and Tech.*, 1989, *63*, 89.
63. Freihaut, J.D. and Proscia, W.M., *Energy & Fuels*, 1989, *3*(5), 625.
64. Solomon, P.R., Serio, M.A., and Markham, J.R., Kinetics of Coal Pyrolysis, Int. Conference on Coal Science Proceedings, IEA, Tokyo, Japan, p. 575, (October 23-27, 1989).
65. Serio, M.A., Solomon, P.R., Charpenay, S., Yu, Z.Z., and Bassilakis, R., *ACS Div of Fuel Chem. Preprints*, 1990, *35*(3), 808.
66. Burnham, A.K., Oh, M.S., Crawford, R.W., and Samoun, A.M., *Energy & Fuel*, 1989, *3*, 42.
67. Stein, S.E., Robauch, D.A., Alfieri, A.D., and Miller, R.E., *J. Am. Chem. Soc.*, 1982, *104*, 6567.
68. Solum, M.S., Pugmire, R.J., Grant, D.M., Fletcher, T.H. and Solomon, P.R., Studies of Coal Char Structure Evolution: 1. Solid State ^{13}C NMR, to be submitted, (1989).
69. Lynch, L.J., Sakurovs, R., Webster, D.S., and Redlich, P.J., *Fuel*, 1988, *67*, 1036.
70. Lynch, L.J., Webster, D.S., Sakurovs, R., Barton, W.A., and Maher, T.P., *Fuel*, 1988, *67*, 579.
71. Barton, W.A. and Lynch, L.J., *Energy & Fuels*, 1989, *3*, 402.
72. Dr. Richard Sakurovs, personal communications.
73. Fong, W.S., Peters, W.A., and Howard, J.B., *Fuel*, 1986, *65*, 251.
74. Sobkowwiak, M., Riesser, B., Given, R., and Painter, P., *Fuel*, 1984, *63*, 1245.
75. Riesser, B., Starsinic, M., Squires, E., Davis, A., and Painter, P., *Fuel*, 1984, *63*, 1253.
76. Solomon, P.R. and Carangelo, R.M., *Fuel*, 1988, *67*, 949.
77. Solomon, P.R., and Carangelo, R.M., *Fuel*, 1982, *61*, 663.
78. Solomon, P.R., Best, P.E., Yu, Z.Z., and Charpenay, S., "A Macromolecular Network Model for Coal Fluidity", to be submitted to Fuel, (1990).
79. Wu, M.M., Robbins, G.A., Winschel, R.A., and Burke, F.P., *Energy & Fuels*, 1988, *2*, 150.
80. Larsen, J.W., *ACS Div. of Fuel Chem. Preprints*, 1988, *33*(1), 400.

Appendix L

Network Models of Coal Thermal Decomposition

Network models of coal thermal decomposition

Peter R. Solomon, David G. Hamblen, Zhen-Zhong Yu and Michael A. Serio

Advanced Fuel Research, Inc., 87 Church Street, East Hartford, CT 06108, USA

(Received 24 July 1989; revised 2 February 1990)

Several groups have considered statistical network fragmentation models to describe coal thermal decomposition. In these models, the coal macromolecule is viewed as a collection of fused aromatic rings (monomers) linked by bridges. During thermal decomposition, existing bridges break and new bridges are formed. The parameters of the models are the geometry of the network, which is expressed as the number of attachments per monomer (the coordination number, $\sigma+1$), and the chemistry of bridge breaking and formation. Given $\sigma+1$ and the instantaneous number of unbroken and formed bridges, the molecular weight distribution can be predicted. The different groups have employed both Monte Carlo methods and percolation theory to describe the network statistics. The former approach has advantages in terms of describing both the depolymerization and crosslinking processes in coal decomposition, since it does not require a constant coordination number. The latter method provides closed form solutions and is computationally less demanding. The models differ in the geometry of the network, the chemistry of bridge breaking and bridge formation (crosslinking) and the mass transport assumptions. This paper considers for three such models: the mathematical schemes; the assumed network geometries; the assumed bond breaking and bond formation chemistries; and the mass transport assumptions. The predictions of three models were compared by comparing the oligomer populations as a function of the number of unbroken bridges per ring cluster. This paper also presents results from a new model which combines the geometry, chemistry and mass transport assumptions of the FG-DVC model with the mathematics of a modified percolation theory.

(Keywords: thermal decomposition; coal; modelling)

Many recent studies have proposed that coal can be thought of as having a macromolecular network structure to which concepts of crosslinked polymers can be applied[1–10]. These concepts have been employed to understand and model such properties of coal as: the insolubility; the equilibrium swelling and penetration of solvents; the viscoelastic properties; similarities between the parent coal and products of hydrogenolysis, or mild oxidation: crosslinking during char formation[11,12]; and the formation of coal tar in pyrolysis[13–17]. With the success of these concepts in describing coal properties, it appears logical to extend macromolecular network concepts to completely describe the thermal decomposition behaviour of coal.

A number of investigators have used statistical methods to predict how the network behaves when subjected to thermally induced bridge breaking, crosslinking, and mass transport processes[17–30]. Gavalas *et al.*[20] employed statistical methods to predict the release of monomers from a randomly connected network. The model of Niksa and Kerstein employed percolation theory in a model called DISARAY[28], which extended their previous model built on chain statistics[24,25]. Grant *et al.*[30] employed percolation theory in a model called chemical percolation devolatilization (CPD). Solomon *et al.*[21–23,27] used Monte Carlo methods in a network model called the depolymerization, vaporization, and crosslinking (DVC) model. This was an extension of their previous model for linear polymers[17,20]. The DVC model was recently combined with their functional group (FG) model[27,29] to produce the general FG-DVC pyrolysis model. This model is currently being applied to model the devolatilization behaviour of Argonne premium coals[31] and to predict the fluidity of coals[32]. Other statistical methods for network behaviour have been employed in the polymer literature[33–38].

In applying network models to coal thermal decomposition, one considers the coal to consist of aromatic ring clusters linked together by bridges in some geometry. The geometry is described by the degree of branching in the network. An unbranched linear network will have one bridge per ring cluster attaching it to the next cluster. Thus each cluster has two attachments and is said to have a coordination number ($\sigma+1$) of two. A highly branched 'fish net' would have two bridges per cluster, attaching it to the neighbouring four clusters and thus a coordination number of four. A branch point is considered to occur at any cluster connected to more than two neighbours (i.e. having more than two attachments).

When the coal is heated, the bridges can break and new bridges can form. Various statistical methods can be employed to predict the concentration of individual aromatic ring clusters (monomers) and linked clusters (oligomers of n clusters, 'n-mers') up to a totally linked network. By assigning an average or distribution of molecular weights to the monomers, the amounts of tar, extractables, liquids or char can then be defined from the distribution of oligomer sizes. The models vary in the assumed chemistry of bridge breaking and crosslinking,

0016-2361/90/060754-10

in the definition of tar, extracts, liquids, and char and in the statistical methods used.

In view of the importance of macromolecular network models to the accurate predictions of coal processing behaviour, this paper assesses the assumptions and limitations of the proposed models. It appears that the way one performs the statistics (Monte Carlo, percolation theory, or other statistical methods) makes little difference. For example, percolation theory methods were substituted for Monte Carlo calculations in the FG-DVC model, and comparable predictions were obtained for appropriately restricted cases. The important differences among models are in the assumptions for: the network geometry (i.e. the degree of branching or coordination number); the chemistry of bridge breaking; the chemistry of crosslink formation; hydrogen utilization; and mass transport. This paper compares the three most recent models (DISARAY, CPD, and FG-DVC) and considers how the assumed network properties relate to behaviours observed for coal.

MACROMOLECULAR NETWORKS

General properties of networks

Figures 1 and *2* present the networks employed in the FG-DVC Monte Carlo calculations and percolation theory, respectively. For the FG-DVC Monte Carlo calculation, linear oligomers of l clusters (shown as the horizontal chains of clusters) of a molecular weight distribution defined by M_{avg} and deviation, ΔM, are linked by m_0 'crosslinks' per monomer[26,29]. These 'crosslinks' are indicated by the vertical double lines as shown in *Figure 1*. The branch points in the network are defined to occur at those clusters where more than two attachments connect a cluster to another cluster. Unless the crosslink occurs at the end of the oligomer, it forms at least one branch point. The term 'crosslink' has previously been used to mean the extra bridges that can form a branch point, and this is the definition employed here[27,29]. During thermal decomposition, bridges break, new crosslinks are added and the molecular weight of the oligomers is calculated by randomly distributing these changes.

For the percolation theory, a Bethe lattice is employed[28,30,39]. Lattices are characterized by the coordination number, $(\sigma+1)$, which is the number of attachment sites for bridges per cluster and the probability, p, that an unbroken bridge occupies the site. *Figure 2* shows lattices at $p=1$ (i.e. all possible bridges occupied) for $\sigma+1=2.2$ and $\sigma+1=4$. The Bethe lattice has no loops, but it has been demonstrated that this lattice is a good approximation to a lattice of equivalent coordination number containing loops[39]. As shown in *Figure 2*, the $\sigma+1=2.2$ lattice has branch points every 5th cluster. This network is close to a linear polymer $\sigma+1=2$ which has no branch points. The $\sigma+1=4$ lattice is much more highly branched, having double branch points on each cluster (this would be the Bethe lattice analogue of the 'fish net'). For values of p less than 1, the bridges are randomly removed from the network. It is important to realize that the statistical distribution of unbroken bridges means that even when the average number of unbranched bridges per cluster is identical for the two networks in *Figure 2*, the $\sigma+1=4$ network can never look like the $\sigma+1=2.2$ network (except for the case $p=0$).

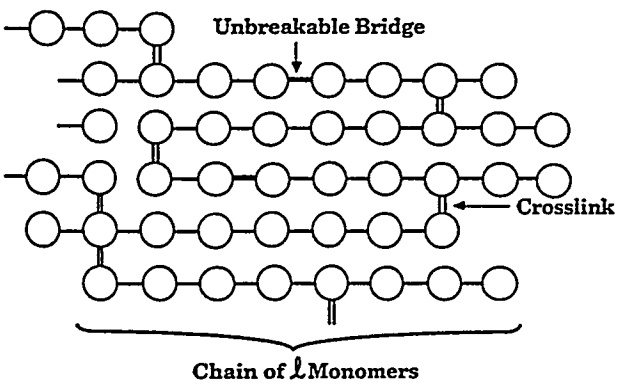

Figure 1 Macromolecular network used in Monte Carlo simulation

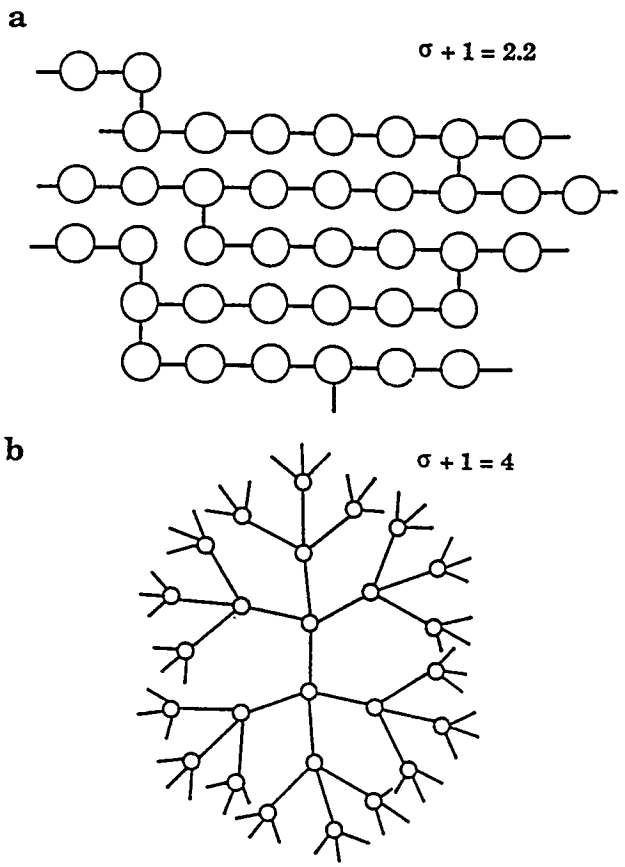

Figure 2 Bethe lattice for a, coordination number 2.2, $p=1$; b, coordination number 4, $p=1$

The loop free geometry of the Bethe lattice allows for the number of free oligomers to be analytically expressed as a function of $\sigma+1$ and the probability p of bonds being unbroken. This is the feature which makes the percolation theory so attractive from the standpoint of computer efficiency and for understanding the behaviour of networks under conditions of varying bridge populations. *Figure 3* shows calculations using percolation theory (for three values of $\sigma+1$) for the monomer, the sum of oligomers up to 3, up to 10, and the sum of all free oligomers as a function of the number of unbroken bridges per ring cluster α, where $\alpha=1/2p\,(\sigma+1)$. The 1/2 enters because $\sigma+1$ is the number of attachments per cluster, which is twice the number of bridges (i.e. each

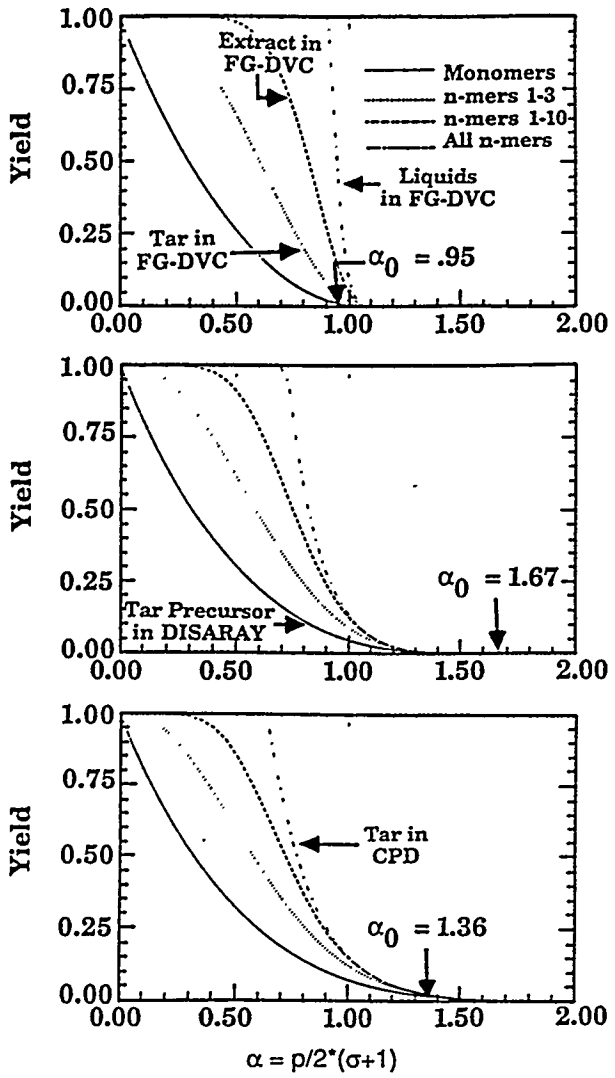

Figure 3 Percolation theory predictions for pyrolysis products (monomers, tar, extracts and total liquids) for three values of the coordination number ($\sigma+1$): a, $\sigma+1=2.2$; b, $\sigma+1=3.25$; c, $\sigma+1=4.6$

bridge forms two attachments). If $\sigma+1$ remains constant during pyrolysis, the molecular weight distribution is a single valued function of α. For ring clusters of molecular weight 300 amu, the sum of 1–3 n-mers corresponds roughly to the potential tar fraction (up to 900 amu), the sum of 1–10 n-mers corresponds to the extractable fraction (up to 3000 amu), and the sum of all oligomers corresponds to the liquids fraction (all free oligomers). It can be seen that, with increasing $\sigma+1$, more broken bridges are required to achieve equivalent fractions of free oligomers. Also, at a fixed value of α, the relative amounts of tar, extracts, and liquids vary with $\sigma+1$.

Network geometries representative of coal

The three important parameters of the network are the average ring cluster size M_{avg}, the coordination number ($\sigma+1$), and the starting probability of bridges being unbroken, p_0. To compare networks of different coordination numbers, it is convenient to use α and α_0 rather than p and p_0. The assumptions of DISARAY, CPD, and FG-DVC are considered below.

Ring cluster size. Ring cluster sizes have been estimated from n.m.r. alone[40], n.m.r. and FT-i.r.[41], mild degradation[42], and the molecular weight distribution of tar[15,16,29]. Based on these results, the average ring cluster size for coals with less than 90% carbon is expected to be between 2 and 3 aromatic rings or a total molecular weight per cluster, including peripheral groups, of 200–400 amu. DISARAY assumes a value of 1400 amu for the monomer which can split into two 700 amu tar fragments. CPD does not specify the monomer molecular weight. For coals with less than 90% carbon, FG-DVC employs a distribution of monomers with an M_{avg} of 256 amu.

Coordination number. Information on the coordination number comes from solvent swelling measurements and recent estimates made using n.m.r. of the number of non-peripheral group attachments to the cluster[40]. There is some controversy about the meaning of the measurements of the solvent swelling ratio. Network theories have, however, been applied[2–9] to relate the solvent swelling ratio, Q, and the average molecular weight of a cluster, M_{avg}, to the average molecular weight between branch points, M_c. The M_c determinations[2–9] suggest that there are between 4 and 8 repeating units (ring clusters) between branch points for coals with less than 90% carbon. (In this work the term crosslink has been used to indicate the bridge which makes a ring cluster into a branch point.) This indicates a value for $\sigma+1$ between 2.13 and 2.25, since $\sigma+1$ is the average number of attachments per cluster (1 bridge makes two attachments). The n.m.r. data suggest that there are between 2 and 3 bridge or loop attachments per cluster (see Figure 8 of Ref. 40). This suggests $\sigma+1$ is between 2 and 3. Based on these two measurements, the coordination number for the starting coal for describing the break up of the network by bridge cleavage should be less than 3, and probably between 2.2 and 2.5. A different value of $\sigma+1$ might be appropriate for describing crosslinking (branch point formation at higher temperature). To model a high volatile bituminous coal, the different models used networks with $(\sigma+1)=3.25$ (DISARAY), 4.6 (CPD), and ≈ 2.1 (FG-DVC).

Initial bridge population. p_0. The starting macromolecular network for FG-DVC is chosen to match the measured extract yield and molecular weight between crosslinks by picking two parameters: the length of the linear oligomer chain, l; and the number of initial crosslinks (branch points) per monomer, m_0. First m_0 is picked such that $m_0 = M_{avg}/M_c$, where M_{avg} is the average ring cluster (monomer) molecular weight and M_c is the molecular weight between crosslinks determined from solvent swelling[2–9]. Then l is chosen so that when the molecule is randomly constructed, the weight per cent of oligomers less than 3000 amu matches the measured extract yield. There is the implicit assumption that the extract yield is due to the unpolymerized fraction of a homogeneous network. Polymethylenes or highly fluid macerals (e.g. exinites), which can be a significant portion of the extracts in coal, should really be treated as separate components but were not in the first version of the FG-DVC model. The initial value of α is approximately $((l-1)/l+m_0)$, which for the Pittsburgh seam coal modelled in Ref. 29 is $\alpha_0 \approx 0.95$. This initial value is indicated in *Figure 3a*. In DISARAY, p_0 is set equal to 1 ($\alpha_0 = 1.63$). This is illustrated in *Figure 3b*.

The starting macromolecular network in the CPD model is chosen by picking two parameters: the coordination number $\sigma+1$, picked to match the average number of all connections (including peripheral groups in addition to bridges and loop attachments) per ring determined by n.m.r.[30,40]; and p_0, the starting probability of unbroken bonds. For the high volatile bituminous coal simulated in Ref. 30, $\alpha_0=1/2\ p_0(\sigma+1)=1.36$. This initial value is indicated in *Figure 3*.

PROCESSES CONTROLLING THE NETWORK DECOMPOSITION

This section considers the important processes in pyrolysis: bridge breaking, and hydrogen utilization; crosslinking (branch point formation); and the mass transport processes which control the distribution of oligomers into tar, extracts, liquids, and solids. The processes are summarized in *Figure 4*.

Bridge breaking and hydrogen utilization

Figure 4a summarizes the bridge breaking assumptions of the three models. Both the FG-DVC and CPD models assume similar (within a factor of 3) bridge breaking rates, $0.86\times10^{15}\ \exp-(55\,400/RT)\ s^{-1}$ for FG-DVC* and $2.6\times10^{15}\ \exp-(55\,400/RT)\ s^{-1}$ for CPD. Both models employ rank independent kinetics. The FG-DVC model rate was determined in experiments in which particle temperatures were directly measured[43]. The rate was recently confirmed within a factor of 2 by Fletcher *et al.*[44] in a second experiment to directly measure particle temperatures. The DISARAY model* assumes a bridge dissociation rate which can produce monomers of $6\times10^{8}\ \exp-(30\,000/RT)\ s^{-1}$. The monomers subsequently decompose at $1.4\times10^{7}\ \exp-(31\,000/RT)\ s^{-1}$ to form tar.

In DISARAY, all the initial bridges can break. In FG-DVC and CPD, there is a process for creating unbreakable bridges associated with the bridge breaking process. The FG-DVC model includes three kinds of bonds: labile bridges, 'unbreakable bridges' (which do not form branch points), and crosslinks (which do form branch points). The unbreakable bridges are represented by the heavy horizontal lines in *Figure 1*. For each broken labile bridge, FG-DVC requires that hydrogen be available to stabilize the free radicals. It is assumed that all the donatable hydrogen (aliphatic plus hydroaromatic) is located in the labile bridges, so that only half the labile bridges can break with the other half becoming unbreakable with the donation of their hydrogen (i.e. there is a 1:1 ratio between the occurrence of bridge breaking and the formation of additional 'unbreakable bridges'). In the FG-DVC model, crosslinks are also considered to be bridges which cannot be broken, but are not in the 'unbreakable bridges' pool. The weight fraction of the initial bridges in the chain of length l which are labile is given by the parameter W_B; the rest are assumed to be unbreakable bridges. W_B is a fitting parameter chosen to make the model fit the pyrolysis data.

In a similar manner, in CPD there are both unbreakable bridges with probability c_0 and labile bridges with probability L_0 ($L_0+c_0=p_0$). As pyrolysis proceeds, the labile bridges can break and react by two possible routes to form unbreakable 'char' bridges or broken bridges. CPD assumes a 0.9:1.0 ratio of broken bridge to char bridge formation. That assumption is almost identical to the 1:1 ratio used in FG-DVC. In

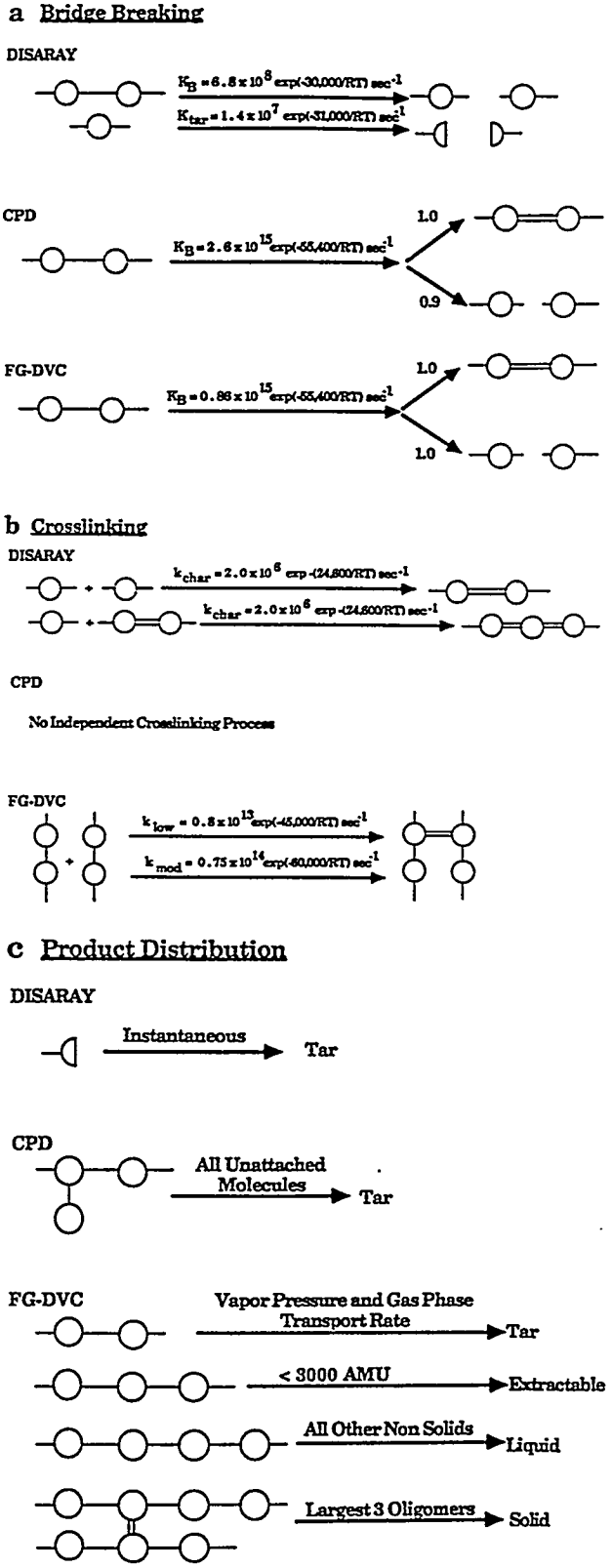

Figure 4 Summary of model assumptions for a, bridge breaking; b, crosslinking; c, product distribution

* Both FG-DVC and DISARAY employ distributed activation energy expressions. The rates quoted above are for the centre of the distribution

CPD there is no distinction between unbreakable bridges and crosslinks. A branch point occurs any place there are three or more attachments per cluster.

Crosslinking

The crosslinking (branch point forming) reactions are summarized in *Figure 4b*. CPD does not define any distinct crosslinking processes. Char forming reactions produce unbreakable bridges as a consequence of bridge breaking. These reactions form branch points (three or more attachments per cluster) randomly depending on the coordination number, $\sigma+1$ and probability, p.

DISARAY assumes char formation occurs at a rate $2\times10^6\exp-(24\,600/RT)\,s^{-1}$. Char formation is assumed to occur by monomers attaching to the original lattice or to each other.

FG-DVC assumes two independent crosslinking reactions. These are the only reactions which can form branch points in the Monte Carlo formulation. One process occurs at low temperature (below that for bridge breaking) for low rank coals and is associated with CO_2 evolution[11,12,45]. Crosslinking also occurs at moderate temperatures, slightly higher than bridge breaking, and is associated with the evolution of CH_4. The model assumes one crosslink is formed for each CH_4 or CO_2 evolved[29]. The mechanistic basis for these assumptions has been discussed elsewhere[45].

Product distribution

The product distribution assumptions are summarized in *Figure 4c*. The identification of different size oligomers with tar, extracts, liquids, and solids is related to their molecular weight. The oligomers which can form tar are the lightest fraction. Tar formation is controlled in part by the vapour pressure of the components. This idea is supported by the observation that tar yields are strongly influenced by external pressure[29,46,47].

Only oligomers with molecular weights less than 1000 amu have sufficient vapour pressure to become gas at typical pyrolysis tempratures, so tar is roughly limited to <1000 amu[47–51]. The extract yield is controlled by the solubility of the oligomers. For coal fragments in pyridine this limit is roughly 3000 amu[47–49,52]. Larger fragments appear to be important to the fluid properties of coal[32].

In FG-DVC, the Monte Carlo calculation is employed to determine the molecular weight distribution in the decomposing char. Then, a mass transport equation is applied to determine the probability of the light n-mers evolving as tar. The transport equation assumes that a molecular weight dependent vapour pressure controls the appearance of these molecules in the gas phase and that they escape the coal particles by convective transport of the gas[29]. Tar is thus the light end of the molecular weight spectrum, i.e. those with sufficiently high vapour pressures. This produces tar with number average molecular weights of 300–400 amu and maximum weights of 800–1000 amu. Thus, in FG-DVC, tar is approximately the sum of 1–3 n-mers in *Figure 3a*. Extractable material is defined as all molecules up to 3000 amu (sum of 1–10 n-mers) and liquids are defined as all molecules not attached to the starting network. An alternative definition, which has been employed here, is to assume the largest three molecules constitute the solid, and all the rest are liquid.

In DISARAY, tar is defined as half the monomer, and the monomer is taken as 1400 amu. Consequently, the tar would be defined as some fraction of the monomer curve in *Figure 3b*. No transport equations are employed in CPD. Tar is defined as all molecules not attached to the infinite lattice. Thus tar is represented by the highest line in *Figure 3c*.

One advantage of the Monte Carlo method over the percolation theory is that, when tar is produced, molecules can be removed from the network. In percolation theory, there is no consistent way to remove molecules from the network and to allow the formation of new bridges such as the crosslinking events in FG-DVC. CPD avoids this problem by excluding any independent crosslinking which would reconnect oligomers. This presents the limitation that independent crosslinking and mass transport cannot be treated with the exact percolation theory expressions.

EXAMPLES OF MODEL CALCULATIONS

Formation of pyrolysis products

The evolution of the macromolecular network in the CPD model is illustrated in *Figure 5*. *Figure 5a* shows the percolation theory predictions for the total of

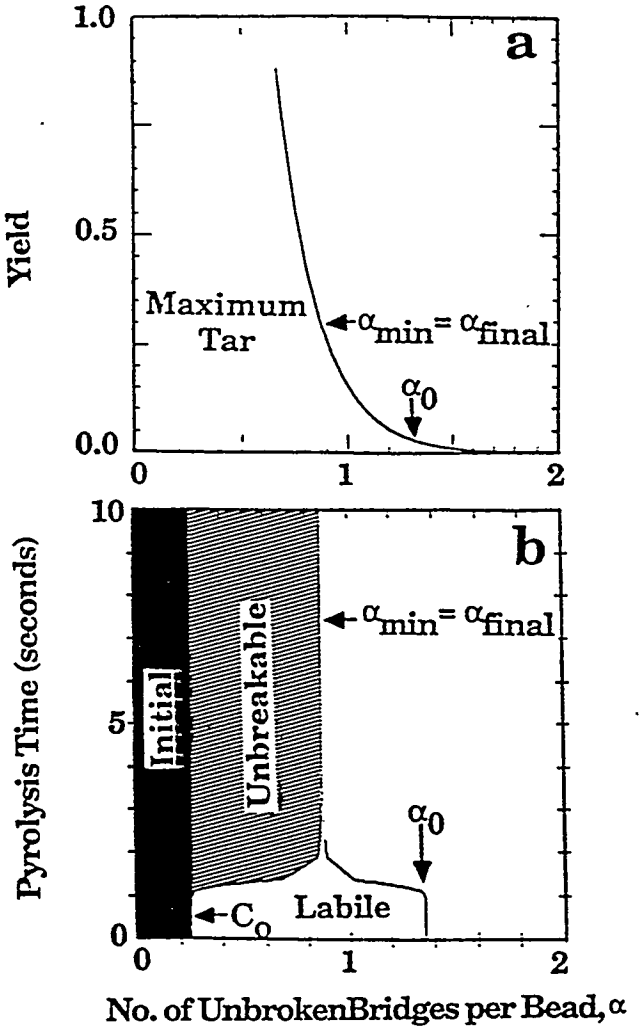

Figure 5 Tar yield for a bituminous coal predicted by the CPD model: a, tar yield versus α; b, variation in α with time, heating at 450°C s^{-1} to 936 K. The shaded areas show the relative amounts of the two types of crosslinks (initial; unbreakable bridge formation)

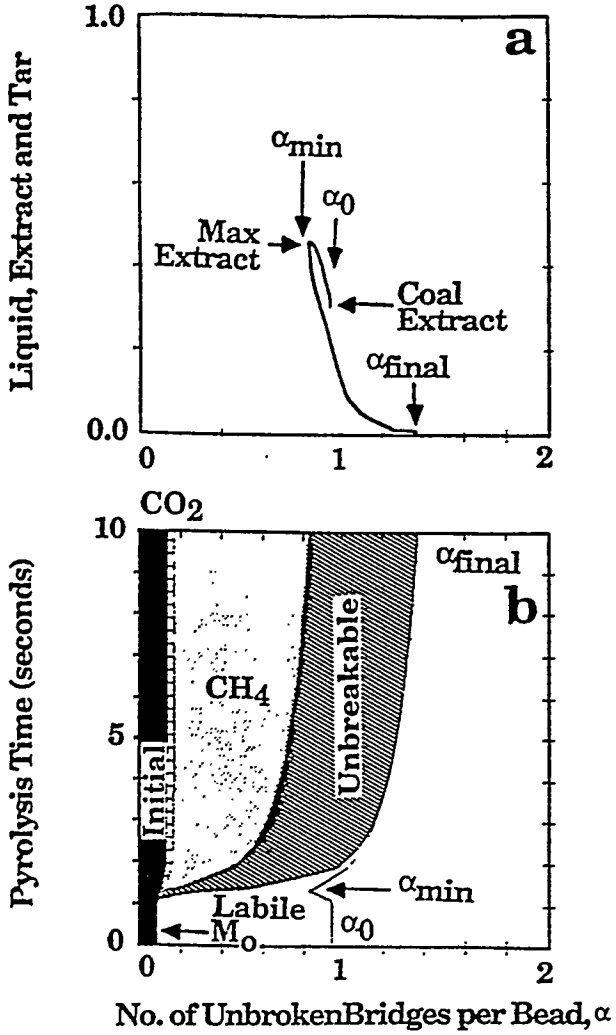

Figure 6 Extract yield for a bituminous coal predicted by the FG-DVC model: a, extract yield versus α; b, variation in α with time, heating at 450°C s^{-1} to 936 K. The shaded areas show the relative amounts of the three types of crosslinks (initial: crosslinks related to gas evolution: unbreakable bridge formation)

unattached oligomers (defined to be the tar) as a function of α. The coal is represented at $p_0=0.59$ or $\alpha_0=1/2p_0(\sigma+1)=1.36$. During pyrolysis, the labile bridges form either broken bridges or unbreakable char bridges in the ratio 0.9 to 1.0. *Figure 5b* shows how α changes during pyrolysis. Pyrolysis proceeds until α_{min} is reached, and all the labile bridges are either broken or have formed unbreakable bridges. Thus

$$\alpha_{min}=1/2(\sigma+1)\,(c_0+(1.0/1.9)L_0)=0.83$$

and the change in α during pyrolysis was 0.53. Note that α can only decrease in the CPD model.

The evolution of the macromolecular network for FG-DVC computed using the Monte Carlo method for a bituminous coal is illustrated in *Figure 6*. *Figure 6a* shows the calculated extract yield as a function of α. The initial probability of unbroken bridges, α_0, starts out at close to 1.0 to produce the measured extract yield (30%). *Figure 6b* shows the computed value of α with its contributions from the initial crosslinks m_0, the conversion of labile bridges to broken bridges and unbreakable bridges and the added crosslinks related to gas evolution. For the bituminous coal, the added crosslinks are almost all due to CH_4 related processes. α goes back up in the FG-DVC model to resolidify the lattice. This is necessary to model fluidity effects[32].

Results of the FG-DVC model applied to a lignite are presented in *Figure 7*. For the lignite, the formation of low temperature crosslinks from CO_2 evolution prevents α from being reduced due to bridge breaking. Thus pyrolysis produces no additional extract yield. The thermosetting behaviour of the low rank coal, and the release of little tar or extracts is related to this low temperature crosslinking process.

Utilization of donatable hydrogen

As discussed above, W_B, the initial fraction of labile bridges, is a parameter of the FG-DVC model. This parameter is related to the fraction of donatable hydrogen by $H(d)=2/28\ W_B$, i.e. there are two donatable hydrogens per labile bridge. This parameter has a strong effect on α_{min} and hence the yield of tar, extracts, and liquids.

There are two ways to estimate the amount of hydrogen donated. During pyrolysis the donation of hydrogen converts two aliphatic or hydroaromatic

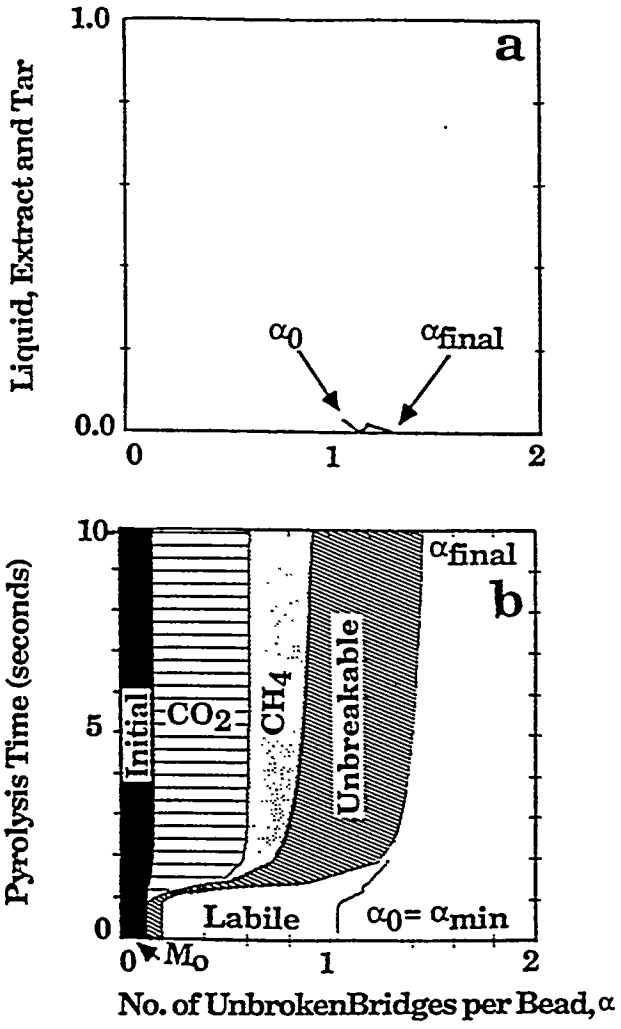

Figure 7 Extract yield for a lignite predicted by the FG-DVC model: a, extract yield versus α; b, variation in α with time, heaing at 450°C s^{-1} to 936 K. The shaded areas show the relative amounts of the three types of crosslinks (initial: crosslinks related to gas evolution: unbreakable bridge formation)

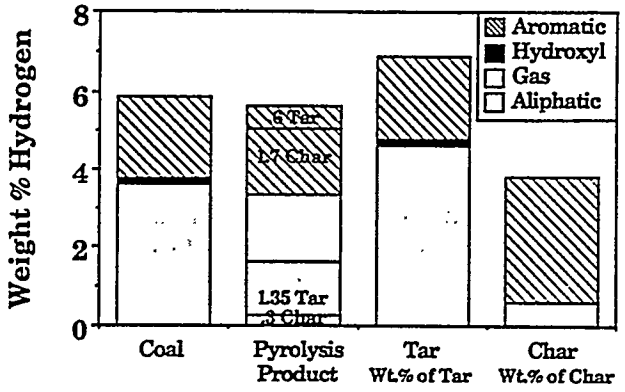

Figure 8 Distribution of hydrogen in coal and pyrolysis products. Pyrolysis produced approximately 53% char, 30% tar and 21% gas

hydrogens into a donated aliphatic hydrogen plus a newly formed aromatic hydrogen. The increase in aromatic hydrogen in the pyrolysis products, and the increase in aliphatic hydrogen in the tar, can both be measured using quantitative FT-i.r. analysis[53,54]. The results for a Pittsburgh seam coal are summarized in *Figure 8*. They show that the aromatic hydrogen in the total pyrolysis products increased from 2.1 to 2.4%, or an increase of 0.3% on a starting coal basis. This increased aromatic content is all in the char. The aromatic content in the tar remains about the same. The tar, which is approximately 30% of the starting coal, increases its aliphatic hydrogen content by about 1% or 0.3% on the starting coal basis. The two numbers are thus consistent: 0.6% aliphatic or hydroaromatic hydrogens in the coal are converted to 0.3% new aromatics plus 0.3% donated aliphatics. If it is assumed that a monomer has a molecular weight of 300 amu, then one breakable bridge per monomer with four aliphatic hydrogens is 1.33%. Half the bridges can break (0.67%) and the other half (0.67%) can donate half its hydrogen (0.34%), in reasonable agreement with the experimentally estimated value of 0.3% hydrogens actually donated. The value assumed[29] in FG-DVC for $H(d)$ for the Pittsburgh seam coal is 0.67%.

The value of $H(d)$ has implications for the CPD model. If there is only one labile bridge per monomer, then

$$\alpha_{min} = 1/2(\sigma+1)(c_0 + (1.0/1.9)L_0)$$
$$= 1/2(4.6)(0.37 + (1.0/1.9)0.22) = 1.11$$

rather than 0.83. In this case, the value of $\sigma+1$ would have to be reduced to match the data. Also, the average molecular weight for the unattached molecules is too high to be identified as tar. If a more reasonable definition of tar is used (e.g. the sum of oligomers up to 3), then $\sigma+1$ has to be reduced still further.

Comparison of Monte Carlo calculation with percolation theory

To further illustrate some of the differences between the FG-DVC Monte Carlo model and percolation theory calculations, the extract yield calculated for a case similar to that in *Figure 6a*, but with tar evolution not permitted, is plotted in *Figure 9* along with the predictions of percolation theory for several values of $\sigma+1$. The FG-DVC Monte Carlo prediction is not a single valued function of α. As pyrolysis proceeds, the increase in extract yield follows $\sigma+1 \approx 2.2$ while the decrease in extract yield follows $\sigma+1 \approx 4$.

It is important to know whether this result is an artefact of the Monte Carlo calculation or a real feature of pyrolysis. Based on what is known to happen in pyrolysis, the result does make sense. For a bituminous coal, the initial process occurring in pyrolysis is bridge breaking. This occurs by breaking bridges in the network described by $\sigma+1$ between 2.1 and 2.5. No crosslinking occurs initially as the solvent swelling ratio is observed to increase during this period[45]. Thus, the coordination number used in CPD, which includes all connections to the ring cluster (bridges, loops, and peripheral groups)[30,40], may not be appropriate to this phase of pyrolysis. Eventually crosslinks start forming, resulting in an increase in the coordination number and in α. There is evidence that crosslinks form at peripheral group sites so that the coordination number used in CPD (the sum of branches and peripheral groups) is appropriate for this phase of the process. Consequently, the network cannot adequately be described by one type of bridge site with a single coordination number. There are bridge sites for labile bridges and for crosslinks, each with their own coordination number. This observation motivated the development of a more general percolation theory model.

LATTICE MODEL WITH TWO BRIDGE BOND TYPES

Two-σ model

To deal with a structure with a time dependent coordination number, a Bethe lattice with two types of bridging bonds is considered, with coordination numbers and probabilities of occupation given by σ_1+1, p, and σ_2+1, q, for the two types, respectively. Such a lattice for $\sigma_1+1=\sigma_2+1=2$ is illustrated in *Figure 10*. The analysis can be carried through using the procedures described previously[30,39], but with extensions to deal with the extra variables. The equations are presented in Appendix A.

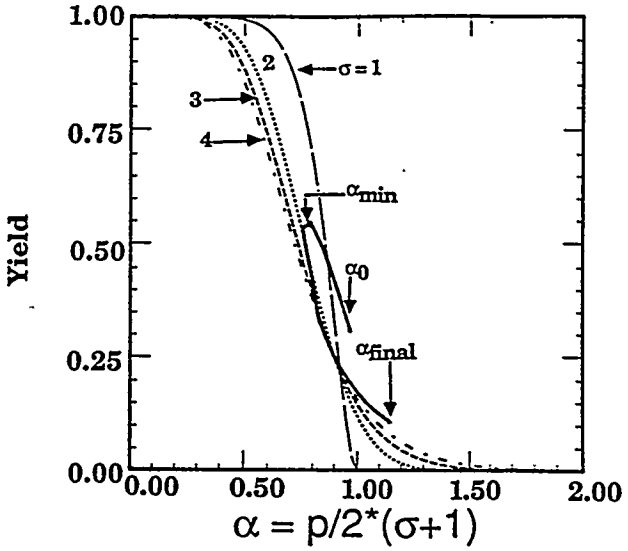

Figure 9 Comparison of extract yield predictions from FG-DVC model with percolation theory for $\sigma=1$, 2, 3 and 4. FG-DVC predictions are for Pittsburgh seam coal heated at 450°C s^{-1} to 936 K with no tar evolved

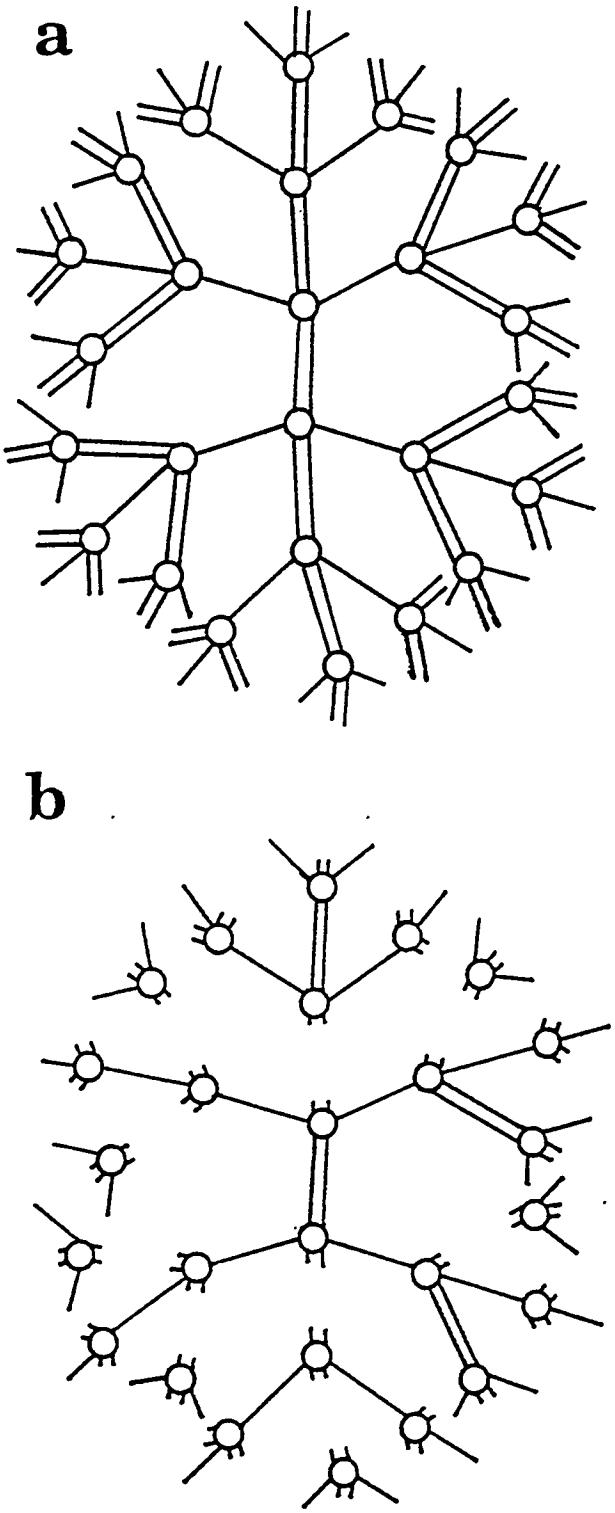

Figure 10 Bethe lattice for two-σ model with $\sigma_1 = 1$ (shown as single bonds) and $\sigma_2 = 1$ (shown as double bonds): a, fully linked case ($p = q = 1$) is like one-σ model with $\sigma = 3$; b, shown with most double bonds (representing the crosslinks) not yet formed to represent the starting coal. This lattice is like a one-σ model with $\sigma = 1$, linear chains

Application of two-σ model

Figure 11 presents a comparison of the predictions for pyrolysis assuming the FG-DVC chemistry, using: the Monte Carlo calculation; the two-σ percolation calculations ($\sigma_1 + 1 = 2$, $\sigma_2 + 1 = 2$); and two cases of the one-σ percolation calculation ($\sigma + 1 = 2.2$ and $\sigma + 1 = 3.2$). The calculations are made under the assumption that no tar is evolved. The tar values in *Figure 11* are the sum of 1–3 *n*-mers remaining in the char. The Monte Carlo calculation in *Figure 11a* is matched best by the two-σ model if liquids are assumed to be the sum of the first 100 *n*-mers (i.e. up to 300 000 amu). The two-σ model has a reasonable value for the initial extract yield but predicts slightly more initial tar. Neither of the one-σ cases is a good match. Use of $\sigma + 1 = 2.2$ is good at low temperature, but overpredicts the maximum values of extracts and liquids and resolidifies the network very abruptly at too low a temperature. Use of $\sigma + 1 = 3.2$ does a much better job at predicting the maximum values of tar, extract and liquids, and resolidifies the network more slowly at a higher temperature, but the initial ratio of tar to extract is not consistent with that observed for coal and the rate of increase of *n*-mers is too slow. It thus appears that the two-σ model can be used instead of the Monte Carlo calculations when no tar is evolved, while one-σ calculations are less accurate.

The real test, however, is how well the models fit the data for coal. A comparison of tar yield is not a sufficient test since α_0 and $\Delta\alpha$ can always be selected in conjunction with the network geometry to fit the data. A critical test requires a careful comparison of how α_0 and $\alpha(t)$ match with measurement of functional group changes in the char (e.g. the transformation of hydrogen functional groups and bridges), solvent swelling behaviour (i.e. crosslink density), and the complete molecular weight distribution as reflected in the amounts of tar, extracts, and fluidity.

COMPARISON OF NETWORK MODELS

A summary of the processes predicted by the three recent network models. CPD, DISARAY and FG-DVC is presented in *Table 1*. All the models predict their primary objective, i.e. the variations in tar and gas yield with time and temperature. All three are capable of predicting

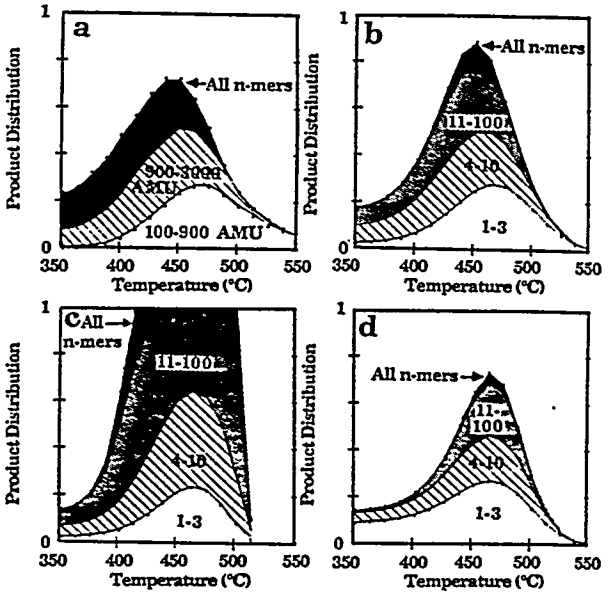

Figure 11 Comparison of distribution of *n*-mers for pyrolysis of upper Freeport coal at 3°C min^{-1}: a, Monte Carlo calculation; b, two-σ model ($\sigma_1 = 1, \sigma_2 = 1$); c, one-$\sigma$ model ($\sigma = 1.2$); d, one-σ model ($\sigma = 2.2$)

Table 1 Comparison of network models

	CPD	DISARAY	FG-DVC Monte-Carlo or 2σ	Relevant model process
Tar yield versus time	Yes	Yes	Yes	Bond breaking
Extract yield versus time	No[a]	No	Yes	Bond breaking
Gas yield versus time	Yes	Yes	Yes	From peripheral groups
Tar yield versus heating rate	Not yet	Yes	Yes	Relative rates of bond breaking and crosslinking
Variation of tar molecular weight with heating rate	No	No	Yes	Relative rates of bond breaking and crosslinking
Molecular weight of tar	No	No	Yes	Mass transport limitation
Tar yields versus pressure	No	No	Yes	Mass transport limitation
Molecular weight versus pressure	No	No	Yes	Mass transport limitation
Solvent swelling of char	No	No	Yes	Crosslinking

[a] All oligomers are defined as tar

variations of tar yield with heating rate, but CPD has not yet done this. All three models are capable of predicting the complete molecular weight distributions of fragments, but only FG-DVC uses this information to predict the extract yield, the tar yield and the tar molecular weight distribution. DISARAY uses only the prediction for monomers (defined as tar precursor) and CPD uses only the prediction for all oligomers (defined as tar). In a recent paper[32], the total oligomer population computed by the FG-DVC model was used to predict coal fluidity behaviour. Only FG-DVC employs a mass transport equation which is necessary to predict tar molecular weights and the variations of yield and molecular weights with pressure. Only FG-DVC predicts the solvent swelling ratio, which is determined by the crosslink density in the char.

CONCLUSIONS

This paper examines the extension of macromolecular network concepts to describe coal thermal decomposition. The statistical methods (Monte Carlo calculations and percolation theories) and the classes of chemical reactions (labile bridge breaking, hydrogen utilization, crosslinking) and mass transport (vaporization and convection) employed by different researchers have been compared. The conclusion are as follows:

1. The application of macromolecular network concepts appears to be a very promising and versatile approach.
2. Monte Carlo methods for computing the network statistics are the most versatile, but are computationally demanding.
3. The use of percolation theory is computationally efficient and helps provide insight into network behaviour, but the use of a fixed coordination number may be inadequate to accurately describe coal thermal decomposition. The network appears to require a coordination number between 2.2 and 2.5 during labile bridge breaking and greater than 3 during crosslinking.
4. Alternatively, a more general percolation theory model for a network with two types of bridging bonds was developed, each with their own $\sigma+1$.
5. When the two-σ percolation model is applied using the FG-DVC chemistry to cases in which tar is not removed, it is much more flexible in matching the Monte Carlo calculations. The one-σ models either decompose at too low a temperature for large values of $\sigma+1$, or decompose too much and resolidify at too low a temperature for small values of $\sigma+1$. Applying percolation theory to cases where tar is removed requires additional approximations.
6. Of the three models compared (CPD, DISARAY, and FG-DVC), FG-DVC is the most complete in treating the molecular weight distribution of network fragments and the processes of vaporization and mass transport to define tar, the tar molecular weight distribution and the extract yield.
7. Of the three models, FG-DVC is the most closely related with the previous concepts of coal as a macromolecular network by requiring that the model predict the coal solvent swelling ratios and measured extract yields. The assumptions which define the parameters of the starting network are open to question and must be explored.
8. Future efforts should focus on identifying the chemistry for the processes of bridge breaking, low temperature crosslinking, moderate temperature crosslinking, and hydrogen utilization.

ACKNOWLEDGEMENTS

The authors acknowledge support for the work provided by the Morgantown Energy Technology Center of the Department of Energy under Contract No. DE-AC21-86MC23075.

REFERENCES

1 van Krevelen, D. W. in 'Coal', Elsevier, Amsterdam, The Netherlands, 1961
2 Green, T. K., Kovac, J. and Larsen, J. W. *Fuel* 1984, 63, 935
3 Brenner, D. *Fuel* 1985, 64, 167
4 Lucht, L. M. and Peppas, N. A. *Fuel* 1987, 66, 803
5 Lucht, L. M., Larsen, J. M. and Peppas, N. A. *Energy & Fuels* 1987, 1, 56
6 Larsen, J. W. *Am. Chem. Soc. Div. Fuel Chem. Prepr.* 1985, 30(4), 444
7 Green, T., Kovac, J., Brenner, D. and Larsen, J. in 'Coal Structure' (Ed. R. A. Meyers), Academic Press, NY, USA, 1982, p. 199
8 Hall, P. J., Marsh, H. and Thomas, K. M. *Fuel* 1988, 67, 863
9 Sanada, Y. and Honda, H. *Fuel* 1966, 45, 295
10 Suuberg, E. M., Yoshi, O. and Deevo, S. *Am. Chem. Soc. Div. Fuel Chem. Prepr.* 1988, 33(1), 387
11 Suuberg, E. M., Lee, D. and Larsen, J. W. *Fuel* 1985, 64, 1668
12 Suuberg, E. M., Unger, P. E. and Larsen, J. W. *Energy & Fuels* 1987, 1, 305
13 Brown, J. K., Dryden, I. G. C., Dunevein, D. H. *et al. J. Inst. Fuel* 1958, 31, 259

14 Orning, A. A. and Greifer, B. *Fuel* 1956, 35, 318
15 Solomon, P. R. and Hamblen, D. G. in 'Chemistry in Coal Conversion' (Ed. R. H. Schlosberg), Plenum Press, New York, USA, chapter 5, p. 121
16 Solomon, P. R. 'New Approaches in Coal Chemistry', ACS Symposium Series 169, ACS, Washington, DC, USA, 1981, p. 61
17 Solomon, P. R. and King, H. H. *Fuel* 1984, 63, 1302
18 Gavalas, G. R. in 'Coal Pyrolysis' Elsevier, NY, USA, 1982, p. 51
19 Gavalas, G. R., Cheong, P. H. and Jain, R. *Ind. Eng. Chem. Fundam.* 1981, 20, 122
20 Squire, K. R., Solomon, P. R., Carangelo, R. M. and DiTaranto, M. B. *Fuel* 1986, 65, 833
21 Squire, K. R., Solomon P. R., DiTaranto, M. B. and Carangelo, R. M. *Am. Chem. Soc. Div. Fuel Chem. Prepr.* 1985, 30(1), 386
22 Solomon, P. R., Squire, K. R. and Carangelo, R. M. 'Proc. Int. Conf. on Coal Science', Pergamon, Sydney, Australia, 1985, p. 945
23 Solomon, P. R. and Squire, K. R. *Am. Chem. Soc. Div. Fuel Chem. Prepr.* 1985, 30(4), 347
24 Niksa, S. and Kerstein, A. R. *Comb. and Flame* 1986, 66, 95
25 Niksa, S. *Comb. and Flame* 1986, 66, 111
26 Solomon, P. R., Hamblen, D. G., Deshpande, G. V. and Serio, M. A. 'Proc. Int. Coal Science Conference', Elsevier, NY, USA, 1987, p. 601
27 Solomon, P. R., Hamblen, D. G., Carangelo, R. M. *et al. Comb. and Flame* 1988, 71, 137
28 Niksa, S. and Kerstein, A. R. *Fuel* 1987, 66, 1389
29 Solomon, P. R., Hamblen, D. G., Carangelo, R. M. *et al. Energy & Fuels* 1988, 2, 405
30 Grant, D. M., Pugmire, R. J., Fletcher, T. H. and Kerstein, A. R. *Energy & Fuels* 1989, 3, 175
31 Serio, M. A., Solomon, P. R., Yu, Z. Z. *et al. Am. Chem. Soc. Div. Fuel Chem. Prepr.* 1988, 33(3), 91
32 Solomon, P. R., Best, P. E., Yu, Z. Z. and Deshpande, G. V. *Am. Chem. Soc. Div. Fuel Chem. Prepr.* 1989, 34(3), 895
33 Nielsen, L. E. in 'Mechanical Properties of Polymers and Composites', Volume 2, Marcel Dekker, Inc., NY, USA, 1974
34 Bartels, C. R., Crist, B., Felters, L. J. and Graessley, W. W. *Macromolecules* 1986, 19, 785
35 Nazem, F. F. *Fuel* 1980, 59, 851
36 Macosko, C. W. *Brit. Polymer Journ.* 1985, 17, 239
37 Flory, P. J. *J. Am. Chem. Soc.* 1941, 63, 3083, 3097; 'Principles of Polymer Chemistry', Cornell University Press, Ithaca, NY, USA, 1953, chapter 9
38 Stockmayer, W. H. *J. Chem. Phys.* 1943, 11, 45; 1944, 12, 125
39 Fisher, M. E. and Essam, J. W. *J. Math. Phys.* 1961, 2, 609
40 Solum, M., Pugmire, R. J. and Grant, D. M. *Energy & Fuels* 1989, 3, 40
41 Gerstein, B. C., Murphy, D. P. and Ryan, L. M. in 'Coal Structure' (Ed. R. A. Meyers), Academic Press, NY, USA, 1982, chapter 4, p. 87
42 Hooker, D. T. II, Lucht, L. M. and Peppas, N. A. *Ind. Eng. Chem. Fundam.* 1986, 25, 103
43 Solomon, P. R., Serio, M. A., Carangelo, R. M. and Markham, J. R. *Fuel* 1986, 65, 182
44 Fletcher, T. H. *Comb. Sci. and Tech.* 1989, 63, 87
45 Solomon, P. R., Serio, M. A., Deshpande, G. V. and Kroo, E. *Energy & Fuels* submitted for publication; Deshpande, G. V., Solomon, P. R. and Serio, M. A. *Am. Chem. Soc. Div. Fuel Chem. Prepr.* 1988, 33(2), 310
46 Unger, P. E. and Suuberg, E. M. '18th Symposium (Int) on Combustion', The Combustion Institute, Pittsburgh, PA, USA, 1981, p. 1203
47 Suuberg, E. M., Unger, P. E. and Lilly, W. D. *Fuel* 1985, 64, 956
48 Unger, P. E. and Suuberg, S. E. *Fuel* 1984, 63, 606
49 Oh, M. S., Peters, W. A. and Howard, J. B. *AIChE J.* 1989, 35(5), 775
50 Serio, M. A. *Ph.D. Thesis* Massachusetts Institute of Technology, Cambridge, MA, USA, 1984
51 Khan, M. R., Serio, M. A., Malhotra, R. and Solomon, P. R. *Am. Chem. Soc. Div. Fuel Chem. Prepr.* 1989, 34(4), 1054
52 Fong, W. S., Peters, W. A. and Howard, J. B. *Fuel* 1986, 65, 251
53 Solomon, P. R. and Carangelo, R. M. *Fuel* 1982, 61, 663
54 Solomon, P. R. and Carangelo, R. M. *Fuel* 1988, 67, 949

APPENDIX A

The probability $F_{s,u}(p, q)$, that a site is a member of a cluster of n sites with s type 1 bridges and u type 2 bridges is given by

$$F_{s,u}(p, q)=a_{s,u}p^s(1-p)^\tau q^u(1-q)^\nu \tag{1}$$

where

$$\begin{aligned} n&=u+s+1 \\ \tau&=(\sigma_1+1)n-2s \\ \nu&=(\sigma_2+1)n-2u \end{aligned} \tag{2}$$

τ and ν are the number of broken bridges of type 1 and 2, respectively, on the perimeter of the cluster, and $a_{s,u}$ is the number of different ways to form such a cluster. Following the procedure used by Fisher and Essam, an expression for the configuration coefficient can be derived

$$a_{s,u}=\frac{(\sigma_1+1)(\sigma_2+1)}{(s+\tau)(u+\nu)}\Gamma(s+\tau+1)\Gamma(u+\nu+1)(u+s+1) \tag{3}$$

where Γ is a gamma function. Note that for $u=0$ (no type 2 bonds), this reduces to the quantity nb_n in Ref. 30. To determine the probability, $F_n(p, q)$ that a given site is a member of a cluster of n sites, i.e. the fraction of n-mers, Equation (1) must be summed over all possible values of s and u that give an n-site cluster:

$$F_n(p, q)=\sum_{s=0}^{n-1} a_{s,u}p^s(1-p)^\tau q^u(1-q)^\nu \qquad u=n-s-1 \tag{4}$$

The total fraction of sites, $F(p, q)$ in finite clusters is the sum over all s and u

$$F(p, q)=\sum_{s=0}^{\infty}\sum_{u=0}^{\infty} F_{s,u}(p, q)=\left(\frac{1-p}{1-p^*}\right)^{\sigma_1+1}\left(\frac{1-q}{1-q^*}\right)^{\sigma_2+1} \tag{5}$$

where p^* and q^* are obtained by finding the least roots of

$$\begin{aligned} p^*(1-p^*)^{\sigma_1-1}(1-q^*)^{\sigma_2+1}-p(1-p)^{\sigma_1-1}(1-q)^{\sigma_2+1}&=0 \\ q^*(1-q^*)^{\sigma_2-1}(1-p^*)^{\sigma_1+1}-q(1-q)^{\sigma_2-1}(1-p)^{\sigma_1+1}&=0 \end{aligned} \tag{6}$$

The critical point at which an infinite lattice begins to form (i.e. $F(p, q)$ begins to decrease) becomes a critical curve which divides the p-q plane into two regions. Note that for $q=0$, the equations all reduce to the single σ case given in Ref. 30.

Appendix M

An Empirical Model for Coal Fluidity Based on a Macromolecular Network Pyrolysis Model

Baxter, L. L., "Turbulent transport of particles," Ph.D. dissertation, Brigham Young University, Provo, UT, (1989).

Baxter, L. L., Smith, P. J. and Smoot, L. D., "Optimization of coal devolatilization model parameters for comprehensive gasifiction and combustion models," Western States Section/The Combustion Institute, Banff, Alberta, Canada, April 27-30, (1986).

Bilger, R. W., "Chemical reaction calculations in turbulent flows: application to a CO-containing turbulent plume," Adv. in Geophysics, 188, 349 (1974).

Bilger, R. W., "Turbulent jet diffusion flames," Prog. Energy Comb. Sci., 1, 87 (1976).

Bird, R. B., Stewart, W. E. and Lightfoot, E. N., Transport phenomena, Wiley, New York (1960).

Borghi, R., "Chemical reaction calculations in turbulent flows: application to a co-containing turbulent plume," Adv. Geophysics, 188, 349 (1974).

Bose, A. C., Dannecker, K. M. and Wendt, J. O. L., "Coal domposition effects on mechamisms governing the destruction of NO and other nitrogenous species during fuel-rich combustion," Energy & Fuels, 2, 301 (1988).

Boussinesq, J., "Theorie de l'ecoulement tourbillant," Mem. Acac. Sci., 23(No. 46), (1877).

Bowman, C. T., "Kinetics of pollutant formation and destruction in combustion," Prog. in Energy Comb. Sci., 1, 1 (1975).

Brewster, B. S., Baxter, L. L. and Smoot, L. D., "Treatment of coal devolatilization in comprehensive combustion modeling," Energy & Fuels, 2, 362-370 (1988).

Brewster, M. Q. and Kunitomo, T., "The optical constants of coal, char, and limestone," J. Heat Trans./Trans. ASME, 106, 678-83 (1984).

Bueters, K. A., Cogoli, J. G. and Habelt, W. E., "Performance prediction of tangentially fired utility furnaces by computer model," Fifteenth Symposium (International) on Combustion, The Combustion Institute, Pittsburgh, PA, 1245-1260 (1974).

Caretto, L. S., "Mathematical modeling pollutant formation," Prog. Energy Comb. Sci., 1, (1976).

Carlson, B. G. and Lathrop, K. D., "Computing methods in reactor physics," Transport theory - the method of discrete ordinates, Eds, Gordon Breach Science Publishers, New York, (1968).

Carnahan, B., Luther, H. A. and Wilkes, J. O., Applied numerical methods, John Wiley and Sons, New York, NY (1969).

Castro, I. P., The numerical prediction of recirculating flows in numerical methods in laminar and turbulent flow, Pentech Press, London (1978).

Chen, S. L., Pershing, D. W. and Martin, G. B., "Influence of coal composition on the fate of volatile and char nitrogen during combustion," Nineteenth Symposium (International) on Combustion, The Combustion Institute, Pittsburgh, PA, 1271 (1982).

Crowe, C. T., Sharma, M. P. and Stock, D. E., "The particle-source-in-cell (PSI-CELL) model for gas-droplet flows," J. Fluids Eng., Trans. of the ASME, 99, 325-332 (1977).

DeMarco, A. G. and Lockwood, F. C., "A new flux model for the calculation of radiation in furnaces," LaRivista dei Combustibili (Italian Flame Day), 29, 184 (1975).

DeSoete, G. G., Overall reaction rates of NO and N2 formation from fuel nitrogen, 15th Symposium (International) on Combustion, The Combustion Institute, Pittsburgh, PA, 1093-1102 (1975).

Field, M. A., Gill, D. W., Morgan, B. B. and Hawksley, P. G. W., Combustion of pulverized coal, The British Coal Utilisation Research Association, Leatherhead, Surrey, England (1967).

Fletcher, T. H., "Theoretical modeling of reacting coal particles in pulverized coal combustion and gasification," M.S. thesis, Brigham Young University, Provo, UT, (1980).

Fletcher, T. H., "A two-dimensional model for coal gasification and combustion," Ph.D. dissertation, Brigham Young University, Provo, UT, (1983).

Freihaut, J. D. and Proscia, W. M., First International Conference on Combustion Technologies for a Clean Environment, Vilamoura (Algarve), Portugal, (1991).

Gallagher, R. H., Oden, J. T., Taylor, C. and Zienkiewicz, O. C., Finite elements in fluids volume 1 and 2, John Wiley and Sons, London (1975).

Ghani, M. U. and Wendt, J. O. L., "Early evolution of coal nitrogen in opposed flow combustion configurations," Twenty-Third Symposium (International) on Combustion, The Combustion Institute, Pittsburgh, Orléans, France, July 22-27, 1281-1288 (1990).

Godridge, A. M. and Read, A. W., "Combustion and heat transfer in large boiler furnaces," Prog. Energy Combust. Sci., 2, 83-95 (1976).

Goetz, G. J., Nsakala, N. Y., Patel, K. L. and Lao, T. C., "Combustion and gasification kinetics of chars from four commercially significant coals of varying rank," Second Annual Conference on Coal Gasification, EPRI, Palo Alto, CA, October, (1982).

Gosman, A. D. and Lockwood, F. C., "Incorporation of a flux method for radiation into a finite-difference procedure for furnace calculations," in Fourteenth Symposium (International) on Combustion, The Combustion Institute, Pittsburgh, PA, University Park, PA, August 20-25, 1972, 661-671 (1973).

Gosman, A. D., Lockwood, F. C. and Salooja, A. P., The prediction of cylindrical furnaces gaseous fueled with premixed and diffusion burners, 17th Symposium (International) on Combustion, The Combustion Institute, (1978).

Gosman, A. D., Pun, W. M., Ruchal, A. K., Spalding, D. B. and Wolfshstein, R., Heat and mass transfer in recirculating flows, Academic Press, London (1969).

Gosman, A. D. and Pun, W. M., Picture notes for course entitled calculation of recirculating Flows, Imperial College, London (December 1973).

Hadvig, S., "Gas emissivity and absorptivity: a thermodynamic study," J. Inst. Fuel, 129-135 (April 1970).

Haussmann, G. J. and Kruger, C. H., "Evolution and reaction of fuel nitrogen during rapid coal pyrolysis and combustion," Western States Section/The Combustion Institute, Livermore, CA, (1989).

Hobbs, M. L., Radulovic, P. T. and Smoot, L. D., "Modeling fixed-bed coal gasifiers," AIChE Journal, 38, 681-702 (1992).

Hottel, H. C. and Sarofim, A. F., Radiative transfer, New York, McGraw-Hill (1967).

Huber, A. M., "Effect of sorbent on sulfur pollutant species in an entrained-flow coal gasifier," M.S. thesis, Brigham Young University, Provo, Utah, (1989).

Iverach, D., Basden, K. S. and Kirov, N. Y., "Formation of nitric oxide in fuel-lean and fuel-rich flames," Fourteenth Symposium (International) on Combustion/The Combustion Institute, Pittsburgh, PA, 767 (1973).

Jamaluddin, A. S. and Smith, P. J., Prediction of radiative heat transfer in cylindrical furnaces, Western States and Canadian Sections, The Combustion Institute, Banff, Canada, April, (1986).

Jamaluddin, A. S. and Smith, P. J., "Predicting radiative transfer in axisymmetric cylindrical enclosures using the discrete ordinates method," Comb. Flame, (1987).

Jayatilleke, C. L. V., "The influence of Prandtl number and surface roughness on the resistance of the laminar sub-layer to momentum and heat transfer," Prog. Heat Mass Trans., 1, 193-237 (1969).

Jones, W. P. and Launder, B. E., "The calculation of low-Reynolds-number phenomena with a two-equation model of turbulence," Int. J. Heat Mass Transfer, 16, 1119-1130 (1973).

Jones, W. P. and Launder, B. E., "The prediction of laminarization with a two-equation model of turbulence," Int. J. Heat Mass Transfer, 15, 301-314 (1972).

Kent, J. H. and Bilger, R. W., "The prediction of turbulent diffusion flame fields and nitric oxide formation," 16th Symp. (International) on Combustion, The Combustion Institute, Pittsburgh, PA, 1643-1656 (1977).

Kent, J. H. and Honnery, D. R., "A soot formation rate map for a laminar ethylene diffusion flame," Comb. Flame, 79, 289-298 (1990).

Khalil, E. E., Spalding, D. B. and Whitelaw, J. H., "The calculation of local flow properties in two-dimensional furnaces," Int. J. Heat and Mass Trans., 18, 775-791 (1975).

Kobayashi, H., "Devolatilization of coal at high temperatures," Ph.D. dissertation, M.I.T., Cambridge, MA, (1976).

Kuo, K. K., Principles of combustion, John Wiley, New York (1986).

Launder, B. E. and Spalding, D. B., Mathematical models of turbulence, Academic Press, London (1972).

Lavoie, G. A., Heywood, J. B. and Keck, J. C., "Experimental and theoretical study of nitric oxide formation in internal combustion engines," Comb. Sci. Tech., 1, 313 (1970).

Leonard, B. P., "A stable and accurate convective modeling procedure based on quadratic upstream interpolation," Computer Methods in Applied Mechanics and Engineering, 19, 59-98 (1979).

Leschiziner, M. A., "Practical evaluation of three finite difference schemes for the computation of steady-State recirculating flows," Computer Methods in Applied Mechanics and Engineering, 23, 293-312 (1980).

Levy, J. M., Chen, L. K., Sarofim, A. F. and Béer, J. M., NO/char reactions at pulverized coal flame conditions, 18th Symposium (International) on Combustion, The Combustion Institute, Pittsburgh, PA, 111-120 (1981).

Libby, P. A., "On turbulent flows with fast chemical reactions part III: two-dimensional mixing with highly dilute reactants," Combust. Sci. Tech., 13, 79-98 (1976).

Lillington, J. N., "Numerical methods in laminar and trubulent flow," A comparison of finite difference methods for the prediction of temperature in recirculating flows in rod cluster geometry, Pentech Press, London, 515-525 (1978).

Lilly, D. G. and Rhode, D. L., A computer code for swirling turbulent axisymmetric recirculating flows in practical isothermal combustor geometries, NASA Contractor Report 3442, prepared for Lewis Research Center under Grant NAG 3-74, (1982).

Lilly, G. P., "Effect of particle size on particle eddy diffusivity," Ind. Eng. Chem. Fund., 12, 268-275 (1973).

Lockwood, F. C. and Naguib, A. S., "The prediction of the fluctuations in the properties of free, round-Jet, turbulent, diffusion flame," Comb. Flame, 24, 109-124 (1975).

Lockwood, F. C., Salooja, A. P. and Syed, S. A., "A prediction method for coal-fired furnaces," Comb. Flame, 38, 1-15 (1980).

Longwell, J. P. and Weiss, M. A., "Mixing and distribution of liquids in high-velocity air streams," Ind. Eng. Chem., 45, 1-15 (1980).

Lowe, A., Wall, T. F. and Stewart, I., "A zoned heat transfer model of large tangentially fired pulverized coal boilers," Fifteenth Symposium (International) on Combustion, The Combustion Institute, Pittsburgh, PA, 1261-1270 (1974).

Lowes, T. M., Bartelds, H., Heap, M. P., Michelfelder, S. and Pai, B. R., "The prediction of radient heat transfer in axisymmetrical systems," Report No. GO2/a/25, International Flame Research Foundation, IJmuiden, The Netherlands, (1973).

Melville, E. K. and Bray, N. C., "A Model of the two-phase turbulent jet," Int. J. Heat and Mass Trans., 22, 647-656 (1979).

Merrick, D., "Mathematical models of the thermal decomposition of coal. 2. Specific heats and heats of reaction," Fuel, 62, 540-546 (1983).

Mie, G., "Optics of turbid media," Ann. Phys., 25, 377-445 (1908).

Miller, J. A. and Bowman, C. T., "Mechanism and modeling of nitrogen chemistry in combustion," Prog. Energy Combust. Sci., 15, 287 (1989).

Mitchell, J. W. and Tarbell, J. M., "A kinetic model of nitric oxide formation during pulverized coal combustion," AIChE J., 28, 302-311 (1982).

Mitchell, R. E., "Determination of the intrinsic reactivities of pulverized-coal chars at high temperature," (1988).

Mitchell, R. E., "The influence of the mineral matter content of coal on the temperatures and burning rates of char particles during pulverized coal combustion," Sixth Annual International Pittsburgh Coal Conference Proceedings, Pittsburgh, PA, September 25-29, 32-52 (1989).

Nicoletti, P. A., METCEC - USER'S MANUAL, Final Report, DOE-METC Contract No. DE-AC21-85MC21353, EG&G WASC, Inc., Morgantown, WV, (1986).

Nicoletti, P. A., METCEC - PROGRAM LOGIC MANUAL, Final Report, DOE-METC Contract No. DE-AC21-85MC21353, EG&G WASC, Inc., Morgantown, WV, (1986).

Patankar, S. V. and Spalding, D. B., "A calculation procedure for heat, mass and momentum transfer in three-dimensional parabolic flows," International Journal of Heat and Mass Transfer, (Oct. 1972).

Patankar, S. V. and Spalding, D. B., Heat and mass transfer in boundary layers, Intertext Books, London (1970).

Patankar, S. V., Numerical heat transfer and fluid flow, Hemisphere Publishing, Washington (1980).

Patanker, S. V., "Studies in converction," in Chapter 1, Numerical prediction of three-dimensional flows, Ed, Academic Press, London, (1975).

Peck, R. E., Glarborg, P. and Johnsson, J. E., Comb. Sci. Tech., 76, 81 (1991).

Pratt, D. T., "Mixing and chemical reaction in continuous combustion," Prog. Energy Comb. Sci, 73-86 (1976).

Pratt, D. T. and Wormeck, J. J., CREK A computer program for calculation of combustion reaction equilibrium and kinetics in laminar or turbulent flows, WSU-COE-B-76-341, Washington State Univ., Pullman, WA, (1976).

Raithby, G. D., "Skew upstream differencing schemes for problems involving fluid flow," Computer Methods in Applied Mechanics and Engineering, 9, 153-164 (1976).

Roache, P. J., Computational fluid dynamics, Hermosa Publishers, Albuquerque, NM (1976).

Sarofim, A. F. and Hottel, H. C., "Radiative transfer in combustion chambers: Influence of alternative fuels," Sixth International Heat Transfer Conference, Toronto, Canada, (1978).

Sarofim, A. F. and Pohl, J. H., "Kinetics of nitric oxide formation in premixed laminar flames," Fourteenth Symposium (International) on Combustion/The Combustion Institute, Pittsburgh, PA, 739 (1973).

Siegel, R. and Howell, J. R., Thermal radiation heat transfer, Hemisphere Publishing, New York (1981).

Silcox, G. D., "Analysis of the SO2-lime reaction system: Mathematical modeling and experimental studies emphasis on stoker applications," Ph.D. dissertation, The University of Utah, (1985).

Sloan, D. G., Smith, P. J. and Smoot, L. D., "Modeling of swirl in turbulent flow systems," Prog. Energy Comb. Sci., 12, 63-250 (1986).

Smith, P. J., "Theoretical modeling of coal and gas-fired turbulent combustion and gasification process," Ph.D. dissertation, Brigham Young University, Provo, UT, (1979).

Smith, P. J., Hill, S. C. and Smoot, L. D., "Theory for NO formation in turbulent coal flames," 19th Symposium (International) on Combustion, The Combustion Institute, Pittsburgh, PA, 1263 (1982).

Smith, P. J., Fletcher, T. H. and Smoot, L. D., "Model for pulverized coal-fired reactors," Eighteenth Symposium (International) on Combustion, The Combustion Institute, Pittsburgh, PA, Waterloo, Canada, Aug 17-22 1980, 1285-1293 (1981).

Smoot, L. D. and Horton, M. D., "Exploratory studies of flame and explosion quenching," Final Report, Bureau of Mines Contract 101220052, Brigham Young University, Provo, UT, (1978).

Smoot, L. D. and Pratt, D. T., Pulverized coal combustion and gasification, Plenum, New York (1979).

Smoot, L. D. and Smith, P. J., Coal combustion and gasification, Plenum, New York (1985).

Smoot, L. D. and Smith, P. J., "Comprehensive modeling of combustion systems," Proceedings of the 1987 ASME/JSME Thermal Engineering Joint Conference, eds. P. J. Marto and I. Tanasawa, American Society of Mechanical Engineers, 1, Honolulu, HI, (1987).

Solomon, P. R., Hamblen, D. G., Carangelo, R. M., Serio, M. A. and Deshpande, G. V., "General model of coal devolatilization," Energy & Fuels, 2, 405-422 (1988).

Solomon, P. R., Serio, M. A., Carangelo, R. M. and Markham, J. R., "Very rapid coal pyrolysis," Fuel, 65, 182-194 (1986).

Spalding, D. B., "Concentration fluctuations in a round turbulent free jet," Chem. Engr. Sci., 26, 95-107 (1971).

Spalding, D. B., "A general theory of turbulent combustion," J. Energy, 2, 16-23 (1978).

Spalding, D. B., Turbulence modeling: solved and unsolved problems, turbulent mixing in nonreactive and reactive flows, Ed, Plenum Press, New York, NY, (1975).

Dave, F. V., "Subroutine for computing the parameters of the electromagnetic radiation scattered by a sphere, 360 D-17, 4.00Z," IBM Corporation, (1968).

Tennekes, H. and Lumley, J. L., A first course in turbulence, The MIT Press, Cambridge, MA (1972).

Thompson, D., Brown, T. D. and Beér, J. M., "Formation of NO in a methane-air flame," Eighteenth Symposium (International) on Combustion/The Combustion Institute, Pittsburgh, PA, 787 (1981).

Truelove, J. S., Differential equation models of radiative heat transfer, AERE R-8364, AERE Harwell, U.K., (1976).

Truelove, J. S., Evaluation of a multi-flux model for radiative heat transfer in cylindrical furnaces, AERE R-9100, AERE Harwell, U.K., (1978).

Truelove, J. S. and Jamaluddin, A. S., "Models for rapid devolatilization of pulverized coal," Combustion and Flame, 64, 369-372 (1986).

Ubhayakar, S. K., Stickler, D. B., von Rosenberg, C. W. and Gannon, R. E., "Rapid devolatilization of pulverized coal in hot combustion gases," 16th Symposium (International) on Combustion, The Combustion Institute, Pittsburgh, PA, 427-436 (1976).

Van Doormaal, J. P. and Raithby, G. D., "Enhancements of the SIMPLE method for predicting incompressible fluid flows," Num. Heat Transf., 7, 147-163 (1984).

Varma, S. A., "Radiative heat transfer in a pulverized-coal flame," Chapter 5 in Pulverized coal combustion and gasification, Eds., Plenum Press, New York, NY, 83-106 (1979).

Varma, S. A. and Pratt, D. T., Anisotropic and multiple scattering of thermal radiation in pulverized coal combustors, 17th Symposium (International) on Combustion, Pittsburgh, PA, (1978).

Walker, P. L. J., Rusinko, F. J. and Austin, L. G., "Gas reactions of carbon," in Eley, D. D., Selwood, P. W. and Weisz, P. B., ed., Advances in catalysis, Volume XI, ed., Academic Press, New York, 133 (1959).

Wallis, G. B., One-dimensional two-phase flow, McGraw-Hill, New York (1969).

Wen, C. Y., Chen, H. and Onozaki, M., User's manual for computer simulation and design of the moving bed coal gasifier, Final report DOE/MC/16474-1390, U.S. Dept. of Energy, Morgantown, WV, (1982).

Wendt, J. O. L., Bose, A. C. and Hein, K. R. G., "Fuel nitrogen mechanisms governing NOx abatement for low and high rank coals," 1988 Joint Symposium on Stationary Combustion NOx Control, San Francisco, CA, March 609, (1989).

Westenberg, A. A., "Kinetics of NO and CO in lean, premixed hydrocarbons air flows," Comb. Sci. Tech., 9, 59 (1971).

Williams, F. A., Combustion theory, Addison-Wesley, Reading, MA (1965).

Wiser, W. H., Hill, G. R. and Kertamus, N. J., Ind. Eng. Chem. Process Des. Develop., 6, 133 (1967).

Wormeck, J. J., "Computer modeling of turbulent combustion in a longwell jet-stirred Reactor," Ph.D. dissertation, Washington State University, (1976).

Yoon, H., "Modeling and analysis of moving bed coal gasifiers," Ph.D. dissertation, University of Delaware, Newark, DE, (1978).

Zeldovich, Y. B., Sadovnikov, P. Y. and Frank-Kamentskii, D. A., "Oxidation of nitrogen in combustion," translated by Academy of Sciences of USSR, (1947).

Appendix A

Description of Subroutines

A description of the routines used in PCGC-2 is given in this appendix. The subroutines are grouped according to function. Entry points are shown with the name of the subroutine to which they belong in parentheses. Descriptions of routines contained in the FG-DVC submodel are found in Chapter 6.

Main Program

PCGC-2	Main driver routine for PCGC-2. Reads basic input data for grid site, inlet conditions, etc. Calls all CALC subroutines for calculating gas variables, as well as PSICT and FLUX. Determines convergence criterion and stops program when converged.

Auxiliary Subroutines

BLOCKDATA	Blockdata subprogram.
CPUTIM	Returns the elapsed CPU time.

FLINT	Initializes flow field so calculations can begin. Also initializes inlet densities.
GRDGRF	Makes visual output of grid for interactive program users.
GRID	Sets up numerical grid used to solve the equations.
GRMAP	Reads location of user-specified grid points from data file. Also writes calculated grid points into data file.
HEATBAL	Calculates wall radiative heat transfer and overall heat and material balances.
INFLOW	Reads flowrates and properties of incoming streams.
INIT	Initializes FORTRAN arrays for all field variables.
PRINT	Prints output according to specified format.
PROFIL	Reads in parameters governing inlet profiles of U (axial velocity), V (radial velocity), W (tangential velocity), TE (turbulence kinetic energy), and ED (eddy dissipation rate), and then initializes the inlet boundary.
PROG	Writes progress file.
RESTRT	This subroutine does all the work necessary for reading and writing information necessary to restart a combustion calculation from a partially converged solution.
VECTOR	Initializes a vector (2-dimensional array) to a uniform value. Can be called on the fly in a symbolic debugger. Useful for program debugging.

Gas-Phase Fluid Mechanics

AIM	Matrix-solving routine. LISOLV is nearly always used instead of AIM. AIM should be considered in cases where convergence is slow or unattainable with LISOLV. AIM takes full-directional coupling into account (5-diagonal matrix). LISOLVE is faster when it works.
CALACJ	Calculates coefficients for Eulerian finite difference equation for ACJ at each grid point.
CALAHJ	Calculates coefficients for Eulerian finite difference equation for AHJ at each grid point.
CALCED	Calculates coefficients for finite difference equation for eddy dissipation and solves for the field values of eddy dissipation at each grid point.
CALCET	Calculates coefficients for finite difference equation for eta (coal gas mixture fraction) and solves for the field values of eta at each grid point.
CALCF	Calculates coefficients for finite difference equation for f (inlet gas mixture fraction) and solves for the field values of f at each grid point.
CALCG	Calculates coefficients for finite difference equation for G (variance of the coal gas mixture fraction) and solves for the field values of G at each grid point.
CALCGE	Calculates coefficients for finite difference equation GETA (variance of the coal gas mixture fraction) and solves for the field values of GETA at each grid point.

CALCH	Calculates coefficients for finite difference equation for H (gas enthalpy) and solves for the field values of H at each grid point.
CALCNJ	Calculates coefficients for finite difference equation for NJ (bulk particle number density for jth particle type) and solves for the field values of NJ at each grid point.
CALCP	Calculates coefficients for finite difference equation for P (pressure) and solves for the field values of P at each grid point (SIMPLER algorithm).
CALCPP	Calculates coefficients for finite difference equation for PP (pressure correction) and solves for the values of PP at each grid point (SIMPLE algorithm).
CALCTE	Calculates coefficients for finite difference equation for K (turbulence kinetic energy) and solves for the field values of K at each grid point.
CALCU	Solves for the field values of U (axial velocity) at each grid point.
CALCV	Solves for the field values of V (radial velocity) at each grid point.
CALCW	Calculates coefficients for finite difference equation for W (tangential velocity) and solves for the field values of W at each grid point.
CALCYFU	Calculates coefficients for finite difference equation for YFU (fuel mass fraction) and solves for the field values of YFU at each grid point.
LISOLV	The tri-diagonal matrix solving routine (Based on Thomas Algorithm). See description of AIM.
MODED (PROMOD)	Modifies coefficients and source terms for boundary nodes so as to take boundary conditions into account for eddy dissipation.

MODETA	Modifies coefficients and source terms for boundary nodes so as to take boundary conditions in to account.
MODF (PROMOD)	Modifies coefficients and source terms for boundary nodes so as to take boundary conditions into account.
MODG (PROMOD)	Modifies coefficients and source terms for boundary nodes so as to take boundary conditions into account.
MODGET (PROMOD)	Modifies coefficients and source terms for boundary nodes so as to take boundary conditions into account for GETA.
MODH	Modifies coefficients and source terms for boundary nodes so as to take boundary conditions into account for H (gas enthalpy).
MODP (PROMOD)	Modifies coefficients and source terms for boundary nodes so as to take boundary conditions into account for P (pressure).
MODPP (PROMOD)	Modifies coefficients and source terms for boundary nodes so as to take boundary conditions into account for PP (pressure correction).
MODTE	Modifies coefficients and source terms for boundary nodes so as to take boundary conditions into account for K (turbulence kinetic energy).
MODU	Modifies coefficients and source terms for boundary nodes so as to take boundary conditions into account for U (axial velocity).
MODV (PROMOD)	Modifies coefficients and source terms for boundary nodes so as to take boundary conditions into account for V (radial velocity).

MODW (PROMOD)	Modifies coefficients and source terms for boundary nodes so as to take boundary conditions into account for W (tangential velocity).
MODYFU (PROMOD)	Modifies coefficients and source terms for boundary nodes so as to take boundary conditions into account for YFU (fuel mass fraction).
MOSOLV	Modified Operator Strongly Implicit (MOSI) Scheme, a fast elliptic solver. Alternative to LISOLV.
UCOEF	Calculates coefficients for finite difference equation for U (axial velocity).
VCOEF	Calculates coefficients for finite difference equation for V (radial velocity).
WALL	Handles intrusion boundary conditions for f (inlet gas mixture fraction), η (coal gas mixture fraction, g_f (variance in inlet gas mixture fraction), g_η (variance in coal gas mixture fraction), y_{fu}, p (pressure), and p' (pressure correction).

Gas-Phase Chemistry

ADCOND	Function which adds (if possible) a pure condensed species or an ideal solution based on lowering Gibbs free energy.
API	Auxiliary function used in thermochemical equilibrium computations.
CALC	Auxiliary subroutine for the CREE thermochemical equilibrium computations.

CHGCON	Replaces the solid phase of a species with the liquid phase of the same species (or vise versa), depending on the current temperature. CHGCON returns .TRUE. if a change was made.
CREE	This is the main controlling routine for the thermochemical equilibrium calculations (Chemically Reacting Equilibrium, from Elemental balances).
CREE0	This is strictly an initializing routine, the sole function of which is to read, store, and process data from input files. The initial statements in CREE0 cause branching to appropriate chapters, depending on which of the key words ELEM, THER, REAC, or a blank field are encountered. Data fields must be in the order given, as element data are needed in order to catalog thermodynamic data.
DGELG	Gaussian elimination subroutine.
DIF	Function that compares two numbers and returns their positive fractional difference.
ERATIO (SPECE)	Calculates fuel/air equivalence ratio given atom numbers using positive and negative oxidation states (valences).
ERF	Calculates the area under the normal curve from a spline fit. This is used for values of intermittency in the turbulent combustion model.
ETAST (TBLFE)	Calculates stoichiometric η (coal gas mixture fraction) for adiabatic reactor.
ETASTH (TBLFEH)	Calculates stoichiometric η (coal gas mixture fraction) for non-adiabatic reactor.
ETASTO (TABLE)	Calls either ETASTH or ETAST.

FAZCHK	Determine whether the current active list of pure condensed phase species violates the phase rule.
FGTABL	Calculates limits of normalized Gaussian PDF.
FRZFE	Calculates gas properties as a function of f (inlet gas mixture fraction) and η (coal gas mixture fraction) using frozen equilibrium scheme when the local equivalence ratio is greater than 2.0 (adiabatic reactor).
FRZFEH	Calculates gas properties as function of f (inlet gas mixture fraction), η (coal gas mixture fraction), and h_r (residual gas enthalpy, using frozen equilibrium scheme when the local equivalence ratio is greater than 2.0.
FSTE	Calculates stoichiometric mixture fraction (adiabatic reactor with no inlet gas mixing).
FSTF	Calculates stoichiometric mixture fraction (gas only and adiabatic reactor).
FSTFE	Calculates stoichiometric mixture fraction (adiabatic reactor with f and η).
FSTFEH	Calculates stoichiometric mixture fraction (using f, η, and h_r).
FSTFH	Calculates stoichiometric mixture fraction using f (inlet gas mixture fraction) and h_r (residual gas enthalpy) (gas only).
GASFIX	Called if a singular matrix is encountered and the latest condensed phase to be added has already been removed. GASFIX changes the moles of all gas phase species whose current moles equals zero to 1.0E-6.

GAUSS	Driver routine for DGELG, the Gaussian elimination subroutine.
GIBCHK	Removes the condensed phase species that have the least contribution to lowering the system's Gibbs free energy. This subroutine is called only if the phase rule is being violated.
GTDELN	Calculates the updates to the species mole numbers for gas and solution species. The update for the pure condensed species comes directly from the solving of the iteration matrix. GTDELN also calls GTETA which calculates the control factor.
GTETA	Calculates the control factor.
HCALC	Calculates HSUB0 from the reactant cards.
HCPS	Calculates specific heat, enthalpy, and entropy for a species at a specified temperature.
MATRIX	Sets up the iteration matrix.
MIXFE	For given mixture fraction (F and ETA), calculates fully mixed product without chemical reaction (adiabatic reactor).
MU	Calculates Gibbs free energy for each species.
PROPS	Calculates gas-phase properties from the cardinal variables, including turbulence effects when appropriate.
RANGOK	Returns .TRUE. if the current temperature is within the temperature range for the specified species.
REMPUR	Removes a pure condensed phase species from the equilibrium calculation. The species status, moles, the number of pure condensed species, and the SOLELE array are also updated.

SOLPOS	Determines the position of a specified solution in the active solution list.
SORTG	Sorts the pure condensed phase species in the active list in order of their contribution to the minimization of Gibbs free energy (from the species with the least contribution to the species with the largest contribution).
SPECE	The chemical equilibrium subroutine.
SYSERR	Called if a fatal error occurs in the equilibrium computations. It prints out a diagnostic message and stops program execution.
TABLE	Sets up table of equilibrium gas properties (ρ_g, M_i, T_g) as a function of f (inlet gas mixture fraction), η (coal gas mixture fraction), and/or h_r (residual gas enthalpy).
TBLE	Sets up gas equilibrium properties table as function of η (coal gas mixture fraction) (adiabatic reactor and no inlet gas mixing).
TBLF	Sets up gas equilibrium properties table as function of f (inlet gas mixture fraction) (gas only and adiabatic reactor).
TBLFE	Sets up table of equilibrium gas properties as function of f (inlet gas mixture fraction) and η (coal gas mixture fraction).
TBLFEH	Sets up table of equilibrium gas properties as a function of f (inlet gas mixture fraction), η (coal gas mixture fraction), and h_r (residual gas enthalpy).
TBLFH	Sets up table of equilibrium gas properties as function of f (inlet has mixture fraction) and h_r (residual gas enthalpy) (gas only).

TBLRSTFE	Reads and writes restart file for table of equilibrium gas properties.
TBLRSFEH	Reads and writes restart file for table of equilibrium gas properties as function of f (inlet gas mixture fraction), η (coal gas mixture fraction), and h_r (residual gas enthalpy).
TUBFEH	Calculates the required change in THIDEL or TMAX for table generation if the upper temperature limit is being exceeded.
UPDATE (TABLE)	Interpolates table values for gas properties.
UPF (TBLF)	Interpolates one-dimensional (f) gas properties table.
UPFE	Interpolates two-dimensional (f and η) gas properties table.
UPFEH	Interpolates three-dimensional (f, η, and h_r) gas properties table.
UPFH	Interpolates two-dimensional (f and h_r) gas properties table.

NO_x Submodel

B	Uses a cubic spline to find the reaction order for the homogeneous NO formation reaction based on the local oxygen concentration.
CALCNO	Calculates coefficients for finite difference equation for YNO (NO mass fraction), and solves for the field values of YNO at each grid point.

CALCO2	Calculates the mean O_2, N_2, and OH concentrations based on species or atomic mass balances.
CALHCN	Computes and assembles finite difference equations for the HCN species continuity equation; solves for the field of predicted HCN concentrations.
CALNH3	Computes and assembles finite difference equations for the NH_3 species continuity equation; solves for the field of predicted NH_3 concentrations.
EQSPEC	Calculates the equilibrium concentrations of nitrogen and oxygen by convolving over the probability density functions of f and eta. This is necessary since there is a possibility that their storage arrays were replaced by other information if "AIM" was used in PCGC2.
FREACT	Calculates the maximum possible concentrations of HCN, NH_3, and NO from fuel nitrogen conversion.
INTGRT	Computes integrated average dry mole fraction at each axial node for final writeout.
NOXMN	Reads input cards for the NO model; controls NO model logical sequence; tests for convergence; prints out intermediate and final results.
NOXDATA	Blockdata subprogram for data initialization.
RATE	Calculates the mean reaction rates and species continuity source terms.
RSTNOX	Reads and writes to restart file.
RXNEXT	Calculates reaction progress variables.
RXNRAT	Manages homogeneous chemical reaction rates for all mechanisms.

Plotting

CLOSDB	Closes a database for the CEQUIL post-processor.
INTP	Interpolates to find vertices from nodes for CEQUIL post-processor.
LOADI	Copies integer elements into their proper place in the output array for the CEQUIL post-processor.
LOADSC	Copies real (scalar) elements into their proper place in the output array for the CEQUIL post-processor.
OVENDB	Opens up a database for either read or write for CEQUIL post-processor.
OVTPUT	Writes out in binary format the essential properties for the CEQUIL post-processor.
PLTWRT	Writes Eulerian output into appropriate output files. The output files can be used later for plotting.
REGRID	Takes irregularly spaced grid values and converts them to equal-spaced, square grid values. Linear interpolation is used.
SPREAD	Subroutine for writing out gas variables for spreadsheet plotting. Can be called on the fly from a symbolic debugger. Useful for program debugging.
STREAM	Calculates stream lines from values of U (axial velocity) and V (radial velocity) for plotting purposes.
VELMAG	Calculates the magnitude of the total velocity vector at each node for plotting.

WRITCO	Writes the control variables for the CEQUIL post-processor.
WRITGE	Writes the x, y, and z values of each of the nodes for the CEQUIL post-processor.
WRITSC	Writes a scalar function for the CEQUIL post-processor.
WRITVE	Writes a vector function for the CEQUIL post-processor.

SO_x/Sorbents Submodel

CALCSJ	Calculates sorbent particle number density.
CALH2S	Solves finite difference equation for H_2S species continuity.
CALSO2	Solves finite difference equation for SO_2 species continuity.
SDNRST	Reads and writes to sorbent particle number density restart file.
SLFRST	Reads and write to sulfur species restart file.
SORB0	Reads in input data and initializes sorbent particle number density.
SORPAR	Main submodel driver. Calculates source terms for SO_2 and H_2S (sulfur entering with the coal or gas inlet streams). Determines if convergence is obtained. Prints out final results.
SOXDATA	Block data subprogram for variable initialization.

SBVALIN (SPROPS)	Writes reasonable values into intrusions which border the flowfield in order to allow for 2-D interpolation of gas properties to sorbent particle position.
SBVALOT (SPROPS)	Replaces boundary values with original values.
SPSICT	Tracks sorbent particles through the reactor. Calculates source terms for sulfur capture.
SULFAT	Calculates the change in conversion of calcined $CaCO_3$ particles to $CaSO_4$ according to the shrinking-core model of Silcox (1985).
SULFHS	Calculates the change in conversion of calcined $CaCO_3$ particles to CaS according to the shrinking-core model of Silcox (1985).

Particle Phase

BVALIN (BPROPS)	Inserts reasonable properties into intrusions which border the flow field in order to allow for particle phase 2-D property interpolation.
BVALOUT (BPROPS)	Replaces boundary values with original properties.
COAL0	Reads input coal parameters and sets up initial coal properties.
COAL1	Calculates gas phase properties at a point in the reactor, such as thermal conductivity, diffusivity, and viscosity. These properties are needed in COAL2.
COAL2	Calculates coal reaction rates and other auxiliary parameters from coal and gas properties at a point.

COAL2S (COAL2)	Calculates coal reaction rates and other auxiliary parameters form coal and gas properties at a point. Used when particle energy equation goes stiff. Pseudo steady-state assumption is used.
EOLP	Driver routine for solving Eulerian or Lagrangian particle equations. Eulerian particles are not debugged in this version of PCGC-2. The Lagrangian option is currently the only viable option.
EULINT (PSICT0)	Initializes Eulerian particle number density fields.
FIND	This is a short extrapolation subroutine used by SIGMAM.
GRAD	Calculates gradient of particle number density for particle dispersion submodel.
PEJ	Function for calculating vapor pressure and enthalpy of vaporization for liquid component of slurry and fuel oils.
PRTSUR	Calculates the surface area of char particles required for heterogeneous-NO decay reactions.
PSCRAT	Calculates rate of homogeneous reactions for intermittent primary, secondary and coal off-gas.
PSICT	Interpolates gas property information for each point of the Lagrangian particle information. Integrates particle velocity to get particle trajectory, and calls PSOLVE to integrate particle continuity and energy equations. Saves particle source terms for gas phase.
PSICT0	Reads initial particle information and initialized particle trajectory parameters.
PSOLVE	Solves particle energy and continuity equations for reacting particles.

PSOLVP (PSOLVE)	This subroutine is used when using an Eulerian particle solution (not currently implemented). Prepares the Eulerian data so that an appropriate call to each of the coal subroutines can be made. Takes the resulting coal computations and stores them in Eulerian arrays. Computes the associated source terms for the gas-particle coupling.
PSOLVS (PSOLVE)	Solves particle energy and continuity equations for reacting particles when the particle energy equation is stiff.
SIGMAD	Used by COAL1 for determining the value of the potential function needed for mass diffusivity as a function of the Lennard-Jones parameters and temperature.
SIGMAM	Used by COAL1 for determining the value of the potential function needed for viscosity and thermal conductivity as a function of the Stockmayer parameters and temperature.

Radiation Submodel

DISORD	Calculates radiant wall heat fluxes and flux-sums to the volume elements using the discrete ordinates approximation.
EICO2	Calculates the emissivity of carbon dioxide from the Hottel charts.
EIH2O	Calculates the emissivity of water vapor from the Hottel charts.
FLUX	Main driver routine to calculate all of the radiation flux sums.

FLUX0	Reads input data for radiation flux subroutines and initializes radiation parameters.
FLUXR	Calculates coefficients for finite difference equation for FR (radial flux sum) and solves for the field values for FR at each grid point.
FLUXT	Calculates FETA (azimuthal flux sum) at each grid point.
FLUXX	Calculates coefficients for finite difference equation for FX (axial flux sum) and solves for field values for FX at each grid point.
RADCOF	Calculates radiation coefficients.
RESULT	Writes the results of the discrete ordinates radiative heat transfer calculation to the output file.
SETUP	Sets up radiation coefficients for FLUX subroutines.

Appendix B

Description of Input Data

FORTRAN Variable	Type	Units	Description and Usual Symbol	Recommended or Typical Value
AF	real	—	A value of 0.0 will use upwind differencing to solve radiation equations in discrete ordinates model. A value of 1.0 will use central differencing. An intermediate value will use a hybrid of upwind and central.	0.0
AL1	real	m	Axial length where axial dimensions of the computational cells begin to shrink.	Greater than the length of the reactor unless it is desired to have cells shrink at the outlet

FORTRAN Variable	Type	Units	Description and Usual Symbol	Recommended or Typical Value
ALJ (J, L)[1]	real	m s^{-1} K^{-n}	Pre-exponential factor for the L^{th} char reaction for the J^{th} particle size/type, A_{jp}.	Depends on the coal type; not needed if use FG-DVC
AMJ (J, M)	real	s^{-1}	Pre-exponential factor for the M^{th} coal reaction for the J^{th} particle size/type, A_{jm}.	Depends on the coal type; not needed if use FG-DVC
AO	real	—	Degree of anisotropicity of scattering in discrete ordinates radiation model.	1.0
ASUB (I, II)	character	—	Name of I^{th} species, II = 1,3.	Depends on species; must correspond to name used in JANAF database
AT (II)	character	—	Element symbols in a species name (e.g., CO_2 has C and O).	Depends on species
ATOM (1, K)	real	kg $kmol^{-1}$	Atomic mass of K^{th} element.	Depends on element
ATOM (2, K)	real	—	Valence of K^{th} element.	Depends on element
ATOMID (K)	character	—	Name of K^{th} element.	Depends on element
B (II)	real	—	Number of molecules of element 'AT' in species name (e.g., CO_2 has 1 and 2).	Depends on species
BETSUR	real	m^2/kg	Sorbent particle BET surface area.	1.E6

[1]Definitions for array subscripts are at end of table.

FORTRAN Variable	Type	Units	Description and Usual Symbol	Recommended or Typical Value
BLANK	ASCII	sec^{-1}	A blank card.	
CHARNO	integer	--	Flag for selecting char-NO decay rate expression: 1=Equation by Levy	1[2]
COMENT(II)	character	—	Comment words for output of particle information.	Arbitrary
DATA(I = 1, 3)	character	—	Molecular symbol or name of species.	Depends on species; must match names in JANAF database
DELRRJ	real	—	Fractional change in total reaction rate that is acceptable for a converged reaction rate.	1.E-6
DELTA(I)	real	—	Stockmayer polar parameter of species I, δ_i.	Depends on species
DELTPJ	real	K	Temperature difference acceptable for convergence when calculating particle temperature from particle enthalpy.	0.01
DIACH	real	m	Diameter of reaction chamber.	Depends on reactor
DIAP	real	m	Diameter of primary duct	Depends on reactor

[2]Only option available for now.

FORTRAN Variable	Type	Units	Description and Usual Symbol	Recommended or Typical Value
DIAS	real	m	Diameter of secondary duct.	Depends on reactor
DT1, DT2	character	—	Date species was put in JANAF database	Depends on species
EDIN(II)	real	m s	Experimental inlet turbulent kinetic energy dissipation rate at radial position RIN(II).	Depends on experimental data
EDPD	logical	—	.TRUE. will use turbulent kinetic energy dissipation rate profile data from an inlet data file for additional inlets (option not presently functional in code).	F
EDPDAT	logical	—	.TRUE. will use turbulent kinetic energy dissipation rate profile data from an inlet data file for the primary tube, and calculates adjusted profiles at the inlet node point. .FALSE. will use theoretical calculations for the profile	F

FORTRAN Variable	Type	Units	Description and Usual Symbol	Recommended or Typical Value
EDSDAT	logical	—	.TRUE. will use turbulent kinetic energy dissipation rate profile data from an inlet data file for the secondary annulus, and calculates adjusted profiles at the inlet node points. .FALSE. will use theoretical calculations for the profile.	F
EK(I)	real	K	Stockmayer parameter for the I^{th} species, ε/k.	Depends on species; must be paired with S(I)
EL(J, L)	real	J kmol^{-1}	Activation energy for the L^{th} char oxidation reaction for the J^{th} particle size/type.	Depends on coal type and oxidizer
ELEM	character	—	Formatted line must contain the letters 'ELEM'.	ELEM
EMJ(J, M)	real	J kmol^{-1}	Activation energy for the M^{th} devolatilization reaction for the J^{th} particle size/type.	Depends on coal type; not needed if use FG-DVC
EMM(J, L)	real	—	Exponent on temperature in kinetic char rate expression, m.	Depends on coal type

FORTRAN Variable	Type	Units	Description and Usual Symbol	Recommended or Typical Value
EMW	real	—	Wall emissivity, ε_w	0.8
EPSD	real	—	Ratio of cell size decrease in radial direction.	0.9
EPSI	real	—	Ratio of cell size increase in radial direction.	1.1
EPSX	real	—	Ratio of cell sites in axial direction (cf AL1).	1.1
EQTEST	real	--	Local equivalence ratio test criterion used to determine the method of estimating atomic oxygen concentration	0.5[3]
FBACK	real	—	Fraction of volatiles enthalpy which is fed directly back to the particle.	0.5
FCTHCN	real	—	Fraction of frozen HCN concentrations used to initialize HCN field in NO_x model.	0.8
FCTNH3	real	—	Fraction of maximum NH_3 used to estimate initial NH_3 concentration in NO_x model.	0.1

[3]The value of `EQTEST` doesn't matter when the recommended option of `RADOXY = 1` is used. For `RADOXY = 0` or 2, the recommended value of `EQTEST` is 0.5.

FORTRAN Variable	Type	Units	Description and Usual Symbol	Recommended or Typical Value
FCTNO	real	—	Fraction of frozen NO concentrations used to initialize NO field in NO_x model.	0.1
FFLOW	real	—	Fraction of reactant stream 1 in NINLET stream.	1.0 for primary and 0.0 for secondary
FGDVC	logical	—	.TRUE. uses the FGDVC submodel for coal devolatilization.	T
FLOW	real	kg s^{-1}	Mass flow rate of gas in NINLET stream.	Depends on flowrate
FN2PRT	real	—	Partitioning factor of coal or char nitrogen between gaseous HCN and NH_3 in NO_x submodel. 0=all nitrogen evolves as NH_3 1=all nitrogen evolves as HCN	1.0 for high-rank coals; something less (0.5?) for low-rank coals

FORTRAN Variable	Type	Units	Description and Usual Symbol	Recommended or Typical Value
FUELNO	integer	—	Flag for choosing fuel NO mechanism: 0=fuel NO not calculated 1=deSoëte kinetics[4] 2=Wendt kinetics[5] 3=Mitchell and Tarbell kinetics	1
GAMMA	real	—	Particle swelling parameter, γ.	1.1
GRDOUT	logical	—	.TRUE. prints a grid (.grd) file.	T
HAØ(J)	real	J kg^{-1}	Heat of formation of the ash in the Jth particle, h^{o}_{aj}.	0.0[6]
HGV(J,M)	real	J kg^{-1}	Heat of reaction for Mth devolatilization reaction for Jth particle.	0.0[7]
HHØ	real	J kg^{-1}	Heat of formation of the char in the Jth particle, h^{o}_{hj}.	0.0[8]

[4]Kinetic parameters have been adjusted at BYU from what deSoëte originally reported.

[5]Has a more theoretical basis than Option 1, but may cause numerical instability.

[6]Since ash is inert, anything could be used here, so using 0.0 is the simplest option.

[7]This is used to calculate volatiles enthalpy when FG-DVC is not used. FG-DVC predicts the volatiles composition and, therefore, the volatiles enthalpy.

[8]This value is based on assuming pure carbon for the char.

FORTRAN Variable	Type	Units	Description and Usual Symbol	Recommended or Typical Value
HLOSS	real	—	Fraction of enthalpy in excess of ambient conditions to be removed from each computational cell. Should be 0.0 if INCALH is set TRUE.	0.0
HTRACK	logical	—	.TRUE. causes hydrogen to be tracked independently from all other elements in the coal offgas when INETA2 is equal to .TRUE.	F[9]
HWØ	real	J kg^{-1}	Heat of formation of the slurry liquid in the J^{th} particle, h^{o}_{wj}.	-1.5866E7[10]
ICALCN	integer	—	Iteration frequency that HCN species continuity is solved in NO_x submodel when `fuelno` = 2 or 3.	1[11]
IDON(I=1,4)	integer	—	Not used.	

[9]This option has not yet been proven and only works when INETA2 = T.

[10]This is the value for water.

[11]Try a value greater than 1 if have convergence problems and FUELNO = 2 or 3.

FORTRAN Variable	Type	Units	Description and Usual Symbol	Recommended or Typical Value
IEUCK	integer	—	Gas thermal conductivity calculated from the Eucken equation if IEUCK = 1, otherwise Sage-Galloway equation is used.	1
IGASV	integer	—	Index for gas property interpolation during Lagrangian particle trajectory integration. If IGASV = 1 no interpolation gas properties are assumed constant in the cell; IGASV = 2, gas properties are interpolated in the axial direction; IGASV = 3, gas properties are interpolated in both axial and radial directions.	3
INCALF	logical	—	.TRUE. will solve the f mixture fraction equation.	T
INCALG	logical	—	.TRUE. will solve g_f equation.	T

FORTRAN Variable	Type	Units	Description and Usual Symbol	Recommended or Typical Value
INCALH	logical	—	.TRUE. will solve gas energy equation (presently under development for particle-laden flows).	T
INCALN	logical	—	.TRUE. will solve n_j equation.	T
INCFP	logical	—	.TRUE. will incorporate correction for particles into gas phase turbulent diffusion coefficients (Eq. 14).	T
INCLET	logical	—	.TRUE. will solve η equation.	T
INCLGE	logical	—	.TRUE. will solve g_η equations.	T
INCLKE	logical	—	.TRUE. solves the k-ε equations.	T
INCNOX	logical	—	.TRUE. will solve NO_x equations.	T
INCOAL	logical	—	.TRUE. will solve coal reaction equations.	T
INCREK	logical	—	.TRUE. will set up gas property table.	T
INCSWP	logical	—	.TRUE. allows for swirl in the primary stream.	F
INCSWS	logical	—	.TRUE. allows for swirl in the secondary stream.	T

FORTRAN Variable	Type	Units	Description and Usual Symbol	Recommended or Typical Value
INCURF	logical	—	.TRUE. will stop program every INDRST/2 iterations, allowing user to change under-relaxation factors.	F
INDPNX	integer	—	Number of iterations of the NO model between writing restart file and intermediate output to the output file.	50
INDPRI	integer	—	Number of iterations in gas phase calculations between intermediate printouts.	>MAXIT to prevent hardcopy output
INDRST	integer	—	Number of iterations between intermediate output of restart information.	50
INEACH	logical	—	.TRUE. will solve particle field equation after each 5 gas phase macro-iterations, .FALSE. will solve particle equations only upon reaching a converged gas phase solution.	F

FORTRAN Variable	Type	Units	Description and Usual Symbol	Recommended or Typical Value
INETA2	logical	—	.TRUE. uses both f and η to track coal offgas.	F[12]
INFSOU	logical	—	.TRUE. will include source term in f equation (should be TRUE for slurry and fuel oil calculations, FALSE otherwise).	F
INHTNX	logical	—	.TRUE. will include heterogeneous NO reduction reaction.	T
INNOZZ	logical	—	.TRUE. will configure computational grid for very small spacing near centerline (typically used w/nozzles or large reactors).	F
INPROG	logical	—	.TRUE. maintains a progress (.prg) file for monitoring convergence at a specific location in the reactor.	F

[12]This option is not fully debugged and is not recommended for the ordinary user.

FORTRAN Variable	Type	Units	Description and Usual Symbol	Recommended or Typical Value
INPRST	logical	—	.TRUE. will use a particle restart file to begin computations and output intermediate particle restart files.	T
INQRL	logical	—	.TRUE. allows for a quarl at the secondary inlet.	T
INRAD	logical	—	.TRUE. will solve radiation equations.	T
INRDGD	logical	—	.TRUE. reads location of user specified grid points from data file.	T
INRST	logical	—	.TRUE. will use a gas restart file to begin computations and output intermediate gas phase restart files.	T
INSIMP	logical	—	.TRUE. uses the SIMPLER algorithm to solve velocity/pressure field. .FALSE. uses the SIMPLE algorithm.	T
INSMPC	logical	—	.TRUE. uses the SIMPLEC algorithm	F

FORTRAN Variable	Type	Units	Description and Usual Symbol	Recommended or Typical Value
INSORB	logical	—	.TRUE. calls the sorbent reactions submodel after converging the main flowfield.	T
INTFRZ	logical	—	.TRUE. uses frozen equilibrium scheme for gas properties when the local equivalence ratio is greater than 2.0.	F
INTRUS	logical	—	.TRUE. will allow intrusions in reactor.	T
IPLTNX	logical	—	.TRUE. will write files for plots from NO model calculations.	T
IPSICT	logical	—	.TRUE. will solve particle equations (should be TRUE for all calculations involving particles).	T
IRSTNO	logical	—	.TRUE. will use a restart file to begin NO model computations and output intermediate NO model restart files.	T

FORTRAN Variable	Type	Units	Description and Usual Symbol	Recommended or Typical Value
ITYNX	integer	—	Number of iterations of the NO model between intermediate typing of the residuals to the screen or log file.	5
KEQ	integer	—	IF KEQ = 1 the linear form of the Field (1967) char oxidation rate expression is used; if KEQ ≠ 1 normal Arrhenius form used (low temperature reactors (< 1400 K) should not use KEQ = 1).	0
KOPED	integer	—	Selection parameter which designates one of several optional equations to be used in calculating a theoretical or experimental turbulent kinetic energy dissipation rate profile for additional inlets.	1

FORTRAN Variable	Type	Units	Description and Usual Symbol	Recommended or Typical Value
KOPEDP	integer	—	Selection parameter which designates one of several optional equations to be used in calculating a theoretical or experimental turbulent kinetic energy dissipation rate profile for the primary.	1
KOPEDS	integer	—	Selection parameter which designates one of several optional equations to be used in calculating a theoretical or experimental turbulent kinetic energy dissipation rate profile for the secondary.	1
KOPTE	integer	—	Selection parameter which designates one of several optional equations to be used in calculating a theoretical or experimental turbulent kinetic energy profile for the additional inlets (option not functional at present).	1

FORTRAN Variable	Type	Units	Description and Usual Symbol	Recommended or Typical Value
KOPTEP	integer	—	Selection parameter which designates one of several optional equations to be used in calculating a theoretical or experimental turbulent kinetic energy profile for the primary.	1
KOPTES	integer	—	Selection parameter which designates one of several optional equations to be used in calculating theoretical or experimental turbulent kinetic energy profile for the primary.	1
KOPU	integer	—	Specifies the angle the flow in the North wall inlet makes with a plane perpendicular to the axis of symmetry. The value is disregarded for the West wall inlets (not presently operational).	90.

FORTRAN Variable	Type	Units	Description and Usual Symbol	Recommended or Typical Value
KOPUP	integer	—	Selection parameter which designates one of several optional equations to be used in calculating a theoretical or experimental axial velocity profile for the primary.	1
KOPUS	integer	—	Selection parameter which designates one of several optional equations to be used in calculating a theoretical or experimental axial velocity profile for the secondary.	1
KOPV	integer	—	Specifies the angle the flow in the West wall inlet makes with the axis of symmetry. KOPV (N) is disregarded for North Wall inlets (not presently operational).	0.

FORTRAN Variable	Type	Units	Description and Usual Symbol	Recommended or Typical Value
KOPVP	integer	—	Selection parameter which designates one of several optional equations to be used in calculating a theoretical or experimental radial velocity profile for the primary.	1
KOPVS	integer	—	Selection parameter which designates one of several optional equations to be used in calculating a theoretical or experimental radial velocity profile for the secondary.	1
KOPW	integer	—	Tangential component of velocity is zero for all additional inlets (not presently operational).	1

FORTRAN Variable	Type	Units	Description and Usual Symbol	Recommended or Typical Value
KOPWP	integer	—	Selection parameter which designates one of several optional equations to be used in calculating a theoretical or experimental tangential velocity profile for the primary.	1
KOPWS	integer	—	Selection parameter which designates one of several optional equations to be used in calculating a theoretical or experimental or tangential velocity profile for the secondary.	1
LAMINAR	logical	—	.TRUE. causes molecular transport properties to be calculated locally, as functions of composition, etc., and invokes the laminarization extension to the k-ε model, if INCLKE = .TRUE.	F

FORTRAN Variable	Type	Units	Description and Usual Symbol	Recommended or Typical Value
LBACK	logical	—	.TRUE. causes a portion (specified by FBACK) of the volatiles enthalpy to be fed back directly to the particle.	T
LBUOY	logical	—	.TRUE. causes the buoyancy term to be included in the axial gas momentum equation.	F
LDISO	logical	—	.TRUE. will solve radiation equations by discrete ordinates method.	T
LEMCOR	logical	—	.TRUE. will incorporate corrections for gas emissivity due to spectral overlap.	T
LEULP	logical	—	.TRUE. solves Eulerian particle equations instead of Lagrangian equations only, .FALSE. is the only currently viable option.	F
LGASE	logical	—	.TRUE. will solve for gas phase emissivity.	T
LPARTP	logical	—	.TRUE. allows for particles in the primary stream.	T

FORTRAN Variable	Type	Units	Description and Usual Symbol	Recommended or Typical Value
LPARTS	logical	—	.TRUE. allows for particles in the secondary stream.	F
LPBOTH	logical	—	.TRUE. allows for particles in both the primary and secondary streams.	F
LPBUG	logical	—	.TRUE. will print out debug information for Lagrangian particle calculations	F
LPOST	logical	—	.TRUE. writes a file for the CQUEL post-processor for plotting.	T
LRBNDS	logical	—	.TRUE. allows sorbent particle to rebound from walls; otherwise they stick	T
LSPBUG	logical	—	.TRUE. will print out debug information for Lagrangian sorbent particle calculations	F
LSPH	logical	—	.TRUE. allows for particle energy source term.	T
LSPM	logical	—	.TRUE. allows for particle mass source term.	T
LSPU	logical	—	.TRUE. allows for particle axial velocity source term.	T

FORTRAN Variable	Type	Units	Description and Usual Symbol	Recommended or Typical Value
LSPV	logical	—	.TRUE. allows for particle radial velocity source term.	T
LSYPS	logical	—	.TRUE. allows the user to specify sorbent particle trajectory starting locations	F
LTBUG	logical	—	.TRUE. allows debug of chemical equilibrium table.	F
LYPS	logical	—	.TRUE. allows user to specify coal particle trajectory starting location, .FALSE. assumes uniform mass flux to calculate starting locations.	F
MAGHJER	logical	—	.TRUE. allows use of the Magnussen-Hjertauger (coal reaction) model.	F
MAXIT	integer	—	Maximum number of gas phase macro-iterations.	200
MAXITP	integer	—	Maximum number of particle phase iterations.	10
MAXITR	integer	—	Maximum number of radiation flux iterations.	10

FORTRAN Variable	Type	Units	Description and Usual Symbol	Recommended or Typical Value
MAXRES	real	—	Maximum normalized value of residual source for convergence of NO_X/SO_X submodels.	1.0E-04
MINITP	integer	—	If gas phase reconverges within MINITP iterations after a particle phase iteration, overall convergence is assumed.	15
MOLE	ASCII	—	Gas stream relative amount flag. When MOLE is 'M', relative amounts of reactant stream are in mole percent. Otherwise, relative amounts are taken to be mass percent.	Either blank or "M"
MXITNX	integer	—	Maximum iterations for NO_X submodel	200
MXITSX	integer	—	Maximum iterations for sorbent reactions submodel	1000
NCARD	integer	—	Number of comment cards to follow.	Variable
NCD	integer	—	Card number.	Variable
NCRXN	integer	—	Number of devolatilization reactions, M.	1 or 2

FORTRAN Variable	Type	Units	Description and Usual Symbol	Recommended or Typical Value
NDIA	real	—	Length of reaction chamber divided by diameter of reaction chamber, L/D.	Depends on reactor; this is how the reactor length is specified
NHRXN	integer	—	Number of char oxidation reactions, L.	1 for fuel-lean and 3 for fuel-rich
NIINQ	integer	—	Number of axial grid points in the quarl region.	5-10
NIWOQ	integer	—	Number of grid points in the axial direction without quarl.	30-100
NJINP	integer	—	Number of grid points in radial direction in primary stream, only used if INNOZZ is .TRUE.	3-5
NJINS	integer	—	Number of grid points in radial direction in the secondary stream.	3-5
NL	integer	—	Cell number associated with AL1.	Depends on AL1 and reactor length; doesn't matter of AL1 is greater than reactor length

FORTRAN Variable	Type	Units	Description and Usual Symbol	Recommended or Typical Value
NPROP	integer	—	Number of particle integration steps before updating gas phase transport properties for particle reaction scheme.	5
NPS	integer	—	Number of fuel particle sizes/types.	5
NPSS	integer	—	Number of sorbent particle sizes/types.	1
NSAY	integer	—	Number of comment cards to follow in main input file.	1-10
NSAYNX	integer	—	Number of comment cards to follow in NO_x input file.	1-10
NSAYNX(II), II=1,NSAYNX	character	—	Comment words for output from NO_x submodel.	Arbitrary
NSAYSX	integer	—	Number of comment cards to follow in sorbent reactions input file.	1-10
NSFORM	integer	—	Form of swirl number equation to be used.	1
NSL	integer	—	Number of particle trajectory starting locations for fuel particles.	10

FORTRAN Variable	Type	Units	Description and Usual Symbol	Recommended or Typical Value
NSLS	integer	—	Number of particle trajectory starting locations for sorbent particles.	1-10
NSTYPE	integer	—	1=SO_2 capture by sorbent 2=H_2S capture by sorbent	1 for fuel-lean systems and 2 for fuel-rich systems
OHADJS	integer	--	Flag for adjusting equilibrium concentration: 1=multiply equilibrium OH concentration by a non-linear temperature expression[13] ≠1=no adjustment made	≠1
OMEGAA(J)	real	—	Initial mass fraction of ash in J^{th} particle, ω_{aj}.	Depends on coal type
OMEGAC(J)	real	—	Initial mass fraction of raw coal in J^{th} particle, ω_{ci}.	Depends on coal type; not needed for FG-DVC

[13]This expression was developed by Wendt et al. (1989) to account for "overshoot" of OH and is specific to their reactor system and fuel-rich coal combustion. It is not appropriate to use this expression unless case-specific fitting parameters are substituted into this expression which appears in subroutines EQSPEC, PSCRAT, and RXNRAT. Therefore, it is recommended that OHADJS ≠ 1.

FORTRAN Variable	Type	Units	Description and Usual Symbol	Recommended or Typical Value
OMEGAH(J)	real	—	Initial mass fraction of char in J^{th} particle, ω_{hj}.	0. unless coal is partially devolatilized
OMEGAW(J)	real	—	Initial mass fraction of liquid in the J^{th} particle, ω_{wj}.	0. unless feeding a slurry[14]
OXYD(L)	character	—	Species identification symbol for the oxidizer for the L^{th} char oxidation reaction.	Always O2; sometimes CO2, H2O, and even H2 as well
PD(J)	real	m	Initial diameter of J^{th} fuel particle, d_i.	Depends on particle size distribution
PDEN	real	kg m^{-3}	Particle/droplet density	1300.
PDS(IPS)	real	m	Initial diameters of sorbent particles.	10.E-6
PECWT	real	—	Relative amounts of each species in each input stream.	Depends on stream composition
PHASE	ASCII	—	Phase of inlet stream species; only gases are allowed except for slurry calculations, which require one stream of liquid.	G

[14]Note that OMEGAW is not used for coal moisture. Coal moisture can only be accounted for adding it to the transporting gas stream. This is equivalent to assuming the moisture evaporates from the coal during transport into the furnace.

FORTRAN Variable	Type	Units	Description and Usual Symbol	Recommended or Typical Value
PHIL(L)	real	—	Ratio of moles of fuel (C) to moles of oxidizer in the L^{th} char oxidation reaction, ϕ_ℓ.	Depends on oxidizer; see discussion in Chapter 2
PLOD(I)	real	—	Coal particle loading (mass of coal particles/mass of primary gas) in the i^{th} stream.	Whatever it is
PLODS(I)	real	—	Sorbent particle loading (mass of sorbent particles/mass of primary gas) in the i^{th} stream.	Whatever it is
PLS	real	m	Local length scale in primary stream.	Not used unless KOPEDP = 3
PMF(J)	real	—	Mass fraction of J^{th} particle type.	Must add up to 1.0
PMFS(J)	real	—	Mass fraction of J^{th} sorbent particle type	Must add up to 1.0
POLLUT	logical	—	.TRUE. solves only NO_x equations without recalculating other Eulerian variables.	F
PRES	real	N m^{-2}	Reactor outlet pressure.	Whatever it is

FORTRAN Variable	Type	Units	Description and Usual Symbol	Recommended or Typical Value
PRHCN	real	—	Turbulent Prandtl/Schmidt number for HCN concentrations.	0.9
PRK(J)	real	—	Turbulent Prandtl/Schmidt number for J^{th} particle type, σ_j^t.	0.35
PRKS(J)	real	—	Turbulent Prandtl/Schmidt number for J^{th} sorbent particle type	0.35
PRNH3	real	—	Turbulent Prandtl/Schmidt number for NH_3.	0.9
PRNOX	real	—	Turbulent Prandtl/Schmidt number for NO.	0.9
PRSO2	real	—	Turbulent Prandtl/Schmidt number for SO_2.	0.9
QHA	real	degrees	Quarl half angle (with centerline).	Depends on reactor geometry
QHC(J)	real	J/kg	Gross heating value (constant volume) for j^{th} fuel particle type.	0.0[15]

[15]If the heating value is known, its value can be given here. The value of "0.0" causes the gross heating value to be estimated from the IGT correlation, based on ultimate analysis.

FORTRAN Variable	Type	Units	Description and Usual Symbol	Recommended or Typical Value
QLX	real	m	Axial length of quarl region.	Depends on reactor geometry
RADOH	integer	--	Flag for choosing quasi-equilibrium expression for estimating radical hydroxide (OH) concentration: 2=assume equilibrium with H_2O and H_2 ≠2=assume equilibrium among all gas species	≠2

FORTRAN Variable	Type	Units	Description and Usual Symbol	Recommended or Typical Value
RADOXY	integer	--	Flag for choosing quasi-equilibrium expression for estimating atomic oxygen concentration 0=allow the code to select the method 1 or 2 at each node based on comparison of `eqtest` with the local equivalence ratio 1=assume equilibrium with O_2 only 2=assume equilibrium with O_2, CO, and CO_2	1[16]
REAC(II) (II=1-10)	character	—	Reactant card, the first four letters on the card must be 'REAC', 36 other ASCII symbols may be included for user description of the reactant stream. These symbols are simply echoed in output.	REAC

[16]Options 0 and 2 have a better theoretical basis, but the expression for Option 2 is not sufficiently developed. If the code included effects of non-equilibrium CO/CO_2, Option 0 might be the recommended choice.

FORTRAN Variable	Type	Units	Description and Usual Symbol	Recommended or Typical Value
RIN(I)	real	m	Radial location of experimental inlet data point.	Depends on data
RP	real	m	Primary tube inside radius for experimental inlet data.	Depends on data
RS1	real	m	Primary tube outside radius for experimental inlet data.	Depends on data
RS2	real	m	Secondary tube radius for experimental inlet data.	Depends on data
S(I)	real	Å	Stockmayer collision diameter, σ_i.	Depends on species; must be paired with EK(I)
SAY (II) (II=1-10)	character	—	Comment words for beginning of output.	Variable
SAYSX(II), II=1,NSAYSX	character	—	Comment words for output from sorbent reactions submodel.	Variable
SLRCMP (I)	character	—	Name of slurry component found in gas (e.g. H_2O) (I = 1, 2, and 3).	H2O
SLS	real	m	Local length scale in secondary stream.	Not used unles KOPEDS=3

FORTRAN Variable	Type	Units	Description and Usual Symbol	Recommended or Typical Value
SORMAX	real	—	Maximum normalized value of residual source sums for convergence of gas phase computations.	0.01
SORMIN	real	—	Minimum normalized value of residual source sums between particle phase iterations for overall convergence.	0.1
SPDEN	real	kg/m^3	Sorbent particle density.	1800.
SPRANG(I)	real	—	Spray angle for initial starting location for particles.	Depends on injection geometry
STRING	character	—	Inlet card. Must contain the string 'INLET'.	INLET
SWIRLN(I)	real	—	Swirl no. for the I^{th} inlet.	Variable
SWIRLS	real	—	Swirl no. for the secondary stream, defined as flux of angular momentum divided by product of axial momentum flux and secondary duct radius.	Variable
TBE	real	K	Temperature boundary condition for the east face of intrusions.	Variable

FORTRAN Variable	Type	Units	Description and Usual Symbol	Recommended or Typical Value
TBN(I)	real	K	Temperature boundary condition for the north (side) wall and north face of intrusions.	Variable
TBW	real	K	Temperature boundary condition for the west (front) wall and west face of intrusions.	Variable
THER	Character	—	Thermo card. Must contain the string 'THER'.	THER
THICK	real	m	Thickness of tube wall between primary and secondary streams.	Depends on the geometry
THIDEL	real	K	Relative (to adiabatic temperature) maximum temperature for table generation.	500. or greater
THIGH	real	K	Upper limit of temperature range for thermodynamic correlations for gas species.	5000.

FORTRAN Variable	Type	Units	Description and Usual Symbol	Recommended or Typical Value
THRMNO	integer	--	Flag for choosing thermal NO mechanism: 0=thermal NO not calculated 1=include forward and reverse rates of extended Zel'dovich mechanism 2=include only forward rates of Zel'dovich mechanism	1 for fuel-rich systems and 2 for fuel-lean systems
TINFLO(I)	real	—	Turbulence intensity of I^{th} inlet stream.	0.10
TIPD	logical	—	.TRUE. will use turbulence intensity profile data from INLET file for the additional inlet tube, and calculates adjusted profiles at the inlet node points (not functional at present). .FALSE. will use theoretical calculations for the profile.	F

FORTRAN Variable	Type	Units	Description and Usual Symbol	Recommended or Typical Value
TIPDAT	logical	—	.TRUE. will use turbulence intensity profile data from INLET file for the primary tube, and calculate adjusted profiles at the inlet node points. .FALSE will use theoretical calculations for the profile.	F
TISDAT	logical	—	.TRUE. will use turbulence intensity profile data from INLET file for the secondary annulus, and calculate adjusted profiles at the inlet node points. .FALSE. will use theoretical calculations for the profile.	F
TLAG(J)	real	—	Ratio of inlet particle temperature (K) to inlet gas temperature (K).	1.0
TLODEL	K	—	Relative (to adiabatic temperature) minimum temperature for table generation.	1500. or more

FORTRAN Variable	Type	Units	Description and Usual Symbol	Recommended or Typical Value
TLOW	real	—	Lower limit for temperature range of thermodynamic correlations for gas species.	300.
TMAX	real	K	Absolute maximum temperature for table generation.	2500. or greater for combustion, 3000. or greater for oxygen-blown gasification
TMIN	real	K	Absolute minimum temperature for table generation.	Lowest of inlet gas temperatures, often 298 K
TMP	real	K	Temperature of inlet stream NSTRM if NSTRM = 1, TMP is temperature of primary gas stream; = 2, temperature of secondary gas stream.	Often room temperature for primary, higher for secondary
TNBP	real	K	Normal boiling point of slurry liquid.	373 K for H_2O at 1 atm
TOUT	real	K	Outlet gas temperature for radiation (0.0 yields adiabatic condition).	0.

FORTRAN Variable	Type	Units	Description and Usual Symbol	Recommended or Typical Value
TURBIN(I)	real	—	Experimental normalized turbulent intensity at radial position RIN(I). (The unnormalized turbulent intensity will be utilized if the selection parameter KOPTE* so specifies).	Depends on data
UIN(I)	real	m/s^{-1}	Experimental axial velocity at radial position RIN(I).	Depends on data
UPD	logical	—	.TRUE. will use axial velocity profile data from an inlet data file for the additional inlet tube, and calculates adjusted profiles at the inlet node points. .FALSE. will use theoretical calculations for the profile (option not functional at present).	T

FORTRAN Variable	Type	Units	Description and Usual Symbol	Recommended or Typical Value
UPDAT	logical	—	.TRUE. will use axial velocity profile data from an inlet data file for the primary tube, and calculates adjusted profiles at the inlet node points. .FALSE. will use theoretical calculations for the profile.	T
UPDWN	real	—	1.0 = co-gravity flow. -1.0 = counter-gravity flow. 0.0 = horizontal flow (gravity effects neglected).	1.0, -1.0, or 0.0
UPLAG(ISL)	real	—	Ratio of inlet particle velocity to inlet gas velocity.	1.0
URFDEN	real	—	Under-relaxation factor for density, λ_ρ.	0.3 for SIMPLE, 0.5 for SIMPLER
URFE	real	—	Under-relaxation factor for eddy dissipation rate, λ_ε.	0.5 for SIMPLE, 0.7 for SIMPLER
URFETA	real	—	Under-relaxation factor for η, λ_η.	0.5 for SIMPLE, 0.7 for SIMPLER
URFF	real	—	Under-relaxation factor for f, λ_f.	0.5 for SIMPLE, 0.7 for SIMPLER

FORTRAN Variable	Type	Units	Description and Usual Symbol	Recommended or Typical Value
URFG	real	—	Under-relaxation factor for g_f, λ_{gf}.	0.5 for SIMPLE, 0.7 for SIMPLER
URFGET	real	—	Under-relaxation factor for g_n, λ_{gn}.	0.5 for SIMPLE, 0.7 for SIMPLER
URFH	real	—	Under-relaxation factor for h, g_h.	0.8 for SIMPLE, 0.9 for SIMPLER
URFHCN	real	—	Under-relaxation factor for HCN in NO_x submodel.	0.9
URFK	real	—	Under-relaxation factor for k, λ_k.	0.5 for SIMPLE, 0.7 for SIMPLER
URFNH3	real	—	Under-relaxation factor for NH_3 in NO_x submodel	0.9
URFNJ	real	—	Under-relaxation factor for n_j, λ_{nj}.	1.0
URFNOX	real	—	Under-relaxation factor for NO in NO_x submodel.	0.9
URFP	real	—	Under-relaxation factor for p, λ_p.	1.0 for SIMPLER, not used for SIMPLE
URFPH	real	—	Under-relaxation factor for S_p^h	0.5 or less, sometimes 0.1

FORTRAN Variable	Type	Units	Description and Usual Symbol	Recommended or Typical Value
URFPM	real	—	Under-relaxation factor for S_n^u, S_n^v, S_n^m.	0.5 or less, but usually not as small as URFPH
URFPP	real	—	Under-relaxation factor for p', λ_p'.	0.8 for SIMPLER, not used for SIMPLE
URFSO2	real	—	Under-relaxation factor for SO_2 or H_2S mole fraction after sorbent reactions.	0.9
URFU	real	—	Under-relaxation factor for u, λ_u.	0.5 for SIMPLE, 0.7 for SIMPLER
URFV	real	—	Under-relaxation factor for v, λ_v.	0.5 for SIMPLE, 0.7 for SIMPLER
URFVIS	real	—	Under-relaxation factor for ν^t, $\lambda_\nu{}^\tau$.	0.3 for SIMPLE, 0.5 for SIMPLER
URFW	real	—	Under-relaxation for w, λ_w.	0.5 for SIMPLE, 0.7 for SIMPLER

FORTRAN Variable	Type	Units	Description and Usual Symbol	Recommended or Typical Value
USDAT	logical	—	.TRUE. will use axial velocity profile data from an inlet data file for secondary annulus, and calculates adjusted profiles at the inlet node points. .FALSE. will use theoretical calculations for the profile.	F
VIN(I)	real	m s^{-1}	Experimental radial velocity at radial position RIN(I).	Depends on data
VISCOS	real	kg m^{-1} s^{-1}	Approximate laminar viscosity for entire reaction chamber.	1.79E-5 for 1 atm
VPD	logical	—	.TRUE. will use radial velocity profile data from an inlet data file for the additional inlet tube, and calculates adjusted profiles at the inlet node points. .FALSE. will use theoretical calculations for the profile (option not presently functional).	T

FORTRAN Variable	Type	Units	Description and Usual Symbol	Recommended or Typical Value
VPDAT	logical	—	.TRUE. will use radial velocity profile data from an inlet data file or the primary tube, and calculates adjusted profiles at the inlet node points. .FALSE. will use theoretical calculations for the profile.	F
VSDAT	logical	—	.TRUE. will use radial velocity profile data from an inlet data file for the secondary annulus, and calculates adjusted profiles at the inlet node points., .FALSE. will use theoretical calculations for the profile.	F
WIC(J, K)	real	—	K^{th} elemental mass fraction of J^{th} particle size, ω_{jk}, specified on a daf basis in order of elements listed in thermodynamic file.	Depends on coal type, not needed for FG-DVC
WIN (I)	real	m s^{-1}	Experimental tangential velocity at radial position RIN(I).	Depends on data

FORTRAN Variable	Type	Units	Description and Usual Symbol	Recommended or Typical Value
WPD	logical	—	.TRUE. will use tangential velocity profile data from an inlet data file for the additional inlet tube, and calculates adjusted profiles at the inlet node points. .FALSE. will use theoretical calculations for the profile (option not presently operational).	T
WPDAT	logical	—	.TRUE. will use tangential velocity profile data from an inlet data file for the primary tube, and calculates adjusted profiles at the inlet node points. .FALSE. will use theoretical calculations for the profile.	F

FORTRAN Variable	Type	Units	Description and Usual Symbol	Recommended or Typical Value
WSDAT	logical	—	.TRUE. will use tangential velocity profile data from an inlet data file for the secondary annulus, and calculates adjusted profiles at the inlet node points. .FALSE. will use theoretical calculations for the profile.	F
XI(J)	real	—	Surface area factor for J^{th} particle type, ζ_j.	1.0
XIANOX	real	—	Fractional change in external char area used in NO model as a result of swelling and fracturing.	≈1.0
XPS(ISL)	real	m	Axial position of the ISL starting location.	0.0 for front wall
YPS (ISL)	real	m	Radial position of the ISL starting location.	Variable
YPSH	real	—	Normalized upper bound for particle starting locations (r/R).	0.95
YPSL	real	—	Normalized lower bound for particle starting locations (r/R).	0.05

FORTRAN Variable	Type	Units	Description and Usual Symbol	Recommended or Typical Value
YY (J, M)	real	—	Volatiles fraction for J^{th} particle with regards to M^{th} devolatilization reaction Y_{jm}.	Depends on coal type
Z (N1, N, I)	real	—	Coefficients for I^{th} species heat capacity equation. For N = 1, the temperature range of the heat capacity is generally 300 K - 1000 K and for N = 2, the temperature range is generally 1000 K - 5000 K (see TLOW and THIGH). In both cases: $\frac{h}{RT} = \left(\sum_{ii=1}^{5} z_{ii} \frac{T^{(ii-1)}}{ii} \right)$ $\frac{S^o}{R} = z_1 \, lnT + \left(\sum_{n=2}^{5} z_{ii} \right.$	Depends on species
ZEDA	real	—	Fractional conversion of devolatilized nitrogen to HCN in the gas phase in NO_x submodel.	1.0

Index Identification

I	Species
ISL	Particle starting location
J	Particle size/type

FORTRAN Variable	Type	Units	Description and Usual Symbol	Recommended or Typical Value
		K	Elements	
		L	Char reaction	
		M	Devolatilization reaction	
		N	Particle component	
		II	Arbitrary	

Appendix C

Sample Script Files for UNIX Operation Systems

Two C-shell scripts are used to run PCGC-2 in the UNIX environment at BYU. The first script (pcf) interacts with the user and assigns the filenames to environment variables which are then passed to the second script (pcgc2.com). The second script performs the file manipulation and runs the program.

Of course, these two scripts are just examples and must be adapted to each individual computer environment. Three environment variables must be defined in the C-shell before these scripts are used. `$PCSRC` is the pathname of the second script (pcgc2.com). `$PCEXE` is the pathname of the executable. `$PCBUG` is the name of the host symbolic debugger. At BYU, these variables are defined in each user's .cshrc file. A partial listing of a sample .cshrc file is also shown to indicate how this can be done.

The first script (pcf) provides several options to the user. To execute this script, type

```
pcf -db -batch -test filename
```

where `filename` is the specific name of the case that you are running. The above command assumes that the script or a link to it exists in the same directory as the input files for the case that is being simulated. Everything after `pcf` is optional. The modifier `-db` runs the program in the symbolic debugger `$PCBUG`. The modifier `-batch` causes the script pcgc2.com to be submitted to a batch queue

rather than being submitted as an interactive process. The modifier `-test` causes a version of the executable in `$PCEXE/test` to be used rather than `$PCEXE`. This feature is useful for code development. If `filename` is absent, the script prompts interactively for the input, thermo, inlet profile, output, and restart filenames separately. Alternatively, they may all be given on the command line. If only a single filename is given as in the example above, all files for the simulation are assumed to have the same root filename with only the filename extension (e.g. .dat, .thm, .inl) being different.

Script File No. 1 - pcf

```
[lola:35]afr >> cat pcf
#!/bin/csh
#script file to run PCGC2 program interactively
#new file names are assigned
#echo "PCAFR is temporarily being worked on.  Try again later."
#exit
unsetenv BATCH
setenv PROGRAM PCAFR
#set echo
set noglob
onintr control_exit
set a1 = $1
set a2 = $2
set a3 = $3
set a4 = $4
set a5 = $5
set a6 = $6
set a7 = $7
start:
if ("$a1" !~ '') then
   if ("$a1" =~ '-db') then
     setenv DEBUG true
```

```
    set a1 = $a2
    set a2 = $a3
    set a3 = $a4
    set a4 = $a5
    set a5 = $a6
    set a6 = $a7
    goto start
  else if ("$a1" =~ '-batch') then
    setenv BATCH true
    set a1 = $a2
    set a2 = $a3
    set a3 = $a4
    set a4 = $a5
    set a5 = $a6
    set a6 = $a7
    goto start
  else if ("$a1" =~ '-test') then
    setenv TEST true
    set a1 = $a2
    set a2 = $a3
    set a3 = $a4
    set a4 = $a5
    set a5 = $a6
    set a6 = $a7
    goto start
  endif
  if ($a2 =~ '') then
#     all data and output file names the same
#     as first file name: read in argument list
    setenv DNAME $cwd/$a1:r
    setenv TNAME $cwd/$a1:r
    setenv INAME $cwd/$a1:r
    setenv ONAME $cwd/$a1:r
    setenv RNAME $cwd/$a1:r
  else
```

```
#     separate file names for each file:
#     read in argument list
      setenv DNAME $cwd/$a1:r
      setenv TNAME $cwd/$a2:r
      setenv INAME $cwd/$a3:r
      setenv ONAME $cwd/$a4:r
      setenv RNAME $cwd/$a5:r
   endif
else
#  prompt and read in each file name
   set a = ''
   set b = ''
   set c = ''
   set d = ''
   set e = ''
   one:
   echo 'Input File'
   set a = ($<)
   if ($a =~ '') goto one
   setenv DNAME $cwd/$a:r
   two:
   echo 'Thermo File'
   set b = ($<)
   if ($b =~ '') goto two
   setenv TNAME $cwd/$b:r
   three:
   echo 'Inlet Profile File'
   set c = ($<)
   if ($c =~ '') goto three
   setenv INAME $cwd/$c:r
   four:
   echo 'Output File'
   set d = ($<)
   if ($d =~ '') goto four
   setenv ONAME $cwd/$d:r
```

```
    five:
    echo 'Restart File'
    set e = ($<)
    if ($e =~ '') goto five
    setenv RNAME $cwd/$e:r
    endif
endif
if ($?BATCH) then
  set oname = $ONAME
  set jobname = $oname:r
  if (`/bin/hostname` =~ "opus") then
    echo "Which queue?  s = short queue (for jobs shorter than 10 minutes)"
    echo "              l = long queue (for long jobs)"
    echo "              v = verylong queue (for very long jobs)"
    echo "              a = acerc queue (routes to acerc queue on lola)"
    echo "              c = caedm queue (routes to caedm queue on lola)"
    echo "              bl = bestl queue (chooses the best queue from among"
    echo "                                  long, acerc, caedm)"
    set queue = ($<)
    goto submit
  else if (`/bin/hostname` =~ "lola") then
    echo "Which queue?  s = short queue (for jobs shorter than 5 minutes)"
    echo "              a = acerc queue (for jobs submitted by acerc group)"
    echo "              c = caedm queue (for jobs submitted by caedm group)"
    echo "              v = verylong queue (for very long jobs)"
    set queue = ($<)
    goto submit
  else
    echo "Can't run batch jobs on" $hostname".  Job terminated."
    goto control_exit
  endif
  submit:
  if ($queue =~ '') set queue = 'bl'
  if ($?TEST) then
    qsub -q $queue -r $PROGRAM\:$jobname:t -o $cwd/$jobname:t.log1\
```

```
      -eo -x $PCEXE/test/pcgc2.com
  else
    qsub -q $queue -r $PROGRAM\:$jobname:t -o $cwd/$jobname:t.log1\
      -eo -x pcgc2.com
  endif
else if ($?TEST) then
  $PCEXE/test/pcgc2.com
else
  $PCEXE/pcgc2.com
endif
control_exit:
exit

[lola:36]afr >>
```

Script File No. 2 - pcgc2.com

```
[lola:37]c2 >> cat pcgc2.com
#!/bin/csh
#script file to run PCGC2 program interactively
#set echo
#    Copy restart files to output, if different from output
if ($RNAME !~ $ONAME) cp $RNAME.rst $ONAME.rst
if ($RNAME !~ $ONAME) cp $RNAME.pso $ONAME.pso
if ($RNAME !~ $ONAME) cp $RNAME.rnx $ONAME.rnx
if ($RNAME !~ $ONAME) cp $RNAME.tbl $ONAME.tbl
#    If generic files exist, remove them
if ( -e PCGCIN) rm PCGCIN
if ( -e THERMO) rm THERMO
if ( -e INLET) rm INLET
if ( -e GRIDS) rm GRIDS
if ( -e INOUT) rm INOUT
if ( -e RSNXIO) rm RSNXIO
if ( -e TBLRST) rm TBLRST
```

```
if ( -e PARSOU) rm PARSOU
#    Link specific input files to generic input files
ln $DNAME.dat $cwd/PCGCIN
ln $TNAME.thm $cwd/THERMO
ln $INAME.inl $cwd/INLET
if ( -e $DNAME.grd ) ln $DNAME.grd $cwd/GRIDS
if ( -e $ONAME.rst ) ln $ONAME.rst $cwd/INOUT
if ( -e $ONAME.rnx ) ln $ONAME.rnx $cwd/RSNXIO
if ( -e $ONAME.tbl ) ln $ONAME.tbl $cwd/TBLRST
if ( -e $ONAME.pso ) ln $ONAME.pso $cwd/PARSOU
#    If output files exist, delete them
if (-e PCGCOT) rm PCGCOT
if (-e TWODDB) rm TWODDB
if (-e output.fg) rm output.fg
#    Run PCGC2
#mkmf "FFLAGS = -O2" PROGRAM=pcgc2 "SUFFIX = .INC:hF"
if (`/bin/hostname` =~ opus) then
  cd $PCEXE
  make program
  back
  echo "Running $PROGRAM on Opus"
  if ($?DEBUG) then
    $PCBUG $PCEXE/pcgc2
    else
      if ($?BATCH) then
        pmd $PCEXE/pcgc2 >& $ONAME.log
        else
          #pmd $PCEXE/pcgc2
          time $PCEXE/pcgc2
        endif
    endif
  else if (`/bin/hostname` =~ 'lola') then
    cd $PCEXE
    #echo "Making $PROGRAM on Lola"
    #make program
```

```
    echo "This script assumes you have already 'made' the program in"
    echo "\$PCEXE.  If not, hit cntrl-C and do so now."
    back
    echo "Running $PROGRAM on Lola"
    if ($?DEBUG) then
      echo "Leaving pcgc2.com to enter $PCBUG"
      $PCBUG $PCEXE/pcgc2
      echo "Back in pcgc2.com after $PCBUG"
      else
        if ($?BATCH) then
          time $PCEXE/pcgc2 >& $ONAME.log
          else
            #pmd $PCEXE/pcgc2
            time $PCEXE/pcgc2
          endif
      endif
  else
    cd $PCEXE
    make program
    back
    if ($?DEBUG) then
      echo "Running $PROGRAM on $hostname in $PCBUG"
      echo "This script assumes you have already compiled the routines"
      echo "you wish to debug with the -g flag."
      echo "If not, hit cntrl-C and compile them now."
      $PCBUG $PCEXE/pcgc2
      else
        echo "Running $PROGRAM on" $hostname
        $PCEXE/pcgc2
      endif
  endif
control_exit:
#    Remove linked generic file names.  Move unlinked generic files
#    to specific files.
echo "Removing linked generic file names"
```

```
rm $cwd/PCGCIN
rm $cwd/THERMO
rm $cwd/INLET
if ( -e $DNAME.grd ) then
  rm $cwd/GRIDS
else
  mv $cwd/GRIDS $DNAME.grd
endif
echo "Moving unlinked generic files to specific files"
if (-e $cwd/PCGCOT) mv $cwd/PCGCOT $ONAME.out
if (-e $cwd/TWODDB) mv $cwd/TWODDB $ONAME.db
if (-e $cwd/output.fg) mv $cwd/output.fg $ONAME.fgo
if ( -e $ONAME.rst ) then
  rm $cwd/INOUT
else
  mv $cwd/INOUT $ONAME.rst
endif
if ( -e $ONAME.rnx ) then
  rm $cwd/RSNXIO
else
  if (-e $cwd/RSNXIO) mv $cwd/RSNXIO $ONAME.rnx
endif
if ( -e $ONAME.tbl ) then
  rm $cwd/TBLRST
else
  mv $cwd/TBLRST $ONAME.tbl
endif
if ( -e $ONAME.pso ) then
  rm $cwd/PARSOU
else
  if (-e $cwd/PARSOU) mv $cwd/PARSOU $ONAME.pso
endif
if (-e $cwd/PPLOT1) mv $cwd/PPLOT1 $ONAME.pp1
if (-e $cwd/PPLOT2) mv $cwd/PPLOT2 $ONAME.pp2
if (-e $cwd/PPLOT3) mv $cwd/PPLOT3 $ONAME.pp3
```

```
if (-e $cwd/PSORB1) mv $cwd/PSORB1 $ONAME.ps1
if (-e $cwd/PSORB2) mv $cwd/PSORB2 $ONAME.ps2
if (-e $cwd/PSORB3) mv $cwd/PSORB3 $ONAME.ps3
if (-e $cwd/GASPLT) mv $cwd/GASPLT $ONAME.gsp
if (-e $cwd/POLPLT) mv $cwd/POLPLT $ONAME.nxp
if (-e $cwd/PRGRSS) mv $cwd/PRGRSS $ONAME.prg
if (-e $cwd/UNIRAS) mv $cwd/UNIRAS $ONAME.uni
if (-e $cwd/UNIREG) mv $cwd/UNIREG $ONAME.unr
exit
[lola:38]c2 >>
```

Script File No. 3 - .cshrc (partial listing)

```
[lola:40]brewster >> cat .cshrc
# .cshrc
set path=(. ~ /usr/ucb /bin /usr/bin /usr/bsd /usr/sbin / /etc /usr/etc)
set notify
set hostname=`hostname`
set user=`whoami`
setenv PCEXE /opus/exe/brewster/pcafr/c2
alias a alias

switch ($hostname)
  case opus:
        setenv PCEXE /opus/exe/brewster/pcafr/c1
        setenv PCBUG csd
        breaksw
  case lola:
        setenv PCEXE /opus/exe/brewster/pcafr/c2
        setenv PCBUG csd
        breaksw
  case banjo:
        setenv PCBUG sdb
```

```
        setenv PCEXE /opus/exe/brewster/pcafr/c2
        a df df -B
        a ll 'ls -alFd'
        setenv PCBUG csd
        breaksw
case steve:
        breaksw
case milo:
        breaksw
case bill:
        setenv PCBUG dbx
        setenv PCEXE /opus/exe/brewster/pcafr/suns
        alias debug 'f77 -c -sun4 -g'
        breaksw
case bink:
        breaksw
case hodg:
        setenv PCEXE /opus/exe/brewster/pcafr/c2
        setenv PCBUG dbx
        source /software/disspla11/setup.csh
        set path=($path /software/disspla11)
        breaksw
case rose:
        setenv PCEXE /opus/exe/brewster/pcgc/suns
        setenv PCSRC /opus/mnt/brewster/pcgc
        setenv PCBUG dbx
        breaksw
case cj:
        breaksw
case rann:
        breaksw
case homer:
        breaksw
case marge:
        source /software/marge_diss/disspla11/setup.csh
```

```
        'set path=($path /software/marge_diss/dissplall)
        breaksw
  case olie:
        breaksw
  case maggie:
        breaksw
  case bart:
        a df 'df | grep -v pid'
        breaksw
  case alaska:
        breaksw
  default:
        setenv PCEXE /opus/exe/brewster/pcafr/suns
        setenv PCEXE /opus/exe/brewster/pcafr/c2
        setenv PCBUG dbx
        breaksw
endsw
```

Appendix D

Sample MAKE File for Program Maintenance on UNIX Systems

Program maintenance can be simplified by using a `Makefile` on UNIX systems. Makefiles contain a description of all of the file dependencies in a program. Then, if one file is updated, all of the files which depend on that file will be updated automatically by issuing the `make` command. For example, if a FORTRAN source file is updated, it will be recompiled automatically by issuing the `make` command. If an INCLUDE file is updated, then all of the FORTRAN source files which incorporate that INCLUDE file will be recompiled automatically. It is possible to include the `make` command in the `pcgc2.com` script file and have the `make` command issued every time the program is run, as shown in Appendix C. A listing of a sample `Makefile` is shown below:

```
[lola:30]test >> cat Makefile
DEST            =

VPATH           =

EXTHDRS         =

HDRS            =

FFLAGS          = -O1 -fi -db
```

```
LDFLAGS         = -fi -db

LIBS            =

LINKER          = fc

MAKEFILE        = Makefile

OBJS            = adcond.o \
                  aim.o \
                  amnt.o \
                  api.o \
                  b.o \
                  b_evlv.o \
                  blockdata.o \
                  bprops.o \
                  calacj.o \
                  calahj.o \
                  calc.o \
                  calced.o \
                  calcet.o \
                  calcf.o \
                  calcg.o \
                  calcge.o \
                  calch.o \
                  calcnj.o \
                  calcno.o \
                  calco2.o \
                  calcp.o \
                  calcpp.o \
                  calcsj.o \
                  calcte.o \
                  calcu.o \
                  calcv.o \
                  calcw.o \
                  calcyfu.o \
                  calh2s.o \
                  calhcn.o \
                  calnh3.o \
                  calso2.o \
                  chgcon.o \
                  closdb.o \
                  coal0.o \
                  coal1.o \
                  coal2.o \
                  cputim.o \
                  cree.o \
                  cree0.o \
                  decod.o \
```

```
dgelg.o \
dif.o \
disord.o \
dwgout.o \
eico2.o \
eih2o.o \
elback.o \
eolp.o \
eqspec.o \
eratio.o \
erf.o \
fazchk.o \
fgdata.o \
fgtabl.o \
find.o \
finfl1.o \
finfl2.o \
fksu.o \
flint.o \
flux.o \
flux0.o \
fluxr.o \
fluxt.o \
fluxx.o \
fnpq.o \
fpq.o \
freact.o \
frzfe.o \
frzfeh.o \
fste.o \
fstf.o \
fstfe.o \
fstfeh.o \
fstfh.o \
gasfix.o \
gauss.o \
getcdf.o \
getkin.o \
getrct0.o \
gibchk.o \
grdgrf.o \
grid.o \
grmap.o \
gtdeln.o \
gteta.o \
hcalc.o \
hcps.o \
heat.o \
heatbal.o \
```

```
inflow.o \
init.o \
inity0.o \
intgrt.o \
intp.o \
kbar.o \
klcalc.o \
lisolv.o \
loadi.o \
loadsc.o \
maknam.o \
matrix.o \
mixfe.o \
modeta.o \
modh.o \
modte.o \
modu.o \
mosolv.o \
mu.o \
netin.o \
netout.o \
nextte.o \
nfcn.o \
ngfun6.o \
nothing.o \
noxdata.o \
noxmn.o \
ovendb.o \
ovtput.o \
pcgc2.o \
pej.o \
per12.o \
per12p.o \
percvap.o \
pltwrt.o \
print.o \
profil.o \
prog.o \
promod.o \
props.o \
prtsur.o \
pscrat.o \
psict.o \
psict0.o \
psolve.o \
pydist.o \
pyrite1.o \
pyrite2.o \
radcof.o \
```

```
rangok.o \
rate.o \
regrid.o \
reinit.o \
rempur.o \
restrt.o \
result.o \
rk6.o \
rstnox.o \
rxnext.o \
rxnrat.o \
sdnrst.o \
setup.o \
sigmad.o \
sigmam.o \
slfrst.o \
solpos.o \
sorb0.o \
sorpar.o \
sortg.o \
soxdata.o \
spece.o \
spread.o \
sprops.o \
spsict.o \
stream.o \
sulfat.o \
sulfhs.o \
swefun6.o \
swelldata.o \
swesub6.o \
syserr.o \
table.o \
tarvap.o \
tble.o \
tblf.o \
tblfe.o \
tblfeh.o \
tblfh.o \
tblrsfeh.o \
tblrstfe.o \
tblrts.o \
ther15p.o \
tubfeh.o \
ucoef.o \
upfe.o \
upfeh.o \
upfh.o \
vcoef.o \
```

```
                vector.o \
                velmag.o \
                viscosp.o \
                volswl.o \
                wall.o \
                wgfun6.o \
                writco.o \
                writge.o \
                writsc.o \
                writve.o \
                wrtout.o

PRINT           = pr

PROGRAM         = ./pcgc2

SRCS            = adcond.f \
                aim.f \
                amnt.f \
                api.f \
                b.f \
                b_evlv.f \
                blockdata.f \
                bprops.f \
                calacj.f \
                calahj.f \
                calc.f \
                calced.f \
                calcet.f \
                calcf.f \
                calcg.f \
                calcge.f \
                calch.f \
                calcnj.f \
                calcno.f \
                calco2.f \
                calcp.f \
                calcpp.f \
                calcsj.f \
                calcte.f \
                calcu.f \
                calcv.f \
                calcw.f \
                calcyfu.f \
                calh2s.f \
                calhcn.f \
                calnh3.f \
                calso2.f \
                chgcon.f \
```

```
closdb.f \
coal0.f \
coal1.f \
coal2.f \
cputim.f \
cree.f \
cree0.f \
decod.f \
dgelg.f \
dif.f \
disord.f \
dwgout.f \
eico2.f \
eih2o.f \
elback.f \
eolp.f \
eqspec.f \
eratio.f \
erf.f \
fazchk.f \
fgdata.f \
fgtabl.f \
find.f \
finfl1.f \
finfl2.f \
fksu.f \
flint.f \
flux.f \
flux0.f \
fluxr.f \
fluxt.f \
fluxx.f \
fnpq.f \
fpq.f \
freact.f \
frzfe.f \
frzfeh.f \
fste.f \
fstf.f \
fstfe.f \
fstfeh.f \
fstfh.f \
gasfix.f \
gauss.f \
getcdf.f \
getkin.f \
getrct0.f \
gibchk.f \
grdgrf.f \
```

```
grid.f \
grmap.f \
gtdeln.f \
gteta.f \
hcalc.f \
hcps.f \
heat.f \
heatbal.f \
inflow.f \
init.f \
inity0.f \
intgrt.f \
intp.f \
kbar.f \
klcalc.f \
lisolv.f \
loadi.f \
loadsc.f \
maknam.f \
matrix.f \
mixfe.f \
modeta.f \
modh.f \
modte.f \
modu.f \
mosolv.f \
mu.f \
netin.f \
netout.f \
nextte.f \
nfcn.f \
ngfun6.f \
nothing.f \
noxdata.f \
noxmn.f \
ovendb.f \
ovtput.f \
pcgc2.f \
pej.f \
per12.f \
per12p.f \
percvap.f \
pltwrt.f \
print.f \
profil.f \
prog.f \
promod.f \
props.f \
prtsur.f \
```

```
pscrat.f \
psict.f \
psict0.f \
psolve.f \
pydist.f \
pyrite1.f \
pyrite2.f \
radcof.f \
rangok.f \
rate.f \
regrid.f \
reinit.f \
rempur.f \
restrt.f \
result.f \
rk6.f \
rstnox.f \
rxnext.f \
rxnrat.f \
sdnrst.f \
setup.f \
sigmad.f \
sigmam.f \
slfrst.f \
solpos.f \
sorb0.f \
sorpar.f \
sortg.f \
soxdata.f \
spece.f \
spread.f \
sprops.f \
spsict.f \
stream.f \
sulfat.f \
sulfhs.f \
swefun6.f \
swelldata.f \
swesub6.f \
syserr.f \
table.f \
tarvap.f \
tble.f \
tblf.f \
tblfe.f \
tblfeh.f \
tblfh.f \
tblrsfeh.f \
tblrstfe.f \
```

```
                tblrts.f \
                ther15p.f \
                tubfeh.f \
                ucoef.f \
                upfe.f \
                upfeh.f \
                upfh.f \
                vcoef.f \
                vector.f \
                velmag.f \
                viscosp.f \
                volswl.f \
                wall.f \
                wgfun6.f \
                writco.f \
                writge.f \
                writsc.f \
                writve.f \
                wrtout.f

all:            $(PROGRAM)

$(PROGRAM):     $(OBJS) $(LIBS)
                echo -n "Loading $(PROGRAM) ... "
                @$(LINKER) $(LDFLAGS) $(OBJS) $(LIBS) -o $(PROGRAM)
                echo "done"

clean:;         rm -f $(OBJS)

depend:;        mkmf -f $(MAKEFILE) PROGRAM=$(PROGRAM) DEST=$(DEST)

index:;         tags -wx $(HDRS) $(SRCS)

install:        $(PROGRAM)
                echo Installing $(PROGRAM) in $(DEST)
                install -s $(PROGRAM) $(DEST)

print:;         $(PRINT) $(HDRS) $(SRCS)

program:        $(PROGRAM)

tags:           $(HDRS) $(SRCS); ctags $(HDRS) $(SRCS)

update:         $(DEST)/$(PROGRAM)

$(DEST)/$(PROGRAM): $(SRCS) $(LIBS) $(HDRS) $(EXTHDRS)
                make -f $(MAKEFILE) DEST=$(DEST) install
###
adcond.o: CECPAR.INC LUTION.INC CPARAM.INC CEQUIL.INC
```

```
aim.o: PARAMETER.INC COEF.INC FLUPR.INC
api.o: CECPAR.INC CPARAM.INC CEQUIL.INC
b_evlv.o: t_ch4.inc
blockdata.o: PARAMETER.INC ADFLO.INC CGSFLO.INC CPART.INC CTABLE.INC \
        CTNBP.INC GEOM.INC HCAP.INC KASET1.INC KRAD.INC LUTION.INC PCOR.INC \
        PROPIN.INC PSCRT1.INC RADCON.INC RCON.INC UVEL.INC difeq.inc
bprops.o: PARAMETER.INC ALL.INC CPARAM.INC CPART.INC CPEUL.INC FLUPR.INC \
        INTRUZ.INC KASET1.INC SAVBP.INC VAR.INC VARR.INC
calacj.o: PARAMETER.INC ADFLO.INC INTRUZ.INC ALL.INC CPART.INC CPSOU.INC \
        VAR.INC GEOM.INC FLUPR.INC COEF.INC TURB.INC PANDS.INC PARD.INC \
        TUBWAL.INC KASET1.INC CPEUL.INC SWPDIR.INC BOUND.INC CFLAG.INC \
        IPPAR.INC EULP.INC
calahj.o: PARAMETER.INC INTRUZ.INC ALL.INC VAR.INC GEOM.INC FLUPR.INC \
        COEF.INC TURB.INC PARD.INC TUBWAL.INC KASET1.INC CPEUL.INC SWPDIR.INC \
        BOUND.INC CFLAG.INC IPPAR.INC EULP.INC CPART.INC CPSOU.INC PANDS.INC
calc.o: PARAMETER.INC CCHEMI.INC CEQUIL.INC CINDEX.INC CMATRI.INC \
        CPARAM.INC CSPECE.INC PRIN.INC
calced.o: PARAMETER.INC AFR.INC ALL.INC TDIS.INC GEOM.INC FLUPR.INC \
        COEF.INC TURB.INC KASET1.INC CPSOU.INC INTRUZ.INC SWPDIR.INC SUSP.INC \
        VAR.INC
calcet.o: PARAMETER.INC AFR.INC CPART.INC ALL.INC CGASMF.INC VAR.INC \
        GEOM.INC FLUPR.INC COEF.INC TURB.INC MIXFR.INC KASET1.INC CPSEF.INC \
        SWPDIR.INC CPSOU.INC INTRUZ.INC
calcf.o: PARAMETER.INC AFR.INC INTRUZ.INC ALL.INC VAR.INC GEOM.INC \
        FLUPR.INC COEF.INC TURB.INC MIXFR.INC CPSOU.INC SWPDIR.INC KASET1.INC \
        TABRIT.INC CGASMF.INC CPSEF.INC
calcg.o: PARAMETER.INC ALL.INC VAR.INC GEOM.INC FLUPR.INC COEF.INC TURB.INC \
        FLUC.INC KASET1.INC CPSOU.INC SWPDIR.INC INTRUZ.INC
calcge.o: PARAMETER.INC ALL.INC CGASMF.INC VAR.INC GEOM.INC FLUPR.INC \
        COEF.INC TURB.INC FLUC.INC KASET1.INC CPSOU.INC SWPDIR.INC INTRUZ.INC
calch.o: PARAMETER.INC CPART.INC AFR.INC PRIN.INC INTRUZ.INC ALL.INC \
        ENTH.INC VAR.INC GEOM.INC FLUPR.INC COEF.INC TURB.INC KASET1.INC \
        CPSOU.INC SWPDIR.INC RADCON.INC TYPE.INC VARR.INC KRAD.INC
calcnj.o: PARAMETER.INC AFR.INC ALL.INC INTRUZ.INC VAR.INC GEOM.INC \
        FLUPR.INC COEF.INC TURB.INC PARD.INC TUBWAL.INC KASET1.INC CPSOU.INC \
        CPART.INC CPEUL.INC SWPDIR.INC CFLAG.INC PANDS.INC IPPAR.INC EULP.INC
calcno.o: PARAMETER.INC ALL.INC INTRUZ.INC VAR.INC GEOM.INC FLUPR.INC \
        COEF.INC TURB.INC FLUC.INC CALCYI.INC NOXMN1.INC NOXRTE.INC NSWPS.INC \
        KASET1.INC RATECM.INC RATPAR.INC SWPDIR.INC TUBWAL.INC CPSOU.INC
calco2.o: PARAMETER.INC ALL.INC CALCYI.INC CGASMF.INC CINDEX.INC INTRUZ.INC \
        PSCCOM.INC RATECM.INC RATPAR.INC VAR.INC
calcp.o: PARAMETER.INC PRIN.INC ALL.INC INTRUZ.INC PCOR.INC VAR.INC \
        GEOM.INC COEF.INC CPSOU.INC SWPDIR.INC SIMPLE.INC FLUPR.INC \
        FLUPR2.INC
calcpp.o: PARAMETER.INC PRIN.INC ALL.INC INTRUZ.INC PCOR.INC VAR.INC \
        GEOM.INC COEF.INC CPSOU.INC SWPDIR.INC SIMPLE.INC SWPALT.INC \
        FLUPR.INC FLUPR2.INC
calcsj.o: PARAMETER.INC ALL.INC EULP.INC INTRUZ.INC VAR.INC GEOM.INC \
        FLUPR.INC COEF.INC TURB.INC PARD.INC TUBWAL.INC KASET1.INC CPSOU.INC \
```

```
        CPART.INC CPEUL.INC SWPDIR.INC CFLAG.INC PANDS.INC IPPAR.INC
calcte.o: PARAMETER.INC AFR.INC ALL.INC INTRUZ.INC GRID1.INC TEN.INC \
        VAR.INC GEOM.INC FLUPR.INC COEF.INC TURB.INC KASET1.INC SUSP.INC \
        CPSOU.INC SWPDIR.INC SWRL.INC
calcu.o: PARAMETER.INC AFR.INC ALL.INC INTRUZ.INC UVEL.INC VAR.INC GEOM.INC \
        COEF.INC KASET1.INC CPSOU.INC SWPDIR.INC SIMPLE.INC FLUPR.INC \
        FLUPR2.INC PARD.INC PCOR.INC
calcv.o: PARAMETER.INC AFR.INC ALL.INC INTRUZ.INC VVEL.INC VAR.INC GEOM.INC \
        COEF.INC KASET1.INC CPSOU.INC SWPDIR.INC SWRL.INC FLUPR.INC \
        FLUPR2.INC PCOR.INC SIMPLE.INC
calcw.o: PARAMETER.INC ALL.INC INTRUZ.INC WVEL.INC VAR.INC GEOM.INC \
        FLUPR.INC COEF.INC KASET1.INC CPSOU.INC SWPDIR.INC
calcyfu.o: PARAMETER.INC ALL.INC CGASMF.INC COEF.INC CPSEF.INC CPSOU.INC \
        FLUPR.INC GEOM.INC INTRUZ.INC KASET1.INC MAGHJ.INC MIXFR.INC \
        SWPDIR.INC SSUM.INC TURB.INC VAR.INC
calh2s.o: PARAMETER.INC ALL.INC COEF.INC CPSOU.INC FLUC.INC FLUPR.INC \
        GEOM.INC INTRUZ.INC KASET1.INC NOXMN1.INC NSWPS.INC RATESX.INC \
        SOXRTE.INC SWPDIR.INC TUBWAL.INC TURB.INC VAR.INC
calhcn.o: PARAMETER.INC ALL.INC INTRUZ.INC VAR.INC GEOM.INC FLUPR.INC \
        COEF.INC TURB.INC FLUC.INC CALCYI.INC NOXMN1.INC NOXRTE.INC NSWPS.INC \
        KASET1.INC RATECM.INC RATPAR.INC SWPDIR.INC TUBWAL.INC CPSOU.INC
calnh3.o: PARAMETER.INC ALL.INC INTRUZ.INC VAR.INC GEOM.INC FLUPR.INC \
        COEF.INC TURB.INC FLUC.INC CALCYI.INC NOXMN1.INC NOXRTE.INC NSWPS.INC \
        KASET1.INC RATECM.INC RATPAR.INC SWPDIR.INC TUBWAL.INC CPSOU.INC
calso2.o: PARAMETER.INC ALL.INC COEF.INC CPSOU.INC FLUC.INC FLUPR.INC \
        GEOM.INC INTRUZ.INC KASET1.INC NOXMN1.INC NSWPS.INC RATESX.INC \
        SOXRTE.INC SWPDIR.INC TUBWAL.INC TURB.INC VAR.INC
chgcon.o: CECPAR.INC LUTION.INC CSPECE.INC CPARAM.INC
coal0.o: PARAMETER.INC TFLOF10.INC MAGHJ.INC AFR.INC ALL.INC BUG.INC \
        CCHEMI.INC CEQUIL.INC CFLAG.INC CGSFLO.INC CHETRX.INC CINDEX.INC \
        CNDXCG.INC CPARAM.INC CPART.INC CPLOT.INC CPSEF.INC CPSOU.INC \
        CSPECE.INC CTNBP.INC CWATER.INC FLUPR.INC GEOM.INC GPARAM.INC \
        HCAP.INC HCAPFG.INC HREF.INC ICON.INC IPPAR.INC KASET1.INC MRCK.INC \
        PANDS.INC PFAC.INC PRIN.INC PVAR.INC RCON.INC RCONT.INC F1AF0.INC \
        RRAT.INC TABRIT.INC TRAJ.INC TUBWAL.INC UNDER.INC VAR.INC difeq.inc \
        elem.inc ffids.inc order.inc reactk.inc
coal1.o: PARAMETER.INC PRIN.INC CSPECE.INC CEQUIL.INC CCHEMI.INC CINDEX.INC \
        CPARAM.INC DIFUS.INC RCON.INC RCONT.INC TRAJ.INC ICON.INC GPARAM.INC
coal2.o: PARAMETER.INC AFR.INC elem.inc CPARAM.INC CCHEMI.INC CEQUIL.INC \
        CINDEX.INC CHETRX.INC CSPECE.INC CPART.INC difeq.inc RCONT.INC \
        GEOM.INC IPPAR.INC HCAP.INC HREF.INC RRAT.INC DIFEQN.INC VARR.INC \
        RADCON.INC OMEGA.INC PECOR.INC PFAC.INC PRIN.INC DIFUS.INC TRAJ.INC \
        ICON.INC RCON.INC GPARAM.INC MRCK.INC dvccomp.inc order.inc pools.inc \
        rates.inc finish.inc tempcm.inc xeffcm.inc CNDXCG.INC
cree.o: PARAMETER.INC CCHEMI.INC CEQUIL.INC CINDEX.INC CPARAM.INC \
        CSPECE.INC LUTION.INC PRIN.INC
cree0.o: PARAMETER.INC CCHEMI.INC CEQUIL.INC CINDEX.INC CMATRI.INC \
        CPARAM.INC CSPECE.INC LUTION.INC PANDS.INC PRIN.INC CNDXCG.INC
decod.o: defs.inc config.inc
```

```
disord.o: PARAMETER.INC ALL.INC BCRAD.INC CPART.INC CSET.INC DISO.INC \
        FLUPR.INC GEOM.INC GRID1.INC INTRUZ.INC KASET1.INC KRAD.INC \
        NOXMN1.INC PARD.INC PRIN.INC RADCON.INC SHERX.INC SWPDIR.INC VARR.INC
dwgout.o: defs.inc config.inc dwgswe.inc order.inc pyrite.inc difeq.inc
elback.o: pyrite.inc
eolp.o: PARAMETER.INC AFR.INC TFLOF10.INC TYPE.INC PRIN.INC ALL.INC \
        INTRUZ.INC VAR.INC GEOM.INC FLUPR.INC COEF.INC TURB.INC PARD.INC \
        TUBWAL.INC KASET1.INC CPSOU.INC CPART.INC CPEUL.INC SWPDIR.INC \
        CFLAG.INC IPPAR.INC EULP.INC VARR.INC CGASMF.INC CGSFLO.INC CPSEF.INC \
        UNDER.INC TIMER.INC PANDS.INC
eqspec.o: PARAMETER.INC AFR.INC ALL.INC AREXP.INC BOUND.INC BUG.INC \
        CALCYI.INC CCHEMI.INC CFLAG.INC CGASMF.INC CGAUSS.INC CINDEX.INC \
        CPARAM.INC CPART.INC CPEUL.INC CPSOU.INC CSPECE.INC CTABLE.INC \
        DENS.INC FLUC.INC FLUPR.INC GEOM.INC GPARAM.INC INTRUZ.INC IPPAR.INC \
        KASET1.INC MOLWT.INC NOXMN1.INC NOXRTE.INC PANDS.INC PROPIN.INC \
        PRIN.INC PSCCOM.INC PVAR.INC RATECM.INC RATEST.INC RATPAR.INC \
        F1AF0.INC RESID.INC RMSCOM.INC TIMER.INC TABRIT.INC TRAJ.INC \
        TUBWAL.INC TURB.INC UPNX.INC VAR.INC XRATE.INC
eratio.o: PARAMETER.INC CCHEMI.INC CEQUIL.INC CINDEX.INC CMATRI.INC \
        CPARAM.INC CSPECE.INC PRIN.INC
fgdata.o: PARAMETER.INC HCAPFG.INC
fgtabl.o: CGAUSS.INC
finfl1.o: PARAMETER.INC order.inc finish.inc difeq.inc elem.inc pyrite.inc
finfl2.o: order.inc finish.inc pyrite.inc
flint.o: PARAMETER.INC TFLOF10.INC CTABLE.INC ADFLO.INC AFR.INC ALL.INC \
        CPART.INC CWATER.INC FLIN.INC GRID1.INC INTRUZ.INC VAR.INC VVEL.INC \
        GEOM.INC FLUPR.INC PANDS.INC F1AF0.INC PVAR.INC KASET1.INC TUBWAL.INC \
        STRFNC.INC CGSFLO.INC NOXMN1.INC PDIM.INC SHERX.INC GMAP.INC \
        CGASMF.INC CPSEF.INC TURB.INC
flux.o: PARAMETER.INC ALL.INC INTRUZ.INC PRIN.INC VARR.INC GEOM.INC \
        RADCON.INC CPART.INC KRAD.INC DISO.INC COEF.INC CSET.INC RADRES.INC
flux0.o: PARAMETER.INC TYPE.INC KASET1.INC SHERX.INC ALL.INC CPART.INC \
        CINDEX.INC PRIN.INC GEOM.INC DISO.INC RADCON.INC BCRAD.INC
fluxr.o: PARAMETER.INC PRIN.INC BCRAD.INC COEF.INC GEOM.INC VARR.INC \
        KRAD.INC CPART.INC SWPDIR.INC CSET.INC RADRES.INC ALL.INC INTRUZ.INC \
        RADCON.INC
fluxt.o: PARAMETER.INC ALL.INC INTRUZ.INC COEF.INC GEOM.INC VARR.INC \
        KRAD.INC CPART.INC SWPDIR.INC CSET.INC RADRES.INC RADCON.INC
fluxx.o: PARAMETER.INC PRIN.INC ALL.INC BCRAD.INC INTRUZ.INC COEF.INC \
        GEOM.INC VARR.INC KRAD.INC CPART.INC SWPDIR.INC CSET.INC RADRES.INC \
        KASET1.INC RADCON.INC
freact.o: PARAMETER.INC ALL.INC CGASMF.INC CGAUSS.INC CINDEX.INC INTRUZ.INC \
        NOXMN1.INC NOXRTE.INC PSCCOM.INC RATECM.INC RATEST.INC RATPAR.INC \
        VAR.INC
frzfe.o: PARAMETER.INC PRIN.INC CPARAM.INC UPNX.INC PVAR.INC DENS.INC \
        TABRIT.INC CTABLE.INC FLUPR.INC RTMTAB.INC
frzfeh.o: PARAMETER.INC PRIN.INC RTMTAB.INC CPARAM.INC CINDEX.INC UPNX.INC \
        PVAR.INC DENS.INC TABRIT.INC BUG.INC CCHEMI.INC CTABLE.INC FLUPR.INC \
        CSPECE.INC
```

```
fste.o: PARAMETER.INC F1AF0.INC PVAR.INC PRIN.INC CPARAM.INC FLUPR.INC \
        CTABLE.INC
fstf.o: PARAMETER.INC F1AF0.INC PRIN.INC CPARAM.INC FLUPR.INC CTABLE.INC
fstfe.o: PARAMETER.INC F1AF0.INC PRIN.INC CPARAM.INC PVAR.INC BUG.INC \
        CTABLE.INC FLUPR.INC
fstfeh.o: PARAMETER.INC F1AF0.INC CPARAM.INC PVAR.INC PRIN.INC BUG.INC \
        CTABLE.INC FLUPR.INC
fstfh.o: PARAMETER.INC F1AF0.INC PRIN.INC CPARAM.INC FLUPR.INC CTABLE.INC
gasfix.o: CECPAR.INC CPARAM.INC LUTION.INC
getcdf.o: config.inc order.inc ffids.inc difeq.inc input.inc t_ch4.inc \
        pyrite.inc
getkin.o: order.inc config.inc ffids.inc input.inc
getrct0.o: reactk.inc
gibchk.o: CECPAR.INC
grid.o: PARAMETER.INC BOUND.INC ALL.INC INTRUZ.INC GRID1.INC GEOM.INC \
        KASET1.INC TUBWAL.INC STRFNC.INC CGSFLO.INC NOXMN1.INC PDIM.INC \
        PRIN.INC
grmap.o: PARAMETER.INC ADFLO.INC ALL.INC INTRUZ.INC GRID1.INC GEOM.INC \
        TUBWAL.INC NOXMN1.INC TIMER.INC PDIM.INC STRFNC.INC GMAP.INC \
        KASET1.INC PRIN.INC
gtdeln.o: CECPAR.INC CEQUIL.INC CPARAM.INC LUTION.INC CSPECE.INC
gteta.o: CECPAR.INC LUTION.INC CPARAM.INC
hcalc.o: CECPAR.INC RCARDS.INC CPARAM.INC COF.INC LUTION.INC CSPECE.INC \
        CEQUIL.INC CCHEMI.INC
hcps.o: CECPAR.INC CPARAM.INC CCHEMI.INC CSPECE.INC CMATRI.INC LUTION.INC
heat.o: PARAMETER.INC HCAPFG.INC CEQUIL.INC order.inc elem.inc DIFEQN.INC \
        difeq.inc dwgswe.inc IPPAR.INC PECOR.INC
heatbal.o: PARAMETER.INC ADFLO.INC ALL.INC BOUND.INC CGSFLO.INC CPART.INC \
        CTABLE.INC DISO.INC ENTH.INC F1AF0.INC FLUPR.INC GEOM.INC HEATCP.INC \
        IPPAR.INC NOXMN1.INC TUBWAL.INC VAR.INC
inflow.o: PARAMETER.INC TFLOF10.INC PRIN.INC ADFLO.INC CGSFLO.INC CPSEF.INC \
        FLIN.INC KASET1.INC PANDS.INC PDIM.INC SWRL.INC
init.o: PARAMETER.INC DISO.INC F1AF0.INC TFLOF10.INC HEATCP.INC CTABLE.INC \
        AFR.INC TURB.INC ALL.INC INTRUZ.INC WVEL.INC VVEL.INC ENTH.INC \
        MAGHJ.INC MIXFR.INC VAR.INC GEOM.INC FLUPR.INC CFLAG.INC KASET1.INC \
        COEF.INC CPSOU.INC CGASMF.INC STRFNC.INC KRAD.INC VARR.INC CGSFLO.INC \
        PANDS.INC CPSEF.INC UVEL.INC PCOR.INC SSUM.INC UNDER.INC
inity0.o: order.inc pyrite.inc
intgrt.o: PARAMETER.INC ALL.INC INTRUZ.INC
intp.o: PARAMETER.INC ALL.INC GEOM.INC
kbar.o: rates.inc pools.inc
klcalc.o: reactk.inc
lisolv.o: PARAMETER.INC COEF.INC SWPDIR.INC TIMER.INC SWPALT.INC
maknam.o: config.inc ffids.inc
matrix.o: CECPAR.INC CCHEMI.INC CEQUIL.INC CMATRI.INC CPARAM.INC CSPECE.INC \
        LUTION.INC
mixfe.o: PARAMETER.INC PRIN.INC CPARAM.INC PVAR.INC DENS.INC CCHEMI.INC \
        BUG.INC CGSFLO.INC PANDS.INC F1AF0.INC TABRIT.INC CTABLE.INC \
        FLUPR.INC
```

```
modeta.o: PARAMETER.INC ADFLO.INC INTRUZ.INC ALL.INC MAGHJ.INC VVEL.INC \
        WVEL.INC PCOR.INC VAR.INC GEOM.INC FLUPR.INC SHERX.INC KASET1.INC \
        SUSP.INC COEF.INC TURB.INC MIXFR.INC SHEAR.INC TUBWAL.INC CGASMF.INC \
        SSUM.INC SWRL.INC TIMER.INC CPSEF.INC UVEL.INC
modh.o: PARAMETER.INC ENTH.INC HEATCP.INC CCHEMI.INC CSPECE.INC CPARAM.INC \
        F1AF0.INC PVAR.INC ADFLO.INC AFR.INC INTRUZ.INC ALL.INC MAGHJ.INC \
        VVEL.INC WVEL.INC PCOR.INC VAR.INC GEOM.INC FLUPR.INC SHERX.INC \
        KASET1.INC SUSP.INC COEF.INC TURB.INC MIXFR.INC SHEAR.INC TUBWAL.INC \
        CGASMF.INC SSUM.INC SWRL.INC TIMER.INC CPSEF.INC UVEL.INC
modte.o: PARAMETER.INC ADFLO.INC AFR.INC INTRUZ.INC ALL.INC MAGHJ.INC \
        VVEL.INC WVEL.INC PCOR.INC VAR.INC GEOM.INC FLUPR.INC SHERX.INC \
        KASET1.INC SUSP.INC COEF.INC TURB.INC MIXFR.INC SHEAR.INC TUBWAL.INC \
        CGASMF.INC SSUM.INC SWRL.INC TIMER.INC CPSEF.INC UVEL.INC
modu.o: PARAMETER.INC ADFLO.INC AFR.INC INTRUZ.INC ALL.INC MAGHJ.INC \
        VVEL.INC WVEL.INC PCOR.INC VAR.INC GEOM.INC FLUPR.INC SHERX.INC \
        KASET1.INC SUSP.INC COEF.INC TURB.INC MIXFR.INC SHEAR.INC TUBWAL.INC \
        CGASMF.INC SSUM.INC SWRL.INC TIMER.INC CPSEF.INC UVEL.INC
mosolv.o: PARAMETER.INC COEF.INC SWPDIR.INC TIMER.INC SWPALT.INC
mu.o: CECPAR.INC LUTION.INC CPARAM.INC CSPECE.INC
netin.o: dvccomp.inc xeffcm.inc difeq.inc percol.inc input.inc
netout.o: dvccomp.inc xeffcm.inc percol.inc
nextte.o: defs.inc tempcm.inc config.inc
nfcn.o: rates.inc pools.inc
noxdata.o: PSCCOM.INC RMSCOM.INC
noxmn.o: PARAMETER.INC AFR.INC ALL.INC AREXP.INC BOUND.INC BUG.INC \
        CALCYI.INC CCHEMI.INC CEQUIL.INC CFLAG.INC CGASMF.INC CGAUSS.INC \
        CINDEX.INC CPARAM.INC CPART.INC CPEUL.INC CPSOU.INC COEF.INC \
        CSPECE.INC CTABLE.INC DENS.INC FLUC.INC FLUPR.INC GEOM.INC GPARAM.INC \
        INTRUZ.INC IPPAR.INC KASET1.INC MOLWT.INC NOXMN1.INC NOXRTE.INC \
        NSWPS.INC PANDS.INC PROPIN.INC PRIN.INC PSCCOM.INC PFAC.INC PVAR.INC \
        RATECM.INC RATEST.INC RATPAR.INC F1AF0.INC RESID.INC RMSCOM.INC \
        SSUM.INC SWPDIR.INC TIMER.INC TABRIT.INC TRAJ.INC TUBWAL.INC TURB.INC \
        UPNX.INC VAR.INC XRATE.INC
ovtput.o: PARAMETER.INC ADFLO.INC ALL.INC COEF.INC FLUPR.INC GEOM.INC \
        GMAP.INC VAR.INC CPEUL.INC INTRUZ.INC VARR.INC STRFNC.INC CPARAM.INC \
        CGASMF.INC
pcgc2.o: PARAMETER.INC ADFLO.INC AFR.INC ALL.INC BOUND.INC BUG.INC \
        CGASMF.INC CGSFLO.INC CINDEX.INC CNDXCG.INC COEF.INC CPARAM.INC \
        CPART.INC CPEUL.INC CPLOT.INC CPSEF.INC CPSOU.INC CSPECE.INC \
        CTABLE.INC CWATER.INC DIRECT.INC DISO.INC ENTH.INC F1AF0.INC FLIN.INC \
        FLUC.INC FLUPR.INC GEOM.INC GPARAM.INC GRID1.INC HEATCP.INC ICON.INC \
        INTRUZ.INC KASET1.INC MAGHJ.INC MIXFR.INC MOLWT.INC PANDS.INC \
        PARD.INC PCOR.INC PDIM.INC PRIN.INC RRAT.INC SHEAR.INC SWRL.INC \
        TDIS.INC TEN.INC TFLOF10.INC TRAJ.INC TURB.INC TYPE.INC UVEL.INC \
        VAR.INC VVEL.INC WVEL.INC TUBWAL.INC PROPIN.INC VARR.INC STRFNC.INC \
        SSUM.INC SWPDIR.INC UNDER.INC DENS.INC SIMPLE.INC NOXMN1.INC \
        TABRIT.INC TIMER.INC PVAR.INC CFLAG.INC PLTVAR.INC RESID.INC \
        CCHEMI.INC SHERX.INC EULP.INC IPPAR.INC GMAP.INC RCON.INC
pej.o: PARAMETER.INC CINDEX.INC CSPECE.INC CTNBP.INC TRAJ.INC HCAP.INC \
```

```
        HREF.INC RCON.INC
percvap.o: dvccomp.inc xeffcm.inc percol.inc pools.inc input.inc t_ch4.inc
pltwrt.o: PARAMETER.INC CINDEX.INC FORMAT.INC MOLWT.INC RESID.INC AFR.INC \
        ALL.INC CGASMF.INC CGSFLO.INC COEF.INC CPARAM.INC CPART.INC CPEUL.INC \
        FLUPR.INC GEOM.INC INTRUZ.INC NOXMN1.INC STRFNC.INC VAR.INC VARR.INC
profil.o: PARAMETER.INC ADFLO.INC ALL.INC VAR.INC GEOM.INC FLUPR.INC \
        KASET1.INC STRFNC.INC CGSFLO.INC TURB.INC NOXMN1.INC TUBWAL.INC \
        PDIM.INC PANDS.INC F1AF0.INC SWRL.INC VVEL.INC
prog.o: PARAMETER.INC ALL.INC FLUC.INC VAR.INC CGASMF.INC FLUPR.INC \
        UVEL.INC VVEL.INC WVEL.INC PCOR.INC ENTH.INC TEN.INC TDIS.INC \
        MIXFR.INC PARD.INC
promod.o: PARAMETER.INC ADFLO.INC AFR.INC INTRUZ.INC ALL.INC MAGHJ.INC \
        VVEL.INC WVEL.INC PCOR.INC VAR.INC GEOM.INC FLUPR.INC SHERX.INC \
        KASET1.INC SUSP.INC COEF.INC TURB.INC MIXFR.INC SHEAR.INC TUBWAL.INC \
        CGASMF.INC SSUM.INC SWRL.INC TIMER.INC CPSEF.INC UVEL.INC
props.o: PARAMETER.INC HEATCP.INC F1AF0.INC TRAJ.INC AFR.INC GPARAM.INC \
        ALL.INC INTRUZ.INC PRIN.INC MAGHJ.INC CPARAM.INC CPART.INC FLUPR.INC \
        PANDS.INC CTABLE.INC BUG.INC VAR.INC GEOM.INC TURB.INC FLUC.INC \
        CGASMF.INC PVAR.INC MOLWT.INC PROPIN.INC DENS.INC TIMER.INC \
        TABRIT.INC BOUND.INC RESID.INC CFLAG.INC CPEUL.INC IPPAR.INC \
        CCHEMI.INC CGAUSS.INC
prtsur.o: PARAMETER.INC ALL.INC CPART.INC INTRUZ.INC CPEUL.INC PFAC.INC \
        AREXP.INC BOUND.INC GEOM.INC
pscrat.o: PARAMETER.INC CINDEX.INC CPARAM.INC CPART.INC CPSOU.INC \
        PSCCOM.INC PVAR.INC PANDS.INC RATPAR.INC RMSCOM.INC TABRIT.INC
psict.o: PARAMETER.INC DIRECT.INC difeq.inc FORMAT.INC PANDS.INC \
        TFLOF10.INC HCAP.INC AFR.INC ALL.INC CEQUIL.INC CFLAG.INC CGASMF.INC \
        CGSFLO.INC CINDEX.INC CNDXCG.INC CPARAM.INC CPART.INC CPEUL.INC \
        CPLOT.INC CPSEF.INC CPSOU.INC CWATER.INC DIFEQN.INC FLUPR.INC \
        GEOM.INC GPARAM.INC ICON.INC INTRUZ.INC IPPAR.INC KASET1.INC \
        MOLWT.INC PECOR.INC PRIN.INC RCONT.INC RRAT.INC SSUM.INC SWRL.INC \
        TRAJ.INC TURB.INC TUBWAL.INC VAR.INC VARR.INC config.inc defs.inc \
        elem.inc input.inc order.inc pools.inc tempcm.inc xeffcm.inc
psict0.o: PARAMETER.INC TFLOF10.INC ADFLO.INC ALL.INC AFR.INC CFLAG.INC \
        CGASMF.INC CGSFLO.INC CPART.INC CPEUL.INC CPLOT.INC CPSEF.INC \
        CPSOU.INC GRID1.INC EULP.INC FLIN.INC FLUPR.INC GEOM.INC INTRUZ.INC \
        IPPAR.INC KASET1.INC PANDS.INC PRIN.INC F1AF0.INC TUBWAL.INC VAR.INC
psolve.o: PARAMETER.INC difeq.inc AFR.INC ALL.INC CPARAM.INC CPART.INC \
        CPSOU.INC TRAJ.INC VAR.INC FLUPR.INC KASET1.INC CGSFLO.INC CPLOT.INC \
        CPEUL.INC MOLWT.INC IPPAR.INC CFLAG.INC RCONT.INC OMEGA.INC EULP.INC \
        PRIN.INC VARR.INC DIFEQN.INC PECOR.INC GEOM.INC
pydist.o: pyrite.inc order.inc
pyrite1.o: pyrite.inc order.inc pools.inc difeq.inc
pyrite2.o: pyrite.inc
radcof.o: PARAMETER.INC ALL.INC CEQUIL.INC CINDEX.INC CPEUL.INC CPART.INC \
        DISO.INC GEOM.INC MOLWT.INC RADCON.INC KRAD.INC FLUPR.INC
rangok.o: CECPAR.INC CPARAM.INC CSPECE.INC
rate.o: PARAMETER.INC AFR.INC ALL.INC AREXP.INC BOUND.INC BUG.INC \
        CALCYI.INC CCHEMI.INC CEQUIL.INC CFLAG.INC CGASMF.INC CGAUSS.INC \
```

```
        CINDEX.INC CPARAM.INC CPART.INC CPEUL.INC CPSOU.INC CSPECE.INC \
        CTABLE.INC DENS.INC FLUC.INC FLUPR.INC GEOM.INC GPARAM.INC INTRUZ.INC \
        IPPAR.INC KASET1.INC MOLWT.INC NOXMN1.INC NOXRTE.INC PANDS.INC \
        PROPIN.INC PRIN.INC PSCCOM.INC PVAR.INC RATECM.INC RATEST.INC \
        RATPAR.INC F1AF0.INC RESID.INC RMSCOM.INC TIMER.INC TABRIT.INC \
        TRAJ.INC TUBWAL.INC TURB.INC UPNX.INC VAR.INC XRATE.INC
regrid.o: PARAMETER.INC
reinit.o: pools.inc order.inc pyrite.inc xeffcm.inc percol.inc plotw.inc \
        input.inc
rempur.o: CECPAR.INC CPARAM.INC CEQUIL.INC
restrt.o: PARAMETER.INC TURB.INC AFR.INC ALL.INC VAR.INC FLUPR.INC \
        MAGHJ.INC KASET1.INC CGASMF.INC KRAD.INC VARR.INC TABRIT.INC FLUC.INC
result.o: PARAMETER.INC ALL.INC FLUPR.INC BCRAD.INC KRAD.INC GEOM.INC \
        DISO.INC VARR.INC PRIN.INC
rstnox.o: PARAMETER.INC ALL.INC CALCYI.INC CGASMF.INC KASET1.INC RATECM.INC
rxnext.o: PARAMETER.INC AFR.INC ALL.INC AREXP.INC BOUND.INC BUG.INC \
        CALCYI.INC CCHEMI.INC CEQUIL.INC CFLAG.INC CGASMF.INC CGAUSS.INC \
        CINDEX.INC CPARAM.INC CPART.INC CPEUL.INC CPSOU.INC CSPECE.INC \
        CTABLE.INC DENS.INC FLUC.INC FLUPR.INC GEOM.INC GPARAM.INC INTRUZ.INC \
        IPPAR.INC KASET1.INC MOLWT.INC NOXMN1.INC NOXRTE.INC PANDS.INC \
        PROPIN.INC PRIN.INC PSCCOM.INC PVAR.INC RATECM.INC RATEST.INC \
        RATPAR.INC F1AF0.INC RESID.INC RMSCOM.INC TIMER.INC TABRIT.INC \
        TRAJ.INC TUBWAL.INC TURB.INC UPNX.INC VAR.INC XRATE.INC
rxnrat.o: PARAMETER.INC AFR.INC ALL.INC AREXP.INC BOUND.INC BUG.INC \
        CALCYI.INC CCHEMI.INC CEQUIL.INC CFLAG.INC CGASMF.INC CGAUSS.INC \
        CINDEX.INC CPARAM.INC CPART.INC CPEUL.INC CPSOU.INC CSPECE.INC \
        CTABLE.INC DENS.INC FLUC.INC FLUPR.INC GEOM.INC GPARAM.INC INTRUZ.INC \
        IPPAR.INC KASET1.INC MOLWT.INC NOXMN1.INC NOXRTE.INC PANDS.INC \
        PROPIN.INC PRIN.INC PSCCOM.INC PVAR.INC RATECM.INC RATEST.INC \
        RATPAR.INC F1AF0.INC RESID.INC RMSCOM.INC TIMER.INC TABRIT.INC \
        TRAJ.INC TUBWAL.INC TURB.INC UPNX.INC VAR.INC XRATE.INC
sdnrst.o: PARAMETER.INC ALL.INC CPART.INC CPEUL.INC
setup.o: PARAMETER.INC ALL.INC CPART.INC COEF.INC GEOM.INC KRAD.INC \
        CSET.INC VARR.INC RADCON.INC
slfrst.o: PARAMETER.INC ALL.INC RATESX.INC SOXRTE.INC
solpos.o: CECPAR.INC LUTION.INC
sorb0.o: PARAMETER.INC ADFLO.INC ALL.INC CFLAG.INC CGASMF.INC CGSFLO.INC \
        CPART.INC CPEUL.INC CPLOT.INC CPSOU.INC EULP.INC F1AF0.INC FLIN.INC \
        FLUPR.INC GEOM.INC INTRUZ.INC IPPAR.INC KASET1.INC PANDS.INC PRIN.INC \
        RATESX.INC SOXRTE.INC SXMISC.INC TFLOF10.INC TUBWAL.INC VAR.INC
sorpar.o: PARAMETER.INC ALL.INC CEQUIL.INC CFLAG.INC CGASMF.INC CGSFLO.INC \
        COEF.INC CINDEX.INC CNDXCG.INC CPARAM.INC CPART.INC CPEUL.INC \
        CPSOU.INC EULP.INC FLUC.INC FLUPR.INC GEOM.INC INTRUZ.INC IPPAR.INC \
        KASET1.INC MOLWT.INC NOXMN1.INC NSWPS.INC PANDS.INC PARD.INC PRIN.INC \
        PVAR.INC RATESX.INC SOXRTE.INC SAVBP.INC SSUM.INC SWPDIR.INC \
        SXMISC.INC TIMER.INC TYPE.INC TUBWAL.INC TURB.INC UNDER.INC VAR.INC \
        VARR.INC
soxdata.o: PARAMETER.INC RATESX.INC
spece.o: CECPAR.INC CCHEMI.INC CEQUIL.INC CMATRI.INC CSPECE.INC CPARAM.INC \
```

```
        LUTION.INC
spread.o: PARAMETER.INC ALL.INC GEOM.INC
sprops.o: PARAMETER.INC ALL.INC CPARAM.INC CPART.INC CPEUL.INC FLUPR.INC \
        INTRUZ.INC KASET1.INC SAVBP.INC VAR.INC VARR.INC
spsict.o: PARAMETER.INC ALL.INC CEQUIL.INC CFLAG.INC CGASMF.INC CGSFLO.INC \
        CINDEX.INC CPARAM.INC CPART.INC CPEUL.INC CPLOT.INC CPSOU.INC \
        FLUPR.INC FORMAT.INC GEOM.INC GPARAM.INC INTRUZ.INC KASET1.INC \
        MOLWT.INC PECOR.INC PRIN.INC RATESX.INC RCONT.INC SOXRTE.INC SSUM.INC \
        TRAJ.INC TURB.INC TUBWAL.INC VAR.INC
stream.o: PARAMETER.INC ALL.INC INTRUZ.INC VAR.INC GEOM.INC FLUPR.INC \
        KASET1.INC TUBWAL.INC STRFNC.INC CGSFLO.INC
sulfat.o: PARAMETER.INC CPART.INC GEOM.INC RATESX.INC TRAJ.INC SOXRTE.INC
sulfhs.o: PARAMETER.INC CPART.INC GEOM.INC RATESX.INC TRAJ.INC SOXRTE.INC
swelldata.o: tempcm.inc
swesub6.o: order.inc tempcm.inc xeffcm.inc dwgswe.inc input.inc dvccomp.inc \
        saveinc.inc
table.o: PARAMETER.INC CPARAM.INC TABRIT.INC TIMER.INC CTABLE.INC
tarvap.o: dvccomp.inc xeffcm.inc percol.inc
tble.o: PARAMETER.INC TFLOF10.INC PVAR.INC PRIN.INC CPARAM.INC FLUPR.INC \
        CCHEMI.INC TABRIT.INC BUG.INC CGSFLO.INC PANDS.INC F1AF0.INC \
        CTABLE.INC
tblf.o: PARAMETER.INC TFLOF10.INC AFR.INC GPARAM.INC TRAJ.INC PRIN.INC \
        CPARAM.INC FLUPR.INC CCHEMI.INC TABRIT.INC BUG.INC CGSFLO.INC \
        PANDS.INC F1AF0.INC CTABLE.INC
tblfe.o: PARAMETER.INC TFLOF10.INC AFR.INC TRAJ.INC PRIN.INC CPARAM.INC \
        UPNX.INC PVAR.INC DENS.INC TABRIT.INC CCHEMI.INC BUG.INC CGSFLO.INC \
        PANDS.INC F1AF0.INC CTABLE.INC FLUPR.INC RTMTAB.INC GPARAM.INC
tblfeh.o: PARAMETER.INC TFLOF10.INC CINDEX.INC CSPECE.INC GPARAM.INC \
        AFR.INC TRAJ.INC PRIN.INC CPARAM.INC RTMTAB.INC PVAR.INC DENS.INC \
        TABRIT.INC CCHEMI.INC BUG.INC CGSFLO.INC PANDS.INC F1AF0.INC \
        CTABLE.INC FLUPR.INC
tblfh.o: PARAMETER.INC CINDEX.INC TFLOF10.INC F1AF0.INC AFR.INC TRAJ.INC \
        GPARAM.INC PRIN.INC CPARAM.INC FLUPR.INC CCHEMI.INC DENS.INC BUG.INC \
        CGSFLO.INC TABRIT.INC CTABLE.INC RTMTAB.INC
tblrsfeh.o: PARAMETER.INC F1AF0.INC AFR.INC PRIN.INC CPARAM.INC PVAR.INC \
        DENS.INC TABRIT.INC CCHEMI.INC BUG.INC CTABLE.INC FLUPR.INC \
        RTMTAB.INC
tblrstfe.o: PARAMETER.INC F1AF0.INC PRIN.INC CPARAM.INC UPNX.INC PVAR.INC \
        DENS.INC CCHEMI.INC BUG.INC TABRIT.INC CTABLE.INC FLUPR.INC \
        RTMTAB.INC
tblrts.o: pools.inc order.inc finish.inc rates.inc
ther15p.o: order.inc pools.inc rates.inc xeffcm.inc difeq.inc percol.inc \
        input.inc t_ch4.inc pyrite.inc defs.inc
tubfeh.o: PARAMETER.INC CPARAM.INC CTABLE.INC F1AF0.INC PVAR.INC RTMTAB.INC
ucoef.o: PARAMETER.INC AFR.INC ALL.INC CPART.INC INTRUZ.INC DIRECT.INC \
        UVEL.INC VAR.INC GEOM.INC COEF.INC KASET1.INC CPSOU.INC SWPDIR.INC \
        SIMPLE.INC FLUPR.INC FLUPR2.INC PCOR.INC
upfe.o: PARAMETER.INC TFLOF10.INC AFR.INC TRAJ.INC PRIN.INC CPARAM.INC \
        UPNX.INC PVAR.INC DENS.INC TABRIT.INC CCHEMI.INC BUG.INC CGSFLO.INC \
```

```
        PANDS.INC F1AF0.INC CTABLE.INC FLUPR.INC RTMTAB.INC GPARAM.INC
upfeh.o: PARAMETER.INC CINDEX.INC CSPECE.INC GPARAM.INC AFR.INC TRAJ.INC \
        PRIN.INC CPARAM.INC RTMTAB.INC PVAR.INC DENS.INC TABRIT.INC \
        CCHEMI.INC BUG.INC CGSFLO.INC PANDS.INC F1AF0.INC CTABLE.INC \
        FLUPR.INC
upfh.o: PARAMETER.INC TFLOF10.INC F1AF0.INC AFR.INC TRAJ.INC GPARAM.INC \
        PRIN.INC CPARAM.INC FLUPR.INC CCHEMI.INC DENS.INC BUG.INC CGSFLO.INC \
        TABRIT.INC CTABLE.INC RTMTAB.INC
vcoef.o: PARAMETER.INC AFR.INC ALL.INC CPART.INC INTRUZ.INC VVEL.INC \
        VAR.INC GEOM.INC COEF.INC KASET1.INC CPSOU.INC SWPDIR.INC SWRL.INC \
        FLUPR.INC FLUPR2.INC PCOR.INC SIMPLE.INC
vector.o: PARAMETER.INC
velmag.o: PARAMETER.INC ALL.INC COEF.INC GEOM.INC GMAP.INC VAR.INC
viscosp.o: xeffcm.inc
volswl.o: dvccomp.inc
wall.o: PARAMETER.INC ALL.INC INTRUZ.INC COEF.INC
wrtout.o: finish.inc ffids.inc config.inc order.inc xeffcm.inc difeq.inc \
        pyrite.inc
[ l o l a : 3 1 ] t e s t                                    > >
```

\

Appendix E

Sample Computer Files for Gaseous Combustion

This sample problem is the combustion of natural gas in the BYU controlled-profile reactor (CPR).

Main Data File (cpr.dat, PCGCIN)

```
 4,                                          !NSAY..(SAY(I),I=1,NSAY) follows:
COMBUSTION OF NATURAL GAS IN AIR - ACERC "EATOUGH" REACTOR
ADIABATIC
SECONDARY SWIRL OF 1.5; APPROXIMATE S.R. OF 1.0
   Case Modeled 7/7/89
T    T    T    T    T                      !INRST,INCALF,INCREK,INCALH,INCALG
F    F    F    F    F                      !IPSICT,INPRST,INEACH,INCLET,INCLGE
T    F    F    F    T                      !INCALN,INCURF,LEULP,INTFRZ,INSIMP
F    T    F                               !INSMPC,INCLKE,LPOST
F    F    T    F    T                      !INCNOX,POLLUT,INQRL,INCSWP,INCSWS
F    F    F    T    F                      !INNOZZ,INFSOU,LTBUG,GRDOUT,INPROG
F    T    T    T    F                      !INCFP,INRAD,INRDGD,INTRUS,MAGHJER
F    F    F    F                           !INETA,HTRACK,FGDVC,LAMINAR
down-fired                                 !CONFIG
```

```
 0.800,0.800,0.800,.950,                  !URFU,URFV,URFW,URFH
 0.850,0.850,0.850,0.850,0.850,           !URFE,URFK,URFF,URFG,URFVIS
 0.500,0.800,0.800,1.000,0.900,0.900,     !URFDEN,URFETA,URFGET,URFNJ,URFPP,URFP
  0.02664460, 0.098425 0.80000    ,       !DIAP,DIAS,DIACH
   3.3125    , 0.00352679,                !NDIA(real),THICK
  1000,-1000,  50,                        !MAXIT,INDPRI,INDRST
   04,   07,  34,                         !NJINP,NJINS,NIWOQ
  100.000, 1.100,45, 1.145, 0.900,        !AL1,EPSX,NL,EPSI,EPSD
  300.0,2500.0,0.0                        !TMIN,TMAX,HLOSS
  1500.0, 500.0,                          !TLODEL,THIDEL
          06,   35.00    , 0.200      ,  !NIINQ,QHA,QLX
     1300.0  ,    1000.000,     1000.00,  !TBN,TBW,TBE
  1.79000E-05,  86000.,            1,     !VISCOS,PRES,IEUCK
   0.0100000,  0.10000000,                !SORMAX,SORMIN
INLET 1                                   !(Primary)
  2.6110E-03, 1.000, 0.000,  0.100,       !FLOW,FFLOW,SWIRLN,TINFLO
INLET 2                                   !(Secondary)
  4.7252E-02, 0.000, 1.450,  0.100,       !FLOW,FFLOW,SWIRLN,TINFLO
                                          !                      (Blank line)
ELEMENTS
THERMO                                    !The react. sect. is formatted
REACTANTS 1
    298.000                               !TMP (unformatted)
C 1.     O 2.       0.       0.     CO2      0.016252         G
C 1.     H 4.       0.       0.     CH4      0.800761         G
C 2.     H 6.       0.       0.     C2H6     0.120040         G
C 3.     H 8.       0.       0.     C3H8     0.054172         G
N 2.       0.       0.       0.     N2       0.008775         G
                                          !                      (Blank line)
REACTANTS 2
    298.000                               !TMP (unformatted)
O 2.       0.       0.       0.     O2       0.23300          G
N 2.       0.       0.       0.     N2       0.76700          G
                                          !                      (Blank line)
 T    T    T    ,  10                     !LDISO,LGASE,LEMCOR,MAXITR
```

```
 0.8000,1200.00                          !EMW,TOUT
 1.0000,0.0000                           !A0,AF
```

Inlet Profile Data File (cpr.inl, INLET)

```
 F    2 F    2
!UPDAT,KOPUP,USDAT,KOPUS,...
 F    0 F    0
!VPDAT,KOPVP,VSDAT,KOPVS,...
 F    4 F    4
!WPDAT,KOPWP,WSDAT,KOPWS,...
 F    1 F    1
!TIPDAT,KOPTEP,TISDAT,KOPTES,...
 F    2 F    2
!EDPDAT,KOPEDP,EDSDAT,KOPEDS,...
  0.00E+00, 0.00E+00,
!PLS,SLS,AILS...
 1       8.50000E+00                              !NSFORM,ALPHA0
  1.00000E-03, 2.00000E-04, 6.10000E-02,  !RP,RS1,RS2,
```

Thermo Data File (cpr.thm, THERMO)

```
C         12.01115      4.0
H         1.00797       1.0
O         15.9994      -2.0
N         14.0067       0.0

CO                J 9/65C  1.O  1.00 0.00 0.G   300.000  5000.000
 0.29840689E 01 0.14891387E-02-0.57899678E-06 0.10364576E-09-0.69353499E-14
-0.14245227E 05 0.63479147E 01 0.37100916E 01-0.16190964E-02 0.36923584E-05
-0.20319673E-08 0.23953344E-12-0.14356309E 05 0.29555340E 01
H2O               J 3/61H  2.O  1.00 0.00 0.G   300.000  5000.000
```

```
 0.27167616E 01 0.29451370E-02-0.80224368E-06 0.10226681E-09-0.48472104E-14
-0.29905820E 05 0.66305666E 01 0.40701275E 01-0.11084499E-02 0.41521180E-05
-0.29637404E-08 0.80702101E-12-0.30279719E 05-0.32270038E 00
N2               J 9/65N  2.0  0.0  0.0  0.G   300.000  5000.000
 0.28963194E 01 0.15154863E-02-0.57235275E-06 0.99807385E-10-0.65223536E-14
-0.90586182E 03 0.61615143E 01 0.36748257E 01-0.12081496E-02 0.23240100E-05
-0.63217520E-09-0.22577253E-12-0.10611587E 04 0.23580418E 01
O2               J 9/65O  2.0  0.0  0.0  0.G   300.000  5000.000
 0.36219521E 01 0.73618256E-03-0.19652219E-06 0.36201556E-10-0.28945623E-14
-0.12019822E 04 0.36150942E 01 0.36255980E 01-0.18782183E-02 0.70554543E-05
-0.67635071E-08 0.21555977E-11-0.10475225E 04 0.43052769E 01
NO               J 6/63N  1.O  1.00 0.00 0.G   300.000  5000.000
 0.31889992E 01 0.13382279E-02-0.52899316E-06 0.95919314E-10-0.64847928E-14
 0.98283242E 04 0.67458115E 01 0.40459509E 01-0.34181783E-02 0.79819174E-05
-0.61139254E-08 0.15919072E-11 0.97453867E 04 0.29974976E 01
H2               J 3/61H  2.0  0.0  0.0  0.G   300.000  5000.000
 0.31001883E 01 0.51119458E-03 0.52644204E-07-0.34909964E-10 0.36945341E-14
-0.87738013E 03-0.19629412E 01 0.30574446E 01 0.26765198E-02-0.58099149E-05
 0.55210343E-08-0.18122726E-11-0.98890430E 03-0.22997046E 01
NH3              J 9/65N  1.H  3.00 0.00 0.G   300.000  5000.000
 0.24165173E 01 0.61871186E-02-0.21785136E-05 0.37599057E-09-0.24448854E-13
-0.64747109E 04 0.77043467E 01 0.35912762E 01 0.49388665E-03 0.83449304E-05
-0.83833385E-08 0.27299092E-11-0.66717070E 04 0.22520962E 01
OH               J 3/66O  1.H  1.00 0.00 0.G   300.000  5000.000
 0.29106417E 01 0.95931627E-03-0.19441700E-06 0.13756646E-10 0.14224542E-15
 0.39353811E 04 0.54423428E 01 0.38375931E 01-0.10778855E-02 0.96830354E-06
 0.18713971E-09-0.22571089E-12 0.36412820E 04 0.49370009E 00
CH4              J 3/61C  1.H  4.00 0.00 0.G   300.000  5000.000
 0.15027056E 01 0.10416795E-01-0.39181514E-05 0.67777872E-09-0.44283706E-13
-0.99787031E 04 0.10707143E 02 0.38261929E 01-0.39794557E-02 0.24558321E-04
-0.22732920E-07 0.69626952E-11-0.10144945E 05 0.86690062E 00
CO2              J 9/65C  1.O  2.00 0.00 0.G   300.000  5000.000
 0.44608040E 01 0.30981717E-02-0.12392566E-05 0.22741323E-09-0.15525948E-13
-0.48961438E 05-0.98635978E 00 0.24007788E 01 0.87350905E-02-0.66070861E-05
 0.20021860E-08 0.63274039E-15-0.48377520E 05 0.96951447E 01
```

```
C2H6              CR2178C   2H   60   00   0G   300.000  5000.000
 1.67107058E+00 1.88078150E-02-6.98943156E-06 1.16385735E-09-7.17707692E-14
-1.14683543E+04 1.26317347E+01 1.92453270E+00 1.68224303E-02-2.24906498E-06
-3.40875417E-09 1.49239675E-12-1.14789269E+04 1.16292438E+01
C3H8               CR2178C  3.H  8.00 0.00 0.G   300.000  5000.000
-0.50780070E+00 3.68142930E-02-1.90689480E-05 3.86411680E-09 0.00000000E-14
 0.00000000E+04 0.00000000E+01-0.50780070E+00 3.68142930E-02-1.90689480E-05
 3.86411680E-09 0.00000000E+00 0.00000000E+000.00000000E+010
C(S)               J 3/61C  1.0  0.0  0.0  0.S   300.000  5000.000
 0.13604937E 01 0.19182237E-02-0.84040386E-06 0.16448705E-09-0.11672670E-13
-0.65713843E 03-0.80070200E 01-0.44778049E 00 0.53690970E-02-0.39775563E-06
-0.40459263E-08 0.21134925E-11-0.94280670E 02 0.16840773E 01

3.59,110.,0.,-1.105E+08      CO
2.641,809.1,1.0,-2.418E+08   H2O
3.681,91.5,0.,0.0            N2
3.433,113.,0.,0.0            O2
3.470,119.,0.,0.0            NO  Note: NO is small and does not affect the enthalpy
2.915,38.,0.,0.0             H2
2.900,558.3,0.,0.0           NH3 does not contribute to the enthalpy
3.000,300.0,0.,0.0           OH concentrations are low and do not contribute to the enthalpy
3.822,137.,0.,-7.485E+07     CH4
3.996,190.,0.,-3.935E+08     CO2
4.418,230.,0.,-8.373E+07     C2H6
5.061,254,0.-1.039E+08       C3H8
3.822,137.,0.,0.             C(S)
```

Appendix F

Sample Computer Files for Coal Combustion with NO_X Formation

This sample problem is the combustion of coal in the BYU controlled-profile reactor (CPR) with NO_X formation.

Main Data File (cprcoal.dat, PCGCIN)

```
 5,                                          !NSAY..(SAY(I),I=1,NSAY) follows:
COAL COMBUSTION OF UTAH BLIND CANYON
Changed temporarily to coal.arg7 because coal.arg4 is not available
BYU-ACERC CONTROLLED PROFILE REACTOR
SECONDARY SWIRL OF 1.4;
Case Modeled 10/2/92
T    T    T    T    T                     !INRST,INCALF,INCREK,INCALH,INCALG
T    T    F    T    T                     !IPSICT,INPRST,INEACH,INCLET,INCLGE
T    F    F    F    T                     !INCALN,INCURF,LEULP,INTFRZ,INSIMP
F    T    T                               !INSMPC,INCLKE,LPOST
F                                         !INSORB
T    F    T    F    T                     !INCNOX,POLLUT,INQRL,INCSWP,INCSWS
F    F    F    T    F                     !INNOZZ,INFSOU,LTBUG,GRDOUT,INPROG
T    T    F    F    F                     !INCFP,INRAD,INRDGD,INTRUS,MAGHJER
F    F    T    F    F                     !INETA2,HTRACK,FGDVC,LAMINAR,LBUOY
1.0                                       !UPDOWN
```

```
 0.800,0.800,0.800,0.95,                  !URFU,URFV,URFW,URFH
 0.850,0.850,0.850,0.850,0.50,          . !URFE,URFK,URFF,URFG,URFVIS
 0.500,0.850,0.850,1.000,1.000,1.000,     !URFDEN,URFETA,URFGET,URFNJ,URFPP,URFP
   0.02664460, 0.098425, 0.80000,          !DIAP,DIAS,DIACH
  3.3125    , 0.00352679,                 !NDIA(real),THICK
  100,-1000,  50,                        !MAXIT,INDPRI,INDRST
   01,   09,  35,                         !NJINP,NJINS,NIWOQ
  100.000, 1.05,55, 1.10, 0.900,         !AL1,EPSX,NL,EPSI,EPSD
  298.0,2900.0,0.0                        !TMIN,TMAX,HLOSS
  1500.0, 1000.0,                          !TLODEL,THIDEL
          20,   35.00    , 0.200      ,  !NIINQ,QHA,QLX
     1250.0  ,    1250.000,    1250.00,    !TBN,TBW,TBE
  1.79000E-05,  101325.,           1,      !VISCOS,PRES,IEUCK
   0.0100000,  0.10000000,                !SORMAX,SORMIN
INLET 1                                   !(Primary)
 4.17000E-03, 1.00, 0.00, 0.10,0.76,0.0 !FLOW,FFLOW,SWIRLN;TINFLO,PLOD,PLODS
INLET 2                                   !(Secondary)
 3.52800E-02, 0.000, 1.4,0.100,0.0,0.0  !FLOW,FFLOW,SWIRLN,TINFLO,PLOD,PLODS
                                          !                       (Blank line)
ELEMENTS
THERMO                                    !The react. sect. is formatted
REACTANTS 1
  298.00,                                 !TMP (unformatted)
N 2.00      0.00     0.00     0.00   N2      0.71982        G
O 2.00      0.00     0.00     0.00   O2      0.21868        G
H 2.00   O 1.00      0.00     0.00   H2O     0.06150        G
                                          !           (Blank line)
REACTANTS 2
  423.00,                                 !TMP (unformatted)
N 2.00      0.00     0.00     0.00   N2      0.76700        G
O 2.00      0.00     0.00     0.00   O2      0.23300        G
                                          !           (Blank line)
 10, 5,                                    !NSL,NPS
  1340.00, 1.0,                           !PDEN,UPDOWN
 0.0,0.0,0.0                              !XPS(ISL),YPS(ISL),SPRANG(ISL)
 0.0,0.0,0.0                              !XPS(ISL),YPS(ISL),SPRANG(ISL)
 0.0,0.0,0.0                              !XPS(ISL),YPS(ISL),SPRANG(ISL)
 0.0,0.0,0.0                              !XPS(ISL),YPS(ISL),SPRANG(ISL)
 0.0,0.0,0.0                              !XPS(ISL),YPS(ISL),SPRANG(ISL)
 0.0,0.0,0.0                              !XPS(ISL),YPS(ISL),SPRANG(ISL)
 0.0,0.0,0.0                              !XPS(ISL),YPS(ISL),SPRANG(ISL)
 0.0,0.0,0.0                              !XPS(ISL),YPS(ISL),SPRANG(ISL)
 0.0,0.0,0.0                              !XPS(ISL),YPS(ISL),SPRANG(ISL)
 0.0,0.0,0.0                              !XPS(ISL),YPS(ISL),SPRANG(ISL)
 1.0000,1.0000,1.0000,1.0000,1.0000,      !UPLAG(IPS),IPS = 1,NPS
 1.0000,1.0000,1.0000,1.0000,1.0000,      !TLAG(IPS),IPS = 1,NPS
 20.0e-06,30.0e-06,40.0e-06,             !PD(IPS),IPS = 1,3
 60.0e-06,70.0e-06,                      !PD(IPS),IPS = 4,NPS
 0.1000,0.2000,0.4000,0.2000,0.1000,      !PMF(IPS),IPS = 1,NPS
```

```
 F    F    T    F    F                    !LDEBUG,LYPS,LPARTP,LPARTS,LBOTH
 T    T    T    T                         !LSPM,LSPU,LSPV,LSPV,LSPH
  3000.,                                  !trbnd
   0.9500,  0.0200,                       !YPSH,YPSL
 10, 1, 3,                                !MAXITP,MINITP,IGASV
 0.35,0.35,0.35,0.35,0.35,                !PRK(IPS),IPS = 1,NPS
coal.arg7.7                               !Functional group composition data
file
kin.arg7.7                                !Functional group kinetics data file
polymr.arg7.7                             !Coal polymer data file
1                                        !NCARD...COMENT(I),I=1,NCARD follows:
              All Particles have the same Properties
 T                                        !INCOAL
  0.2, 0.2,                               !URFPM,urfph
  1   1   5   0   0                      !NCRXN,NHRXN,NPROP,KEQ,NSHRNK
  1.000E-02, 1.000E-06, 0.000    ,        !DELTPJ,DELRRJ,GAMMA
   1.0000                                 !XI(J)
  0.00000E+00, 0.00000E+00,-1.50400E+07, !QHC(J),HHO(J),HAO(J)
 -1.58800E+07,  373.15    ,              !HWO(J),TNBP
  0.8609    , 0.0, 0.1391,               !OMEGAC(J),OMEGAH(J),OMEGAA(J)
  0.000,                                  !OMEGAW(J)
  4.30000E+14, 2.29000E+08, 0.40000    , !AMJ(J,M),EMJ(J,M),YY(J,M)
  0.00000E+00,                            !HGV(J,M)
 O2                                       !OXYD(L),L = 1,NHRXN
 1.74,                                   !PHIL(L)  L = 1,NHRXN
 298.0    , 1.49E+08,  1.0000    ,     !AL(J,L),EL(J,L),EMM(J,L)
rct.arg6
 0.6961,   0.0526,     0.0940,        !(WIC(J,K)  K = 1,3)
 0.0133,   0.0048,                    !(WIC(J,K)  K = 4,NLM)
 H2O                                     !SLRCMP
 0.5,T                                 !FBACK,LBACK
 T    T    T    ,  10,                   !LDISO,LGASE,LEMCOR,MAXITR
 0.9000,   786.00,                       !EMW,TOUT
 1.0000,0.00000,                         !AO,AF
```

Grid Data File (cprcoal.grd, GRIDS)

```
NODE
  55  49
  5  14
  6  6
  20  21  30
              X              XU              TBN
   1     -5.0000E-03     -1.0000E-02     1.2500E+03
   2      5.0000E-03      0.0000E+00     1.2500E+03
   3      1.5000E-02      1.0000E-02     1.2500E+03
```

4	2.5000E-02	2.0000E-02	1.2500E+03
5	3.5000E-02	3.0000E-02	1.2500E+03
6	4.5000E-02	4.0000E-02	1.2500E+03
7	5.5000E-02	5.0000E-02	1.2500E+03
8	6.5000E-02	6.0000E-02	1.2500E+03
9	7.5000E-02	7.0000E-02	1.2500E+03
10	8.5000E-02	8.0000E-02	1.2500E+03
11	9.5000E-02	9.0000E-02	1.2500E+03
12	1.0500E-01	1.0000E-01	1.2500E+03
13	1.1500E-01	1.1000E-01	1.2500E+03
14	1.2500E-01	1.2000E-01	1.2500E+03
15	1.3500E-01	1.3000E-01	1.2500E+03
16	1.4500E-01	1.4000E-01	1.2500E+03
17	1.5500E-01	1.5000E-01	1.2500E+03
18	1.6500E-01	1.6000E-01	1.2500E+03
19	1.7500E-01	1.7000E-01	1.2500E+03
20	1.8500E-01	1.8000E-01	1.2500E+03
21	1.9500E-01	1.9000E-01	1.2500E+03
22	2.0500E-01	2.0000E-01	1.2500E+03
23	2.1602E-01	2.1051E-01	1.2500E+03
24	2.2818E-01	2.2210E-01	1.2500E+03
25	2.4158E-01	2.3488E-01	1.2500E+03
26	2.5635E-01	2.4896E-01	1.2500E+03
27	2.7263E-01	2.6449E-01	1.2500E+03
28	2.9059E-01	2.8161E-01	1.2500E+03
29	3.1038E-01	3.0048E-01	1.2500E+03
30	3.3220E-01	3.2129E-01	1.2500E+03
31	3.5625E-01	3.4423E-01	1.2500E+03
32	3.8277E-01	3.6951E-01	1.2500E+03
33	4.1201E-01	3.9739E-01	1.2500E+03
34	4.4424E-01	4.2812E-01	1.2500E+03
35	4.7977E-01	4.6200E-01	1.2500E+03
36	5.1894E-01	4.9936E-01	1.2500E+03
37	5.6213E-01	5.4054E-01	1.2500E+03
38	6.0974E-01	5.8593E-01	1.2500E+03
39	6.6222E-01	6.3598E-01	1.2500E+03
40	7.2009E-01	6.9116E-01	1.2500E+03
41	7.8388E-01	7.5198E-01	1.2500E+03
42	8.5420E-01	8.1904E-01	1.2500E+03
43	9.3173E-01	8.9297E-01	1.2500E+03
44	1.0172E+00	9.7447E-01	1.2500E+03
45	1.1114E+00	1.0643E+00	1.2500E+03
46	1.2153E+00	1.1634E+00	1.2500E+03
47	1.3298E+00	1.2726E+00	1.2500E+03
48	1.4561E+00	1.3930E+00	1.2500E+03
49	1.5953E+00	1.5257E+00	1.2500E+03
50	1.7487E+00	1.6720E+00	1.2500E+03
51	1.9179E+00	1.8333E+00	1.2500E+03
52	2.1044E+00	2.0111E+00	1.2500E+03

53	2.3100E+00	2.2072E+00	1.2500E+03
54	2.5367E+00	2.4233E+00	1.2500E+03
55	2.7633E+00	2.6500E+00	1.2500E+03
	Y	YV	
1	-1.4815E-03	-2.9630E-03	
2	1.4815E-03	0.0000E+00	
3	4.4448E-03	2.9632E-03	
4	7.7164E-03	6.0806E-03	
5	1.1328E-02	9.5224E-03	
6	1.5316E-02	1.3322E-02	
7	1.9304E-02	1.7310E-02	
8	2.3292E-02	2.1298E-02	
9	2.7280E-02	2.5286E-02	
10	3.1267E-02	2.9274E-02	
11	3.5255E-02	3.3261E-02	
12	3.9243E-02	3.7249E-02	
13	4.3231E-02	4.1237E-02	
14	4.7219E-02	4.5225E-02	
15	5.1206E-02	4.9213E-02	
16	5.5593E-02	5.3400E-02	
17	6.0418E-02	5.8006E-02	
18	6.5726E-02	6.3072E-02	
19	7.1565E-02	6.8645E-02	
20	7.7987E-02	7.4776E-02	
21	8.5052E-02	8.1519E-02	
22	9.2823E-02	8.8937E-02	
23	1.0137E-01	9.7097E-02	
24	1.1077E-01	1.0607E-01	
25	1.2112E-01	1.1595E-01	
26	1.3249E-01	1.2681E-01	
27	1.4501E-01	1.3875E-01	
28	1.5878E-01	1.5189E-01	
29	1.7392E-01	1.6635E-01	
30	1.9058E-01	1.8225E-01	
31	2.0890E-01	1.9974E-01	
32	2.2906E-01	2.1898E-01	
33	2.4922E-01	2.3914E-01	
34	2.6736E-01	2.5829E-01	
35	2.8368E-01	2.7552E-01	
36	2.9838E-01	2.9103E-01	
37	3.1160E-01	3.0499E-01	
38	3.2350E-01	3.1755E-01	
39	3.3421E-01	3.2886E-01	
40	3.4386E-01	3.3904E-01	
41	3.5253E-01	3.4819E-01	
42	3.6034E-01	3.5644E-01	
43	3.6737E-01	3.6385E-01	
44	3.7369E-01	3.7053E-01	
45	3.7939E-01	3.7654E-01	

```
 46       3.8451E-01       3.8195E-01
 47       3.8912E-01       3.8682E-01
 48       3.9327E-01       3.9120E-01
 49       4.0673E-01       4.0000E-01
                    ***REACTOR BOUNDARIES AND FLOW DOMAIN***
    1  2  3  4  5  6  7  8  9 10 11 12 13 14 15 16 17 18 19 20 21 22 23 24 ...
49  X  X  X  X  X  X  X  X  X  X  X  X  X  X  X  X  X  X  X  X  X  X  X  X ...
48  X  X  X  X  X  X  X  X  X  X  X  X  X  X  X  X  X  X  X  X  X  O  O  O ...
47  X  X  X  X  X  X  X  X  X  X  X  X  X  X  X  X  X  X  X  X  X  O  O  O ...
46  X  X  X  X  X  X  X  X  X  X  X  X  X  X  X  X  X  X  X  X  X  O  O  O ...
45  X  X  X  X  X  X  X  X  X  X  X  X  X  X  X  X  X  X  X  X  X  O  O  O ...
44  X  X  X  X  X  X  X  X  X  X  X  X  X  X  X  X  X  X  X  X  X  O  O  O ...
43  X  X  X  X  X  X  X  X  X  X  X  X  X  X  X  X  X  X  X  X  X  O  O  O ...
42  X  X  X  X  X  X  X  X  X  X  X  X  X  X  X  X  X  X  X  X  X  O  O  O ...
41  X  X  X  X  X  X  X  X  X  X  X  X  X  X  X  X  X  X  X  X  X  O  O  O ...
40  X  X  X  X  X  X  X  X  X  X  X  X  X  X  X  X  X  X  X  X  X  O  O  O ...
39  X  X  X  X  X  X  X  X  X  X  X  X  X  X  X  X  X  X  X  X  X  O  O  O ...
38  X  X  X  X  X  X  X  X  X  X  X  X  X  X  X  X  X  X  X  X  X  O  O  O ...
37  X  X  X  X  X  X  X  X  X  X  X  X  X  X  X  X  X  X  X  X  X  O  O  O ...
36  X  X  X  X  X  X  X  X  X  X  X  X  X  X  X  X  X  X  X  X  X  O  O  O ...
35  X  X  X  X  X  X  X  X  X  X  X  X  X  X  X  X  X  X  X  X  X  O  O  O ...
34  X  X  X  X  X  X  X  X  X  X  X  X  X  X  X  X  X  X  X  X  X  O  O  O ...
33  X  X  X  X  X  X  X  X  X  X  X  X  X  X  X  X  X  X  X  X  X  O  O  O ...
32  X  X  X  X  X  X  X  X  X  X  X  X  X  X  X  X  X  X  X  X  X  O  O  O ...
31  X  X  X  X  X  X  X  X  X  X  X  X  X  X  X  X  X  X  X  X  X  O  O  O ...
30  X  X  X  X  X  X  X  X  X  X  X  X  X  X  X  X  X  X  X  X  X  O  O  O ...
29  X  X  X  X  X  X  X  X  X  X  X  X  X  X  X  X  X  X  X  O  O  O  O  O ...
28  X  X  X  X  X  X  X  X  X  X  X  X  X  X  X  X  X  O  O  O  O  O  O  O ...
27  X  X  X  X  X  X  X  X  X  X  X  X  X  X  X  O  O  O  O  O  O  O  O  O ...
26  X  X  X  X  X  X  X  X  X  X  X  X  X  O  O  O  O  O  O  O  O  O  O  O ...
25  X  X  X  X  X  X  X  X  X  X  X  O  O  O  O  O  O  O  O  O  O  O  O  O ...
24  X  X  X  X  X  X  X  X  X  X  O  O  O  O  O  O  O  O  O  O  O  O  O  O ...
23  X  X  X  X  X  X  X  X  O  O  O  O  O  O  O  O  O  O  O  O  O  O  O  O ...
22  X  X  X  X  X  X  X  O  O  O  O  O  O  O  O  O  O  O  O  O  O  O  O  O ...
21  X  X  X  X  X  X  O  O  O  O  O  O  O  O  O  O  O  O  O  O  O  O  O  O ...
20  X  X  X  X  X  O  O  O  O  O  O  O  O  O  O  O  O  O  O  O  O  O  O  O ...
19  X  X  X  X  O  O  O  O  O  O  O  O  O  O  O  O  O  O  O  O  O  O  O  O ...
18  X  X  X  O  O  O  O  O  O  O  O  O  O  O  O  O  O  O  O  O  O  O  O  O ...
17  X  X  X  O  O  O  O  O  O  O  O  O  O  O  O  O  O  O  O  O  O  O  O  O ...
16  X  X  O  O  O  O  O  O  O  O  O  O  O  O  O  O  O  O  O  O  O  O  O  O ...
15  X  O  O  O  O  O  O  O  O  O  O  O  O  O  O  O  O  O  O  O  O  O  O  O ...
14  S  O  O  O  O  O  O  O  O  O  O  O  O  O  O  O  O  O  O  O  O  O  O  O ...
13  S  O  O  O  O  O  O  O  O  O  O  O  O  O  O  O  O  O  O  O  O  O  O  O ...
12  S  O  O  O  O  O  O  O  O  O  O  O  O  O  O  O  O  O  O  O  O  O  O  O ...
11  S  O  O  O  O  O  O  O  O  O  O  O  O  O  O  O  O  O  O  O  O  O  O  O ...
10  S  O  O  O  O  O  O  O  O  O  O  O  O  O  O  O  O  O  O  O  O  O  O  O ...
 9  S  O  O  O  O  O  O  O  O  O  O  O  O  O  O  O  O  O  O  O  O  O  O  O ...
 8  S  O  O  O  O  O  O  O  O  O  O  O  O  O  O  O  O  O  O  O  O  O  O  O ...
 7  S  O  O  O  O  O  O  O  O  O  O  O  O  O  O  O  O  O  O  O  O  O  O  O ...
```

```
 6 X O O O O O O O O O O O O O O O O O O O O O O O ...
 5 P O O O O O O O O O O O O O O O O O O O O O O O ...
 4 P O O O O O O O O O O O O O O O O O O O O O O O ...
 3 P O O O O O O O O O O O O O O O O O O O O O O O ...
 2 P O O O O O O O O O O O O O O O O O O O O O O O ...
 1 P O O O O O O O O O O O O O O O O O O O O O O O ...
0 NOTE: THE JPRIM,JSEC,JTUBID,JTUBOD,NJINS,JQUARL
AND IQUARL ARE SUPERSEDED BY THE X AND P AND S IN THE MAP
WHEN INTRUS=.TRUE.  NI and NJ are not superseded.
```

NO_x Data File (cprcoal.nox, NOXIN)

```
  4,                                         !NSAYNX..(SAYNX(I),I=1,NSAYNX)
follows:
      ***************************   PCNOX   *****************************
      **** NOX POLLUTANT CALCULATION USING OUTPUT FROM PCGC-2 FOR THE ****
      *****  PHASE AND PARTICLE PROPERTIES THROUGHOUT THE FLOW FIELD *****
      ***************************  BASECASE   ****************************
  2.0                                       !FUELNO FLG =1 HSS; =2 MT; =0 no fuelno
  0.0                                     !THRMNO FLG =1 f&r; =2 f only; =0 no calc
  1.0, 0.5, 0, 0,                            !RADOXY,eqtest,radoh,ohadj
  1.0                                        !CHARNO
  0.90, 0.90, 0.90, 0.05, 0.80, 0.000,      !PRNOX,PRHCN,PRNH3,FCTNO,FCTHCN,FCTNH3
    20,    2,  100, 1,                        !MXITNX,ITYNX,INDPNX,icalcn
   1.0000    ,  1.0000    , 0.5,1.00000E-04, !XIANOX,ZEDA,fn2prt,MAXRES
  0.95, 0.95, 0.75,                          !urfnox,urfhcn,utfnh3
 F    T    T                                 !IRSTNo,IPLTNX,INHTNX
```

Log File (cprcoal.log)

```
This script assumes you have already 'made' the program in
\/mag/brewster/afr/pcgc2/sun.  If not, hit cntrl-C and do so now.
Running PCAFR on marge
  v
  COAL COMBUSTION OF UTAH BLIND CANYON
  Changed temporarily to coal.arg7 because coal.arg4 is not available
  BYU-ACERC CONTROLLED PROFILE REACTOR
  SECONDARY SWIRL OF 1.4;
  Case Modeled 10/2/92

 THIACT CHANGED FROM      3.52679E-03 TO      3.98780E-03


                                                    55
              49 ______________________________________
                  I                                    >
                  I                                    >
               ___I 21, 30                              >
```

```
          14 _I                                                  >
           6                                                     >
           5 ]                                                   >
             ....................................................

 NITER SORCE      RESORU          RESORV          RESORW          RESORM        NCREE
                  RESORP          RESORH          RESORF          RESOET

    polymer file:   polymr.arg7.7
  N-tar =   4  N-ext =   13
  W-average =     256.000
Calling FG-DVC input data finished

WARNING:  Elemental coal composition is taken from coal data file rather than main data file when
using FG-DVC devolatilization option.
Values calculated.......
  1   0.829815   0.306192
  2   0.808327   0.295413
  3   0.796922   0.288745
  4   0.784649   0.280553
  5   0.780928   0.277786
     *****   SIMPLER ALGORITHM INITIATED  *****
  1   1.306E-01   5.891E-03  0   3.741E-03  0   7.446E-04  0   5.489E-03 19    0
                  8.723E-03  2   1.306E-01  1   4.422E-03  0   2.899E-02  0

  5   4.871E-02   5.909E-03  0   2.144E-03  0   7.402E-04  0   6.127E-03 20    0
                  4.299E-03  6   4.871E-02  2   3.748E-03  0   6.416E-03  0

 10   3.356E-02   3.982E-03  0   1.247E-03  0   6.901E-04  0   4.120E-03 15    0
                  2.330E-03  9   3.356E-02  2   3.046E-03  0   5.179E-03  0

 15   2.294E-02   2.481E-03  0   9.325E-04  0   6.634E-04  0   2.833E-03 11    0
                  1.558E-03 13   2.294E-02  2   2.783E-03  0   4.405E-03  0

 20   1.616E-02   1.548E-03  0   6.449E-04  0   5.972E-04  0   1.817E-03  9    0
                  1.134E-03 13   1.616E-02  2   2.373E-03  0   3.805E-03  0

 25   1.212E-02   1.221E-03  0   5.487E-04  0   5.221E-04  0   1.696E-03  6    0
                  1.518E-03  8   1.212E-02  3   2.017E-03  0   3.426E-03  0

 30   9.764E-03   9.673E-04  0   3.949E-04  0   4.435E-04  0   1.264E-03  9    0
                  1.535E-03  3   9.764E-03  3   1.764E-03  0   3.195E-03  0

ONJITER  SORCE              RESNJ'S
   5    1.342E-03          1.153E-03 1.183E-03 1.238E-03 1.324E-03 1.342E-03

 SCATTER ITER: 0 ITERATION:  1 FRAC CHANGE IN TOT NET WALL FLUX:   1.000E+00
 SCATTER ITER: 0 ITERATION:  2 FRAC CHANGE IN TOT NET WALL FLUX:   7.570E-02
 SCATTER ITER: 0 ITERATION:  3 FRAC CHANGE IN TOT NET WALL FLUX:   5.319E-03
 SCATTER ITER: 0 ITERATION:  4 FRAC CHANGE IN TOT NET WALL FLUX:   3.640E-04
 SCATTER ITER: 0 ITERATION:  5 FRAC CHANGE IN TOT NET WALL FLUX:   2.380E-05
 SCATTER ITER: 0 ITERATION:  6 FRAC CHANGE IN TOT NET WALL FLUX:   1.602E-06
 SCATTER ITER: 1 ITERATION:  1 FRAC CHANGE IN TOT NET WALL FLUX:   2.192E-02
 SCATTER ITER: 1 ITERATION:  2 FRAC CHANGE IN TOT NET WALL FLUX:   5.666E-04
 SCATTER ITER: 1 ITERATION:  3 FRAC CHANGE IN TOT NET WALL FLUX:   2.464E-05
 SCATTER ITER: 1 ITERATION:  4 FRAC CHANGE IN TOT NET WALL FLUX:   1.902E-06
 REBOUNDING COLLISIONS ALLOWED FOR WALLS WHEN WALL TEMPERATURE IS BELOW    3000.0K
 TRAJECTORY ISL= 1,   IPS= 1  RECIRCULATES
  ISL= 1, IPS= 1, TERMINATED AT: IV= 54, JU=31  TIME=  8.377E+00  NPOINT=  714
 TRAJECTORY ISL= 1,   IPS= 2  RECIRCULATES
  ISL= 1, IPS= 2, TERMINATED AT: IV= 54, JU=31  TIME=  8.219E+00  NPOINT=  705
 TRAJECTORY ISL= 1,   IPS= 3  RECIRCULATES
  ISL= 1, IPS= 3, TERMINATED AT: IV= 54, JU=31  TIME=  8.125E+00  NPOINT=  701
 TRAJECTORY ISL= 1,   IPS= 4  RECIRCULATES
  ISL= 1, IPS= 4, TERMINATED AT: IV= 54, JU=32  TIME=  7.758E+00  NPOINT=  736
 TRAJECTORY ISL= 1,   IPS= 5  RECIRCULATES
  ISL= 1, IPS= 5, TERMINATED AT: IV= 54, JU=32  TIME=  7.429E+00  NPOINT=  731
 TRAJECTORY ISL= 2,   IPS= 1  RECIRCULATES
```

```
 ISL= 2, IPS= 1, TERMINATED AT: IV= 54, JU=31  TIME=  8.234E+00  NPOINT=  520
TRAJECTORY ISL= 2,  IPS= 2  RECIRCULATES
 ISL= 2, IPS= 2, TERMINATED AT: IV= 54, JU=31  TIME=  8.019E+00  NPOINT=  563
TRAJECTORY ISL= 2,  IPS= 3  RECIRCULATES
 ISL= 2, IPS= 3, TERMINATED AT: IV= 54, JU=31  TIME=  7.957E+00  NPOINT=  615
TRAJECTORY ISL= 2,  IPS= 4  RECIRCULATES
 ISL= 2, IPS= 4, TERMINATED AT: IV= 54, JU=32  TIME=  7.844E+00  NPOINT=  957
TRAJECTORY ISL= 2,  IPS= 5  RECIRCULATES
 ISL= 2, IPS= 5, TERMINATED AT: IV= 54, JU=30  TIME=  9.384E+00  NPOINT= 1289
TRAJECTORY ISL= 3,  IPS= 1  RECIRCULATES
 ISL= 3, IPS= 1, TERMINATED AT: IV= 54, JU=32  TIME=  7.609E+00  NPOINT=  513
TRAJECTORY ISL= 3,  IPS= 2  RECIRCULATES
 ISL= 3, IPS= 2, TERMINATED AT: IV= 54, JU=32  TIME=  7.675E+00  NPOINT=  498
TRAJECTORY ISL= 3,  IPS= 3  RECIRCULATES
 ISL= 3, IPS= 3, TERMINATED AT: IV= 54, JU=31  TIME=  7.789E+00  NPOINT=  513
TRAJECTORY ISL= 3,  IPS= 4  RECIRCULATES
 ISL= 3, IPS= 4, TERMINATED AT: IV= 54, JU=29  TIME=  1.001E+01  NPOINT=  874
TRAJECTORY ISL= 3,  IPS= 5  RECIRCULATES
 ISL= 3, IPS= 5, TERMINATED AT: IV= 54, JU=32  TIME=  7.282E+00  NPOINT=  535
TRAJECTORY ISL= 4,  IPS= 1  RECIRCULATES
 ISL= 4, IPS= 1, TERMINATED AT: IV= 54, JU=33  TIME=  7.046E+00  NPOINT=  462
TRAJECTORY ISL= 4,  IPS= 2  RECIRCULATES
 ISL= 4, IPS= 2, TERMINATED AT: IV= 54, JU=33  TIME=  6.974E+00  NPOINT=  471
TRAJECTORY ISL= 4,  IPS= 3  RECIRCULATES
 ISL= 4, IPS= 3, TERMINATED AT: IV= 54, JU=30  TIME=  8.784E+00  NPOINT=  623
TRAJECTORY ISL= 4,  IPS= 4  RECIRCULATES
 ISL= 4, IPS= 4, TERMINATED AT: IV= 54, JU=29  TIME=  9.455E+00  NPOINT=  788
TRAJECTORY ISL= 4,  IPS= 5  RECIRCULATES
 ISL= 4, IPS= 5, TERMINATED AT: IV= 54, JU=30  TIME=  9.122E+00  NPOINT=  804
TRAJECTORY ISL= 5,  IPS= 1  RECIRCULATES
 ISL= 5, IPS= 1, TERMINATED AT: IV= 54, JU=33  TIME=  6.721E+00  NPOINT=  483
TRAJECTORY ISL= 5,  IPS= 2  RECIRCULATES
 ISL= 5, IPS= 2, TERMINATED AT: IV= 54, JU=33  TIME=  6.612E+00  NPOINT=  416
TRAJECTORY ISL= 5,  IPS= 3  RECIRCULATES
 ISL= 5, IPS= 3, TERMINATED AT: IV= 54, JU=33  TIME=  6.701E+00  NPOINT=  611
TRAJECTORY ISL= 5,  IPS= 4  RECIRCULATES
 ISL= 5, IPS= 4, TERMINATED AT: IV= 54, JU=33  TIME=  6.685E+00  NPOINT=  565
TRAJECTORY ISL= 5,  IPS= 5  RECIRCULATES
 ISL= 5, IPS= 5, TERMINATED AT: IV= 54, JU=31  TIME=  8.439E+00  NPOINT=  763
TRAJECTORY ISL= 6,  IPS= 1  RECIRCULATES
 ISL= 6, IPS= 1, TERMINATED AT: IV= 54, JU=34  TIME=  6.269E+00  NPOINT=  491
TRAJECTORY ISL= 6,  IPS= 2  RECIRCULATES
 ISL= 6, IPS= 2, TERMINATED AT: IV= 54, JU=34  TIME=  6.329E+00  NPOINT=  441
TRAJECTORY ISL= 6,  IPS= 3  RECIRCULATES
 ISL= 6, IPS= 3, TERMINATED AT: IV= 54, JU=34  TIME=  6.251E+00  NPOINT=  442
TRAJECTORY ISL= 6,  IPS= 4  RECIRCULATES
 ISL= 6, IPS= 4, TERMINATED AT: IV= 54, JU=35  TIME=  6.142E+00  NPOINT=  555
TRAJECTORY ISL= 6,  IPS= 5  RECIRCULATES
 ISL= 6, IPS= 5, TERMINATED AT: IV= 54, JU=33  TIME=  6.755E+00  NPOINT=  771
 ISL= 7, IPS= 1, TERMINATED AT: IV= 54, JU=34  TIME=  6.182E+00  NPOINT=  510
TRAJECTORY ISL= 7,  IPS= 2  RECIRCULATES
 ISL= 7, IPS= 2, TERMINATED AT: IV= 54, JU=34  TIME=  6.156E+00  NPOINT=  497
TRAJECTORY ISL= 7,  IPS= 3  RECIRCULATES
 ISL= 7, IPS= 3, TERMINATED AT: IV= 54, JU=34  TIME=  6.119E+00  NPOINT=  468
TRAJECTORY ISL= 7,  IPS= 4  RECIRCULATES
 ISL= 7, IPS= 4, TERMINATED AT: IV= 54, JU=34  TIME=  6.205E+00  NPOINT=  760
TRAJECTORY ISL= 7,  IPS= 5  RECIRCULATES
 ISL= 7, IPS= 5, TERMINATED AT: IV= 54, JU=34  TIME=  6.256E+00  NPOINT=  744
 ISL= 8, IPS= 1, TERMINATED AT: IV= 54, JU=35  TIME=  5.898E+00  NPOINT=  714
TRAJECTORY ISL= 8,  IPS= 2  RECIRCULATES
 ISL= 8, IPS= 2, TERMINATED AT: IV= 54, JU=35  TIME=  5.861E+00  NPOINT=  579
TRAJECTORY ISL= 8,  IPS= 3  RECIRCULATES
 ISL= 8, IPS= 3, TERMINATED AT: IV= 54, JU=35  TIME=  5.894E+00  NPOINT=  593
TRAJECTORY ISL= 8,  IPS= 4  RECIRCULATES
 ISL= 8, IPS= 4, TERMINATED AT: IV= 54, JU=36  TIME=  5.556E+00  NPOINT=  566
TRAJECTORY ISL= 8,  IPS= 5  RECIRCULATES
 ISL= 8, IPS= 5, TERMINATED AT: IV= 54, JU=37  TIME=  5.405E+00  NPOINT=  467
 ISL= 9, IPS= 1, TERMINATED AT: IV= 54, JU=36  TIME=  5.746E+00  NPOINT=  904
 ISL= 9, IPS= 2, TERMINATED AT: IV= 54, JU=36  TIME=  5.744E+00  NPOINT=  619
TRAJECTORY ISL= 9,  IPS= 3  RECIRCULATES
```

```
 ISL= 9, IPS= 3, TERMINATED AT: IV= 54, JU=35  TIME=  5.889E+00  NPOINT=  462
TRAJECTORY ISL= 9,  IPS= 4  RECIRCULATES
 ISL= 9, IPS= 4, TERMINATED AT: IV= 54, JU=37  TIME=  5.598E+00  NPOINT=  453
TRAJECTORY ISL= 9,  IPS= 5  RECIRCULATES
 ISL= 9, IPS= 5, TERMINATED AT: IV= 54, JU=36  TIME=  5.504E+00  NPOINT=  673
 ISL=10, IPS= 1, TERMINATED AT: IV= 54, JU=37  TIME=  5.495E+00  NPOINT=  458
 ISL=10, IPS= 2, TERMINATED AT: IV= 54, JU=36  TIME=  5.595E+00  NPOINT=  468
 ISL=10, IPS= 3, TERMINATED AT: IV= 54, JU=36  TIME=  5.594E+00  NPOINT=  536
TRAJECTORY ISL=10,  IPS= 4  RECIRCULATES
 ISL=10, IPS= 4, TERMINATED AT: IV= 54, JU=37  TIME=  5.542E+00  NPOINT=  516
TRAJECTORY ISL=10,  IPS= 5  RECIRCULATES
 ISL=10, IPS= 5, TERMINATED AT: IV= 54, JU=37  TIME=  5.614E+00  NPOINT=  685
 FRACTION OF DAF COAL DEVOLATILIZED =  0.54439
0              SUM OF SOLID PHASE COUPLING
               SSPE =   4.342E-04
               SSPF =   0.000E+00
               SSPM =   4.342E-04
               SSPUu =   5.374E-02
               SSPUp =  -2.660E-02
               SSPV =  -1.249E-07
               SSPH =  -2.295E+03

 ******* CUMULATIVE COAL BURNOUT ********

          AT X =   0.00  , COAL BURNOUT = 0.0000
          AT X =   0.01  , COAL BURNOUT = 0.1956
          AT X =   0.02  , COAL BURNOUT = 0.3842
          AT X =   0.03  , COAL BURNOUT = 0.3969
          AT X =   0.04  , COAL BURNOUT = 0.4262
          AT X =   0.05  , COAL BURNOUT = 0.4323
          AT X =   0.06  , COAL BURNOUT = 0.4675
          AT X =   0.07  , COAL BURNOUT = 0.4785
          AT X =   0.08  , COAL BURNOUT = 0.5106
          AT X =   0.09  , COAL BURNOUT = 0.5405
          AT X =   0.10  , COAL BURNOUT = 0.5521
          AT X =   0.11  , COAL BURNOUT = 0.5732
          AT X =   0.12  , COAL BURNOUT = 0.5950
          AT X =   0.13  , COAL BURNOUT = 0.6142
          AT X =   0.14  , COAL BURNOUT = 0.6287
          AT X =   0.15  , COAL BURNOUT = 0.6432
          AT X =   0.16  , COAL BURNOUT = 0.6564
          AT X =   0.17  , COAL BURNOUT = 0.6681
          AT X =   0.19  , COAL BURNOUT = 0.6858
          AT X =   0.20  , COAL BURNOUT = 0.6980
          AT X =   0.21  , COAL BURNOUT = 0.7110
          AT X =   0.22  , COAL BURNOUT = 0.7257
          AT X =   0.23  , COAL BURNOUT = 0.7433
          AT X =   0.24  , COAL BURNOUT = 0.7651
          AT X =   0.26  , COAL BURNOUT = 0.7916
          AT X =   0.27  , COAL BURNOUT = 0.8183
          AT X =   0.29  , COAL BURNOUT = 0.8456
          AT X =   0.31  , COAL BURNOUT = 0.8699
          AT X =   0.33  , COAL BURNOUT = 0.8917
          AT X =   0.36  , COAL BURNOUT = 0.9108
          AT X =   0.38  , COAL BURNOUT = 0.9275
          AT X =   0.41  , COAL BURNOUT = 0.9438
          AT X =   0.44  , COAL BURNOUT = 0.9565
          AT X =   0.48  , COAL BURNOUT = 0.9634
          AT X =   0.52  , COAL BURNOUT = 0.9691
          AT X =   0.56  , COAL BURNOUT = 0.9742
          AT X =   0.61  , COAL BURNOUT = 0.9792
          AT X =   0.66  , COAL BURNOUT = 0.9839
          AT X =   0.72  , COAL BURNOUT = 0.9887
          AT X =   0.78  , COAL BURNOUT = 0.9922
          AT X =   0.85  , COAL BURNOUT = 0.9962
          AT X =   0.93  , COAL BURNOUT = 0.9982
          AT X =   1.02  , COAL BURNOUT = 0.9989
          AT X =   1.11  , COAL BURNOUT = 0.9992
          AT X =   1.22  , COAL BURNOUT = 0.9994
```

```
          AT X =   1.33  , COAL BURNOUT = 0.9998
          AT X =   1.46  , COAL BURNOUT = 1.0000
          AT X =   1.60  , COAL BURNOUT = 1.0000
          AT X =   1.75  , COAL BURNOUT = 1.0000
          AT X =   1.92  , COAL BURNOUT = 1.0000
          AT X =   2.10  , COAL BURNOUT = 1.0000
          AT X =   2.31  , COAL BURNOUT = 1.0000
          AT X =   2.54  , COAL BURNOUT = 1.0000
>>>>EOLP COMPLETE, END OF PARTICLE ITERATION #  1

 NITER SORCE      RESORU          RESORV          RESORW          RESORM       NCREE
                  RESORP          RESORH          RESORF          RESOET

  1   1.095E-01   5.603E-03  0    3.468E-03  0    7.669E-04  0    5.040E-03 12    0
                  8.131E-03  2    1.095E-01  1    3.798E-03  0    2.645E-02  0

  5   3.222E-02   5.813E-03  0    2.380E-03  0    7.904E-04  0    7.738E-03  7    0
                  4.871E-03  5    3.222E-02  1    2.899E-03  0    7.022E-03  0

 10   1.664E-02   2.886E-03  0    1.201E-03  0    6.981E-04  0    3.932E-03  6    0
                  2.395E-03  5    1.664E-02  2    2.328E-03  0    4.789E-03  0

 15   9.674E-03   1.630E-03  0    7.574E-04  0    5.012E-04  0    2.216E-03  5    0
                  2.003E-03  4    9.674E-03  2    1.947E-03  0    3.879E-03  0

ONJITER  SORCE              RESNJ'S
   5    1.048E-03          1.048E-03 1.029E-03 1.025E-03 9.619E-04 9.388E-04

 SCATTER ITER: 0 ITERATION:  1 FRAC CHANGE IN TOT NET WALL FLUX:   1.000E+00
 SCATTER ITER: 0 ITERATION:  2 FRAC CHANGE IN TOT NET WALL FLUX:   7.571E-02
 SCATTER ITER: 0 ITERATION:  3 FRAC CHANGE IN TOT NET WALL FLUX:   5.320E-03
 SCATTER ITER: 0 ITERATION:  4 FRAC CHANGE IN TOT NET WALL FLUX:   3.642E-04
 SCATTER ITER: 0 ITERATION:  5 FRAC CHANGE IN TOT NET WALL FLUX:   2.380E-05
 SCATTER ITER: 0 ITERATION:  6 FRAC CHANGE IN TOT NET WALL FLUX:   1.628E-06
 SCATTER ITER: 1 ITERATION:  1 FRAC CHANGE IN TOT NET WALL FLUX:   2.191E-02
 SCATTER ITER: 1 ITERATION:  2 FRAC CHANGE IN TOT NET WALL FLUX:   5.671E-04
 SCATTER ITER: 1 ITERATION:  3 FRAC CHANGE IN TOT NET WALL FLUX:   2.450E-05
 SCATTER ITER: 1 ITERATION:  4 FRAC CHANGE IN TOT NET WALL FLUX:   1.897E-06
 REBOUNDING COLLISIONS ALLOWED FOR WALLS WHEN WALL TEMPERATURE IS BELOW    3000.0K
 TRAJECTORY ISL= 1,  IPS= 1  RECIRCULATES
  ISL= 1, IPS= 1, TERMINATED AT: IV= 54, JU=31  TIME=  8.302E+00  NPOINT=  656
 TRAJECTORY ISL= 1,  IPS= 2  RECIRCULATES
  ISL= 1, IPS= 2, TERMINATED AT: IV= 54, JU=31  TIME=  8.015E+00  NPOINT=  716
 TRAJECTORY ISL= 1,  IPS= 3  RECIRCULATES
  ISL= 1, IPS= 3, TERMINATED AT: IV= 54, JU=31  TIME=  7.922E+00  NPOINT=  705
 TRAJECTORY ISL= 1,  IPS= 4  RECIRCULATES
  ISL= 1, IPS= 4, TERMINATED AT: IV= 54, JU=32  TIME=  7.778E+00  NPOINT=  788
 TRAJECTORY ISL= 1,  IPS= 5  RECIRCULATES
  ISL= 1, IPS= 5, TERMINATED AT: IV= 54, JU=32  TIME=  7.400E+00  NPOINT=  767
 TRAJECTORY ISL= 2,  IPS= 1  RECIRCULATES
  ISL= 2, IPS= 1, TERMINATED AT: IV= 54, JU=31  TIME=  8.233E+00  NPOINT=  523
 TRAJECTORY ISL= 2,  IPS= 2  RECIRCULATES
  ISL= 2, IPS= 2, TERMINATED AT: IV= 54, JU=31  TIME=  7.949E+00  NPOINT=  559
 TRAJECTORY ISL= 2,  IPS= 3  RECIRCULATES
  ISL= 2, IPS= 3, TERMINATED AT: IV= 54, JU=31  TIME=  7.946E+00  NPOINT=  934
 TRAJECTORY ISL= 2,  IPS= 4  RECIRCULATES
  ISL= 2, IPS= 4, TERMINATED AT: IV= 54, JU=32  TIME=  7.593E+00  NPOINT=  899
 TRAJECTORY ISL= 2,  IPS= 5  RECIRCULATES
  ISL= 2, IPS= 5, TERMINATED AT: IV= 54, JU=32  TIME=  7.398E+00  NPOINT= 1009
 TRAJECTORY ISL= 3,  IPS= 1  RECIRCULATES
  ISL= 3, IPS= 1, TERMINATED AT: IV= 54, JU=32  TIME=  7.548E+00  NPOINT=  532
 TRAJECTORY ISL= 3,  IPS= 2  RECIRCULATES
  ISL= 3, IPS= 2, TERMINATED AT: IV= 54, JU=32  TIME=  7.661E+00  NPOINT=  503
 TRAJECTORY ISL= 3,  IPS= 3  RECIRCULATES
  ISL= 3, IPS= 3, TERMINATED AT: IV= 54, JU=31  TIME=  7.725E+00  NPOINT=  463
 TRAJECTORY ISL= 3,  IPS= 4  RECIRCULATES
  ISL= 3, IPS= 4, TERMINATED AT: IV= 54, JU=29  TIME=  9.984E+00  NPOINT=  863
 TRAJECTORY ISL= 3,  IPS= 5  RECIRCULATES
  ISL= 3, IPS= 5, TERMINATED AT: IV= 54, JU=32  TIME=  7.240E+00  NPOINT=  641
```

```
 TRAJECTORY ISL= 4,  IPS= 1  RECIRCULATES
  ISL= 4, IPS= 1, TERMINATED AT: IV= 54, JU=33  TIME=  7.039E+00  NPOINT=  445
 TRAJECTORY ISL= 4,  IPS= 2  RECIRCULATES
  ISL= 4, IPS= 2, TERMINATED AT: IV= 54, JU=33  TIME=  7.087E+00  NPOINT=  467
 TRAJECTORY ISL= 4,  IPS= 3  RECIRCULATES
  ISL= 4, IPS= 3, TERMINATED AT: IV= 54, JU=32  TIME=  7.161E+00  NPOINT=  430
 TRAJECTORY ISL= 4,  IPS= 4  RECIRCULATES
  ISL= 4, IPS= 4, TERMINATED AT: IV= 54, JU=32  TIME=  7.292E+00  NPOINT=  525
 TRAJECTORY ISL= 4,  IPS= 5  RECIRCULATES
  ISL= 4, IPS= 5, TERMINATED AT: IV= 54, JU=31  TIME=  7.815E+00  NPOINT=  599
 TRAJECTORY ISL= 5,  IPS= 1  RECIRCULATES
  ISL= 5, IPS= 1, TERMINATED AT: IV= 54, JU=33  TIME=  6.694E+00  NPOINT=  486
 TRAJECTORY ISL= 5,  IPS= 2  RECIRCULATES
  ISL= 5, IPS= 2, TERMINATED AT: IV= 54, JU=33  TIME=  6.742E+00  NPOINT=  416
 TRAJECTORY ISL= 5,  IPS= 3  RECIRCULATES
  ISL= 5, IPS= 3, TERMINATED AT: IV= 54, JU=33  TIME=  6.649E+00  NPOINT=  615
 TRAJECTORY ISL= 5,  IPS= 4  RECIRCULATES
  ISL= 5, IPS= 4, TERMINATED AT: IV= 54, JU=33  TIME=  6.553E+00  NPOINT=  573
 TRAJECTORY ISL= 5,  IPS= 5  RECIRCULATES
  ISL= 5, IPS= 5, TERMINATED AT: IV= 54, JU=31  TIME=  8.156E+00  NPOINT=  694
 TRAJECTORY ISL= 6,  IPS= 1  RECIRCULATES
  ISL= 6, IPS= 1, TERMINATED AT: IV= 54, JU=34  TIME=  6.216E+00  NPOINT=  459
 TRAJECTORY ISL= 6,  IPS= 2  RECIRCULATES
  ISL= 6, IPS= 2, TERMINATED AT: IV= 54, JU=34  TIME=  6.321E+00  NPOINT=  434
 TRAJECTORY ISL= 6,  IPS= 3  RECIRCULATES
  ISL= 6, IPS= 3, TERMINATED AT: IV= 54, JU=34  TIME=  6.445E+00  NPOINT=  438
 TRAJECTORY ISL= 6,  IPS= 4  RECIRCULATES
  ISL= 6, IPS= 4, TERMINATED AT: IV= 54, JU=35  TIME=  6.185E+00  NPOINT=  594
 TRAJECTORY ISL= 6,  IPS= 5  RECIRCULATES
  ISL= 6, IPS= 5, TERMINATED AT: IV= 54, JU=33  TIME=  6.742E+00  NPOINT=  756
  ISL= 7, IPS= 1, TERMINATED AT: IV= 54, JU=34  TIME=  5.999E+00  NPOINT=  518
 TRAJECTORY ISL= 7,  IPS= 2  RECIRCULATES
  ISL= 7, IPS= 2, TERMINATED AT: IV= 54, JU=34  TIME=  6.232E+00  NPOINT=  441
 TRAJECTORY ISL= 7,  IPS= 3  RECIRCULATES
  ISL= 7, IPS= 3, TERMINATED AT: IV= 54, JU=33  TIME=  6.932E+00  NPOINT=  506
 TRAJECTORY ISL= 7,  IPS= 4  RECIRCULATES
  ISL= 7, IPS= 4, TERMINATED AT: IV= 54, JU=34  TIME=  6.313E+00  NPOINT=  772
 TRAJECTORY ISL= 7,  IPS= 5  RECIRCULATES
  ISL= 7, IPS= 5, TERMINATED AT: IV= 54, JU=36  TIME=  5.841E+00  NPOINT=  547
  ISL= 8, IPS= 1, TERMINATED AT: IV= 54, JU=35  TIME=  5.886E+00  NPOINT=  723
 TRAJECTORY ISL= 8,  IPS= 2  RECIRCULATES
  ISL= 8, IPS= 2, TERMINATED AT: IV= 54, JU=35  TIME=  5.944E+00  NPOINT=  581
 TRAJECTORY ISL= 8,  IPS= 3  RECIRCULATES
  ISL= 8, IPS= 3, TERMINATED AT: IV= 54, JU=35  TIME=  5.809E+00  NPOINT=  587
 TRAJECTORY ISL= 8,  IPS= 4  RECIRCULATES
  ISL= 8, IPS= 4, TERMINATED AT: IV= 54, JU=36  TIME=  5.691E+00  NPOINT=  581
 TRAJECTORY ISL= 8,  IPS= 5  RECIRCULATES
  ISL= 8, IPS= 5, TERMINATED AT: IV= 54, JU=37  TIME=  5.422E+00  NPOINT=  438
  ISL= 9, IPS= 1, TERMINATED AT: IV= 54, JU=36  TIME=  5.842E+00  NPOINT=  460
  ISL= 9, IPS= 2, TERMINATED AT: IV= 54, JU=36  TIME=  5.692E+00  NPOINT=  598
  ISL= 9, IPS= 3, TERMINATED AT: IV= 54, JU=35  TIME=  5.748E+00  NPOINT=  483
 TRAJECTORY ISL= 9,  IPS= 4  RECIRCULATES
  ISL= 9, IPS= 4, TERMINATED AT: IV= 54, JU=37  TIME=  5.594E+00  NPOINT=  474
 TRAJECTORY ISL= 9,  IPS= 5  RECIRCULATES
  ISL= 9, IPS= 5, TERMINATED AT: IV= 54, JU=37  TIME=  5.651E+00  NPOINT=  681
  ISL=10, IPS= 1, TERMINATED AT: IV= 54, JU=37  TIME=  5.445E+00  NPOINT=  530
  ISL=10, IPS= 2, TERMINATED AT: IV= 54, JU=36  TIME=  5.616E+00  NPOINT=  439
  ISL=10, IPS= 3, TERMINATED AT: IV= 54, JU=36  TIME=  5.646E+00  NPOINT=  469
 TRAJECTORY ISL=10,  IPS= 4  RECIRCULATES
  ISL=10, IPS= 4, TERMINATED AT: IV= 54, JU=36  TIME=  5.855E+00  NPOINT=  694
 TRAJECTORY ISL=10,  IPS= 5  RECIRCULATES
  ISL=10, IPS= 5, TERMINATED AT: IV= 54, JU=37  TIME=  5.561E+00  NPOINT=  699
 FRACTION OF DAF COAL DEVOLATILIZED =  0.54595
0               SUM OF SOLID PHASE COUPLING
                SSPE =   4.342E-04
                SSPF =   0.000E+00
                SSPM =   4.342E-04
                SSPUu =   5.218E-02
                SSPUp =  -2.575E-02
                SSPV =  -1.222E-07
```

```
                SSPH =  -2.291E+03

******* CUMULATIVE COAL BURNOUT ********

          AT X =   0.00  , COAL BURNOUT = 0.0000
          AT X =   0.01  , COAL BURNOUT = 0.1949
          AT X =   0.02  , COAL BURNOUT = 0.3868
          AT X =   0.03  , COAL BURNOUT = 0.3995
          AT X =   0.04  , COAL BURNOUT = 0.4293
          AT X =   0.05  , COAL BURNOUT = 0.4361
          AT X =   0.06  , COAL BURNOUT = 0.4698
          AT X =   0.07  , COAL BURNOUT = 0.4933
          AT X =   0.08  , COAL BURNOUT = 0.5118
          AT X =   0.09  , COAL BURNOUT = 0.5374
          AT X =   0.10  , COAL BURNOUT = 0.5556
          AT X =   0.11  , COAL BURNOUT = 0.5841
          AT X =   0.12  , COAL BURNOUT = 0.5998
          AT X =   0.13  , COAL BURNOUT = 0.6104
          AT X =   0.14  , COAL BURNOUT = 0.6292
          AT X =   0.15  , COAL BURNOUT = 0.6483
          AT X =   0.16  , COAL BURNOUT = 0.6591
          AT X =   0.17  , COAL BURNOUT = 0.6720
          AT X =   0.19  , COAL BURNOUT = 0.6863
          AT X =   0.20  , COAL BURNOUT = 0.6984
          AT X =   0.21  , COAL BURNOUT = 0.7107
          AT X =   0.22  , COAL BURNOUT = 0.7245
          AT X =   0.23  , COAL BURNOUT = 0.7421
          AT X =   0.24  , COAL BURNOUT = 0.7617
          AT X =   0.26  , COAL BURNOUT = 0.7861
          AT X =   0.27  , COAL BURNOUT = 0.8104
          AT X =   0.29  , COAL BURNOUT = 0.8349
          AT X =   0.31  , COAL BURNOUT = 0.8597
          AT X =   0.33  , COAL BURNOUT = 0.8828
          AT X =   0.36  , COAL BURNOUT = 0.9036
          AT X =   0.38  , COAL BURNOUT = 0.9227
          AT X =   0.41  , COAL BURNOUT = 0.9407
          AT X =   0.44  , COAL BURNOUT = 0.9543
          AT X =   0.48  , COAL BURNOUT = 0.9614
          AT X =   0.52  , COAL BURNOUT = 0.9671
          AT X =   0.56  , COAL BURNOUT = 0.9720
          AT X =   0.61  , COAL BURNOUT = 0.9767
          AT X =   0.66  , COAL BURNOUT = 0.9812
          AT X =   0.72  , COAL BURNOUT = 0.9861
          AT X =   0.78  , COAL BURNOUT = 0.9901
          AT X =   0.85  , COAL BURNOUT = 0.9941
          AT X =   0.93  , COAL BURNOUT = 0.9961
          AT X =   1.02  , COAL BURNOUT = 0.9977
          AT X =   1.11  , COAL BURNOUT = 0.9985
          AT X =   1.22  , COAL BURNOUT = 0.9992
          AT X =   1.33  , COAL BURNOUT = 0.9998
          AT X =   1.46  , COAL BURNOUT = 1.0000
          AT X =   1.60  , COAL BURNOUT = 1.0000
          AT X =   1.75  , COAL BURNOUT = 1.0000
          AT X =   1.92  , COAL BURNOUT = 1.0000
          AT X =   2.10  , COAL BURNOUT = 1.0000
          AT X =   2.31  , COAL BURNOUT = 1.0000
          AT X =   2.54  , COAL BURNOUT = 1.0000
>>>>EOLP COMPLETE, END OF PARTICLE ITERATION #  2

 15

NITER SORCE      RESORU          RESORV          RESORW          RESORM        NCREE
                 RESORP          RESORH          RESORF          RESOET

 1   1.067E-01   5.827E-03  0    3.612E-03  0    8.049E-04  0    5.555E-03  6    0
                 9.710E-03  2    1.067E-01  1    4.504E-03  0    2.925E-02  0

 5   2.090E-02   4.458E-03  0    2.401E-03  0    1.035E-03  0    6.050E-03 11    0
                 3.473E-03 17    2.090E-02  2    3.129E-03  0    7.288E-03  0
```

```
 10   1.156E-02   1.944E-03  0   1.027E-03  0   7.091E-04  0   2.189E-03 10    0
                  1.630E-03  7   1.156E-02  2   2.654E-03  0   5.357E-03  0

ONJITER  SORCE              RESNJ'S
   5    1.157E-03          1.020E-03 1.056E-03 1.103E-03 1.143E-03 1.157E-03

 SCATTER ITER: 0 ITERATION:  1 FRAC CHANGE IN TOT NET WALL FLUX:   1.000E+00
 SCATTER ITER: 0 ITERATION:  2 FRAC CHANGE IN TOT NET WALL FLUX:   7.572E-02
 SCATTER ITER: 0 ITERATION:  3 FRAC CHANGE IN TOT NET WALL FLUX:   5.322E-03
 SCATTER ITER: 0 ITERATION:  4 FRAC CHANGE IN TOT NET WALL FLUX:   3.645E-04
 SCATTER ITER: 0 ITERATION:  5 FRAC CHANGE IN TOT NET WALL FLUX:   2.362E-05
 SCATTER ITER: 0 ITERATION:  6 FRAC CHANGE IN TOT NET WALL FLUX:   1.708E-06
 SCATTER ITER: 1 ITERATION:  1 FRAC CHANGE IN TOT NET WALL FLUX:   2.191E-02
 SCATTER ITER: 1 ITERATION:  2 FRAC CHANGE IN TOT NET WALL FLUX:   5.679E-04
 SCATTER ITER: 1 ITERATION:  3 FRAC CHANGE IN TOT NET WALL FLUX:   2.467E-05
 SCATTER ITER: 1 ITERATION:  4 FRAC CHANGE IN TOT NET WALL FLUX:   1.974E-06
 REBOUNDING COLLISIONS ALLOWED FOR WALLS WHEN WALL TEMPERATURE IS BELOW    3000.0K
 TRAJECTORY ISL= 1,  IPS= 1  RECIRCULATES
  ISL= 1, IPS= 1, TERMINATED AT: IV= 54, JU=31  TIME=  8.169E+00  NPOINT=  665
 TRAJECTORY ISL= 1,  IPS= 2  RECIRCULATES
  ISL= 1, IPS= 2, TERMINATED AT: IV= 54, JU=31  TIME=  8.110E+00  NPOINT=  693
 TRAJECTORY ISL= 1,  IPS= 3  RECIRCULATES
  ISL= 1, IPS= 3, TERMINATED AT: IV= 54, JU=31  TIME=  8.192E+00  NPOINT=  684
 TRAJECTORY ISL= 1,  IPS= 4  RECIRCULATES
  ISL= 1, IPS= 4, TERMINATED AT: IV= 54, JU=32  TIME=  7.787E+00  NPOINT=  718
 TRAJECTORY ISL= 1,  IPS= 5  RECIRCULATES
  ISL= 1, IPS= 5, TERMINATED AT: IV= 54, JU=32  TIME=  7.544E+00  NPOINT=  721
 TRAJECTORY ISL= 2,  IPS= 1  RECIRCULATES
  ISL= 2, IPS= 1, TERMINATED AT: IV= 54, JU=31  TIME=  8.026E+00  NPOINT=  512
 TRAJECTORY ISL= 2,  IPS= 2  RECIRCULATES
  ISL= 2, IPS= 2, TERMINATED AT: IV= 54, JU=31  TIME=  8.120E+00  NPOINT=  579
 TRAJECTORY ISL= 2,  IPS= 3  RECIRCULATES
  ISL= 2, IPS= 3, TERMINATED AT: IV= 54, JU=31  TIME=  7.980E+00  NPOINT=  873
 TRAJECTORY ISL= 2,  IPS= 4  RECIRCULATES
  ISL= 2, IPS= 4, TERMINATED AT: IV= 54, JU=29  TIME=  1.004E+01  NPOINT= 1276
 TRAJECTORY ISL= 2,  IPS= 5  RECIRCULATES
  ISL= 2, IPS= 5, TERMINATED AT: IV= 54, JU=32  TIME=  7.304E+00  NPOINT=  904
 TRAJECTORY ISL= 3,  IPS= 1  RECIRCULATES
  ISL= 3, IPS= 1, TERMINATED AT: IV= 54, JU=32  TIME=  7.394E+00  NPOINT=  500
 TRAJECTORY ISL= 3,  IPS= 2  RECIRCULATES
  ISL= 3, IPS= 2, TERMINATED AT: IV= 54, JU=32  TIME=  7.592E+00  NPOINT=  544
 TRAJECTORY ISL= 3,  IPS= 3  RECIRCULATES
  ISL= 3, IPS= 3, TERMINATED AT: IV= 54, JU=31  TIME=  7.794E+00  NPOINT=  455
 TRAJECTORY ISL= 3,  IPS= 4  RECIRCULATES
  ISL= 3, IPS= 4, TERMINATED AT: IV= 54, JU=32  TIME=  7.674E+00  NPOINT=  575
 TRAJECTORY ISL= 3,  IPS= 5  RECIRCULATES
  ISL= 3, IPS= 5, TERMINATED AT: IV= 54, JU=30  TIME=  9.309E+00  NPOINT=  861
 TRAJECTORY ISL= 4,  IPS= 1  RECIRCULATES
  ISL= 4, IPS= 1, TERMINATED AT: IV= 54, JU=33  TIME=  6.943E+00  NPOINT=  444
 TRAJECTORY ISL= 4,  IPS= 2  RECIRCULATES
  ISL= 4, IPS= 2, TERMINATED AT: IV= 54, JU=33  TIME=  7.108E+00  NPOINT=  471
 TRAJECTORY ISL= 4,  IPS= 3  RECIRCULATES
  ISL= 4, IPS= 3, TERMINATED AT: IV= 54, JU=32  TIME=  7.242E+00  NPOINT=  598
 TRAJECTORY ISL= 4,  IPS= 4  RECIRCULATES
  ISL= 4, IPS= 4, TERMINATED AT: IV= 54, JU=30  TIME=  9.459E+00  NPOINT=  764
 TRAJECTORY ISL= 4,  IPS= 5  RECIRCULATES
  ISL= 4, IPS= 5, TERMINATED AT: IV= 54, JU=30  TIME=  8.941E+00  NPOINT=  815
 TRAJECTORY ISL= 5,  IPS= 1  RECIRCULATES
  ISL= 5, IPS= 1, TERMINATED AT: IV= 54, JU=33  TIME=  6.602E+00  NPOINT=  495
 TRAJECTORY ISL= 5,  IPS= 2  RECIRCULATES
  ISL= 5, IPS= 2, TERMINATED AT: IV= 54, JU=33  TIME=  6.553E+00  NPOINT=  426
 TRAJECTORY ISL= 5,  IPS= 3  RECIRCULATES
  ISL= 5, IPS= 3, TERMINATED AT: IV= 54, JU=33  TIME=  6.685E+00  NPOINT=  660
 TRAJECTORY ISL= 5,  IPS= 4  RECIRCULATES
  ISL= 5, IPS= 4, TERMINATED AT: IV= 54, JU=33  TIME=  6.531E+00  NPOINT=  533
 TRAJECTORY ISL= 5,  IPS= 5  RECIRCULATES
  ISL= 5, IPS= 5, TERMINATED AT: IV= 54, JU=33  TIME=  6.778E+00  NPOINT=  489
 TRAJECTORY ISL= 6,  IPS= 1  RECIRCULATES
  ISL= 6, IPS= 1, TERMINATED AT: IV= 54, JU=34  TIME=  6.275E+00  NPOINT=  455
```

```
 TRAJECTORY ISL= 6,  IPS= 2  RECIRCULATES
  ISL= 6, IPS= 2, TERMINATED AT: IV= 54, JU=34  TIME=  6.431E+00  NPOINT=  420
 TRAJECTORY ISL= 6,  IPS= 3  RECIRCULATES
  ISL= 6, IPS= 3, TERMINATED AT: IV= 54, JU=34  TIME=  6.249E+00  NPOINT=  438
 TRAJECTORY ISL= 6,  IPS= 4  RECIRCULATES
  ISL= 6, IPS= 4, TERMINATED AT: IV= 54, JU=33  TIME=  6.803E+00  NPOINT=  755
 TRAJECTORY ISL= 6,  IPS= 5  RECIRCULATES
  ISL= 6, IPS= 5, TERMINATED AT: IV= 54, JU=33  TIME=  6.724E+00  NPOINT=  786
  ISL= 7, IPS= 1, TERMINATED AT: IV= 54, JU=34  TIME=  6.032E+00  NPOINT=  455
 TRAJECTORY ISL= 7,  IPS= 2  RECIRCULATES
  ISL= 7, IPS= 2, TERMINATED AT: IV= 54, JU=34  TIME=  6.130E+00  NPOINT=  489
 TRAJECTORY ISL= 7,  IPS= 3  RECIRCULATES
  ISL= 7, IPS= 3, TERMINATED AT: IV= 54, JU=35  TIME=  6.104E+00  NPOINT=  528
 TRAJECTORY ISL= 7,  IPS= 4  RECIRCULATES
  ISL= 7, IPS= 4, TERMINATED AT: IV= 54, JU=34  TIME=  6.388E+00  NPOINT=  724
 TRAJECTORY ISL= 7,  IPS= 5  RECIRCULATES
  ISL= 7, IPS= 5, TERMINATED AT: IV= 54, JU=34  TIME=  6.246E+00  NPOINT=  750
  ISL= 8, IPS= 1, TERMINATED AT: IV= 54, JU=35  TIME=  5.808E+00  NPOINT=  726
 TRAJECTORY ISL= 8,  IPS= 2  RECIRCULATES
  ISL= 8, IPS= 2, TERMINATED AT: IV= 54, JU=35  TIME=  5.817E+00  NPOINT=  583
 TRAJECTORY ISL= 8,  IPS= 3  RECIRCULATES
  ISL= 8, IPS= 3, TERMINATED AT: IV= 54, JU=35  TIME=  5.892E+00  NPOINT=  543
 TRAJECTORY ISL= 8,  IPS= 4  RECIRCULATES
  ISL= 8, IPS= 4, TERMINATED AT: IV= 54, JU=36  TIME=  5.684E+00  NPOINT=  587
 TRAJECTORY ISL= 8,  IPS= 5  RECIRCULATES
  ISL= 8, IPS= 5, TERMINATED AT: IV= 54, JU=37  TIME=  5.422E+00  NPOINT=  440
  ISL= 9, IPS= 1, TERMINATED AT: IV= 54, JU=36  TIME=  5.844E+00  NPOINT=  455
  ISL= 9, IPS= 2, TERMINATED AT: IV= 54, JU=36  TIME=  5.815E+00  NPOINT=  613
  ISL= 9, IPS= 3, TERMINATED AT: IV= 54, JU=35  TIME=  5.743E+00  NPOINT=  479
 TRAJECTORY ISL= 9,  IPS= 4  RECIRCULATES
  ISL= 9, IPS= 4, TERMINATED AT: IV= 54, JU=35  TIME=  5.738E+00  NPOINT=  452
 TRAJECTORY ISL= 9,  IPS= 5  RECIRCULATES
  ISL= 9, IPS= 5, TERMINATED AT: IV= 54, JU=36  TIME=  5.619E+00  NPOINT=  690
  ISL=10, IPS= 1, TERMINATED AT: IV= 54, JU=37  TIME=  5.455E+00  NPOINT=  894
  ISL=10, IPS= 2, TERMINATED AT: IV= 54, JU=36  TIME=  5.590E+00  NPOINT=  441
  ISL=10, IPS= 3, TERMINATED AT: IV= 54, JU=36  TIME=  5.644E+00  NPOINT=  465
 TRAJECTORY ISL=10,  IPS= 4  RECIRCULATES
  ISL=10, IPS= 4, TERMINATED AT: IV= 54, JU=36  TIME=  5.678E+00  NPOINT=  679
 TRAJECTORY ISL=10,  IPS= 5  RECIRCULATES
  ISL=10, IPS= 5, TERMINATED AT: IV= 54, JU=37  TIME=  5.563E+00  NPOINT=  682
 FRACTION OF DAF COAL DEVOLATILIZED =  0.54653
0               SUM OF SOLID PHASE COUPLING
                SSPE =   4.342E-04
                SSPF =   0.000E+00
                SSPM =   4.342E-04
                SSPUu =   5.329E-02
                SSPUp =  -2.636E-02
                SSPV =  -1.242E-07
                SSPH =  -2.325E+03

 ******* CUMULATIVE COAL BURNOUT ********


          AT X =   0.00  , COAL BURNOUT = 0.0000
          AT X =   0.01  , COAL BURNOUT = 0.1948
          AT X =   0.02  , COAL BURNOUT = 0.3875
          AT X =   0.03  , COAL BURNOUT = 0.4005
          AT X =   0.04  , COAL BURNOUT = 0.4300
          AT X =   0.05  , COAL BURNOUT = 0.4366
          AT X =   0.06  , COAL BURNOUT = 0.4708
          AT X =   0.07  , COAL BURNOUT = 0.4946
          AT X =   0.08  , COAL BURNOUT = 0.5142
          AT X =   0.09  , COAL BURNOUT = 0.5324
          AT X =   0.10  , COAL BURNOUT = 0.5556
          AT X =   0.11  , COAL BURNOUT = 0.5775
          AT X =   0.12  , COAL BURNOUT = 0.5995
          AT X =   0.13  , COAL BURNOUT = 0.6178
          AT X =   0.14  , COAL BURNOUT = 0.6324
          AT X =   0.15  , COAL BURNOUT = 0.6488
          AT X =   0.16  , COAL BURNOUT = 0.6620
```

```
          AT X =   0.17  , COAL BURNOUT = 0.6770
          AT X =   0.19  , COAL BURNOUT = 0.6881
          AT X =   0.20  , COAL BURNOUT = 0.7000
          AT X =   0.21  , COAL BURNOUT = 0.7129
          AT X =   0.22  , COAL BURNOUT = 0.7271
          AT X =   0.23  , COAL BURNOUT = 0.7449
          AT X =   0.24  , COAL BURNOUT = 0.7650
          AT X =   0.26  , COAL BURNOUT = 0.7902
          AT X =   0.27  , COAL BURNOUT = 0.8153
          AT X =   0.29  , COAL BURNOUT = 0.8415
          AT X =   0.31  , COAL BURNOUT = 0.8667
          AT X =   0.33  , COAL BURNOUT = 0.8903
          AT X =   0.36  , COAL BURNOUT = 0.9117
          AT X =   0.38  , COAL BURNOUT = 0.9300
          AT X =   0.41  , COAL BURNOUT = 0.9483
          AT X =   0.44  , COAL BURNOUT = 0.9623
          AT X =   0.48  , COAL BURNOUT = 0.9686
          AT X =   0.52  , COAL BURNOUT = 0.9735
          AT X =   0.56  , COAL BURNOUT = 0.9776
          AT X =   0.61  , COAL BURNOUT = 0.9819
          AT X =   0.66  , COAL BURNOUT = 0.9858
          AT X =   0.72  , COAL BURNOUT = 0.9898
          AT X =   0.78  , COAL BURNOUT = 0.9930
          AT X =   0.85  , COAL BURNOUT = 0.9959
          AT X =   0.93  , COAL BURNOUT = 0.9975
          AT X =   1.02  , COAL BURNOUT = 0.9985
          AT X =   1.11  , COAL BURNOUT = 0.9990
          AT X =   1.22  , COAL BURNOUT = 0.9994
          AT X =   1.33  , COAL BURNOUT = 0.9997
          AT X =   1.46  , COAL BURNOUT = 1.0000
          AT X =   1.60  , COAL BURNOUT = 1.0000
          AT X =   1.75  , COAL BURNOUT = 1.0000
          AT X =   1.92  , COAL BURNOUT = 1.0000
          AT X =   2.10  , COAL BURNOUT = 1.0000
          AT X =   2.31  , COAL BURNOUT = 1.0000
          AT X =   2.54  , COAL BURNOUT = 1.0000
 >>>>EOLP COMPLETE, END OF PARTICLE ITERATION #  3

  13

 NITER SORCE      RESORU          RESORV          RESORW          RESORM       NCREE
                  RESORP          RESORH          RESORF          RESOET

  1   9.512E-02   5.240E-03  0   3.185E-03  0   8.074E-04  0   4.657E-03 20    0
                  7.311E-03  2   9.512E-02  1   4.715E-03  0   3.157E-02  0

 CONVERGED BY SORMIN CRITERION
  5   1.630E-02   3.203E-03  0   1.984E-03  0   7.639E-04  0   4.120E-03 10    0
                  3.205E-03  8   1.630E-02  2   3.447E-03  0   6.693E-03  0

 10   9.664E-03   2.015E-03  0   1.189E-03  0   5.167E-04  0   2.092E-03  9    0
                  1.609E-03  7   9.664E-03  2   3.272E-03  0   4.607E-03  0

 ONJITER  SORCE              RESNJ'S
    5    1.110E-03          9.489E-04 9.807E-04 1.030E-03 1.072E-03 1.110E-03

  SCATTER ITER: 0 ITERATION:  1 FRAC CHANGE IN TOT NET WALL FLUX:   1.000E+00
  SCATTER ITER: 0 ITERATION:  2 FRAC CHANGE IN TOT NET WALL FLUX:   7.573E-02
  SCATTER ITER: 0 ITERATION:  3 FRAC CHANGE IN TOT NET WALL FLUX:   5.322E-03
  SCATTER ITER: 0 ITERATION:  4 FRAC CHANGE IN TOT NET WALL FLUX:   3.644E-04
  SCATTER ITER: 0 ITERATION:  5 FRAC CHANGE IN TOT NET WALL FLUX:   2.372E-05
  SCATTER ITER: 0 ITERATION:  6 FRAC CHANGE IN TOT NET WALL FLUX:   1.603E-06
  SCATTER ITER: 1 ITERATION:  1 FRAC CHANGE IN TOT NET WALL FLUX:   2.188E-02
  SCATTER ITER: 1 ITERATION:  2 FRAC CHANGE IN TOT NET WALL FLUX:   5.678E-04
  SCATTER ITER: 1 ITERATION:  3 FRAC CHANGE IN TOT NET WALL FLUX:   2.445E-05
  SCATTER ITER: 1 ITERATION:  4 FRAC CHANGE IN TOT NET WALL FLUX:   1.882E-06
  REBOUNDING COLLISIONS ALLOWED FOR WALLS WHEN WALL TEMPERATURE IS BELOW    3000.0K
  TRAJECTORY ISL= 1,  IPS= 1  RECIRCULATES
   ISL= 1, IPS= 1, TERMINATED AT: IV= 54, JU=31  TIME=  8.281E+00  NPOINT=  722
  TRAJECTORY ISL= 1,  IPS= 2  RECIRCULATES
```

```
 ISL= 1, IPS= 2, TERMINATED AT: IV= 54, JU=31  TIME=  8.018E+00  NPOINT=  785
TRAJECTORY ISL= 1,  IPS= 3  RECIRCULATES
 ISL= 1, IPS= 3, TERMINATED AT: IV= 54, JU=31  TIME=  7.942E+00  NPOINT=  723
TRAJECTORY ISL= 1,  IPS= 4  RECIRCULATES
 ISL= 1, IPS= 4, TERMINATED AT: IV= 54, JU=29  TIME=  1.012E+01  NPOINT= 1053
TRAJECTORY ISL= 1,  IPS= 5  RECIRCULATES
 ISL= 1, IPS= 5, TERMINATED AT: IV= 54, JU=32  TIME=  7.410E+00  NPOINT=  773
TRAJECTORY ISL= 2,  IPS= 1  RECIRCULATES
 ISL= 2, IPS= 1, TERMINATED AT: IV= 54, JU=31  TIME=  8.159E+00  NPOINT=  572
TRAJECTORY ISL= 2,  IPS= 2  RECIRCULATES
 ISL= 2, IPS= 2, TERMINATED AT: IV= 54, JU=31  TIME=  8.127E+00  NPOINT=  559
TRAJECTORY ISL= 2,  IPS= 3  RECIRCULATES
 ISL= 2, IPS= 3, TERMINATED AT: IV= 54, JU=31  TIME=  7.864E+00  NPOINT=  619
TRAJECTORY ISL= 2,  IPS= 4  RECIRCULATES
 ISL= 2, IPS= 4, TERMINATED AT: IV= 54, JU=32  TIME=  7.652E+00  NPOINT=  991
TRAJECTORY ISL= 2,  IPS= 5  RECIRCULATES
 ISL= 2, IPS= 5, TERMINATED AT: IV= 54, JU=32  TIME=  7.435E+00  NPOINT=  921
TRAJECTORY ISL= 3,  IPS= 1  RECIRCULATES
 ISL= 3, IPS= 1, TERMINATED AT: IV= 54, JU=31  TIME=  7.855E+00  NPOINT=  613
TRAJECTORY ISL= 3,  IPS= 2  RECIRCULATES
 ISL= 3, IPS= 2, TERMINATED AT: IV= 54, JU=32  TIME=  7.465E+00  NPOINT=  488
TRAJECTORY ISL= 3,  IPS= 3  RECIRCULATES
 ISL= 3, IPS= 3, TERMINATED AT: IV= 54, JU=31  TIME=  7.603E+00  NPOINT=  467
TRAJECTORY ISL= 3,  IPS= 4  RECIRCULATES
 ISL= 3, IPS= 4, TERMINATED AT: IV= 54, JU=29  TIME=  1.003E+01  NPOINT=  901
TRAJECTORY ISL= 3,  IPS= 5  RECIRCULATES
 ISL= 3, IPS= 5, TERMINATED AT: IV= 54, JU=30  TIME=  9.318E+00  NPOINT=  868
TRAJECTORY ISL= 4,  IPS= 1  RECIRCULATES
 ISL= 4, IPS= 1, TERMINATED AT: IV= 54, JU=33  TIME=  6.833E+00  NPOINT=  441
TRAJECTORY ISL= 4,  IPS= 2  RECIRCULATES
 ISL= 4, IPS= 2, TERMINATED AT: IV= 54, JU=33  TIME=  7.131E+00  NPOINT=  476
TRAJECTORY ISL= 4,  IPS= 3  RECIRCULATES
 ISL= 4, IPS= 3, TERMINATED AT: IV= 54, JU=32  TIME=  7.273E+00  NPOINT=  726
TRAJECTORY ISL= 4,  IPS= 4  RECIRCULATES
 ISL= 4, IPS= 4, TERMINATED AT: IV= 54, JU=32  TIME=  7.258E+00  NPOINT=  558
TRAJECTORY ISL= 4,  IPS= 5  RECIRCULATES
 ISL= 4, IPS= 5, TERMINATED AT: IV= 54, JU=32  TIME=  7.229E+00  NPOINT=  527
TRAJECTORY ISL= 5,  IPS= 1  RECIRCULATES
 ISL= 5, IPS= 1, TERMINATED AT: IV= 54, JU=33  TIME=  6.709E+00  NPOINT=  489
TRAJECTORY ISL= 5,  IPS= 2  RECIRCULATES
 ISL= 5, IPS= 2, TERMINATED AT: IV= 54, JU=33  TIME=  6.554E+00  NPOINT=  399
TRAJECTORY ISL= 5,  IPS= 3  RECIRCULATES
 ISL= 5, IPS= 3, TERMINATED AT: IV= 54, JU=33  TIME=  6.634E+00  NPOINT=  621
TRAJECTORY ISL= 5,  IPS= 4  RECIRCULATES
 ISL= 5, IPS= 4, TERMINATED AT: IV= 54, JU=33  TIME=  6.634E+00  NPOINT=  567
TRAJECTORY ISL= 5,  IPS= 5  RECIRCULATES
 ISL= 5, IPS= 5, TERMINATED AT: IV= 54, JU=31  TIME=  7.946E+00  NPOINT=  682
TRAJECTORY ISL= 6,  IPS= 1  RECIRCULATES
 ISL= 6, IPS= 1, TERMINATED AT: IV= 54, JU=34  TIME=  6.276E+00  NPOINT=  503
TRAJECTORY ISL= 6,  IPS= 2  RECIRCULATES
 ISL= 6, IPS= 2, TERMINATED AT: IV= 54, JU=34  TIME=  6.455E+00  NPOINT=  428
TRAJECTORY ISL= 6,  IPS= 3  RECIRCULATES
 ISL= 6, IPS= 3, TERMINATED AT: IV= 54, JU=34  TIME=  6.265E+00  NPOINT=  440
TRAJECTORY ISL= 6,  IPS= 4  RECIRCULATES
 ISL= 6, IPS= 4, TERMINATED AT: IV= 54, JU=35  TIME=  6.064E+00  NPOINT=  587
TRAJECTORY ISL= 6,  IPS= 5  RECIRCULATES
 ISL= 6, IPS= 5, TERMINATED AT: IV= 54, JU=33  TIME=  6.666E+00  NPOINT=  751
 ISL= 7, IPS= 1, TERMINATED AT: IV= 54, JU=34  TIME=  5.999E+00  NPOINT=  525
TRAJECTORY ISL= 7,  IPS= 2  RECIRCULATES
 ISL= 7, IPS= 2, TERMINATED AT: IV= 54, JU=34  TIME=  6.244E+00  NPOINT=  494
TRAJECTORY ISL= 7,  IPS= 3  RECIRCULATES
 ISL= 7, IPS= 3, TERMINATED AT: IV= 54, JU=34  TIME=  6.055E+00  NPOINT=  528
TRAJECTORY ISL= 7,  IPS= 4  RECIRCULATES
 ISL= 7, IPS= 4, TERMINATED AT: IV= 54, JU=34  TIME=  6.430E+00  NPOINT=  732
TRAJECTORY ISL= 7,  IPS= 5  RECIRCULATES
 ISL= 7, IPS= 5, TERMINATED AT: IV= 54, JU=34  TIME=  6.215E+00  NPOINT=  737
 ISL= 8, IPS= 1, TERMINATED AT: IV= 54, JU=35  TIME=  5.808E+00  NPOINT=  726
TRAJECTORY ISL= 8,  IPS= 2  RECIRCULATES
 ISL= 8, IPS= 2, TERMINATED AT: IV= 54, JU=35  TIME=  5.952E+00  NPOINT=  583
TRAJECTORY ISL= 8,  IPS= 3  RECIRCULATES
```

```
 ISL= 8, IPS= 3, TERMINATED AT: IV= 54, JU=35  TIME=  5.937E+00  NPOINT=  572
TRAJECTORY ISL= 8,  IPS= 4  RECIRCULATES
 ISL= 8, IPS= 4, TERMINATED AT: IV= 54, JU=36  TIME=  5.667E+00  NPOINT=  607
TRAJECTORY ISL= 8,  IPS= 5  RECIRCULATES
 ISL= 8, IPS= 5, TERMINATED AT: IV= 54, JU=36  TIME=  5.805E+00  NPOINT=  733
 ISL= 9, IPS= 1, TERMINATED AT: IV= 54, JU=36  TIME=  5.843E+00  NPOINT=  460
 ISL= 9, IPS= 2, TERMINATED AT: IV= 54, JU=36  TIME=  5.697E+00  NPOINT=  599
 ISL= 9, IPS= 3, TERMINATED AT: IV= 54, JU=35  TIME=  5.889E+00  NPOINT=  481
TRAJECTORY ISL= 9,  IPS= 4  RECIRCULATES
 ISL= 9, IPS= 4, TERMINATED AT: IV= 54, JU=37  TIME=  5.477E+00  NPOINT=  449
TRAJECTORY ISL= 9,  IPS= 5  RECIRCULATES
 ISL= 9, IPS= 5, TERMINATED AT: IV= 54, JU=36  TIME=  5.591E+00  NPOINT=  692
 ISL=10, IPS= 1, TERMINATED AT: IV= 54, JU=37  TIME=  5.625E+00  NPOINT=  888
 ISL=10, IPS= 2, TERMINATED AT: IV= 54, JU=36  TIME=  5.615E+00  NPOINT=  431
 ISL=10, IPS= 3, TERMINATED AT: IV= 54, JU=36  TIME=  5.726E+00  NPOINT=  546
TRAJECTORY ISL=10,  IPS= 4  RECIRCULATES
 ISL=10, IPS= 4, TERMINATED AT: IV= 54, JU=37  TIME=  5.456E+00  NPOINT=  530
TRAJECTORY ISL=10,  IPS= 5  RECIRCULATES
 ISL=10, IPS= 5, TERMINATED AT: IV= 54, JU=37  TIME=  5.585E+00  NPOINT=  690
 FRACTION OF DAF COAL DEVOLATILIZED =  0.54539
0               SUM OF SOLID PHASE COUPLING
                SSPE =   4.342E-04
                SSPF =   0.000E+00
                SSPM =   4.342E-04
                SSPUu =   5.329E-02
                SSPUp =  -2.637E-02
                SSPV =  -1.265E-07
                SSPH =  -2.318E+03

 ******* CUMULATIVE COAL BURNOUT ********

          AT X =   0.00  , COAL BURNOUT = 0.0000
          AT X =   0.01  , COAL BURNOUT = 0.1948
          AT X =   0.02  , COAL BURNOUT = 0.3712
          AT X =   0.03  , COAL BURNOUT = 0.3850
          AT X =   0.04  , COAL BURNOUT = 0.4146
          AT X =   0.05  , COAL BURNOUT = 0.4211
          AT X =   0.06  , COAL BURNOUT = 0.4559
          AT X =   0.07  , COAL BURNOUT = 0.4656
          AT X =   0.08  , COAL BURNOUT = 0.5002
          AT X =   0.09  , COAL BURNOUT = 0.5318
          AT X =   0.10  , COAL BURNOUT = 0.5442
          AT X =   0.11  , COAL BURNOUT = 0.5772
          AT X =   0.12  , COAL BURNOUT = 0.5989
          AT X =   0.13  , COAL BURNOUT = 0.6110
          AT X =   0.14  , COAL BURNOUT = 0.6303
          AT X =   0.15  , COAL BURNOUT = 0.6451
          AT X =   0.16  , COAL BURNOUT = 0.6642
          AT X =   0.17  , COAL BURNOUT = 0.6748
          AT X =   0.19  , COAL BURNOUT = 0.6904
          AT X =   0.20  , COAL BURNOUT = 0.7027
          AT X =   0.21  , COAL BURNOUT = 0.7153
          AT X =   0.22  , COAL BURNOUT = 0.7302
          AT X =   0.23  , COAL BURNOUT = 0.7477
          AT X =   0.24  , COAL BURNOUT = 0.7690
          AT X =   0.26  , COAL BURNOUT = 0.7934
          AT X =   0.27  , COAL BURNOUT = 0.8196
          AT X =   0.29  , COAL BURNOUT = 0.8449
          AT X =   0.31  , COAL BURNOUT = 0.8701
          AT X =   0.33  , COAL BURNOUT = 0.8934
          AT X =   0.36  , COAL BURNOUT = 0.9118
          AT X =   0.38  , COAL BURNOUT = 0.9282
          AT X =   0.41  , COAL BURNOUT = 0.9446
          AT X =   0.44  , COAL BURNOUT = 0.9567
          AT X =   0.48  , COAL BURNOUT = 0.9634
          AT X =   0.52  , COAL BURNOUT = 0.9692
          AT X =   0.56  , COAL BURNOUT = 0.9747
          AT X =   0.61  , COAL BURNOUT = 0.9800
          AT X =   0.66  , COAL BURNOUT = 0.9852
```

```
          AT X =   0.72  , COAL BURNOUT = 0.9899
          AT X =   0.78  , COAL BURNOUT = 0.9941
          AT X =   0.85  , COAL BURNOUT = 0.9972
          AT X =   0.93  , COAL BURNOUT = 0.9991
          AT X =   1.02  , COAL BURNOUT = 0.9998
          AT X =   1.11  , COAL BURNOUT = 0.9999
          AT X =   1.22  , COAL BURNOUT = 1.0000
          AT X =   1.33  , COAL BURNOUT = 1.0000
          AT X =   1.46  , COAL BURNOUT = 1.0000
          AT X =   1.60  , COAL BURNOUT = 1.0000
          AT X =   1.75  , COAL BURNOUT = 1.0000
          AT X =   1.92  , COAL BURNOUT = 1.0000
          AT X =   2.10  , COAL BURNOUT = 1.0000
          AT X =   2.31  , COAL BURNOUT = 1.0000
          AT X =   2.54  , COAL BURNOUT = 1.0000
 >>>>EOLP COMPLETE, END OF PARTICLE ITERATION #  4

  10
TOTAL MASS IN (kg/s) =     4.26192E-02

TOTAL MASS OUT (kg/s) =     4.32478E-02


TOTAL MASS OUT - TOTAL MASS IN (kg/s) =     6.28643E-04
*************************MASS BALANCE CLOSURE**********************************
PERCENT OF TOTAL MASS IN =     1.47502
*******************************************************************************
       ***************************   PCNOX   ***************************
       **** NOX POLLUTANT CALCULATION USING OUTPUT FROM PCGC-2 FOR THE **
       *****  PHASE AND PARTICLE PROPERTIES THROUGHOUT THE FLOW FIELD ***
       ***************************   BASECASE   ************************


    nox pollutant calculations called following convergence of pcgc2


    nitnox       maxsor         resnox     reshcn     resnh3     ncree

        2      3.776E+01      5.164E-01 3.721E+01 3.776E+01       20
        4      3.718E+01      5.732E-01 3.718E+01 1.356E+00       20
        6      3.718E+01      4.814E-01 3.718E+01 4.816E-01       20
        8      3.718E+01      4.322E-01 3.718E+01 2.865E-01       20
       10      4.090E-01      4.090E-01 1.066E-01 2.141E-01       20
       12      3.892E-01      3.892E-01 6.261E-02 1.737E-01       20
       14      3.748E-01      3.748E-01 6.232E-02 1.468E-01       20
       16      3.683E-01      3.683E-01 6.178E-02 1.263E-01       20
       18      3.675E-01      3.675E-01 6.093E-02 1.098E-01       20
       20      3.667E-01      3.667E-01 5.972E-02 9.620E-02       20
0 at x = 2.53667   noxavg =      55.01 ppm   hcnavg =     912.43 ppm   nh3avg =       0.12 ppm

    THIS IS A CONVERGED CASE


Removing linked generic file names
rm: /mag/brewster/afr/cpr/SOXIN: No such file or directory
Moving unlinked generic files to specific files
mv: /mag/brewster/afr/cpr/YSO21: Cannot access: No such file or directory
mv: /mag/brewster/afr/cpr/YH2S1: Cannot access: No such file or directory
mv: /mag/brewster/afr/cpr/SORDN1: Cannot access: No such file or directory
```

Appendix G

Sample Computer Files for Coal Gasification with Sidewall Sorbent Injection and Sulfur Capture

This sample problem is the gasification of coal in the BYU gasifier with sidewall injection of sorbent.

Main Data File (ill.dat, PCGCIN)

```
  2,                                          !NSAY..(SAY(I)=!,NSAY) follows:
  BYU gasifier
  Huber case I9 12-2 3
F     T     T     T     T                      !INRST,INCALF,INCREK,INCALH,INCALG
T     T     F     T     T                      !IPSICT,INPRST,INEACH,INCLET,INCLGE
T     F     F     F     T                      !INCALN,INCURF,LEULP,INTFRZ,INISMP
T     T     F                                  !INSMPC,INCLKE,LPOST
T                                              !INSORB
F     F     T     F     F                      !INCNOX,POLLUT,INQRL,INCSWP,INCSWS
F     F     F     F     F                      !INNOZZ,INFSOU,LTBUG,GRDOUT,INPROG
T     T     T     T     F                      !INCFP,INRAD,INRDGD,INTRUS,MAGHJER
F     F     T     F     F                      !INETA2,HTRACK,FGDVC,LAMINAR,LBUOY
```

```
1.0                                         !UPDOWN
 0.700,0.700,0.700,0.950,                   !URFU,URFV,URFW,URFH
 0.700,0.700,0.700,0.700,0.500,             !URFE,URFK,URFF,URFG,URFVIS
  0.50,0.900,0.900,1.000,1.0000,1.0000,     !URFDEN,URFETA,URFGET,URFNJ,URFPP,URFP
  1.31e-02,  2.87e-02,  0.20000,            !DIAP,DIAS,DIACH
   9.91,  1.0e-04,                          !NDIA(real),THICK
 300,-1000, 50,                             !MAXIT,INDPRI,INDRST
   2,   5,  80,                             !NJINP,NJINS,NIWOQ
 100.000,  1.100,25,  1.100,  0.9200,       !AL1,EPSX,NL,EPSI,EPSD
     300.00,     4050.00, 0.000000e+00,     !TMIN,TMAX,HLOSS
 1500.00,2050.00,                           !TLODEL,THIDEL
 3,      36.3, 5.100000e-02,                !NIINQ,QHA,QLX
 1100.000, 1100.000, 1000.000,              !TBN,TBW,TBE
     1.79e-05,        183389, 1,            !VISCOS,PRES,IEUCK
     0.02,     0.8,                         !SORMAX,SORMIN
INLET 1                                     !(Primary)
 1.110000e-03, 1.00, 0.00, 0.10,7.508,0.0  !FLOW,FFLOW,SWIRLN,TINFLO
INLET 2                                     !(Secondary)
 5.250000e-03, 0.00, 0.00, 0.10,0.0,0.0        !FLOW,FFLOW,SWIRLN,TINFLO
INLET 3                                     !(Sidewall)
 0.0013, 1.00, 0.00, 0.10,0.0,12.0          !FLOW,FFLOW,SWIRLN,TINFLO
                                            !            (Blank line)
ELEMENTS
THERMO                                      !The react. sect. is formatted
REACTANTS 1
  356.00,                                   !TMP (unformatted)
AR1.00      0.00      0.00      0.00   AR      1.00000M        G
                                            !            (Blank line)
REACTANTS 2
  589.00,                                   !TMP (unformatted)
O 2.00      1.00      0.00      0.00   O2      1.00000M        G
                                            !            (Blank line)
 10, 5,                                     !NSL,NPS
   1340.00, -1.0                            !PDEN,UPDOWN
 0.0,0.0,0.0                                !XPS(ISL),YPS(ISL),SPRANG(ISL)
 0.0,0.0,0.0                                !XPS(ISL),YPS(ISL),SPRANG(ISL)
 0.0,0.0,0.0                                !XPS(ISL),YPS(ISL),SPRANG(ISL)
 0.0,0.0,0.0                                !XPS(ISL),YPS(ISL),SPRANG(ISL)
 0.0,0.0,0.0                                !XPS(ISL),YPS(ISL),SPRANG(ISL)
 0.0,0.0,0.0                                !XPS(ISL),YPS(ISL),SPRANG(ISL)
 0.0,0.0,0.0                                !XPS(ISL),YPS(ISL),SPRANG(ISL)
 0.0,0.0,0.0                                !XPS(ISL),YPS(ISL),SPRANG(ISL)
 0.0,0.0,0.0                                !XPS(ISL),YPS(ISL),SPRANG(ISL)
 0.0,0.0,0.0                                !XPS(ISL),YPS(ISL),SPRANG(ISL)
 1.0000,1.0000,1.0000,1.0000,1.0000,        !UPLAG(IPS),IPS = 1,NPS
 1.0000,1.0000,1.0000,1.0000,1.0000,        !TLAG(IPS),IPS = 1,NPS
  5.0e-06,13.0e-06,32.0e-06,                !PD(IPS),IPS = 1,3
  50.0e-06,100.0e-06,                       !PD(IPS),IPS = 4,NPS
 0.2000,0.2000,0.2000,0.2000,0.2000,        !PMF(IPS),IPS = 1,NPS
```

```
 F    F    T    F    F                    !LDEBUG,LYPS,LPARTP,LPARTS,LBOTH
 T    T    T    T                         !LSPM,LSPU,LSPV,LSPH
 3000.,                                   !trbnd
   0.9500,  0.0200,                       !YPSH,YPSL
 30, 1, 3,                                !MAXITP,MINITP,IGASV
 0.35,0.35,0.35,0.35,0.35,                     !PRK(IPS),IPS = 1,NPS
coal.arg3.7                             !Functional group composition data file
kin.arg3.7                              !Functional group kinetics data file
polymr.arg3.7                           !Coal polymer data file
 1                                        !NCARD...COMENT(I),I=1,NCARD follows:
              All Particles have the same Properties
  T                                      !INCOAL
  0.2,0.2                                !urfpm,urfph
  1   3   5   0   1                      !NCRXN,NHRXN,NPROP,KEQ,NSHRNK
  1.000E-02, 1.000E-06, 0.000      !DELTPJ,DELRRJ,GAMMA,URFPM
   1.0000                                !XI(J)
  0.00000E+00, 0.00000E+00,-1.50400E+07, !QHC(J),HH0(J),HA0(J)
 -1.58800E+07,  373.15    ,              !HW0(J),TNBP
  0.941    , 0.000, 0.059,               !OMEGAC(J),OMEGAH(J),OMEGAA(J)
  0.000,                                 !OMEGAW(J)
  4.30000E+14, 2.29000E+08, 0.40000    , !AMJ(J,M),EMJ(J,M),YY(J,M)
  0.00000E+00,                           !HGV(J,M)
 O2  CO2 H2O                             !OXYD(L),L = 1,NHRXN
  1.74, 1.0, 1.0                         !PHIL(L)  L = 1,NHRXN
   2.30    , 9.29E+07,  1.0000    ,      !AL(J,L),EL(J,L),EMM(J,L)
   3.419   , 1.30E+08,  1.0000    ,      !AL(J,L),EL(J,L),EMM(J,L)
   208.0   , 2.40E+08,  1.0000    ,      !AL(J,L),EL(J,L),EMM(J,L)
rct.arg6
  0.7770,    0.0500,     0.1370,         !(WIC(J,K)  K = 1,3)
  0.0140,    0.0220, 0.0,                  !(WIC(J,K)  K = 4,NLM)
 H2O                                     !SLRCMP
  0.5,T                                  !FBACK,LBACK
  T    T    T    ,  10,                  !LDISO,LGASE,LEMCOR,MAXITR
  0.9000,    0.00,                       !EMW,TOUT
  1.0000,0.00000,                        !A0,AF
```

Inlet Profile Data File (ill.inl, INLET)

```
 F   1 F   1 F   0                       !UPDAT,KOPUP,USDAT,KOPUS,...
 F   0 F   0 F   0                       !VPDAT,KOPVP,VSDAT,KOPVS,...
 F   0 F   0 F   1                       !WPDAT,KOPWP,WSDAT,KOPWS,...
 F   1 F   1 F   0                       !TIPDAT,KOPTEP,TISDAT,KOPTES,...
 F   2 F   2 F   1                       !EDPDAT,KOPEDP,EDSDAT,KOPEDS,...
  0.00E+00, 0.00E+00,                    !PLS,SLS,AILS...
1       8.50000E+00                      !NSFORM,ALPHA0
  1.25500E-02, 1.25500E-02, 6.50000E-02, !RP,RS1,RS2,
```

Thermo Data File (ill.thm, THERMO)

```
C         12.01115       4.0
H         1.00797        1.0
O         15.9994       -2.0
N         14.0067        0.0
S         32.06          4.0
AR        39.94800       0.0

AR                L 5/66AR 1.00 0.00 0.00 0.G   300.000  5000.000
1
 0.25000000E 01     0.00000000     0.00000000     0.00000000     0.00000000
2
-0.74537502E 03 0.43660006E 01 0.25000000E 01     0.00000000     0.00000000
3
     0.00000000     0.00000000-0.74537498E 03 0.43660006E 01
CO2               J 9/65C  1.O  2.00 0.00 0.G   300.000  5000.000
 0.44608040E 01 0.30981717E-02-0.12392566E-05 0.22741323E-09-0.15525948E-13
-0.48961438E 05-0.98635978E 00 0.24007788E 01 0.87350905E-02-0.66070861E-05
 0.20021860E-08 0.63274039E-15-0.48377520E 05 0.96951447E 01
H2O               J 3/61H  2.O  1.00 0.00 0.G   300.000  5000.000
 0.27167616E 01 0.29451370E-02-0.80224368E-06 0.10226681E-09-0.48472104E-14
-0.29905820E 05 0.66305666E 01 0.40701275E 01-0.11084499E-02 0.41521180E-05
-0.29637404E-08 0.80702101E-12-0.30279719E 05-0.32270038E 00
N2                J 9/65N  2.0  0.0  0.0  0.G   300.000  5000.000
 0.28963194E 01 0.15154863E-02-0.57235275E-06 0.99807385E-10-0.65223536E-14
-0.90586182E 03 0.61615143E 01 0.36748257E 01-0.12081496E-02 0.23240100E-05
-0.63217520E-09-0.22577253E-12-0.10611587E 04 0.23580418E 01
O2                J 9/65O  2.0  0.0  0.0  0.G   300.000  5000.000
 0.36219521E 01 0.73618256E-03-0.19652219E-06 0.36201556E-10-0.28945623E-14
-0.12019822E 04 0.36150942E 01 0.36255980E 01-0.18782183E-02 0.70554543E-05
-0.67635071E-08 0.21555977E-11-0.10475225E 04 0.43052769E 01
CO                J 9/65C  1.O  1.00 0.00 0.G   300.000  5000.000
 0.29840689E 01 0.14891387E-02-0.57899678E-06 0.10364576E-09-0.69353499E-14
-0.14245227E 05 0.63479147E 01 0.37100916E 01-0.16190964E-02 0.36923584E-05
-0.20319673E-08 0.23953344E-12-0.14356309E 05 0.29555340E 01
H2                J 3/61H  2.0  0.0  0.0  0.G   300.000  5000.000
 0.31001883E 01 0.51119458E-03 0.52644204E-07-0.34909964E-10 0.36945341E-14
-0.87738013E 03-0.19629412E 01 0.30574446E 01 0.26765198E-02-0.58099149E-05
 0.55210343E-08-0.18122726E-11-0.98890430E 03-0.22997046E 01
CH4               J 3/61C  1.H  4.00 0.00 0.G   300.000  5000.000
 0.15027056E 01 0.10416795E-01-0.39181514E-05 0.67777872E-09-0.44283706E-13
-0.99787031E 04 0.10707143E 02 0.38261929E 01-0.39794557E-02 0.24558321E-04
-0.22732920E-07 0.69626952E-11-0.10144945E 05 0.86690062E 00
H2S               J12/65H  2.S  1.00 0.00 0.G   300.000  5000.000
```

```
 0.28479090E 01 0.38415990E-02-0.14099360E-05 0.24278735E-09-0.15783280E-13
-0.34469788E 04 0.74781399E 01 0.38811293E 01-0.13211856E-03 0.36517713E-05
-0.21820441E-08 0.28783779E-12-0.36350916E 04 0.25161505E 01
SO2               J 6/61S  1.O  2.00 0.00 0.G   300.000  5000.000
 0.52451363E 01 0.19704204E-02-0.80375759E-06 0.15149969E-09-0.10557998E-13
-0.37558227E 05-0.10873518E 01 0.32665329E 01 0.53237863E-02 0.68437544E-06
-0.52809987E-08 0.25590450E-11-0.36908145E 05 0.96513472E 01
C(S)               J 3/61C  1.0  0.0  0.0  0.S   300.000  5000.000
 0.13604937E 01 0.19182237E-02-0.84040386E-06 0.16448705E-09-0.11672670E-13
-0.65713843E 03-0.80070200E 01-0.44778049E 00 0.53690970E-02-0.39775563E-06
-0.40459263E-08 0.21134925E-11-0.94280670E 02 0.16840773E 01

AR
3.542,93.3,0.,0.,AR
CO2
3.996,190.,0.,-3.935E+08,CO2
H2O
2.641,809.1,1.0,-2.418E+08,H2O
N2
3.681,91.5,0.,0.,N2
O2
3.433,113.,0.,0.,O2
CO
3.59,110.,0.,-1.105E+08,CO
H2
2.915,38.,0.,0.,H2
CH4
3.758,148.6,0.0,-7.485E+07,CH4
H2S
3.49,343.0,0.21,-2.017E+07,H2S
SO2
4.04,347.0,0.42,-2.969E+08,SO2
C(S)
3.822,137.,0.,0.,C(S)
```

SO_x Data File (ill.sox, SOXIN)

```
 3,                                    !NSAYSX..(SAYNX(I),I=1,NSAYSX) follows:
    ***************************   PCSORB  ******************************
    ***************** SOX/H2S-SORBENT REACTIONS SUBMODEL    *************
    ************************             ******************************
 2                                     !nstype (SO2=1,H2S=2)
 1,1                                   !NSLS,NPSS
 1793.,                                !SPDEN
100000.,                               !SORBENT BET SURFACE AREA (m^2/g)
0.65024,0.100,0.0,                          !XPS(ISL),YPS(ISL),SPRANG(ISL)
```

```
10.600E-06,                          !PDS(IPS),IPS = 1,NPSS
1.0000,                             !PMFS(IPS),IPS = 1,NPSS
F    T    F    F    F               !LSPBUG,LSYPS,LPARTP,LPARTS,LPBOTH
F                                    !LRBNDS
0.9500,0.0200,                       !YPSH,YPSL
0.3500,                              !PRKS(IPS),IPS = 1,NPSS
 0.90,                               !PRSO2
 1000,0.0010,                          !MXITSX,MAXRES
 0.90000,                            !URFSO2
```

Grid Data File (ill.grd, GRIDS)

```
NODE
        100          37
          6          11
          7           6
          3           4          23
             X              XU           TBN
   1    -8.5000E-03    -1.7000E-02    1100.
   2     8.5000E-03     0.0000E+00    1100.
   3     2.5500E-02     1.7000E-02    1100.
   4     4.2500E-02     3.4000E-02    1100.
   5     5.9500E-02     5.1000E-02    1100.
   6     7.6500E-02     6.8000E-02    1100.
   7     9.3500E-02     8.5000E-02    1100.
   8     1.1050E-01     1.0200E-01    1100.
   9     1.2750E-01     1.1900E-01    1100.
  10     1.4450E-01     1.3600E-01    1100.
  11     1.6150E-01     1.5300E-01    1100.
  12     1.7850E-01     1.7000E-01    1100.
  13     1.9550E-01     1.8700E-01    1100.
  14     2.1250E-01     2.0400E-01    1100.
  15     2.2950E-01     2.2100E-01    1100.
  16     2.4650E-01     2.3800E-01    1100.
  17     2.6350E-01     2.5500E-01    1100.
  18     2.8050E-01     2.7200E-01    1100.
  19     2.9750E-01     2.8900E-01    1100.
  20     3.1450E-01     3.0600E-01    1100.
  21     3.3150E-01     3.2300E-01    1100.
  22     3.4850E-01     3.4000E-01    1100.
  23     3.6550E-01     3.5700E-01    1100.
  24     3.8250E-01     3.7400E-01    1100.
  25     3.9950E-01     3.9100E-01    1100.
  26     4.1650E-01     4.0800E-01    1100.
  27     4.3350E-01     4.2500E-01    1100.
  28     4.5050E-01     4.4200E-01    1100.
```

29	4.6750E-01	4.5900E-01	1100.
30	4.8450E-01	4.7600E-01	1100.
31	5.0150E-01	4.9300E-01	1100.
32	5.1680E-01	5.0915E-01	1100.
33	5.3057E-01	5.2368E-01	1100.
34	5.4296E-01	5.3677E-01	1100.
35	5.5412E-01	5.4854E-01	1100.
36	5.6416E-01	5.5914E-01	1100.
37	5.7319E-01	5.6867E-01	1100.
38	5.8132E-01	5.7726E-01	1100.
39	5.8864E-01	5.8498E-01	1100.
40	5.9522E-01	5.9193E-01	1100.
41	6.0115E-01	5.9819E-01	1100.
42	6.0649E-01	6.0382E-01	1100.
43	6.1129E-01	6.0889E-01	1100.
44	6.1561E-01	6.1345E-01	1100.
45	6.1950E-01	6.1755E-01	1100.
46	6.2300E-01	6.2125E-01	1100.
47	6.2615E-01	6.2457E-01	1100.
48	6.2898E-01	6.2757E-01	1100.
49	6.3154E-01	6.3026E-01	1100.
50	6.3383E-01	6.3268E-01	1100.
51	6.3590E-01	6.3487E-01	1100.
52	6.3776E-01	6.3683E-01	1100.
53	6.3943E-01	6.3860E-01	1100.
54	6.4094E-01	6.4019E-01	1100.
55	6.4230E-01	6.4162E-01	1100.
56	6.4352E-01	6.4291E-01	1100.
57	6.4461E-01	6.4407E-01	1100.
58	6.4560E-01	6.4511E-01	1100.
59	6.4649E-01	6.4605E-01	1100.
60	6.4729E-01	6.4689E-01	1100.
61	6.4801E-01	6.4765E-01	1100.
62	6.4866E-01	6.4834E-01	1100.
63	6.4925E-01	6.4895E-01	1100.
64	6.4977E-01	6.4951E-01	1100.
65	6.5024E-01	6.5001E-01	1100.
66	6.5067E-01	6.5046E-01	1100.
67	6.5105E-01	6.5086E-01	1100.
68	6.5152E-01	6.5129E-01	1100.
69	6.5209E-01	6.5181E-01	1100.
70	6.5279E-01	6.5244E-01	1100.
71	6.5363E-01	6.5321E-01	1100.
72	6.5467E-01	6.5415E-01	1100.
73	6.5593E-01	6.5530E-01	1100.
74	6.5747E-01	6.5670E-01	1100.
75	6.5935E-01	6.5841E-01	1100.
76	6.6165E-01	6.6050E-01	1100.
77	6.6444E-01	6.6304E-01	1100.

78	6.6786E-01	6.6615E-01	1100.
79	6.7202E-01	6.6994E-01	1100.
80	6.7710E-01	6.7456E-01	1100.
81	6.8330E-01	6.8020E-01	1100.
82	6.9086E-01	6.8708E-01	1100.
83	7.0008E-01	6.9547E-01	1100.
84	7.1134E-01	7.0571E-01	1100.
85	7.2507E-01	7.1820E-01	1100.
86	7.4182E-01	7.3344E-01	1100.
87	7.6225E-01	7.5203E-01	1100.
88	7.8718E-01	7.7472E-01	1100.
89	8.1760E-01	8.0239E-01	1100.
90	8.5470E-01	8.3615E-01	1100.
91	8.9997E-01	8.7734E-01	1100.
92	9.5520E-01	9.2759E-01	1100.
93	1.0226E+00	9.8890E-01	1100.
94	1.1048E+00	1.0637E+00	1100.
95	1.2051E+00	1.1549E+00	1100.
96	1.3274E+00	1.2663E+00	1100.
97	1.4767E+00	1.4021E+00	1100.
98	1.6588E+00	1.5678E+00	1100.
99	1.8810E+00	1.7699E+00	1100.
100	2.1520E+00	2.0165E+00	1100.

	Y	YV
1	-5.7790E-04	-1.1558E-03
2	5.7790E-04	0.0000E+00
3	1.7339E-03	1.1559E-03
4	2.9798E-03	2.3569E-03
5	4.3226E-03	3.6512E-03
6	5.7700E-03	5.0463E-03
7	7.3300E-03	6.5500E-03
8	8.8900E-03	8.1100E-03
9	1.0450E-02	9.6700E-03
10	1.2010E-02	1.1230E-02
11	1.3570E-02	1.2790E-02
12	1.5130E-02	1.4350E-02
13	1.6846E-02	1.5988E-02
14	1.8734E-02	1.7790E-02
15	2.0810E-02	1.9772E-02
16	2.3094E-02	2.1952E-02
17	2.5606E-02	2.4350E-02
18	2.8370E-02	2.6988E-02
19	3.1410E-02	2.9890E-02
20	3.4754E-02	3.3082E-02
21	3.8432E-02	3.6593E-02
22	4.2479E-02	4.0455E-02
23	4.6929E-02	4.4704E-02
24	5.1825E-02	4.9377E-02
25	5.7211E-02	5.4518E-02

```
 26        6.2597E-02        5.9904E-02
 27        6.7551E-02        6.5074E-02
 28        7.2110E-02        6.9830E-02
 29        7.6303E-02        7.4207E-02
 30        8.0161E-02        7.8232E-02
 31        8.3711E-02        8.1936E-02
 32        8.6976E-02        8.5343E-02
 33        8.9981E-02        8.8478E-02
 34        9.2745E-02        9.1363E-02
 35        9.5288E-02        9.4016E-02
 36        9.7627E-02        9.6457E-02
 37        1.0237E-01        9.9999E-02
                          ***REACTOR BOUNDARIES AND FLOW DOMAIN***
    1  2  3  4  5  ...60 61 62 63 64 65 66 67 68 69 70 ...95 96 97 98 99 100
37  X  X  X  X  X  ... X  X  X  X  1  X  X  X  X  X  X  ...X  X  X  X  X  X
36  X  O  O  O  O  ... O  O  O  O  O  O  O  O  O  O  O  ...O  O  O  O  O  O
35  X  O  O  O  O  ... O  O  O  O  O  O  O  O  O  O  O  ...O  O  O  O  O  O
34  X  O  O  O  O  ... O  O  O  O  O  O  O  O  O  O  O  ...O  O  O  O  O  O
33  X  O  O  O  O  ... O  O  O  O  O  O  O  O  O  O  O  ...O  O  O  O  O  O
32  X  O  O  O  O  ... O  O  O  O  O  O  O  O  O  O  O  ...O  O  O  O  O  O
31  X  O  O  O  O  ... O  O  O  O  O  O  O  O  O  O  O  ...O  O  O  O  O  O
30  X  O  O  O  O  ... O  O  O  O  O  O  O  O  O  O  O  ...O  O  O  O  O  O
29  X  O  O  O  O  ... O  O  O  O  O  O  O  O  O  O  O  ...O  O  O  O  O  O
28  X  O  O  O  O  ... O  O  O  O  O  O  O  O  O  O  O  ...O  O  O  O  O  O
27  X  O  O  O  O  ... O  O  O  O  O  O  O  O  O  O  O  ...O  O  O  O  O  O
26  X  O  O  O  O  ... O  O  O  O  O  O  O  O  O  O  O  ...O  O  O  O  O  O
25  X  O  O  O  O  ... O  O  O  O  O  O  O  O  O  O  O  ...O  O  O  O  O  O
24  X  O  O  O  O  ... O  O  O  O  O  O  O  O  O  O  O  ...O  O  O  O  O  O
23  X  O  O  O  O  ... O  O  O  O  O  O  O  O  O  O  O  ...O  O  O  O  O  O
22  X  O  O  O  O  ... O  O  O  O  O  O  O  O  O  O  O  ...O  O  O  O  O  O
21  X  O  O  O  O  ... O  O  O  O  O  O  O  O  O  O  O  ...O  O  O  O  O  O
20  X  O  O  O  O  ... O  O  O  O  O  O  O  O  O  O  O  ...O  O  O  O  O  O
19  X  O  O  O  O  ... O  O  O  O  O  O  O  O  O  O  O  ...O  O  O  O  O  O
18  X  O  O  O  O  ... O  O  O  O  O  O  O  O  O  O  O  ...O  O  O  O  O  O
17  X  O  O  O  O  ... O  O  O  O  O  O  O  O  O  O  O  ...O  O  O  O  O  O
16  X  O  O  O  O  ... O  O  O  O  O  O  O  O  O  O  O  ...O  O  O  O  O  O
15  X  O  O  O  O  ... O  O  O  O  O  O  O  O  O  O  O  ...O  O  O  O  O  O
14  X  O  O  O  O  ... O  O  O  O  O  O  O  O  O  O  O  ...O  O  O  O  O  O
13  X  O  O  O  O  ... O  O  O  O  O  O  O  O  O  O  O  ...O  O  O  O  O  O
12  X  O  O  O  O  ... O  O  O  O  O  O  O  O  O  O  O  ...O  O  O  O  O  O
11  S  O  O  O  O  ... O  O  O  O  O  O  O  O  O  O  O  ...O  O  O  O  O  O
10  S  O  O  O  O  ... O  O  O  O  O  O  O  O  O  O  O  ...O  O  O  O  O  O
 9  S  O  O  O  O  ... O  O  O  O  O  O  O  O  O  O  O  ...O  O  O  O  O  O
 8  S  O  O  O  O  ... O  O  O  O  O  O  O  O  O  O  O  ...O  O  O  O  O  O
 7  S  O  O  O  O  ... O  O  O  O  O  O  O  O  O  O  O  ...O  O  O  O  O  O
 6  P  O  O  O  O  ... O  O  O  O  O  O  O  O  O  O  O  ...O  O  O  O  O  O
 5  P  O  O  O  O  ... O  O  O  O  O  O  O  O  O  O  O  ...O  O  O  O  O  O
 4  P  O  O  O  O  ... O  O  O  O  O  O  O  O  O  O  O  ...O  O  O  O  O  O
 3  P  O  O  O  O  ... O  O  O  O  O  O  O  O  O  O  O  ...O  O  O  O  O  O
```

```
  2  P  O  O  O  O  ... O  O  O  O  O  O  O  O  O  O  O  ...O  O  O  O  O  O
  1  P  O  O  O  O  ... O  O  O  O  O  O  O  O  O  O  O  ...O  O  O  O  O  O
0 NOTE: THE JPRIM,JSEC,JTUBID,JTUBOD,NJINS,JQUARL
AND IQUARL ARE SUPERSEDED BY THE X AND P AND S IN THE MAP
WHEN INTRUS=.TRUE.  NI and NJ are not superseded.
```

Appendix H

Major FORTRAN Variables

FORTRAN Variable	FORTRAN Dimensions	FORTRAN Common Block or Routine	User's Manual Nomenclature	Units	User's Manual Eq. Nos.	Definition
a0	--	COMMON diso		--		Degree of anisotropicity of scattering in discrete ordinates radiation submodel
a1frwd	--	COMMON rmscom				Zel'dovich forward rate 1f pre-exponential
a1rev	--	COMMON rmscom				Zel'dovich reverse rate 1r pre-exponential (has no T depend.)
a2frwd	--	COMMON rmscom				Zel'dovich forward rate 2f pre-exponential
a2rev	--	COMMON rmscom				Zel'dovich reverse rate 2r pre-exponential

FORTRAN Variable	FORTRAN Dimensions	FORTRAN Common Block or Routine	User's Manual Nomenclature	Units	User's Manual Eq. Nos.	Definition
a3frwd	--	COMMON rmscom				Zel'dovich forward rate 3f pre-exponential (has no T depend.)
a3rev	--	COMMON rmscom				Zel'dovich reverse rate 3r pre-exponential
acj	numxpt, numypt, numpar	COMMON eulp	A_{ci}		--	Eulerian value of mass of coal in k^{th} particle
ae	numxpt, numypt	COMMON coef	A_E		3-61	Coefficient
ae	numxpt,numypt	COMMON coef	A_E		3-81	East neighbor coefficient
af	--	COMMON diso		--		A value of 0.0 will use upwind differencing to solve radiation equations in discrete ordinates model. A value of 1.0 will use central differencing. An intermediate value will use a hybrid of upwind and central.
afbar	--	COMMON cgauss				Mean value of mixture fraction
aq	--	COMMON cgauss				Variance of mixture fraction

FORTRAN Variable	FORTRAN Dimensions	FORTRAN Common Block or Routine	User's Manual Nomenclature	Units	User's Manual Eq. Nos.	Definition
agsic	numxpt, numypt	COMMON krad				Absorption coefficient for gases
ahj	numxpt, numypt, numpar	COMMON eulp	A_{hi}		--	Eulerian value of mass of char in k^{th} particle
ahss1	--	COMMON rmscom				DeSoete rate 1 pre-exponential
ahss2	--	COMMON rmscom				DeSoete rate 2 pre-exponential
ahss3	--	COMMON rmscom				DeSoete rate 3 pre-exponential
ahss4	--	COMMON rmscom				DeSoete rate 4 pre-exponential
AJ	--	COAL2	A_i	m^2	2-131	Particle external surface area.
al	numele, numspe	COMMON cequil		--		al(i,j) is the stoichiometric coefficient of the i^{th} element in the j^{th} species
all	--	COMMON grid1		m		Axial location where cell spacing begins to shrink
alfaa0	numpar	COMMON ippar		kg		Initial mass of ash in a particle
alfac0	numpar	COMMON ippar		kg		Initial mass of raw coal in a particle
alfah0	numpar	COMMON ippar		kg		Initial mass of char in a particle

FORTRAN Variable	FORTRAN Dimensions	FORTRAN Common Block or Routine	User's Manual Nomenclature	Units	User's Manual Eq. Nos.	Definition
alfaj	numpar	COMMON cflag		kg		Particle mass
alfas	numpar	COMMON cflag		kg		Sorbent particle mass
alfaw0	numpar	COMMON ippar		kg		Initial mass of slurry liquid in a droplet
ALFC	--	PROPS	α_c		2-80	Intermittency of pure coal offgas
alj	numpar,numoxd	COMMON rrat				Char reaction pre-exponential
alphaa	--	COMMON difeqn		kg		Mass of ash in particle
alphac	--	COMMON difeqn		kg		Mass of raw coal in particle
alphah	--	COMMON difeqn		kg		Mass of char in particle
alphat	--	COMMON difeqn		kg		Total particle mass
alphaw	--	COMMON difeqn		kg		Mass of slurry liquid in particle
altot	--	COMMON qrid1		m		Location at which axial nodes start to shrink
amj	numpar,numdev	COMMON rrat				Coal reaction pre-exponential
amt1	--	COMMON rmscom				Mitchell and Tarbell rate 1 pre-exponential

FORTRAN Variable	FORTRAN Dimensions	FORTRAN Common Block or Routine	User's Manual Nomenclature	Units	User's Manual Eq. Nos.	Definition
amt2a	--	COMMON rmscom				Mitchell & Tarbell rate 2a pre-exponential
amt2b	--	COMMON rmscom				Mitchell & Tarbell rate 2b pre-exponential
amt3	--	COMMON rmscom				Mitchell & Tarbell rate 3 pre-exponential
amt4	--	COMMON rmscom				Mitchell & Tarbell rate 4 pre-exponential (has no T depend.)
an	numxpt, numypt	COMMON coef	A_N		3-63	Coefficient
an	numxpt,numypt	COMMON coef	A_N		3-79	North neighbor coefficient
aoxyeq	--	COMMON rmscom				Equilibrium constant
aoxype	--	COMMON rmscom				Equilibrium constant
ap	numxpt, numypt	COMMON coef	A_P		3-75	Coefficient
ap	numxpt, numypt	COMMON coef	A_P		3-75	p-node coefficient
apsic	numxpt, numypt	COMMON krad				Absorption coefficient for char and ash particles
arexp	numxpt,numypt	COMMON arexp		$m^2\ kg^{-1}$		Specific external surface area of particles

FORTRAN Variable	FORTRAN Dimensions	FORTRAN Common Block or Routine	User's Manual Nomenclature	Units	User's Manual Eq. Nos.	Definition
as	numxpt, numypt	COMMON coef	A_S		3-64	Coefficient
as	numxpt,numypt	COMMON coef	A_S		3-80	South neighbor coefficient
asub	numspe, numnam	COMMON cparam		--		Species name
at	maxrea,5	COMMON rcards		--		Atomic names of atoms in each reacant
atom	2, numele	COMMON cequil		kg kmol^{-1}, --		atom(1,j) is the atomic weight of the j^{th} element atom(2,j) is the valence of the j^{th} element
atomid	numele	COMMON cequil		--		atomid(j) is the name of the j^{th} element
aue	numxpt, numypt	COMMON flupr2		--		East neighbor coefficient for u equation
aun	numxpt, numypt	COMMON flupr2		--		North neighbor coefficient for u equation
aup	numxpt, numypt	COMMON flupr2		--		Coefficient for u-cell node in u equation
aus	numxpt, numypt	COMMON flupr2		--		South neighbor coefficient for u equation

FORTRAN Variable	FORTRAN Dimensions	FORTRAN Common Block or Routine	User's Manual Nomenclature	Units	User's Manual Eq. Nos.	Definition
auw	numxpt, numypt	COMMON flupr2		--		West neighbor coefficient for u equation
ave	numxpt, numypt	COMMON flupr2		--		East neighbor coefficient in v equation
avgawt	numpar	COMMON hcap		kg kmol^{-1}		Average atomic weight for raw coal
avn	numxpt, numypt	COMMON flupr2		--		North neighbor coefficient in v equation
avp	numxpt, numypt	COMMON flupr2		--		v-cell coefficient in v equation
avs	numxpt, numypt	COMMON flupr2		--		South neighbor coefficient in v equation
avw	numxpt, numypt	COMMON flupr2		--		West neighbor coefficient in v equation
aw	numxpt, numypt	COMMON coef	A_W		3-62	Coefficient
aw	numxpt,numypt	COMMON coef	A_W		3-82	West neighbor coefficient
awdt1	--	COMMON rmscom				Wendt rate 1 pre-exponential
awdt2	--	COMMON rmscom				Wendt rate 2 pre-exponential
awj	numxpt, numypt, numpar	COMMON eulp				Eulerian value of mass of slurry liquid in kth particle

FORTRAN Variable	FORTRAN Dimensions	FORTRAN Common Block or Routine	User's Manual Nomenclature	Units	User's Manual Eq. Nos.	Definition
b0	--	COMMON cparam		kg-atom i kg^{-1}		Mole numbers of each element
bbar	--	COMMON radcon	$\bar{b}$	--	2-148	Backward-scattered component of radiation
bcc	--	COMMON ratpar		kg-atom kg^{-1}		bct for carbon
bch	--	COMMON ratpar		kg-atom kg^{-1}		bct for hydrogen
bcn	--	COMMON ratpar		--		Fraction of nitrogen in the coal
bct	numele	COMMON pvar		kg-atom kg^{-1}		Atom nos. for coal offgas
betsur	--	COMMON ratesx		$cm^2\ g^{-1}$		BET surface area of calcined sorbent
bf0	numele	COMMON flaf0		kg-atom i kg^{-1}		Mole nos. for f=0 stream
bf1	numele	COMMON flaf0		kg-atom i kg^{-1}		Mole nos. for f=1 stream
binlet	numlet, numele	COMMON adflo		kg-atoms i kg^{-1}		Atom nos. for additional inlet
bjm	--	COMMON traj		--		Particle blowing parameter for mass transfer
bp	numele	COMMON fluc		kg-atom i kg^{-1}		Atom nos. for primary gas
bs	numele	COMMON fluc		kg-atom i kg^{-1}		Atom nos. for secondary gas

FORTRAN Variable	FORTRAN Dimensions	FORTRAN Common Block or Routine	User's Manual Nomenclature	Units	User's Manual Eq. Nos.	Definition
burnot	numxpt	COMMON cflag		--		Fractional burnout of coal and char particles
c1, c2, c3, c4	numxpt, numypt	COMMON cset			2-157	Radiation coefficients
c1, c2	--	COMMON turb	C_1, C_2	--	2-11	Turbulence model constants
cappa	--	COMMON turb				von Karmann constant
ccpa	numpar, numcoe	COMMON hcap				Heat capacity coefficients for ash
ccpc	numpar, numcoe	COMMON hcap				Heat capacity coefficients for raw coal
ccph	numpar, numcoe	COMMON hcap				Heat capacity coefficients for char
cd	--	COMMON turb				
ceiu	--	COMMON bcrad				$\varepsilon_w/(2-\varepsilon_w)$
ceo	--	COMMON bcrad				$\varepsilon_w/(2-\varepsilon_w)$ for exit plane
cfpdbg	--	COMMON dens1		--		Debug flag for correction factor for turbulence due to particles
CG	--	COAL2		kmol m^3		Total gas concentration

FORTRAN Variable	FORTRAN Dimensions	FORTRAN Common Block or Routine	User's Manual Nomenclature	Units	User's Manual Eq. Nos.	Definition
cg1,cg2	--	COMMON turb	$C_{\varepsilon 1}$,$C_{\varepsilon 2}$	--	2-43	Turbulent combustion model constants
ch2s	nsnode	COMMON ratesx		mol cm^{-3}		H_2S concentration at sorbent particle subshell
cint	numxpt, numypt, 4,5	COMMON diso				Directional intensity at each control volume
cmu	--	COMMON turb	C_μ	--	2-8	Turbulence model constant
concrit	--	COMMON cparam		--		Convergence for temperature (compare with crit)
control	--	COMMON cparam		--		Convergence for molar composition (compare with tol)
cpcoef	42,4	COMMON hcapfq				Heat capacity coefficients for FG-DVC volatiles
cpgg	--	COMMON gparam		J kg^{-1} K^{-1}		Gas mixture heat capacity
cpm	numxpt, numypt	COMMON heatcp		J kg^{-1} K^{-1}		Gas mixture heat capacity
cpmix	--	COMMON kaset1		J kg^{-1} K^{-1}		Mixture heat capacity
cpsct	--	COMMON pvar		kg kmol^{-1}		Coal offgas heat capacity
cpsf0	--	COMMON f1af0		J mol^{-1} K^{-1}		Heat capacity for f=0 stream

FORTRAN Variable	FORTRAN Dimensions	FORTRAN Common Block or Routine	User's Manual Nomenclature	Units	User's Manual Eq. Nos.	Definition
cpsf1	--	COMMON f1af0		J mol^{-1} K^{-1}		Heat capacity for f=1 stream
cpsinlet	numlet	COMMON adflo		J kg^{-1} K^{-1}		Heat capacity for additional inlet
cpsmh	--	COMMON magnussen		J kg^{-1} K^{-1}		Product stream heat capacity (Magnussen-Hjertager method)
cpsp	--	COMMON pands		J kg^{-1}		Primary stream heat capacity
cpss	--	COMMON pands		J kg^{-1}		Secondary stream heat capacity
cpsum	--	COMMON cchemi		J kg^{-1} K^{-1}		Heat capacity of gas
cso2	nsnode	COMMON ratesx		mol cm^{-3}		SO_2 concentration at sorbent particle subshell
delrrj	--	COMMON rcont				Tolerance for reaction rate
delta	numspe	COMMON gparam		--		Stockmayer parameter
deltpj	--	COMMON rcont		K		Tolerance for particle temperature
den	numxpt, numypt	COMMON flupr	ρ	kg m^{-3}	2-55	Gas mixture density
densct	--	COMMON pvar		kg kmol^{-1}		Coal offgas density
densf0	--	COMMON f1af0	\	kg m^{-3}		Density of f=0 stream

FORTRAN Variable	FORTRAN Dimensions	FORTRAN Common Block or Routine	User's Manual Nomenclature	Units	User's Manual Eq. Nos.	Definition
densf1	--	COMMON flaf0		kg m^{-3}		Density of f=1 stream
densinlet	numlet	COMMON adflo		kg m^{-3}		Density for additional inlet
densmh	--	COMMON magnussen		kg m^{-3}		Density of stoichiometric product (Magnussen-Hjertager method)
densp	--	COMMON pands		kg m^{-3}		Primary stream density
denss	--	COMMON pands		kg m^{-3}		Secondary stream density
diach	--	COMMON gridl		m		Reactor chamber diameter
diap	--	COMMON noxmn1		m		Primary tube diameter
dias	--	COMMON pdim		m		Secondary tube diameter
difm	numspe	COMMON difus		m^2 s^{-1}		Species molecular diffusivity
disbuq	--	COMMON diso		--		Debug flag for discrete ordinates submodel
DP1	--	COAL2		m		Particle diameter
dp1	--	COMMON traj		m		Particle diameter

FORTRAN Variable	FORTRAN Dimensions	FORTRAN Common Block or Routine	User's Manual Nomenclature	Units	User's Manual Eq. Nos.	Definition
dt	--	COMMON pecor		s		Time step of integration along a particle trajectory
du	numxpt, numypt	COMMON pcor				
dum1,..., dum8	numxpt, numypt	COMMON fluprz		--		Dummy arrays for debugging
dv	numxpt, numypt	COMMON pcor				
dxep	numxpt	COMMON geom		m		Distance between p-node and its east neighbor
dxepu	numxpt	COMMON uvel		m		Distance between u-velocity node and its east neighbor
dxpw	numxpt	COMMON geom		m		Distance between p-node and its west neighbor
dxpwu	numypt	COMMON uvel		m		Distance between u-velocity node and its west neighbor
dynp	numypt	COMMON geom		m		Distance between p-node and its north neighbor
dynpv	numypt	COMMON vvel		m		Distance between v velocity node and north neighbor
dyps	numypt	COMMON geom		m		Distance between p-node and its south neighbor

FORTRAN Variable	FORTRAN Dimensions	FORTRAN Common Block or Routine	User's Manual Nomenclature	Units	User's Manual Eq. Nos.	Definition
dypsv	numypt	COMMON vvel		m		Distance between v velocity node and south neighbor
e	numxpt, numypt	COMMON fluc		--		Equivalence ratio
e1frwd	--	COMMON rmscom		cal K^{-1}		Zel'dovich forward rate 1f activation energy
e2frwd	--	COMMON rmscom		cal K^{-1}		Zel'dovich foward rate 2f activation energy
e2rev	--	COMMON rmscom		cal K^{-1}		Zel'dovich reverse rate 2r activation energy
e3rev	--	COMMON rmscom		cal K^{-1}		Zel'dovich reverse rate 3r activation energy
ebi	--	COMMON bcrad		W m^{-2} K		Blackbody emissive power for west wall
ebo	--	COMMON bcrad		W m^{-2} K		Blackbody emissive power for exit plane
eboe	--	COMMON bcrad				Blackbody emissive power for east wall
ebu	--	COMMON bcrad		W m^{-2} K		Blackbody emissive power for north wall
ed	numxpt, numypt	COMMON var				Eddy dissipation of turbulent energy
efac	numxpt	COMMON geom		--		Geometric factor
ehss1	--	COMMON rmscom		cal K^{-1}		DeSoete rate 1 activation energy

FORTRAN Variable	FORTRAN Dimensions	FORTRAN Common Block or Routine	User's Manual Nomenclature	Units	User's Manual Eq. Nos.	Definition
ehss2	--	COMMON rmscom		cal K^{-1}		DeSoete rate 2 activation energy
ehss3	--	COMMON rmscom		cal K^{-1}		DeSoete rate 3 activation energy
ehss4	--	COMMON rmscom		cal K^{-1}		DeSoete rate 4 activation energy
ek	numspe	COMMON gparam		K		Lennard-Jones parameter
el	numpar,numoxd	COMMON rrat		J K^{-1}		Char reaction activation energy
elog	--	COMMON turb		--		Constant in law of the wall
emj	numpar,numdev	COMMON rrat		J kg^{-1}		Coal reaction activation energy
emm	numpar,numoxd	COMMON rrat				Reaction rate parameter for char reaction
emt1	--	COMMON rmscom		cal K^{-1}		Mitchell and Tarbell rate 1 activation energy
emt2a	--	COMMON rmscom		cal K^{-1}		Mitchell & Tarbell rate 2a activation energy
emt2b	--	COMMON rmscom		cal K^{-1}		Mitchell & Tarbell rate 2b activation energy
emt3	--	COMMON rmscom		cal K^{-1}		Mitchell & Tarbell rate 3 activation energy
emw	--	COMMON bcrad				Wall emissivity

FORTRAN Variable	FORTRAN Dimensions	FORTRAN Common Block or Routine	User's Manual Nomenclature	Units	User's Manual Eq. Nos.	Definition
enfac	numypt	COMMON geom		--		Geometric factor
eoxyeq	--	COMMON rmscom				Equilibrium constant
eoxyqe	--	COMMON rmscom				Equilibrium constant
epsd	--	COMMON grid1		--		Radial cell contraction factor
epsdp	--	COMMON grid1		--		Cell expansion factor
epsi	--	COMMON grid1		--		Radial cell expansion factor
epsic	numxpt, numypt	COMMON krad				Blackbody emissive power
epsx	--	COMMON grid1		--		Axial cell expansion factor
eqtest	--	COMMON ratpar		--		Local equivalence ratio test criterion used to determine the method used to estimate atomic oxygen concentrations
er	--	COMMON cparam				Equivalence ratio
erct	--	COMMON pvar		--		Coal offgas equivalence ratio
erf0	--	COMMON f1af0				Equivalence ratio of f=0 stream
erf1	--	COMMON f1af0				Equivalence ratio of f=1 stream

FORTRAN Variable	FORTRAN Dimensions	FORTRAN Common Block or Routine	User's Manual Nomenclature	Units	User's Manual Eq. Nos.	Definition
ermh	--	COMMON magnusse n		--		Equivalence ratio of product stream (Magnussen-Hjertager method)
erp	--	COMMON pands		--		Primary stream equivalence ratio
ers	--	COMMON pands		--		Secondary stream equivalence ratio
eta	--	COMMON cmatri		--		Under-relaxation factor for Newton-Raphson correction variables
eta	--	COMMON cmatri		--		Under-relaxation for Newton-Raphson correction variables
eta	numxpt, numypt	COMMON cgasmf				Coal gas mixture fraction
etastm	--	COMMON magnusse n		--		Stoichiometric value of η
ewdt1	--	COMMON rmscom		cal K^{-1}		Wendt rate 1 activation energy
ewdt2	--	COMMON rmscom		cal K^{-1}		Wendt rate 2 activation energy
exvoid	--	COMMON ratesx		--		Sorbent particle void fraction
f	numxpt, numypt	COMMON var		--		Mixture fraction

FORTRAN Variable	FORTRAN Dimensions	FORTRAN Common Block or Routine	User's Manual Nomenclature	Units	User's Manual Eq. Nos.	Definition
fback	--	COMMON rrat		--		Fraction of volatiles enthalpy fed back directly to the particle
fbar	--	COMMON radcon	$\overline{f}$	--	2-148	Forward-scattered component of radiation
fcthcn	--	COMMON nxmisc		--		Fraction of frozen HCN concentrations used to initialize HCN field throughout the coal reactor
fctno	--	COMMON nxmisc		--		Fraction of frozen NO concentrations used to initialize NO field throughout the coal reactor
fgdvc	--	COMMON afr				.TRUE. = FG-DVC submodel used for devolatilization .FALSE. = simple weight-loss submodel used
flo	numlet	COMMON adflo		kg s^{-1}		Mass flowrate of additional inlets
floc	numlet	COMMON adflo				Character representation of additional inlets ('1', etc.)

FORTRAN Variable	FORTRAN Dimensions	FORTRAN Common Block or Routine	User's Manual Nomenclature	Units	User's Manual Eq. Nos.	Definition
flof	numlet	COMMON adflo				Mixture fraction in additional inlets
flot	numlet	COMMON adflo				Additional inlet flow type (north wall, west wall)
flowin	--	COMMON kaset1		$kg \cdot s^{-1}$		Total gas flow entering the reactor
flown	--	COMMON flin		$kg\ s^{-1}$		The flow into the chamber from the north wall
FLOWPR	--	Common CGSFLO	$\dot{m}_p$	$kg\ s^{-1}$		Mass flowrate of primary gas
flowpr	--	COMMON cgsflo		$kg\ s^{-1}$		Primary gas flowrate
flowse	--	COMMON cgsflo		$kg\ s^{-1}$		Secondary gas flowrate
floww	--	COMMON flin		$kg\ s^{-1}$		The flow into the chamber from the west wall additional inlets
fmu	numxpt,n umypt	COMMON turb		--		Function in laminarization extenstion to turbulence submodel
fn2prt	--	COMMON ratpar		--		Partitioning factor of coal or char nitrogen between gaseious HCN and NH_3

FORTRAN Variable	FORTRAN Dimensions	FORTRAN Common Block or Routine	User's Manual Nomenclature	Units	User's Manual Eq. Nos.	Definition
fpract	--	COMMON flin		kg s^{-1}		The real flowrate in the primary calculated by the program
fprim	--	COMMON flin		--		Mixture fraction in primary (normally 1.0)
fr	numxpt,numypt	COMMON varr		J m^{-2} s^{-1}		Radial radiation flux sum
frch2s	numxpt, numypt	COMMON ratesx		--		Fraction of sulfur forming H_2S
frcso2	numxpt, numypt	COMMON ratesx		--		Fraction of sulfur forming SO_2
fsec	--	COMMON flin		--		Mixture fraction in secondary (normally 0.0)
fsl	numstr	COMMON cpart		--		Fraction of particles for each starting location
fsls	numstr	COMMON cpart		--		Fraction of sorbent particles for each starting locations
fsto	--	COMMON fluc		--		Stoichiometric value of *f*
fsum	--	COMMON pecor		J m^{-2} s^{-1}		Radiation flux sum
ftheta	numxpt,numypt	COMMON varr		J m^{-2} s^{-1}		Tangential radiation flux sum
fuelno	--	COMMON ratpar		--		.TRUE. causes fuel NO to be calculated

FORTRAN Variable	FORTRAN Dimensions	FORTRAN Common Block or Routine	User's Manual Nomenclature	Units	User's Manual Eq. Nos.	Definition
fupper	--	COMMON cgauss				Adjusted value of afbar
fx	numxpt,numypt	COMMON varr		J m^{-2} s^{-1}		Axial radiation flux sum
g	numxpt,numypt	COMMON var		--		Variance in mixture fraction
gam	numxpt,numypt	COMMON cset				
gamma	--	COMMON pecor		--		Particle swelling coefficient
gasmw	--	COMMON traj		kg $kmol^{-1}$		Gas mol. wt.
gen	numxpt,numypt	COMMON turb				Generation of turbulent kinetic energy
geta	numxpt, numypt	COMMON cgasmf				Variance in coal gas mixture fraction
GMW	--	Common GPARAM	M_g	kg $kmol^{-1}$	2-131	Gas mixture mol. wt.
gmw	--	COMMON gparam		kg $kmol^{-1}$		Gas mixture molecular weight
qrdout	--	COMMON grid1		--		.TRUE. causes a grid file to be written
qreat	--	COMMON all				A large number
gupper	--	COMMON cgauss				Adjusted value of ag
h	numxpt,numypt	COMMON var	h	J kg^{-1}	2-89	Gas enthalpy

FORTRAN Variable	FORTRAN Dimen-sions	FORTRAN Common Block or Routine	User's Manual Nomen-clature	Units	User's Manual Eq. Nos.	Definition
h0	numspe	COMMON cspece				Molar enthalpy of each species
ha	--	COMMON traj		J kg^{-1}		Ash component enthalpy
ha0	numpar	COMMON href		J kg^{-1}		Heat form. for ash
haex	--	COMMON hcap		J kg^{-1}		Ash enthalpy at 298 K
hc	--	COMMON traj		J kg^{-1}		Coal component enthalpy
hc0	numpar	COMMON href		J kg^{-1}		Heat form. for raw coal
hcex	--	COMMON hcap		J kg^{-1}		Raw coal enthalpy at 298 K
hcg0	42	COMMON hcapfg		J kg^{-1}		Std. heat comb. for FG-DVC volatiles
hcnmw	--	COMMON intrat		kg kmol^{-1}		HCN mol. wt.
hcnmw	--	COMMON psccom		kg kmol^{-1}		HCN mol. wt.
hevolv	--	COMMON afr				Hydrogen evolution parameter
HF0	--	Common FLUPR				Enthalpy of f=0 stream
hf0	--	COMMON flaf0		J kg^{-1}		Enthalpy of f=0 stream
HF1	--	Common FLUPR		J kg^{-1}		Enthalpy of f=1 stream
hf1	--	COMMON flaf0		J kg^{-1}		Enthalpy of f=1 stream

FORTRAN Variable	FORTRAN Dimensions	FORTRAN Common Block or Routine	User's Manual Nomenclature	Units	User's Manual Eq. Nos.	Definition
hfg0	42	COMMON hcapfg		J kg^{-1}		Std. heat form. for FGDVC volatiles
hform	numspe	COMMON gparam		J kmol^{-1}		Species standard heat of formation
hg	numpar	COMMON difeqn		J kg^{-1}		Coal offgas enthalpy
hgv	numpar, numdev	COMMON chetrx		J kg^{-1}		hgv(j,i) is the heat of reaction of the ith devolatilization reaction for the jth particle
HH	--	Common TRAJ	h_{hj}		2-125	Char enthalpy for the jth particle classification.
hh	--	COMMON traj		J kg^{-1}		Char component enthalpy
hh0	numpar	COMMON href		J kg^{-1}		Heat form. for char
hhex	--	COMMON hcap		J kg^{-1}		Char enthalpy at 298 K
hinc	numxpt	COMMON diso		kw m^{-2}		Incident radiation heat flux on north wall
hinlet	numlet	COMMON adflo		J kg^{-1}		Enthalpy for additional inlet
hloss	--	COMMON bug		--		Specified heat loss factor for ihloss=.TRUE.

FORTRAN Variable	FORTRAN Dimensions	FORTRAN Common Block or Routine	User's Manual Nomenclature	Units	User's Manual Eq. Nos.	Definition
hmh	--	COMMON magnussen		J kg^{-1}		Enthalpy of stoichiometric product (Magnussen-Hjertager method)
hnet	numxpt	COMMON diso		kw m^{-2}		Net radiation heat flux on side walls
hp, hp2, hp3, hp4	--	COMMON difeqn		J kg^{-1}		Particle enthalpy
hp0	numpar	COMMON ippar		J kg^{-1}		Initial particle enthalpy
hp0t	--	COMMON pvar		J kg^{-1}		Coal offgas enthalpy
HPRIM	--	Common FLUPR		J kg^{-1}		Enthalpy of primary gas
hprim	--	COMMON fluc		J kg^{-1}		Enthalpy of primary gas
hresid	numxpt,numypt	COMMON resid		J kg^{-1}		Residual enthalpy
hrfm	--	COMMON buq		J kg^{-1}		Fully mixed enthalpy assuming complete burnout and no heat loss
HSEC	--	Common FLUPR		J kg^{-1}		Enthalpy of secondary gas
hsec	--	COMMON fluc		J kg^{-1}		Enthalpy of secondary gas

FORTRAN Variable	FORTRAN Dimensions	FORTRAN Common Block or Routine	User's Manual Nomenclature	Units	User's Manual Eq. Nos.	Definition
hspex	numspe	COMMON spece		J kmol^{-1}		Relative enthalpy of each species at 298 K
HSUB0	--	Common CPARAM		J kg^{-1}		Mixture enthalpy
hsub0	--	COMMON cparam		J kg^{-1}		Enthalpy
hsum	--	COMMON cmatri				Reduced total enthalpy (hsub0/rgas/tk)
hsum	--	COMMON cmatri				Reduced total enthalpy (hsub0/rt)
htrack	--	COMMON afr				.TRUE. = f tracks H; η tracks C, O, N, and S in coal offgas .FALSE. = η tracks coal volatiles; f tracks char oxidation offgas (C)[1]
huge1	numspe*n uminc*nu minc*num ele	COMMON rtmtab				Auxilliary array for gas physical properties table

[1] ineta2 must be .TRUE. for either option of htrack.

FORTRAN Variable	FORTRAN Dimensions	FORTRAN Common Block or Routine	User's Manual Nomenclature	Units	User's Manual Eq. Nos.	Definition
huge2	7*numinc *numinc* numele	COMMON rtmtab				Auxilliary array for gas physical properties table
huge3	9*numinc	COMMON rtmtab				Auxilliary array for gas physical properties table
huge4	2*numinc *numinc	COMMON rtmtab				Auxilliary array for gas physical properties table
hw	--	COMMON traj		$J\ kg^{-1}$		Slurry liquid component enthalpy
hw0	numpar	COMMON href		$J\ kg^{-1}$		Heat form. for slurry liquid
hwex	--	COMMON hcap		$J\ kg^{-1}$		Slurry liquid enthalpy at 298 K
idc2h2	--	COMMON cndxcg		--		Species id for C_2H_2
idc2h2	--	COMMON cndxcg		--		Species id no. for C_2H_2
idc2h4	--	COMMON cndxcg		--		Species id for C_2H_4
idc2h4	--	COMMON cndxcg		--		Species id no. for C_2H_4
idch4	--	COMMON cindex		--		Species id for CH_4
idco	--	COMMON cindex		--		Species id for CO
idco2	--	COMMON cindex		--		Species id for CO_2
idcos	--	COMMON cindex		--		Species id for COS

FORTRAN Variable	FORTRAN Dimensions	FORTRAN Common Block or Routine	User's Manual Nomenclature	Units	User's Manual Eq. Nos.	Definition
idcs	--	COMMON cindex	--			Species id for idcs
idcs2	--	COMMON cindex	--			Species id for CS_2
idh2	--	COMMON cindex	--			Species id for H_2
idh2o	--	COMMON cindex	--			Species id for H_2O
idh2ol	--	COMMON cindex	--			Species id for $H_2O(l)$
idh2s	--	COMMON cindex	--			Species id for H_2S
idn2	--	COMMON cindex	--			Species id for N_2
idnh3	--	COMMON cindex	--			Species id for NH_3
idno	--	COMMON cindex	--			Species id for NO
ido2	--	COMMON cindex	--			Species id for O_2
idoh	--	COMMON cindex	--			Species id for OH
ids2	--	COMMON cndxcg	--			Species id for S_2
ids2	--	COMMON cndxcg	--			Species id no. for S_2
idslgs	--	COMMON cindex	--			Species id for evaporated slurry liquid

FORTRAN Variable	FORTRAN Dimensions	FORTRAN Common Block or Routine	User's Manual Nomenclature	Units	User's Manual Eq. Nos.	Definition
idsllq	--	COMMON cindex		--		Species id for condensed slurry liquid
idso2	--	COMMON cindex		--		Species id for SO_2
idso3	--	COMMON cindex		--		Species id for SO_3
ieuck	--	COMMON icon		--		Flag for gas thermal conductivity eq. 1= Eucken 0= Sage-Galloway
igasv	--	COMMON cpart		--		0=Constant gas properties across a cell 1=1-D interpolation 2=2-D interpolation
ihcps	--	COMMON cindex		--		Flag for calculating entropy of formation in subroutine hcps
ihi	numlet	COMMON adflo				i node boundary for additional inlet
ihlos	--	COMMON bug				.TRUE. calculates external heat loss using a specified, uniform heat loss factor
ilc	--	COMMON cindex		--		Element id for C

FORTRAN Variable	FORTRAN Dimensions	FORTRAN Common Block or Routine	User's Manual Nomenclature	Units	User's Manual Eq. Nos.	Definition
ilh	--	COMMON cindex	--			Element id for H
iln	--	COMMON cindex	--			Element id for N
ilo	--	COMMON cndxcg	--			Element id for O
ilo	--	COMMON cndxcg	--			Element id no. for oxygen
ilow	numlet	COMMON adflo				i node boundary for additional inlet
ils	--	COMMON cndxcg	--			Element id for S
ils	--	COMMON cndxcg	--			Element id no. for sulfur
imat	--	COMMON cindex	--			Matrix dimension in equilibrium calculations
imon	--	COMMON pard	--			Axial node for monitor cell
imstif	--	COMMON pecor	--			.TRUE. means the particle enthalpy equation has gone stiff
inaimp	--	COMMON pcor	--			.TRUE. calls aim subroutine to solve finite difference equations

FORTRAN Variable	FORTRAN Dimensions	FORTRAN Common Block or Routine	User's Manual Nomenclature	Units	User's Manual Eq. Nos.	Definition
inaimu	--	COMMON uvel		--		.TRUE. uses aim routine to solve u-velocity finite difference equations
incald	--	COMMON turb		--		.TRUE. causes ed to be calculated
incalf	--	COMMON tabrit		--		.TRUE. includes f calculations
incalg	--	COMMON fluc		--		.TRUE. results in g_f being calculated
incalk	--	COMMON turb		--		.TRUE. causes te to be calculated
incaln	--	COMMON eulp		--		Flag for performing particle no. density calculations
incalp	--	COMMON simple		--		.TRUE. for calculating pressure equation
incalv	--	COMMON simple		--		.TRUE. for calculating radial velocity
incalyfu	--	COMMON magnusse n		--		.TRUE. causes yfu to be calculated (Magnussen-Hjertager method)
incfp	--	COMMON propin		--		.TRUE. causes gas phase turbulence to be corrected for particles
inclet	--	COMMON tabrit		--		.TRUE. includes eta calculations

FORTRAN Variable	FORTRAN Dimensions	FORTRAN Common Block or Routine	User's Manual Nomenclature	Units	User's Manual Eq. Nos.	Definition
inclge	--	COMMON tabrit	--			.TRUE. includes geta calculations
includ	--	PARAMETER	--			Flag indicating that a species or solution if currently included in the equilibrium system
incnox	--	COMMON type	--			.TRUE. causes NO_x calculations to be performed
incoal		COMMON cflag	--			.TRUE. means the condensed phase contains reacting coal or char
increk	--	COMMON fluc	--			.TRUE. causes a physical properties table to be generated
incrs	--	COMMON pecor	--			Flag for increasing the step size for integrating particle trajectories
incswp	--	COMMON swrl	--			.TRUE. includes swirl in the primary
incsws	--	COMMON swrl	--			.TRUE. includes swirl in the secondary
inden	--	COMMON propin	--			.TRUE. causes gas density to be calculated

FORTRAN Variable	FORTRAN Dimensions	FORTRAN Common Block or Routine	User's Manual Nomenclature	Units	User's Manual Eq. Nos.	Definition
indpnx	--	COMMON nxmisc		--		Number of iterations of the NO model between intermediate printouts
indpri	--	COMMON eulp		--		Frequency of printout
ineta2	--	COMMON afr				.TRUE. = both f and η used to track coal offgas .FALSE = f tracks primary gas and η tracks coal offgas
infsou	--	COMMON cpsef		--		.TRUE. causes source term to be included in f equation
inhtnx	--	COMMON ratpar		--		.TRUE. will include heterogeneous NO reduction reaction
initpr	--	COMMON propin		--		Calculational control variable
innozz	--	COMMON grid1		--		.TRUE. causes the nozzle option to be used for grid generation
inprim	--	COMMON strfnc		--		.TRUE. if there is a primary stream
inprin	--	COMMON prin		--		.TRUE. causes printout to be printed

FORTRAN Variable	FORTRAN Dimensions	FORTRAN Common Block or Routine	User's Manual Nomenclature	Units	User's Manual Eq. Nos.	Definition
inprst	--	COMMON cpeul		--	--	.TRUE. reads a particle restart file
inqrl	--	COMMON grid1		--		.TRUE. includes a quarl region
inrad	--	COMMON varr		--		.TRUE. solves radiation equations
inrdgd	--	COMMON grid1		--		.TRUE. causes a grid file to be read
inrst	--	COMMON flin		--		.TRUE. will call restrt subroutine
insec	--	COMMON strfnc		--		.TRUE. if there is a secondary stream
insimp	--	COMMON simple		--		.TRUE. for SIMPLER algorithm
insmpc	--	COMMON simple		--		.TRUE. for including SIMPLEC approximation
insorb		COMMON cflag		--		.TRUE. results in the sorbent particle reactions submodel being called after convergence of the gas and particle flowfield
INSTEP	Logical	Common TUBWAL	--		--	True if DIAS ≠ DIACH
instep	--	COMMON tubwal		--		.TRUE. means dias is smaller than diach

FORTRAN Variable	FORTRAN Dimensions	FORTRAN Common Block or Routine	User's Manual Nomenclature	Units	User's Manual Eq. Nos.	Definition
intabl	--	COMMON propin		--		.TRUE. causes gas physical properties table to be calculated
intfrz	--	COMMON buq				.TRUE. uses "frozen" equilibrium properties
intime	--	COMMON calcyi		--		.TRUE. writes cpu time information for NO_x calculations in log file
intr	numxpt, numypt	COMMON intruz		--		1=intrusion (wall) 0=flowfield or inlet
intrst	--	COMMON bug				.TRUE. uses a table restart file
intrus	--	COMMON intruz		--		.TRUE. allows for intrusions to be read in
intube	--	COMMON tubwal		--		.TRUE. means there is a primary tube
ipltnx	--	COMMON nxmisc		--		.TRUE. will write files for plots from NO model calculations
ipref	--	COMMON pcor		--		Axial node of pressure reference cell
iprintr	--	COMMON varr		--		Frequency of printing radiation calculations intermediate results

FORTRAN Variable	FORTRAN Dimensions	FORTRAN Common Block or Routine	User's Manual Nomenclature	Units	User's Manual Eq. Nos.	Definition
ipsict	--	COMMON type	--			.TRUE. causes particle calculations to be performed
iquarl	--	COMMON gridl	--			Axial node at edge of quarl
ireduc	--	COMMON pecor	--			Flag for reducing the step size for integrating particle trajectories
irstno	--	COMMON nxmisc	--			.TRUE. will use a restart file to begin NO model computations and output intermediate NO model restart files
istep	--	COMMON kaset1	--			First axial node outside the quarl
istm1	--	COMMON gridl	--			Last axial node in the quarl region
istrt	--	COMMON flin	--			0 will read restrt information from file 1 will write restrt information to file
it	--	COMMON all				Maximum possible no. of x nodes
iter	--	COMMON cindex	--			Iteration counter

FORTRAN Variable	FORTRAN Dimensions	FORTRAN Common Block or Routine	User's Manual Nomenclature	Units	User's Manual Eq. Nos.	Definition
itynx	--	COMMON nxmisc		--		Number of iterations of the NO model between intermediate typing of the residuals
itype	--	COMMON pard		--		Frequency of printout
ius	numstr	COMMON cpart		--		U-cell no. for particle trajectory starting locations
ivs	numstr	COMMON cpart		--		V-cell no. for particle trajectory starting locations
iwall	numypt	COMMON bound				Axial node location of the wall for each radial node
jhi	numlet	COMMON adflo				j node boundary for additional inlet
jlow	numlet	COMMON adflo				j node boundary for additional inlet
jmon	--	COMMON pard		--		Radial node for monitor cell
jpref	--	COMMON pcor		--		Radial node of pressure reference cell
jprim	--	COMMON noxmn1		--		Outermost radial node in primary duct
jquarl	--	COMMON grid1		--		Radial node at edge of quarl

FORTRAN Variable	FORTRAN Dimensions	FORTRAN Common Block or Routine	User's Manual Nomenclature	Units	User's Manual Eq. Nos.	Definition
jsec	--	COMMON noxmn1		--		Outermost radial node in secondary duct
jstep	--	COMMON kaset1		--		First radial node in the wall outside the primary and secondary
jstp1	--	COMMON kaset1		--		jstep+1
jt	--	COMMON all				Maximum possible no. of y nodes
jtubid	--	COMMON tubwal		--		No. of the innermost radial node in the primary tube wall
jtubod	--	COMMON tubwal		--		No. of the outermost radial node in the primary tube wall
jus	numstr	COMMON cpart		--		j-nodes for u-cells for particle starting locations
jvs	numstr	COMMON cpart		--		j-nodes for v-cells for particle starting locations
jwall	numxpt	COMMON bound				Radial node location of the wall for each axial node
KCJ	NUMOXD	COAL2	k_{ci}	m s^{-1}	2-134	Mass transfer coefficient.

FORTRAN Variable	FORTRAN Dimensions	FORTRAN Common Block or Routine	User's Manual Nomenclature	Units	User's Manual Eq. Nos.	Definition
keq	--	COMMON icon		--		1=linear form of Field eq. used for char oxidation when T>1400 K
kq	--	COMMON gparam		$J\ m^{-1}\ K^{-1}\ s^{-1}$		Gas mixture thermal conductivity
ki	numspe	COMMON gparam		$J\ m^{-1}\ K^{-1}\ s^{-1}$		Species thermal conductivity
KL	--	COAL2	k_{il}	$m\ s^{-1}$	2-132	Char reaction kinetic rate coefficient.
ksootab	numxpt, numypt	COMMON krad				Radiation coefficient for soot
ksootem	numxpt, numypt	COMMON krad				Radiation coefficient for soot
laminar	--	COMMON afr				.TRUE. = laminar transport properties calculated locally .FALSE. = laminar transport properties approximated globally or neglected
lbuoy	--	COMMON afr				.TRUE. = gas buoyancy included in axial direction .FALSE. = gas buoyancy neglected

FORTRAN Variable	FORTRAN Dimensions	FORTRAN Common Block or Routine	User's Manual Nomenclature	Units	User's Manual Eq. Nos.	Definition
lconvg	--	COMMON cchemi	--			.TRUE. = convergence was obtained in equilibrium algorithm
ldebug	--	COMMON cparam	--			Debug print flag
ldiso	--	COMMON diso	--			.TRUE. calls the discrete ordinates radiation submodel
lemcor	--	COMMON radcon	--			.TRUE. incorporates correction to gas emissivity due to spectral overlap
leulp	--	COMMON eulp	--			Flag for performing Eulerian particle calculations
lgase	--	COMMON radcon	--			.TRUE. includes gas radiation
lmoles	--	COMMON rcards	--			.TRUE. causes stream composition to be taken in terms of mole fraction
lmrck	--	COMMON mrck	--			Merrick heat capacity model used if .TRUE.
lmrcka	--	COMMON mrck	--			Merrick heat capacity model used for ash if .TRUE.

FORTRAN Variable	FORTRAN Dimensions	FORTRAN Common Block or Routine	User's Manual Nomenclature	Units	User's Manual Eq. Nos.	Definition
lmrckc	--	COMMON mrck		--		Merrick heat capacity model used for coal if .TRUE.
lmrckh	--	COMMON mrck		--		Merrick heat capacity model used for char if .TRUE.
lnjcon	--	COMMON pard		--		.TRUE. when particle no. density eqns. converged
logs2	numspe	COMMON cparam				log(s2)
lpartp	--	COMMON cpart		--		.TRUE. if particles in primary stream
lparts	--	COMMON cpart		--		.TRUE. if particles in secondary stream
lpbug	--	COMMON cpart		--		Debug flag for particle submodel
lplaw	--	COMMON swpdir		--		.TRUE. for power-law differencing
lplot	--	COMMON cpart		--		Plotting flag
lprop	--	COMMON dens1		--		Flag for calculating gas-phase properties
lrbnd	--	COMMON cpart		--		.TRUE. = particles rebound when they hit the wall .FALSE. = particles stick when they hit the wall

FORTRAN Variable	FORTRAN Dimensions	FORTRAN Common Block or Routine	User's Manual Nomenclature	Units	User's Manual Eq. Nos.	Definition
lrbnds	--	COMMON cpart		--		.TRUE. = sorbent particle rebound from the wall .FALSE. = sorbent particles stick to the wall
lreact	--	COMMON afr				.TRUE. = char reactivity based on char structure .FALSE. = char reactivity calculated from empirical kinetics
lrlam	--	COMMON afr				.TRUE. = laminarization terms included in k-ε submodel .FALSE. = laminarization terms neglected
lsoot	--	COMMON radcon		--		.TRUE. includes soot radiation (soot based on equilibrium solid carbon).
lspbug	--	COMMON cpart		--		Debug flag for sorbent particles
lsph	--	COMMON cpart		--		Flag for calculating sph
lsplot	--	COMMON cpart		--		Plotting flag for sorbent particles

FORTRAN Variable	FORTRAN Dimensions	FORTRAN Common Block or Routine	User's Manual Nomenclature	Units	User's Manual Eq. Nos.	Definition
lspm	--	COMMON cpart	--			Flag for calculating spm
lspu	--	COMMON cpart	--			Flag for calculating spu
lspv	--	COMMON cpart	--			Flag for calculating spv
lswpew, lswpns	--	COMMON swpalt	--			.TRUE. for east-west or north-south sweep direction
lswpwe, lswpsn	--	COMMON swpdir	--			.TRUE. for west-east or south-north sweep direction
lsyps	--	COMMON cpart	--			.TRUE. allows the user to specify sorbent starting locations
ltbuq	--	COMMON bug				.TRUE. turns on debugging for table generation
ltmptq	--	COMMON traj	--			.TRUE. allows small particles to follow the gas temp. after heatup
lwans	--	COMMON cpart	--			.TRUE. causes particle source terms and density to be written to restart file
lyps	--	COMMON cpart	--			.TRUE. allows the user to specify starting locations

FORTRAN Variable	FORTRAN Dimensions	FORTRAN Common Block or Routine	User's Manual Nomenclature	Units	User's Manual Eq. Nos.	Definition
maghjer	--	COMMON magnusse n	--			.TRUE. performs Magnussen-Hjertager calculations for gas properties
maxels	--	PARAMETE R	--			Same as numele
maxit	--	COMMON pard	--			Max. no. gas iterations
maxitp	--	COMMON cpart	--			Maximum no. of particle iterations
maxitr	--	COMMON radcon	--			Max. iterations for radiation submodel
maxpur	--	PARAMETE R	--			Maximum number of pure condensed phase species allowed in the system
maxres	--	COMMON nxmisc	--			Maximum normalized value of residual source for convergence of NO_x/SO_x submodels
maxres	--	COMMON sxmisc	--			Max. residual source sum for convergence of SO_x/NO_x calculations

FORTRAN Variable	FORTRAN Dimensions	FORTRAN Common Block or Routine	User's Manual Nomenclature	Units	User's Manual Eq. Nos.	Definition
maxsol	--	PARAMETER		--		Maximum no. of solutions allowed (including the gas phase as a solution)
maxsp	--	PARAMETER		--		Same as numspe
MH	NUMPAR	Common PFAC	M_{hi}	kg kmol^{-1}	2-131	Average atomic wt. of raw coal in each particle size.
mh	numpar	COMMON pfac		kg kmol^{-1}		Mol. wt. of the char
minitp	--	COMMON cpart		--		Maximum no. of gas iterations for overall convergence
mu	numspe	COMMON gparam		kg m^{-1} s^{-1}		Species viscosity
muq	--	COMMON gparam		kg m^{-1} s^{-1}		Gas mixture viscosity
mwfg	42	COMMON hcapfg		kg kmol^{-1}		Mol. wt. of FG-DVC volatiles
mxitjt	--	COMMON all				Maximum of it and jt
mxitnx	--	COMMON noxrte		--		Max. iterations for NO_x submodel
mxitsx	--	COMMON soxrte		--		Max.SO_x iterations
n1	--	COMMON cindex		--		nlm+1
n2	--	COMMON cindex		--		nlm+2

FORTRAN Variable	FORTRAN Dimensions	FORTRAN Common Block or Routine	User's Manual Nomenclature	Units	User's Manual Eq. Nos.	Definition
n3	--	COMMON cindex	--			nlm+3
na	--	COMMON cindex	--			ns+3
nc	--	COMMON ctable	--			No. of components (gas species)
ncncal	--	COMMON cparam	--			No. of pure species in the calculation
ncond	--	COMMON cparam	--			No. of pure species
ncrxn	--	COMMON icon	--			No. of coal reactions
ndebug	--	COMMON cparam	--			Debug print: Higher the number, the more the print
ndia	--	COMMON grid1	--			Length of reactor in no. of chamber diameters
nhrxn	--	COMMON icon	--			No. of char reactions
ni	--	COMMON all				No. of x nodes
niinq	--	COMMON grid1	--			No. of axial nodes in quarl region
nim1	--	COMMON all				No. of x nodes minus 1
ninlet	--	COMMON adflo				No. of additional inlets (beyond the primary and secondary)

FORTRAN Variable	FORTRAN Dimensions	FORTRAN Common Block or Routine	User's Manual Nomenclature	Units	User's Manual Eq. Nos.	Definition
niter	--	COMMON all				No. of gas iterations
niterp	--	COMMON cpart		--		No. of particle iterations
nitnox	--	COMMON noxrte		--		Iter no. for NO_x submodel
nitsox	--	COMMON soxrte		--		No. SO_x iterations
niwoq	--	COMMON grid1		--		No. of axial nodes outside quarl region
nix	numstr,numpar	COMMON cplot		--		No. plotting points for a particle trajectory
nj	--	COMMON all				No. of y nodes
njinp	--	COMMON grid1		--		No. of radial nodes in primary duct
njins	--	COMMON grid1		--		No. of radial nodes in secondary duct
njm1	--	COMMON all				No. of y nodes minus 1
nl	--	COMMON grid1		--		No. of axial nodes to the location all
nlm	--	COMMON cparam		--		No. of elements
notc	--	COMMON pecor		--		1=Raw coal not present in the particle
noth	--	COMMON pecor		--		1=Char not present in the particle

FORTRAN Variable	FORTRAN Dimen-sions	FORTRAN Common Block or Routine	User's Manual Nomen-clature	Units	User's Manual Eq. Nos.	Definition
notw	--	COMMON pecor	--			1=Slurry liquid not present in the particle
noxyd	numoxd	COMMON icon	--			Species id no. for oxidizer
npoint	--	COMMON pecor	--			No. of integration steps along a particle trajectory
nprop	--	COMMON rcont	--			No. of times that coall is called
nps	--	COMMON cpart	--			No. of particle sizes
npss	--	COMMON cpart	--			No. of particle sizes for sorbent
nq	--	COMMON cindex	--			ns+2
nrange	--	PARAMETER	--			Number of temperature intervals in JANAF data
ns	--	COMMON cparam	--			Total no. of species
nsl	--	COMMON cpart	--			No. of particle starting locations
nsls	--	COMMON cpart	--			No. of starting locations for sorbent particles
nsm	--	COMMON cindex	--			ns+1
nsnode	--	PARAMETER	--			Number of nodes in the sorbent particle

FORTRAN Variable	FORTRAN Dimensions	FORTRAN Common Block or Routine	User's Manual Nomenclature	Units	User's Manual Eq. Nos.	Definition
nsol	--	COMMON lution	--			No. of solutions used in equilibrium algorithm
nsswpd	--	COMMON tdis	--			No. of lisolv sweeps for calculating ed
nstype	--	COMMON soxrte	--			1=SO_2 capture 2=H_2S capture
nsubsh	--	PARAMETER	--			Number of sorbent particle subshells
nswpcn	--	COMMON nswps	--			No. lisolv sweeps for HCN
nswpet	--	COMMON cgasmf	--			No. of sweeps by line solver for eta
nswpf	--	COMMON mixfr	--			No. lisolv sweeps for f
nswpq	--	COMMON fluc	--			No. of sweeps for calculating g_f
nswpge	--	COMMON cgasmf	--			No. of sweeps by line solver for geta
nswph	--	COMMON enth	--			No. of line solver sweeps for enthalpy equation
nswpk	--	COMMON ten	--			No. lisolv swee;s for te
nswpnh	--	COMMON nswps	--			No. lisolv sweeps for NH_3
nswpnj	--	COMMON pard	--			No. lisolv sweeps for parden
nswpno	--	COMMON nswps	--			No. lisolv sweeps for NO

FORTRAN Variable	FORTRAN Dimensions	FORTRAN Common Block or Routine	User's Manual Nomenclature	Units	User's Manual Eq. Nos.	Definition
nswpp	--	COMMON pcor	--			No. lisolv sweeps for pp
nswpu	--	COMMON uvel	--			No. lisolv sweeps for u velocity
nswpv	--	COMMON vvel	--			No. lisolv sweeps for v velocity
nswpw	--	COMMON wvel	--			No. lisolv sweeps for w velocity
numdev	--	PARAMETER	--			Maximum number of devolatilization reactions
numele	--	PARAMETER	--			Maximum number of elements
numinc	--	PARAMETER	--			Number of increments used in table routine
numintr	--	PARAMETER	--			Maximum no. of intrusions (including north and west edges)
numlet	--	PARAMETER	--			Maximum no. of additional inlets
numnam	--	PARAMETER	--			Number of words to store species name in
numoxd	--	PARAMETER	--			Maximum no. of oxidation reactions

FORTRAN Variable	FORTRAN Dimensions	FORTRAN Common Block or Routine	User's Manual Nomenclature	Units	User's Manual Eq. Nos.	Definition
numpar	--	PARAMETER		--		Maximum no. of particle sizes
numsol	--	COMMON solution		--		No. solutions defined in equilibrium algorithm
numspe	--	PARAMETER		--		Maximum no. of species
numstr	--	PARAMETER		--		Maximum no. of particle starting locations
numxpt	--	PARAMETER		--		Maximum no. of axial nodes
numypt	--	PARAMETER		--		Maximum no. of radial nodes
o2mw	--	COMMON intrat		kg kmol^{-1}		O_2 mol. wt.
ohadjs	--	COMMON ratpar		--		Flag for adjusting equilibrium concentration
omegaa	--	COMMON omega		--		Mass fraction of ash
omegac	--	COMMON omega		--		Mass fraction of raw coal
omegah	--	COMMON omega		--		Mass fraction of char
omegaw	--	COMMON omega		--		Mass fraction of slurry liquid
omegaw	numpar	COMMON cwater		--		Mass fraction of water in particles

FORTRAN Variable	FORTRAN Dimensions	FORTRAN Common Block or Routine	User's Manual Nomenclature	Units	User's Manual Eq. Nos.	Definition
opl	--	COMMON radcon		m		Optical length
p	numxpt,numypt	COMMON var		Pa		Pressure
pa	--	COMMON cparam		Pa		Pressure
parden	numxpt,numypt,numpar	COMMON cpeul	$\bar{n}_j$		2-35	Particle no. density
pcell	numxpt, numypt	COMMON gmap		--		X = wall cell O = flowfield cell P = primary cell S = secondary cell 1,2,3 = additional inlets
pd	numpar	COMMON cpart		m		Particle sizes
pden	--	COMMON cpart		kg m^3		Particle density
pds	numpar	COMMON cpart		m		Sorbent particle sizes
pecwt	maxrea	COMMON rcards		--		Percent of each reactant in each stream
pfunc	--	COMMON turb				Extra resistance to heat transfer at the wall that arises due to the difference in σ_h and $\sigma_{h,t}$

FORTRAN Variable	FORTRAN Dimensions	FORTRAN Common Block or Routine	User's Manual Nomenclature	Units	User's Manual Eq. Nos.	Definition
PHIL	NUMOXD	Common RRAT	ϕ_1	--	2-96	Moles of carbon required per mole of oxidizer.
phil	numoxd	COMMON rrat		--		Moles of fuel per mole of oxidizer for heterogeneous reaction
pi	--	COMMON geom		--		The number pi
PIE						3.14159
piehcn	numxpt, numypt	COMMON ratecm		--		Deviation from equilibrium for HCN
pien2	numxpt, numypt	COMMON ratecm		--		Deviation from equilibrium for N_2
pienh3	numxpt, numypt	COMMON ratecm		--		Deviation from equilibrium for NH_3
pienof	numxpt, numypt	COMMON ratecm		--		Deviation from equilibrium for NO
pienot	numxpt, numypt	COMMON ratecm		--		Deviation from equilibrium for NO
pieo2	numxpt, numypt	COMMON ratecm		--		Deviation from equilibrium for O_2
pieoh	numxpt, numypt	COMMON ratecm		--		Deviation from equilibrium for OH
pload	--	COMMON cpart		kg kg^{-1}		Total particle loading
ploada	numlet	COMMON cgsflo		kg kg^{-1}		Coal particle loading in additional inlet

FORTRAN Variable	FORTRAN Dimensions	FORTRAN Common Block or Routine	User's Manual Nomenclature	Units	User's Manual Eq. Nos.	Definition
ploadas	numlet	COMMON cgsflo		kg kg^{-1}		Sorbent particle loading in additional inlet
ploadp	--	COMMON cgsflo		kg kg^{-1}		Primary coal particle loading
ploadps	--	COMMON cgsflo		kg kg^{-1}		Primary sorbent particle loading
ploads	--	COMMON cgsflo		kg kg^{-1}		Secondary coal particle loading
ploadss	--	COMMON cgsflo		kg kg^{-1}		Secondary sorbent particle loading
pmf	numpar	COMMON cpart		--		Fraction of particles in each size group
pmfs	numpar	COMMON cpart		--		Particle mass fraction for each size
pmpvr	numxpt,numypt	COMMON arexp				
pnfr	numstr, numpar	COMMON cpart		s^{-1}		Particle no. flowrate
pnfrs	numstr, numpar	COMMON cpart		s^{-1}		Particle no. flowrate for sorbent
pp	numxpt,numypt	COMMON var		Pa		Pressure correction
ppln	--	COMMON cchemi				Natural logarithm of pressure in atm
pprg	--	COMMON gparam		--		Gas mixture Prandtl no.
pred	--	COMMON turb		--		Turbulent Prandtl no. for ed
pres	--	COMMON fluc		Pa		Pressure

FORTRAN Variable	FORTRAN Dimensions	FORTRAN Common Block or Routine	User's Manual Nomenclature	Units	User's Manual Eq. Nos.	Definition
PRESP	--	Common TRAJ		Pa		Local gas pressure (assumed constant across a cell)
presp	--	COMMON traj		Pa		Gas pressure
preta	--	COMMON cgasmf		--		Prandtl no. for eta
prf	--	COMMON turb		--		Turbulent Prandtl no. for f
prg	--	COMMON turb		--		Turbulent Prandtl no. for g
prgeta	--	COMMON cgasmf		--		Prandtl no. for geta
prh2s	--	COMMON ratesx		--		Prandtl no. for H_2S
prhcn	--	COMMON calcyi		--		Prandtl no. for HCN transport
prht	--	COMMON turb		--		Turbulent Prandtl no. for h
prhtl	numxpt, numypt	COMMON fluc		--		Laminar Prandtl no. for heat transfer
prhtlf0	--	COMMON flaf0		--		Prandtl no. for f=0 stream
prhtlf1	--	COMMON flaf0		--		Prandtl no. for f=1 stream
prhtlinlet	numlet	COMMON adflo				Laminar Prandtl no. for additional inlet
prhtlp	--	COMMON pands		--		Primary stream laminar Prandtl no.

FORTRAN Variable	FORTRAN Dimensions	FORTRAN Common Block or Routine	User's Manual Nomenclature	Units	User's Manual Eq. Nos.	Definition
prhtls	--	COMMON pands		--		Secondary stream laminar Prandtl no.
prhtlsct	--	COMMON pvar		kg kmol^{-1}		Coal offgas laminar Prandtl no.
prk	numpar	COMMON cpeul	σ_i^t	--	2-28	Turbulent Prandtl (Schmidt) no. for coal particle diffusion
prks	--	COMMON cpeul		--		Turbulent Prandtl (Schmidt) no. for sorbent particle diffusion
prnh3	--	COMMON calcyi		--		Prandtl no. for NH_3
prnox	--	COMMON calcyi		--		Prandtl no. for NO_x transport
prso2	--	COMMON ratesx		--		Prandtl no. for SO_2
prte	--	COMMON turb		--		Turbulent Prandtl no. for te
pw	numstr	COMMON cpart		kg s^{-1}		Total particle mass flowrate for a starting location
qab	numpar	COMMON radcon		--		Particle absorption coefficient
qcflxe	numxpt, numypt	COMMON heatcp		J m^{-2} s^{-1}		Convective heat flux to east faces of intrusions
qcflxs	numxpt, numypt	COMMON heatcp		J m^{-2} s^{-1}		Convective heat flux to south faces of intrusions

FORTRAN Variable	FORTRAN Dimensions	FORTRAN Common Block or Routine	User's Manual Nomenclature	Units	User's Manual Eq. Nos.	Definition
qct	--	COMMON enth		$J\ s^{-1}$		Total enthalpy lost by convection
qha	--	COMMON grid1		°		Quarl half-angle
qinc	4, numxpt, numypt	COMMON diso		$J\ s^{-1}\ m^{-2}$		Incident radiation flux on west wall (I=2,NJ-1), north wall (I=NJ+2,NJ+NI-1), and east wall (I=NJ+NI+2,NJ+NI+ NJ-1)
qlx	--	COMMON grid1		m		Length of reactor
qnet	4, numxpt, numypt	COMMON diso		$J\ s^{-1}\ m^{-2}$		Net radiation heat flux on west wall (I=2,NJ-1), north wall (I=NJ+2,NJ+NI-1), and east wall (I=NJ+NI+2,NJ+NI+ NJ-1)
qp	--	COMMON difeqn		$J\ s^{-1}$		Convection and conduction from particle to the gas
qrgt	--	COMMON enth		$J\ s^{-1}$		Total enthalpy gained by the gas by radiation
qrpk	--	COMMON pecor		$J\ s^{-1}$		Net radiation to the particle

FORTRAN Variable	FORTRAN Dimensions	FORTRAN Common Block or Routine	User's Manual Nomenclature	Units	User's Manual Eq. Nos.	Definition
qrpt	--	COMMON enth		$J\ s^{-1}$		Total enthalpy gained by the particles by radiation
qsc	numpar	COMMON radcon		--		Particle scattering coefficient
r	numypt	COMMON geom		m		Radial location of p-node
ra	numypt	COMMON geom		m		Radial location of north face of v-cell
radg	--	COMMON ratesx		cm		Initial sorbent grain radius
radoh	--	COMMON ratpar		--		Flag for choosing quasi-equilibrium expression for estimating radical hydroxide (OH) concentrations
radoxy	--	COMMON ratpar		--		Flag for choosing quasi-equilibrium expression for estimating atomic oxygen concentration
rangin	--	COMMON cparam		--		Flag to identify if all species are within temperature range
rate1c	--	COMMON rmscom				
rate1p	--	COMMON rmscom				

FORTRAN Variable	FORTRAN Dimensions	FORTRAN Common Block or Routine	User's Manual Nomenclature	Units	User's Manual Eq. Nos.	Definition
rate1s	--	COMMON rmscom				
rate2c	--	COMMON rmscom				
rate2p	--	COMMON rmscom				
rate2s	--	COMMON rmscom				
rate3c	--	COMMON rmscom				
rate3p	--	COMMON rmscom				
rate3s	--	COMMON rmscom				
rate4c	--	COMMON rmscom				
rate4p	--	COMMON rmscom				
rate4s	--	COMMON rmscom				
rate5c	--	COMMON rmscom				
rate5p	--	COMMON rmscom				
rate5s	--	COMMON rmscom				
rchsec	--	COMMON grid1		--		Ratio of diach to dias
rcj	numxpt, numypt, numpar	COMMON eulp				Reaction term for acj

FORTRAN Variable	FORTRAN Dimensions	FORTRAN Common Block or Routine	User's Manual Nomenclature	Units	User's Manual Eq. Nos.	Definition
rco2mw	--	COMMON psccom		kg kmol^{-1}		CO_2 mol. wt.
rcomw	--	COMMON psccom		kg kmol^{-1}		CO mol. wt.
rcor	nsubsh	COMMON ratesx		cm		Radius of unreacted CaO in grains at sorbent particle subshell
rcv	numypt	COMMON vvel		m		Radial location of south face of v-cell
resacj	numpar	COMMON eulp				Residual source sum for acj
resahj	numpar	COMMON eulp				Residual source sum for ahj
resawj	numpar	COMMON eulp				Residual source sum for awj
resh2s	--	COMMON soxrte		--		Residual source sum for H_2S
reshcn	--	COMMON noxrte		--		Residual source sum for HCN
resnh3	--	COMMON noxrte		--		Residual source sum for NH_3
resnjn	numpar	COMMON eulp				Residual source sum for Eulerian particle no. density
resnox	--	COMMON noxrte		--		Residual source sum for NO_x
resoet	--	COMMON cgasmf		--		Residual source sum for eta
resoge	--	COMMON cgasmf		--		Residual source sum for geta

FORTRAN Variable	FORTRAN Dimensions	FORTRAN Common Block or Routine	User's Manual Nomenclature	Units	User's Manual Eq. Nos.	Definition
resore	--	COMMON tdis		--		Max. residual source sum for ed
resorf	--	COMMON mixfr		--		Residual source sum for f
resorq	--	COMMON fluc	g_f	--		Residual source sum for variance in f
resorh	--	COMMON enth				Residual sorce sum for gas enthalpy
resork	--	COMMON ten		--		Max. residual source sum for te
resorm	--	COMMON pcor		--		Residual source sum for mass (continuity)
resorn	--	COMMON pard		--		Residual source sum
resorp	--	COMMON pcor		--		Pressure residual source sum
resorr	--	COMMON radres		--		Residual source sum for radiation in radial direction
resoru	--	COMMON uvel				Residual source sum for u velocity
resorv	--	COMMON vvel				Residual source sum for v velocity
resorw	--	COMMON wvel				Residual source sum for w velocity
resorx	--	COMMON radres		--		Residual source sum for radiation in axial direction

FORTRAN Variable	FORTRAN Dimensions	FORTRAN Common Block or Routine	User's Manual Nomenclature	Units	User's Manual Eq. Nos.	Definition
resoyfu	--	COMMON magnussen		--		Residual source sum for yfu
resso2	--	COMMON soxrte				Residual source sum for SO_2
rf	--	COMMON magnussen		--		Stoichiometric mass ratio of oxident to fuel (Magnussen-Hjertager method)
rgas	--	COMMON cchemi		J kmol^{-1} K^{-1}		Universal gas constant
rgasin	--	COMMON cchemi		kmol K J^{-1}		Inverse of rgas
rgc	--	COMMON rcon		J kmol^{-1} K		Real gas constant
rgi	nsubsh	COMMON ratesx		cm		Extended grain radius of sorbent subshell
rh	--	COMMON difeqn		kg s^{-1}		Total char reaction rate
rh2omw	--	COMMON psccom		--		H_2O mol. wt.
rhj	numxpt, numypt, numpar	COMMON eulp				Reaction term for ahj
RHL	--	COAL2	$\sum_l r_{hjl}$		2-125	Total char reaction rate due to all oxidizer reactions for the j^{th} particle classification.

FORTRAN Variable	FORTRAN Dimensions	FORTRAN Common Block or Routine	User's Manual Nomenclature	Units	User's Manual Eq. Nos.	Definition
rhochs	--	COMMON ratesx		kg m^{-3}		CaS density
rhoco	--	COMMON ratesx		g cm^{-3}		Density of CaO
rhocs	--	COMMON ratesx		g cm^{-3}		Density of $CaSO_4$
rhog	--	COMMON traj		kg m^{-3}		Gas density
rhop	--	COMMON cparam		kg m^3		Gas phase density
rint0	5	COMMON diso				
rmwchs	--	COMMON ratesx		kg $kmol^{-1}$		CaS mol. wt.
rmwco	--	COMMON ratesx		kg $kmol^{-1}$		CaO mol. wt.
rmwcs	--	COMMON ratesx		kg $kmol^{-1}$		$CaSO_4$ mol. wt.
rmwh2s	--	COMMON ratesx		kg $kmol^{-1}$		H_2S mol. wt.
rmwso2	--	COMMON ratesx		kg $kmol^{-1}$		SO_2 mol. wt.
rmxhcn	--	COMMON noxrte				Max. HCN concentration
rmxnh3	--	COMMON noxrte				Max. NH_3 concentration
rmxnox	--	COMMON noxrte				Maximum NO_x concentration
rn2mw	--	COMMON psccom		kg $kmol^{-1}$		N_2 mol. wt.

FORTRAN Variable	FORTRAN Dimensions	FORTRAN Common Block or Routine	User's Manual Nomenclature	Units	User's Manual Eq. Nos.	Definition
rnh3mw	--	COMMON psccom		kg kmol^{-1}		NH_3 mol. wt.
rnomw	--	COMMON intrat		kg kmol^{-1}		NO mol. wt.
rnomw	--	COMMON psccom		kg kmol^{-1}		NO mol. wt.
ro2mw	--	COMMON psccom		kg kmol^{-1}		O_2 mol. wt.
rohmw	--	COMMON psccom		kg kmol^{-1}		OH mol. wt.
rprim	--	COMMON grid1		m		Radius of primary tube
rps	--	COMMON ratesx		cm		Sorbent particle radius
rrc	--	COMMON difeqn		kg s^{-1}		Total coal reaction rate
RRJ	--	Common DIFEQN	r_i	kg/s	2-129	Particle reaction rate to gas phase.
rrj	--	COMMON difeqn		kg s^{-1}		Particle reaction rate to the gas phase
rsec	--	COMMON grid1		m		Radius of secondary tube
rtcnsp	numxpt, numypt	COMMON calcyi		kg m^{-3} s^{-1}		"S_p" source term for HCN
rtcnsu	numxpt, numypt	COMMON calcyi		kg HCN m^{-3} s^{-1}		"S_u" source term for HCN
rthssp	numxpt, numypt	COMMON ratesx		--		Linearized source term for H_2S

FORTRAN Variable	FORTRAN Dimensions	FORTRAN Common Block or Routine	User's Manual Nomenclature	Units	User's Manual Eq. Nos.	Definition
rthssu	numxpt, numypt	COMMON ratesx		--		Linearized source term for H_2S
rtnhsp	numxpt, numypt	COMMON calcyi		kg m^{-3} s^{-1}		"S_p" source term for NH_3
rtnhsu	numxpt, numypt	COMMON calcyi		kg NH_3 m^{-3} s^{-1}		"S_u" source term for NH_3
rtnosp	numxpt, numypt	COMMON calcyi		kg m^{-3} s^{-1}		"S_p" source term for NO
rtnosu	numxpt, numypt	COMMON calcyi		kg NO m^{-3} s^{-1}		"S_u" source term for NO
rtsosp	numxpt, numypt	COMMON ratesx		--		Linearized source term for SO_2
rtsosu	numxpt, numypt	COMMON ratesx		--		Linearized source term for SO_2
rv	numypt	COMMON geom		m		Same as yv
rw	--	COMMON difeqn		kg s^{-1}		Change of slurry liquid mass per unit time
s	numspe	COMMON gparam		Å		Lennard-Jones parameter
s0	numspe	COMMON spece				Molar entropy of each species
s2	numspe	COMMON cparam		kmol i kg^{-1}		Mole numbers of each species
sbar	--	COMMON radcon	$\bar{s}$	--	2-148	Side-scattered component of radiation
sconv	nsubsh	COMMON ratesx		--		Sorbent subshell conversion

FORTRAN Variable	FORTRAN Dimensions	FORTRAN Common Block or Routine	User's Manual Nomenclature	Units	User's Manual Eq. Nos.	Definition
sew	numxpt	COMMON geom		m		East-west width of p-cell
sewu	numxpt	COMMON uvel		--		Width of u-cell
sf	numxpt,numypt	COMMON strfnc		--		Stream function
sfac	numypt	COMMON geom		--		Geometric factor
SHHJ	--	COAL2	$\frac{\sum_l r_{hjl} h g_{hil}}{\sum_l r_{hjl}}$		2-125	Total heat of reaction for all oxidation reactions for the j^{th} particle classification normalized to the total rate of mass loss due to all oxidizer reactions.
SHVJ	--	COAL2	\I\SU(m ,,r_{vjm}h g vjm)		2-125	Total heat of devolatilization for all devolatilization reactions for the j^{th} particle classification.
sigma	--	COMMON radcon		J m^{-2} s^{-1} K^{-4}		Stefan-Boltzmann constant
SM	--	Common CPARAM		kmol kg^{-1}		Inverse of molecular weight
smct	--	COMMON pvar		kmol kg^{-1}		Coal offgas inverse mol. wt.

FORTRAN Variable	FORTRAN Dimensions	FORTRAN Common Block or Routine	User's Manual Nomenclature	Units	User's Manual Eq. Nos.	Definition
smf0	--	COMMON f1af0		kmol kg-1		Value of sm for f=0 stream
smf1	--	COMMON f1af0		kmol kg^{-1}		Value of sm for f=1 stream
sminlet	numlet	COMMON adflo		kmol kg^{-1}		Inverse of mol. wt. for additional inlet
sminv	--	COMMON cchemi		kg $kmol^{-1}$		Inverse of sm
smmh	--	COMMON magnusse n		kmol kg^{-1}		Inverse of mol. wt. for product stream (Magnussen-Hjertager method)
smp	--	COMMON pands		kmol kg^{-1}		Primary stream inverse mol. wt.
sms	--	COMMON pands		kmol kg^{-1}		Secondary stream inverse mol. wt.
smw	numspe	COMMON spece				Species mol. wt.
sns	numypt	COMMON geom		m		North-south height of p-cell
snsv	numypt	COMMON vvel		m		Height of v-cell
so2cap	numxpt, numypt	COMMON ratesx		kg s^{-1}		SO_2 capture rate

FORTRAN Variable	FORTRAN Dimensions	FORTRAN Common Block or Routine	User's Manual Nomenclature	Units	User's Manual Eq. Nos.	Definition
solele	numele	COMMON cequil		--		solele(i) = the number of active pure condensed phase species that contain element i (used for phase rule checking)
solmol	maxsol	COMMON lution		--		Total moles in solution in equilibrium algorithm
solnam	numnam, maxsol	COMMON lution		--		Names of the solutions in equilibrium algorithm
solsta	maxsol	COMMON lution		--		Status of solution in equilibrium algorithm (omit or includ)
sorden	numxpt, numypt, numpar	COMMON cpeul		m^{-3}		Sorbent particle number density
sormax	--	COMMON pard		--		Convergence criterion for max. residual source sum
sp	numxpt, numypt	COMMON coef	S_P		3-71	Source coefficient
sp	numxpt, numypt	COMMON coef	S_P		3-71	Source term
spden	--	COMMON cpart		kg m^{-3}		Sorbent particle density

FORTRAN Variable	FORTRAN Dimensions	FORTRAN Common Block or Routine	User's Manual Nomenclature	Units	User's Manual Eq. Nos.	Definition
specct	numspe	COMMON pvar	--	kmol i kg^{-1}	--	Equilibrium species composition for pure coal offgas
specf0	numspe	COMMON f1af0		kmol i kg^{-1}		Value of s2 for f=0 stream
specf1	numspe	COMMON f1af0		kmol i kg^{-1}		Value of s2 for f=1 stream
specf1	numspe	COMMON react		kmol i kg^{-1}		Species mole numbers in the f=1 stream (usually the primary)
specie	numxpt, numypt, numspe	COMMON flupr		kmol i $kmol^{-1}$		Species mole fractions in the bulk gas
specinlet	numlet, numspe	COMMON adflo		kmol i kg^{-1}		Species mole nos. for additional inlet
specmh	numspe	COMMON magnussen				Product stream species mole nos. (Magnussen-Hjertager method)
specp	numspe	COMMON pands				Species mole numbers in the primary stream
specs	numspe	COMMON pands				Secondary stream mol. nos.
sph	numxpt,numypt	COMMON cpsou				Particle enthalpy source term

FORTRAN Variable	FORTRAN Dimensions	FORTRAN Common Block or Routine	User's Manual Nomenclature	Units	User's Manual Eq. Nos.	Definition
sphold	numxpt,numypt	COMMON under				Old values of sph
spm	numxpt,numypt	COMMON cpsou				Total particle mass source term
spme	numxpt,numypt	COMMON cpsef				Particle mass source term for eta
spmeold	numxpt,numypt	COMMON under				Old values of spme
spmf	numxpt,numypt	COMMON cpsef				Particle mass source term for f
spmfold	numxpt,numypt	COMMON under				Old values of spmf
spmh2s	numxpt, numypt	COMMON ratesx		kg s^{-1}		Capture source term for H_2S
spmold	numxpt,numypt	COMMON under				Old values of spm
spmso2	numxpt, numypt	COMMON ratesx		kg s^{-1}		Capture source term for SO_2
sprang	numstr	COMMON cpart		°		Spray angle
spsic	numxpt, numypt	COMMON krad				Scattering coefficient for char and ash particles
spstat	numspe	COMMON cparam		--		species status (tomit, includ)
spup	numxpt,numypt	COMMON cpsou				Particle momentum source term coefficient for u velocity

Reprinted from ENERGY & FUELS, 1992, 6.

An Empirical Model for Coal Fluidity Based on a Macromolecular Network Pyrolysis Model

P. R. Solomon,* P. E. Best,† Z. Z. Yu, and S. Charpenay

Advanced Fuel Research, Inc., 87 Church Street, East Hartford, Connecticut 06108

Received May 22, 1991. Revised Manuscript Received November 26, 1991

We have developed a phenomenological model for coal fluidity based on a macromolecular network model for the decomposition and condensation of the network under the influence of bond breaking and cross-linking reactions. The macromolecular network model is the previously published FG-DVC model of coal pyrolysis. It employs a network consisting of aromatic ring clusters linked by bridges. The bond scissions are described by a single first-order reaction with a distribution of activation energies. Cross-linking is related to CO_2 and CH_4 formation which are described in multiple first-order reactions with distributions of activation energies. The fluidity is described by an empirical equation which depends on the relative amounts of the liquid (molecules detached from the network) and solid (the remaining network) and on the fluidity of the liquid component. The FG-DVC model predicts the yield of liquids. The fluidity of the liquid component is described by a second phenomenological equation which depends only on the temperature. The advantage of this model is that it is based on a previously demonstrated methodology which allows the incorporation of rank-dependent kinetics, cross-linking, weathering, and extraction phenomena into the fluidity predictions. Excellent agreement has been obtained between the model predictions and low-temperature fluidity measurements of Oxley and Pitt, van Krevelen, and Gieseler plastometer measurements for the Argonne premium coal samples. The trends for changes in the fluidity with weathering or extraction are predicted as well. Good agreement has been obtained at high temperatures between the model predictions and measurements of Fong for the onset of the fluidity. The loss of fluidity, however, is predicted to occur sooner than is indicated by the data and the maximum value of fluidity is overpredicted. The data cover over 5 orders of magnitude in fluidity, and eight coals with carbon concentration between 80 and 90%. This agreement is obtained using coal-independent equations for the dependence of the fluidity on the liquid fraction and the liquid fluidity. The coal-dependent variables are the kinetic rates for bond breaking and cross-linking and the extent of cross-linking as determined from laboratory pyrolysis measurements using a TG-FTIR (thermogravimetric analyzer with Fourier transform infrared analysis of evolved products). There are only two adjustable parameters in the model.

Introduction

When bituminous coals are heated, they become liquid. Those in the range of 82–89% carbon achieve the highest fluidities,[1,2] but even lignites, if heated rapidly enough, can exhibit some fluidity.[3] The understanding and ability to predict a coal's fluid properties are important in many processes. In liquefaction, highly fluid coals dissolve quickly in the process solvent, so that further chemistry occurs by liquid–liquid interactions, while nonfluid coals must undergo slower solid–liquid interactions. In combustion or gasification, fluidity controls particle swelling,[4] agglomeration of particles, intrinsic char reactivity,[5] and subsequent fragmentation[6] of char. In coke making, fluidity controls the coke properties.[7,8] Fluidity also affects the growth of carbon products made from coal tars.

There are a number of factors which contribute to the fluidity of coal liquid. They include (i) the fluidity of the liquid fraction, with and without molecular entanglements; (ii) the dependence of this fluidity on temperature; (iii) the contributions of suspended solids in the liquid, both "chunks" of char and mineral particles; and (iv) the formation of bubbles due to trapped gases.

Several models for coal liquid viscosity have been proposed which consider all of the influences except the bubbles. The models were based on the two step process described by van Krevelen and co-workers,[1,9] which assume the following reactions to occur on heating.

$$\text{coal} \xrightarrow{k_1} \text{metaplast} \xrightarrow{k_2} \text{coke}$$

where k_1 and k_2 are reaction rate constants. In the viscosity models, the change of fluidity is assumed to result from the change in solids mass fraction, ϕ_s (coal and coke), in the melt. The metaplast is the liquid fraction. Thus Bronowski et al.[10] used an expression in which fluidity was directly proportional to the liquid fraction $(1 - \phi_s)$. Expanding on this, Fitzgerald[11,12] used an equation which described the relative fluidity as depending on liquid fraction raised to a power n (where n was chosen to be 2.5). This power law expression was based on earlier work by Roscoe[13] and Brinkman.[14] Frankel and Acrivos[15] used an

† Physics Department and Institute of Material Science, University of Connecticut, Storrs, CT 06268.

(1) van Krevelen, D. W. *Coal*; Elsevier: Amsterdam, 1961.
(2) Sanada, Y.; Honda, H. *Fuel* 1966, *45*, 295.
(3) Solomon, P. R.; Serio, M. A.; Carangelo, R. M.; Markham, J. R. *Fuel* 1986, *65*, 182.
(4) Solomon, P. R.; Hamblen, D. G. *Chemistry of Coal Conversion*; Schlosberg, R. H., Ed.; Plenum Publishing: New York, 1985; Chapter 5, pp 121–251.
(5) Serio, M. A.; Solomon, P. R.; Bassilakis, R.; Suuberg, E. M. *Prepr. Pap.–Am. Chem. Soc., Div. Fuel Chem.* 1989, *34* (1), 9.
(6) Helble, J. J.; Sarofim, A. F. *Combust. Flame* 1989, *76*, 183.
(7) Marsh, H. *Fuel* 1973, *52*, 205.
(8) Marsh, H.; Neavel, R. C. *Fuel* 1980, *59*, 511.
(9) Chermin, H. A. G.; van Krevelen, D. W. *Fuel* 1957, *36*, 85.
(10) Bronowski, J.; Fitzgerald, D.; Gillings, D. W.; Rhys-Jones, D. C. *Nature* 1953, *171*, 389.
(11) Fitzgerald, D. *Fuel* 1956, *35*, 178.
(12) Fitzgerald, D. *Trans. Faraday Soc.* 1956, *52*, 362.
(13) Roscoe, Brit. *J. Appl. Phys.* 1952, *3*, 267.
(14) Brinkman, J. *J. Chem. Phys.* 1952, *20*, 571.
(15) Frankel, N. A.; Acrivos, A. *Chem. Eng., Sci.* 1976, *22*, 847.

0887-0624/92/2506-0143$03.00/0

expression in which the fluidity also depends on a power of the liquid fraction. Their model has the extra feature of a critical solids volume fraction at which fluidity disappears. This critical value occurs at the maximum volume fraction that the solids can occupy as limited by particle–particle interaction. At this critical value, the liquid fraction is insufficient to separate the solid particles. Its value is 0.64 for randomly close-packed spheres, while it ranges from 0.5 to 0.9 for other systems, depending on particle shape and state of agglomeration.[16] Viscosity models predict that the fluidity vanishes for solid volume fractions equal to or greater than the critical value, and we refer to this critical value as the inhomogeneous gel point.

Fong et al.[17] employed the power law of Frankel and Acrivos;[15] however, the chosen critical solids volume fraction value in Fong's model was unity, somewhat higher than usual.[16] A similar model was used by Oh.[18] The above models gave good fits to data, although in each case, four model parameters (k_1, k_2, n, and the critical solids volume fraction) were chosen to fit the data for a particular coal studied in a limited number of experiments covering a narrow range of heating rates, or holding temperatures.

On the basis of the observation that coal can be considered as a macromolecular network to which theories of cross-linked polymers may be applied,[1,2,19–26] we have examined the polymer literature of viscosity in polymer melts to determine the range of assumptions which have been employed.[17,27–32] For nonreacting melts of branched polymers at molecular sizes below those sufficiently large for entanglements, there is experimental and theoretical support for viscosities which depend exponentially on side-arm molecular mass.[27] These same authors determined temperature-dependent activation energies for viscosity, for temperatures below 200 °C. For inhomogeneous polymer melts, theories with an inhomogeneous gel point have been employed.[17,32]

In reacting melts, the manner in which average molecular weight varies with extent of reaction in a homogeneous melt has been considered in the branching theory described by Macosko and co-workers.[29] Insofar as it describes molecular weight distributions, this theory duplicates and extends the results of older combinatorial methods developed by Flory[30] and by Stockmayer.[31] A particular result of Macosko's work is that measured viscosity correlates well with the weight average molecular weight of the longest linear path through the molecules. This theory predicts that the homogeneous gel-point (the point at which the viscosity goes to infinity) appears at the first occurrence of a solid phase (i.e., the gel point is at $\phi_s = 0$).

While Macosko's approach appears to be good for homogeneous polymer melts, it does not appear to be appropriate for coal, since coal is typically an inhomogeneous reacting melt. The inhomogeneities result from several factors including starting with a powdered solid (which would be sufficient to insure inhomogeneity) and having a material consisting of diverse maceral types and mineral grains. Because of these inhomogeneities, it is thought that theories which describe the viscosity of a suspension of a solid in a liquid are the most appropriate for coal, and in this work we have pursued the two phase approach with a gel point at a critical ϕ_s value where $\phi_s > 0$.

To improve upon the prediction of the liquid fraction, we have employed polymer concepts to describe the molecular weight distribution during pyrolysis, from which a liquid and solid fraction can be determined. This work is based on a theory initially employing linear chain statistics[33,34] and subsequently employing network statistics.[35–38] Our DVC macromolecular network decomposition model includes the processes of *depolymerization* (bond breaking), *vaporization* (mass transport), and cross-linking. This model was combined with our *functional group* (FG) model for gas evolution[4,39,40] to provide the general FG-DVC coal pyrolysis model.[41–43] In the combined model, the cross-linking process in the DVC model is related to the evolution of CO_2 and CH_4 in the FG model. The FG-DVC model employs Monte Carlo methods to compute the network properties. More recently, network models of thermal decomposition have been proposed employing percolation theory.[44,45] We have also employed a modified percolation theory for the statistical calculations in the FG-DVC model.[43,46,47]

The fluidity model presented here employs the FG-DVC model to predict the molecular weight distribution of the decomposing macromolecular network. From this distribution, a solid fraction ϕ_s and a liquid fraction $(1 - \phi_s)$ are defined. These parameters are employed using the concepts of inhomogeneous mixtures to predict the fluidity from the solid fraction, the liquid viscosity, and the tem-

(16) Nielsen, L. E. *Mechanical Properties of Polymers and Composites*; Marcel Dekker: New York, 1974; Vol. 2.
(17) Fong, W. S.; Khalil, Y. F.; Peters, W. A.; Howard, J. B. *Fuel* 1986, *65*, 195.
(18) Oh, M. S.; Peters, W. A.; Howard, J. B. *AIChE J.* 1989, *35* (5), 775.
(19) Green, T. K.; Kovac, J.; Larsen, J. W. *Fuel* 1984, *63*, 935.
(20) Green, T. K.; Kovac, J.; Larsen, J. W. *Coal Structure*; Meyers, R. A., Ed.; Academic Press: New York, 1982.
(21) Nelson, J. R. *Fuel* 1983, *62*, 112.
(22) Lucht, L. M.; Peppas, N. A. *Fuel* 1987, *66*, 803.
(23) Lucht, L. M.; Larsen, J. M.; Peppas, N. A. *Energy Fuels* 1987, *1*, 56.
(24) Green, T.; Kovac, J.; Brenner, D.; Larsen, J. *Coal Structure*; Meyers, R. A., Ed.; Academic: New York, 1982; p 199.
(25) Hall, P. J.; Marsh, H.; Thomas, K. M. *Fuel* 1988, *67*, 863.
(26) Hirsch, P. B. *Proc. R. Soc.* 1954, *A226*, 143.
(27) Bartels, C. R.; Crist, B.; Felters, L. J.; Graessley, W. W. *Macromolecules* 1986, *19*, 785.
(28) Nazem, F. F. *Fuel* 1980, *59*, 851.
(29) Macosko, C. W. *Brit. Polymer J.* 1985, *17*, 239; and references therein.
(30) Flory, P. J. *J. Am. Chem. Soc.* 1941, *63*, 3083, 3097. See also: *Principles of Polymer Chemistry*; Cornell University Press: Ithaca, NY, 1953; Chapter 9.
(31) Stockmayer, W. H. *J. Chem. Phys.* 1943, *11*, 45; 1944, *12*, 125.
(32) Mooney, M. *J. Colloid Sci.* 1951, *6*, 162.
(33) Solomon, P. R.; King, H. H. *Fuel* 1984, *63*, 1302.
(34) Squire, K. R. Carangelo, R. M.; DiTaranto, M. B.; Solomon, P. R. *Fuel* 1986, *65*, 833.
(35) Squire, K. R.; Solomon, P. R.; DiTaranto, M. B.; Carangelo, R. M. *Prepr. Pap.—Am. Chem. Soc., Div. Fuel Chem.* 1985, *30* (1), 386.
(36) Solomon, P. R.; Squire, K. R.; Carangelo, R. M. *Int. Conf. Coal Sci., Proc., Sydney, Australia* 1985, 945.
(37) Solomon, P. R.; Squire, K. R. *Prepr. Pap.—Am. Chem. Soc., Div. Fuel Chem.* 1985, *30* (4), 347.
(38) Solomon, P. R.; Hamblen, D. G.; Carangelo, R. M.; Serio, M. A.; Deshpande, G. V. *Combust. Flame* 1988, *71*, 137.
(39) Solomon, P. R.; Hamblen, D. G.; Carangelo, R. M.; Krause, J. L. *Nineteenth Symposium (International) on Combustion*; The Combustion Institute: Pittsburgh, PA, 1982; p 1139.
(40) Serio, M. A.; Hamblen, D. G.; Markham, J. R.; Solomon, P. R. *Energy Fuels* 1987, *1*, 138.
(41) Solomon, P. R.; Hamblen, D. G.; Deshpande, G. V.; Serio, M. A. A General Model of Coal Devolatilization, In *International Conference on Coal Science Proceedings*; Elsevier: Amsterdam, The Netherlands, 1987; p 601.
(42) Solomon, P. R.; Hamblen, D. G.; Carangelo, R. M.; Serio, M. A.; Deshpande, G. V. *Energy Fuels* 1988, *2*, 405.
(43) Solomon, P. R.; Hamblen, D. G.; Serio, M. A.; Yu, Z. Z.; Charpenay, S., Storch Award Symposium Lecture, *Prepr. Pap.—Am. Chem. Soc., Div. Fuel Chem.* 1991, *36* (1), 267.
(44) Niksa, S.; Kerstein, A. R. *Fuel* 1987, *66*, 1389.
(45) Grant, D. M.; Pugmire, R. J.; Fletcher, T. H.; Kerstein, A. R. *Energy Fuels* 1989, *3*, 175.
(46) Solomon, P. R.; Hamblen, D. G.; Yu, Z. Z.; Serio, M. A. Network Models of Coal Thermal Decomposition *Fuel* 1990, *69*, 754.
(47) Solomon, P. R.; Serio, M. A.; Hamblen, D. G.; Yu, Z. Z.; Charpenay, S. *Prepr. Pap.—Am. Chem. Soc., Div. Fuel Chem.* 1990, *35* (2), 479.

Table I

	ILL	UTAH	UPK	PIT	UPF	POC	PSOC815
volatile matter (daf), %	47.4	48.1	37.6	41.7	31.6	19.5	31.5
C % (daf)	77.7	80.7	82.6	83.2	85.6	91.1	85.6
O % (daf)	13.5	11.6	9.8	8.8	7.5	2.5	7.8
bond breaking							
E_{BB}/R	26000	27000	27250	27500	28250	29000	28250
A_{BB}	1.0×10^{14}	1.0×10^{14}	1.0×10^{14}	1.0×10^{14}	1.0×10^{14}	1.0×10^{14}	1.0×10^{14}
σ_{BB}/R	750	1250	1000	1250	1250	750	1250
BB rate at 650 °C	2.4×10^{-2}	6.0×10^{-3}	4.3×10^{-3}	3.0×10^{-3}	1.1×10^{-3}	3.8×10^{-4}	1.1×10^{-3}
methane cross-linking							
$E_{CH_4\text{-}L}/R$	28000	28000	28000	28000	28750	29500	28500
$A_{CO_2\text{-}L}$	3.0×10^{13}	3.0×10^{13}	3.0×10^{13}	3.0×10^{13}	3.0×10^{13}	3.0×10^{13}	3.0×10^{13}
$\sigma_{CO_2\text{-}L}/R$	1800	1500	1200	1300	800	750	1000
CH_4 L Rate at 650 °C	4.5×10^{-4}	4.5×10^{-4}	4.5×10^{-4}	4.5×10^{-4}	1.6×10^{-4}	5.7×10^{-5}	2.3×10^{-4}
CO_2 cross-linking							
$E_{CO_2\text{-}L}/R$	24750	25000	26000	26500	27000	28000	26750
$A_{CO_2\text{-}L}$	5.0×10^{12}	5.0×10^{12}	5.0×10^{12}	5.0×10^{12}	5.0×10^{12}	5.0×10^{12}	5.0×10^{12}
$\sigma_{CO_2\text{-}L}/R$	1750	1250	3000	3000	3000	2500	3000
CO_2 L rate at 650 °C	6.8×10^{-3}	4.8×10^{-3}	1.2×10^{-3}	6.0×10^{-4}	3.0×10^{-4}	7.6×10^{-5}	4.3×10^{-4}
M_0 (cross-link/ring cluster)	0.21	0.21	0.13	0.08	0.08	0.128	0.08
l (oligomer length)	4	4	8	8	10	10	8
H(al), %	0.51	0.55	0.67	0.62	0.55	0.35	0.51

perature.[17,28,32] The effect of bubbles has not been specifically considered but are included implicitly since bubbling occurs under conditions of the experiments whose fitting was used to devise the empirical equations. The model predictions are compared with measurements made with a Gieseler plastometer[1,48-53] and with the high-temperature fluidity measurements of Fong et al.[17]

Experimental Section

The low-temperature fluidity data employed in this paper were obtained with a Gieseler plastometer. Data were obtained from the literature[1,48-52] and from Commercial Testing and Engineering.[53] Descriptions of the apparatus and operation may be found in the literature.[54,55] The viscosity is determined by measuring the rotation rate of a stirrer in the sample when constant torque is applied.

The high-temperature data were obtained by Fong et al.[17] in a device designed for rapid heating. Coal is contained in a pancake-shaped cavity in which a disk is driven at constant rotation. The torque was related to viscosity in poise using standards of known viscosity.

There are many problems of translating stirrer rotation speed to viscosity in poise, and most researchers simply report data in degrees/min or dial divisions/min (DDPM) where one DDPM = 3.6°/min. However, the Gieseler plastometer was calibrated in absolute units of viscosity by Stevens[56] and by Soth and Russel[57] who obtained the calibration DDPM/min = 10^{-7} rhe's, where 1 rhe = 1/poise. We have employed this relationship as a convenience so that data of van Krevelen (at constant temperature) and Fong[17] (both of whom related the experimental observations on rotation speed and torque to viscosity and thus reported data in viscosity units) could be directly compared with the other data reported in DDPM. To the extent that the coal melt is a Newtonian fluid, and the presence of bubbles and ash can be ignored, the same proportionality factor should also be applicable to the viscosity data obtained at both constant torque and constant rotation. We calibrated our model parameters using Gieseler plastometer data. The agreement for the other sets of data suggest that the conversion factors agree to within an order of magnitude. If the absolute magnitude of the van Krevelen data is ignored, the conversion factor is unimportant.

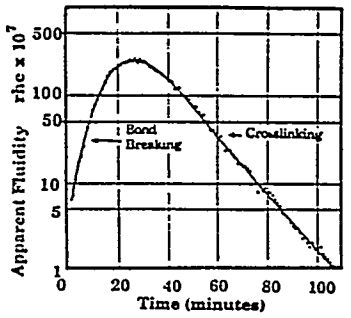

Figure 1. Apparent fluidity as a function of time at 407 °C for a typical coking coal (34.4% dry ash free volatile matter, coal rank code no. 401b). From ref 49.

Table II

experiments	Fong	Oxley and Pit	van Krevelen
volatile matter (daf), %	45.2	30.3	24
C % (daf)	79	N/A	N/A
coal used for modeling	Pitts 8	Upper Kanawha	Upper Freeport
volatile matter (daf), %	41.7	37.6	31.6
C % (daf)	83.2	82.6	85.6
parameters modified from Argonne coal			
E_{BB}/R			29000
M_o (cross-links/bead)		0.17	0.07
l (oligomer length)		6	
H(al), %		0.59	0.19

In making fluidity measurements on coal, it has been found that there is an initial softening of coal on heating which is reversible, and this has been associated with melting and hydrogen bond breaking. This is followed by a sharp rise in fluidity due to the decomposition of the macromolecular network by covalent bond breaking. This sharp rise is illustrated in Figure 1 which presents the measured fluidity of a bituminous coal as a function of time as the coal was heated from 300 °C at 3 °C/min to 407 °C and held at constant temperature.[49] The slower fall in fluidity with time is due to cross-linking which resolidifies the network.

The model we present employs both the coal composition parameters and the kinetic rates for bond breaking and gas evolution. For the Argonne coals, the rates and composition parameters were determined using a thermogravimetric analyzer with analysis of evolved products by Fourier transform Infrared

(48) Oxley, G. R.; Pitt, G. J. *Fuel* 1958, *37*, 19.
(49) Fitzgerald, D. *Fuel* 1956, *35*, 178.
(50) Waters, P. L. *Fuel* 1962, *41*, 3.
(51) Seki, H.; Kumagai, J.; Matsuda, M.; Ito, O.; Iino, M. *Fuel* 1989, *68*, 978.
(52) Wu, M. M.; Robbins, G. A.; Winschel, R. A.; Burke, F. P. *Energy Fuels* 1988, *2*, 150.
(53) The Gieseler Plastometer data was supplied by Mr. George Engelke from Commercial Testing and Engineering Co.
(54) Lowry, H. H. *Chemistry of Coal Utilization*; Wiley: New York, 1963.
(55) ASTM D 2639-74 (reapproved, 1980).
(56) Stevens, J. N. CSIRO Division of Coal Research, Investigation Report No. 12, 1957.
(57) Soth, G. C.; Russell, C. C. *Proc. Am. Soc. Test. Mater.* 1943, *43*, 1176.
(58) Solomon, P. R.; Serio, M. A.; Deshpande, G. V.; Kroo, E. *Energy Fuels* 1990, *4*, 42.

spectroscopy (TG-FTIR). The TG-FTIR analysis of the Argonne coals and the determination of kinetic rates are presented in detail elsewhere.[41-43,59,60] Table I presents the parameters for the Argonne oals and PSOC 815 used by Seki et al.[51] for which fluidity data and samples were available. Since it was not possible to obtain samples for the other coals used for the fluidity measurements reported in the literature[1,48,50] we have selected from the Argonne coal samples those which best match the reported coals in carbon concentration and volatile matter. Table II presents the available data on the coals whose fluidities have been reported in the literature and the Argonne coals chosen to represent them. More complete composition data for the Argonne coals were presented by Vorres[61] and for PSOC 815 by Seki et al.[51]

Model

The model of coal fluidity consists of two parts: (i) a macromolecular network model (FG-DVC) to predict the liquid fraction as a function of time and temperature (this prediction includes all the rank-dependent bond breaking and cross-linking behavior and effects of weathering or extraction); and (ii) rank-independent empirical expressions to predict fluidity from the liquid fraction, and the temperature.

The Macromolecular Network Decomposition Model. To predict the liquid fraction and its average molecular weight, we employ the FG-DVC model which describes the decomposition or condensation of the macromolecular network under the influence of bond breaking and cross-linking reactions.[38,41-43,58] The model employs a sample macromolecular network in the computer, consisting of aromatic ring clusters (monomers) linked by bridges. The molecular weights of the ring clusters is estimated from FIMS data[42] and ^{13}C NMR.[62] The bridges are either stable and remain unbroken or are broken by bond scission reactions. New bridges are formed by cross-linking. As discussed previously,[38,43,58] cross-linking occurs at low temperatures for low-rank coals by a process apparently associated with CO_2 evolution. Cross-linking at moderate temperatures occurs by a process associated with CH_4 evolution. This is based on an experimentally observed correlation between the evolution of CH_4 and the appearance of new cross-links in the macromolecular network (as determined by the solvent swelling ratio). A possible explanation for this observation is that the methane is formed by an ipso substitution reaction in which a methyl group is replaced by a free radical attached to the network or to a network fragment. It is the latter process which leads to the reduction of fluidity shown in Figure 1.

An example of the model is shown in Figure 2. Figure 2a shows the starting molecule. The network is formed from linear oligomer chains of length l (horizontal) joined by random cross-links (vertical). The network is characterized by the molecular weight of the ring clusters and the average number of attachments per cluster. When more than two attachments are present per cluster a cross-link or branch point occurs. During the initial development of the model, the number of initial branch points (verticle doubled lines) per monomer, m_0, was chosen to match values of molecular weight between cross-links reported in the literature.[38,41-43] This parameter,

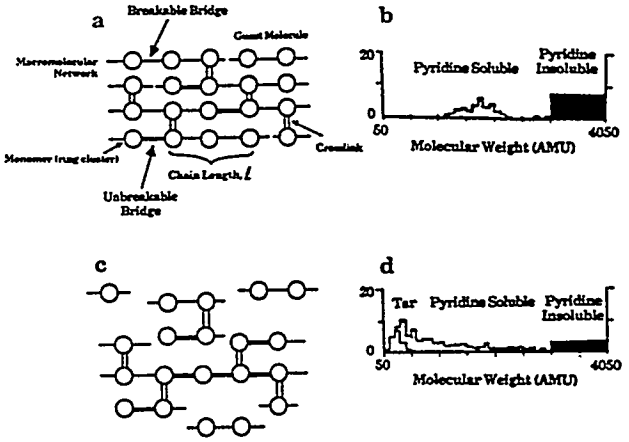

Figure 2. Representation of a coal molecular network in a Monte Carlo simulation (a and c) and corresponding molecular weight distribution (b and d). In the molecule, the circles represent monomers (ring clusters with their peripheral groups). The molecular weight distributions of the network are shown as histograms in b and d. The histogram is divided into tar, pyridine-soluble and pyridine-insoluble fractions. The area under the histogram corresponds to the weight percent of the oligomers.

which is derived from solvent swelling, is, however, not well known and so instead of fixing it from swelling data, it became one of the two adjustable parameters used to fit the fluidity data. The parameter is within the range of reported values. The second parameter is the length of the linear oligomer chains l, which are cross-linked to form the network. This parameter is selected so that the fraction of unattached small monomer cluster matches the measured fraction of pyridine solubles. With a fixed number of cross-links, m_0, the smaller the vale of l, the lower the probability that a given oligomer will be attached to the network and thus the higher the value of unattached "extractables". This parameter l is thus fixed for a fixed value of m_0, but varies with the choice of m_0. The final parameter in the model is the fraction of donatable hydrogens H(al) in the network. It is assumed that all the donatable hydrogens are in the labile ethylene (C_2H_4) bridges, so H(al) determines the number of breakable bridges. These are randomly distributed in the linear oligomer chains. All other bridges in the chains are assumed to be unbreakable. The unbreakable bridges are indicated by heavy horizontal lines and the breakable bonds by thin horizontal lines. Cross-links once formed are also assumed to be unbreakable. As in the case of m_0, H(al), is not easily measured and has become the second adjustable parameter.

With the parameters m_0, l, and H(al) determining the number and type of bonds, the position of the bonds is randomly chosen and the molecular weight distribution of the initial coal molecule is computed. The result is shown in Figure 2b.

To simulate pyrolysis, the rates of bond breaking and cross-linking are determined at each time step and the appropriate changes in bridge concentration are randomly distributed in the molecule. When bonds are broken, more small molecules are formed as shown in Figure 2, c and d. For each labile bridge broken, a second labile bridge is converted to an unbreakable bride (C_2H_2) as its hydrogen is used to stabilize the free radicals. The light molecules evaporate and become tar. The value of H(al) thus determines the total number of bridges which can be broken and, thus, the extent to which the network comes apart. The parameter m_0 determines the efficiency with which the network is fragmented. The larger the value of m_0, the more bonds must be broken to produce fragments, and the

(59) Solomon, P. R.; Serio, M. A.; Carangelo, R. M.; Bassilakis, R.; Gravel, D.; Baillargeon, M.; Baudais, F.; Vail, G. *Energy Fuels* 1990, *4* (3), 319.
(60) Serio, M. A.; Solomon, P. R.; Charpenay, S.; Yu, Z. Z.; Bassilakis, R. *Prepr. Pap.—Am. Chem. Soc., Div. Fuel Chem.* 1990, *35* (3), 808.
(61) Vorres, K. *Prepr. Pap.—Am. Chem. Soc., Div. Fuel Chem.* 1987, *32* (4), 221.
(62) Solum, M. S.; Pugmire, R. J.; Grant, D. M. *Energy Fuels* 1989, *3*, 187.

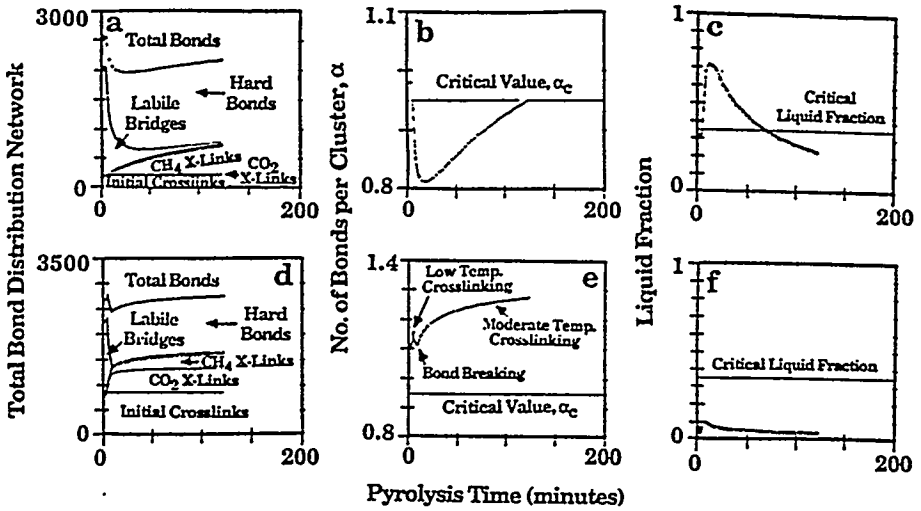

Figure 3. Comparison of the variation in the unbroken bond concentration, bonds/cluster, α, and liquid fraction with time at constant temperature of 440 °C for (a–c) Upper Freeport bituminous coal and (d–f) Wyodak subbituminous coal.

smaller the fragments. Thus, m_0 determines the ratio of small to large fragments.

To illustrate the model's predictions, we consider in Figure 3 the break up of the network as a function of time at a temperature of 440 °C. Figure 3 compares, for a subbituminous and a bituminous coal, the variation with time at constant temperature in the total number of unbroken bonds (bridges and cross-links), the number of unbroken bonds per cluster α, and the liquid fraction. Also shown are the individual contributions to the total bond count. Both networks experience a minimum in α as bonds are cleaved and then reconnected through cross-linking reactions. This leads to a maximum in the liquid fraction shown in Figure 3, c and f. As discussed below, the viscosity is related to the liquid fraction produced during the break-up of the network. The liquid fraction consists of all molecules detached from the starting macromolecular network (the solid fraction). Operationally, we count the largest three molecules as belonging to the solid fraction and all others as belonging to the liquid fraction. This is a convenient approximation which gives results that agree reasonably well with experiment and do not depend on the molecular weight of the starting computer molecule. We have also used just the largest molecule as the solid fraction and found that computed results are similar but noisier.

An important feature of a network model is that the break-up or solidification of the network occurs near a "gel point" where the number of unbroken bonds per ring cluster (monomer), α, reaches a critical low value. In a homogeneous network model, this gel point for a polymerizing melt occurs at the first appearance of the solid (or in the case of a decomposing network when the liquid fraction goes to 1.0), since the solid in a homogeneous melt extends throughout the entire melt. For most network geometries, the break-up of the network occurs between $\alpha = 1.0$ and $\alpha = 0.8$.

For an inhomogeneous melt (such as expected for a liquefying powdered coal sample), the solids can appear as isolated particles (instead of extending across the whole sample as in a homogeneous melt), so the gel point occurs at a higher solid fraction (lower liquid fraction). Based on the inhomogeneous model of fluidity discussed below, the liquid fraction must only exceed 0.35 before there is sufficient liquid to separate the solid particles, and appreciable fluidity can occur. With the network geometry assumed for this model, this minimum liquid fraction is achieved at a critical value α_c of approximately 0.95. For bituminous coals, this critical value can be achieved in pyrolysis and the coal melts and becomes fluid as illustrated in Figure 3c. For low-rank coals, the effect of low-temperature cross-linking is to increase α (see Figure 3e), so that in some cases the network cannot come apart by normal pyrolytic reactions. For the subbituminous coal, shown in Figure 3, the value of α has a sharp increase at low temperatures due to CO_2 related cross-linking. This can be seen by the appearance of CO_2 related bonds in Figure 3d. These bonds are a significant fraction of the total bonds connecting the network. With this large number of additional bonds, the value of α never achieves the critical value ($\alpha_c = 0.95$) and the solid fraction of the coal remains too high to liquefy (see Figure 3f). On the other hand, α for the bituminous coal is not increased by CO_2 related cross-linking. The value of α falls below the critical value and sufficient liquid is produced for the network to disintegrate and become fluid.

The Viscosity Model. Because of the inhomogeneous and complicated nature of coals, the viscosity model which we developed is purely phenomenological. The previous literature was employed to suggest the important parameters and appropriate relationships, but the final choice of the model was arrived at by finding the simplest expressions capable of fitting the available data. The viscosity model used here has terms that depend on the coal liquid temperature, and the volume fraction of solids, with an inhomogeneous gel-point.

In common with previous studies of coal viscosity, a two-phase model is used. The particular equation chosen is that put forward by Mooney[17,32]

$$\ln(\eta/\eta_{liq}) = \left[\frac{k_E\phi_s}{1-\phi_s/\phi_c}\right] \quad (1)$$

where η is the viscosity of the suspension, η_{liq} the viscosity of the liquid, k_E is the Einstein coefficient, and ϕ_s is the volume fraction of solids, having a critical value ϕ_c at which η goes to ∞.

The viscosity of the liquid phase is given by the Andrade equation

$$\eta_{liq} = C\exp(E_\eta/RT^*) \quad (2)$$

which on combining with eq 1 leads to

$$\eta = C\exp(E_\eta/RT^*)\exp\left[\frac{k_E\phi_s}{1-\phi_s/\phi_c}\right] \quad (3)$$

The constants used in the viscosity theory are as follows:

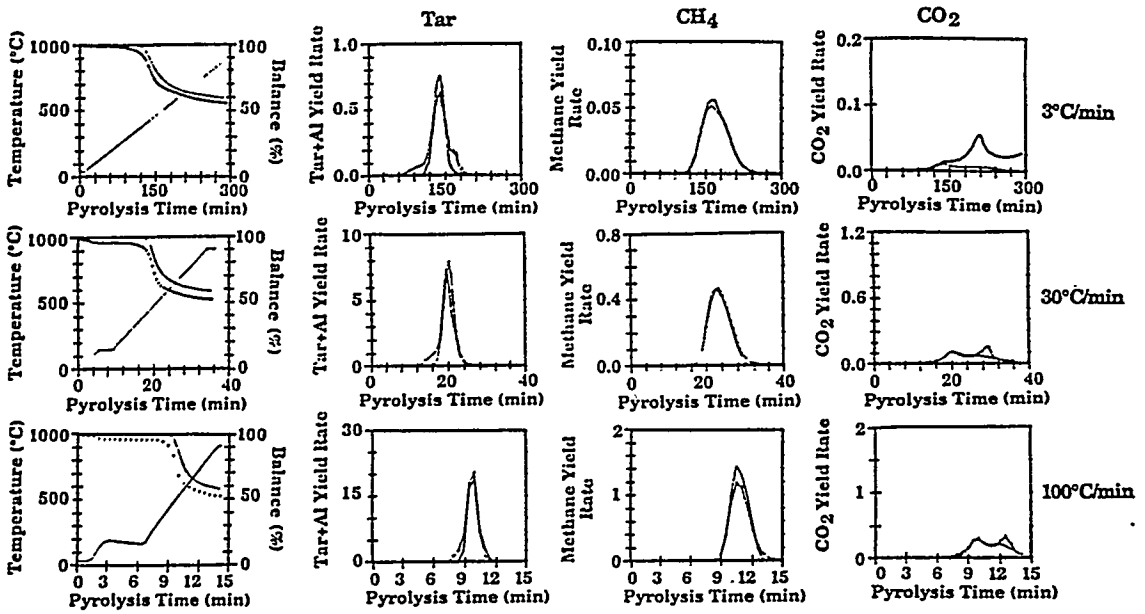

Figure 4. Kinetic analysis for Utah Blind Canyon coal for weight loss, tar evolution, methane evolution, and CO_2 evolution at three heating rates. Experiment (*) and theory (solid line) using the FG-DVC Model[41-43] with the kinetic rates reported in Table I.

k_E, Einstein coefficient, $k_E = 5.0$; ϕ_c, volume fraction of the solid phase at the gel-point, $\phi_c = 0.65$; η_{liq}, viscosity of the liquid phase; $\eta_{liq} = C_1 \exp(E_{\eta 1}/RT^*) = 7.5 \times 10^{-31} \exp(100\,000/RT^*)$ for $T \leq 708$ K, and $\eta_{liq} = C_2 \exp(E_{\eta 2}/RT^*) = 1.623 \times 10^{-15} \exp(50\,000/RT^*)$ for $T \geq 708$ K; T^*: Absolute temperature, cutoff at $T^c = 750$ K, i.e., $T^* = T$ for $T \leq T^c$ K, and $T^* = T^c$ for $T > T^c$ K; R: gas constant, $R = 1.98$ cal mol^{-1} K^{-1}.

The value of $k_E = 5$ was arrived at empirically, i.e., to fit the data. This value, however, matches the situation in which liquid is entrapped within large agglomerates of solid.[63] The value of the activation energies for coal was chosen based on measured liquid viscosities (from 50 to 100 kcal/mol) determined by Waters.[50] It should be noted that this is higher than that typically used for polymers and is probably describing chemical reactions and instrument-dependent effects as well as true viscosity. The use of a cutoff temperature T^c follows the concept introduced by Oh et al.[18]

Results

Volatile Evolution. There are two aspects to validating the model by comparison with data. The first is that the FG-DVC model should provide good predictions for pyrolysis products. This validates the coal-dependent kinetic rates for bond breaking and cross-linking and the amount of cross-linking. The second comparison of predictions is to fluidity data. Extensive comparisons of the FG and FG-DVC models have been made by Solomon et al. and Serio et al.[39-41] These comparisons show reasonable agreement between theory and experiment using rank-independent kinetics for the Argonne coals and several other coals. There are, however, some variations of kinetic rates with rank[59] and these differences particularly affect the viscosity predictions. We have consequently adopted rank-dependent kinetics for the FG-DVC model in making the fluidity predictions. We have employed the volatile evolution profiles from the TG-FTIR analysis to determine the rates by adjusting the rate constants to make the theory fit the data. Figure 4 compares the observed and predicted weight loss, tar evolution, methane evolution, and CO_2 evolution profiles at heating rates of 0.05, 0.5, and

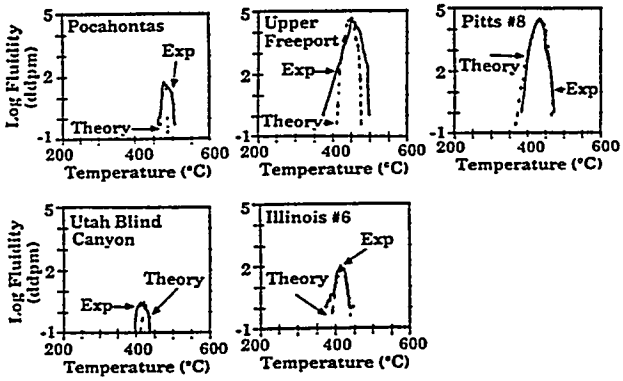

Figure 5. Comparison of measured and predicted fluidity for five Argonne coals: (*) experiment; (---) theory.

1.67 °C/s for Utah bituminous coal. The agreement is good for all three heating rates. The same procedure was employed for all eight Argonne coals.[43,59,60] A discussion of the procedure and a complete tabulation of rates appears elsewhere.[43,60] For PSOC 815 the results were fit from the 30 °C/min data only, assuming the same preexponential values used for the Argonne coals. The results are presented in Table I for E, k_0, and σ which are the parameters of rate equations of the form

$$k_n = k_0 \exp(-((E/R) \pm (\sigma/R))/T)$$

with k_0 in s^{-1}, E/R in K, and, σ/R in K.[41,42] The accuracy of the activation energies is estimated to be within ±2 kcal. With a fixed activation energy, the accuracy of the preexponential k_0 is ±25% and of σ is ±10%. These rates appear to provide good predictions when applied to fit data taken at much higher heating rates (5000 °C/s) as well.[43,60] The bond-breaking rates are in reasonable agreement with the tar evolution rates derived by Burnham et al.[64]

Viscosity Predictions for the Argonne Coals. All the viscosity data were fitted using the same viscosity equations and same viscosity model constants. The kinetic rates for bond breaking and the amount and rates of CO_2 and CH_4 evolution are determined from the TG-FTIR analysis. The only adjustable parameters for each coal

(63) Lewis, T. B.; Nielsen, L. E. *Trans. Soc. Rheol.* 1968, *12*, 421.

(64) Burnham, A. K.; Oh, M. S.; Crawford, R. W.; Samoun, A. M. *Energy Fuels* 1989, *3*, 42.

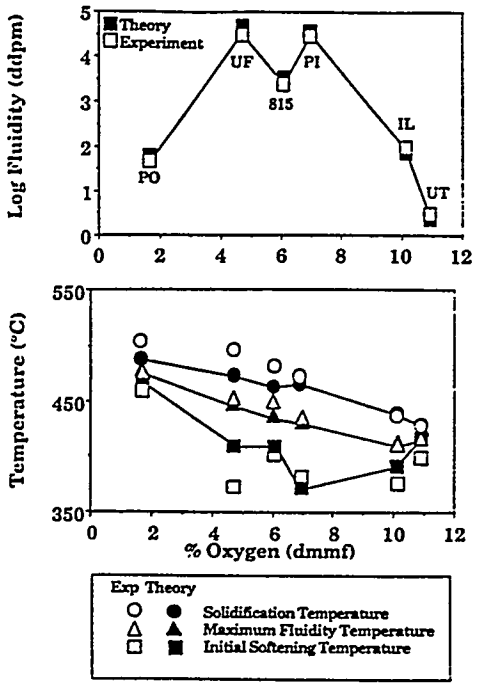

Figure 6. Fluidity behavior as a function of coal rank: theory and experiment. (a) Maximum fluidity values and (b) fluidity temperatures.

were the number of initial cross-links per monomer, m_0, and the percent of donatable hydrogen H(al). The value of l is obtained from the extracted amount and the value chosen for m_0. The cross-linking efficiency for CH_4 and CO_2 is one cross-link formed per CH_4 or CO_2 evolved.

Figure 5 compares the theoretical and experimental Gieseler plastometer curves[53] for the five Argonne coals for which data were available. The low-rank Argonne coals, Zap and Wyodak, showed no fluidity and the Lewis-Stockton coal was not measured. Figure 6 compares the maximum fluidity, solidification temperature, maximum fluidity temperature, and initial softening temperature as a function of the coal's oxygen concentration. In general, the data are in good agreement with the model. The agreement is the worst for the Upper Freeport initial softening and solidification temperatures. The maximum fluidities as a function of carbon concentration match the trends summarized by Whitehurst,[65] with maximum fluidity achieved between 4–8% 0 DMMF (84 and 88% C).

Considering that there are only two adjustable parameters required to fit the Gieseler curve, it appears that the model is more than just curve fitting. Further comparisons which allow predictions of other conditions lend further credence to the model's accuracy in simulating the chemical and physical processes in fluidity. One such comparison is of the predicted liquid yield compared with M_{2T} values derived by Lynch et al.[66] The M_{2T} parameter is a measure of the hydrogens attached to nonmobile molecules. As coal is heated M_{2T} is observed to decrease as pyrolysis begins, reaching a minimum value (which coincides with the maximum fluidity temperature), and then to increase. We find that our predicted solid fractions have a similar dependence on temperature when compared to the M_{2T} data for the Argonne coals.[67] Comparison of our

(65) Whitehurst, D. D.; Mitchell, T. O.; Farcasiu, M. *Coal Liquefaction: The Chemistry and Technology of Thermal Processes*; Academic Press: New York, 1980.

(66) Lynch, L. J.; Webster, D. S.; Sakurovs, R.; Barton, W. A.; Maher, T. P. *Fuel* 1988, *67*, 579.

(67) Sakurovs, Richard. Private communication.

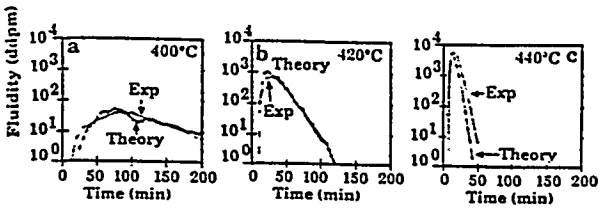

Figure 7. Comparison of experiment and theory for fluidity of a high-rank coal at constant temperatures of (a) 400 °C, (b) 420 °C, and (c) 440 °C. The experiment is for a coal which has 30% volatile matter content[48] and theory is for Upper Kanawha (see Tables I and II).

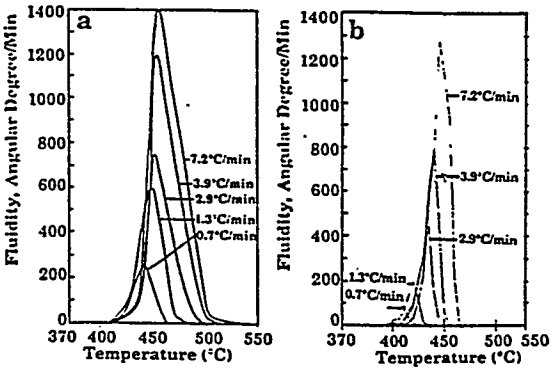

Figure 8. Fluidity at constant heating rate: (a) experimental data of van Krevelen[1] for 24% volatile coal and (b) theory for Upper Freeport coal (see Tables I and II).

model with the M_{2T} data will be the subject of a future publication. Other fluidity conditions which can be compared to the model are discussed below.

Viscosity Predictions for Literature Data. The first example of the application of the model to predict fluidity for literature data is shown in Figure 7. The data are from Oxley and Pitt[48] obtained by heating to constant temperatures of 400, 420, and 440 °C. The coal is believed to be closest in behavior to the Lewis–Stockton since it has comparable volatile weight loss, and the parameters for this coal, except for a different amount of CH_4 and slightly different network parameters, were employed (see Table II). The agreement is excellent in following the increase and decrease in fluidity due to bond breaking and cross-linking, suggesting that these processes are accurately modeled. The magnitude of the fluidity is accurately predicted at all temperatures.

Results for a higher rank coal studied by van Krevelen[1] at constant heating rates are presented in Figure 8a. Considering fluidity data and volatile matter, this coal's rank seemed to be between Upper Freeport and Pocahontas coals. The coal composition and kinetic parameters picked to represent the coal were that of Upper Freeport. The bond-breaking rate was, however, chosen to be the same as for Pocahontas in order to match the amount of fluidity (see Table II). The theoretical predictions in Figure 8b are in reasonable agreement with the data. The data, however, shows a narrower range of initial softening than the simulation, suggesting a greater influence of melting for this coal.

Data from isothermal experiments for the same Van Krevelen coal are presented in Figure 9a. The theory in Figure 9b show the right increase in fluidity with temperature. The model, however, does not predict the very early rise in fluidity at low temperature (400 and 408 °C), which is probably related to the breakage of hydrogen bonds and consequent melting. The loss of fluidity is also predicted to occur sooner than is indicated by the data. Additional effort to determine the sources of error was not made because the coals were not available to accurately

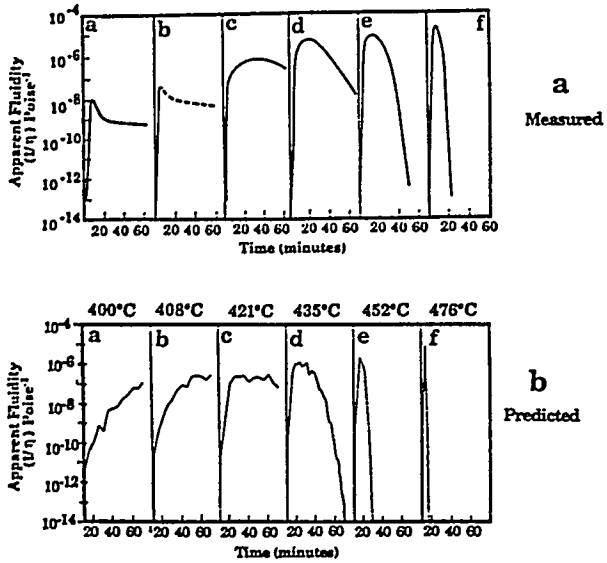

Figure 9. Fluidity at constant temperature: (a) experimental data of van Krevelen[1] for 24% volatile coal and (b) theory for Upper Freeport coal (see Tables I and II).

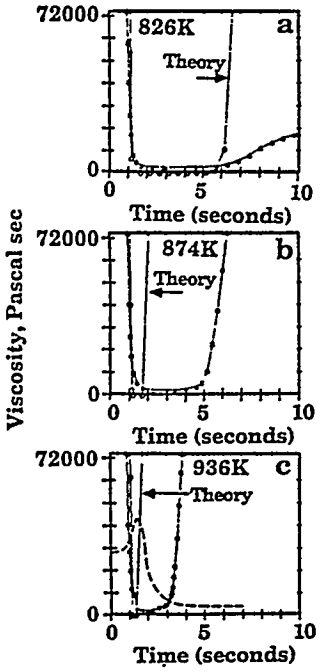

Figure 10. Viscosity at high temperatures. Symbols connected by line are data of Fong et al.[17] Lines without symbols are theory. Dashed line in (c) is the extract yield.

determine the kinetic and composition parameters.

Results for a Pittsburgh Seam coal obtained at high heating rates by Fong et al.[17] are presented in Figure 10 as the symbols connected by lines. The theory is shown as the solid lines. There is good agreement between theory and experiment for the onset of fluidity. The maximum fluidity is overpredicted by about 1 order of magnitude, possibly because the model based the prediction on the Argonne Pittsburgh No. 8, instead of the Pittsburgh coal from Fong's experiment (see Table II). Another possibility is that Fong's calibration relating disk rotation velocity to fluidity is not fully consistent with the calibration made for the Gieseler plastometer by Stevens[56] and Soth and Russel.[57] Since the model constants were calibrated using Gieseler plastometer data in which rotation is measured at constant torque, the discrepancy may suggest that there are non-Newtonian effects or consequences due to bubbles

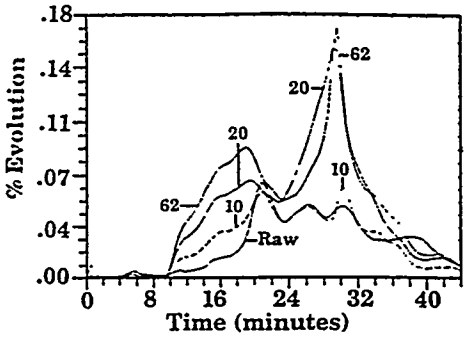

Figure 11. CO_2 evolution curves for raw coal and 10, 20, and 62 days oxidized coals.

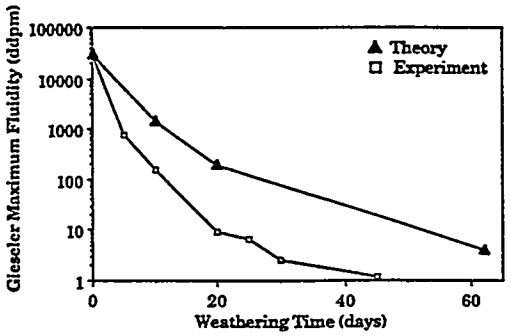

Figure 12. Comparison of predicted and measured fluidity for oxidized Pittsburgh coal (data from Wu et al.[52]).

or ash. The loss of fluidity is also predicted to occur much sooner than expected. The extract yield obtained by Fong et al.[17] in a heated grid experiment is also shown as a dashed line. The disappearance of fluidity predicted by our model does appear to coincide with the disappearance of the extract yield. This is as expected, since the model is dependent on the liquid fraction. The fact that the fluidity and extract data do not agree may suggest that there are differences in temperature between the two apparatuses employed by Fong.

Effect of Oxidation on Fluidity. It is well known that oxidation of coal rapidly destroys its fluidity. A systematic study of the effect of coal weathering on fluidity was recently reported by Wu et al.[52] The maximum fluidity for a Pittsburgh Seam coal was reduced from 30 000 DDPM to a little over 1 DDPM by oxidation for 40 days at a temperature of 80 °C and to a little over 10 DDPM by weathering for 380 days at 50 °C.

Oxidation of a Pittsburgh Seam coal in our laboratory was performed at 80 °C for 10, 20, and 62 days. In our model, the loss of fluidity with increasing oxygen concentration is related to the increase in CO_2 evolution and, hence, increases in low-temperature cross-linking. To determine the CO_2 evolution at low temperatures, measurements were made in the TG-FTIR.[59] The data in Figure 11 show that the low-temperature CO_2 evolution was significantly increased, becoming comparable to that for Illinois No. 6 after 10 days of oxidation, and becoming larger than that for the Utah bituminous coal after 20 days. After 3 months at 110 °C the CO_2 evolution was comparable to that of a lignite. When these increased CO_2 yields were incorporated in the simulation for the oxidized Pittsburgh Seam coal's fluidity, the maximum fluidity was reduced.

We compare our predicted maximum fluidity with the measurement of Wu et al.[52] for comparable coal and oxidation treatment in Figure 12. The agreement is quite reasonable considering the difference in coal samples. Also, the work of Wu et al. suggests that some of the loss of

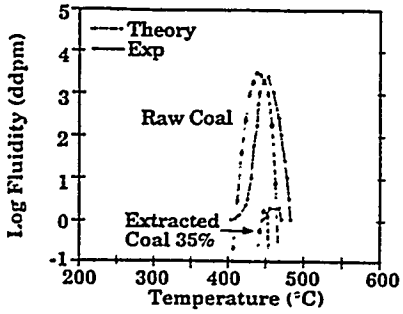

Figure 13. Comparison of predicted and measured fluidity for raw PSOC 815 coal and 35% extracted coal (data from Seki et al.[51]).

fluidity is caused by weathering of the pyrite which is not included in our model.

Effect of Extraction on Fluidity. The extraction of coal with organic solvents has been shown to affect the caking property of the coal residue.[68] To study this effect, Seki et al. measured the fluidity of a coal and a set of residua after extractions in a mix of CS_2–pyridine and CS_2–NMP solvents.[51] Their results in Figure 13 show that extracting the coal reduces the fluidity.

In our model, extraction of the coal reduces the fluid fraction and hence the fluidity. To model their results, we obtained a sample of PSOC 815 and determined the composition and kinetic parameters for the model by performing TG-FTIR and solvent swelling analysis experiments. Based on these data, the computed liquid percentage of the room temperature sample of raw PSOC 815 is 40%. The predicted fluidity for the raw coal is shown as the dashed line in Figure 13. The agreement with the data is good. To model the residua after extraction, the oligomer length l was varied to reduce the liquid fraction in the starting residue by the amount extracted. For the case in which 30% of the coal was extracted, the starting liquid amount was reduced from 40% to 10%. The fluidity calculated for the 30% extract yield case shown in Figure 13 agrees well with the measured values.

Discussion

The comparisons presented above demonstrate that the model which we have developed fits fluidity data for all ranks of coal and predicts the proper trends with heating rate, weathering, or extraction. In evaluating the usefulness of any model, there are, however, a number of additional questions which should be addressed. (1) Does the model extrapolate to other conditions? (2) Are the number of adjustable parameters manageable? (3) Is the model really describing the physical and chemical processes, or simply curve fitting? (4) How unique is the model?

With regard to the first question, all of the kinetic rates were derived from low heating rate data, but the one comparison to high heating rate fluidity[17] seems reasonable. Also, extrapolations of the model to predict tar and gas yields at high heating rates are good.[60,69,70]

With regard to the second question, the fluidity part of the model has seven parameters: $C = C_1$ or C_2 depending on temperature, K_E; $E_\eta = E_{\eta 1}$ or $E_{\eta 2}$ depending on temperature; ϕ_c, and T^c, but these are fixed for all coals and conditions. The FG-DVC model has many coal composition and kinetic parameters, but these are fixed based on the TG-FTIR analysis except for three parameters related to the macromolecular network geometry (m_0, l, and H(al)). Two of these can be independently adjusted to fit the fluidity, tar evolution, and solvent extraction data. We believe that two adjustable parameters is reasonable.

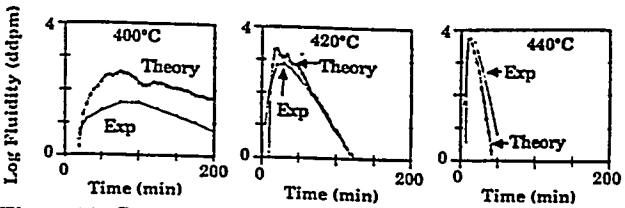

Figure 14. Comparison of Oxley and Pitt Data[48] with predictions using E_η = 50 kcal.

With regard to the third question, the description of the decomposition and resolidification of the macromolecular network appears sound in concept, since the model fits fluidity, extract yields, tar evolution, gas evolution, and M_{2T} measurements.[66,67] The network model appears to provide a good parameter, the solid fraction, ϕ_s, upon which the fluidity equations are based. This parameter incorporates all of the rank-dependent bond breaking and cross-linking phenomena and the effects of weathering or extraction. On the other hand, the fluidity equations are empirical and do not have any obvious relationships to physical phenomena. Their functional form is consistent with those employed in previous investigations.

A further test is whether the network parameters make any sense. This is related to the fourth question of how unique is the choice of these parameters. To address these issues we have performed a sensitivity analysis, considered the variation in the parameters with rank, and considered the meaning of the parameters. These issues are discussed below.

Sensitivity Analysis. A sensitivity analysis was conducted in which the predictions of the model were determined using variations in the values of the fluidity model parameters, k_E, E_η, ϕ_c, and T^c, and the coal network parameters H(al), m_0, and l. The parameter C is simply a proportionality constant.

Variations in E_η and T^c. Variations in the assumed value of E_η were made between the extremes reported by Waters of 50–100 kcal/mol. Also, T^c (cutoff temperature) was varied between 708 and 750 K. The network parameters were readjusted in each case to get the best fit. Good fits were achieved for all the Argonne coals for values of 50, 80, and 100 kcal/mol. In this case, since the data were taken for a single heating rate, there is only one value of the temperature for maximum fluidity for each coal. Potential errors in choosing the wrong value of E can be overcome by adjusting the network parameters. Thus, if just the Argonne data at 3 °C/min are used, then the model is insensitive to the choices of E_η and T^c.

The same comparisons at 50, 80, and 100 kcal and variable T^c were made in simulating the data of Oxley and Pitt and van Krevelen which provide data for several temperatures of maximum fluidity for each coal. Figure 14 presents the Oxley and Pitt predictions for E_η = 50 kcal with the critical temperature T^c = 750 K. The highest value of E_η (100 kcal/mol) in Figure 7 gave a better fit, especially for low temperatures, suggesting a high value of E_η.

The Oxley and Pitt data were insensitive to the value of the critical temperatures T^c, since all the experiments were done at temperature lower than 713 K. The van Krevelen data, which describe the behavior of a coal up

(68) Dormans, H. N. M.; van Krevelen, D. W. *Fuel* 1960, *39*, 273.
(69) Serio, M. A.; Solomon, P. R.; Yu, Z. Z.; Bassilakis, R. *Prepr. Pap.—Am. Chem. Soc., Div. Fuel Chem.* 1989, 34 (4), 1324.
(70) Solomon, P. R.; Serio, M. A.; Markham, J. R. Kinetics of Coal Pyrolysis *Int. Conf. Coal Sci., Proc., IEA, Tokyo, Jpn. October 23–27*; 1989, 575.

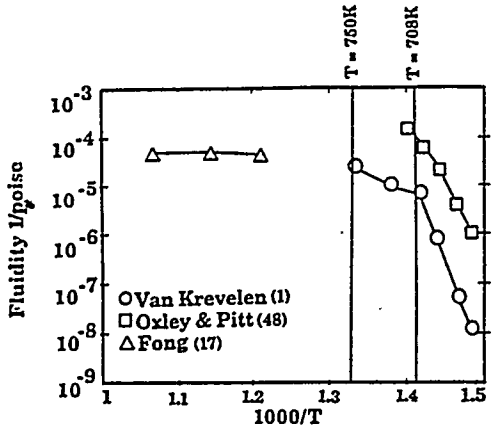

Figure 15. Maximum fluidity for three experiments.

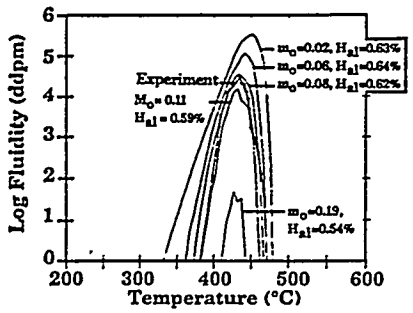

Figure 16. Comparison of measured fluidity for Pittsburgh No. 8 coal with predictions using different values of m_0 (initial cross-link density).

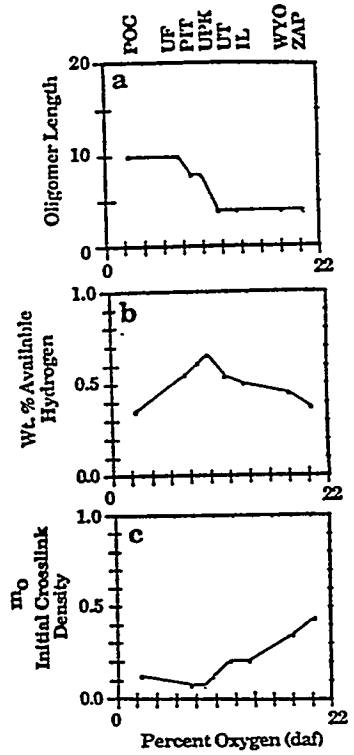

Figure 17. Variation of network parameters with rank: (a) starting oligomer length l; (b) weight percent hydrogen H(al); and (c) initial cross-link density, m_0. Cross-links/cluster (note: one cross-link connects two monomers).

to 749 K, were also well predicted using $E_\eta = 100$ kcal at low temperatures (up to 708 K). However, at higher temperatures the fluidity was overpredicted. Figure 15 which presents the maximum fluidity achieved as a function of temperature seems to indicate a change in E_η at about 708 K. To take this into account we reduced E_η from 100 to 50 kcal for temperatures between 708 and 750 K and adjusted C accordingly. This change does not have any influence on Argonne coal fluidity predictions and Oxley and Pitt predictions, since in these cases fluidity is present at temperatures generally lower than 708 K. While this choice of reducing E_η is only based on one experiment, it gave good predictions for all available data including van Krevelen's. Further experiments on variations in fluidity with temperature should be performed and compared.

Variations in k_E. We varied k_E between 2.5 and 5. $k_E = 5$ gave a better fit by allowing a wide range of fluidity values since it emphasizes the role of the amount of liquid fraction. This helped us fit low-rank coals like Illinois No. 6, which have a large tar amount but low fluidity.

Variations in ϕ_c. As mentioned earlier in the Introduction, the critical solid volume fraction ϕ_c has a value of 0.64 for randomly close packed spheres and is thought to range between 0.5 and 0.9 for other systems. As a first approximation, we chose ϕ_c to be 0.65 and were able to fit all the available data. We believe that other parameters (initial cross-link density and the proportionally constant for the viscosity) can compensate for the choice of ϕ_c and values between 0.60 and 0.70 could be used equally well.

Variations with m_0 and H(al) and l. Having fixed the parameters in the fluidity model, tests were made of the sensitivity of the model to the assumed values of m_0, H(al), and l. Figure 16 presents predictions for the fluidity of the Pittsburgh Seam coal for different values of m_0. The simulations were performed with the following rules: (1) a value of m_0 was picked, (2) H(al) was adjusted to give the correct tar yield in the TG/plus experiment, (3) l was picked to give the correct extract yield for the starting coal. The fluidity predictions were then compared with the data. Figure 16 demonstrates that the model requires a unique value of m_0 and H(al). The simulation required a value of $m_0 = 0.08 \pm 0.01$, a value of $l = 8 \pm 2$, and a value for H(al) of 0.62%. This value of m_0 will be chemically meaningful if the viscosity parameters (especially E_η) have been correctly chosen. The same result is achieved if H(al) is varied and m_0 and l are adjusted to give the correct tar yield and extract yield.

Variation of Network Parameters with Rank. The three parameters of the model, l, H(al), and m_0, have been determined for the Argonne coals. These are plotted in Figure 17a–c as a function of the oxygen in the coal. Also plotted in Figure 18 is the molecular weight between cross-links M_c derived from m_0 and the average molecular weight of a ring cluster, the measured solvent swelling ratio, and the extract yield.

The network parameters show systematic variations with rank. The molecular weight between cross-links and the oligomer length both decrease with decreasing rank. This suggests the low-rank coals are more highly branched (large m_0) to yield low extractable amounts while the highest rank coals have fewer branches but longer chains (large l) to yield low extractable amounts. The high fluidity coals must have low values of m_0 to yield a high fluid fraction, but also must have small amounts of low-temperature cross-linking so that the amount of branching remains low prior to cross-linking. The starting cross-link density for low-rank coals (Zap, Wyodak) presents some uncertainty, since there is no apparent fluidity to better define the network parameters.

Figure 18b presents the molecular weight between cross-links, M_c, determined by our model,

$$M_c = M_{avg}/2m_0$$

where M_{avg} is the average molecular weight of a cluster.

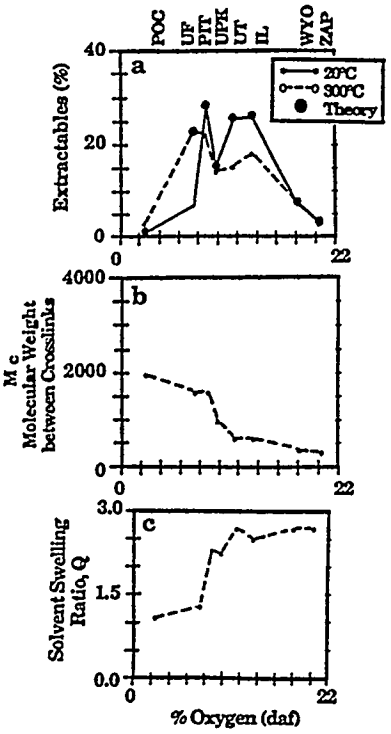

Figure 18. Variation of network parameters with rank: (a) extractables, (b) molecular weight between cross-links; (c) solvent swelling ratio, Q.

The factor of 2 occurs because each cross-link connects two clusters. We have not determined M_c from solvent swelling theories[71,72] because of the uncertainty in the proper way to calculate the solvent swelling and uncertainties in the values of the interaction parameter χ. Our values of M_c for Pittsburgh, Lewis Stockton, Illinois No. 6, and Utah coals are within the range of those predicted from current theories of solvent swelling.[71,72] Our values for Pocahontas and Upper Freeport are, however, much higher than what would be calculated from their very low solvent swelling ratios (1.12 and 1.32, respectively) using any of the theories for M_c and acceptable χ values.[71,72] It is probable, however, that van der Waals forces or π—π bonding in these coals (not cross-linking) limit the swelling.[73] When heated to 400 °C, for example, the solvent swelling of the cooled Upper Freeport increases from 1.32 to 2.13.[57] Little chemistry has occurred, but the π—π bonding may have been disrupted.

The problems of π—π bonding may also affect the determination of the value of the l parameter. For the six lowest rank Argonne coals, pyridine swells the coal between a factor of 2 and 3. With the coals swollen to roughly the same large amount, it is expected that most of the loose molecules which are soluble in pyridine can be removed. On the other hand, the Upper Freeport and Pocahontas coals only have Q values of 1.32 and 1.12, and extract yields of 10% and 1%. The question is: are these coals covalently cross-linked, or is pyridine not able to break other noncovalent bonds such as the stacking interactions, or π—π bonds discussed by Larsen.[73] If the latter were the case, much of the loose material may be trapped. One indication that this is the case is the observation that after heating to 300 °C the extract yield from the more easily swollen Upper Freeport went from 10 to 23%. We have, therefore, chosen to employ the extract yield after heating to 300 °C

(71) Larsen, J. W.; Kovac, J. *ACS Symp. Ser.* 1978, *71*, 36.
(72) Lucht, L. M.; Peppas, N. A. *ACS Symp. Ser.* 1981, *169*, 43.
(73) Larsen, J. W. *Prepr. Pap.—Am. Chem. Soc., Div. Fuel Chem.* 1988, *33* (1), 400.

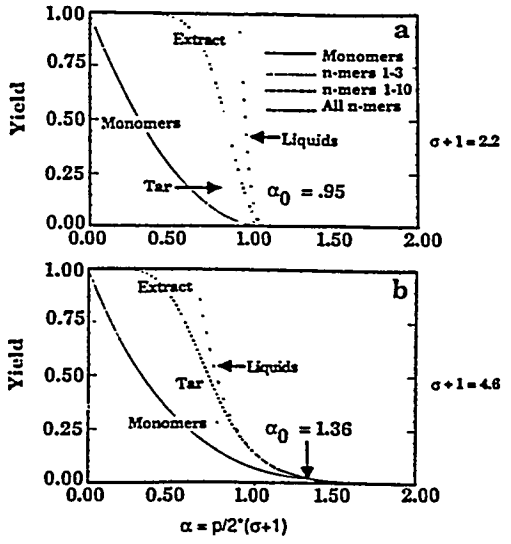

Figure 19. Percolation theory predictions for pyrolysis products (monomers, tar, extracts, and total liquids) for two values of coordination number: (a) $\sigma + 1 = 2.2$ and (b) $\sigma + 1 = 4.6$.

to determine a better value of l. This procedure may not give the complete extractable, so the value of l may still be in error. Also, it is possible that π—π bonding could affect the viscosity itself, so that C_1 and C_2 could be rank dependent. These effects could explain why the temperature predictions for Upper Freeport in Figure 6 are the worst of all the coals.

The values of H(al) are between 0.3 and 0.7%. This is within the range of expected concentrations for donatable hydrogen (the total aliphatic or hydroaromatic hydrogen (2–3%) minus the hydrogen in methyl groups (~1%) and other aliphatic peripheral groups or guest molecules (~1%).

Meaning of the Network Parameters. To understand the relationship between the network parameters and the pyrolysis behavior, it is useful to consider an alternative to the Monte Carlo method to compute the molecular weight distributions. The alternative is percolation theory employed by several research groups to describe the network fragmentation.[43-47] The percolation theory has the advantage that it is much faster to calculate than the Monte Carlo method, since the molecular weights are predicted by closed form analytical expressions. In addition, the relationship between the network parameters and the pyrolysis behavior is more transparent for the percolation theory than it is for the Monte Carlo method.

Figure 19 compares the predictions of the n-mer distribution (proportional to molecular weight distributions) for two networks with coordination numbers of 2.2 and 4.6. The coordination number designated by $(\sigma + 1)$ is the number of *possible* attachments per ring cluster. A linear polymer has $\sigma + 1 = 2$, while a "fish net" has $\sigma + 1 = 4$. The *actual* number of bridges per ring cluster α is defined by the probability p that bridges are unbroken, where $\alpha = (p/2)(\sigma + 1)$.

The importance of the coordination number is its effect on the n-mer distribution as a function of α. For low values of $\sigma + 1$, the liquid fraction is a strong function of α. For the $\sigma + 1 = 2.2$ network, there are large changes in the liquid yield for small change in α. Also, the ratio of liquids (all n-mers) to monomers, to n-mers up to 3 (representing the tar for a ring cluster molecular weight of 300), and to n-mers up to 10 (representing the extracts) is large. In contrast, for $\sigma + 1 = 4.6$ the liquid yield goes up more slowly with decreasing α and the ratio of liquids to the other products is much smaller.

By examining the percolation theory it is possible to see how the three parameters l, H(al), and m_0 are constrained. The ratio of liquid yield (to match the fluidity) to the measured tar yield constrains the value of $\sigma + 1$. In the Monte Carlo model, this is equivalent to constraining m_0. A high ratio of liquids to tar requires a low $\sigma + 1$ and a low m_0. Thus, referring to the rank dependence of the parameters in Figures 17 and 18, it is the decrease in the cross-linking during the process of maturation and the reduction in the low-temperature cross-linking which keeps the coordination number low prior to bond breaking. That allows the coals to become fluid.

From this discussion it is now possible to understand why weathering (oxidation) is so effective in reducing fluidity. It has always been puzzling why a small amount of oxygen uptake (which sometimes cannot even be measured) leads to large changes in fluidity. The apparent reason is that oxidation leads to low-temperature cross-linking, thus increasing the coordination number and reducing the liquid yield for the same number of bonds broken.

Conclusion

1. An empirical model for fluidity of coal has been developed based on a previously published macromolecular network model for coal pyrolysis.
2. The network model is used to predict the fraction of liquids under the combined effects of bond breaking and cross-linking.
3. The empirical model for an inhomogeneous melt assumes the fluidity to depend on the liquid fraction in the melt, and on the viscosity of the liquid.
4. Good agreement is obtained with fluidity data for eight coals which covers 5 orders of magnitude in fluidity and several hundred degrees in temperature. This agreement is obtained with fixed parameters in the empirical fluidity equations, with kinetics and volatile amounts fixed by TG-FTIR data, but with two adjustable parameters, the number of initial cross-links per monomer, m_0, and the percent of donatable hydrogens H(al). The third parameter l is fixed by the extract yield.
5. The model predicts the observed trends to lower fluidity with oxidation or extraction.
6. A sensitivity analysis suggests that the model is most sensitive to the three network parameters: the cross-link density m_0, the amount of donatable hydrogen H(al), and the oligomer length of l. These parameters appear to have some physical and chemical significance.
7. The effect of π—π bonding appears to be important for high-rank coals, reducing the accuracy of the predictions. Additional study is required to account for these effects.
8. Additional tests of the model using fluidity data derived for the Argonne coals over a wider range of heating rates would be important to further improve the model.

Acknowledgment. We gratefully acknowledge the support for the work provided by the Morgantown Energy Technology Center of the Department of Energy under Contract DE-AC21-86MC23075, Dr. Richard Johnson, Contract Monitor. We thank Mr. George Engelke from Commercial Testing and Engineering Co. who provided us with the Gieseler plastometer data for the Argonne coals.

Appendix N

Analysis of the Argonne Premium Coal Samples by Thermogravimetric Fourier Transform Infrared Spectroscopy

Reprinted from ENERGY & FUELS, 1990, 4.

Analysis of the Argonne Premium Coal Samples by Thermogravimetric Fourier Transform Infrared Spectroscopy

P. R. Solomon,* M. A. Serio, R. M. Carangelo, and R. Bassilakis

Advanced Fuel Research, Inc., 87 Church Street, East Hartford, Connecticut 06108

D. Gravel, M. Baillargeon, F. Baudais, and G. Vail

Bomem, Inc., 450 rue St. Baptiste, Quebec City, Quebec, Canada

Received October 19, 1989. Revised Manuscript Received April 2, 1990

We have developed a TG-FTIR instrument that combines thermogravimetric analysis (TGA) with evolved product analysis by Fourier transform infrared (FT-IR) spectroscopy. FT-IR analysis of evolved products has advantages over mass spectroscopy in allowing analysis of very heavy products and over gas chromatography in speed. This paper describes the most recent improvements in the apparatus and presents its application in characterizing the Argonne premium coal samples. The TG-FTIR apparatus for pyrolysis, oxidation of pyrolysis products, and oxidation of the sample is described. To analyze coal, a sequence of drying, pyrolysis, and combustion is employed to obtain proximate analysis, volatile composition, volatile kinetics, and relative char reactivity. Pyrolysis results are presented for the eight Argonne coals, several demineralized coals, and two oxidized samples of Pittsburgh Seam coal. A kinetic analysis was applied to species evolution data collected at several different heating rates. There is a systematic variation in rate with rank. The rate for tar evolution from Pittsburgh Seam coal is in good agreement with that of Burnham et al. using a similar set of data. Analysis of the amounts of evolved products also show a systematic variation with rank consistent with the coal's elemental and functional group comositions. Postoxidation of the volatile products has been successful in providing elemental composition information on the volatile products as well as showing the evolution of H_2, which is not infrared active, and H_2S (in the postoxidized SO_2 profile), which is a weak infrared absorber. Oxidation of the char yields an ash amount as well as two measures of the char's reactivity, the oxygen absorbed by the char and the temperature at which significant oxidation of the char occurs.

Introduction

Thermogravimetric analysis (TGA) has been employed in coal science to perform a number of characterizations including proximate analysis,[1] kinetics of weight loss,[2,3] char reactivity,[4-9] and gas adsorption measurements.[10] A complimentary technique, evolved-product analysis, has been employed to study pyrolysis product distributions

0887-0624/90/2504-0319$02.50/0

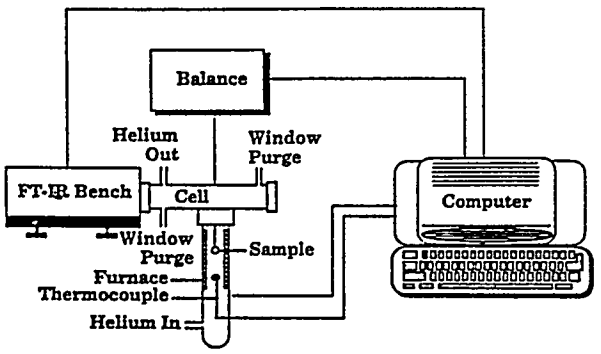

Figure 1. Schematic of TG/plus.

and kinetics,[11-18] functional group compositions,[14,19-21] and temperature-programmed desorption.[22-24] We have developed a TG-FTIR instrument which combines TGA with evolved-product analysis by Fourier transform infrared (FT-IR) spectroscopy. FT-IR analysis of evolved products has advantages over mass spectroscopy in allowing analysis of very heavy products and over gas chromatography in speed.

The application of TG-FTIR to coal and petroleum source rock has recently been described.[25,26] To analyze coal, a sequence of drying, pyrolysis, and combustion is employed to obtain proximate analysis, volatile composition, volatile kinetics, and relative char reactivity. By

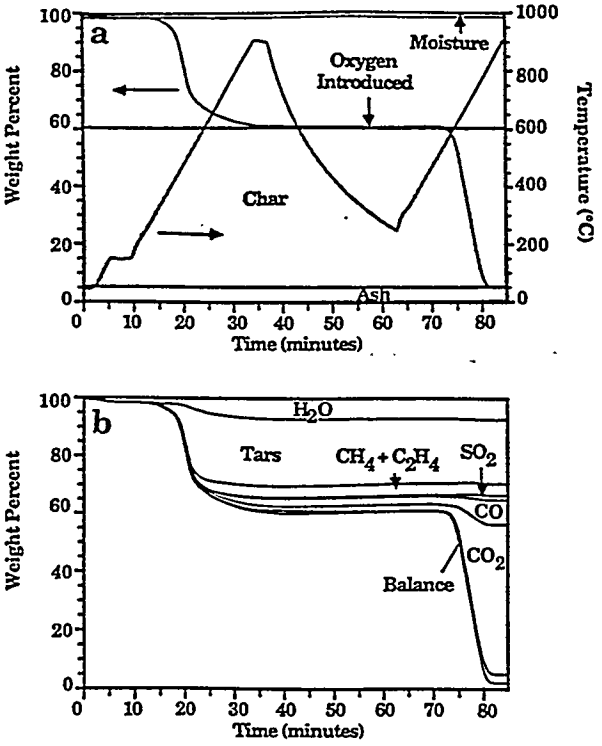

Figure 2. TG-FTIR analysis of Pittsburgh Seam coal. (a) Temperature history and weight loss. (b) Species contributions to weight loss.

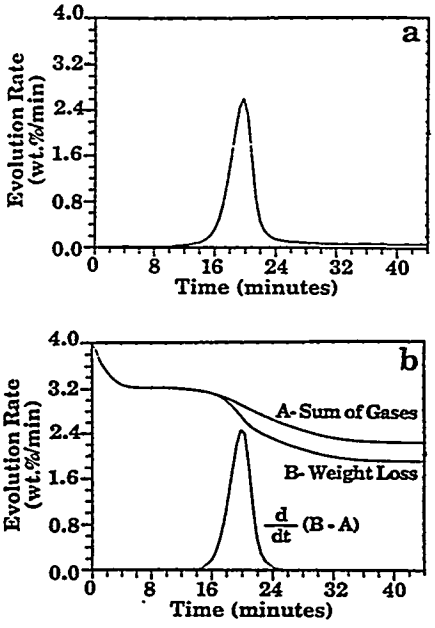

Figure 3. Calibration of tar absorptivity. (a) Tar absorption profile. (b) Weight loss minus the sum of gases.

employing several different heating rates, kinetic rate constants have been obtained.[27,28] The apparatus has been very useful in studying the effects of pretreatments such

(1) Ottaway, W. *Fuel* 1982, *61*, 713.
(2) Ciuryla, V. T.; Weimer, R. F.; Bivans, A.; Motika, S. A. *Fuel* 1979, *58*, 748.
(3) van Krevelen, D. W.; van Heerden, C.; Huntjens, F. J. *Fuel* 1951, *30*, 253.
(4) Solomon, P. R.; Serio, M. A.; Heninger, S. G. *Prepr. Pap.—Am. Chem. Soc., Div. Fuel Chem.* 1986, *31* (3), 200.
(5) Best, P. E.; Solomon, P. R.; Serio, M. A.; Suuberg, E. M.; Mott, W. R., Jr.; Bassilakis, R. *Prepr. Pap—Am. Chem. Soc., Div. Fuel Chem.* 1987, *32* (4) 138.
(6) Serio, M. A.; Solomon, P. R.; Bassilakis, R.; Suuberg, E. M. *Prepr. Pap—Am. Chem. Soc., Div. Fuel Chem.* 1989, *34* (1), 9.
(7) Serio, M. A.; Solomon, P. R.; Suuberg, E. M. The Variation in Char Reactivity with Pyrolysis Conditions and Coal Type. To be submitted.
(8) Jenkins, R. G.; Nandi, S. P.; Walker, P. L., Jr. *Fuel* 1973, *52*, 228.
(9) Sahu, R.; Levendis, Y. A.; Flagan, R. C.; Gavalas, G. R. *Fuel* 1988, *67*, 275.
(10) Suuberg, E. M.; Calo, J. M.; Wojtowicz, W. *Prepr. Pap.—Am. Chem. Soc., Div. Fuel Chem.* 1986, *31* (3), 186.
(11) Juntgen, H.; van Heek, K. H. *Fuel Process. Technol.* 1979, *2*, 261.
(12) Winans, R. E.; McBeth, R. L.; Neill, P. H. *Prepr. Pap.—Am. Chem. Soc., Div. Fuel Chem.* 1988, *33* (3), 85.
(13) Chakravarty, T.; Windig, W.; Hill, G. R.; Meuzelaar, H.L.C. *Energy Fuels* 1988, *2*, 400.
(14) Solomon, P. R.; Hamblen, D. G. *Finding Order in Coal Pyrolysis Kinetics*; Topical Report submitted to U.S. Department of Energy under Contract No. DE-AC21-81FE05122, 1983; also *Prog. Energy Combust. Sci.* 1983, *9*, 323.
(15) Fitzgerald, D.; van Krevelen, D. W. *Fuel* 1959, *38*, 17.
(16) Campbell, J. H. *Fuel* 1978, *57*, 217.
(17) Burnham, A. K.; Oh, M. S.; Crawford, R. W.; Samoun, A. M. *Energy Fuels* 1989, *3*, 42.
(18) Weimer, R. F.; Ngan, D. Y. *Prepr. Pap.—Am. Chem. Soc., Div. Fuel Chem.* 1979, *24* (3), 129.
(19) Attar, A.; Dupuis, F. *Prepr. Pap.—Am. Chem. Soc., Div. Fuel Chem.* 1978, *23* (2), 44.
(20) Attar, A.; Hendrickson, G. G. *Coal Structure*; Meyers, R. A., Ed.; Academic Press: New York, 1982; Chapter 5, p 131.
(21) LaCount, R. B.; Anderson, R. R.; Friedman, S.; Blaustein, B. D. *Fuel* 1987, *66*, 873.
(22) Hall, P. J.; Calo, J. M. *Energy Fuels* 1989, *3*, 370.
(23) Zhang, Z. G.; Kyotani, T.; Tomita, A. *Energy Fuels* 1989, *3*, 566.
(24) Kyotani, T.; Zhang, Z. G.; Hayashi, S.; Tomita, A. *Energy Fuels* 1988, *2*, 1136.
(25) Carangelo, R. M.; Solomon, P. R.; Gerson, D. G. *Fuel* 1987, *66*, 960.
(26) Whelan, J. K.; Solomon, P. R.; Deshpande, G. V.; Carangelo, R. M. *Energy Fuels* 1988, *2*, 65.
(27) Serio, M. A.; Solomon, P. R.; Yu, Z. Z.; Deshpande, G. V. An Improved Model of Coal Devolatilization. In *International Conference on Coal Science Proceedings*; IEA: Tokyo, Japan, 1989; p 209.
(28) Serio, M. A.; Solomon, P. R.; Yu, Z. Z.; Bassilakis, R.; Markham, J. R.; Klapheke, J. G. *Prepr. Pap.—Am. Chem. Soc., Div. Fuel Chem.* 1989, *34* (4), 1324.

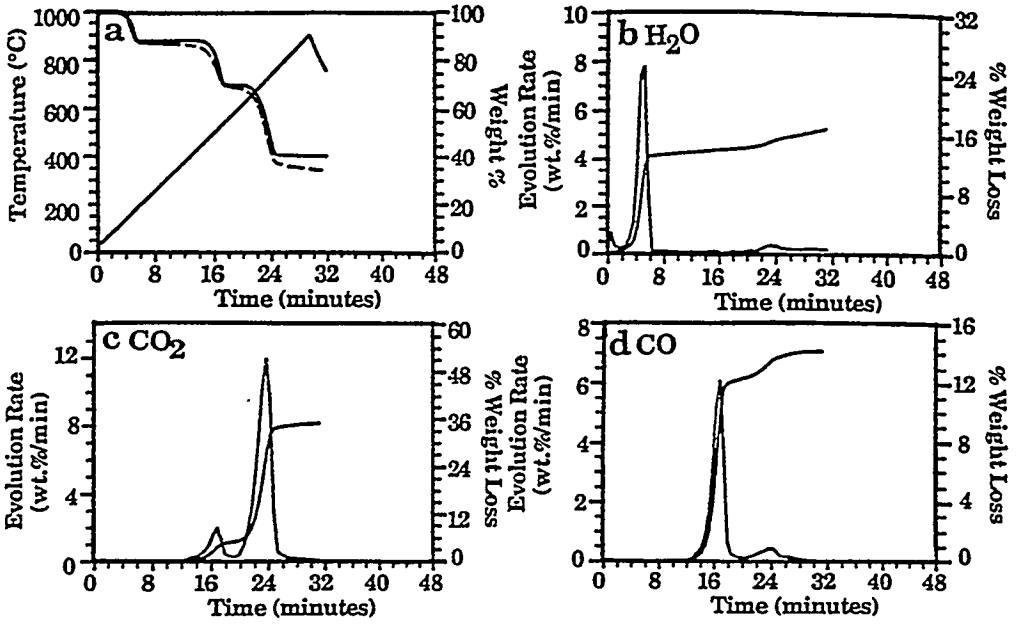

Figure 4. Pyrolysis of calcium oxylate. (a) Weight loss (solid), sum of evolved products (dashed), and temperature profile. (b) H_2O evolution and integrated amount evolved. (c) CO_2 evolution and integrated amount evolved. (d) CO evolution and integrated amount evolved.

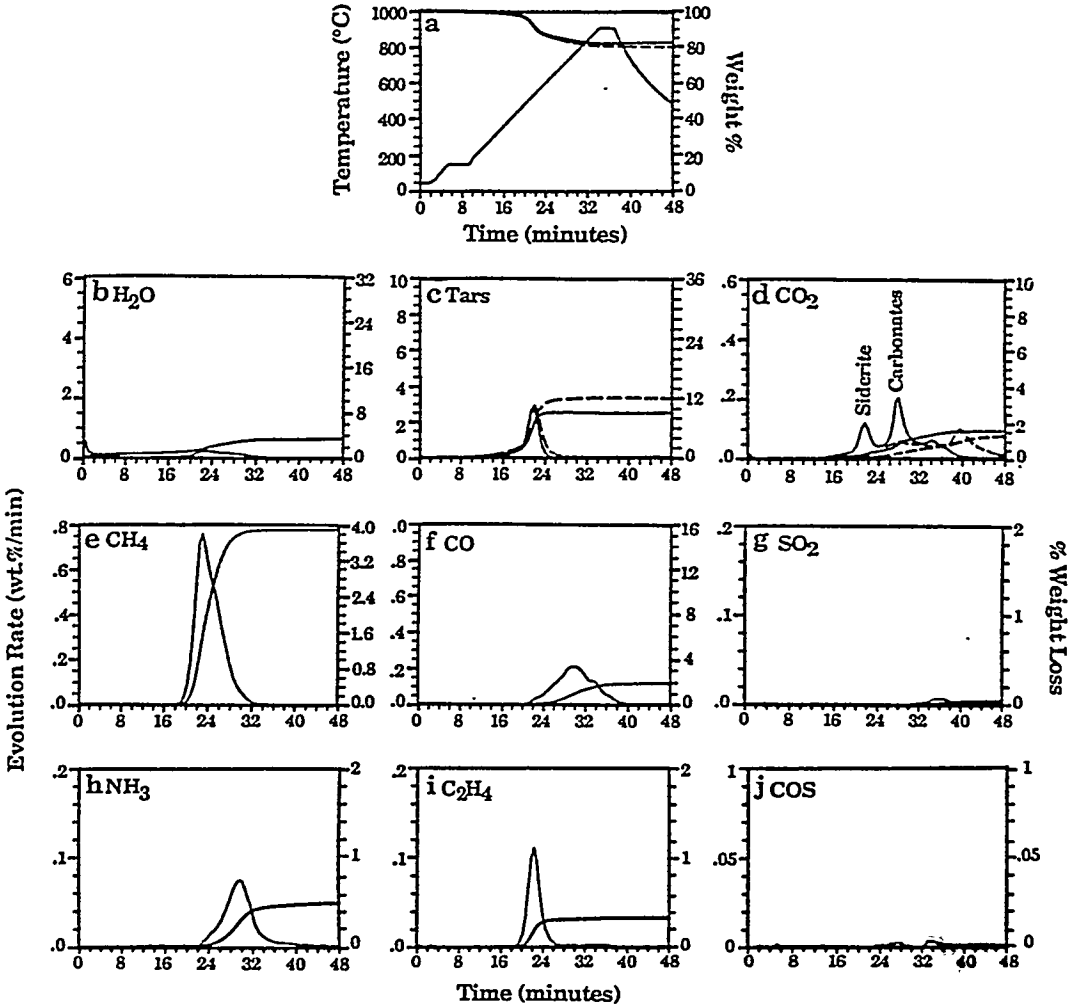

Figure 5. TG-FTIR analysis of raw and demineralized Pocahontas coal during the pyrolysis cycle. (a) weight loss (solid), sum of evolved products (dashed), and temperature profile. (b) H_2O evolution rate and integrated amount evolved. (c) Tar evolution rate and integrated amount evolved (raw coal (solid line); demineralized coal (dashed line)). (d) CO_2 evolution rate and integrated amount evolved (raw coal (solid line); demineralized coal (dashed line)). (e) Methane evolution rate and integrated amount evolved. (f) CO evolution rate and integrated amount evolved. (g) SO_2 evolution rate and integrated amount evolved. (h) NH_3 evolution rate and integrated amount evolved. (i) C_2H_4 evolution rate and integrated amount evolved. (j) COS evolution rate and integrated amount evolved. All weight losses are on an as received basis.

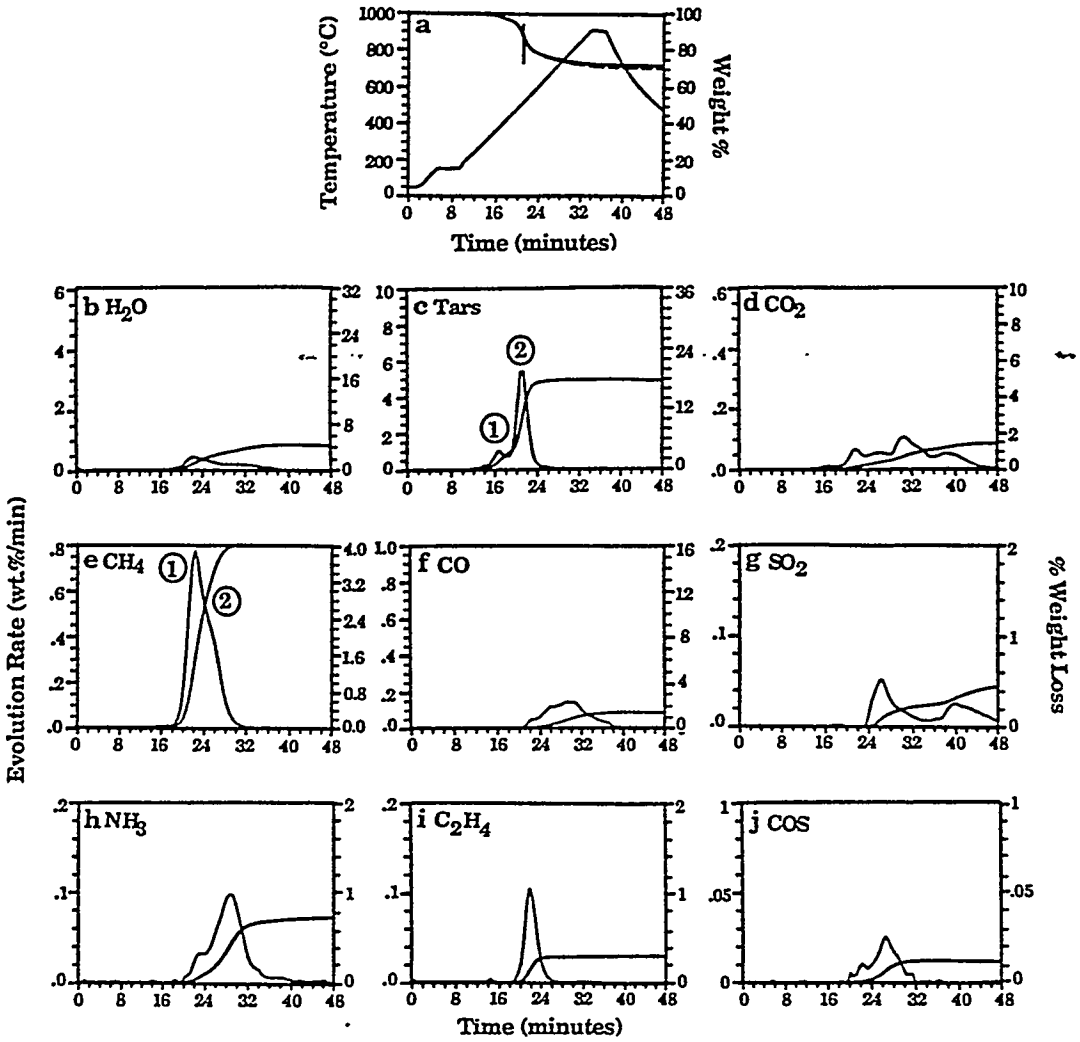

Figure 6. TG-FTIR analysis of Upper Freeport coal during the pyrolysis cycle. (a) Weight loss (solid), sum of evolved products (dashed), and temperature profile. (b) H_2O evolution rate and integrated amount evolved. (c) Tar evolution rate and integrated amount evolved. (d) CO_2 evolution rate and integrated amount evolved. (e) Methane evolution rate and integrated amount evolved. (f) CO evolution rate and integrated amount evolved. (g) SO_2 evolution rate and integrated amount evolved. (h) NH_3 evolution rate and integrated amount evolved. (i) C_2H_4 evolution rate and integrated amount evolved. (j) COS evolution rate and integrated amount evolved. All weight losses are on an as received basis.

as catalytic preliquefaction,[29] demineralization,[30] ion exchange,[30] methylation,[30,31] or oxidation[31] on the volatile product distribution. Temperature-programmed desorption has also been performed to study oxidation and gasification mechanisms.[32] The purpose of this paper is to describe the most recent improvements in the apparatus and present its application in characterizing the Argonne premium coal samples. The technique is being employed to obtain the kinetic and composition parameters to be employed in a recently developed general model of coal pyrolysis.[33]

Table I. Normalized Adsorptivity for Coal Tar

coal	% oxygen (maf)	rel absorptivity[a] at 30 °C/min
Pocahontas No. 3	2.47	0.60
Upper Freeport	7.51	0.82
Pittsburgh No. 8	8.83	0.95
Upper Kanawha	9.83	0.87
Utah Blind Canyon	11.58	1.04
Illinois No. 6	13.51	0.70
Wyodak	18.02	1.32
Beulah Zap	20.34	1.28

[a] Relative to a Pittsburgh No. 8 Seam tar spectrum.

Experimental Section

Apparatus. A schematic of the instrument is presented in Figure 1. Its components are as follows: a DuPont 951 TGA; a hardware interface (including a furnace power supply); an Infrared Analysis 16 pass gas cell with transfer optics; a MICHELSON 110 FT-IR; (resolution, 4 cm^{-1}; detector, MCT). A helium sweep gas (250 cm^3/s) is employed to bring evolved products from the TGA directly into the gas cell. A window purge

(29) Solomon, P. R.; Serio, M. A.; Deshpande, G. V.; Kroo, E.; Schobert, H.; Burgess, C. *Prepr. Pap.—Am. Chem. Soc., Div. Fuel Chem.* 1989, *34* (3), 803.
(30) Serio, M. A.; Solomon, P. R.; Kroo, E.; Bassilakis, R.; Malhotra, R.; McMillen, D. *Prepr. Pap.—Am. Chem. Soc., Div. Fuel Chem.* 1990, *35* (1), 61.
(31) Solomon, P. R.; Serio, M. A.; Deshpande, G. V.; Kroo, E. *Energy Fuels* 1990, *4*, 42.
(32) Serio, M. A.; Solomon, P. R.; Bassilakis, R.; Suuberg, E. M. The Effects of Minerals on Coal Reactivity. In *International Conference on Coal Science Proceedings*; IEA: Tokyo, Japan, 1989; p 341.
(33) Solomon, P. R.; Hamblen, D. G.; Carangelo, R. M.; Serio, M. A.; Deshpande, G. V. *Energy Fuels* 1988, *2*, 405.

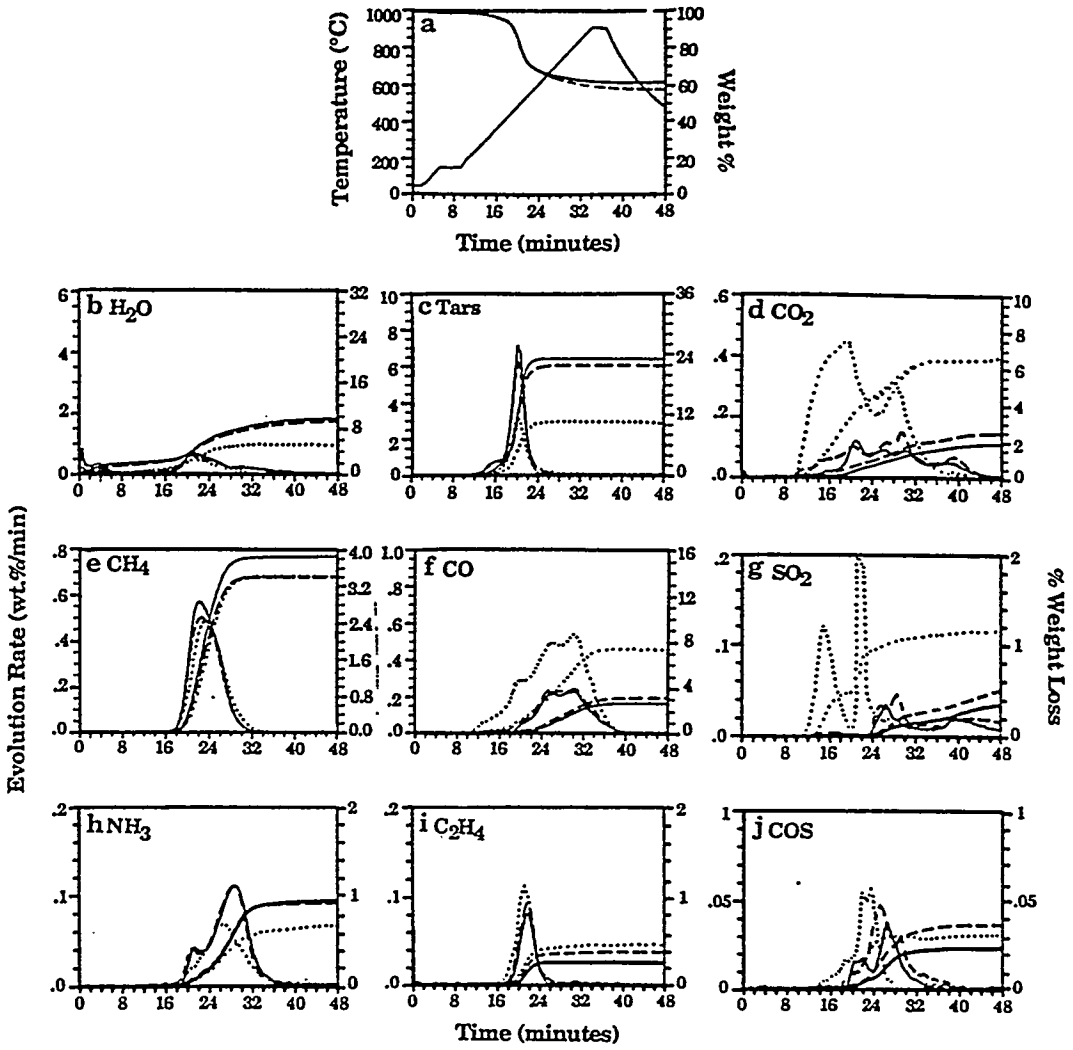

Figure 7. TG-FTIR analysis of raw and oxidized Pittsburgh No. 8 coal during the pyrolysis cycle: solid line, raw coal; dashed line, oxidized 3 days; and dotted line, oxidized 3 months. (a) Weight loss for raw coal (solid), sum of evolved products for raw coal (dashed), and temperature profile. (b) H_2O evolution rate and integrated amount evolved. (c) Tar evolution rate and integrated amount evolved. (d) CO_2 evolution rate and integrated amount evolved. (e) Methane evolution rate and integrated amount evolved. (f) CO evolution rate and integrated amount evolved. (g) SO_2 evolution rate and integrated amount evolved. (h) NH_3 evolution rate and integrated amount evolved. (i) C_2H_4 evolution rate and integrated amount evolved. (j) COS evolution rate and integrated amount evolved. All weight losses are on an as received basis.

of 700 cm^3/s was employed at each end of the cell. The system is operated at atmospheric pressure. This instrument package is now available commercially as the TG/plus from Bomem, Inc.

The most difficult volatiles to analyze are the heavy decomposition products that condense at room temperature, such as tars from coal. In the TG/plus, the high-conductivity helium sweep gas and the rapid cooling cause these products to form an aerosol that is fine enough to follow the gas through the analysis cell. The cell is connected without restrictions to the sample area. The aerosol is also fine enough that there is only a little scattering of the infrared beam, and it is thus attenuated almost as though the tar was in the gas phase. On the basis of the aerosol's Rayleigh scattering of infrared radiation, the diameter of the aerosol droplets is less than 1.0 μm.

Procedure. As an example of the analysis procedure, the pyrolysis and oxidation of a coal is described. More detail can be found in refs 25 and 26. Figure 2a illustrates the weight loss from this sample and the temperature history. A 35-mg sample of Pittsburgh Seam coal, loaded in the sample basket of the DuPont 951, is taken on a 30 °C/min temperature excursion in the helium sweep gas, first to 150 °C to dry for 240 s and then at 30 °C/min to 900 °C for pyrolysis. Upon reaching 900 °C, the sample is immediately cooled to 250 °C over a 20-min period. After cooling, a small flow of O_2 (0.3 cm^3/s) is added to the helium sweep gas at the 57-min mark and the temperature is ramped to 700 °C at 30 °C/min (or as high as 1000 °C) for oxidation.

During this excursion, infrared spectra are obtained once every 41 s. As discussed previously,[25,26] the spectra show absorption bands for CO, CO_2, CH_4, H_2O, SO_2, COS, C_2H_4, and NH_3. The spectra above 250 °C also show aliphatic, aromatic, hydroxyl, carbonyl, and ether bands from tar. The evolution of gases derived from the IR absorbance spectra are obtained by a quantitative analysis program that employs a database of integration regions and calibration spectra for different compounds. The routine employs regions of each calibration spectrum that permit the best quantitation with the least interferences. The routine is fast, so the product analysis is displayed on the computer screen during the actual experiment.

Figure 2b illustrates the integral of the evolution curves to obtain cumulative evolved-product amounts. Because the data are quantitative, the sum of these curves matches the weight loss as determined by the TGA balance. Discrepancies occur in this match because of missing components such as H_2 which cannot be seen by IR. Also, when O_2 is introduced, the balance shows a net gain in weight due to O_2 chemisorption.

Calibration. To calibrate the instrument, known flows of calibration gases were mixed with a fixed flow of sweep gas and passed through the gas cell. Reference spectra were collected and the flow rate was varied to provide spectra over the range of expected concentrations. For water calibration, a TGA pan was

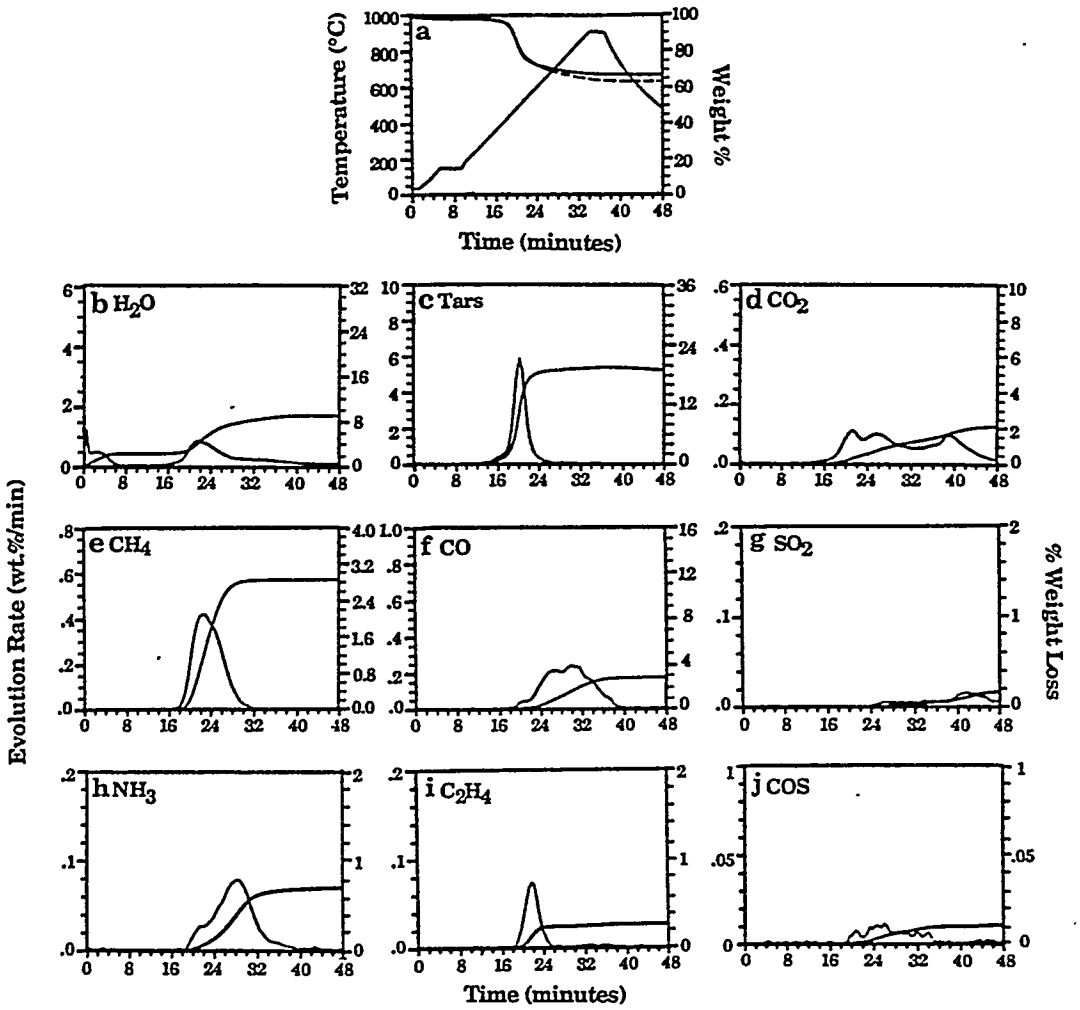

Figure 8. TG-FTIR analysis of Lewis-Stockton Seam coal during the pyrolysis cycle. (a) Weight loss (solid), sum of evolved products (dashed), and temperature profile. (b) H_2O evolution rate and integrated amount evolved. (c) Tar evolution rate and integrated amount evolved. (d) CO_2 evolution rate and integrated amount evolved. (e) Methane evolution rate and integrated amount evolved. (f) CO evolution rate and integrated amount evolved. (g) SO_2 evolution rate and integrated amount evolved. (h) NH_3 evolution rate and integrated amount evolved. (i) C_2H_4 evolution rate and integrated amount evolved. (j) COS evolution rate and integrated amount evolved. All weight losses are on an as received basis.

filled with water and the furnace temperature set to obtain the desired flow rate as measured by the TGA weight loss. The quantitative analysis program employs the spectrum that most closely matches the experimental amplitudes, since Beer's law (absorption is proportional to concentration) is not valid for many light gases.

Calibration spectra cannot be employed in the same way for tar since the absorptivity of any band varies with the tar compositions. Instead, the evolution of tar is derived by using the spectrum of a Pittsburgh Seam coal tar as a calibration standard. This coal tar has all the functional group features characteristic of coal tars. Its use as a reference spectrum, therefore, employs the important tar functional group regions whose amplitudes provide a qualitative tar evolution profile for other coals. The tar's evolution determined in this manner typically exhibits a sharply peaked function with increasing temperature as shown in Figure 3a.

To quantitatively determine the tar loss, it is assumed that the qualitative tar evolution profile is proportional to the rate of loss of tar. This will be true when the functional group composition of the tar does not change with temperature, a condition that holds over most of the tar evolution profile as shown by comparison of the infrared spectra at different temperatures. To determine the constant of proportionality for each coal sample, the tar loss profile is compared to the rate of weight loss from the balance minus the rate of weight loss for all the gases. This difference is presented in Figure 3b. The proportionality constant is picked by performing a least-squares fit between the two curves over the region of tar evolution, except for temperatures where other gases are evolving quickly and might introduce error. Table I compares the absorptivities for the eight coals normalized by the absorptivity of the reference Pittsburgh Seam tar. The measured spectral areas divided by the absorptivities yield the concentration of tar. The absorptivities are averages over several runs at 0.5 °C/s. There is a systematic trend of increasing absorptivity with decreasing rank. There are two factors that affect the absorptivity. One is that the oxygen functionalities, which are highly absorbing, become more important with decreasing rank. The second is that the aliphatic peak in tar generally increases with decreasing rank. The exception to the trend is the absorptivity for Illinois No. 6 coal. The Illinois No. 6 tar absorbance spectra indicate that its C_{ar}/C_{al} resembles that of a higher rank coal.

Routine calibration of the instrument is performed on a monthly basis by use of calcium oxalate. A typical evolution profile is presented in Figure 4. The calcium oxalate has three weight loss regions yielding H_2O, CO_2, and CO. When the gas calibration constants and the sweep gas flow rate are correct, then the sum of gases matches the weight loss. The temperature of gas evolution peaks compared to a known reference validates the accuracy of the thermocouple temperature measurement. To check for possible leaks in the system and the absence of oxygen in the helium sweep gas, graphite is run periodically. If there are no leaks and the helium is of high purity, no appreciable weight loss or CO_2 evolution is experienced during the pyrolysis cycle.

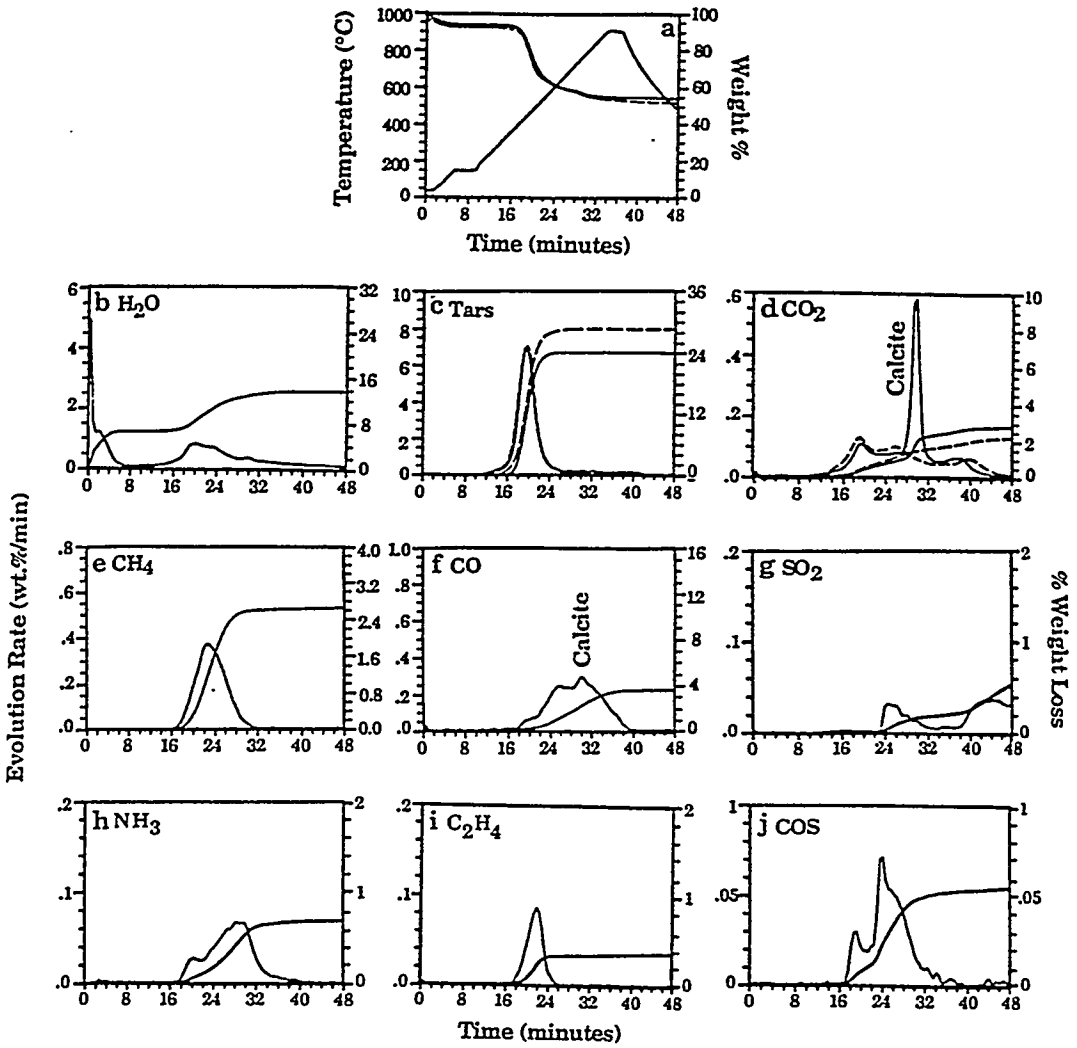

Figure 9. TG-FTIR analysis of raw and demineralized Illinois No. 6 coal during the pyrolysis cycle. (a) Weight loss (solid), sum of evolved products (dashed), and temperature profile. (b) H_2O evolution rate and integrated amount evolved. (c) Tar evolution rate and integrated amount evolved (raw coal (solid line); demineralized coal (dashed line)). (d) CO_2 evolution rate and integrated amount evolved (raw coal (solid line); demineralized coal (dashed line)). (e) Methane evolution rate and integrated amount evolved. (f) CO evolution rate and integrated amount evolved. (g) SO_2 evolution rate and integrated amount evolved. (h) NH_3 evolution rate and integrated amount evolved. (i) C_2H_4 evolution rate and integrated amount evolved. (j) COS evolution rate and integrated amount evolved. All weight losses are on an as received basis.

Samples. The coals analyzed were Argonne premium coal samples. The characterization of these samples has appeared elsewhere.[34] In addition, demineralized samples of the same coals were produced according to the technique of Bishop and Ward.[35] This technique removes both discrete minerals as well as organically bound alkali and alkaline-earth metals. Oxidized samples were prepared in air in an oven at 110 °C or at room temperature.

Results and Discussion

Analysis of Volatile Products from Eight Argonne Coals. The results of eight Argonne coals for the pyrolysis cycle are presented in Figures 5–12. Figures 5a–12a present the weight losses and temperature profiles. Also presented (dashed line) is the sum of species (tar, CH_4, H_2O, CO_2, CO, SO_2, NH_3, C_2H_4, and COS). In general, the sum of species is within a few percent of the weight loss.

Water evolution is presented in Figures 5b–12b. Water appears first at low temperature when the coal's moisture is evolved. For all coals, a prominent water peak also occurs simultaneously with the tar peak. This suggests that the chemistry responsible for this peak is related to either the free radicals produced or the increase in fluidity (and hence mobility for bimolecular interactions), both of which occur during tar formation. Burnham et al.[17] report the coincidence of the tar peak with the low-temperature peaks for CO_2 and H_2S. There is also a higher temperature H_2O peak and a lower temperature peak or shoulder accompanying CO_2 evolution in low rank coals. In Figure 11b, these peaks are labeled 1 (moisture), 2 (water extra loose, associated with early CO_2 evolution), 3 (water loose, associated with tar evolution), and 4 (water tight).

The evolution of tar and aliphatic gases is presented in Figures 5c–12c. These tar evolution profiles typically consist of a low-temperature peak or shoulder followed by a narrow larger peak. The low-temperature peak is believed to be due to the evaporation of unattached "guest" molecules (or the term used by Marzec,[36] the "molecular

(34) Vorres, K. S. *Users Handbook for the Argonne Premium Coal Sample Program*; Supported by US DOE, Contract No. W-31-109-ENG-238, 1989.

(35) Bishop, M.; Ward, D. L. *Fuel* 1958, *37*, 191.

(36) Marzec, A. *Fuel* 1989, *68*, 1104.

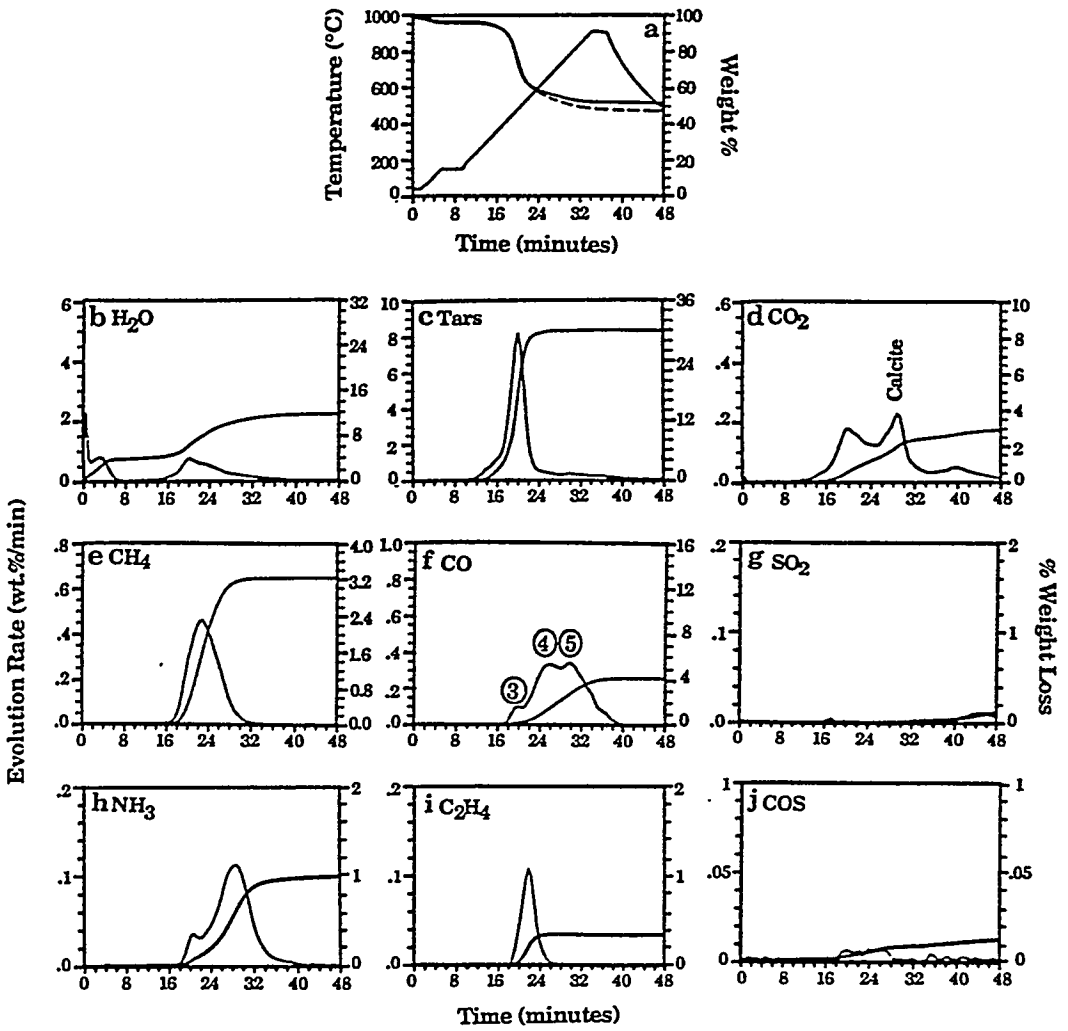

Figure 10. TG-FTIR analysis of Utah Blind Canyon coal during the pyrolysis cycle. (a) Weight loss (solid), sum of evolved products (dashed), and temperature profile. (b) H_2O evolution rate and integrated amount evolved. (c) Tar evolution rate and integrated amount evolved. (d) CO_2 evolution rate and integrated amount evolved. (e) Methane evolution rate and integrated amount evolved. (f) CO evolution rate and integrated amount evolved. (g) SO_2 evolution rate and integrated amount evolved. (h) NH_3 evolution rate and integrated amount evolved. (i) C_2H_4 evolution rate and integrated amount evolved. (j) COS evolution rate and integrated amount evolved. All weight losses are on an as received basis.

phase"). This early tar evolution peak is also evident in the data of Burnham et al.[17] using the Rock-Eval and Meuzelaar et al.[37] using pyrolysis-FIMS. The higher temperature peak is due to the release of coal fragments by bond breaking, evaporation and transport.[33] In Figure 6c, these peaks are labeled 1 (molecular phase) and 2 (pyrolysis).

Figures 5d–12d present the results for CO_2. Wyodak (Figure 11d), which is typical of low-rank coals, shows three peaks between 200 and 900 °C labeled 2 (CO_2 extra loose associated with H_2O), 3 (CO_2 loose associated with tar evolution and H_2O evolution), and 4 (CO_2 tight). There is also a very low temperature peak labeled 1 (occurring only for the lowest rank coals) whose origin appears to be the low-temperature tail of the CO_2 extra loose. The peak occurs because of the constant temperature of the drying cycle. Higher rank coals usually have peaks 3 and 4 but not peak 2 unless they are oxidized. Peak 2 is one of the regions affected most by oxidation. In addition, the evolution of CO_2 is often complicated in high-rank coals by the evolution of CO_2 from carbonates such as calcite (Figure 9d) and siderite (Figure 5d).

Methane evolution is presented in Figures 5e–12e. Methane evolution occurs in two closely spaced peaks. The low-temperature peak is initiated coincident with the initiation of tar evolution but reaches a maximum at a slightly higher temperature than the maximum tar evolution rate. The temperature for the maximum evolution varies little with rank, but the temperature of initiation of methane evolution decreases with decreasing rank. It has been suggested that the low-temperature evolution of methane occurs by ipso-substitution reactions involving free radicals on macromolecular fragments or hydrogen free radicals, both of which are produced during the decomposition of the macromolecular network.[31,38-40] This is consistent with the observation that the early methane evolution peak is initiated coincident with the tar peak.

(37) Meuzelaar, H. L. C.; Yun, Y.; Simmleit, N.; Schulten, H. R. *Prepr. Pap.—Am. Chem. Soc., Div. Fuel Chem.* 1989, *34* (3), 693.

(38) Solomon, P. R.; Best, P. E.; Yu, Z. Z.; Deshpande, G. V. *Prepr. Pap.—Am. Chem. Soc., Div. Fuel Chem.* 1989, *34* (3), 895.

(39) Squire, K. R.; Solomon, P. R.; Carangelo, R. M.; DiTaranto, M. B. *Fuel* 1986, *65*, 833.

(40) Squire, K. R.; Solomon, P. R.; DiTaranto, M. B.; Carangelo, R. M. *Prepr. Pap.—Am. Chem. Soc., Div. Fuel Chem.* 1985, *30* (1), 386.

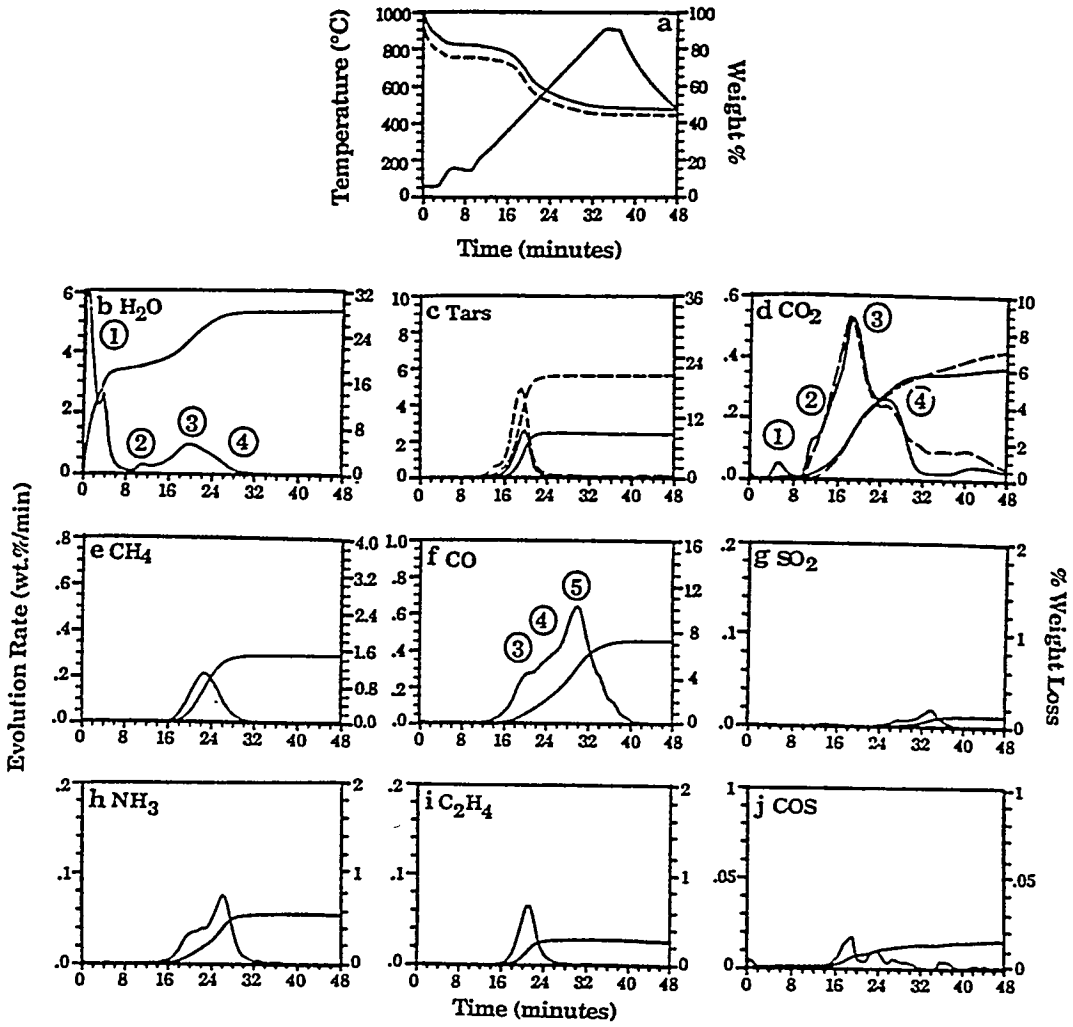

Figure 11. TG-FTIR analysis of raw and demineralized Wyodak subbituminous coal during the pyrolysis cycle. (a) Weight loss (solid), sum of evolved products (dashed), and temperature profile. (b) H_2O evolution rate and integrated amount evolved. (c) Tar evolution rate and integrated amount evolved (raw coal (solid line); demineralized coal (dashed line)). (d) CO_2 evolution rate and integrated amount evolved (raw coal (solid line); demineralized coal (dashed line)). (e) Methane evolution rate and integrated amount evolved. (f) CO evolution rate and integrated amount evolved. (g) SO_2 evolution rate and integrated amount evolved. (h) NH_3 evolution rate and integrated amount evolved. (i) C_2H_4 evolution rate and integrated amount evolved. (j) COS evolution rate and integrated amount evolved. All weight losses are on an as received basis.

The second peak appears as a shoulder on the high-temperature side of the first peak. This peak may be due to methane formed by homolytic cleavage of methyl groups or by ipso substitution associated with H radicals released during ring condensation. In Figure 6e, these peaks are labeled 1 (methane loose) and 2 (methane tight).

The evolution of CO is presented in Figures 5f–12f. Low-rank coals exhibit three peaks labeled 3, 4, and 5 as shown in Figure 10f. Peaks 3 and 4 coincide with the CO_2 peaks 3 and 4, while peak 5 has no accompanying peaks for H_2O or CO_2. CO peaks also can be seen accompanying the CO_2 calcite peak (see Figure 9). High-rank coals appear to have only the high-temperature peak 5.

Results for other gases are presented in parts g–i of Figures 5–12. The C_2H_2 evolution shown in Figures 5g–12g occurs as a narrow peak which lags the tar peak, but which precedes the methane. The ammonia evolution in Figures 5h–12h appears to coincide with the start of CO evolution (Figures 5f–12f). The SO_2 peak near 28 min (Figures 5i–12i) appears to coincide with one of the COS peaks (Figures 5j–12j).

The evolution peaks in Figures 5–12 are currently being examined to elucidate the chemistry responsible for their formation. For example, there are certain evolution peaks that match in shape and temperature for more than one species, suggesting that there is common chemistry responsible for the evolution of these species. Also, certain evolution peaks (i.e., CH_4 and CO_2) are observed to coincide with cross-linking[31,33] and certain peaks show correlations such as decreases in tar yield with increases in CO_2 due to oxidation[31] or increases in tar yield associated with decreases in CO_2 due to demineralization[30] (as discussed below) or preliquefaction.[29]

Analysis of Argonne Chars in the Combination Cycle. Sample results for the combustion cycle are presented in Figures 13 and 14. Since oxygen is added, the reported weight loss is for the elements C, H, and S, not the oxide. This will make the sum of the elements (C, H, and S) lost less than the total measured weight loss, the difference being the oxygen in the char. The combustion cycle is dominated by the evolution of CO_2, CO, and SO_2. The sum of the C, H, and S in these species is in reasonable agreement with the weight loss. As discussed below, the reactivity of the char affects the weight gain when oxygen is introduced and also affects the temperature of initiation of the combustion reactions. The higher the reactivity, the

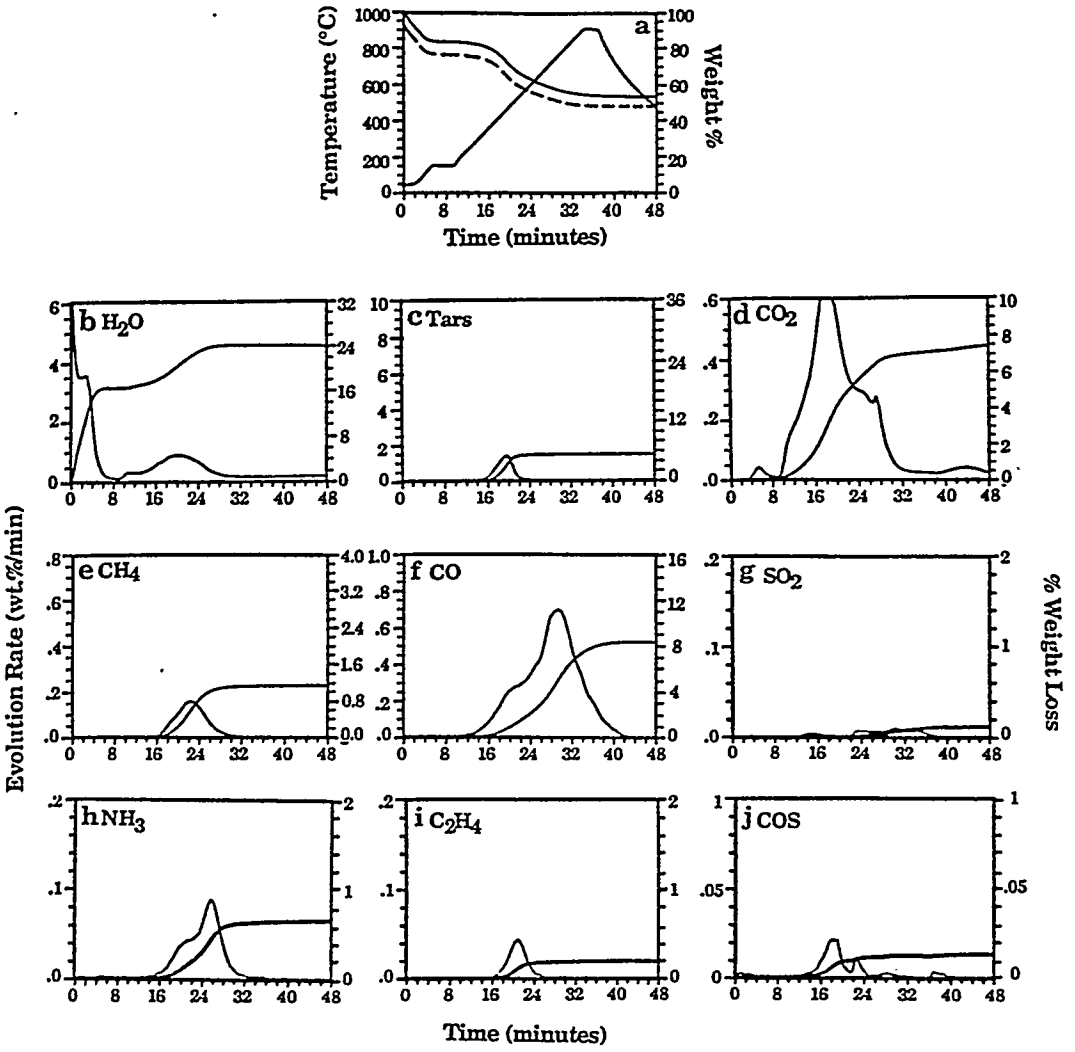

Figure 12. TG-FTIR analysis of Zap lignite during the pyrolysis cycle. (a) Weight loss (solid), sum of evolved products (dashed), and temperature profile. (b) H_2O evolution rate and integrated amount evolved. (c) Tar evolution rate and integrated amount evolved. (d) CO_2 evolution rate and integrated amount evolved. (e) Methane evolution rate and integrated amount evolved. (f) CO evolution rate and integrated amount evolved. (g) SO_2 evolution rate and integrated amount evolved. (h) NH_3 evolution rate and integrated amount evolved. (i) C_2H_4 evolution rate and integrated amount evolved. (j) COS evolution rate and integrated amount evolved. All weight losses are on an as received basis.

more oxygen is adsorbed and the lower is the reaction temperature.

Analysis of Minerals. The identification of evolution peaks due to minerals was made by performing TG/plus analysis of reference minerals and demineralized coals. Figure 15 presents the data for calcite. The major reaction is the evolution of CO_2 near 800 °C. There are also small amounts of CO and H_2O evolved. Reference spectra for kaolin (now shown) exhibit a 14% weight loss caused by a large water evolution peak at 550 °C and small CO_2 peaks at 518 and 884 °C. Evolution profiles for montmorillonite and illite (not shown) exhibit smaller weight losses (6–8%) primarily due to water loss near 650 °C and smaller CO_2 losses.

The CO_2 peak exhibited by calcite is almost identical in shape and position with that exhibited by the Illinois No. 6 coal in Figure 9d. When the Illinois coal was demineralized (dashed line in Figure 9d) the 800 °C CO_2 peak disappeared. Several high-rank coals (Pocahontas, Upper Freeport, and Pittsburgh) showed CO_2 peaks at about 525 °C which disappeared with demineralization. Figure 5, which shows the evolution profiles for demineralized Pocahontas (dashed line), is an example, showing removal of the CO_2 peaks at 520 and 760 °C. The 520 °C peak appears to be due to siderite on the basis of the discussion by Raask.[41] However, the TG/plus results on a reference siderite sample obtained from Copper Lake in Nova Scotia showed the CO_2 peak at 580 °C. Another possible source is dolomite, which decomposes in this range. The high-temperature CO_2 peak is most likely a carbonate, although it is at a different temperature from the reference calcite.

Effects of Minerals on Other Volatile Products. Besides the changes observed in the CO_2 yields, demineralization also affects the tar yield. Figures 5c and 9c show 20–30% increases in tar yield for Pocahontas and Illinois No. 6 upon demineralization. This is larger than can be attributed to the weight percent adjustment from an as-received basis to a daf basis. More than a 100% increase in the tar was observed for Wyodak coal (Figure 11c). Similar results were obtained for Zap lignite.[30] The tar increases in both the low-rank coals were accompanied by reductions in the early release of CO_2 as discussed by

(41) Raask, E. *Mineral Impurities in Coal Combustion; Behavior, Problems, and Remedial Measures*; Hemisphere: New York, 1985.

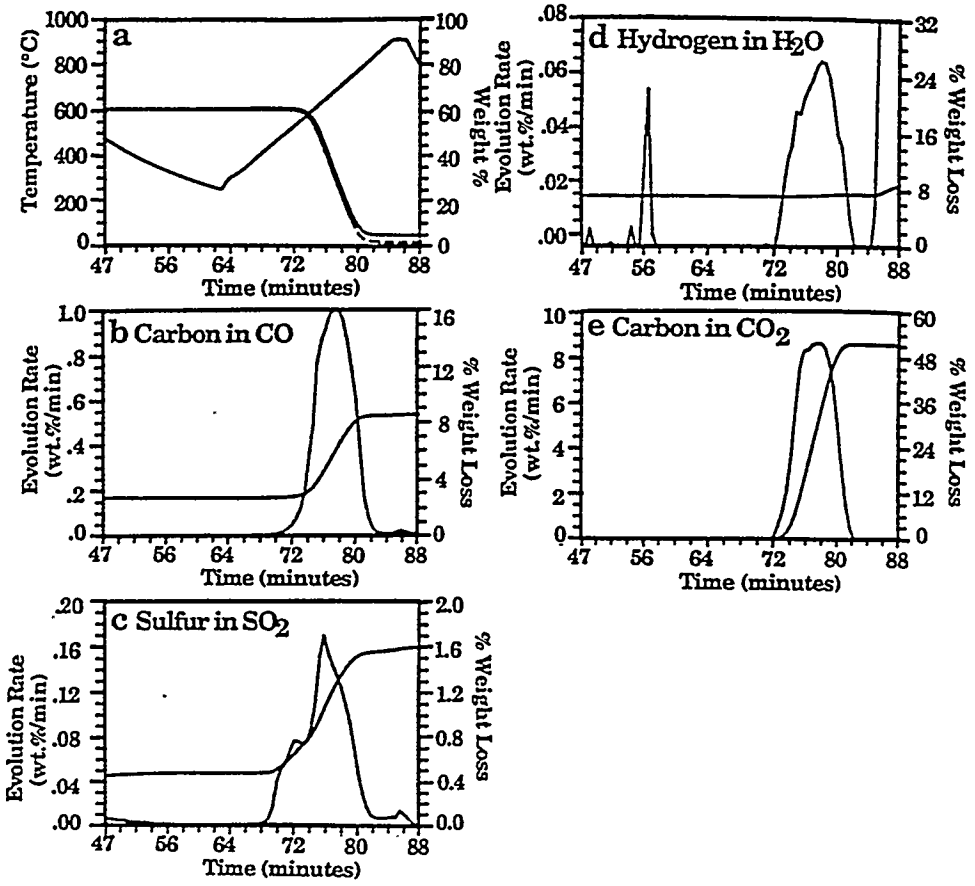

Figure 13. TG-FTIR analysis of Pittsburgh Seam coal during the combustion cycle. (a) Weight loss (solid), sum of evolved products (dashed), and temperature profile. (b) Carbon in CO evolution rate and integrated amount evolved. (c) Sulfur in SO_2 evolution rate and integrated amount evolved. (d) Hydrogen in H_2O evolution rate and integrated amount evolved. (e) Carbon in CO_2 evolution rate and integrated amount evolved.

Serio et al.[30] This result is further confirmation of the concept of low-temperature cross-linking related to CO_2 evolution.[31] For low-rank coals, changes are also observed in the CO profile with demineralization, but little change was observed in any of the other species. The effect of demineralization and other pretreatments on the evolution profiles is discussed in more detail by Serio et al.[30]

Effect of Coal Oxidation on Volatile Evolution. The effect of coal oxidation on the volatile product evolution was also examined. Figure 7 compares the evolution curves for a raw Pittsburgh Seam bituminous (solid line) to those for samples oxidized in air at 110 °C for 3 days (dashed line) and 3 months (dotted lines). The 3-day oxidation resulted in minor changes in the evolution curves. A difference can be seen in increased CO_2 released at low temperatures. Major changes occur for the 3-month sample. Large increases are observed in the CO_2, CO, and SO_2 yields while a large reduction (50%) is seen in the tar. Similar results on the increase in early CO_2 evolution and reduction in tar yield have been presented as evidence for low-temperature cross-linking associated with CO_2 evolution.[31] The reduction in tar yield upon oxidation is consistent with the usual observation of reduced fluidity and deterioration of liquefaction behavior with oxidation. Of interest is the surprising reduction in the H_2O yield. Smaller changes are observed for other species.

Proximate Analysis. The cycle of drying, pyrolysis, and oxidation, illustrated in Figure 2a, simulates the conditions for the proximate analysis. Table II compares the moisture (measured at the end of the drying period), the volatile matter (measured at the end of the pyrolysis period), and the ash (measured at the end of the combustion cycle) with the proximate analysis values published by Argonne National Laboratory.[34] The agreement is within 1% or 2% except for moisture, which varies with the laboratory conditions, and ash, which may vary because of the small sample size (35 mg) used in the TG/plus analysis.

Table II. Proximate Analysis by TG/plus; ASTM Values in Parentheses

coal	moisture	volatile matter	fixed carbon	ash
Pocahontas No. 3	0.2 (0.7)	20.6 (18.5)	73.4 (76.1)	6.3 (4.7)
Upper Freeport	0.4 (1.1)	25.2 (27.1)	60.0 (58.7)	14.4 (13.0)
Pittsburgh No. 8	1.1 (1.7)	35.9 (37.2)	49.5 (52.1)	13.4 (9.1)
Stockton	1.5 (2.4)	31.8 (29.4)	43.2 (48.8)	23.4 (19.4)
Illinois No. 6	2.0 (8.0)	39.3 (36.9)	43.4 (40.9)	15.3 (14.3)
Utah	2.3 (4.6)	43.5 (43.7)	47.8 (47.2)	6.3 (4.5)
Wyodak	25.7 (28.1)	33.0 (32.2)	34.8 (33.4)	6.5 (6.3)
Beulah Zap	30.6 (32.2)	28.4 (30.5)	33.7 (30.7)	7.3 (6.6)

Volatile Kinetics. The TG-FTIR analysis can be used to study product evolution kinetics. Since tar and hydrocarbon gases are the most important contributors to the weight loss, we have compared, in Figure 16a, the temperature for the maximum hyrocarbon evolution rate for the Argonne coals as a function of rank at 0.05, 0.5, 0.83, and 1.67 °C/s. Duplicate runs were all within ±4 °C. The peak temperatures as well as the shape of the tar peaks are in good agreement with the results of Burnham et al.[17] obtained by using a Rock-Eval analyzer and a triple-

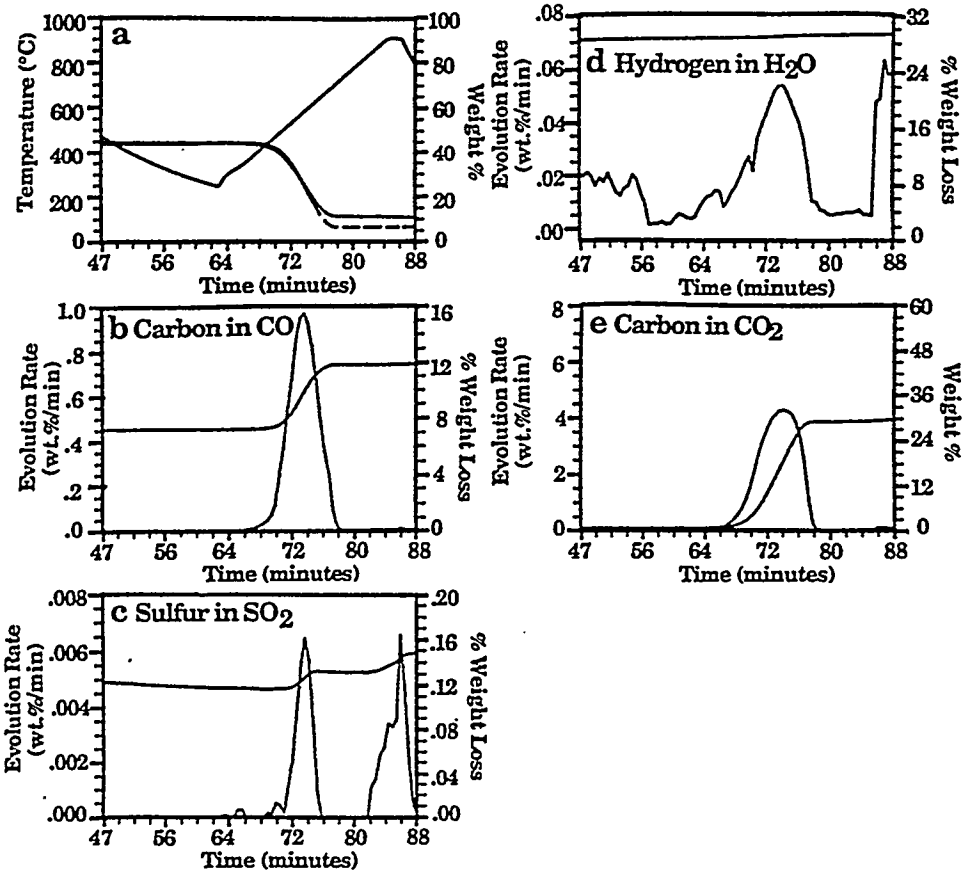

Figure 14. TG-FTIR analysis of Wyodak subbituminous coal during the combustion cycle. (a) Weight loss (solid), sum of evolved products (dashed), and temperature profile. (b) Carbon in CO evolution rate and integrated amount evolved. (c) Sulfur in SO_2 evolution rate and integrated amount evolved. (d) Hydrogen in H_2O evolution rate and integrated amount evolved. (e) Carbon in CO_2 evolution rate and integrated amount evolved.

quadrupole mass spectrometer (TQMS) at similar heating rates. The kinetic rate for hydrocarbon evolution shows a systematic variation with rank. The variation in the rate of thermal decomposition is in part responsible for the variation of ignition behavior with rank.[42]

The peak shift with heating rate has been employed by Serio et al. to derive rates for tar evolution.[27,28] The 50–65 °C shift in temperatures with heating rate corresponds to activation energies approximately between 45 and 60 kcal/mol. Recently, we have employed the TG/plus volatile evolution profiles to determine rank-dependent rates to employ in the FG-DVC model of coal pyrolysis.[33] The rates are determined by adjusting the rate constants to make the theory fit the data. Figure 17 compares the observed and predicted weight loss, tar evolution, and methane evolution profiles at heating rates of 0.05, 0.5, and 1.67 °C/s for Pittsburgh Seam coal. The agreement is good for all three heating rates. To obtain these fits, the following rates were employed for the Pittsburgh Seam coal:

$$k_{\text{bond breaking}} = 1.28 \times 10^{12} \exp(-(24000 \pm 1200)/T)\ \text{s}^{-1}$$

$$k_{\text{CH}_4\text{ loose}} = 7.95 \times 10^{13} \exp(-(29000 \pm 1500)/T)\ \text{s}^{-1}$$

$$k_{\text{CH}_4\text{ tight}} = 4.5 \times 10^{12} \exp(-(30000 \pm 2000)/T)\ \text{s}^{-1}$$

The rate equation is of the form $k_n = k_0 \exp(-((E/R) \pm (\sigma/R))/T)$, with k_0 in s^{-1}, E/R in K, and σ/R in K. The accuracy of the activation energies is estimated to be within ±2 kcal. With a fixed activation energy, the accuracy of the preexponential is ±25% and that of σ is ±10%. These rates appear to provide good predictions when applied to fit data taken at much higher heating rates (5000 °C/s) as well. The bond-breaking rate is in good agreement with the approximate rate of $3.1 \times 10^{12} \exp(-(24942 \pm 1250)/T)$ derived by Burnham et al.[17] The above rates can be compared to the rank-independent rates employed previously:[33]

$$k_{\text{bond breaking}} = 8.6 \times 10^{15} \exp(-(27700 \pm 1500)/T)\ \text{s}^{-1}$$

$$k_{\text{CH}_4\text{ loose}} = 7.5 \times 10^{13} \exp(-(30000 \pm 2000)/T)\ \text{s}^{-1}$$

$$k_{\text{CH}_4\text{ tight}} = 3.4 \times 10^{11} \exp(-(3000 \pm 2000)/T)\ \text{s}^{-1}$$

The activation energy for bond breaking is smaller, the rate for CH_4 loose is similar, and the rate for CH_4 tight is about a factor of 10 faster.

Functional Group Composition. The TG-FTIR analysis provides information on the coal's functional group composition since it is the functional group composition that gives rise to the variation in gas yields. Figure 16b shows the variation in oxygen-containing products with rank. Low-rank coals have a high content of oxygen functional groups and thus produce higher yields of oxygenated species. The trends are in agreement with the data of Burnham et al.[17] The results of the present work are, however, higher for high-rank coals and lower for low-rank coals.

(42) Solomon, P. R.; Chien, P. L.; Carangelo, R. M.; Best, P. E.; Markham, J. R. *Twenty-Second Symposium (International) on Combustion*; The Combustion Institute: Pittsburgh, PA, (1988); p 211.

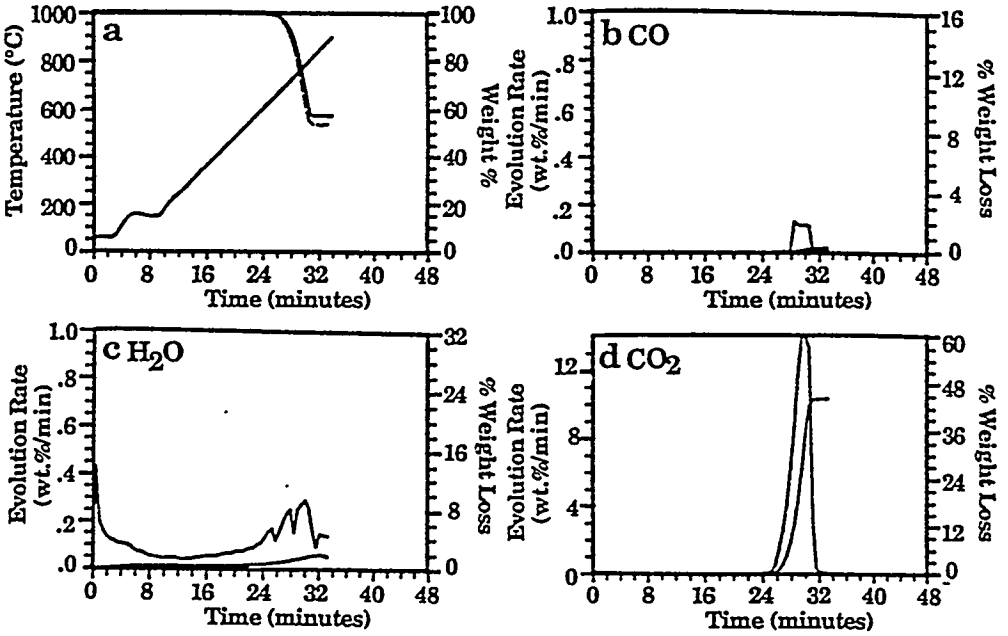

Figure 15. TG-FTIR analysis of calcium carbonate during the pyrolysis cycle. (a) Weight loss (solid), sum of evolved products (dashed), and temperature profile. (b) Tar evolution rate and integrated amount evolved. (c) Methane evolution rate and integrated amount evolved. (d) H_2O evolution rate and integrated amount evolved. (e) CO_2 evolution rate and integrated amount evolved. (f) CO evolution rate and integrated amount evolved.

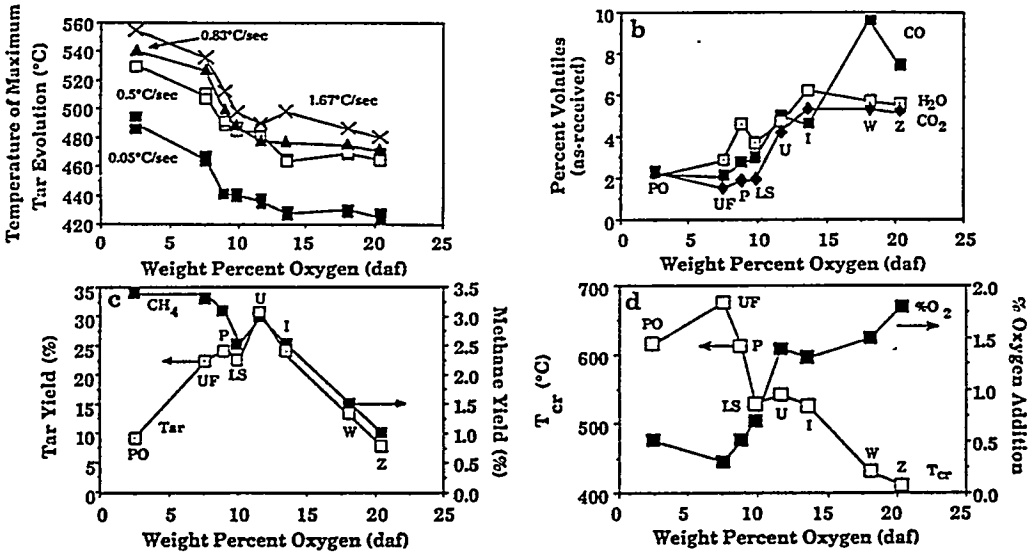

Figure 16. Variation of coal pyrolysis properties with rank. (a) Rank variation of tar evolution temperature. (b) Rank variation of oxygenated gases CO and CO_2 and pyrolysis water. (c) Rank variation of CH_4 and hydrocarbons. (d) Rank variation of T_{cr} and oxygen chemisorption. Results are on an as received basis.

Figure 16c presents the data for tar and CH_4 yields. Methane increases systematically with increasing rank. The trend also agrees with the results of Burnham et al.[17] The amounts are comparable for the high-rank coals, but our results for low-rank coals are lower than those of Burnham et al. For example, we get 1.0 wt % for Zap lignite while Burnham et al. get 2.4 wt %.

Tar yields are low for both high- and low-rank coals, with high-volatile bituminous coals having the most tar. The tar amounts are in good quantitative agreement with the S_2 peak reported by Burnham et al.[17] from Rock-Eval analysis. Tar yields are related to soot formation in combustion,[42] to fluidity,[38] and to liquid yields in liquefaction[30] or mild gasification.[43] The tar functional group composition can also be obtained from the infrared spectra during tar evolution.

Char Reactivity. As discussed above, the TG-FTIR analysis provides two measurements related to char reactivity. The first is the weight gain of the char which occurs when oxygen is added early in the combustion cycle (see Figure 2b). This weight gain is proportional to the concentration of active sites that are accessible to O_2. The second measurement is of the temperature required to produce a specified rate of weight loss during the oxidation cycle. As discussed previously, this critical temperature T_{cr} is related to the reactivity.[4-7] The higher the reactivity, the lower is T_{cr}.

Figure 16d compares both the oxygen chemisorbed and T_{cr} as functions of the oxygen in the coal. There is a systematic decrease in T_{cr} and an increase in oxygen chemisorbed with increasing oxygen. The interplay of

(43) Khan, M. R.; Serio, M. A.; Malhotra, R.; Solomon, P. R. *Prepr. Pap.—Am. Chem. Soc., Div. Fuel Chem.* 1989, *34* (4), 1054.

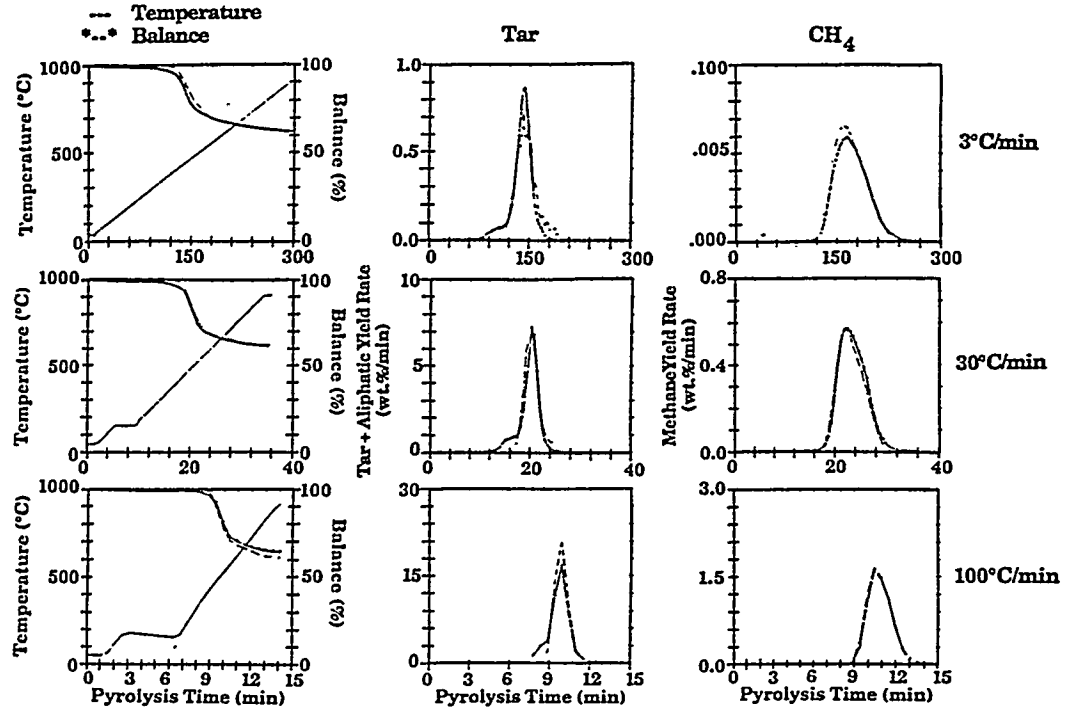

Figure 17. Kinetic analysis for Pittsburgh Seam coal for weight loss, tar evolution, and methane evolution at three heating rates. Experiment (solid line) and theory (dashed line) using the FG-DVC Model 33 with the kinetic rates reported in this paper.

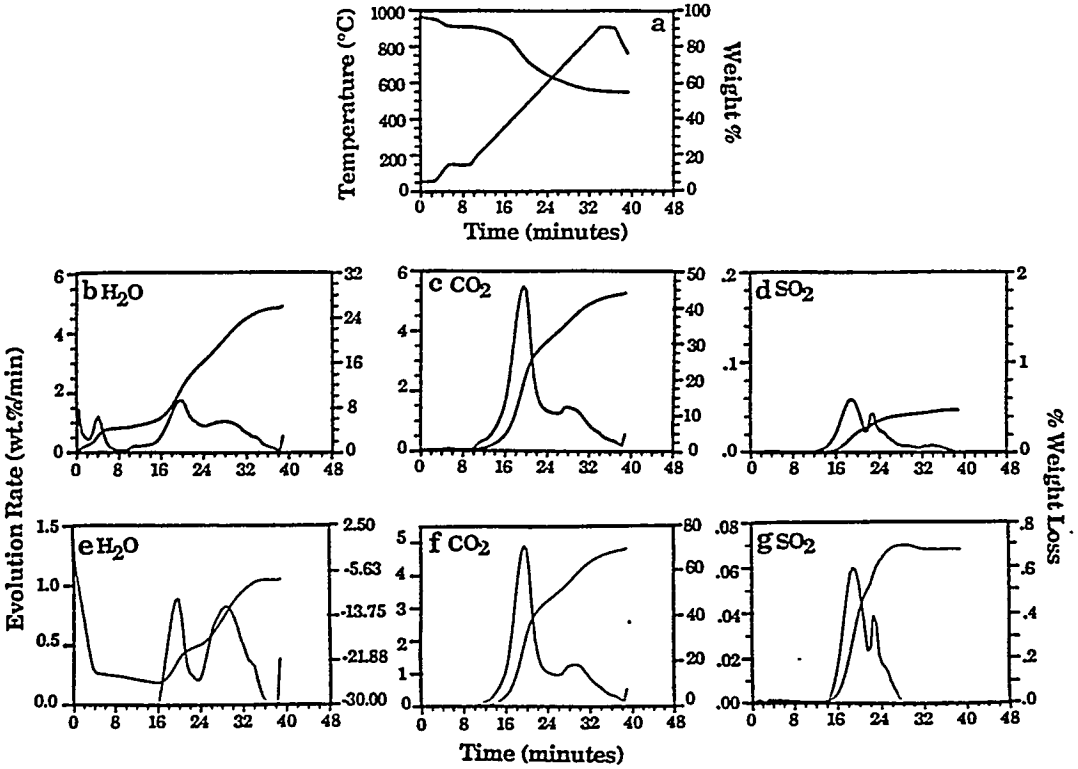

Figure 18. TG-FTIR analysis with postoxidizer. (a) Weight loss and temperature profile. (b) H_2O evolution rate and integrated amount evolved. (c) CO_2 evolution rate and integrated amount evolved. (d) SO_2 evolution rate and integrated amount evolved. (e) H_2O postoxidizer profile minus pyrolysis profile. (f) CO_2 postoxidizer profile minus pyrolysis profile. (g) SO_2 postoxidizer profile minus pyrolysis profile.

reactivity and decomposition kinetics control the ignition behavior and burnout in combustion or gasification.[42]

Postoxidation. It is possible to perform a (C, H, N, S) elemental analysis of the volatile products by adding heat and oxygen to the product stream after the furnace but before the analysis cell. This step has the added benefit of indicating the presence of products like H_2 that are not infrared active or H_2S that are very weak infrared absorbers.

The hardware modification is made by inserting a quartz tube section about 3 cm long between the quartz tube leaving the furnace section and the multipass cell. The

insert has an input line for oxygen addition and a platinum heater. An oxygen flow of 10 cm^3/min and a temperature of about 800 °C in the platinum heater were employed.

Results are presented for a Zap lignite in Figure 18. Figure 18a presents the weight loss, which is almost identical with that in Figure 12a. Parts b, c, and d of Figure 18 present the yields of H_2O, CO_2, and SO_2, which are the primary oxidation products of the volatile species. We could not see significant amounts of NO in the combustion products. The other volatile species (tar, CH_4, C_2H_4, CO, NH_3, and COS) have also been oxidized and are thus absent from the spectra.

To analyze the results, the H_2O, CO_2, and SO_2 observed in pyrolysis (Figure 12) have been subtracted from the curves in Figure 18b–d and the results presented in Figure 18e–g. The H_2O, CO_2, and SO_2 difference curves now have peaks that match the tar evolution peak in Figure 12c. These data determine the C, H, and S composition of the tar. In addition, the H_2O evolution profile has a wide peak at elevated temperatures believed to result from the oxidation of hydrogen. The CO_2 has a high-temperature peak from the oxidation of CO. The SO_2 has peaks at 449 and 565 °C related to the release of H_2S. The peak at 565 °C is close to that for a sample of pure pyrite run in the TG-FTIR.

Thus, the postoxidation section adds significant new information to the analysis.

Summary and Conclusions

A single TG-FTIR analysis provides an extensive characterization of coal with regard to the decomposition kinetics, char reactivity, functional group compositions, and conversion behavior. The paper presents the following:

1. The TG-FTIR apparatus for pyrolysis, oxidation of pyrolysis products, and oxidation of the sample is described.

2. Pyrolysis results are presented for the eight Argonne coals, several demineralized coals, and two oxidized samples of Pittsburgh Seam coal.

3. There are certain evolution peaks that match in shape and temperature for more than one species, suggesting common chemistry responsible for the evolution of these species.

4. Several peaks in the CO_2 evolution have been identified with mineral decomposition.

5. Increases in tar yield are observed for the demineralized coals (especially low-rank coals) while decreases in tar yield are observed for the oxidized samples.

6. A kinetic analysis was applied to species evolution data collected at several different heating rates. There is a systematic variation in rate with rank. The rate for tar evolution from Pittsburgh Seam coal is in good agreement with that of Burnham et al.[17] using a similar set of data.

7. Analyses of the amounts of evolved products also show a systematic variation with rank consistent with the coal's elemental and functional group compositions.

8. Postoxidation of the volatile products has been successful in providing elemental composition information on the volatile products as well as showing the evolution of H_2, which is not infrared active, and H_2S (in the postoxidized SO_2 profile), which is a weak infrared absorber.

9. Oxidation of the char yields the ash amount as well as two measures of the char's reactivity, the oxygen absorbed by the char, and the temperature at which significant oxidation of the char occurs.

Acknowledgment. This work was supported by the U.S. Department of Energy, Morgantown Energy Technology Center, under Contract No. DE-AC21-86MC23075 and the National Science Foundation, Grant No. ISI-8703520. We acknowledge the contributions of Z. Z. Yu and S. Charpenay on the modeling of the TG-FTIR data. We also thank Jean Whelan of Woods Hole Oceanographic Institute for supplying the siderite sample.

Appendix O

Analysis of Coal by Thermogravimetry—Fourier Transform Infrared Spectroscopy and Pyrolysis Modeling

Journal of Analytical and Applied Pyrolysis, 19 (1991) 1–14
Elsevier Science Publishers B.V., Amsterdam

Analysis of coal by thermogravimetry–Fourier transform infrared spectroscopy and pyrolysis modeling

P.R. Solomon [a,*], M.A. Serio [a], R.M. Carangelo [a], R. Bassilakis [a], Z.Z. Yu [a], S. Charpenay [a] and J. Whelan [b]

[a] *Advanced Fuel Research, Inc., 87 Church Street, East Hartford, CT 06108 (U.S.A.)*
[b] *Woods Hole Oceanographic Institute, Woods Hole, MA 02543 (U.S.A.)*

(Received June 29, 1990; accepted in final form February 8, 1991)

ABSTRACT

We have developed a TG–FT-IR instrument which combines thermogravimetric analysis (TGA) with evolved product analysis by Fourier Transform Infrared (FT-IR) spectroscopy. FT-IR analysis of evolved products has an advantage over mass spectroscopy in allowing analysis of very heavy products, and over gas chromatography in speed. This paper describes the most recent improvements in the apparatus and presents its application in characterizing coal. The emphasis in this work is on employing the TG–FT-IR system to obtain kinetic rates for species evolution under easily obtained laboratory conditions. These rates can then be extrapolated to predict the conversion behavior of the hydrocarbon at higher heating rates and temperatures in practical conversion processes or at lower heating rates and temperatures in geological conversion processes. For several coal samples, a kinetic analysis was applied to species evolution data collected at several different heating rates. For coal, there is a systematic variation in rate with rank for almost all volatile species. Extrapolation to high temperatures shows excellent agreement with high temperature coal pyroloysis data. Extrapolation to low temperatures is consistent with the expected changes induced by bed temperatures over geological times.

Argonne coals; coal; Fourier transform infrared spectroscopy; pyrolysis; thermogravimetric analysis.

INTRODUCTION

For the characterization of hydrocarbons, thermogravimetric (TG) analysis techniques have proved to be very useful. However, TG analysis by itself does not identify the decomposition products. When TG analysis is coupled with evolved product analysis, a great deal of additional information regard-

ing the composition of pyrolysis and oxidation products can be obtained. We have recently employed Fourier transform infrared (FT-IR) spectroscopy to perform such evolved product analysis. FT-IR has an advantage over mass spectroscopy in allowing analysis of very heavy products, and over gas chromatography in speed. The application of TG–FT-IR to coal and petroleum source rock has been described in two recent publications [1,2].

The effluents most difficult to analyze are the heavy decomposition products which condense at room temperature. These condensates, such as tars from coal, are the major evolved products from most hydrocarbons. A recently designed TG–FT-IR apparatus, the Bomem TG/plus allows these products to be analyzed by condensing them into an aerosol which is fine enough to follow the gas through the infrared analysis cell, which is connected without restrictions to the sample area. The aerosol is also fine enough so that there is only a little scattering of the infrared beam and it is thus attenuated almost as though the tar was in the gas phase. The quantitative analysis of both gases and tars allows the mass balance to be closed within a few percent.

The TG/plus apparatus has been applied to the analysis of the Argonne premium coal samples to determine their pyrolysis behavior [3]. In addition, kinetic rate coefficients for the evolution of specific products have been obtained by employing several heating rates between 0.05 K s^{-1} and 1.67 K s^{-1} [4]. These rate coefficients are employed in the FG-DVC model for coal devolatilization [5–9] to allow predictions of pyrolysis at other heating rates and temperatures. This general model combines a functional group (FG) model for gas evolution [10.11] and a statistical depolymerization, vaporization, and crosslinking (DVC) model for tar formation [12–14]. The FG model describes the evolution of gases from sources in the coal, char and tar. The DVC model describes the decomposition and condensation of a macromolecular network under the influence of bond breaking and crosslinking to predict (using statistical methods) the molecular weight distribution of the network fragments. Both Monte Carlo [5,8] and percolation statistics [9] have been employed. Tar is formed from the light fraction of the network fragments which vaporizes and is transported by the light gases. The crosslinking reactions are related to the evolution of CO_2 at low temperature and CH_4 at moderate temperature [5,14,15].

In this paper, we explore how well the kinetic rate coefficients determined at moderate heating rates can be extrapolated to conversion processes at high heating rates ($\approx 40\,000$ K s^{-1}) and natural maturation processes at 10 K per million years. The kinetic rate coefficients and composition parameters derived using the TG/plus applied to the Argonne coals [3,4] were employed in the FG-DVC model which was used to simulate high heating rate pyrolysis experiments and natural maturation. The simulations for coal are compared with high heating rate data previously obtained for Illinois

No. 6 coal [11] and with the natural maturation represented by the Argonne premium sample collection.

EXPERIMENTAL

The TG/plus apparatus has been described previously [3,16]. Its components are as follows: a Du Pont™ 951 TGA; an Infrared Analysis 16 pass gas cell with transfer optics; a MICHELSON 110 FT-IR; (resolution: 4 cm^{-1}, detector: MCT). A typical analysis is performed as follows: a sample (typically 5–200 mg) is taken on a 30°C min^{-1} temperature excursion in the helium sweep gas, first to 150°C to dry for 240 s, then at 30°C min^{-1} to 900°C for pyrolysis. Upon reaching 900°C, the sample is cooled to 250°C over a 20 minute period. After cooling, a small flow of O_2 (0.3 cc s^{-1}) is added to the helium sweep gas and the temperature is ramped to 700°C (or as high as 1000°C) at 30°C min^{-1} for oxidation.

During this excursion, IR spectra are obtained once every 41 s. As discussed previously [1–3,15], the spectra show absorption bands for CO, CO_2, CH_4, H_2O, SO_2, COS, C_2H_4 and NH_3. The spectra above 250°C also show aliphatic, aromatic, hydroxyl, carbonyl and ether bands from tar. The evolution of gases derived from the IR absorbance spectra are obtained by a quantitative analysis program. Gas calibrations were performed using known flows of individual gases. The calibration for CO_2, CO, and H_2O is checked on a routine basis using a sample of calcium oxalate, as described previously [3,16]. The tar absorptivity for each run is obtained by comparing a qualitative evolution curve for the appearance of tar functional groups with the sample weight loss minus the sum of gases.

Samples

The coals analyzed were Argonne premium coal samples. Table 1 presents their ultimate and proximate analysis. More complete characterization of these samples has appeared elsewhere [17].

RESULTS

Determination of kinetic rate coefficients

The TG–FT-IR results for the Illinois No. 6 coal at three heating rates are presented in Fig. 1. The broken lines are the prediction of the FG-DVC model [5–9] while the experimental data are plotted as asterisks connected by solid lines. The left-hand set of curves is for the cumulative weight loss from the balance. Superimposed on each of these plots is the time–tempera-

TABLE 1

Analytical data; ultimate (elemental) and proximate analyses

Coal	UF	WY	IL	PITT	POC	UT	WV	ND
AR H_2O	1.13	28.09	7.97	1.65	0.65	4.63	2.42	32.24
AR Ash	13.03	6.31	14.25	9.10	4.74	4.49	19.36	6.59
Dry Ash	13.18	8.77	15.48	9.25	4.77	4.71	19.84	9.72
Dry VM	27.45	44.73	40.05	37.82	18.60	45.84	30.17	44.94
Dry S	2.32	0.63	4.83	2.19	0.66	0.62	0.71	0.80
Pyritic S	1.77	0.17	2.81	1.37	0.15	0.24	0.16	0.14
Sulfate S	0.01	0.03	0.01	0.01	0.03	0.03	0.03	0.03
Organic S	0.54	0.43	2.01	0.81	0.48	0.35	0.52	0.63
MAF C	85.50	75.01	77.67	83.20	91.05	80.69	82.58	72.94
MAF H	4.70	5.35	5.00	5.32	4.44	5.76	5.25	4.83
MAF N	1.55	1.12	1.37	1.64	1.33	1.57	1.56	1.15
MAF Org S	0.74	0.47	2.38	0.89	0.50	0.37	0.65	0.70
MAF O	7.51	18.02	13.51	8.83	2.47	11.58	9.83	20.34

ture profile. Except for very low heating rates, the coal is heated first to 150°C for drying before heating at the designated rate to 900°C. The agreement between the experimental and predicted weight predictions is quite good at each of the three heating rates. The predicted weight loss is the sum of the tar evolution and the major gases (CO, CO_2, H_2, H_2O, CH_4, paraffins, olefins) which are included in the FG-DVC model. The theoretical curves have been shifted downwards to account for the moisture loss which is not modeled.

The second set of curves in Fig. 1 is for the tar evolution. The prediction of tar evolution is based on the breaking of weak linkages between an assumed polymeric structure for coal followed by transport of the molecule out of the coal if it meets the volatility criteria [5–9]. The position and shape of the main tar peak is predicted very well.

The evolution of CH_4 is also well predicted. The CH_4 evolution is modeled using two sources which evolve in a manner such that the peaks are usually merged into a single peak [6,11]. The evolution of CO_2 is reasonably well predicted at the highest heating rates, but a slight oxidation at the lowest heating rate produces more CO_2 than predicted. Note that the large CO_2 peak observed at high temperatures is due to calcite, not the organic portion of the coal.

The evolution profiles show a systematic shift with increasing heating rate. The change in the temperature for the maximum evolution rate (T_{max}) with temperature can be used in a preliminary analysis to derive kinetic parameters [18,19]. We have used this approach to obtain a preliminary estimate of the mean values of the distributed activation energy parameters. The parameters are further refined by using the FG-DVC model to best fit the complete evolution profiles at each of four heating rates. A similar

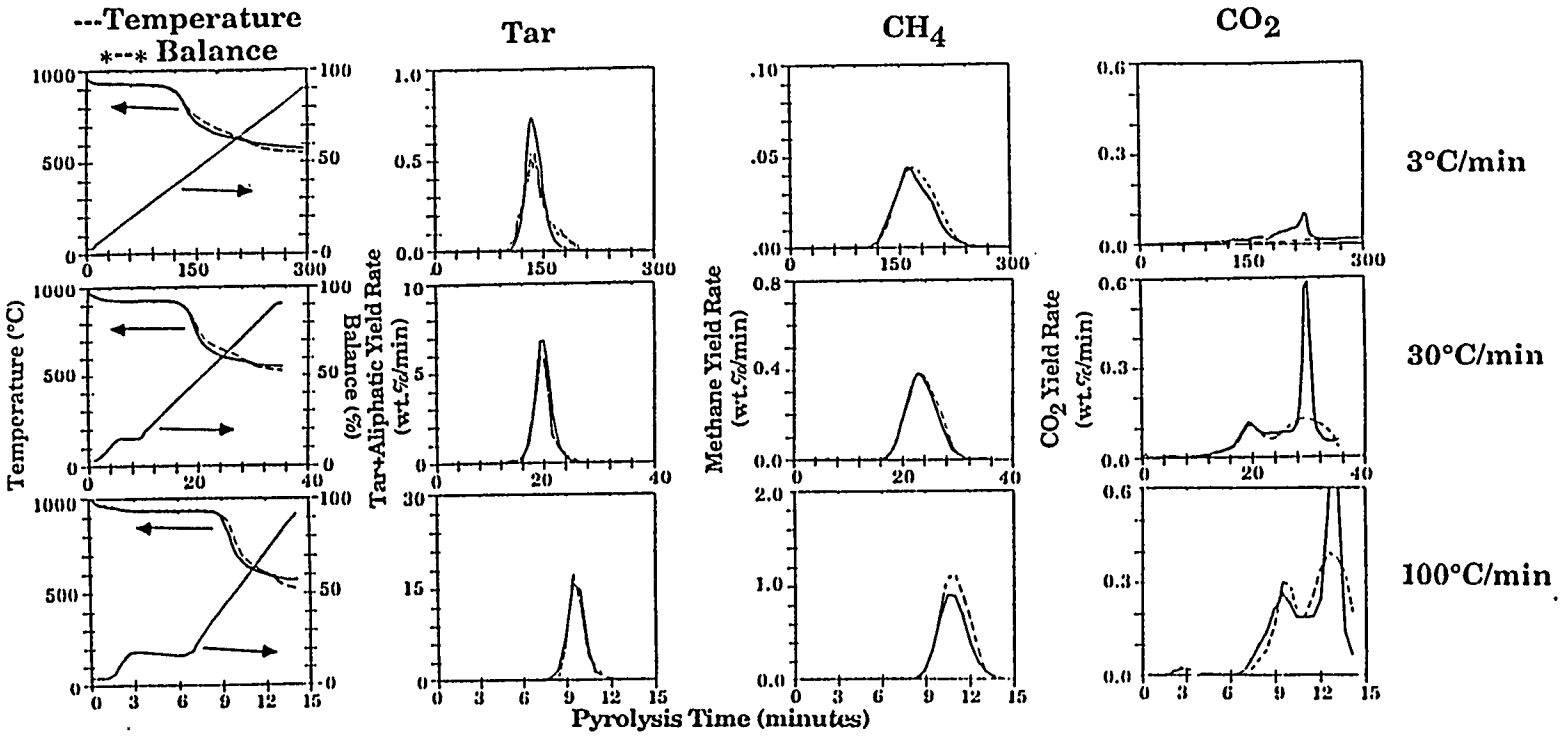

Fig. 1. Kinetic analysis for Illinois No. 6 coal for weight loss, tar evolution, methane evolution and CO_2 evolution at three heating rates. Experiment (solid line) and theory (broken line) using the FG-DVC model with kinetic rates reported in the paper.

analysis was performed for the Zap lignite [4]. The kinetic rate coefficients determined for bond breaking, methane, and CO_2 evolution for Illinois No. 6 and Zap lignite are as follows:

Illinois No. 6

$$k_{\text{bond breaking}} = 1.6 \times 10^{13} \exp[-(25\,000 \pm 1250)/T] \text{ s}^{-1}$$

$$k_{\text{CH}_4\text{-loose}} = 1.5 \times 10^{14} \exp[-(30\,000 \pm 2000)/T] \text{ s}^{-1}$$

$$k_{\text{CH}_4\text{-light}} = 1.9 \times 10^{12} \exp[-(30\,000 \pm 2000)/T] \text{ s}^{-1}$$

$$k_{\text{CO}_2\text{ extra loose}} = 2.0 \times 10^{13} \exp[-(22\,500 \pm 3000)/T] \text{ s}^{-1}$$

$$k_{\text{CO}_2\text{ loose}} = 8.0 \times 10^{17} \exp[-(33\,850 \pm 2000)/T] \text{ s}^{-1}$$

$$k_{\text{CO}_2\text{ light}} = 1.25 \times 10^{14} \exp[-(38\,315 \pm 5000)/T] \text{ s}^{-1}$$

Zap Lignite

$$5 \times 10^{15} \exp[-(30\,000 \pm 1500)/T] \text{ s}^{-1}$$

$$7 \times 10^{13} \exp[-(30\,000 \pm 3000)/T] \text{ s}^{-1}$$

$$2.1 \times 10^{12} \exp[-(30\,000 \pm 3000)/T] \text{ s}^{-1}$$

$$6.2 \times 10^{12} \exp[-(22\,500 \pm 3000)/T] \text{ s}^{-1}$$

$$1.6 \times 10^{17} \exp[-(33\,850 \pm 3000)/T] \text{ s}^{-1}$$

$$2.1 \times 10^{16} \exp[-(38\,315 \pm 3000)/T] \text{ s}^{-1}$$

The rate equation is of the form $k_n = k_0 \exp\{-[(E/R) \pm (\sigma/R)]/T\}$, with k_0 in reciprocal seconds, E/R in kelvins, and σ/R in kelvins. The accuracy of the activation energies is estimated to be within ± 2 kcal. With a fixed activation energy, the accuracy of the pre-exponential factor is $\pm 25\%$ and of σ is $\pm 10\%$. The bond breaking rate is in good agreement with the approximate rate of $3.1 \times 10^{12} \exp[-(24{,}942 \pm 1250)/T]$ derived by Burnham et al. [20].

Simulation of high heating rate experiments

A good test of the validity of the kinetic parameters derived using the TG–FT-IR over a range of low heating rates is the ability to use these parameters to extrapolate to high heating rate conditions. An example is shown in Fig. 2, where the kinetic parameters for the Illinois No. 6 coal were used to simulate previously obtained high heating rate ($\approx 40\,000$ K s^{-1}) data for pyrolysis of another Illinois No. 6 coal with somewhat higher oxygen content [11]. The agreement is excellent except for the amount of CO_2. The contribution from calcite (not included in the model) and the higher oxygen content in this sample (16.5% compared to 11% of the Argonne coal) are the problem.

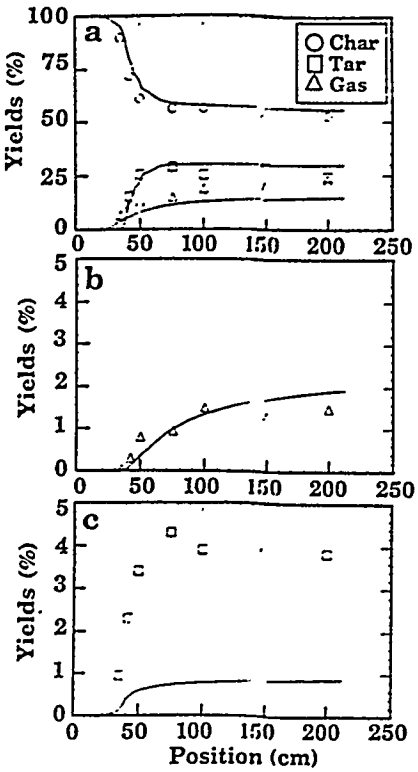

Fig. 2. Pyrolysis of Illinois No. 6 coal in a heated tube reactor at a heating rate of 40000 K s^{-1}; (a) char (○), tar (□), and gas (△), (b) CH_4, and (c) CO_2.

Variations in kinetic rates and compositions with rank

TG/plus analyses have been performed for the other seven Argonne coals to determine their product evolution profile and kinetic rate coefficients [3,4]. Results for the evolution curves for the major evolved species, tar, CH_4, CO_2, CO, and H_2O, are presented in Figs. 3(a)–7(a). For most evolution curves there is a systematic shift in the evolution curves to higher temperatures with increasing rank. There are also systematic decreases in the amounts of CO_2, CO, and H_2O, and a systematic increase in the amount of methane found with increasing rank. With increasing rank, tar increases reaching a maximum for Pittsburgh Seam coal and then decreases.

Simulation of natural maturation

The FG-DVC model was employed to determine whether the shifts in the evolution curves as a function of rank could be predicted by the FG-DVC model. We assume that coals of increasing rank are the products from lower rank coals pyrolyzed under natural conditions at increased times and temperatures. Based on the work of Welte et al. on profiling of the deep basin in Western Canada [21], it is assumed that high rank coals have been subjected to temperatures up to 180 °C while low rank coals have not been

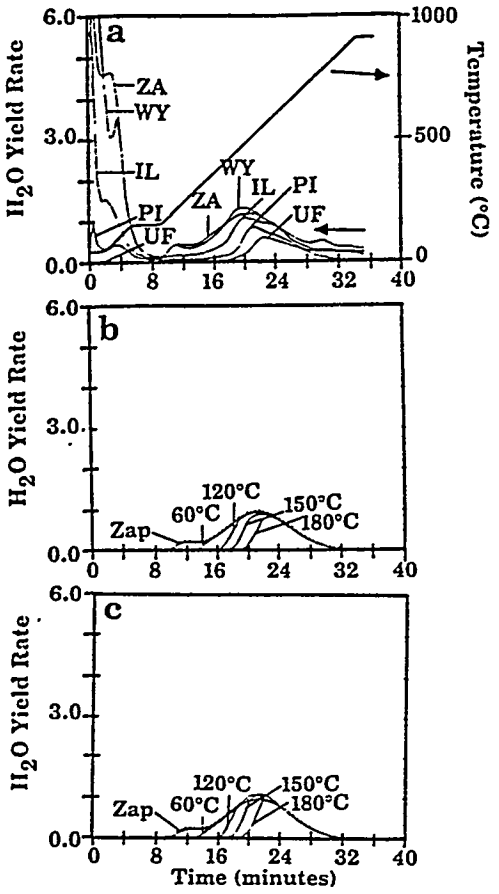

Fig. 3. Evolution curves for H_2O for five coals from the Argonne premium samples collected at 30 °C min^{-1} (UF, Upper Freeport; PI, Pittsburgh; IL, Illinois; WY, Wyodak; ZA, Zap Lignite); (a) measured in TG/Plus, (b) predicted using FG-DVC pyrolysis model, and (c) predicted using FG-DVC maturation model.

elevated above 100 °C. This is also the range suggested by van Krevelen [22]. The pressures were assumed to be 100 atm. during pyrolysis.

The evolution curves assuming a constant heating rate of 10°C per 10^6 years to temperatures of 60, 120, 150, and 180°C are presented in Figs. 3(b)–7(b). The starting coal (i.e. the coal that we employ in the simulation of natural pyrolysis) was the Zap lignite. The predicted evolution curves for water (Fig. 3(b)) show reasonable agreement with the trends measured for water. The CO and CO_2 in Figs. 4(b) and 5(b), however, do not show sufficient removal compared to the natural sequence. The removal of total oxygen is also too slow compared to the removal of hydrogen. This is illustrated in Fig. 8, on a plot of H/C vs. O/C for the maturation prediction compared to the natural maturation. In addition, the model does not predict the increase in tar (Fig. 6(b)) or methane yield (Fig. 7(b)) with maturation. Clearly, the simulation based on the pyrolytic reaction derived using the TG/plus does not represent the natural occurrence.

The question of simulating natural maturation has been discussed by Lewen [23] and Landais and co-workers [24–26]. They observe that labora-

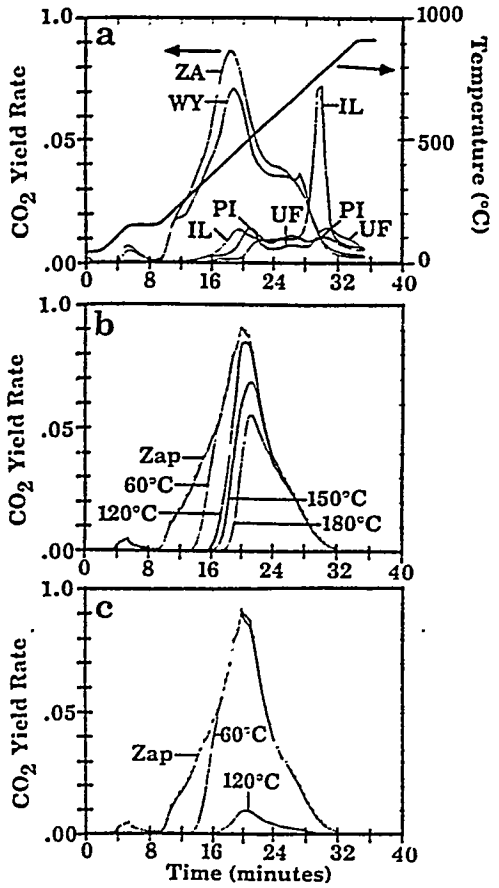

Fig. 4. Evolution curves for CO_2 for five coals from the Argonne premium samples collected at 30 °C min^{-1} (UF, Upper Freeport; PI, Pittsburgh; IL, Illinois; WY, Wyodak; ZA, Zap Lignite); (a) measured in TG/Plus, (b) predicted using FG-DVC pyrolysis model, and (c) predicted using FG-DVC maturation model.

tory pyrolysis under conditions where the pyrolysis products can escape (open system pyrolysis) (such as in the TG/plus) does not represent natural maturation. Landais has proposed that a system termed "confined pyrolysis" is a good simulation of natural maturation. In confined pyrolysis, the coal is subjected to high pressures in a tightly confined tube without dead volume. Lewen has proposed that the hydrous pyrolysis in which the sample is confined with water at high pressure is a better laboratory representation of natural maturation.

These results suggest that the FG-DVC model derived from open system laboratory data should not accurately simulate natural maturation, and so we have explored what changes might be made in the model to simulate the chemistry of the natural system. Based on the TG/plus analysis, we have assumed that the functional group sources for CO and CO_2 are removed by a higher rate process not observed in the TG/plus experiment, but which may occur in confined systems at high pressures in the presence of water. This assumption is consistent with the observation of Lewen [23] that large amounts of CO_2 are produced in hydrous pyrolysis. It is assumed that under

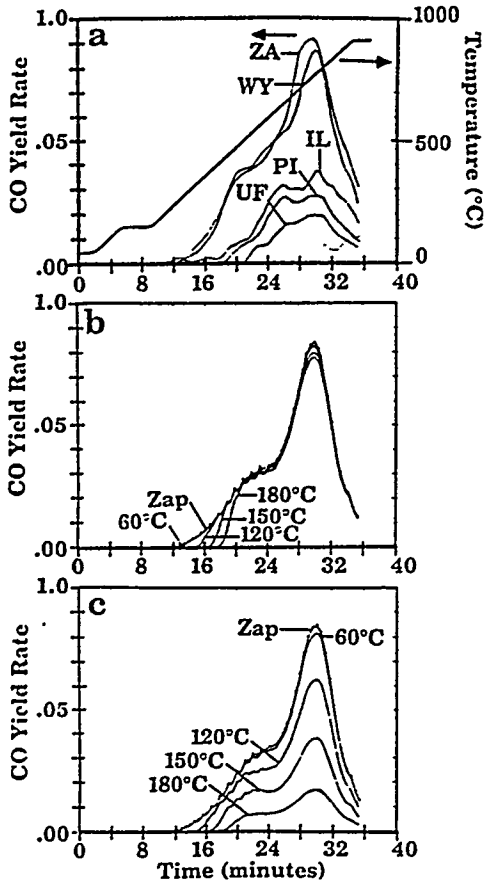

Fig. 5. Evolution curves for CO for five coals from the Argonne premium samples collected at 30 °C min^{-1} (UF, Upper Freeport; PI, Pittsburgh; IL. Illinois; WY, Wyodak; ZA, Zap Lignite); (a) measured in TG/Plus, (b) predicted using FG-DVC pyrolysis model, and (c) predicted using FG-DVC maturation model.

these conditions, all the CO sources are reduced at a kinetic rate $3.5 \times 10^{14} \exp[-(27\,500 \pm 2500)/T)]$ while the CO_2 sources are reduced at a rate $1.5 \times 10^{12} \exp[-(22\,500 \pm 750)/T]$. These rates are chosen to fit the CO and CO_2 profiles in Figs. 4(a) and 5(a). Based on the values of water T_{max}, the temperature maximum in the basin for each coal was assumed to be 60, 120, 150, and 180°C for the Wyodak, Illinois, Pittsburgh, and Upper Freeport coals, respectively. It is also assumed that neither process involves the formation of crosslinks. Under these assumptions, the curves in Fig. 3(c)–7(c) are obtained, as well as the broken curve in Fig. 8. As can be seen, these changes in the assumed chemistry for natural maturation give a much better simulation of the natural maturation sequence for CO and CO_2 (as expected), but, in addition, improvements are made in the predictions for the tar, the O/C vs. H/C ratio, and the systematic variation in kinetic rates with coal rank.

These results suggest that natural maturation provides an additional mechanism for the removal of carboxyl groups and ether linkages (which are believed to be the sources for CO_2 and CO [5, 10]) which is faster than that

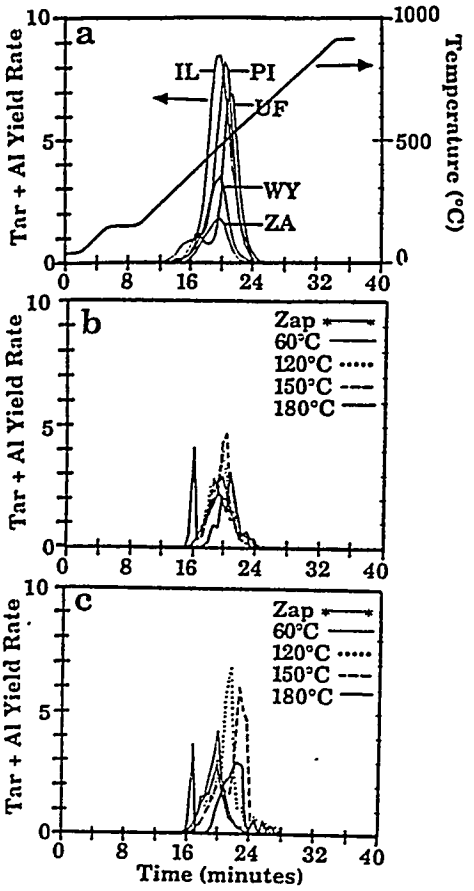

Fig. 6. Evolution curves for tar for five coals from the Argonne premium samples collected at 30 °C min^{-1} (UF, Upper Freeport; PI, Pittsburgh; IL, Illinois; WY, Wyodak; ZA, Zap Lignite); (a) measured in TG/Plus, (b) predicted using FG-DVC pyrolysis model, and (c) predicted using FG-DVC maturation model.

observed under laboratory conditions in an open system. These reactions do not result in the formation of crosslinks as is observed to accompany CO_2 formation under open laboratory conditions. While the rates we have picked are highly speculative, it is clear that some reactions of the kind described do occur in the natural aging process, but not in open system pyrolysis.

There are, however, still some problems with the model. The increase in methane is not predicted. It appears that maturation chemistry must include some process for adding methyl groups. Also, the shift in the T_{max} for tar are somewhat too large ($\approx 70°C$) compared to what is observed ($\approx 50°C$). This may be due to the fact that the T_{max} values for the low rank coals (Zap and Wyodak) are too high due to the domination in these peaks of polymethylenes.

CONCLUSIONS

The TG/plus provides an extensive analysis of the pyrolysis behavior of coals.

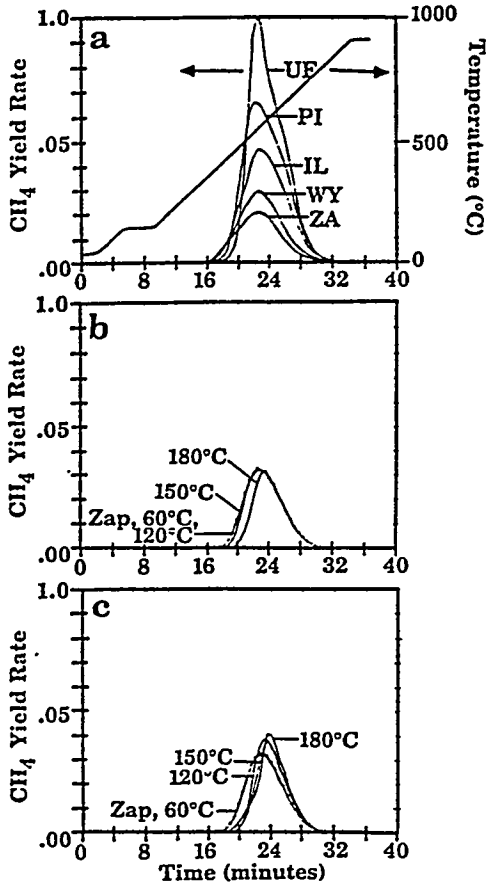

Fig. 7. Evolution curves for CH_4 for five coals from the Argonne premium samples collected at 30 °C min^{-1} (UF, Upper Freeport; PI, Pittsburgh; IL, Illinois; WY, Wyodak; ZA, Zap Lignite); (a) measured in TG/Plus, (b) predicted using FG-DVC pyrolysis model, and (c) predicted using FG-DVC maturation model.

Kinetic rate coefficients have been derived for the evolution of tar, CH_4, CO_2, CO, and H_2O for an Illinois No. 6 bituminous coal and a Zap lignite using data from the TG/plus at 0.05, 0.5, 0.83, and 1.67 at K s^{-1}.

The kinetic rate coefficients for Illinois No. 6 were employed in the FG-DVC coal pyrolysis model to simulate pyrolysis of Illinois No. 6 coal at 20 000 K s^{-1}. There is good agreement with the data.

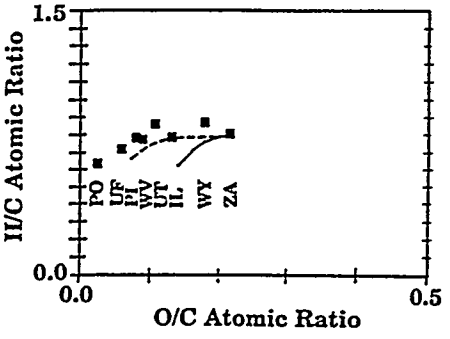

Fig. 8. Maturation of coal. Comparison of predictions for FG-DVC pyrolysis model (solid), FG, DVC maturation model (broken) and the data for the Argonne coals (symbols).

The kinetic rate coefficients for Zap lignite were employed in the FG-DVC model to simulate natural maturation at 10 K per 10^6 years. Except for the H_2O prediction, the simulations based on the chemical reactions determined from experiments performed in the laboratory in open systems do not match the variations in evolution curves with rank for the Argonne premium sample collection.

Two changes were made in the FG-DVC model to account for the possible differences between the laboratory open pyrolysis and confined natural maturation in the presence of H_2O at high pressure: (a) a decarboxylation reaction is assumed to occur which removes the sources of CO_2 at a higher rate than originally predicted and without the formation of crosslinks usually associated with CO_2 evolutions; and (b) ether groups are removed (thus removing the source for CO evolution) at a higher rate than originally predicted.

With these two changes made and the rates for these reactions picked so that the predicted CO_2 and CO evolution profiles match the natural sequence, the model predicts the proper variation in H/C ratio vs. O/C ratio, the correct variation with rank of the tar yield and the nearly correct variation with rank in kinetic rates for product evolution. The increase in methane with increasing rank is not properly predicted, suggesting some additional chemistry in the natural sequence which forms methyl groups.

ACKNOWLEDGEMENT

Support from NSF Grant No. ISI-8703520 and DOE Contract Nos. DE-AC21-86MC23075 and DE-AC22-89PC89878 is gratefully acknowledged.

REFERENCES

1 R.M. Carangelo, P.R. Solomon and D.J. Gerson, Fuel, 66 (1987) 960.
2 J.K. Whelan, P.R. Solomon, G.V. Deshpande and R.M. Carangelo, Energy and Fuels, 2 (1988) 65.
3 P.R. Solomon, M.A. Serio, R.M. Carangelo, R. Bassilakis, D. Gravel, M. Baillargeon, F. Baudais and G. Vail, Energy & Fuels, 4 (3) (1990) 319.
4 M.A. Serio, P.R. Solomon, S. Charpenay, Z.Z. Yu and R. Bassilakis, Kinetics of Volatile Product Evolution from the Argonne Premium Coals, ACS Div. Fuel Chem. Preprints, Washington, DC, 35 (1990) to be presented.
5 P.R. Solomon, D.G. Hamblen, R.M. Carangelo, M.A. Serio and G.V. Deshpande, Energy and Fuel, 2 (1988) 405.
6 P.R. Solomon, M.A. Serio, D.G. Hamblen, Z.Z. Yu and S. Charpenay, ACS Div. Fuel Chem. Preprints, 35 (2) (1990) 479.
7 P.R. Solomon, D.G. Hamblen, Z.Z. Yu and M.A. Serio, Fuel, 69 (1990) 754.

8 M.A. Serio, P.R. Solomon, Z.Z. Yu and G.V. Deshpande, An Improved Model of Coal Devolatilization, Int. Conf. on Coal Science Proceedings, IEA, October 23–27, 1989, Tokyo, Japan, p. 209.
9 P.R. Solomon, M.A. Serio, D.G. Hamblen, Z.Z. Yu and S. Charpenay, ACS Div. Fuel Chem. Preprints, 35 (2) (1990) 479.
10 P.R. Solomon and D.G. Hamblen, "Pyrolysis", in R.H. Schlosberg (Editor), Chemistry of Coal Conversion, Plenum, New York, NY, (1985) pp. 121–251.
11 M.A. Serio, D.G. Hamblen, J.R. Markham, P.R. Solomon, Energy and Fuel, 1 (1987) 138.
12 P.R. Solomon and H.H. King, Fuel, 63 (1984) 1302.
13 K.R. Squire, R.M. Carangelo, M.B. DiTaranto, and P.R. Solomon, Fuel, 65 (1986) 833.
14 P.R. Solomon, D.G. Hamblen, R.M. Carangelo, M.A. Serio and G.V. Deshpande, Combustion and Flame, 71 (1988) 137.
15 P.R. Solomon, M.A. Serio, G.V. Deshpande and E. Kroo, Energy and Fuels, 4 (1) (1990) 42.
16 R.M. Carangelo, P.R. Solomon, R. Bassilakis, D. Gravel, M. Baillargeon, F. Baudais and G. Vail, Applications of TG–FT-IR in the Analytical Lab, American Laboratory, (1990) p. 51.
17 K. Vorres, Am. Chem. Soc. Div. Fuel Chem. Preprints, 32 (4) (1987) 221, see also Users Handbook for the Argonne Premium Coal Sample Program, Argonne National Lab. (September 1989).
18 H. Jüntgen, and K.H. Van Heek, Fuel, 47 (1968) 103; Progress Made in the Research of Bituminous Coal, paper given at the annual meeting of the DGMK, Salzburg, (1968), Translated by Belov and Associates, Denver, CO, APTIC-TR-0779 (1970).
19 R.L. Braun, and A.K. Burnham, Energy and Fuels, 1 (1987) 153.
20 A.K. Burnham, M.S. Oh, R.W. Crawford, and A.M. Samoun, Energy and Fuels, 3 (1989) 42.
21 D.H. Welte, R.G. Schaefer, W. Stoessinger, and W. Radke, Mitt, Geol. Palaontol Inst. Univ. Hamb. 56 (1984) 263.
22 van Krevelen, Coal, Elsevier, Amsterdam 1961.
23 M.D. Lewen, in M.H. Engel and S.A. Macko, (Editor), Organic Geochemistry, Plenum, NY, Chapter 24, to be published.
24 P. Landais, R. Michels, and B. Poty, J. Anal. and Appl. Pyrol. 16 (1989) 103.
25 P. Landais, J.C. Monin, M. Monthioux, B. Poty, and P. Zaugg, C.R. Acad. Sci. Paris, t, 308, Serie II, 1989 p. 1161.
26 M. Monthioux, and P. Landais, Energy and Fuels, 2 (1988) 794.

User's Forum

You are invited to submit your comments concerning the clarity, accuracy, and usefulness of this manual. Constructive critical comments are most welcome and will help us continue our efforts to generate quality user documentation. Please list the page number for questions and comments. Use other side if necessary.

From:
Name_____ Title_____
Company_____ Date_____
Address and Phone No._____
Mail to:

Dr. Andy M. Eaton
45 Crabtree Building
Brigham Young University
Provo, UT 84602